



**University of
Nottingham**

UK | CHINA | MALAYSIA

Investigating the role of Y-box binding protein 1 in medulloblastoma tumour progression and drug resistance

Louisa Taylor MSci, MRes

Thesis submitted to the University of Nottingham for the degree of
Doctor of Philosophy

January 2022



Declaration

I confirm that the work presented in this thesis is my own work except where stated in the text.

The material and figures included in Sections 1.4.1 - 1.4.4 draw heavily on my previously published literature review (Taylor et al., 2021) and are presented in line with the article reuse permissions policies of AACR journals.

I understand the nature of plagiarism and that it is a serious academic offence. I confirm that no material in this project has been plagiarised.

Name: Louisa Taylor

Signed: 

Date: 10th January 2022

Abstract

Introduction: Medulloblastoma relapse represents the most significant unmet clinical challenge in childhood cancer. In spite of this, our understanding of the molecular biology of relapsed medulloblastoma is limited. Evidence is emerging, however, that the biology of medulloblastoma at relapse differs significantly from the disease at diagnosis. Such genetic divergence may arise through the emergence and expansion of a therapy-resistant sub-population of cells. Thus, the identification of targets that either mark therapy resistant cell populations, or drive the proliferation of resistant medulloblastoma cells, may improve treatment strategies for relapsed disease. YB-1, a transcription factor encoded by the *YBX1* gene, has been extensively researched in non-CNS tumours where elevated expression is associated with tumour progression and drug resistance. However, little is known regarding the significance of YB-1 in paediatric brain tumours. This study, therefore, set out to examine the functional role of YB-1 in medulloblastoma tumourigenesis. Particular attention was paid to the multi-drug transporter ABCB1, a putative YB-1 target, which our studies have shown to be associated with cancer cell therapy resistance and high-risk medulloblastoma.

Methods and Results: Genomic analysis of medulloblastoma patient datasets demonstrated elevated *YBX1* expression across all four core molecular medulloblastoma subgroups, which was associated with poor overall survival and metastasis. In support of this, genetic knockdown of *YBX1* diminished the invasive capability of medulloblastoma cells in 3D *in vitro* invasion assays. To build a global picture of YB-1 transcriptional control in medulloblastoma, whole transcriptome sequencing of *YBX1* knockdown cell lines was employed. Ingenuity Pathway Analysis indicated YB-1 involvement in key cellular processes including lipid metabolism, the Sirtuin signalling pathway and the activation of MYC and mTOR pathway components; revealing novel, pro-tumourigenic functions for YB-1 in medulloblastoma cells.

To assess the association between YB-1 and *ABCB1* transcriptional regulation, chromatin immunoprecipitation (ChIP) assays were undertaken, confirming strong YB-1 interaction within the distal *ABCB1* promoter region. Accordingly, YB-1 depletion was associated with decreased *ABCB1* expression and concomitant increased sensitivity to vincristine – an *ABCB1* substrate. Further investigation of the association between YB-1 and drug response, this time with cisplatin, a non-*ABCB1* substrate, revealed YB-1 nuclear expression was elevated in medulloblastoma cells following short-term cisplatin treatment, indicative of YB-1 involvement in the acute cisplatin stress response. ChIP sequencing of cisplatin-tolerant cell lines was used to identify YB-1 target genes associated with a chronic cisplatin-tolerant phenotype. This highlighted an additional function for YB-1 in the acquisition of cisplatin resistance in medulloblastoma cells.

In order to better understand general mechanisms surrounding drug resistance in medulloblastoma, 3'mRNA sequencing of stable cisplatin- and vincristine tolerant cell lines was also undertaken. Notably, differential gene expression analysis identified the existence of a drug-tolerant gene expression signature – a gene set common to all sequenced drug-tolerant lines, irrespective of subgroup or treatment type. These genes likely represent novel mediators of the medulloblastoma drug-tolerant state and thus may present new opportunities for therapeutic targeting.

Conclusion: This study has characterised the role of YB-1 in medulloblastoma and has demonstrated clear associations between YB-1 expression and various aspects of medulloblastoma tumorigenesis, including invasion, *MYC* activity and lipid metabolism. Importantly, we also provide evidence to support a function for YB-1 in both acute drug response and acquired drug resistance and identify YB-1 as a transcriptional regulator of drug resistance-related gene *ABCB1*. Finally, we identify therapeutically targetable hits implicated in the acquisition of drug-tolerance, both directly regulated by and independent from YB-1, which may inform future pre-clinical investigations to establish more effective therapeutic options for the treatment of high-risk medulloblastoma.

Acknowledgements

I cannot quite believe that, after almost four and a half years, my PhD has finally come to a close. For every challenge and failed experiment there have been so many more brilliant memories and rewarding experiences and I feel very grateful to have been given such an opportunity. Of course, this research would not have been possible without the support and guidance of so many and for that I am truly thankful.

I would first like to thank my wonderful supervisor, Dr Beth Coyle, for her continued encouragement and advice throughout my PhD. I could not have asked for a kinder or more supportive supervisor, thank you for inspiring and motivating me. To my supervisor, Dr Ian Kerr, your support and reassurance has helped me grow and given me confidence as a researcher. You have been a constant source of advice and knowledge (and humour!) and it has been a pleasure to work with you, thank you.

I would also like to express my gratitude to the BBSRC Doctoral Training Partnership who funded my PhD and The Stoneygate Children's Brain Tumour Research Fund who provided additional funding for key parts of this research project.

I feel incredibly lucky to have made lifelong friends during my PhD. To my lab group – Macha, Hannah, James, Sophie, Christine, Pippa and Alice – you have supported me and made me laugh every day of my PhD, I am so grateful for all of you. To Michaela and Alina, travelling to Boston with you for our first international conference is one of my PhD highlights, thank you for being such wonderful friends. To Alex J and Alex

P, thank you for always being there to make me smile, I am so happy that I have been able to share this experience with you both.

I would also like to thank all other members of the CBTRC who have made the lab such a friendly and happy working environment, especially Phoebe, Catherine, Lou, Rebeca and Susie. I would like to extend a special thank you to Dr Franziska Linke. Your drive, knowledge and skill is truly inspiring - thank you for your being so helpful and generous with your time.

Lastly, I would like to thank my loved ones. To Hayden, thank you for always being there for me, for helping me to believe in myself and for understanding how important my scientific career is to me. You are my best friend and greatest support and you have helped me more than you will ever know. To my brother Eddie, you are a constant source of entertainment – thank you for keeping me laughing. Finally, to my brilliant parents, Andrew and Fiona, I cannot put into words how much I value you both. I would not be where I am today without your endless support, love and encouragement. I'm not sure if I will ever be able to thank you enough for everything you have done for me, but I wanted to say the biggest thank you anyway, I hope I have made you proud.

Table of Contents

Declaration	i
Abstract	ii
Acknowledgements	iv
Table of Contents	vi
List of Figures	xiv
List of Tables	xx
List of Common Abbreviations	xxii
Chapter 1 Introduction	2
1.1 Paediatric Cancer.....	2
1.2 Paediatric Brain Cancer	4
1.2.1 Medulloblastoma	6
1.3 ABC Transporters.....	24
1.3.1 ABCB1 and Cancer.....	24
1.3.2 ABCB1 and Medulloblastoma	27
1.3.3 Inhibition of ABCB1	28
1.4 Y-Box Binding Protein 1 (YB-1)	31
1.4.1 Structural Organisation of YB-1	33
1.4.2 Regulation of YB-1.....	36
1.4.3 YB-1 and Brain Tumours.....	45
1.4.4 YB-1 and Paediatric Brain Tumours in the Clinic.....	56
1.5 Aims	62
Chapter 2 Materials and Methods	65
2.1 Identification of candidate <i>ABCB1</i> interactors.....	65
2.2 Genomic analysis of large-scale publicly available datasets.....	67
2.2.1 Survival analysis of large-scale publicly available datasets	67
2.3 Patient Analysis	69
2.3.1 Paediatric medulloblastoma Nottingham tumour microarray	69
2.3.2 Paediatric medulloblastoma Birmingham tumour microarray.....	69
2.4 Cell Maintenance.....	70

2.4.1	Culturing Adherent Cells	70
2.4.2	Culturing Semi-Adherent Cells	71
2.4.3	Culturing Suspension Cells	71
2.4.4	Cell Counting	72
2.4.5	Cell Storage	73
2.4.6	Culturing Cells From Frozen	74
2.4.7	Mycoplasma Testing	74
2.5	Drug Treatments.....	74
2.5.1	Drugs used in this Study.....	74
2.5.2	Drug response assays for IC ₅₀ value calculation	75
2.5.3	Optimisation of puromycin selection condition	76
2.5.4	Assessment of YB-1 localisation in response to drug treatment.....	77
2.6	Generation of stable knockdown cell lines	78
2.6.1	Determination of relative transduction efficiency	79
2.6.2	Transduction of target cells	82
2.7	Generation of drug-tolerant (DT)-cell lines.....	83
2.7.1	Generation of stable drug tolerant cell lines	84
2.7.2	Maintenance of drug tolerant cell lines.....	84
2.8	Modified Boyden chamber invasion and migration assay	86
2.8.1	Quantification of cell invasion/migration	87
2.9	Molecular Biology.....	88
2.9.1	Chromatin Immunoprecipitation (ChIP)	88
2.9.2	Optimisation of ChIP cross-linking and sonication conditions.....	88
2.9.3	RNA Isolation.....	91
2.9.4	Complementary DNA (cDNA) Synthesis.....	92
2.9.5	Temperature gradient optimisation of primers.....	93
2.9.6	qRT-PCR for Gene Expression Analysis	94
2.9.7	Immunoblotting	95
2.9.8	Immunofluorescence	100
2.9.9	Immunohistochemistry	105
2.10	Next-generation Sequencing.....	110
2.10.1	Whole Transcriptome Sequencing.....	110

2.10.2	3'mRNA Sequencing.....	116
2.10.3	ChIP Sequencing.....	122
Chapter 3	The identification and characterisation of a potential regulator of <i>ABCB1</i> in medulloblastoma.....	127
3.1	Introduction.....	127
3.2	Identification of YB-1 and NFE2L2 as targets for further investigation	129
3.2.1	Search for potential regulators of the <i>ABCB1</i> gene.....	129
3.3	Analysis of YB-1 and NFE2L2 expression across publicly available large-scale medulloblastoma datasets	137
3.3.1	<i>YBX1</i> and <i>NFE2L2</i> are highly expressed in paediatric brain tumours and across medulloblastoma subgroups	137
3.3.2	High <i>YBX1</i> expression correlates with poor overall survival and metastasis	141
3.4	Analysis of YB-1 expression in a medulloblastoma cell line model.....	148
3.4.1	YB-1 is expressed across various medulloblastoma cell lines.....	148
3.4.2	YB-1 localises predominantly to the cytoplasm in medulloblastoma cell lines	150
3.5	Investigation of YB-1 expression and localisation across patient medulloblastoma tumour microarrays	152
3.5.1	The majority of medulloblastoma patients exhibit high YB-1 protein levels and significant YB-1 nuclear accumulation.	155
3.5.2	YB-1 expression does not appear to correlate with metastatic status at time of diagnosis in medulloblastoma.....	159
3.6	Summary.....	160
Chapter 4	Examination of YB-1 as a regulator of <i>ABCB1</i> in medulloblastoma	162
4.1	Introduction.....	162
4.2	Examination of the YB-1- <i>ABCB1</i> functional interaction	164
4.2.1	<i>ABCB1</i> expression is highest amongst SHH and Group 3 cell lines....	164
4.2.2	YB-1 interacts directly with an inverted CCAAT box in the <i>ABCB1</i> promoter.....	166
4.2.3	YB-1 represents a potential regulator of the <i>ABCB1</i> gene in medulloblastoma	169
4.3	Analysis of the effect of drug treatment on YB-1 subcellular localisation in medulloblastoma.....	171

4.3.1	Optimisation of chemotherapy drug concentration.....	171
4.3.2	Treatment of Group 3 medulloblastoma cell lines with cisplatin but not vincristine elevates levels of nuclear YB-1.....	175
4.4	Study of <i>ABCB1</i> expression in response to drug treatment.....	189
4.4.1	<i>ABCB1</i> expression is elevated following treatment with vincristine, not cisplatin	189
4.4.2	YB-1 enrichment at the <i>ABCB1</i> promoter is likely altered dependent on the chemotherapeutic agent employed.....	193
4.5	Summary.....	196
Chapter 5 Functional analysis of the role of YB-1 in drug resistance and metastasis in medulloblastoma		199
5.1	Introduction.....	199
5.2	shRNA-mediated knockdown of <i>YBX1</i> expression in medulloblastoma Group 3 cell lines	201
5.2.1	Optimisation of shRNA knockdown	201
5.2.2	Generation of stable <i>YBX1</i> knockdown cell lines.....	205
5.2.3	Validation of Group 3 <i>YBX1</i> knockdown cell lines	208
5.3	Effect of YB-1 depletion on cellular sensitivity to anti-cancer agents	213
5.3.1	YB-1 depletion sensitises medulloblastoma Group 3 cell lines to vincristine.....	213
5.3.2	YB-1 depletion results in significantly reduced expression of drug-efflux pump <i>ABCB1</i>	216
5.3.3	YB-1 depletion sensitises medulloblastoma Group 3 cell line HDMB-03 to HDAC inhibitor panobinostat and BET bromodomain inhibitor JQ1	218
5.3.4	YB-1 depletion impedes the invasive capacity of medulloblastoma cells	225
5.4	Whole transcriptome sequencing of <i>YBX1</i> -knockdown medulloblastoma Group 3 cell lines	228
5.4.1	Sample preparation and sequencing	228
5.4.2	Mapping of sequencing data.....	229
5.4.3	Differential gene expression analysis	231
5.4.4	Analysis of significantly differentially expressed genes arising from <i>YBX1</i> knockdown.....	236
5.4.5	Ingenuity Pathway Analysis (IPA) of gene expression profiles following in <i>YBX1</i> knockdown.....	239

5.5	Summary.....	254
Chapter 6	Examination of the route to drug tolerance in medulloblastoma	257
6.1	Introduction.....	257
6.2	Generation of drug-tolerant medulloblastoma cell lines.....	259
6.2.1	Long-term drug treatment with continuous selection promotes increased tolerance to cisplatin in medulloblastoma Group 3 cell lines.....	259
6.2.2	Group 3 cell lines are unable to develop tolerance to vincristine following continuous selection and dose escalation.....	264
6.2.3	Continuous vincristine selection facilitates tolerance in SHH cell line DAOY	265
6.2.4	Drug-tolerant cell lines express altered levels of ABC transporters ..	267
6.2.5	Drug-tolerant cell lines display reduced levels of <i>YBX1</i>	269
6.3	Analysis of the transcriptomic changes that occur upon the acquisition of drug tolerance in medulloblastoma Group 3 and SHH cell lines	272
6.3.1	Sample preparation and sequencing	273
6.3.2	Mapping of sequencing data.....	273
6.3.3	Differential Gene Expression Analysis	274
6.3.4	Analysis of significantly differentially expressed genes arising from the development of drug-tolerance	281
6.3.5	Gene ontology analysis of gene expression profiles in drug-tolerant cell lines	290
6.4	Identification of YB-1 downstream targets upon acute and chronic drug exposure	294
6.4.1	ChIP sample preparation.....	295
6.4.2	Mapping of ChIP-Seq Samples	300
6.4.3	Peak Calling	305
6.4.4	Integration of ChIP-Seq and 3'mRNA-Seq datasets reveals potential YB-1 targets implicated in drug resistance in medulloblastoma cell lines.	310
6.5	Summary.....	315
Chapter 7	Discussion	318
7.1	<i>YBX1</i> expression has oncogenic implications in medulloblastoma patients ..	318
7.1.1	High <i>YBX1</i> expression correlates with poor overall survival in medulloblastoma patients.....	319

7.1.2	YB-1 exhibits substantial nuclear accumulation in a medulloblastoma patient cohort	320
7.2	YB-1 may represent a novel regulator of metastasis in medulloblastoma	321
7.2.1	<i>YBX1</i> expression correlates with metastatic disease.....	321
7.2.2	<i>YBX1</i> knockdown impedes the invasive capacity of medulloblastoma Group 3 cell lines	322
7.3	Whole transcriptome sequencing reveals a function for <i>YBX1</i> in numerous key cellular pathways in Group 3 medulloblastoma	324
7.3.1	<i>YBX1</i> knockdown dysregulates various aspects of lipid metabolism, highlighting a novel function of YB-1 in medulloblastoma	325
7.3.2	<i>YBX1</i> knockdown alters cell death and survival pathways in Group 3 medulloblastoma	327
7.4	3'mRNA-Seq of medulloblastoma drug-tolerant cell lines identifies novel drug-tolerant gene signatures.....	332
7.4.1	A seven gene signature defines all drug-tolerant cell lines sequenced, regardless of parental line or treatment type	333
7.5	YB-1 mediates intrinsic vincristine tolerance in Group 3 medulloblastoma cells by the transcriptional regulation of the <i>ABCB1 gene</i>	336
7.5.1	Binding site prediction software identified a Y-Box binding site within the <i>ABCB1</i> promoter region	337
7.5.2	YB-1 represents a novel transcriptional regulator of <i>ABCB1</i> in medulloblastoma	338
7.5.3	YB-1 depletion increases cellular sensitivity to vincristine in medulloblastoma Group 3 cell lines	339
7.5.4	Vincristine treatment promotes elevated <i>ABCB1</i> expression, likely mediated by pre-existing nuclear YB-1.....	340
7.6	YB-1 may regulate multiple genes implicated in acquired cisplatin resistance in Group 3 medulloblastoma	342
7.6.1	Acute cisplatin treatment triggers elevated YB-1 nuclear levels in Group 3 medulloblastoma cell lines	342
7.6.2	YB-1 may represent a transcriptional regulator of numerous genes implicated in chronic cisplatin tolerance in Group 3 medulloblastoma	346
7.6.3	ChIP-Seq data analysis identifies direct transcriptional targets of YB-1 implicated in the acquisition and maintenance of a chronic cisplatin-tolerant state	347
7.7	Concluding Statement	355

References	356
Appendix	389
Appendix A: Chapter 3 – The identification and characterisation of a potential regulator of <i>ABCB1</i> in medulloblastoma.....	389
Appendix A1.....	389
Appendix A2.....	391
Appendix A3.....	392
Appendix A4.....	394
Appendix A5.....	395
Appendix A6.....	394
Appendix A7.....	396
Appendix A8.....	396
Appendix B: Chapter 4 – Examination of YB-1 as a regulator of <i>ABCB1</i> in medulloblastoma.	397
Appendix B1.....	397
Appendix B2.....	398
Appendix B3.....	399
Appendix B4.....	400
Appendix B5.....	401
Appendix B6.....	402
Appendix B7.....	403
Appendix C: Chapter 5 – Functional analysis of the role of YB-1 in drug resistance and metastasis in medulloblastoma.	404
Appendix C1.....	404
Appendix C2.....	405
Appendix C3.....	406
Appendix C4.....	407
Appendix C5.....	407
Appendix D: Chapter 6 - Examination of the route to drug tolerance in medulloblastoma.....	409
Appendix D1.....	409
Appendix D2.....	410

Appendix D3.....	411
Appendix D4.....	414
Appendix D5.....	415
Appendix D6.....	416
Appendix D7.....	417
Appendix D8.....	418
Appendix D9.....	419
Appendix D10.....	420
Appendix D11.....	422
Appendix D12.....	426
Appendix D13.....	426
Appendix D14.....	427
Appendix E: Chapter 7 – Discussion	428
Appendix E1	428
PhD Project Outputs.....	429
Laboratory Rotations.....	429
List of publications.....	430
Grant Awards.....	430
Presentations.....	431
Oral Presentations.....	431
Poster Presentations.....	431
Awards.....	431
Professional Internship for PhD Students (PIPS)	432
PIPS Reflective Statement.....	432

List of Figures

Figure 1.1 Childhood cancer five-year actuarial survival.	3
Figure 1.2 Histological subtypes of medulloblastoma.	10
Figure 1.3 Molecular subgroups of medulloblastoma and their various clinical, histological and genetic features.	11
Figure 1.4 WNT and SHH pathways and medulloblastoma.	12
Figure 1.5 Location of medulloblastoma tumours.....	18
Figure 1.6 A simplified model of ABC transporter-mediated efflux from the cell.....	26
Figure 1.7 Summary of core YB-1 functions.....	32
Figure 1.8 YB-1 protein domain organisation.	35
Figure 1.9 Regulation of YB-1 expression.	39
Figure 1.10 Proposed mechanisms of YB-1 nuclear translocation.	44
Figure 1.11 Proposed oncogenic functions of YB-1 in brain tumours.	49
Figure 2.1 <i>ABCB1</i> GXT_26193608 Promoter.....	66
Figure 2.2 Mapping of GIPZ lentiviral shRNA constructs onto <i>YBX1</i> mRNA sequence.	81
Figure 2.3 Simplified flow diagram depicting generation of drug-tolerant (DT)-cell lines.	85
Figure 2.4 Schematic of ChIP assay.....	90
Figure 2.5 Simplified workflow depicting the calculation of nuclear staining intensity using binary masks in Fiji (ImageJ).	104
Figure 2.6 Colour deconvolution and quantification of cytoplasmic/nuclear staining intensity using IHC Profiler.....	109
Figure 2.7 Whole transcriptome sequencing.....	115
Figure 2.8 3'RNA-Seq workflow using Lexogen Quant-Seq sequencing library methodology.	118
Figure 2.9 QuantSeq 3'mRNA-Seq data integrated data analysis pipeline using the BlueBee genomics platform.	121
Figure 2.10 Overview of ChIP-Seq analysis process.....	125
Figure 3.1 Workflow of Genomatix MatInspector Software.	131

Figure 3.2 Identification of candidate regulators of the ABCB1 promoter.....	134
Figure 3.3 <i>YBX1</i> expression is elevated in paediatric brain cancer and across all four subgroups of medulloblastoma.	139
Figure 3.4 <i>NFE2L2</i> expression is elevated in paediatric brain cancer and across all four subgroups of medulloblastoma.....	140
Figure 3.5 <i>YBX1</i> expression correlates with poor survival in medulloblastoma.....	145
Figure 3.6 <i>YBX1</i> gene expression is elevated in metastatic tumours.	147
Figure 3.7 <i>YBX1</i> and YB-1 are expressed in a range of medulloblastoma cell lines.	149
Figure 3.8 YB-1 localises mainly to the cytoplasm in untreated medulloblastoma cell lines.	151
Figure 3.9 Medulloblastoma patient TMAs display differential YB-1 protein expression.	154
Figure 3.10 YB-1 is expressed in medulloblastoma patient tissue samples.	157
Figure 3.11 Medulloblastoma patients display significant YB-1 nuclear accumulation.	158
Figure 4.1 <i>ABCB1</i> expression is highest in SHH cell lines.....	165
Figure 4.2 YB-1 binds to an inverted CCAAT box upstream of the Genomatix MatInspector predicted binding site in <i>ABCB1</i> promoter..	168
Figure 4.3 YB-1 is strongly enriched at an inverted CCAAT box in the <i>ABCB1</i> promoter in Group 3 medulloblastoma cell lines.	170
Figure 4.4 Cisplatin cytotoxicity in SHH and Group 3 cell lines.....	173
Figure 4.5 Vincristine cytotoxicity in SHH and Group 3 cell lines.	174
Figure 4.6 Treatment of Group 3 cell line HDMB-03 with cisplatin promotes YB-1 nuclear localisation.	176
Figure 4.7 Cisplatin treatment does not alter total YB-1 protein level in HDMB-03 cells.....	177
Figure 4.8 Treatment of Group 3 cell line HDMB-03 with standard-of-care medulloblastoma chemotherapeutic cisplatin results in elevated nuclear YB-1 expression.	180
Figure 4.9 Treatment of Group 3 cell line HDMB-03 with standard-of-care medulloblastoma chemotherapeutic vincristine does not alter YB-1 expression or localisation.	181

Figure 4.10 Treatment of Group 3 cell line D283 with cisplatin results in elevated nuclear and cellular YB-1 expression 1 and 6 hours post-cisplatin exposure.....	183
Figure 4.11 Treatment of Group 3 cell line D283 with standard-of-care medulloblastoma chemotherapeutic vincristine does not alter YB-1 expression or localisation.	184
Figure 4.12 Treatment of Group 3 cell line D458 with cisplatin does not alter nuclear or cellular YB-1 expression.....	187
Figure 4.13 Treatment of D458 cells with vincristine decreases cellular YB-1 expression.	188
Figure 4.14 <i>ABCB1</i> expression remains unchanged following cisplatin treatment.	191
Figure 4.15 <i>ABCB1</i> expression increases following vincristine treatment.	192
Figure 4.16 Cisplatin treatment may lessen YB-1 enrichment at the <i>ABCB1</i> promoter	195
Figure 4.17 Graphical Summary.....	196
Figure 5.1 Calculation of lentiviral shRNA transduction efficiency in HDMB-03 and D283 cell lines.	203
Figure 5.2 Incubation with polybrene enhances transduction efficiency in the D283 cell line.	204
Figure 5.3 Comparison of lentiviral construct infection efficiencies within the HDMB-03 cell line.	206
Figure 5.4 Comparison of lentiviral construct infection efficiencies within the D283 cell line.	207
Figure 5.5 shRNA-mediated knockdown of <i>YBX1</i> effectively depletes <i>YBX1</i> mRNA expression in HDMB-03 and D283 Group 3 medulloblastoma cell lines.....	209
Figure 5.6 shRNA-mediated knockdown of <i>YBX1</i> effectively depletes YB-1 protein expression in HDMB-03 and D283 Group 3 medulloblastoma cell lines.	210
Figure 5.7 Depletion of YB-1 does not alter the proliferative capacity of HDMB-03 or D283 Group 3 medulloblastoma cell lines.	212
Figure 5.8 YB-1 depletion sensitises HDMB-03 and D283 cells to vincristine but not cisplatin treatment.....	215
Figure 5.9 <i>YBX1</i> knockdown reduces <i>ABCB1</i> expression in Group 3 medulloblastoma cell lines.....	217

Figure 5.10 YB-1 depletion sensitises HDMB-03 cells to HDAC inhibitor panobinostat.	220
Figure 5.11 YB-1 depletion sensitises HDMB-03 cells to BET bromodomain inhibitor JQ1.....	221
Figure 5.12 <i>YBX1</i> knockdown has little effect on c-MYC expression in HDMB-03 and D283 Group 3 cell lines.	224
Figure 5.13 <i>YBX1</i> knockdown significantly impedes the invasive capacity of Group 3 medulloblastoma cell lines.	227
Figure 5.14 Principle component (PC) analysis of <i>YBX1</i> knockdown whole transcriptome sequencing samples.	233
Figure 5.15 Unsupervised clustering of <i>YBX1</i> -knockdown and non-silencing control D283 cell lines.....	235
Figure 5.16 Unsupervised clustering of <i>YBX1</i> -knockdown and non-silencing control HDMB-03 cell lines.	235
Figure 5.17 Significantly up-regulated genes upon <i>YBX1</i> knockdown in Group 3 medulloblastoma cell lines.	237
Figure 5.18 Significantly down-regulated genes upon <i>YBX1</i> knockdown in Group 3 medulloblastoma cell lines.	238
Figure 5.19 Significantly altered molecular and cellular functions upon <i>YBX1</i> knockdown in medulloblastoma Group 3 cell lines.	241
Figure 5.20 Significantly altered canonical pathways upon YB-1 depletion in HDMB-03 and D283 cells..	243
Figure 5.21 YB-1 may play a role in the regulation of a number of pathways implicated in lipid metabolism in paediatric brain tumours.....	244
Figure 5.22 <i>YBX1</i> -knockdown results in inactivation of the Sirtuin Signalling Pathway in HDMB-03 cells.	248
Figure 5.23 <i>YBX1</i> -knockdown has an activational effect on the Senescence Pathway in D283 cells.	249
Figure 5.24 YB-1 depletion results in functional inhibition of MYC-, RPTOR- and RICTOR-associated pathways in medulloblastoma Group 3 cell lines.....	253
Figure 5.25 Graphical Summary of the YB-1 transcriptome in Group 3 medulloblastoma.	254

Figure 6.1 Continuous selection of D458, D283 and HDMB-03 Group 3 cell lines with cisplatin..	262
Figure 6.2 Continuous selection of SHH cell line DAOY with vincristine.	266
Figure 6.3 ABC transporter expression is altered in drug-tolerant medulloblastoma cell lines.....	268
Figure 6.4 <i>YBX1</i> and YB-1 expression is either reduced or unaltered in drug tolerant medulloblastoma cell lines..	271
Figure 6.5 Principal component (PC) analysis of drug-tolerant cell line 3'mRNA sequencing samples..	276
Figure 6.6 Unsupervised clustering of DT-D283-CIS and DT-D283-DMF cell lines. .	277
Figure 6.7 Unsupervised clustering of DT-D458-CIS and DT-D458-DMF cell lines. .	278
Figure 6.8 Unsupervised clustering of DT-HDMB-03-CIS and DT-HDMB-03-DMF cell lines.	279
Figure 6.9 Unsupervised clustering of DT-DAOY-VIN and DT-DAOY-DMSO cell lines.	280
Figure 6.10 Significantly up-regulated genes detected in drug-tolerant cell lines compared to vehicle-treated control cell lines.....	284
Figure 6.11 Significantly down-regulated genes detected in drug-tolerant cell lines compared to vehicle-treated control cell lines.....	287
Figure 6.12 Significantly DEGs are shared between cisplatin-tolerant and <i>YBX1</i> knockdown Group 3 medulloblastoma cell lines.....	289
Figure 6.13 Different cell lines exhibit different altered biological processes upon the acquisition of drug-tolerance.....	291
Figure 6.14 Significantly enriched GO terms overlap between drug-tolerant medulloblastoma cell lines of different subgroups and treatment types.	293
Figure 6.15 DNA fragment profiles of test libraries.	299
Figure 6.16 Fingerprint plots revealed unexpected enrichment in input control samples.	304
Figure 6.17 Peak annotation of YB-1 binding regions in drug-tolerant medulloblastoma cell lines.	309
Figure 6.18 Integration of DT-HDMB-03-CIS ChIP-Seq and 3'mRNA-Seq datasets reveals common genes.	313

Figure 6.19 Integration of DT-D283-CIS ChIP-Seq and 3'mRNA-Seq datasets reveals a common gene.	314
Figure 6.20 Summary Venn diagrams displaying overlapping genes identified upon integration of RNA-Seq, 3'mRNA-Seq and ChIP-Seq datasets.	315
Figure 7.1 Graphical summary of YB-1 function in medulloblastoma cell invasion.	324
Figure 7.2 Graphical summary of YB-1 cellular functions in medulloblastoma, as identified by whole-transcriptome sequencing.	332
Figure 7.3 Graphical summary of 3'mRNA-Seq data analysis.	336
Figure 7.4 Graphical summary of proposed YB-1 function in response to short-term vincristine treatment.	339
Figure 7.5 Graphical summary of the function of YB-1 in the response to acute and chronic treatment with cisplatin.	352
Figure 7.6 Graphical summary of YB-1 functions in medulloblastoma as elucidated by this study.	354

List of Tables

Table 1-1 Genetic syndromes associated with a pre-disposition to paediatric brain tumours.....	5
Table 1-2 Medulloblastoma clinical risk stratification.....	19
Table 1-3 Standard medulloblastoma chemotherapeutics and their association with ABC transporters.....	28
Table 1-4 Experimentally confirmed transcriptional, translational and post-translational regulators of human <i>YBX1</i> / <i>YB-1</i>	40
Table 1-5 Summary of tumourigenic features experimentally associated with <i>YB-1</i> expression.....	46
Table 2-1 Gene expression dataset information.....	67
Table 2-2 Cell lines utilised in this study.....	70
Table 2-3 Culture media information for cell lines utilised in this study.....	72
Table 2-4 Drugs used in this study.....	75
Table 2-5 Calculated IC_{50} for chemotherapeutic agents used in this study.....	76
Table 2-6 Optimised puromycin kill concentrations.....	77
Table 2-7 GIPZ lentiviral <i>YBX1</i> shRNA constructs.....	79
Table 2-8 Maintenance doses for the culture of drug-tolerant cell lines.....	84
Table 2-9 Cross-linking conditions for the cell lines used in this study.....	89
Table 2-10 Antibodies used in ChIP assay immunoprecipitation.....	89
Table 2-11 Primers used for qRT-PCR/qPCR.....	93
Table 2-12 Buffers used for immunoblotting.....	98
Table 2-13 Preparation of SDS-Gels.....	99
Table 2-14 Antibodies used for immunoblotting.....	99
Table 2-15 Antibodies used for immunofluorescence.....	102
Table 3-1 <i>YB-1</i> and <i>NFE2L2</i> predicted binding sites in the <i>ABCB1</i> promoter.....	136
Table 3-2 Output of the Mantel-Haenszel log-rank test for <i>YBX1</i> expression.....	144
Table 3-3 Output of the Cox's Proportional Hazard's Model for <i>YBX1</i> expression, age and metastatic status.....	144

Table 3-4 YB-1 expression does not associate with metastatic status in medulloblastoma patients.	159
Table 5-1 Quantification of RNA concentration and integrity in whole transcriptome sequencing samples.	229
Table 5-2 Mapping of whole transcriptome sequencing data.....	230
Table 6-1 Differential gene expression profiles of drug-tolerant cell lines.	282
Table 6-2 Association between shared up-regulated genes and recorded roles in tumour progression and drug resistance.....	285
Table 6-3 Mapping of CHIP-Seq data.....	303
Table 6-4 Number of individual and shared peaks within IP biological replicates..	306

List of Common Abbreviations

ABC	ATP-Binding Cassette
ANOVA	analysis of variance
ATP	adenosine triphosphate
BTIC	brain tumour initiating cell
CGNP	cerebellar granule neuron precursors
ChIP	chromatin immunoprecipitation
CIS	cisplatin
CNS	central nervous system
CSD	cold shock domain
CSF	cerebrospinal fluid
DMF	dimethylformamide
DMSO	dimethylsulfoxide
DN	desmoplastic/nodular
DT	drug-tolerant
ECM	extracellular matrix
FBS	foetal bovine serum
FDA	Food and Drug Administration
FDR	false discovery rate
GFP	green fluorescent protein
GO	gene ontology
H3K4me3	tri-methylation at Lysine 4 of the Histone 3 protein
IC₅₀	half-maximal inhibitory concentration

IHC	immunohistochemistry
IP	immunoprecipitation
KD	knockdown
LC/A	large cell/anaplastic
MBEN	medulloblastoma with extensive nodularity
MDR	multi-drug resistance
MMP	matrix-metalloproteinase
mRNA	messenger RNA
NGS	next-generation sequencing
NS	non-silencing
PCA	principal component analysis
SEM	standard error of the mean
SHH	Sonic Hedgehog
shRNA	small hairpin RNA
siRNA	small interfering RNA
TP53	Tumour Protein 53
TSS	transcription start site
VIN	vincristine
WHO	World Health Organisation
WNT	Wingless-related integration site
WT	wild type
YB-1	Y-Box Binding Protein 1 (protein)
YBX1	Y-Box Binding Protein 1 (gene)

Chapter 1

Introduction

Chapter 1 Introduction

1.1 Paediatric Cancer

Paediatric cancer, a term used to describe cancers that occur between birth and 15 years of age, is rare and occurs with an incidence of around 1,900 cases in the UK every year; equivalent to around 5 cases every day (Cancer Research UK, 2020). Yet, despite their rarity, cancers remain the most common cause of death for children aged 1 – 15 years, accounting for approximately one-fifth of deaths in this age group in the UK (Public Health England, 2018).

Recent advances in the diagnosis and treatment of paediatric cancers have seen survival rates improve significantly. Indeed, paediatric cancer 10-year survival in the UK (Figure 1.1) has increased from 36% to 84% in just 40 years (National Cancer Intelligence Network, 2012; NCRAS, 2018). Of particular note, lymphomas, hepatic tumours and leukaemia have all seen significant increases in survival. However, due to their early onset, paediatric cancers frequently result in a drastic loss of quality-adjusted life years (QUALYs), both from death and from the lifelong cognitive and functional complications that arise from current treatment strategies in surviving patients.

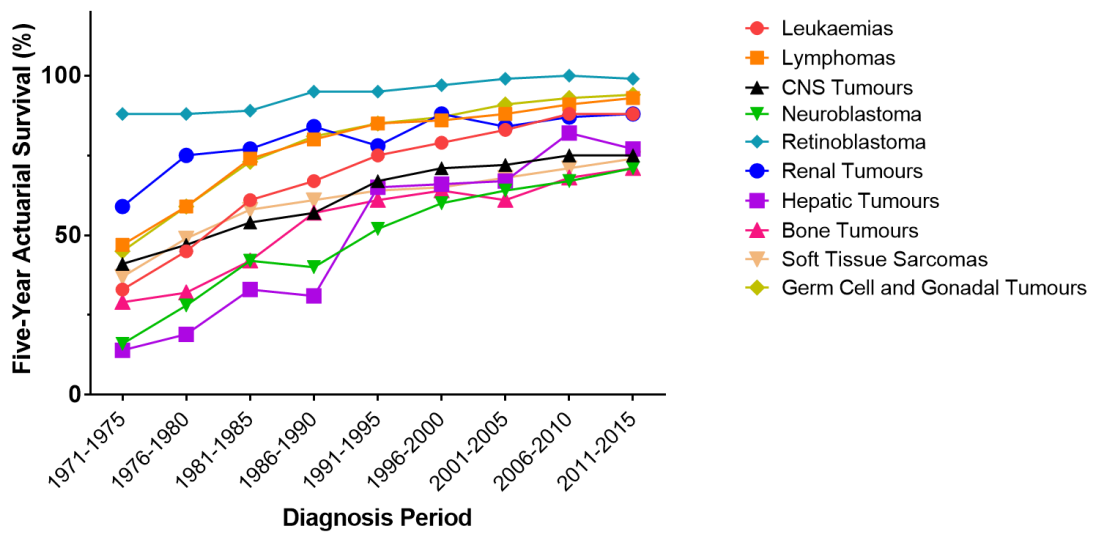


Figure 1.1 Childhood Cancer Five-Year Actuarial Survival. Five-year survival rates have increased for all childhood cancer groups, however improvements are greater in some cancer types than others. Raw data obtained from (National Cancer Intelligence Network, 2012; NCRAS, 2018).

1.2 Paediatric Brain Cancer

Brain and central nervous system (CNS) tumours are the most common solid tumour of childhood and represent the second most prevalent cancer in children after leukaemia. Making up 21% of all paediatric cancers, they remain the leading cause of cancer-related mortality and morbidity in childhood (Northcott et al., 2012; Ward et al., 2014).

There are over 100 different subtypes of brain and central nervous system tumour. As is true for most solid childhood cancers, the majority of brain tumours arise sporadically with no known cause. However, a small percentage of neoplasms are known to be associated with several genetic syndromes, as outlined in Table 1-1 (Abubakar & Traunecker, 2014; Malbari & Lindsay, 2020; Wilne et al., 2007). Furthermore, exposure to ionising radiation therapy during the treatment of other childhood cancer types is a significant risk factor for the development of a CNS tumour (Neglia, 2006).

Due to recent advances in neurosurgical techniques, radiation therapy and the use of combination chemotherapy, five-year survival for children with brain and CNS tumours in the UK now lies at approximately 75% (NCRAS, 2018). However, by cause of the lesion itself, its surgical removal and subsequent treatment, it is thought that 60% of brain tumour survivors go on to suffer significant, long-term difficulties including physical, cognitive, neurological and endocrine complications (Wilne et al., 2007). In addition, owing to the rarity of brain tumours, as well as the variability and non-specificity of clinical symptoms at onset, the diagnosis of brain and CNS tumours is often delayed. This may in turn have a detrimental effect on the acute

management and ultimate prognosis of the patient (Kariyawasam, 2015; Wilne et al., 2007). New resources such as HeadSmart (www.headsmart.org.uk), a guideline to advise health professionals and the public on symptoms that could be caused by a brain tumour, have worked to address this issue. In fact, since accreditation in 2011, HeadSmart has reduced diagnosis time for children with brain tumours in the UK from 12-13 weeks to 6.5 weeks (Shanmugavadivel et al., 2020). However, further research is still required, both to better understand the symptom pattern of brain and CNS malignancies, as well as to further improve survival rates and reduce complications associated with current therapies.

Table 1-1 Genetic syndromes associated with a pre-disposition to paediatric brain tumours.

Genetic Syndrome	Prevalence (UK new-borns)	Germline Mutation	Brain/CNS Tumour Type
Gorlin Syndrome	1 in 31,000	Chr. 9q22, <i>PTCH1</i> Chr.10q24, <i>SUFU</i>	Medulloblastoma (SHH subgroup)
Li-Fraumeni Syndrome	Very Rare	Chr. 17p13, <i>TP53</i>	Multiple malignant brain/CNS tumours including medulloblastoma
Neurofibromatosis I	1 in 2,500 – 3000	Chr. 17q11, <i>NF1</i>	Pilocytic astrocytoma, low-grade glioma
Neurofibromatosis II	1 in 25,000	Chr.22q12, <i>NF2</i>	Meningiomas, neurilemmomas, ependymomas
Tuberous Sclerosis	1 in 6000	Chr.9q34, <i>TSC1</i> Chr. 16p13, <i>TSC2</i>	Subependymal giant cell astrocytomas, low-grad glioma.
Turcot Syndrome I	Very Rare	Chr.7p22, <i>PMS2</i> Chr.3p22, <i>MLH1</i> Chr. 2p21-16, <i>MSH2</i> Chr.2p16, <i>MSH6</i>	High grade glioma
Turcot syndrome II	Very Rare	Chr.5q21-22, <i>APC</i>	Medulloblastoma (WNT subgroup)
Von Hippel-Lindau Disease	1 in 36,000	Chr.3p25-56, <i>VHL</i>	Haemangioblastomas

Abbreviations: Chr. = chromosome, p = short arm, q = long arm.

1.2.1 Medulloblastoma

Medulloblastoma is the most frequent malignant brain tumour of childhood comprising up to 15-20% of all paediatric CNS tumour cases (Massimino et al., 2016). By definition, medulloblastoma must arise in the posterior fossa, with 80% of paediatric patients presenting with tumours in the fourth ventricle. Medulloblastoma occurs at all ages, with incidence peaking at 6 – 8 years and declining with increasing age, consistent with the embryonal origin of the tumour (Northcott et al., 2019).

Most early medulloblastoma symptomatology is related to blockage of cerebral spinal fluid (CSF) and resultant accumulation of CSF in the brain. As such, patients suffering with medulloblastoma commonly present with symptoms indicative of increased intracranial pressure and cerebellar dysfunction; including vomiting, macrocephalus, headaches, ataxia, lethargy and visual impairment (PDQ® Pediatric Treatment Editorial Board, 2020). Magnetic resonance imaging (MRI) typically demonstrates a midline or paramedian cerebellar mass, often with compression of the fourth ventricle and dilation of the lateral and third ventricles because of CSF flow. Patients may also display evidence of metastases, as assessed by spinal MRI and cytological assessment of the lumbar CSF (Gerber et al., 2014).

1.2.1.1 Aetiology/Risk Factors

For many medulloblastoma patients, the aetiology of the disease is unknown. However, rare familial tumour syndromes Gorlin and Turcot predispose to medulloblastoma development (Table 1-1) and as such have provided insight into some of the genes and pathways involved in medulloblastoma pathogenesis. Gorlin syndrome cases exhibit an increased risk of medulloblastoma due to inherited

mutations of the *patched 1 (PTCH1)* or *suppressor of fused homolog (SUFU)* tumour suppressor genes - associated with the negative regulation of the Sonic Hedgehog (SHH) signalling pathway (Figure 1.4). Both genes are mutated, somatically and in the germ line in medulloblastoma, establishing a causative role for SHH signalling in medulloblastoma pathogenesis. Meanwhile, type II Turcot syndrome patients possess inactivating mutations in *adenomatous polyposis coli (APC)*, a tumour suppressor gene implicated in wingless (WNT) signalling (Figure 1.4). Likewise, deficient WNT signalling is associated with medulloblastoma development, with *APC* germline mutations and *Beta catenin 1 (CTNNB1)* somatic mutations detected in ~1% and ~7% of patients, respectively (Northcott et al., 2019).

Notably, a recent study of 1,022 medulloblastoma patients identified damaging and pathogenetic germline mutations in *APC*, *Breast Cancer Gene 2 (BRCA2)*, *Partner And Localizer Of BRCA2 (PALB2)*, *PTCH1*, *SUFU* and *Tumour Protein P53 (TP53)* and estimated that these mutations accounted for 6% of medulloblastoma diagnoses in the retrospective cohort (Waszak et al., 2018). Different germline mutations were associated with different patient characteristics (such as age), molecular subgroups (Section 1.2.1.4) and clinical outcomes (Waszak et al., 2018).

1.2.1.2 Medulloblastoma Tumour Classification

Traditionally, medulloblastoma was stratified based upon various clinical factors, which allowed the characterisation of patients into different risk groups, ultimately determining treatment strategy and intensity. The 2007 edition of the *WHO Classification of Tumours of the Central Nervous System* aimed to move towards a

biological sub-grouping approach, with medulloblastoma divided into groups based on histological features (Louis et al., 2007).

1.2.1.3 Histological Subgroups

Medulloblastoma morphologies distinguished in the 2007 WHO brain tumour classification include desmoplastic/nodular (DN), large cell/anaplastic (LC/A) and classic (Figure 1.2). Due to important clinicopathological correlates, a further group of DN tumours in the infant population was denoted as medulloblastoma with extensive nodularity (MBEN) (Louis et al., 2007; Orr, 2020).

Desmoplastic/nodular tumours are comprised of nodular, reticulin¹-free balls of tumour cells surrounded by a reticulin-rich stroma. Tumours of this pathology represent 7% of all medulloblastoma and are associated with a favourable outcome, especially in young children. MBEN medulloblastoma differs from the desmoplastic/nodular variant through its expanded, lobular structure, which arises due to unusually elongated reticulin-free zones and reduced reticulin-rich internodular zones. MBEN tumours comprise just 3% of medulloblastoma and, like the desmoplastic/nodular variant, are indicative of favourable clinical outcome. LC/A medulloblastoma is a variant consisting of cells with large, round nuclei, prominent nucleoli and abundant cytoplasm. Such cells are commonly found in sheets, interspersed with anaplastic cells, characterised by marked nuclear pleomorphism, cell-cell wrapping and nuclear moulding. The LC/A variant comprises 10 – 22% of medulloblastoma and is often associated with a significantly worse prognosis.

¹ Reticulin describes a type of fibre in connective tissue composed of type III collagen, which cross-links to form a fine meshwork.

Tumours of classic histology constitute the remaining 66% of medulloblastoma. Classic tumours are made up of sheets of small, densely packed, rounded cells with a high nuclear to cytoplasmic ratio (Louis et al., 2007; Massimino et al., 2016; Taylor et al., 2012).

1.2.1.4 Molecular Subgroups

Although the aforementioned histological variants partially reflect underlying molecular heterogeneity, they do not tell us the whole story (Figure 1.3). Advances in molecular and genetic profiling uncovered substantial heterogeneity within medulloblastoma and led to the identification of four core distinct molecular subgroups - Wingless (WNT), Sonic Hedgehog (SHH), Group 3 and Group 4 - which differ in their patient demographics, prognoses and metastatic status (Northcott et al., 2012; Taylor et al., 2012). As such, the revised 2016 and recently published 2021 WHO *Classification of Tumours of the Central Nervous System* defines medulloblastoma both histologically and genetically (Louis et al., 2016; Louis et al., 2021). Additionally, based on significant intra-subgroup heterogeneity, variances in age of onset and disparate prognoses, the existence of additional subtypes beyond the four consensus subgroups has been reported (Cavalli et al., 2017; Northcott et al., 2017; Schwalbe et al., 2017; Sharma et al., 2019). Only the four core molecular subgroups will, however, be extensively discussed in this report.

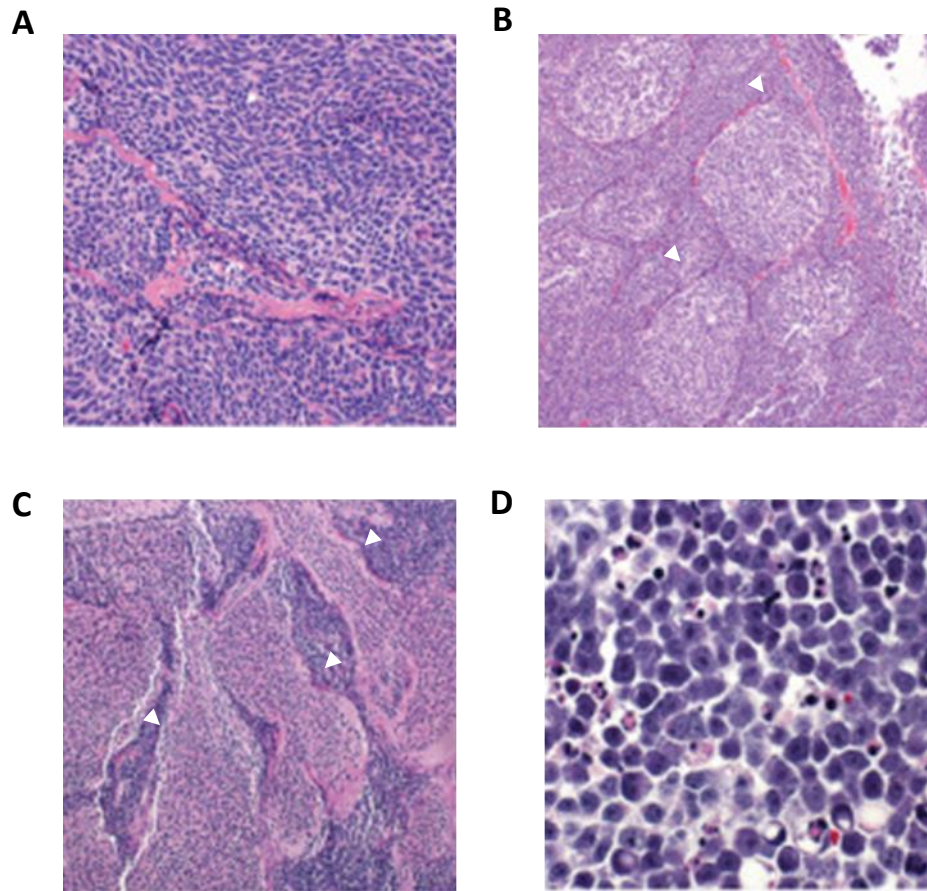


Figure 1.2 Histological subtypes of medulloblastoma. Medulloblastoma is widely considered as four main histological variants. A) Classic, characterised by densely packed, small cells with round to ovoid nuclei surrounded by sparse cytoplasm. B) Desmoplastic/nodular (DN), characterised by reticulin-free nodules (arrowed) surrounded by densely packed, mitotically active cells, which produce a reticulin-positive network of fibres. C) Medulloblastoma with extensive nodularity (MBEN), characterised by unusually elongated reticulin-free zones (arrowed) containing a population of small cells with round nuclei. D) Large cell/anaplastic (LC/A), characterised by “large” round cells mixed with cells with marked nuclear pleomorphism and nuclear moulding (anaplastic). Figure adapted from (Orr, 2020).

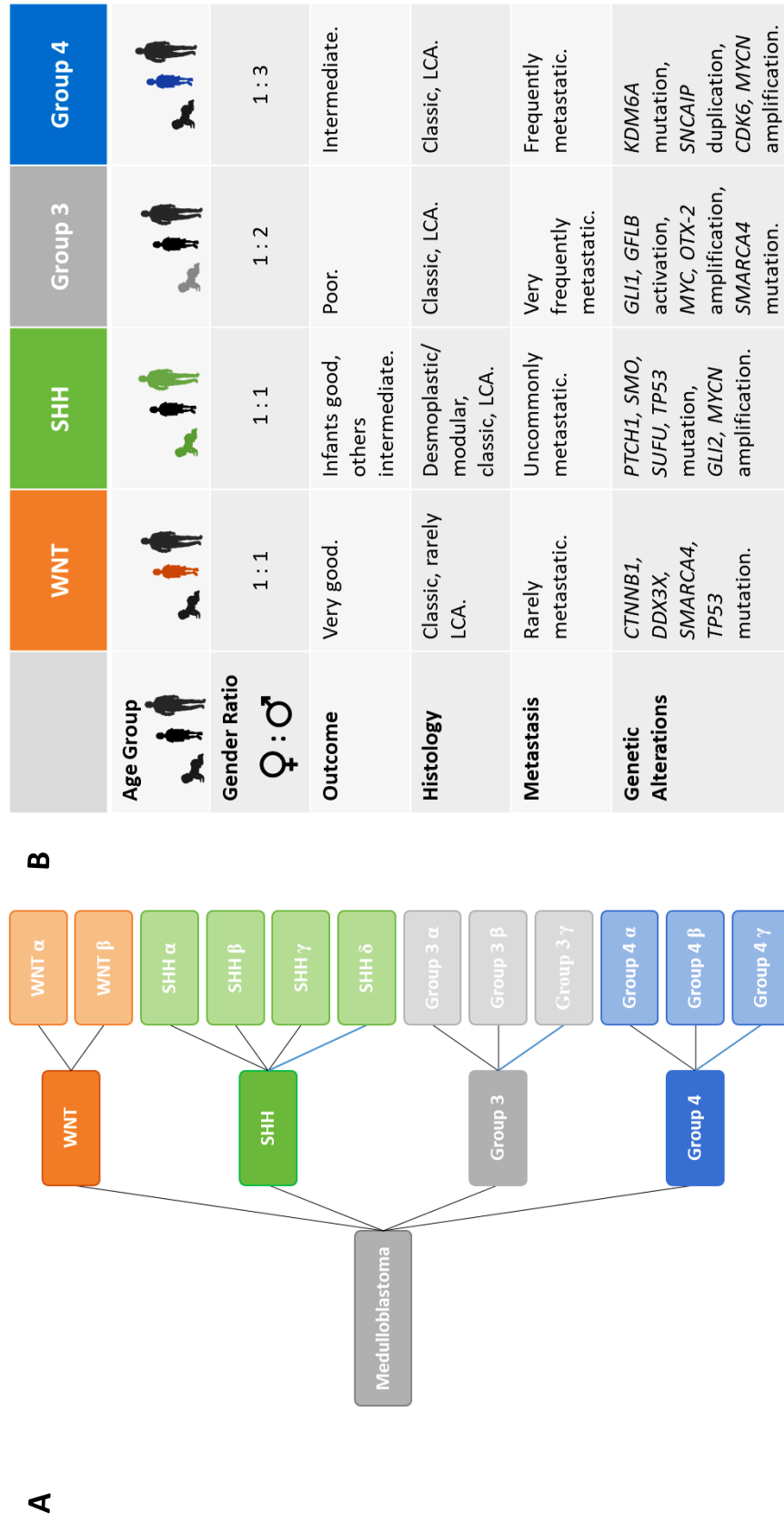


Figure 1.3 Molecular subgroups of medulloblastoma and their various clinical, histological and genetic features. A) Classification of medulloblastoma tumours. Currently, four main subgroups exist: WNT, SHH, Group 3 and Group 4. It is thought that each subgroup can be further divided into distinct sub-types, which differ biologically and clinically from other sub-types within the same subgroup. Variations of “second-generation” medulloblastoma sub-typing have been performed. Here we present sub-types identified by Cavalli et al. in 2017. B) Comparison of various medulloblastoma subgroups. Adapted from (Taylor et al., 2012).

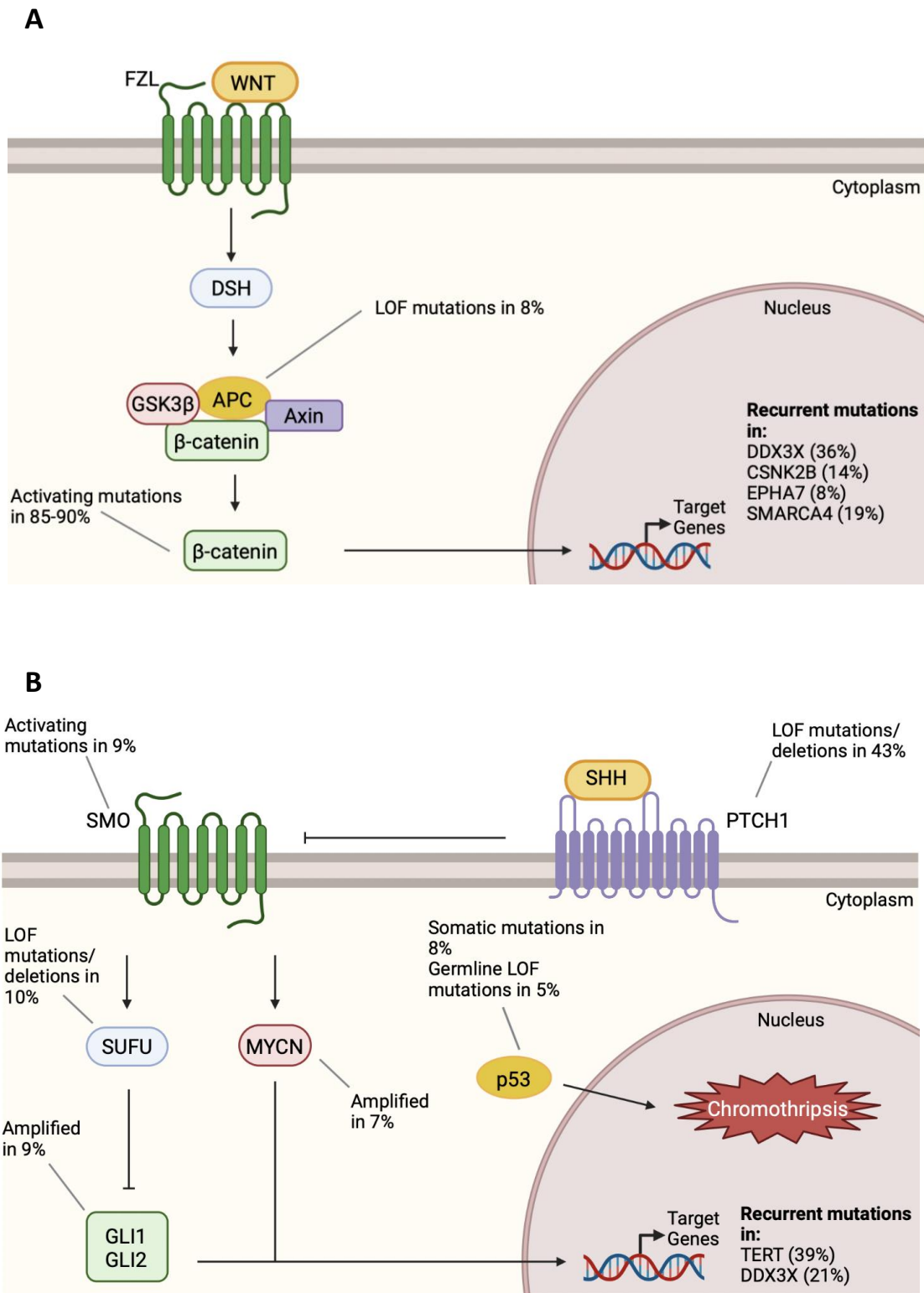


Figure 1.4 WNT and SHH pathways and medulloblastoma. Genes of canonical WNT (A) and SHH (B) signalling pathways are frequently altered in patients with WNT and SHH subgroup medulloblastoma, respectively. LOF (loss of function); FZL (Frizzled); DSH (Dishevelled); APC (Adenomatous Polyposis Coli); GSK3 β (Glycogen synthase kinase-3 β); DDX3X (ATP-dependent RNA helicase DDX3X); CSNK2B (Casein kinase II subunit beta); EPHA7 (Ephrin type-A receptor 7); PTCH1 (Protein patched homolog 1); SUFU (Suppressor of fused homolog); GLI1/2 (Zinc finger protein GLI1); SMO (Smoothened). Figure adapted from (Northcott et al., 2019).

1.2.1.4.1 WNT

WNT subgroup medulloblastoma has the best prognosis of all four subgroups, with a survival rate of >95%. This is likely attributed to alterations in the brain vasculature in these patients, resulting in a “leaky” blood-brain barrier and thus high levels of intra-tumoural chemotherapy (Phoenix et al., 2016). Histologically, these tumours generally exhibit classic histology (Figure 1.2 A), occur in the midline of the brain, occupying the fourth ventricle (Figure 1.5) and are infrequently metastatic (Massimino et al., 2016; Northcott et al., 2012).

Around 10% of medulloblastomas exhibit aberrant WNT signalling; with 85-90% of WNT tumours harbouring somatic activating mutations in exon 3 of *CTNNB1*. Such mutations result in stabilisation and nuclear accumulation of the β -catenin protein, hyper-activation of the WNT pathway and a concurrent increase in the transcription of proliferative genes, including *Cyclin D1* and *MYC* (Figure 1.4 A). *CTNNB1* wild-type patients frequently present with pathogenetic loss-of-function variants of *APC*, a TSG that functions in a complex which promotes degradation of β -catenin (Northcott et al., 2019). Somatic mutations in *DDX3X* (36% of tumours), *CSNK2B* (14%), *EPHA7* (8%), and subunits of the SWI/SNF nucleosome-remodelling complex *SMARCA4* (19%) have also been recorded (Northcott et al., 2017; Northcott et al., 2019). Less frequent are heterozygous somatic mutations in the *TP53* gene, which, unlike in other subgroups, are not prognostic (Zhukova et al., 2013). Cytogenetically, WNT tumours often exhibit loss of chromosome 6, a genomic signature observed almost exclusively in WNT tumours (Jones et al., 2012).

1.2.1.4.2 SHH

SHH tumours account for approximately 30% of medulloblastoma. SHH tumours can have classic, LC/A and desmoplastic/nodular histology (Figure 1.2), with the desmoplastic/nodular variant exclusively classified to this group. SHH tumours commonly present in a hemispheric location (Figure 1.5) in the cerebellum (Massimino et al., 2016; Northcott et al., 2012).

Genetically, this subgroup is among the best understood. As the name suggests, the SHH subgroup arises from aberrations in the SHH signalling pathway. As such, this group describes patients harbouring germline or somatic mutations in any critical SHH signalling pathway gene leading to constitutive ligand-independent activation of SHH signalling and the upregulation of SHH-responsive genes implicated in cell growth and proliferation (Figure 1.4 B). This includes loss-of-function mutations/deletions of *PTCH1* (43% of patients), loss-of-function mutations/deletions of *SUFU* (10%), activating mutations in *SMO* (9%), *GLI1/GLI2* amplifications (9%) and *MYCN* amplification (7%). Interestingly, SHH tumours are genetically distinct in infants (iSHH) and children. Accordingly, germline and somatic *SUFU* mutations and activating *SMO* mutations are enriched in infants, while childhood/adolescent cases frequently harbour *TP53* loss-of-function mutations and deletions, which commonly co-occur alongside *MYCN* and *GLI2* amplifications and LC/A histology (Kool et al., 2014; Northcott et al., 2017). Likewise, *telomerase reverse transcriptase (TERT)* promoter mutations, also demonstrate an age-associated bias, characterising the majority of adult tumours (98%) but appearing less frequently in children (21%) and infants (13%) (Kool et al., 2014; Lindsey et al., 2014; Remke et al., 2013).

Cytogenetically, deletion of chromosomes 9q and 10q are common in SHH medulloblastoma, perhaps unsurprisingly due to the location of *PTCH1* at chromosome 9q22 and *SUFU* located at 10q24 (Northcott et al., 2010; Taylor et al., 2012).

SHH tumours have an intermediate prognosis, with an overall survival rate of 60-80% (Northcott et al., 2012). However, unlike WNT tumours, SHH patients harbouring germline or somatic *TP53* mutations have very poor survival (Zhukova et al., 2013) and as such are considered a very high-risk group (Section 1.2.1.5).

1.2.1.4.3 Group 3

Group 3 medulloblastoma accounts for approximately 25% of all medulloblastoma cases and carries the worst prognosis of all four subgroups, with 5-year survival rates standing at less than 50% (Kool et al., 2012). Group 3 tumours present a predominantly classic histology, although this group also has a high ratio of LC/A histology (Figure 1.2 A and D), especially in infants (Kool et al., 2012). Tumours are usually located in the IV ventricle, against the brainstem (Figure 1.5). Notably, Group 3 medulloblastoma is considered the most aggressive of all four subgroups, with almost half of all tumours metastatic at diagnosis and relapse frequent (Hill et al., 2020).

No germline mutations have been associated with a pre-disposition to Group 3 medulloblastoma and somatic nucleotide variants are rare. The most frequent genetic alteration is focal, high-level amplification of the *MYC* proto-oncogene, which occurs in ~17% of Group 3 patients and yet is rare in other subgroups. Other frequent somatic mutations include *GFI1B* (11% of patients), *SMARCA4* (9%), *KBTBD4* (6%),

CTDNEP1 (5%), *KMT2D* (5%) and *MYCN* (5%) which represent the only genes mutated in $\geq 5\%$ of Group 3 patients (Northcott et al., 2017; Northcott et al., 2019). Interestingly, pathway analysis of recurrent genetic events in Group 3 patients has highlighted significant over-representation of genes implicated in Notch and TGF β signalling, indicative of a possible role of deregulated Notch and TGF β pathways in Group 3 pathogenesis (Northcott et al., 2017).

The Group 3 medulloblastoma genome is highly unstable with extensive aneuploidy characterised by frequent isochromosome 17q (loss of the short arm of chromosome 17 (17p) and duplication of the long arm (17q); 42% of patients), gain of chromosome 1q (35%), gain of chromosome 7 (55%) and loss of chromosomes 8p (33%), 10q (49%), 16q (50%) (Kool et al., 2012). Further chromosomal abnormalities including tetraploidy and chromothripsis are also common. In addition to metastasis, both *MYC* amplification and the presence of isochromosome 17q are separately considered risk factors for this group. Accordingly, absence of these markers is associated with favourable prognosis (Shih et al., 2014).

1.2.1.4.4 Group 4

Group 4 medulloblastoma represents the most common medulloblastoma subgroup. Histologically, most patients exhibit classic histology, although some tumours may exhibit LC/A characteristics (Figure 1.2 A and D). Tumours of this type frequently disseminate, with one-third of patients exhibiting metastases at diagnosis (Northcott et al., 2012).

As with Group 3 medulloblastoma, no genetic predisposition has been recorded for Group 4 medulloblastoma and again, somatic nucleotide variants are rare. One of the

most significant driver events in this subgroup involves the activation of *PRDM6* via “enhancer hijacking”², which is found in ~17% of Group 4 patients and notably, is strongly associated with focal tandem duplication of *alpha-synuclein interacting protein (SNCAIP)* (Northcott et al., 2017; Northcott Shih, et al., 2012). Other notable somatic mutations in Group 4 medulloblastoma include amplification of the proto-oncogene *MYCN* (6% of patients) and cyclin dependant kinase *CDK6* (6%), which appear to occur mutually exclusively to *SNCAIP* tandem duplication.

Cytogenetically, the most common structural alteration in Group 4 medulloblastoma is isochromosome 17q, which is found in 80% of cases. Further common large-scale chromosomal aberrations include chromosome 7 gain (40-50% of patients) and chromosome 8 (40-50%) and 11 (30%) deletions (Northcott et al.,2012). Similar to Group 3, the Group 4 medulloblastoma genome is commonly tetraploid and interestingly, most female Group 4 tumours lose one copy of the X chromosome, suggesting the existence of one or more TSGs on this chromosome (Jones et al., 2012; Northcott et al.,2012).

² Enhancer hijacking describes the misplacement of an active enhancer such that it regulates genes other than its original targets e.g. oncogenes. This can occur through chromosomal re-arrangements or micro-amplification of genomic regions.

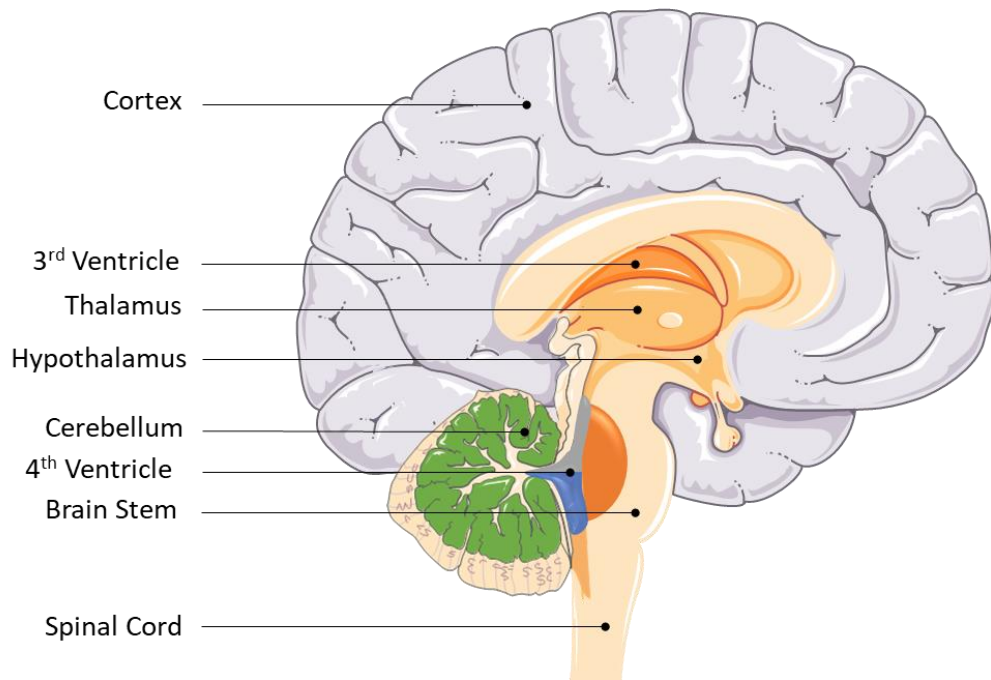


Figure 1.5 Location of medulloblastoma tumours. Sagittal section of the cerebellum and brainstem showing common diagnostic locations for medulloblastoma subgroups: **WNT** (orange); **SHH** (green), Group 3 (grey) and **Group 4** (blue). Adapted from (Northcott et al., 2019).

1.2.1.5 Clinical Risk Stratification

Until recently, risk stratification criteria for medulloblastoma relied primarily on clinicopathological variables relating to age, metastatic status, extent of surgical resection and occasionally other genetic and pathological factors including the presence of *MYC/MYCN* gene amplifications and if tumours presented with LC/A pathology. However, in recent years, the identification of molecular subgroups has promoted the re-evaluation of medulloblastoma risk stratification (Juraschka & Taylor, 2019; Ramaswamy et al., 2016). Patients are now ascribed to one of four risk groups ranging from low- to very high-risk according to subgroup status and genetic/cytogenetic aberrations (Table 1-2).

Table 1-2 Medulloblastoma clinical risk stratification

Risk Category	Low-Risk	Standard-Risk	High-Risk	Very High-Risk
Survival	>90%	75-90%	50-75%	<50%
Subgroup, clinical and molecular characteristics	Non-metastatic	Non-metastatic, <i>TP53</i> WT + no <i>MYCN</i> amplification	Metastatic +/or <i>MYCN</i> amplification	<i>TP53</i> mutation
		Non-metastatic + no <i>MYC</i> amplification		
	Non-metastatic + Chr. 11 loss	Non-metastatic + No Chr. 11 loss	Metastatic	Metastatic

Clinical and molecular criteria for each risk group is described. Box colour represents molecular subgroup: **WNT** (orange); **SHH** (green); Group 3 (grey) and **Group 4** (blue). WT = wild type. Table adapted from (Juraschka & Taylor, 2019).

1.2.1.6 Relapsed Medulloblastoma

As outlined in Sections 1.2.1.4 and 1.2.1.5, recent advances in our understanding of medulloblastoma genetics and cytogenetics at diagnosis has enhanced subgrouping and risk stratification. Comparatively, much less is understood regarding the pathways and mechanisms that drive medulloblastoma relapse, largely arising from the rarity of biopsy performed at disease recurrence. Accordingly, patient management at relapse predominantly focuses on quality of remaining life rather than curative strategies. As such, relapse following conventional treatment represents the single, most adverse event in medulloblastoma. 30% of medulloblastoma patients will go on to relapse and of these over 95% will die, accounting for 10% of all childhood cancer deaths (Hill et al., 2015; Pizer & Clifford, 2009).

In recent years, the assembly of relapsed patient cohorts has facilitated the investigation of the landscape of relapsed medulloblastoma. Tumour biology, as well as therapeutic strategy, appears to heavily influence the nature and outcome of relapsed disease. Factors associated with a decreased time to relapse include Group 3 disease, withholding of upfront craniospinal irradiation, LC/A histology and *MYC* amplification. Both *MYC* amplification and lack of tumour resection at relapse are also associated with decreased overall survival following relapse (Hill et al., 2020). Combined *MYC* family amplifications and P53 pathway defects frequently occur at disease relapse across all molecular subgroups and are associated with rapidly progressive disease (Hill et al., 2015).

Although molecular subgroups and novel sub-types are largely stable over disease course, a recent large-scale study of relapsed medulloblastoma genetics revealed significant genetic divergence at relapse (Richardson et al., 2021). In the study, approximately 40% of genetic driver events were found to emerge at relapse and these acquired changes differed significantly between sub-groups. Interestingly, Group 4 patients demonstrated the greatest genetic divergence at relapse, enriched for CDK co-amplifications and several novel events including mutations in *USH2A*, a gene encoding basement membrane protein usherin. Comparatively, recurrent genetic events were rare in Group 3 patients. iSHH and non-infant SHH medulloblastoma were found to display distinct genetic landscapes at relapse, with a greater proportion of chromosomal arm-level CNV changes acquired in non-infant SHH patients, and an increased acquisition of driver gene mutations in iSHH patients (Richardson et al., 2021).

The high frequency of relapse in medulloblastoma, combined with the poor outcome post-relapse of medulloblastoma patients treated with conventional therapy supports the hypothesis that a number of patients maintain or acquire cellular traits associated with chemo-/radio-resistance. Accordingly, a number of recent studies are focussing on elucidating mechanisms towards therapy resistance in medulloblastoma, with the aim to reduce the rate of relapse for which outcome is so dire (Bortolozzi et al., 2020; Daggubati et al., 2021; Mo et al., 2021; Sreenivasan et al., 2020; Yuan et al., 2021).

1.2.1.7 Medulloblastoma Treatment Protocols

Contemporary medulloblastoma treatment protocols begin with surgical resection of the primary tumour. The extent of surgical resection is important and represents a prognostic factor, with gross total resection (GTR) and near total resection (NTR; <1.5 cm² residual tumour) associated with a significant survival benefit when compared with subtotal resection (STR; ≥ 1.5cm²) (Thompson et al., 2016).

Following surgery, patients are given radiotherapy followed by post-radiation adjuvant chemotherapy. The most successful radiation approach includes craniospinal irradiation (CSI) with a focal boost to the primary tumour site. On account of the significant and inimical effects of CSI, radiation-sparing approaches, particularly in young children, have been proposed. Irradiation-avoiding strategies seems feasible for iSHH patients (in particular the second-generation iSHH-II subtype), however alternative strategies will be required for high-risk/non-SHH patients, for which reduced-intensity approaches have not been successful (Hicks et al., 2021; Robinson et al., 2018; Yeo et al., 2019).

A number of studies have confirmed improved patient outcome with the addition of chemotherapy compared with surgery and radiotherapy alone (Taylor et al., 2003). Maintenance chemotherapy post-radiotherapy rather than pre-radiotherapy also results in a clear survival advantage in medulloblastoma patients (Kortmann et al., 2000). Although the dose, combination and number of courses of chemotherapy employed by different treatment regimens remains variable, the most widely used chemotherapy agents are cisplatin, carboplatin, vincristine, lomustine and cyclophosphamide (Packer et al., 2006; Packer et al., 2013). The aforementioned

chemotherapeutics are always used in combination, which both facilitates maximum cancer cell killing at tolerated drug doses and attempts to minimise the evolution of drug resistance, which can occur through alterations of the apoptotic pathway, changes in cellular repair mechanisms and increased expression/activity of drug transporters (Section 1.3).

1.2.1.7.1 Landscape of Current Clinical Trials

A major obstacle in the effective treatment of medulloblastoma has been its continued management as a uniform disease. With the advent of molecular subgroups and the identification of molecular markers, it is now imperative to design treatment plans based on molecular and clinical risk features. Only one current clinical trial (NCT01878617) takes into account both subgroups and risk stratification. In this trial, low risk WNT patients, receive de-escalated treatment with the aim to reduce treatment-related morbidities, while skeletally mature standard- and high-risk SHH patients receive standard-of-care therapy with the addition of smoothed receptor inhibitors. Standard and high risk non-SHH/-WNT patients are then prioritised for intensified treatment (Juraschka & Taylor, 2019). A further 11 current clinical trials take into account molecular subgroups, with a focus on irradiation reduction/removal in WNT subgroup medulloblastoma. Just two current trials consider Group 3 or Group 4 patients (NCT04023669 and NCT03434262). The continued definition of driver events in Group 3, Group 4 and relapsed medulloblastoma will likely impact and inform future molecular- and risk-stratified trials, likely including less toxic, targeted therapies for medulloblastoma (Thompson et al., 2020).

1.3 ABC Transporters

ATP-binding cassette (ABC) transporters are essential proteins found in all living organisms. The human ABC transporter superfamily is composed of 48 genes subdivided into 7 subfamilies, from ABCA to ABCG (Dean, 2005). Located in the plasma membrane of prokaryotes and eukaryotes, and in the organellar membrane of eukaryotes, core ABC transporters typically consist of two hydrophobic transmembrane domains and two water-soluble nucleotide-binding domains (Figure 1.6). The transmembrane domains determine transport substrate specificity, while the nucleotide binding domains are responsible for ATP binding and hydrolysis, facilitating substrate translocation irrespective of concentration gradient (Nobili et al., 2020).

Twelve ABC transporters have been implicated in the transport of cancer drugs in laboratory studies (Szakacs et al., 2006), however *in vivo* evidence only supports roles for three of these in chemoresistance: ABCB1 (also known as P-glycoprotein or MDR1), ABCG2 (also known as BCRP) and ABCC1 (also known as MRP1). These proteins appear to have protective/secretory roles, with expression high in organ-vasculature sites. Consequently, expression of ABCB1, ABCC1 and ABCG2 can alter pharmacokinetic parameters and as such, under FDA requirement novel drugs must now be tested as transport substrates for these pumps (Fletcher et al., 2016; Robey et al., 2018; Theodoulou & Kerr, 2015).

1.3.1 ABCB1 and Cancer

ABCB1 was the first ABC transporter to be associated with multi-drug resistance, characterised in 1976 as a surface glycoprotein capable of modulating drug

permeability (Juliano & Ling, 1976). In humans, the *ABCB1* gene on chromosome 7q21.12 encodes for ABCB1. ABCB1 is capable of transporting a wide range of substrates with different chemical structures, molecular weights and properties. ABCB1 substrates are typically hydrophobic/amphipathic with a planar, commonly aromatic ring system and positive charge, or are unmodified neutral compounds (Gomez-Zepeda et al., 2020; Schinkel, 1999). ABCB1 has been implicated in the translocation of numerous cancer drugs including anthracyclines (e.g. doxorubicin), vinca alkaloids (e.g. vincristine), taxanes (e.g. paclitaxel), epipodophyllotoxins (e.g. etoposide) and tyrosine kinase inhibitors (e.g. gefitinib) (Ambudkar et al., 1999; Szakacs et al., 2006). Accordingly, elevated expression levels of ABCB1 can promote the efflux of chemotherapy agents (Table 1-3), leading to sub-optimal intracellular drug levels and concurrent drug insensitivity, often to multiple agents (both through broad substrate specificity and cross-resistance) - a phenomenon known as multi-drug resistance (MDR). Consequently, numerous clinical studies have reported correlation between ABCB1 tumour expression and patient response rates. For example, ABCB1 expression is associated with early relapse and reduced overall and event free survival in ependymoma patients (Sabnis et al., 2019). ABCB1 expression also negatively correlates with response to chemotherapy in small cell lung cancer (Triller et al., 2006). Similarly, an extensive meta-analysis of studies examining ABCB1 in epithelial ovarian cancer revealed that ABCB1 expression is significantly associated with chemoresistance and poor prognosis (Sun et al., 2016).

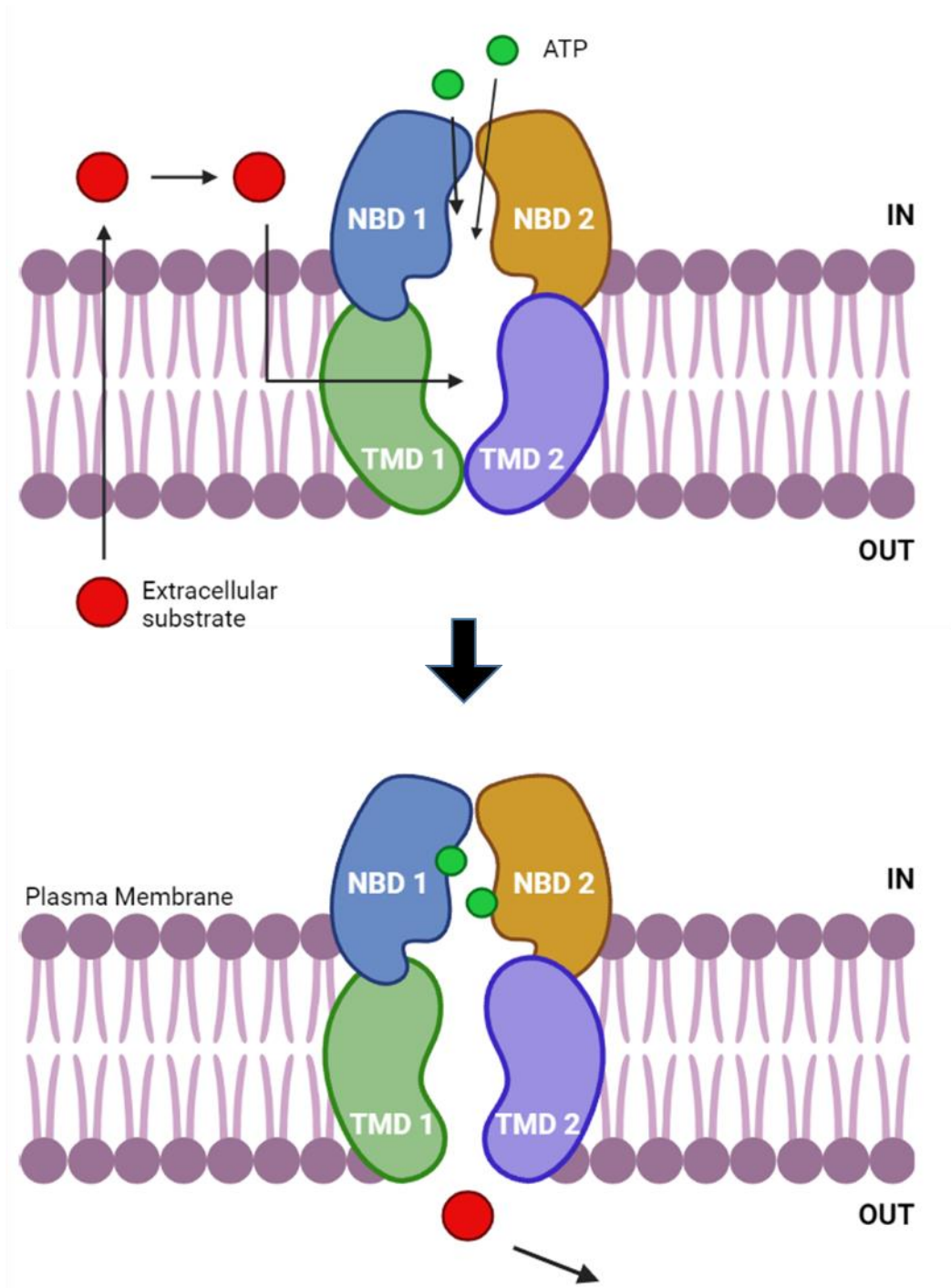
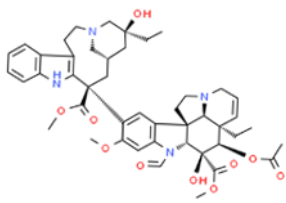
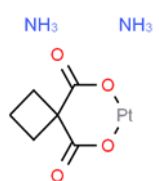
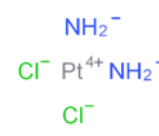
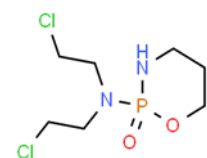
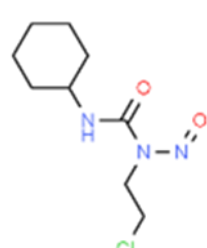


Figure 1.6 A simplified model of ABC transporter-mediated efflux from the cell. As shown, a substrate such as a drug molecule (red) enters the cell. Next, the ABC transporter binds the substrate, either from the cytoplasm or the inner leaflet of the lipid bilayer. In response to the binding of ATP molecules (green) to the ABC transporter nucleotide-binding domains (NBD), the transmembrane domain (TMD) undergoes a conformational alteration, opening towards the extracellular space and releasing the drug to the extracellular milieu. ATP hydrolysis, ADP/Pi release and NBD dissociation resets the transporter to the closed conformation. Figure adapted from (Weinberg, 2014).

1.3.2 ABCB1 and Medulloblastoma

In medulloblastoma, as in other solid tumours, high ABCB1 expression has been associated with chemoresistance and adverse prognosis (Chou et al., 1995). More recently, a significant correlation between ABCB1 expression and high-risk medulloblastoma and metastatic disease has been demonstrated (Nasir et al., 2021; Othman et al., 2014). Notably, key medulloblastoma chemotherapeutics vincristine and cyclophosphamide, currently used to treat both primary and recurrent medulloblastoma, are substrates of ABCB1 (Table 1-3). It has, therefore been postulated that treatment with these drugs may promote the survival of a resistant, ABCB1-expressing sub-population of cells that over time may result in tumour relapse (Hussein et al., 2011; Othman et al., 2014). For this reason, further study of ABCB1 and indeed how ABCB1 is regulated, represents an important avenue of medulloblastoma research.

Table 1-3 Standard medulloblastoma chemotherapeutics and their association with ABC transporters.

Drug	Mechanism of action	ABC Transporter	Reference
Vincristine 	Vinca alkaloid/anti-tubulin Primarily acts by binding to tubulin and inhibiting microtubule formation. This causes mitosis to arrest at metaphase through the disruption of mitotic spindle formation.	ABCB1 ABCC1	(Balayssac et al., 2005) (Akan et al., 2005)
Carboplatin 	Alkylating Agent Platinum compounds covalently bind to DNA causing intra- and inter-strand adducts. This inhibits DNA replication and transcription and causes cell cycle arrest and programmed cell death.	None reported.	n/a
Cisplatin 		None reported.	n/a
Cyclophosphamide 	Alkylating Agent Nitrogen mustard derivative metabolised in the liver to an active phosphoramidate alkylating agent that cross-links DNA and RNA, resulting in inhibition of protein synthesis and programmed cell death.	ABCB1	(Patutina et al., 2012)
Lomustine 	Alkylating Agent A nitrosoureas agent that is metabolised spontaneously to alkylating and carbomyloating compounds. Transfer of the chloroethyl group of the nitrosourea to O-6 methyl guanine causes DNA cross-linking, which inactivates DNA synthesis and causes cell death.	None reported.	n/a

1.3.3 Inhibition of ABCB1

Due to various anti-cancer therapies representing ABCB1 substrates, competitive and non-competitive ABC transporter inhibitors have been investigated, with the aim to

improve tumour drug delivery. First generation inhibitors utilised drugs already in clinical use and included verapamil, quinidine, amiodarone and cyclosporine. These agents were either not potent or highly toxic at the doses required to attenuate ABCB1 function (Gottesman et al., 2002). The second generation of inhibitors, derivatives of first generation agents such as valsopodar and dexverapamil, were more successful, however significantly limited the metabolism and excretion of cytotoxic agents, resulting in unacceptable toxicity (Leonard et al., 2002). Third generation inhibitors, novel agents which included, zosuquidar, tariquidar and elacridar, were developed specifically as ABCB1 inhibitors with high transporter selectivity. Unfortunately, despite early successes (Fox et al., 2015; List et al., 2001; Minderman et al., 2004), the majority of clinical trials for third generation ABCB1 modulators did not confirm clinical benefit (Robey et al., 2018). Despite such issues, targeting ABCB1 with specific inhibitors is still considered a promising therapeutic strategy to overcome drug resistance. Indeed, at the time of writing there exists >100 clinical trials investigating ABCB1 inhibitors. These include new generation, selective ABCB1 inhibitors such as Encequidar (HM30181; 21 clinical trials) and CBT-1[®] (tetrandrine; 51 clinical trials), which have recently entered clinical trials in combination with different chemotherapeutic drugs and have proved to negatively interfere with ABC transporters at tolerable doses (Kelly et al., 2012; Smolinski et al., 2021).

In recent years, other FDA-approved drugs have also been investigated for their ABCB1-targeting activity. This led to the identification of phosphodiesterase inhibitors including vardenafil and sildenafil, clinically used in the treatment of male erectile dysfunction. Sildenafil has now been actively studied in cancer treatment and appears to significantly sensitise ABCB1-overexpressing cells to ABCB1 substrates

colchicine, vinblastine, and paclitaxel (Shi et al., 2011) . Likewise, vardenafil has been demonstrated to selectively inhibit ABCB1, potentiating the cytotoxicity of paclitaxel and vincristine in ABCB1-overexpressing cells (Ding et al., 2011).

Alternative approaches to targeting ABCB1 have also been suggested. At a protein level, antibodies and small molecule peptides have demonstrated significant inhibitory effects on ABCB1-mediated drug efflux and warrant further exploration (Goda et al., 2007; Luo et al., 2020). Oligonucleotide-based inhibition of *ABCB1* has also shown promising results *in vitro*, encapsulation of which into lipid-based nanoparticles may represent a viable option for delivery *in vivo* (Susa et al., 2010; Zhu et al., 2013). Selective down-regulation of the *ABCB1* gene represents a further therapeutic strategy. *ABCB1* regulation is highly complex and not yet fully understood. If mechanisms regulating *ABCB1* expression were mediated via cancer-specific pathways, these could be exploited, with minimal effect on constitutive expression in non-cancer cell types (Szakacs et al., 2006). One strategy for selective gene regulation involves designed zinc finger proteins that selectively bind to the *ABCB1* promoter, resulting in *ABCB1* transcriptional repression and elevated cellular chemosensitivity (Bartsevich & Juliano, 2000; Xu et al., 2002).

Further investigation of ABCB1 regulatory elements and translational/transcriptional control mechanisms may provide further opportunities for alternative strategies for *ABCB1* inhibition. Indeed, many possible transcriptional factor binding sequences, such as those for Y-box binding protein 1 (YB-1; Section 1.4), have been identified in the *ABCB1* promoter region, highlighting possible regulatory mechanisms which remain to be therapeutically explored.

1.4 Y-Box Binding Protein 1 (YB-1)

YB-1, encoded for by the *YBX1* gene on chromosome 1p34.2, is a member of the large, cold-shock protein superfamily that shares an evolutionarily conserved nucleic acid binding motif denoted the “cold-shock domain”. YB-1 was first identified in 1988 by its ability to bind specifically to Y-boxes, 5'-CTGATTGG ^{T/c}/_c AA-3' sequences, in MHC class II promoters (Didier et al., 1988). It has since been clarified that YB-1 can bind to a wide variety of DNA sequences (Hasegawa et al., 1991) and as such, numerous YB-1 target genes have now been described. *Epidermal growth factor receptor (EGFR)* (Hyogotani et al., 2012; Stratford et al., 2007), *ABCB1* (Bargou et al., 1997; Kamura et al., 1999; Oda et al., 1998; Saji et al., 2003; Xu & Hu, 2016) and *Cyclin A, B1 and D1 (CCNA1, CCNB1, CCND1)* (Harada et al., 2014; Jurchott et al., 2003) all represent putative YB-1 target genes.

YB-1 is able to bind RNA as well as DNA and as such is considered a multi-functional protein with extensive roles beyond its transcription factor functionality. In fact, YB-1 has been implicated in almost all DNA- and mRNA-dependent processes within the cell, including mRNA translation and packaging, DNA repair, proliferation and pre-mRNA splicing (Figure 1.7). Due to the multi-functional nature of YB-1 and its position upstream of numerous cellular signalling pathways, it is perhaps not surprising that YB-1 has been heavily linked to cancer. YB-1 is over-expressed in many malignancies (Section 1.4.3), where elevated expression often strongly correlates with cancer progression, poor prognosis, metastasis and drug resistance.

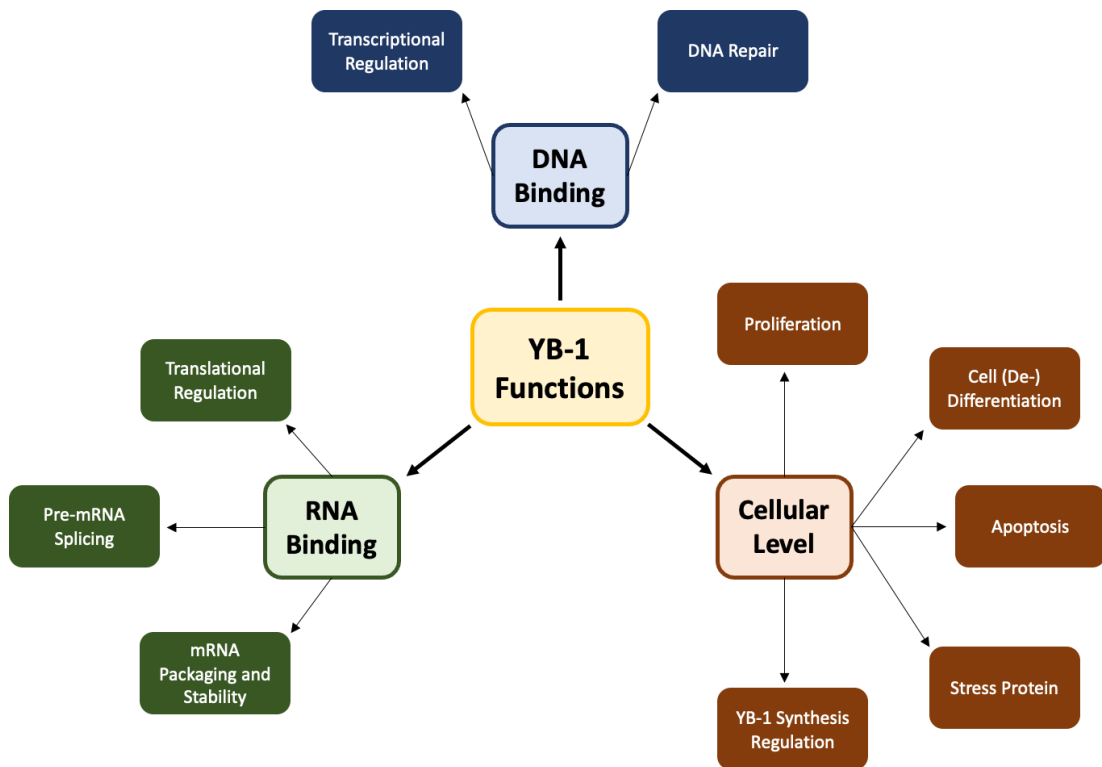


Figure 1.7 Summary of core YB-1 functions. YB-1 is a multi-functional protein with both DNA and RNA binding capabilities. YB-1 DNA-associated functions are denoted by blue shading, RNA-associated functions are denoted by green shading and cellular level functions denoted by brown shading.

1.4.1 Structural Organisation of YB-1³

YB-1 is a 324 amino acid protein with a molecular mass of 35.9 kDa (Figure 1.8). It comprises three domains: a short alanine/proline-rich (A/P) N-terminal domain, a highly conserved cold shock domain (CSD), and an elongated C-terminal domain (CTD) with alternating clusters of positively and negatively charged amino acid residues (Lyabin et al., 2014). The three-dimensional structure of the CSD domain has been resolved by NMR spectroscopy and is known to adopt a classical oligonucleotide/oligosaccharide (OB)-fold consisting of a closed five-stranded anti-parallel β -barrel (Kloks et al., 2002). The CSD contains ribonucleoprotein (RNP)-1 and RNP-2 RNA binding motifs and is responsible for both specific and non-specific RNA binding and specific ssDNA binding. Recently, it was demonstrated that the YB-1 CSD forms a homodimer, both in a crystal structure as well as in solution. This has been proposed to facilitate the RNA binding ability of YB-1 and its multimerisation through the CTD - a process involved in mRNA packaging and translational control (Yang et al., 2019).

Contrastingly, the 3D structures of both the CTD and A/P domain are unknown, likely due to their predicted intrinsically disordered nature (Guryanov et al., 2012). The A/P domain contains binding sites for various proteins, including serine/arginine rich splicing factor 9 (SRP30C; also interacts with the CSD), cyclin D1, actin and P53 (Khandelwal et al., 2009; Okamoto et al., 2000; Raffetseder et al., 2003; Ruzanov et

³ The material and figures included in Sections 1.4.1, 1.4.2, 1.4.3 and 1.4.4 draw heavily on the author's previously published literature review Taylor, L., Kerr, I. D., & Coyle, B. (2021). Y-Box Binding Protein-1: A Neglected Target in Pediatric Brain Tumors? *Mol Cancer Res*, 19(3), 375-387. <https://doi.org/10.1158/1541-7786.MCR-20-0655> and is presented in line with the article reuse permissions policies of AACR journals.

al., 1999). Likewise, the CTD has been reported to bind a number of proteins, including P53, DNA repair protein NEIL2 and YB-1 itself (Das et al., 2007; Izumi et al., 2001; Skabkin et al., 2004; Skabkina et al., 2005). The CTD also contains several proposed nuclear localisation signals (NLS), all of which are denoted in Figure 1.8. Originally, the YB-1 NLS was identified at residues 183 – 202 aa (Bader & Vogt, 2005). More recently, a further set of NLS have been proposed: NLS-1 at residues 149 – 156 aa, NLS-2 at residues 185 – 194 aa and NLS-3 at residues 276 – 292 aa (van Roeyen et al., 2013). Finally, a proline-tyrosine(PY)-NLS, was identified at residues 174 – 202 aa, closely matching the position of the originally identified NLS (Mordovkina et al., 2016). Two cytoplasmic retention signals (CRS) have also been suggested, residing at residues 247 – 267 aa and 264 – 290 aa (Bader & Vogt, 2005; Woolley et al., 2011). The CTD also has nucleic acid binding capabilities. While the CSD appears to have a more significant role in RNA binding, it is thought that DNA binds with highest affinity to the CTD (Tanabe et al., 2015).

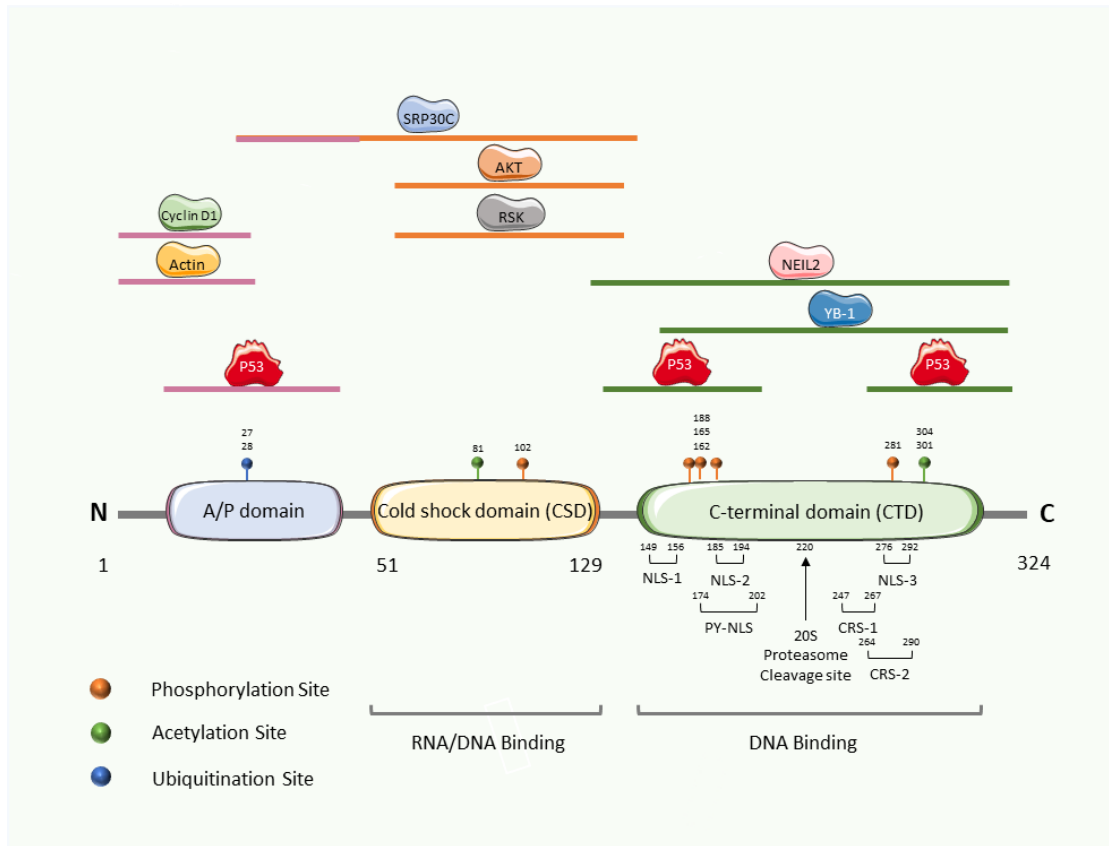


Figure 1.8 YB-1 protein domain organisation. YB-1 has a disordered alanine/proline-rich (A/P) domain, a universally conserved cold shock domain (CSD) and an elongated, disordered C-terminal domain (CTD) comprising alternating clusters of positive and negatively charged amino acids. Each domain contains binding sites for various protein interactors, some of which are illustrated. Within the CTD there exists a number of proposed nuclear localisation signals (NLS) and two proposed cytoplasmic retention signals (CRS). The CTD also contains a peptide bond linkage between Glu219 and Gly220 which is targeted by the 20S proteasome. Notable phosphorylation (orange), acetylation (green) and ubiquitination (blue) sites are also shown.

1.4.2 Regulation of YB-1

1.4.2.1 Regulation of YB-1 Expression

In spite of interest in YB-1 and its functions, our understanding of the regulation of *YBX1* expression remains vague. An overview of YB-1 transcriptional and translational regulation is presented in Figure 1.9. Several transcription factors have been shown to regulate *YBX1* through interaction with a number of different motifs throughout both the *YBX1* promoter and 5'untranslated (UTR) region (Table 1-4). Correspondingly, the control of *YBX1* expression is likely to be highly context-dependent and may be triggered in response to various stimuli. Six E-boxes are located throughout the *YBX1* promoter. The E-box binding transcription factor c-MYC has been shown to interact with the *YBX1* promoter and drive transcription in a P73-dependent manner in response to DNA-damaging stimuli (Uramoto et al., 2002). Additionally, basic-helix-loop-helix transcription factor TWIST1 has been implicated in E-box dependent *YBX1* transcriptional control (Shiota et al., 2008), a finding further validated by the involvement of TWIST1 binding proteins p300/CBP-associated factor (PCAF) in *YBX1* transcriptional activation and Programmed Cell Death Protein 4 (PCDP4) in *YBX1* down-regulation (Shiota et al., 2009; Shiota et al., 2010). A 5'UTR GGATAA element has also been shown to activate the *YBX1* gene promoter through binding of both GATA-1 and GATA-2 to this region, although interestingly not to GATA elements present within the promoter (Yokoyama et al., 2003).

Post-transcriptional regulatory mechanisms of YB-1 are better described (Table 1-4). YB-1 translation is controlled by an auto-regulatory feedback loop in which YB-1 binds to a ~80-nucleotide regulatory element in the 3'UTR of its own mRNA, which

encompasses overlapping binding sites for both YB-1 and poly(A)-binding protein (PABP). PABP binds to a 50-nucleotide A-rich sequence within the regulatory element, stimulating *YBX1* mRNA translation in a poly(A) tail-independent manner. Conversely, YB-1 selectively inhibits its own synthesis through interaction with two sequences within the regulatory element, both containing the same 8-nucleotide motif - UCCAG/ACAA. The binding sites of YB-1 and PABP overlap, meaning that the two proteins compete for *YBX1* mRNA binding (Skabkina et al., 2003; Skabkina et al., 2005). YB-1 is a major protein in both polysomal and free messenger RNPs (mRNPs) and plays an extensive role in the regulation of overall protein synthesis within the cell, depending on the amount of YB-1 associated with mRNA. In the complete absence of YB-1, or conversely at high YB-1 concentrations where mRNA is saturated with YB-1, translation is suppressed; whereas at relatively low YB-1 levels, translation is stimulated (Eliseeva et al., 2011). Thus, YB-1 appears to auto-regulate its own synthesis at a concentration that is optimal for the translation of other cellular mRNAs.

Moreover, YB-1 translation also appears to be sensitive to signalling through the mTOR pathway, dictated by sequences in the 5'UTR of *YBX1* mRNA. Regulation in this way appears to be highly dependent on cell division rate. When cells are slow-dividing/serum starved, mTOR signalling is attenuated and hence YB-1 translation is inhibited (Lyabin et al., 2012). Various families of non-coding RNA (ncRNA) have also been implicated in the regulation of *YBX1* expression, including miR-137 and miR-216a and the lncRNA GAS5 and MIR22HG, reviewed in (Johnson et al., 2019).

YB-1 is known to undergo various post-translational modifications (Figure 1.8; Table 1-4), with phosphorylation being the focus of the majority of research to date. Indeed, there is evidence to suggest that phosphorylation “activates” YB-1, promoting both nuclear transport and facilitating DNA binding. The most extensively studied phosphorylation site in YB-1 is serine-102 (S102) in the CSD, which kinases AKT and RSK have been shown to target, implicating both the MAP kinase pathway and PI3K cascade in the control of YB-1 activation (Stratford et al., 2008; Sutherland et al., 2005). Other confirmed phosphorylation sites include: S165 (CSD), which appears to be crucial for transcriptional activation of nuclear factor kappa (NF-κB); tyrosine-162 (Y162) (CTD), phosphorylation of which is mediated by fibroblast growth factor receptor 1 (FGFR1) and Y188 and Y281 (CTD), where Y281 phosphorylation appears to correlate with YB-1 nuclear shuttling (Prabhu et al., 2015). Acetylation sites have also been reported, including lysine-81 (K81) in the CSD as well as K301 and K304 in the CTD. Although the functional significance of K81 acetylation is unknown, acetylation at positions K301 and K304 has been suggested to promote microvesicle-mediated secretion of YB-1 from the cell (Frye et al., 2009; Prabhu et al., 2015). Ubiquitination sites have also been identified in YB-1 and retinoblastoma binding protein 6 (RBBP6), an E3 ubiquitin ligase, has been shown to interact with YB-1, leading to ubiquitination and proteasomal degradation (Prabhu et al., 2015). Additionally, the peptide bond linkage between glutamate-219 (Glu219) and glycine-220 (Gly220) has been reported to be targeted by the 20S proteasome for endoproteolytic cleavage in an ubiquitin-independent manner and may also be involved in YB-1 nuclear shuttling (Sorokin et al., 2005; van Roeyen et al., 2013).

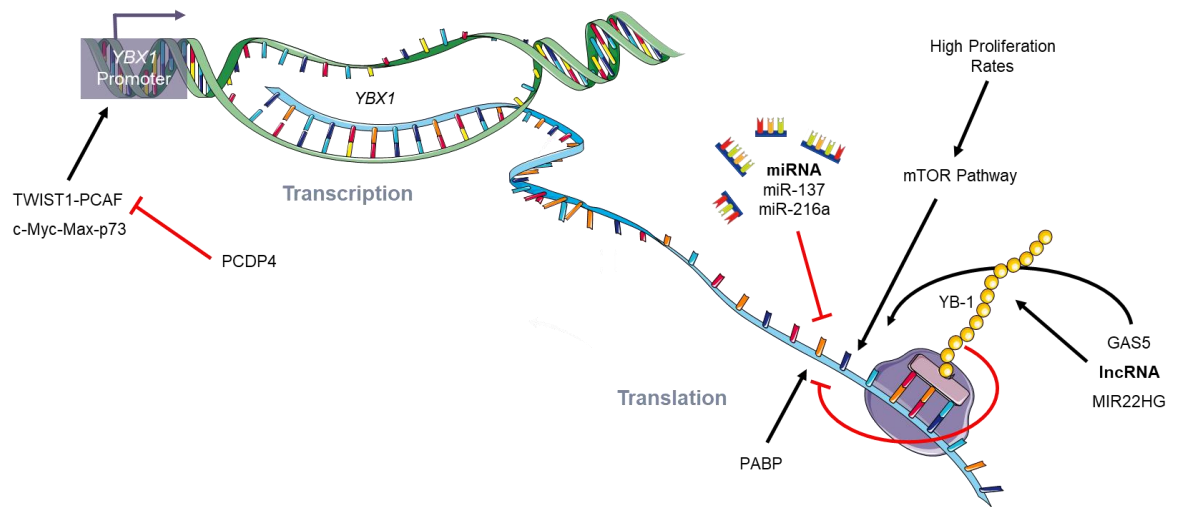


Figure 1.9 Regulation of YB-1 expression. A number of factors regulate YB-1 expression at both transcriptional and translational levels. E-box binding proteins TWIST1 and c-Myc-Max bind to one of six E-boxes in the *YBX1* promoter to initiate transcription. *YBX1* mRNA is down-regulated by various miRNA, including miR-137 and miR-216a. YB-1 translation is stimulated by mTOR, which itself is influenced by cellular proliferation. Additionally, YB-1 protein function and expression are regulated by lncRNA such as GAS5 and MIR22HG. YB-1 protein can auto-regulate translation by binding to sites within the YB-1 regulatory element in the 3'UTR, inhibiting translation at the initiation stage. PABP competes with YB-1 for binding in this area, displacing YB-1 to stimulate translation. Adapted from (Johnson et al., 2019).

Table 1-4 Experimentally confirmed transcriptional, translational and post-translational regulators of human YBX1/YB-1.

Level	Regulator	Effect	Reference
Transcriptional	C-MYC/P73	Stimulates transcription.	(Uramoto et al., 2002)
	TWIST1	Stimulates transcription.	(Shiota et al., 2008)
	PCAF	Stimulates transcription (via Twist1 acetylation).	(Shiota et al., 2010)
	PDCD4	Inhibits transcription (via direct Twist1 interaction).	(Shiota et al., 2009)
	GATA-1/GATA-2	Stimulates transcription.	(Yokoyama et al., 2003)
Translational	mTOR (mTOR Pathway)	Stimulates translation (influenced by proliferation rate).	(Lyabin et al., 2012)
	YB-1	Inhibits translation.	(Skabkina et al., 2005)
	PABP	Stimulates translation.	(Skabkina et al., 2003)
Post-Translational	AKT (PI3K/AKT Pathway)	Activation (via phosphorylation of S102 site).	(Sutherland et al., 2005)
	RSK (MAPK/ERK Pathway)	Activation (via phosphorylation of S102 site).	(Stratford et al., 2008)
	FGFR1	Unknown	Reviewed in (Prabhu et al., 2015)
	RBBP6	Degradation (via ubiquitination-driven proteasomal cleavage).	

Red fonts denote regulators with an inhibitory role while green fonts describe regulators with an activation role. Regulators with grey fonts have a currently unknown effect.

1.4.2.2 Regulation of YB-1 Sub-cellular Localisation

YB-1 is a cytoplasmic-nuclear shuttling protein. In non-malignant cells, over 90% of YB-1 is located in the cytoplasm where it is associated with mRNPs. The NLS and CRS located in the CTD of YB-1 appear to regulate YB-1 distribution between the nucleus

and the cytoplasm. The CRS is thought to be dominant, which combined with the affinity of YB-1 to mRNA and its interaction with cytoplasmic partner proteins, is responsible for YB-1 cytoplasmic retention (Skabkin et al., 2004). The exact mechanism of YB-1 translocation to the nucleus is not fully understood (Figure 1.10) and appears to be a dynamic process that occurs on account of YB-1 being able to undergo structural rearrangements in response to various stimuli, resulting in exposure of NLS to transport proteins. Indeed, transportin-1 has been proposed to mediate YB-1 nuclear import through interaction with the PY-NLS (Mordovkina et al., 2016).

It has been suggested that changes in YB-1 nuclear localisation occur in a cell cycle-dependent manner, with nuclear accumulation observed during the G1/S transition. Two regions in the CTD, encompassing NLS-2 and NLS-3, were shown to mediate translocation in this context (Jurchott et al., 2003). YB-1 subcellular localisation may also be mediated, in part, by interaction with other proteins. YB-1 is known to play a role in pre-mRNA splicing; however, YB-1 appears to interact directly with splicing factor SRP30C via the A/P domain in an RNA-independent manner. Co-localisation of YB-1 and SRP30C has been shown to promote significant nuclear shuttling of YB-1 in HeLa cells, an effect that is reversed upon sequestering of SRP30C into stress-induced nuclear bodies following heat-shock (Raffetseder et al., 2003). Another study, undertaken in breast cancer cells, highlighted the importance of WAVE3, a member of the WASP/WAVE actin-cytoskeleton remodelling protein family. The WAVE3-YB-1 interaction appears to facilitate the nuclear translocation of YB-1, which in this context promoted the transcriptional regulation of cancer stem cell (CSC)-specific genes implicated in self-renewal and expansion (Bledzka et al., 2017).

Clear evidence exists for YB-1 nuclear translocation in response to cellular stress, for example upon exposure to UV radiation, oxidative stress, hyperthermia and chemotherapeutics (Fujita et al., 2005; Koike et al., 1997; Stein et al., 2001; Tanaka et al., 2021). A 2005 study revealed that wild-type, transcriptionally active P53 is necessary for efficient nuclear translocation of YB-1, likely via the trans-activation of a P53 target 'effector' gene (Homer et al., 2005). Comparatively, a 2006 study suggested that YB-1 accumulates in the nucleus by complexing directly with P53 and WRN, a process thought to facilitate WRN-mediated DNA repair (Guay et al., 2006). As previously described (Section 1.4.2.1), proteolytic cleavage between Glu219 and Gly220 by the 20S-proteasome under cellular stress may also trigger YB-1 nuclear localisation through the production of a fragmented YB-1 protein lacking a CRS (Sorokin et al., 2005; van Roeyen et al., 2013). However, the proteasomal theory of YB-1 nuclear accumulation is still disputed, largely due to the lack of a suitable YB-1 antibody (Section 1.4.4.1) (Cohen et al., 2010; Woolley et al., 2011).

Lastly, RSK1 and RSK2 have been shown to directly phosphorylate YB-1 at S102, with knockdown/drug-mediated inhibition diminishing YB-1 promoter binding (Stratford et al., 2008). Experiments using breast and ovarian cancer cell lines have shown phosphorylation by AKT at S102 promotes nuclear translocation; disruption of which, both by mutation or inhibition, prevents nuclear localisation and negatively affects cell growth and the expression of drug resistance genes (Basaki et al., 2007; Sutherland et al., 2005). Contrastingly, some groups have found no evidence of phosphorylation at S102 influencing cellular localisation at all, with mutation of the S102 site resulting in unchanged nuclear/cytoplasmic distribution of YB-1 (Bader & Vogt, 2008; Evdokimova et al., 2006). Alternatively, phosphorylation at Y281 within

NLS-3 may act dominantly on the subcellular localization of YB-1, promoting nearly exclusive nuclear localization of full-length YB-1 (van Roeyen et al., 2013). Another recent conflicting report proposed that rather than cytoplasmic RSK promoting the phosphorylation and resultant nuclear shuttling of YB-1, nuclear-phosphorylated YB-1 (pYB-1) is instead a product of the nuclear translocation of RSK, which then phosphorylates and activates pre-existing nuclear YB-1 in response to cellular stress (Tiwari et al., 2018).

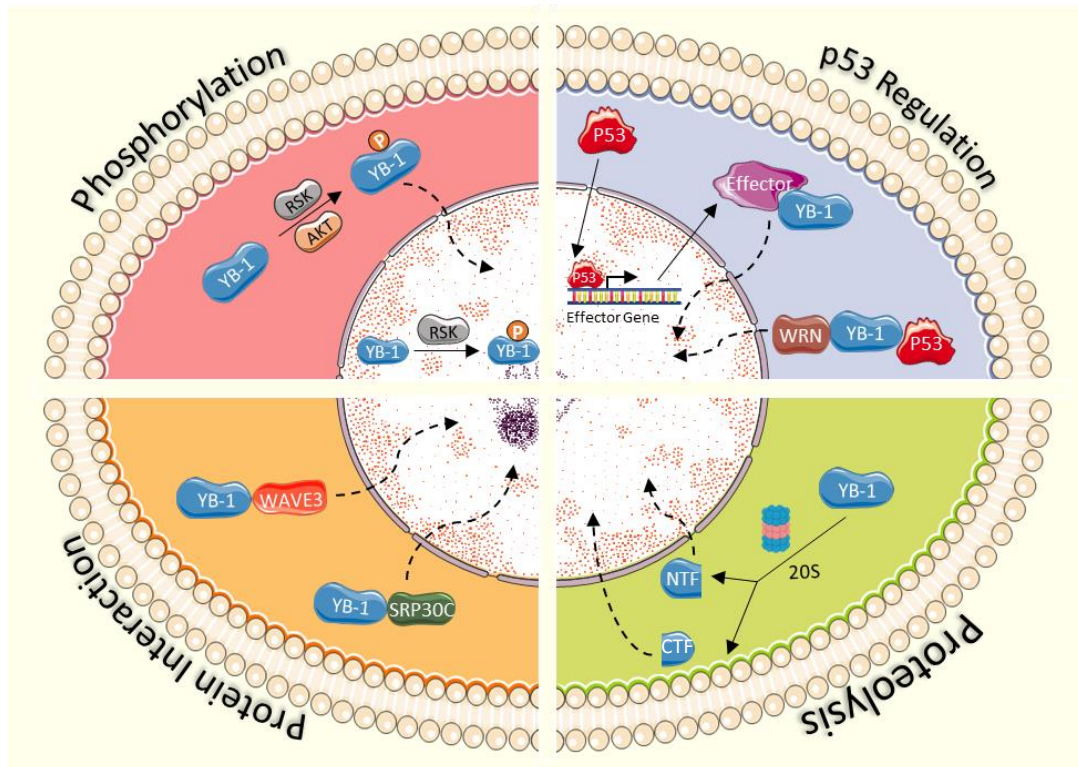


Figure 1.10 Proposed mechanisms of YB-1 nuclear translocation. Simplified overview of potential YB-1 nuclear transport mechanisms. YB-1 has been suggested to translocate to the nucleus upon phosphorylation by RSK/AKT or conversely is activated within the nucleus by nuclear-translocated RSK. Interaction with different proteins including splicing factor SRP30C or actin-remodelling protein WAVE3 may also promote nuclear localisation. Involvement of the 20S proteasome has also been proposed, producing either a C- or N-terminal fragment (CTF; NTF) which translocates to the nucleus. Functional P53 protein has also been suggested to promote nuclear translocation, both by direct interaction with YB-1 and by the transcriptional activation of an “effector protein” which then facilitates YB-1 nuclear transport. Dashed lines represent nuclear translocation.

1.4.3 YB-1 and Brain Tumours

Many of the cellular signalling pathways regulated by YB-1, including E2F, PI3K/AKT/mTOR, RAS/RAF/MEK/ERK and P53 are exploited in cancer cells (discussed extensively in (Lasham et al., 2013)). YB-1 over-expression has been widely described in various cancers including renal cell carcinoma (Y. Wang et al., 2015), breast cancer (Janz et al., 2002; X. Wang, X. B. Guo, et al., 2015), osteosarcoma (Fujiwara-Okada et al., 2013), head and neck squamous cell carcinoma (Kolk et al., 2011), colorectal carcinoma (Shibao et al., 1999), prostate cancer (Giménez-Bonafé et al., 2004), glioma (Zheng et al., 2016) and non-small cell lung cancer (Shibahara et al., 2001). Frequently, elevated expression strongly correlates with cancer progression, poor prognosis, aggressive disease, chemoresistance and increased metastatic potential.

Despite considerable research in solid tumours, there is a significant lack of studies exploring the role of YB-1 in paediatric brain tumours or indeed in brain and CNS tumours in general. However, elevated *YBX1* expression has been reported in both paediatric glioblastoma (Faury et al., 2007) and medulloblastoma (Dey et al., 2016; Kloetgen et al., 2020) indicating that it may represent a target worthy of further investigation. Sections 1.4.3.1 - 1.4.3.4 (summarised in Table 1-5) will describe our current understanding of the function of YB-1 in various aspects of tumorigenesis, with a specific focus on known and likely functions in medulloblastoma and other paediatric brain tumours.

Table 1-5 Summary of tumourigenic features experimentally associated with YB-1 expression.

YB-1 Tumour-Related Role	Cancer Where Observed	Experimental Model	Reference
Proliferation/ Apoptosis	Ovarian Cancer	<i>In vitro</i> cell lines	Basaki et al., 2007
	Cervical Cancer	<i>In vitro</i> cell lines	Jurchott et al., 2003
	Lung adenocarcinoma/ Melanoma	<i>In vitro</i> cell lines	Lasham et al., 2003
	Breast cancer	<i>In vitro</i> cell lines/ <i>in vivo</i> mouse models	Lee et al., 2008
	Medulloblastoma	<i>In vitro</i> cell lines/ <i>in vivo</i> mouse models	Dey et al., 2016; Kloetgen et al., 2020
	Glioblastoma	<i>In vitro</i> cell lines/ <i>in vivo</i> mouse models	Gao et al., 2009; Tong et al., 2019
Invasion/ Metastasis	Breast Cancer	Patient tissue samples/ <i>in vitro</i> cell lines/ <i>in vivo</i> mouse models	Evdokimova et al., 2009; Lasham et al., 2012; Lim et al., 2017; Lovett et al., 2010;
	Cervical Cancer	<i>In vitro</i> cell lines	Pang et al., 2017
	Pancreatic Cancer	Patient tissue samples; <i>in vitro</i> cell lines	Lu et al., 2017
	Melanoma	Patient tissue samples; <i>in vitro</i> cell lines	Schittek et al., 2007
	Glioblastoma	<i>In vitro</i> cell lines/ <i>in vivo</i> mouse models	Gao et al., 2009; Tong et al., 2019
Multi-drug Resistance	Melanoma	<i>In vitro</i> cell lines	Schittek et al., 2007
	Neuroblastoma	<i>In vitro</i> cell lines	Wang et al., 2017
	Hepatocellular Carcinoma	<i>In vivo</i> mouse models	Tao et al., 2019
	B-cell Lymphoma	Patient tissue samples; <i>in vitro</i> cell lines	Miao et al., 2016
	Glioblastoma	<i>In vitro</i> cell lines/ <i>in vivo</i> mouse models	Gao et al., 2009; Mantwill et al., 2013; Tong et al., 2019
Tumour Initiating Cells	Breast Cancer	<i>In vitro</i> cell lines/ <i>in vivo</i> mouse models	To et al., 2010; F. Yang et al., 2019
	Melanoma	<i>In vitro</i> cell lines	F. Yang et al., 2019
	Glioblastoma	Patient tissue samples/ <i>in vitro</i> cell lines/ <i>in vivo</i> mouse models	Fotovati et al., 2011; Mantwill et al., 2013

Blue highlighting denotes functions demonstrated experimentally in paediatric and adult brain tumour models.

1.4.3.1 YB-1 and Proliferation

Sustaining proliferative signalling via dysregulation of the cell cycle is arguably the most important hallmark of a tumour cell. Reduction of YB-1 results in diminished proliferation and apoptosis in cancer cell lines and *in vivo* models, with a number of studies revealing a reduction in cyclin and cyclin-dependent kinase (CDK) level upon YB-1 knockdown (Basaki et al., 2007; Jurchott et al., 2003; Lasham et al., 2003; Lee et al., 2008). In medulloblastoma, YB-1 appears to be critical for sustaining proliferation both in cells and tissues derived from SHH medulloblastoma mouse models and in cerebellar granule neuron precursors (CGNPs; the proposed cells-of-origin for SHH medulloblastoma) *in vitro* and *ex vivo* (Dey et al., 2016). Likewise, a study examining the oncogenic functions of YB-1 in paediatric glioblastoma revealed silencing of YB-1 significantly reduced SF188 cell growth in monolayer and soft agar and delayed tumour growth in mice (Gao et al., 2009).

Several pathways that promote cancer cell proliferation are activated by YB-1 (Figure 1.11 A), including E2F, PI3K/AKT/MTOR and RAS/RAF/MEK/ERK (Lasham et al., 2013). A prime example is the activational role played by YB-1 in the regulation of *IGF2* expression in CGNPs and medulloblastoma cells (Dey et al., 2016). The Insulin-like Growth Factor (IGF) signalling pathway has been reported in medulloblastoma, is required for SHH medulloblastoma formation and medulloblastoma proliferation control and has been associated with metastatic progression (Hartmann et al., 2005; Wu et al., 2012). For example, activation of the IGF receptor by IGF1/2 results in downstream activation of PI3K signalling, leading to inhibition of GSK3 β , a kinase responsible for blocking cell cycle progression in CGNPs (Dey et al., 2016; Hartmann et al., 2005). Interestingly, in the aforementioned study, YB-1 was shown to be

induced by Sonic Hedgehog (Shh) in CGNPs, demonstrating co-operation between SHH and IGF-mediated PI3K signalling and identifying the SHH:YB-1:IGF2 axis as a powerful target for therapeutic intervention in medulloblastoma. Furthermore, a 2007 study assessing molecular pathways in paediatric glioblastoma identified at least two disease subsets, one poor prognosis associated with a proliferative phenotype and RAS and AKT pathway activation and one good prognosis without. Of particular interest, the subset with RAS and AKT pathway activation exhibited nuclear YB-1 expression, which was associated with elevated *EGFR* expression, while the good prognosis subset exhibited predominantly cytoplasmic YB-1 expression. Thus, in paediatric glioblastoma YB-1 may undergo AKT-mediated phosphorylation, resulting in nuclear translocation and concordant transcription factor functionality while relieving translational repression of numerous pro-mRNAs, hence contributing to increased *EGFR* levels, RAS activity and gliomagenesis (Faury et al., 2007). A similar finding was reported in a lung cancer study, where nuclear YB-1 localisation was associated with *EGFR* expression and poor prognosis (Hyogotani et al., 2012).

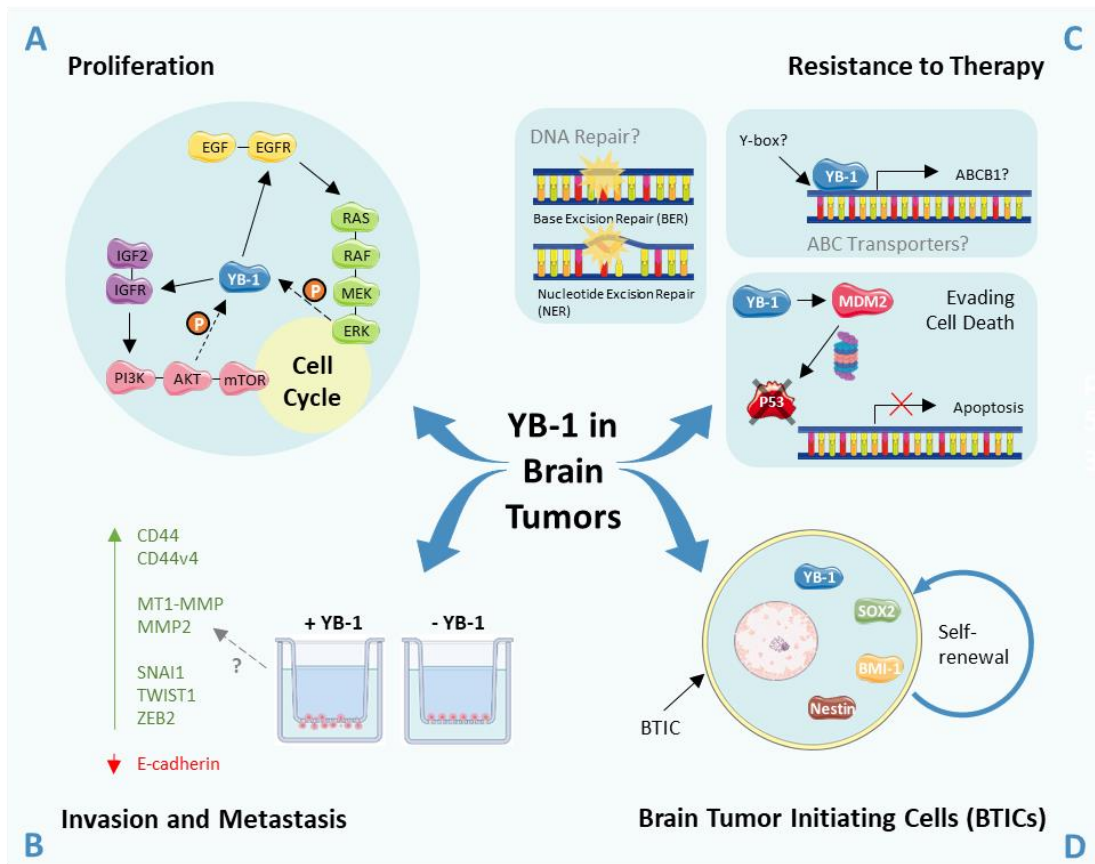


Figure 1.11 Proposed oncogenic functions of YB-1 in brain tumours. YB-1 has been shown to facilitate the advancement of several key malignant phenotypes in brain tumours, including: proliferation, invasion, resistance to therapy and the maintenance of brain tumour initiating cells (BTICs). Oncogenic functions presented in black type have been proven experimentally in brain tumour patient samples and cell lines, whereas those in grey type have been investigated in other tumour types but are yet to be explored in brain tumours.

1.4.3.2 YB-1 and Invasion/Metastasis

Metastasis is the leading cause of cancer mortality. At the point of diagnosis up to 40% of medulloblastoma patients and 17% of paediatric glioblastoma patients display clinically detectable metastatic disease (Das & Kumar, 2017; Wu et al., 2012). Metastasis is a complex process requiring a number of events that can vary between cancer types, however common to all are changes in cell-cell and cell matrix adhesion, cell polarity and cytoskeletal organisation. A number of studies have revealed a clear role for YB-1 in invasion and metastasis. Bioinformatic analysis of a large breast cancer micro-array displayed a strong association between *YBX1* mRNA expression and distant metastasis formation (Lasham et al., 2012). *In vitro* studies have demonstrated that YB-1 depletion impedes the invasive capabilities of several cancer cell lines (Lim et al., 2017; Lu et al., 2017). Likewise, knockdown of YB-1 both stably and transiently in paediatric glioblastoma cell line SF188 significantly reduces cell invasion in transwell invasion assays (Gao et al., 2009). The mechanisms underlying this process have not been studied in paediatric glioblastoma, perhaps owing to the fact that the molecular pathways involved in metastasis in paediatric brain tumours remain largely unclear. However, in other cancer types YB-1 has been shown to regulate multiple stages of the metastatic cascade at the level of transcription, pre-mRNA splicing and translation (Figure 1.11 B).

One of the first steps in metastatic dissemination is loss of polarity and cellular adhesion within the primary tumour mass. A key step in the loss of adhesion in epithelial cells is the inactivation of adherens junction protein E-cadherin by epithelial to mesenchymal (EMT)-inducing transcription factors, such as SNAI1 and TWIST. Although only recently has the EMT process in non-epithelial tumours been

considered important for tumour progression, contemporary glioma research has named the EMT a key player in glioma invasion, with “mesenchymal” a known glioblastoma subtype associated with poor outcome (Phillips et al., 2006). Interestingly, malignant CNS tumours frequently exhibit minimal E-cadherin expression, with one study demonstrating a marked reduction in E-cadherin in adult and paediatric high-grade glioma and medulloblastoma compared to low-grade gliomas, perhaps indicative of the highly aggressive, malignant nature of these tumours (Motta et al., 2008). Gain- and loss-of-function studies in cervical and breast cancer lines have revealed that YB-1 plays a key role in the translational regulation of proteins implicated in the acquisition of a migratory mesenchymal phenotype including SNAI1/2, ZEB2 and TWIST1 (Evdokimova et al., 2009; Pang et al., 2017). Correspondingly, over-expression of YB-1 in breast cancer cells is associated with loss of E-Cadherin and tight junction protein ZO-1, increased expression of N-cadherin and vimentin and the emergence of a mesenchymal phenotype (Evdokimova et al., 2009). As both SNAI1 and ZEB2 have been associated with invasion, migration and EMT in paediatric and adult glioma and glioblastoma, studying the role of YB-1 in this context in brain tumours may yield interesting results (Myung et al., 2014; Qi et al., 2012).

The basement membrane (BM) and extracellular matrix (ECM) represent a substantial physical barrier to the migration of cancer cells. Basement membranes in the CNS include the pial basement membrane, the vascular basement membrane and the basement membranes that are associated with Schwann cells. Both medulloblastoma and paediatric glioblastoma can disseminate through passive shedding into the cerebral spinal fluid (CSF) system (Birzu et al., 2020; Low et al.,

2020). Although the mechanism by which this occurs is not fully understood, for invading cells to extend into the CSF they would have to cross one or more CNS basement membranes. To do this, multiple proteolysis pathways are likely to become activated. Studies have shown YB-1 to regulate the expression of numerous matrix metalloproteinases. YB-1 knockdown in pancreatic and melanoma cancer cell lines results in significant down-regulation of MMP-11, MMP-14 and MMP-2 (Lu et al., 2017; Schitteck et al., 2007). Moreover, in ER-positive breast cancer cells, YB-1 appears to enhance the presentation of membrane type-1 (MT1)-MMP at the sites of cell invasion, namely the cell membrane, where it can degrade the ECM (Lovett et al., 2010). MMPs have been shown to be associated with glioblastoma and medulloblastoma invasiveness. In particular, (MT1)-MMP expression is increased in >75% of medulloblastoma tumour samples and MMP2 expression is associated with paediatric high-grade gliomas (Gu et al., 2009; Ozen et al., 2004).

1.4.3.3 YB-1 and Multi-Drug Resistance

As previously described (Section 1.3.1), the development and acquisition MDR in cancer cells remains a major obstacle in the treatment of metastatic disease. YB-1 knockdown has been shown to increase cellular sensitivity to numerous cytotoxic drugs including cisplatin and etoposide in neuroblastoma and melanoma cell types (Schitteck et al., 2007; Wang et al., 2017). Correspondingly, YB-1 knockdown in paediatric glioblastoma SF188 cells, as well as glioblastoma U251 cells renders cells sensitive to both temozolomide and taxol in an O⁶-methylguanine-DNA methyltransferase (MGMT)-independent manner (Gao et al., 2009). As previously mentioned (Section 1.4.2.2), exposure of various epithelial cancer lines to UV radiation, oxidative stress, hyperthermia and chemotherapeutics promotes YB-1

nuclear localisation (Fujita et al., 2005; Koike et al., 1997; Stein et al., 2001; Tanaka et al., 2021). Moreover, in brain tumour initiating cell (BTIC) lines derived from patients with primary glioblastoma, YB-1 is highly phosphorylated and localised to the nucleus in temozolomide-resistant lines, whereas in temozolomide-sensitive lines, YB-1 is predominantly located in the cytoplasm (Mantwill et al., 2013). Such observations indicate that cancer cells may increase nuclear YB-1 expression/promote nuclear YB-1 translocation as a protective measure in response to extracellular stress (Figure 1.11 C).

Perhaps the best-known mechanism for the development of MDR is the enhanced synthesis of certain members of the ATP-binding cassette family (Section 1.3.1). Of particular note, correlation between ABCB1 expression and nuclear YB-1 translocation has been demonstrated in breast cancer patients treated with paclitaxel and in prostate cancer patients following neo-adjuvant hormone therapy (Fujita et al., 2005; Giménez-Bonafé et al., 2004). Early studies suggested YB-1 may transcriptionally regulate *ABCB1* expression by interacting with a Y-box element present in the *ABCB1* promoter region in response to cellular stress (Ohga et al., 1998; Stein et al., 2001). Additional YB-1 binding sites within the *ABCB1* promoter have since been identified and confirmed by co-immunoprecipitation and luciferase assays (Ghatak et al., 2021; Shen et al., 2011). Controversially, other studies have disputed interaction between YB-1 and the *ABCB1* gene. A 2016 study using triple-negative breast cancer lines demonstrated that although high YB-1 expression correlates with increased resistance, this occurs in an ABCB1-independent manner (Lasham et al., 2016). Likewise, others have argued that there exists more evidence to support nuclear factor Y (NF-Y) as a Y-box element-binding transcription factor in

cancer cells, suggesting a post-transcriptional role for YB-1 in the regulation of *ABCB1*/other Y-box element containing genes (Dolfini & Mantovani, 2013).

Another mechanism of resistance to cytotoxic therapy is the activation of DNA repair mechanisms and the evasion of drug-induced apoptosis. In recent years, YB-1 has been shown to preferentially bind to cisplatin-modified DNA and DNA containing abasic sites/mismatches and possesses intrinsic exo- and endo-nuclease activity (Gaudreault et al., 2004; Ise et al., 1999). It also interacts with several key components of base- and nucleotide-excision repair pathways (Eliseeva et al., 2011). Such observations, combined with observed YB-1 nuclear translocation in response to cytotoxic therapy, supports the theory that YB-1 is involved in the repair of DNA lesions imparted by genotoxic therapy. YB-1 has also been proposed to regulate key pro-apoptotic and immune response genes including *FAS*, *MHC Class I* and *II* and notably key tumour suppressor gene *TP53*. Indeed, *YBX1* knockdown in SHH medulloblastoma cell lines promotes apoptosis through the de-regulation of heterochromatin-regulated genes associated with inflammatory response, apoptosis and death receptor signalling. This occurs through a concurrent reduction in CDX5 expression, a heterochromatin-associated protein regulated post-transcriptionally by YB-1, which represses transcription of apoptosis-related genes through Histone 3 K9 trimethylation (H3K9me3) interaction (Kloetgen et al., 2020).

Perhaps counterintuitively given the role of P53 in YB-1 nuclear translocation (Section 1.4.2.2), YB-1 can both repress transcription of *TP53* and inhibit the ability of P53 to transactivate cell death genes *BAX* (Bcl2-associated X protein) and *NOXA* (NADPH oxidase activator) (Homer et al., 2005; Lasham et al., 2003). The mechanism by which

this occurs likely requires direct interaction between P53 and YB-1, reducing its affinity for promoter binding and causing promoters with a low binding affinity for P53 (i.e. pro-apoptotic genes) to be disabled (Homer et al., 2005). More recently, over-expression of YB-1 in glioblastoma cell lines U87 and DK-MG was shown to promote temozolomide resistance through direct interaction with the MDM2/P53 signalling pathway. YB-1 over-expression results in MDM2 activation and the resultant ubiquitination and proteasomal degradation of P53, inhibiting P53-mediated apoptosis (Tong et al., 2019). In support of this, overexpression of MDM2 was recorded in 67% of patients in a paediatric high-grade astrocytoma cohort, with P53 tumour suppressor pathway inactivation taking place in >95% cases (Sung et al., 2000). Furthermore, *in vivo* studies have highlighted a role played by MDM2 in connecting SHH and P53 pathways in CGNPs, suggesting that MDM2 may be required for SHH medulloblastoma tumorigenesis (Malek et al., 2011). Notably, SHH patients harbouring germline *TP53* mutations represent a very high-risk group in medulloblastoma, with survival rates of less than 50%; further highlighting the importance of P53 pathway disruption in medulloblastoma. Taken together, targeting genes implicated in the P53 tumour suppressor pathway, such as *YBX1*, is likely to be of high therapeutic value for the treatment of paediatric brain tumours.

1.4.3.4 YB-1 and Brain Tumour Initiating Cells

As previously described (Section 1.2.1.6), frequent relapse represents a serious obstacle to paediatric brain tumour survival. A number of factors are associated with poor responses to therapy and concurrent relapse, including the presence of BTICs, referred to in some studies as brain cancer stem cells (Figure 1.11 D). BTICs are multipotent, have the ability to self-renew, form neurospheres and initiate tumour

development (Fotovati et al., 2011). YB-1 was first associated with TICs in 2010, where it was reported to induce breast TICs to express CD44 and CD49f, leading to enhanced cell growth and drug resistance (To et al., 2010). Both PI3K/AKT and RAS/MAPK pathways are activated in BTICs, in which YB-1 is a downstream phosphorylation substrate. Correspondingly, in BTIC lines derived from primary glioblastoma patients, both total and phosphorylated YB-1 was highly elevated compared to normal CNS tissue (Mantwill et al., 2013). This is supported by a comprehensive glioblastoma study by Fotovati *et al* (Fotovati et al., 2011). YB-1 was found to co-localise with neural stem cell markers Nestin, SOX2 and BMI-1 in SF188 paediatric glioblastoma cells cultured as neurospheres, as well as glioblastoma patient-derived BTIC isolates. YB-1 knockdown was associated with loss of neural stem cell markers, reduced proliferation and differentiation in SF188 neurospheres, while forced differentiation of primary BTICs resulted in loss of YB-1 expression. Importantly, high and co-ordinated expression of YB-1, SOX2 and BMI-1 was detected in 67% of glioblastoma cases that subsequently went on to relapse (Fotovati et al., 2011). Collectively, these studies imply that targeting YB-1 will stimulate BTICs to undergo differentiation and suppress their proliferative capacity and hence further supports the development of YB-1 targeted therapies as a novel approach in the management of aggressive paediatric glioblastoma.

1.4.4 YB-1 and Paediatric Brain Tumours in the Clinic

1.4.4.1 YB-1 as a Biomarker

A number of studies have proposed YB-1 as a novel biomarker of glioma progression. In glioblastoma patient samples, YB-1 protein expression has been shown to increase

with tumour stage (Fotovati et al., 2011). Likewise, in a larger study, YB-1 protein/mRNA levels were shown to differ significantly between tumour grades, with Grade I/II tumours presenting with mainly cytoplasmic staining and Grade III/IV presenting with abundant nuclear and cytoplasmic staining, which was found correlate with poor overall survival (Zheng et al., 2016). Of particular note, YB-1 was significantly elevated in the CSF of Grade III/IV patients compared to that of Grade I/II patients, indicating that YB-1 may also represent a promising CSF marker for distinguishing malignant gliomas (Zheng et al., 2016). The aforementioned studies demonstrated that overall YB-1 over-expression is associated with poor prognosis; however it may also be important to consider YB-1 subcellular localisation when determining the prognostic value of YB-1 expression. For example, although YB-1 was found to be up-regulated in 86% of patient samples in a paediatric glioblastoma cohort, high nuclear expression was associated with an AKT-active poor prognosis subgroup, whereas samples exhibiting predominantly cytoplasmic expression were associated with a better prognosis, AKT-inactive subgroup (Faury et al., 2007).

A potential barrier to the use of YB-1 as a prognostic marker in paediatric brain tumours, or indeed in other cancer types in the clinic, has been the variability in available antibodies. As previously reported, controversy exists surrounding the function of proteolysis in the regulation of YB-1 nuclear translocation (Section 1.4.2.2), due to cross-reaction between N-terminal YB-1 antibodies and another protein called heterogeneous nuclear ribonucleoprotein A1 (hnRNPA1) (Cohen et al., 2010). The hnRNPA1 protein is present in both nuclear and cytoplasmic compartments and migrates at ~37 kDa (YB-1 migrates at ~49 kDa), meaning immunostaining products produced by such cross-reaction are very difficult to

interpret (Cohen et al., 2010; Woolley et al., 2011). Despite this issue being raised by research and review articles alike (Cohen et al., 2010; Johnson et al., 2019; Lasham et al., 2013; Woolley et al., 2011), one commercially available N-terminal cross-reactive antibody (abcam; ab12148) continues to be used, with 13 references between 2020 and 2021. Further to this, disparities have also been demonstrated in the ability of YB-1 antibodies to detect nuclear YB-1 protein in addition to cytoplasmic YB-1, a finding that may prove important if the quantification of nuclear expression specifically is required to assess prognosis (Woolley et al., 2011). Standardisation of one properly validated antibody is of fundamental importance in order to develop effective prognostic screens using YB-1 as a biomarker.

1.4.4.1.1 YB-1 as a Therapeutic Target

Given the multi-functional nature of YB-1 and its position upstream of numerous tumour-promoting molecular pathways, YB-1 represents an attractive therapeutic target. One potential therapeutic approach to directly target YB-1 is through oligonucleotide-based methods including siRNA and miRNA. YB-1 knockdown by siRNA has proven effective *in vitro*, resulting in reduced proliferative and migratory capability and increased drug sensitivity in paediatric brain tumour cells (Fotovati et al., 2011; Gao et al., 2009). However, the delivery of siRNA to tumour cells in the human body, especially those that have metastasised, represents a major challenge. Unmodified siRNA is rapidly degraded in the bloodstream, does not readily enter cells and can be immunogenic. The blood-brain barrier (BBB), comprised of a tight arrangement of endothelial cells, represents a further challenge for efficient siRNA delivery. There are a number of systems, which may represent viable options to deliver oligonucleotide-based therapy to brain tumours, including lipid-based,

inorganic and polymeric nanoparticles. Poly(β -amino ester) (PBAE)-based nanoparticles have successfully been used to deliver and efficiently release siRNA in a patient-derived glioblastoma mouse model without systemic toxicity (Karlsson et al., 2019). Dual-modified cationic liposome nanoparticles incorporating CD133-targeting ligands and encompassing paclitaxel and survivin siRNA have also proven successful in *in vitro* and *in vivo* glioma studies, displaying high specificity for glioma stem cells and low toxicity to brain endothelial cells (Sun et al., 2018). As an alternative to larger nanoparticles, which frequently accumulate in the reticuloendothelial system of the liver and spleen, a recent study proposed an alternative oligonucleotide stabilisation approach using Y-shaped block cationomers (YBCs). Notably, the number of positive charges in the YBC can be adjusted to match that of negative charges in each oligonucleotide strand, facilitating selective pairing in the bloodstream. The resultant complex is stable in the blood stream and incredibly small (~18nm), allowing efficient delivery in an *in vivo* patient-derived glioblastoma model (Watanabe et al., 2019). Although further pre-clinical and clinical trials are required, such studies show oligonucleotide-based therapy, both by nanoparticles and alternative approaches, to be a promising brain tumour treatment strategy.

A number of groups have proposed that the transcription factor functionality of YB-1 is activated by phosphorylation. For this reason, disruption of YB-1 phosphorylation may represent another approach to targeting YB-1 activity. The most widely characterised phosphorylation site in YB-1 is S102 (Figure 1.8). Blocking the S102 site by way of a decoy cell permeable peptide led to inhibition of *EGFR* expression and reduced growth in prostate and breast cancer cell lines, without affecting non-

malignant cells (Law et al., 2010). Upstream inhibitors targeting RSK and AKT may also be an option, fisetin is a dietary flavonoid, which is able to bind directly with RSK, both suppressing RSK kinase ability and promoting interaction between fisetin and the YB-1 CSD. Together, this led to a decrease in YB-1 phosphorylation and down regulation of total YB-1 protein, with a concurrent decrease in MMP-2, MMP-9 and ABCB1 expression and reduced cell viability in a melanoma model (Sechi et al., 2018). However, it must be noted that some groups have found no evidence of YB-1 phosphorylation influencing nuclear translocation (Section 1.4.2.2). Further study of the validity of the phosphorylation theory of YB-1 nuclear localisation and as well as in which cancer types/cell types this theory holds true will be required prior to the development of this therapeutic approach.

Over recent years, virotherapy has emerged as an alternative treatment for cancer. The recent FDA approval of oncolytic herpes virus T-VEC (Talimogene laherparepvec) for the treatment of metastatic melanoma has confirmed the possibility of using viruses in the clinic. As such, a promising novel treatment approach for brain tumour therapy is YB-1 targeted virotherapy. YB-1 is known to play an important role in the adenovirus life cycle, where post-adenovirus infection, YB-1 can translocate to the nucleus where it regulates the expression of viral polymerase (Holm et al., 2002). This finding raised the possibility of targeting YB-1 nuclear accumulation with YB-1 dependent oncolytic adenoviruses. Ad-Delo3-RGD is a recombinant adenovirus in which the transactivation domain CR3 of the E1A protein is ablated to enable viral replication solely in YB-1-positive cancer cells. The Ad-Delo3-RGD virus induced significant cell lysis in various glioblastoma cell lines (Holzmüller et al., 2011). Of particular note, due to the YB-1 nuclear translocation induced by certain cytotoxic

drugs, co-treatment with cisplatin and temozolomide significantly enhanced tumour cell killing *in vitro* and reduced tumour growth rate in a xenograft glioma mouse model (Holzmüller et al., 2011). Likewise, Ad-Delo3-RGD mediated substantial cytolysis in glioblastoma patient-derived BTIC lines, with significantly reduced viral replication in non-malignant astrocyte cells (Mantwill et al., 2013). Although Ad-Delo3-RGD is yet to be tested in paediatric brain tumour lines/models, other oncolytic viruses have yielded promising results in paediatric high-grade glioma, supporting the development of YB-1 targeting oncolytic viruses for patients with these tumours (Martínez-Vélez et al., 2019).

1.5 Aims

Relapse following conventional treatment is the single most adverse event in medulloblastoma. Recent studies have revealed that genetic drivers of medulloblastoma progression are both maintained and emerge at relapse. Such genetic divergence following therapy may be indicative of the development and expansion of a cancer cell population with increased therapy tolerance, and thus a better understanding of tumour cell mechanisms towards drug resistance is critical.

ABCB1 is a multi-drug transporter associated with therapy resistance in a range of cancer types. In medulloblastoma, ABCB1 expression correlates with high-risk disease. We hypothesise that treatment of medulloblastoma cells with certain chemotherapeutics may facilitate the survival of a resistant, ABCB1-expressing sub-population of cells that over time may promote tumour relapse. Investigating potential regulators of the *ABCB1* gene, in the context of medulloblastoma, therefore represents an important avenue of research. Multi-functional transcription factor YB-1 may represent one such transcriptional regulator. Although widely researched in adult and solid tumours, where high expression correlates with drug resistance, metastasis and adverse prognosis, much less is known about YB-1 in the context of brain tumours, particularly medulloblastoma. Accordingly, the aims of this study were as follows:

1. Investigate the expression, localisation and prognostic significance of potential *ABCB1* regulator YB-1 in medulloblastoma patient cohorts and cell lines.

2. Validate whether YB-1 represents a bona fide regulator of the *ABCB1* gene by way of functional assays.
3. Assess YB-1 involvement in various aspects of medulloblastoma tumorigenesis by stable depletion of *YBX1* in medulloblastoma cell lines.
4. Generate a better understanding of mechanisms surrounding the acquisition and maintenance of drug tolerance in medulloblastoma cells, identifying both global targets/pathways in addition to those regulated by YB-1.

Chapter 2

Materials and Methods

Chapter 2 Materials and Methods

2.1 Identification of candidate *ABCB1* interactors

In order to identify potential regulators of the *ABCB1* gene, transcription factor binding site prediction software tool Genomatix MatInspector (software version 8.1; <http://www.genomatix.de/>) was employed. MatInspector software uses a large library of weight matrices based on known *in vivo* binding sites to predict transcription factor binding sites in nucleotide sequences of unlimited length.

First, the Genomatix EIDorado Genome database was utilised in order to extract all annotated promoter sequences and the transcripts that they control from the *ABCB1* gene. Following the selection of *ABCB1* promoter sequence GXP_5138817 (Figure 2.1) and the setting of search parameters, the MatInspector software then searched for all matrices within the core promoter. Extensive screening for literature-based evidence and binding site functionality was then employed in order to identify promising candidates with which to carry forward for further study.

```

5' CGTGGTGGCGGGAGCCTGTAGTCCCAGCTACCTGGGAGGCTGAGGCAGGAGAATGGTG
TGAACCCGGGAGGCGGAGCTTGCAGTGAGCCGAGATCCTGCCACTGCACTCCAGCCTGGG
CGACAAAGCAAGACTCCGTCTCAAAAAGAAAAAGAAAAGAAAAACAAAAGAAAACCTTCA
TTGTATTGTAAGCCAAGAACAAAATATATCAAGATAAGGAAAATTTGTAGTCAAGAATA
GAAAAAATTATGGCTTTGAAGTATGAGTTATTTAAAGAAAGTGGAAACATCCTCAGACT
ATGCAGTAAAAACAAAGTGATTTTCTTCTTCTAAACTTATGCAATAAACTGATAGGTAA
TATGTGAAAGTCATAGAATGTAGACTAGAGGATACAACAAACCTATTTCCCTCTATGTTCA
TAAGAAGTAAGAAAAGCTCTGATGTGAGTTAGCATTGCTTTACAATTTTGAATTGTGCAG
ATTGCACGTACTTTTCCTCAGTTTGAAGTAAATAGTGGACAGGAAAAATATTAATGTT
GGCAGTAAATATGGAAGGAAATTACAACCTAATGTAATATGCTAAAACATGCTATGTTTAT
TTACTAATTTGAATTAATAATGTAAGAATTTAAAATGCCCTGGAAAAACACGGGCATTGA
TCTGACGTCTGAAGTTTTAAAATATTACACACTTTGAAATAGCATTGTACCTTGAAATA
CCTGTCTCTATATATTTTTTAAAACCTCCTTTTTCTTTTCATTCCATTTATCATCAAATAA
AGGATGAACAGATGTAACCTCAGAACTGTCAAGCATGCTGAAGAAAGACCACTGCAGAAA
AATTTCTCCTAGCCTTTTCAAAGGTGTTAGGAAGCAGAAAGGTGATACAGAAATTGGAGAG
GTCGGAGTTTTTGTATTAACCTGTATTAATGCGAATCCCGAGAAAATTTCCCTTAACTAC
GTCCTGTAGTTATATGGATATGAAGACTTATGTGAACTTTGAAAGACGTGTCTACATAAG
TTGAAATGTCCTCCCAATGATTCAGCTGATGCGGTTTCTCTACTTGCCCTTTCTAGAGAGG
TGCAACGGAAGCCAGAACATTCCTCCTGGAAATTC AACCTGTTTCGCAGTTTCTCGAGGA
ATCAGCATTCAGTCAATCCGGGCCGGGAGCAGTCATCTGTGGTGAGGCTGATTGGCTGGG
CAGGAACAGCGCCGGGGCGTGGGCTGAGCACAGCCGCTTCGCTCTCTTTGCCACAGGAAG
CCTGAGCTCATTCGAGTAGCGGCTCTTCCAAGCTCAAAGAAGCAGAGGCCGCTGTTTCGTT
TCCTTTAGGTCTTTCCACTAAAG 3'

```

Figure 2.1 ABCB1 GXT_26193608 Promoter. The GXT_26193608 ABCB1 promoter was identified using the Genomatix EIDorado Genome database. The promoter consists of 1341 base pairs, with the transcription start site located at position 1079. Genomatix MatInspector predicted binding sites are annotated in red (YB-1) and green (NFE2L2). Manually predicted binding sites are annotated in blue (YB-1).

2.2 Genomic analysis of large-scale publicly available datasets

Gene expression data was obtained from R2: Genomics Analysis and Visualisation Platform (<http://r2.amc.nl>) for a number of large-scale medulloblastoma, ependymoma and paediatric glioma patient datasets. Information for each dataset can be found in Table 2-1.

Table 2-1 Gene expression dataset information

Author	Tissue/Tumour Type	Sample Size	Normalisation	Platform	Reference
Cavalli	Medulloblastoma	763	rma_sketch	hugene11t	(Cavalli et al., 2017)
Pfister	Medulloblastoma	223	MAS5.0	u133p2	(Northcott et al., 2017)
Roth	Normal Cerebellum	9	MAS5.0	u133p2	(Roth et al., 2006)
Paugh	Paediatric Glioma	53	MAS5.0	u133p2	(Paugh et al., 2010)
Pfister	Ependymoma	209	MAS5.0	u133p2	(Pajtler et al., 2015)
Wang	Medulloblastoma	22	rma_sketch	hugene20t	(X. Wang, A. M. Dubuc, et al., 2015)
Harris	Normal Brain (Prefrontal Cortex)	44	MAS5.0	u133p2	n/a

2.2.1 Survival analysis of large-scale publicly available datasets

2.2.1.1 Mantel-Haenszel Log-rank Test

The association between gene expression and 5-year overall survival was investigated using the Kaplan-Meier method, with the Mantel-Haenszel log-rank test employed to assess statistical differences in patients' survival depending on high/low

gene expression. A P-value of less than 0.05 was considered statistically significant. This analysis was carried out using GraphPad Prism 8 (GraphPad Software. La Jolla, California, USA).

2.2.1.2 Cox's Proportional Hazards Model

The effect of multiple confounding factors on outcome was assessed by way of Cox's Proportional Hazards Model in order to determine the robustness of *YBX1* as an independent predictor of survival. In addition to *YBX1* expression (high/low), the continuous covariate age and the categorical covariate metastatic status (M+/M0) were included in the Cox regression model. This allowed output of an age- and metastatic status-adjusted hazard ratio and associated 95% confidence interval. A P-value of less than 0.05 was considered statistically significant. Data analyses were performed with IBM SPSS 26.0 for Windows (IBM Corp. Armonk, NY, USA).

2.3 Patient Analysis

2.3.1 Paediatric medulloblastoma Nottingham tumour microarray

The Nottingham tumour microarray (TMA) screened in this study comprised of 20 medulloblastoma tumour samples obtained from patients treated within the Nottingham University Hospitals NHS Trust, diagnosed between 1985 and 2007. The median age of patients in the cohort at diagnosis was 7.2 years, with ages ranging from 0.8 to 14.4 years. Treatment was non-standardised, with patients receiving chemotherapy and radiotherapy both alone and in combination. All samples were taken from primary tumours with the exception of one sample which was taken from a secondary tumour.

2.3.2 Paediatric medulloblastoma Birmingham tumour microarray

The Birmingham tumour microarray (TMA) screened in this study comprised of 68 medulloblastoma tumour samples obtained from patients treated within the Birmingham University Hospitals NHS Trust, diagnosed between 2004 and 2016. The median age of patients in the cohort at diagnosis was 6 years with ages ranging from 1.6 to 15.1 years. As in the Nottingham TMA, treatment was non-standardised.

Both the Nottingham and Birmingham studies and related experimental protocols were reviewed and approved by the National Research Ethics Service Committee East Midlands – Nottingham 2 and the Ethics Committee of the Burdenko Neurosurgical Institute (Ethical vote number 563/6-16). Accordingly, informed consent was obtained from either the patient (or legal guardian where the patient was under 18 years of age) prior to their inclusion in the studies.

2.4 Cell Maintenance

Nine cell lines were utilised in this study, clinicopathological information on which can be found in Table 2-2. Cells were cultured at 37°C and 5% CO₂ using the appropriate media and flasks as detailed in Table 2-3. Cells were passaged at 70% confluence as follows.

Table 2-2 Cell lines utilised in this study

Cell Line	Cancer Type	Growth Type	Metastatic Stage	Source	Reference
D283	Group 3/4 MB ¹	Semi-adherent	Metastatic (M2)	ATCC HTB-185™	(Friedman et al., 1985)
D458	Group 3 MB	Semi-adherent	Metastatic (M+; cells isolated from recurrent tumour)	John R. Silber (University of Washington, Seattle)	(Bigner et al., 1990)
HDMB-03	Group 3 MB	Semi-adherent	Metastatic (M3)	Till Milde (DKFZ, Heidelberg, Germany)	(Milde et al., 2012)
CHLA-01*	Group 4 MB	Suspension	Non-metastatic (M3)	Geoff Pilkington (University of Portsmouth, UK)	(Xu et al., 2015)
CHLA-01R*	Group 4 MB	Suspension	Metastatic (M2; cells isolated from recurrent tumour)		
ONS-76	SHH MB	Adherent	Metastatic (M2)	Annette Künkele (Charité Universitätsmedizin, Berlin)	(Yamada et al., 1989)
DAOY	SHH MB	Adherent	Non-metastatic (M0)	ATCC HTB-186™	(Jacobsen et al., 1985)
UW-228-3	SHH MB	Adherent	Non-metastatic (M0)	John R. Silber (University of Washington, Seattle)	(Keles et al., 1995)
U87	Glioblastoma	Adherent	Unknown	ATCC HTB-14™	n/a

¹MB = medulloblastoma; *cell line with matched primary and metastatic pairs. Font colour represents MB molecular subgroup: SHH (green); Group 3 (grey) and Group 4 (blue).

2.4.1 Culturing Adherent Cells

The SHH cell lines DAOY, ONS-76 and UW-228-3 grew adherently in standard culture.

To sub-culture cells, growth media (Table 2-3) was removed and discarded and cells

washed once in Hank's Balanced Salt Solution (HBSS; Gibco; 14170). Cells were detached by incubation for 5 minutes at 37°C in pre-warmed 1x Trypsin-EDTA (TE; 10x; Sigma-Aldrich; T4174). Trypsinisation was inhibited by the addition of a double volume of pre-warmed medium and the cell suspension centrifuged at 123 x *g* for 5 minutes. The resultant pellet was re-suspended in growth medium and seeded into new tissue culture treated T-75 flasks (Corning; 430641U) at a ratio of 1:10 to 1:20.

2.4.2 Culturing Semi-Adherent Cells

The Group 3 medulloblastoma cell lines HDMB-03, D283 and D458 grew semi-adherently in standard culture, with populations of adherent, semi-adherent, and suspension cells within the flask. To sub-culture these cells, growth media (Table 2-3) was removed and retained. Cells were then washed twice with HBSS and washes combined with the retained growth media. Cells were detached by incubation for 5 minutes at 37°C in 1x TE. Trypsinisation was inhibited by the addition of a double volume of pre-warmed medium and the resultant cell suspension pooled with previously retained growth media and washes and centrifuged at 123 x *g* for 5 minutes. The resultant pellet was re-suspended in growth medium and seeded into new tissue culture treated T-75 flasks at a ratio of 1:3 to 1:6 (D283) and 1:10 to 1:20 (D458 and HDMB-03).

2.4.3 Culturing Suspension Cells

The Group 4 medulloblastoma cell lines CHLA-01-MED and CHLA-01R-MED grew as clusters and single cells in suspension in standard culture. Bi-weekly, a half volume of growth media (Table 2-3) was removed and replaced with fresh media. Aspirated media was either discarded or used to further expand the cell line. Weekly, the full

volume of growth media and suspension cells was spun down at 123 x g for 5 min and three-quarters growth media removed. The resulting media and cells were then re-suspended in fresh media and seeded into non-treated T-75 flasks (Corning; 431464U).

Table 2-3 Culture media information for cell lines utilised in this study

Cell Line	Media	Flask Type
D283	Dulbecco's Modified Eagle Serum (DMEM; Gibco; 31885) + 10% foetal bovine serum (FBS; HyClone; SH30541.03)	Treated
D458	DMEM + 10% FBS	Treated
HDMB-03	Roswell Park Memorial Institute-1640 (RPMI-1640; Sigma-Aldrich; R8758) + 10% FBS	Treated
CHLA-01	DMEM F12 + 2% B27 (Gibco, 17504044) + 20ng/mL recombinant human basic fibroblast growth factor (bFGF; Gibco; PHG0266) + 20ng/mL recombinant human epidermal growth factor (EGF; Gibco, PHG0315)	Non-treated
CHLA-01R	DMEM-F12 + 2% B27 + FGF + EGF	Non-treated
ONS-76	RPMI-1640 + 10% FBS	Treated
DAOY	DMEM + 10% FBS	Treated
UW-228-3	DMEM-F12 + 15% FBS + 1% Sodium Pyruvate (Gibco; 11360070)	Treated
U87	DMEM + 10% FBS	Treated

Font colour represents molecular subgroup: SHH (green); Group 3 (grey) and Group 4 (blue).

2.4.4 Cell Counting

For cell counting, cells were first washed, trypsinised and pelleted; after which they were suspended in an appropriate volume of growth media. Equal volumes of trypan blue (Sigma-Aldrich, T8154) and cell suspension were gently mixed. 10 µl of combined solution was then applied to a Neubauer Counting Chamber (VWR; 718605). The number of viable cells (cells that do not absorb trypan blue solution) in the four corner squares and one centre square of the counting chamber were

counted. In order to calculate the number of viable cells and the number of cells per mL of cell suspension, the following equations were utilised.

$$\text{average count viable cells} = \frac{\text{count 1} + \text{count 2} + \text{count 3} + \text{count 4} + \text{count 5}}{5}$$

$$\text{cells / ml} = \text{average count viable cells} \times \text{dilution factor} \times 10^4$$

Where the dilution factor has a value of 2 and 10^4 represents the counting chamber value.

$$\text{total cell number} = \text{cell concentration} \times \text{volume of cell suspension}$$

To calculate the viability of cells in suspension, the following equation was used.

$$\text{cell viability (\%)} = \frac{\text{average count viable cells}}{\text{average count of all cells (dead+viable)}} \times 100$$

2.4.5 Cell Storage

To store cells, cells were washed and trypsinised as previously described. The resulting pellet was re-suspended in Cellbanker® 2 Cryopreservation Media (AMS Biotechnology Ltd; 11891) at a concentration of 2×10^6 cells/ml (Section 2.4.4). 0.5 mL aliquots of cell suspension were then transferred to FluidX tubes (Brooks Life Sciences; 68-0703). For short-term storage samples were kept at -80°C (as tolerated in Cellbanker® media), whilst for long-term storage vials were transferred to liquid nitrogen.

2.4.6 Culturing Cells From Frozen

To culture cells from frozen, FluidX tubes containing stored cells were removed from liquid nitrogen/-80°C and immediately transferred to a water bath set at 37°C. As soon as cells appeared defrosted they were transferred to a treated (adherent/semi-adherent cell line) or non-treated (suspension cell line) T-25 flask (Eppendorf; 0030710126; 0030710029) containing pre-warmed media and incubated at 37°C and 5% CO₂ overnight. After incubation for 24 hrs, cells were transferred to a T-75 flask and passaged when appropriate.

2.4.7 Mycoplasma Testing

Mycoplasma testing was performed monthly using a Plasmotest™ Mycoplasma Detection kit (InvivoGen; rep-pt1) as per the manufacturer's instructions. All tested cells had been growing in culture for 7 days and collected media had been in contact with cells for 48 hours prior to testing. Cells growing in antibiotic-containing media were transferred to antibiotic-free media for 7 days prior to testing.

2.5 Drug Treatments

2.5.1 Drugs used in this Study

Details of the chemotherapeutics and antibiotics utilised in this study can be found in Table 2-4.

Table 2-4 Drugs used in this study

Drug	Stock Concentration	Vehicle	Product Details
Vincristine	100 μ M	DMSO	Selleckchem, S1241
Cisplatin	10 mM	DMF	Selleckchem, S1166
Puromycin	92 mM	Cell Culture Grade H ₂ O	Sigma, P8833
Panobinostat	100 μ M	DMSO	Selleckchem, LBH589
JQ1	10 mM	DMSO	Selleckchem, S7110

2.5.2 Drug response assays for IC₅₀ value calculation

Drug response assays were utilised to assess cell viability in response to treatment with various chemotherapeutics. Cells were plated in complete medium at densities described in Table 2-5 in clear-bottomed, black-walled 96-well plates (Greiner; 655096) and left to settle for 24 hours. Cells were then treated with the chosen chemotherapeutic at a range of concentrations (Table 2-5) and incubated at 37°C and 5% CO₂ for 72 hours. Following treatment, surviving cells were assayed with PrestoBlue (Thermo Fisher; A13262) at a final dilution of 1:10 for 30 - 60 minutes (dependent on cell line) at 37°C and 5% CO₂ and fluorescence measured at 560/590 nm using a FLUOstar Omega microplate reader.

In order to calculate the half maximal inhibitory concentration (IC₅₀), fluorescent measurements were exported to Microsoft Excel and the data normalised against a blank (media only) control. Cell viability was then calculated as a percentage relative to the vehicle-treated control. These values were exported into GraphPad Prism 8 and drug concentrations transformed into log form, following which dose-response curves and IC₅₀ values were generated by non-linear regression analysis using a three-

parameter dose-response equation. The calculated IC₅₀ values were then used to inform treatment doses for future experiments.

Table 2-5 Calculated IC₅₀ for chemotherapeutic agents used in this study

Cell Line	Seeding Density / Cells per Well	Chemotherapeutic	Concentration Range	Calculated IC ₅₀
HDMB-03	5,000	Vincristine	0 – 100 nM	3.4 nM
		Cisplatin	0 – 10 µM	1.4 µM
		Panobinostat	0 – 100 nM	17.6 nM
		JQ1	0 – 50 µM	5.6 µM
D283	10,000	Vincristine	0 – 500 nM	1.0 nM
		Cisplatin	0 – 50 µM	1.6 µM
		Panobinostat	0 – 100 nM	14.3 nM
		JQ1	0 – 50 µM	13.1 µM
D458	10,000	Vincristine	0 – 100 nM	3.1 nM
		Cisplatin	0 – 10 µM	0.4 µM
DAOY	1,000	Vincristine	0 – 100 nM	1.3 nM
		Cisplatin	0 – 10 µM	0.6 µM

2.5.3 Optimisation of puromycin selection condition

In order to determine the minimum amount of puromycin required to eliminate non-transduced cells devoid of a puromycin resistance construct (Section 2.6), a puromycin kill curve was generated. Cells were plated in complete medium at densities described in Table 2-6 in clear-bottomed, black-walled 96-well plates and left to settle for 24 hours. Cells were then treated with puromycin at a range of concentrations (Table 2-6) and incubated at 37°C and 5% CO₂ for 48 hours. Following treatment, surviving cells were assayed with PrestoBlue (at a final dilution of 1:10)

for 30 - 60 minutes at 37°C and 5% CO₂ and the fluorescence measured at 560/590 nm. Kill curves were generated by non-linear regression analysis as previously described (Section 2.5.2) and the optimal puromycin concentration was selected by choosing the minimum concentration of puromycin that causes complete cell death.

Table 2-6 Optimised puromycin kill concentrations

Cell Line	Seeding Density / Cells per Well	Puromycin Concentration Range	100% Kill Concentration
HDMB-03	5,000	0 – 8 µM	2 µg/mL
D283	10,000	0 – 5 µM	2 µg/mL

2.5.4 Assessment of YB-1 localisation in response to drug treatment

The effect of chemotherapeutic treatment on YB-1 localisation/expression was studied both by protein and immunofluorescence analysis. For protein analysis (nuclear/cytoplasmic fractionation and immunoblotting), cells were seeded in complete medium in six-well plates (Corning; CLS3516) at a density of 500,000 cells / well (HDMB-03). Following overnight incubation, cells were treated with chosen chemotherapeutics at previously calculated IC₅₀ concentrations (Table 2-5). Samples were then collected at 0, 1, 2 and 6 hour time points. To harvest samples, media was removed from wells and cells washed with ice-cold HBSS. Ice-cold 1 x TE was then added to wells and cells trypsinised on ice until cells appeared rounded and had begun to detach. Samples were then combined with previously retained media and washes and pelleted at 130 x g. Pellets were immediately snap frozen in liquid nitrogen and stored at -80°C for downstream use (Section 2.9.7).

For immunofluorescence, cells were seeded in complete medium in chamber slides (Ibidi; 80841) at 25,000 cells/well (HDMB-03) or 40,000 cells/well (D283 and D458). Following overnight incubation, cells were treated with the chosen chemotherapeutic at previously calculated IC₅₀ concentrations (Table 2-5). Samples were then fixed at 0, 1, 6 and 12 hour time points in order to determine which time point resulted in maximal YB-1 nuclear localisation. On account of their semi-adherent nature, HDMB-03-, D283- and D458-containing chamber slides were removed from the incubator 15 minutes prior to fixing to allow suspension cells to settle, after which 70% of media was removed in order to leave a thin layer in each chamber containing the suspension cell population. Sterile-filtered 4% paraformaldehyde (PFA) was then added for 20 minutes at room temperature to fix adherent, semi-adherent and suspension cells to the chamber slide surface. Following fixation, chamber slides were either washed with PBS and used immediately for immunofluorescence (Section 2.9.8) or wrapped in parafilm and stored at 4°C for use within 4 weeks.

2.6 Generation of stable knockdown cell lines

Cell lines with stable knockdown of *YBX1* expression were generated through shRNA-mediated gene silencing using the GIPZ Lentiviral particle starter kit for *YBX1* (Horizon Discovery; VGH5526-EG4904 with components VGH5518-200223966, VGH5518-200227422 and VGH5518-200263203). The sequences for each GIPZ lentiviral shRNA construct are displayed in Table 2-7 and are mapped onto the *YBX1* mRNA sequence (transcript variant 1) in Figure 2.2.

Table 2-7 GIPZ lentiviral YBX1 shRNA constructs

shRNA Construct Product Code	shRNA Construct Thesis Code	Target Region	Sequence (mature antisense)
VGH5518-200227422	YBX1_A	Open-reading frame (ORF)	ACAAATACATCTTCCTTGG
VGH5518-200223966	YBX1_B	ORF	AAGGTGGGAACCTTCGCCT
VGH5518-200263203	YBX1_C	3'untranslated region (UTR)	TTATTAACAGGTGCTTGCA

2.6.1 Determination of relative transduction efficiency

Prior to transduction, relative transduction efficiency was calculated for each cell line to be used as recommended in the GIPZ™ lentiviral shRNA manual (Horizon Discovery). This is important as lentiviral titers provided with GIPZ™ lentiviral particles were calculated using HEK293T cells and transduction efficiency is likely to be significantly less in other cells lines. Relative transduction efficiency can be estimated through calculation of a functional titer of the non-silencing control virus (Horizon Discovery; #RHS4348) in each cell line of interest. In brief, a 24-well tissue culture plate (Corning; CLS3527) was seeded with HDMB-03 or D283 cells at 5×10^4 cells per well in complete medium and cells left to settle overnight. The next day, a series of five-fold dilutions up to 390,625-fold of the non-silencing control shRNA viral stock were made in serum-free medium. Plated cells were re-suspended in 225 μ L serum-free media and cells transduced by adding 25 μ L diluted control shRNA lentivirus to labelled wells. Transduced cultures were then incubated at 37°C for 6 hours, following which 1 mL of complete media was added.

Following a 72 hour incubation period, each well containing a dilution of the non-silencing control shRNA stock was imaged using a Nikon TiE inverted fluorescence

microscope. TurboGFP expressing cells/colonies of cells were counted for each viral dilution, following which the functional titer (Transducing Units per ml (TU/mL)) was determined using the formula below:

$$TU / mL = \# TurboGFP \text{ colonies} \times \text{dilution factor} \times 40$$

Where 40 refers to 25 μ L diluted virus added to cells (1/40th of a mL)

The functional titer was then used to calculate the relative transduction efficiency of each cell type using the following formula:

$$\text{Relative transduction efficiency} = \frac{\text{Functional titer of non - silencing control shRNA in cell line}}{\text{Titer of non - silencing control shRNA in HEK293T}}$$

The relative transduction efficiency of each cell type was then used to generate an extrapolated functional titer for each *YBX1* shRNA viral particle by multiplying the relative transduction efficiency by the titer for each particle as calculated in HEK293T cells, thus optimising the volume of virus particle required to achieve each multiplicity of infection (MOI) for transduction.

5' ATTCTCGCTAGTTCGATCGGTAGCGGGAGCGGAGAGCGGACCCCAGAGAGCCCTGAGCAGCCCCACCG
 CCGCCGCGGCTAGTTACCATCACACCCCGGGAGGAGCCGCAGCTGCCGCAGCCGGCCCCAGTCACCAT
 CACCGCAACCATGAGCAGCGAGGCCGAGACCCAGCAGCCGCCGCCGCCGCCGCCGCCGCCCTC
 AGCGCCGCGACACCAAGCCCGCACTACGGGCAGCGGCGCAGGGAGCGGTGGCCCGGGCGGCCTCACA
 TCGGCGGCGCCTGCCGGCGGGGACAAGAAGGTCATCGCAACGAAGTTTTGGGAACAGTAAAATGGTTC
 AATGTAAGGAACGGATATGGTTTCATCAACAGGAATGACA**CCAAGGAAGATGTATTGT**ACACCAGACTG
 CCATAAAGAAGAATAACCCAGGAAGTACCTTCGCAGTGTAGGAGATGGAGAGACTGTGGAGTTTGATGT
 TGTTGAAGGAGAAAAGGGTGCAGGAGGCAGCAAATGTTACAGGTCCTGGTGGTGTTCAGTTCAAGGCAG
 TAAATATGCAGCAGACCGTAACCATTATAGACGCTATCCACGTCGTAGGGGTCCTCCACGCAATTACCAGC
 AAAATTACCAGAATAGTGAGAGTGGGGAAAAGAACGAGGGATCGGAGAGTGTCTCCGAAGGCCAGGCC
 AACACGCCGCGCCCTACCGC**AGGCGAAGGTTCCACCTT**ACTACATGCGGAGACCTATGGGCGTCGACC
 ACAGTATCCAACCTCCTGTGCAGGGAGAAGTGATGGAGGGTGCTGACAACCAGGGTGCAGGAGAACA
 AGGTAGACCAGTGAGGCAGAATATGTATCGGGGATATAGACCACGATTCCGCAGGGGCCCTCCTCGCCAA
 AGACAGCCTAGAGAGGACGGCAATGAAGAAGATAAAGAAAATCAAGGAGATGAGACCCAAGGTCAGCA
 GCCACCTCAACGTCGGTACCGCCGCAACTTCAATTACCGACGCAGACGCCAGAAAACCTAAACCACAAG
 ATGGCAAAGAGACAAAAGCAGCCGATCCACCAGCTGAGAATTCGTCCGCTCCCGAGGCTGAGCAGGGCG
 GGGCTGAGTAAATGCCGGCTTACCATCTCTACCATCATCCGTTTTAGTCATCCAACAAGAAGAAATATGAA
 ATTCCAGCAATAAGAAATGAACAAAAGATTGGAGCTGAAGACCTAAAGTGCTTGCTTTTTGCCGTTGACC
 AGATAAATAGAATCTATGCATTATCTATGCAGCATGGGGTTTTTATTATTTTACCTAAAGACGTCTCTTT
 TGGAATAACAAACGTGTTTTTAAAAAAGCCTGGTTTTTCTCAATACGCCTTAAAGTTTTTAAATTGTTT
 CATATCTGGTCAAGTTGAGATTTTAAAGAACTCATTTTTAATTTGTAATAAAAGTTTACAACCTGATTTTTT
 AAAAAAGTCAACAAAC**TGCAAGCACCTGTTAATAA**AGGCTTAAATAATTGCTTTGTGTAAATTTGTCTA
 GTTTTGCTTTAGTTTGAAGTATTTAGCTATTTATAGGACCTTAGCTTGACCCAGTCTACAAATAGATGATG
 CTCACTGGTAATCCCTCAGGTAAAATGTCTCAAAATCTCTAATCCTTAAAGTGGCATGCCTGTGGGCCAT
 ACTAAAAATTAGAAAATACATACTCTGATAACCTGGCCATTTTTTATTGAAGGATTTAGCTCATTTGTAAGA
 AAGATTGAGTGTAGATTTTGGGTGGGTCCTTTGGCTGTGAGGCATTGTTTAAAGGGCATTGCTCTAGCC
 TAGACCGACCAGACTCTCATCCTGCTCCACTTAGTTTTGTCACCTGGGAGAATTTGTTTCAGTGTGCAATT
 GAAGATGCCAATTGAAGTGTAGGACAACCTGTCACTGCCTGGTGTGGTCATCAAATATTGGTTCAGCT
 CCTTATGTCCTAGAGATGGAACAAGTAATATAAAACCCATGGGAAAGCTGCTTAGGAACATGGAGGTTG
 GTGAGCTTGTAATTATGTGGTTCTCAACACCTAAATCCTAAGCCTAGTCTGGCTGATCTTTCTCTTTTGA
 GACGGAGTCTTGTCTGTCATCAGGCTGGAGTACAGTGGCACAATCTTGGCTACTGCAACCTCCACCTCTA
 GGTTAAGCGATTCTCCTGCCTCGGCCACCTTAGTAGCTGGGAGTACAGGTGCGTGCCACCACACCCAGCT
 AATTTTTGTATTTTAAATAGAGATGGGGTGCAGTGTGTTAGCCAGGATGGTCTTGATCTCTTGACCTTGTG
 ATCCGCCCGCCTCAGCTCCCAAAGTGCTGGGATTACAGGTGTGAGCCACCGCACCTGGCCTCTCTGGCTT
 TTGTTTTCTAATGTTTTGTTAGATGTTCTTTGGCTTGCTTTGTGAAATAGTCATGTAGTTGATAGTACTGCT
 GCCCCGAAACTCCAGATCATCCTGGCCAGCTATCAGGGCCAGGGGAAGCAGACAGTAGGGGTCCGGG
 AGTAGGCCAGAGTGGCACATCAGGAATCCTGCAGTGTGTGGAAGTCATCTCCTGCTTGGGACTAACTCTT
 TGCAGAGGACTTGATAAGAGACTACTCAAAAAAATTTTTTAAACCCTACTTAGTGAAATATCTGTACTGC
 AGAAGTGAGTTAGCCTATTTCTGCTGGTGTTCATGAAAATACTGTGTTGGCAAGAGTGCAGTGGACCTGA
 AACTTCAACTGTTGGTAGCATCTAACTGTTACTTACAACCTGCAGACGCACACAGTCCCTGACTTAAACAGT
 GTTTTGACTTAGGGGCTTTTAGTGGGGTTACGGTTTCTACTGAATCAACATTGTTTTCATGGCATCACAGAG
 TTGAAAAATCATAAATGAAACCATTGTAAGTTGACTGCAGTGTGCCAACATTAATGCAGTTTCAACTTAA
3'

Figure 2.2 Mapping of GIPZ lentiviral shRNA constructs onto YBX1 mRNA sequence. YBX1_A (orange), YBX1_B (blue) and YBX1_C (green) shRNA constructs are displayed mapped onto the YBX1 transcript variant 1 mRNA sequence (NM_004559.5). The ORF nucleotide sequence is underlined.

2.6.2 Transduction of target cells

Transduction of D283 and HDMB-03 cell lines was achieved following the GIPZ™ lentiviral shRNA manual (Horizon Discovery). In brief, 5×10^4 cells were seeded in 24-well plates and incubated at 37°C and 5% CO₂ overnight to allow cells to settle. Subsequently, complete media was removed, cells were washed with HBSS and media and washes were combined and centrifuged at 123 x *g* for 5 minutes. Resulting pellets were re-suspended in 1 mL serum-free media and an appropriate amount of virus added to achieve the required MOI for transduction. To improve transduction efficiency in the D283 cell line, polybrene – a polycation that neutralizes the charge repulsion between the virus and cell target surface – was added simultaneously at a concentration of 8 µg/mL. Six hours post-transduction, an additional 1 mL of complete media was added. 72 hours post-transduction, cells were examined microscopically for the presence of lentiviral reporter gene (TurboGFP) expression. Selection of transfected cells was achieved by adding an optimised concentration of puromycin (2 µg/mL), as previously described (Section 2.5.3). Transduced D283 and HDMB-03 cells were gradually expanded from 24-well plates to T-75 culture flasks and cells either frozen as stocks for long-term storage (Section 2.4.5) or pelleted and snap frozen in liquid nitrogen for downstream analysis. *YBX1* knockdown was later confirmed by both qRT-PCR (Section 2.9.6) and western blot (Section 2.9.7).

2.7 Generation of drug-tolerant (DT)-cell lines

In order to generate cell lines tolerant to vincristine and cisplatin, a continuous model of selection was chosen where cells were grown continually in presence of the drug and the treatment dose escalated upon cell proliferation (McDermott et al., 2014).

To optimise the dose of drug used for selection, vincristine and cisplatin drug response assays (Section 2.5.2) were carried out to determine the IC_{50} for each cell line (HDMB-03, D458 and D283). Cells were passaged in T-25 flasks in duplicate to account for any issues arising in one of the flasks. To account for morphological and physiological changes arising from long-term culture, vehicle controls were passaged alongside drug-treated flasks.

For each cell line, T-25 flasks at 60% confluence were treated at $1/100 IC_{50}$ for either cisplatin or vincristine. Growth was monitored by microscopy daily until cells exhibited proliferation, at which point cells were challenged with increasing doses of cisplatin/vincristine (Figure 2.3). Upon dose escalation, cells were passaged and stocks were generated. DMF/DMSO-treated vehicle flasks were passaged bi-weekly.

To confirm the acquisition of drug resistance, drug response assays were repeated as previously described (Section 2.5.2). For all drug response assays, cells were grown in drug-free media for 5 days prior to testing. Cell lines were considered resistant when the IC_{50} value of the treated cells had exceeded the treatment dose and the cell lines exhibited a significant increase in fold resistance, as calculated below.

$$\text{Fold resistance} = \frac{IC_{50} \text{ of resistant cell line}}{IC_{50} \text{ of parental cell line}}$$

2.7.1 Generation of stable drug tolerant cell lines

To establish a reliable cell line model of cisplatin/vincristine resistance, the resistance phenotype should be stable following a freeze/thaw cycle. To assess this, stocks were generated as previously described (Section 2.4.5). Following a minimum of 48 hours in -80°C storage, cells were thawed and passaged twice in drug-free media before repeating drug response assays. IC₅₀ values were then compared to assess whether the resistant phenotype had been retained following the freeze/thaw cycle.

2.7.2 Maintenance of drug tolerant cell lines

To ensure consistency between experiments, drug-tolerant lines were cultured continuously in the appropriate chemotherapeutic at the dose used for cell line selection. Maintenance doses can be found in Table 2-8. Prior to cell viability assays/downstream applications, cells were cultured in drug-free media for 3-5 days.

Table 2-8 Maintenance doses for the culture of drug-tolerant cell lines

Cell Line	Maintenance Chemotherapeutic Dose	
	Chemotherapeutic	Concentration
DT-D283-CIS	Cisplatin	1.6 µM
DT-D458-CIS	Cisplatin	0.6 µM
DT-HDMB-03-CIS	Cisplatin	0.5 µM
DT-DAOY-VIN	Vincristine	2 nM

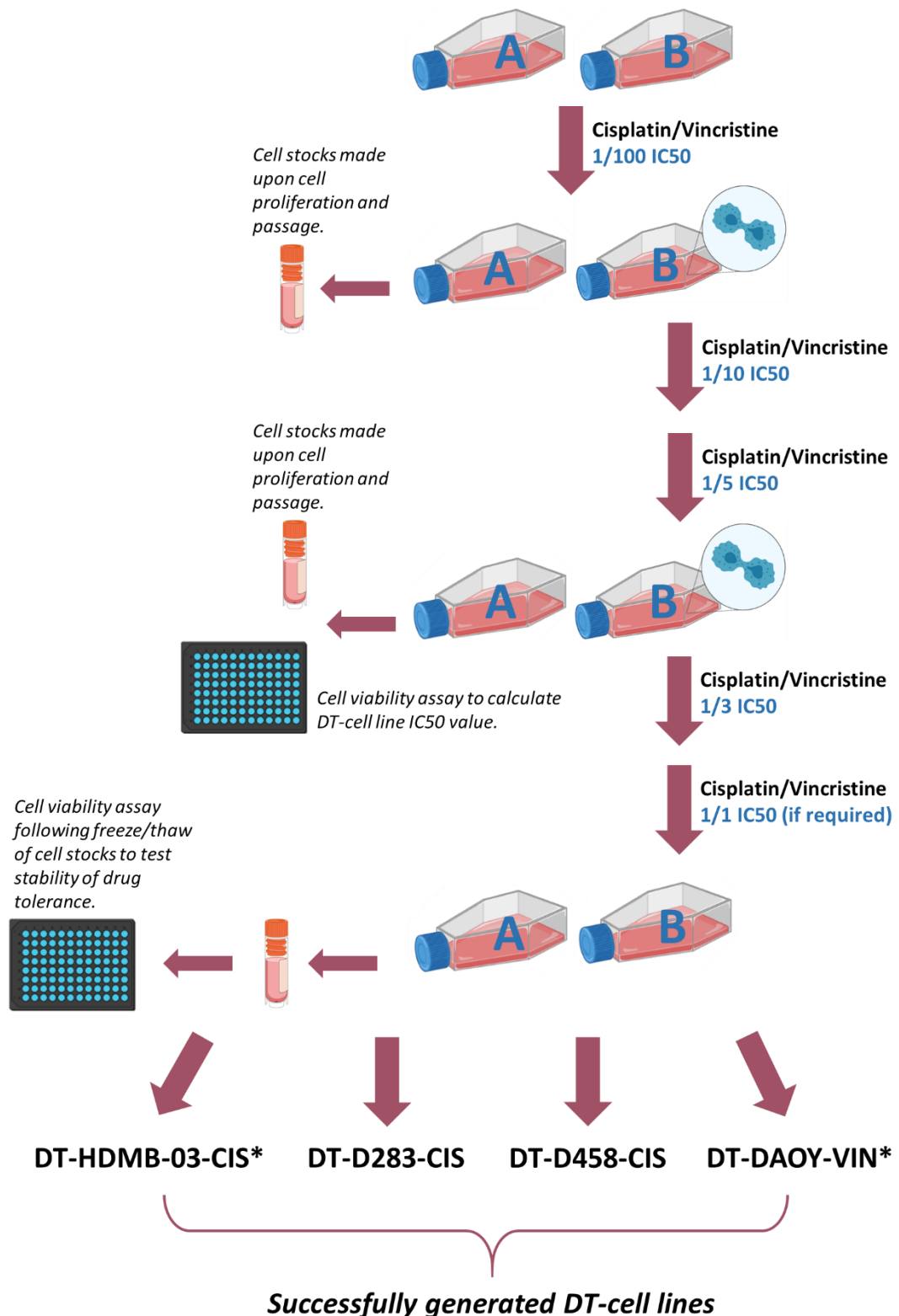


Figure 2.3 Simplified flow diagram depicting generation of drug-tolerant (DT)-cell lines. A continuous model of selection was chosen to generate vincristine/cisplatin-tolerant cell lines whereby cells were grown continually in the presence of the drug and the treatment dose escalated upon cell proliferation. Cell stocks were made frequently and cell viability assays undertaken regularly to assess if drug tolerance had been reached. To test the stability of drug tolerance, cells were frozen as stocks and thawed, following which cell viability assays were repeated. *Gift from Dr Gianpiero Di Leva; University of Salford.

2.8 Modified Boyden Chamber Invasion and Migration Assay

Cell migration and invasion were measured using a modified Boyden chamber assay as follows. 24 hours prior to cell seeding and assay commencement, cell lines of choice were starved in reduced-serum (2% FBS) media. Alongside, 8 μm 24-well plate transwell inserts (Greiner; 662641) were placed in a 24-well plate and coated with 50 μL 10 $\mu\text{g}/\text{mL}$ mouse collagen IV (Cultrex; 3410-010-02). Coated inserts were dried in a tissue culture hood overnight.

The following day, 50 μL of 100 $\mu\text{g}/\text{mL}$ Laminin III stock was added to each coated insert, which was then partially dried in a tissue culture hood for 1 hour. Meanwhile, starved cells were counted as previously described (Section 2.4.4) and diluted to a concentration of 1×10^6 cells/ mL in serum-free (0% FBS) media. After 1 hour, any remaining Laminin III solution was removed from the inserts. The resultant collagen IV/laminin III coated inserts are designed to model medulloblastoma cell invasion through the basement membrane. To assess cell migration alone, non-coated inserts were instead utilised. 100 μL of the aforementioned cell suspension (1×10^5 cells) was then seeded into each insert. Following this, 600 μL of complete cell culture media (10% FBS) was pipetted into the lower chamber – generating an FBS concentration gradient. The invasion assay was then incubated for 48 hours at 37°C and 5% CO_2 to assess migration and invasion.

After 48 hours of incubation, media was aspirated from the lower chamber of each well. The upper chamber was carefully blotted to remove any non-invaded cells. Invaded/migrated cells were dissociated in 300 μL 1x cell dissociation solution (AMS-Bio; 3455-05-03) containing PrestoBlue for 1 hour at 37°C and 5% CO_2 . Cell

dissociation solution was then transferred to a clear-bottomed, black-walled 96-well plate and fluorescence read at 560/590 nm using a FLUOstar Omega microplate reader.

2.8.1 Quantification of Cell Invasion/Migration

In order to calculate the number of invaded/migrated cells, a standard curve of known cell numbers (ranging from 5,000 to 100,000 cells) was prepared for each biological replicate in 1 x cell dissociation solution at the time of cell seeding. Cells were seeded in triplicate in a clear-bottomed, black-walled 96-well plate and PrestoBlue added to a final dilution of 1:10. Cells were incubated for 1 hour at 37°C and 5% CO₂ and fluorescence read at 560/590 nm using a FLUOstar Omega microplate reader.

2.9 Molecular Biology

2.9.1 Chromatin Immunoprecipitation (ChIP)

In order to assess protein-DNA interactions, ChIP assays were undertaken (Figure 2.4). ChIP assays have five main stages which are as follows:

1. Cross-linking of cells to fix proteins to DNA.
2. Cell lysis to release and isolate nuclear DNA/protein complexes.
3. Sonication to shear chromatin into small fragments.
4. Immunoprecipitation to “pull-down” DNA cross-linked to proteins of interest.
5. Reversal of cross-links and DNA purification to isolate bound DNA.

Prior to assay commencement, it is important to optimise cross-linking and sonication conditions, as optimal conditions will likely vary between cell lines (Section 2.9.2). For the resultant ChIP assay, Magna ChIP A/G Immunoprecipitation kits, Magna G ChIP kits (Sigma Aldrich; 17-10085 and 17-611) and ChIP-IT High Sensitivity Kits (Active Motif; 53040) were used according to manufacturer’s instructions, in each case using 5×10^6 cells. Antibodies employed for immunoprecipitation are displayed in Table 2-10.

2.9.2 Optimisation of ChIP cross-linking and sonication conditions

In order to determine the optimum conditions for a desired cell line, cells were counted and 1×10^6 cells per condition (9 conditions in total) isolated. Each sample was then re-suspended in 4 mL PBS. Following this, 4 mL of either 2 %, 1.5 % or 1 % fresh PFA was added and each sample was incubated for either 7, 10 or 15 min at room temperature (RT) on a roller table. Cross-linking and cell lysis were then undertaken according to ChIP kit manufacturer’s instructions. Samples were then

sonicated using a water bath sonicator (Bioruptor Pico; Diagenode) over a sonication time course (e.g. of 5-10-15 sonication cycles 30'' ON/30'' OFF), following which samples were centrifuged to pellet cell debris.

To analyse sheared chromatin fragment size, sonication test samples were removed from the sheared lysate and prepared according to ChIP kit manufacturer's instructions. Following sample purification by either ethanol precipitation (Active Motif) or spin column purification (Magna), purified samples were visualised by agarose gel electrophoresis (1.5% (w/v) agarose gel) and the condition which gave the strongest, cleanest band between 200 – 500 bp, with the least smearing above 1000 bp and below 200 bp, was selected as the cross-linking condition for that particular cell line (Table 2-9).

Table 2-9 Cross-linking conditions for the cell lines used in this study

Cell Line	PFA Concentration			Cross-Linking Incubation Time		
	Magna A/G	Magna G	Active Motif	Magna A/G	Magna G	Active Motif
D283	0.75 %	1 %	1 %	7 min	10 min	10 min
HDMB-03	1 %	1 %	1 %	10 min	10 min	10 min

Table 2-10 Antibodies used in ChIP assay immunoprecipitation

Immunoprecipitating Antibody	ChIP Validated?	Supplier
YB-1	No	Santa Cruz; SC101198
Immunoglobulin (IgG) G1	Yes	Cell Signalling; 5415
Histone H3K4me3	Yes	Active Motif; 61379

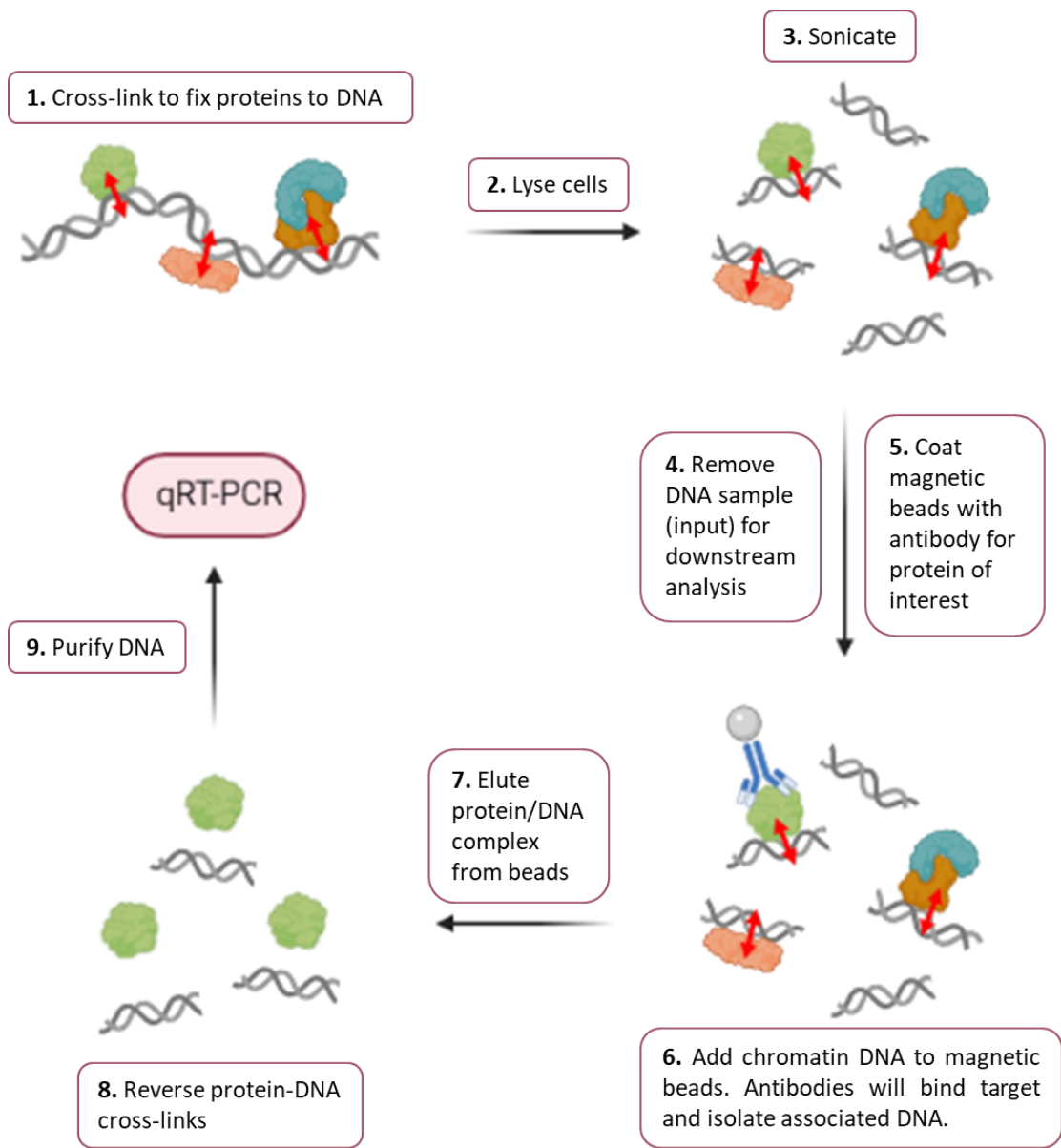


Figure 2.4 Schematic of ChIP assay.

2.9.2.1 qPCR for ChIP Analysis

To determine the level of protein enrichment of the gene promoter of interest, qPCR with SYBR-green chemistry was utilised. To each reaction, 3 µl ChIP sample (IP and input), 1 µM forward and reverse primers (targeting the protein binding sequence in the gene of interest; Table 2-11) and 7.5 µL of iQ™ SYBR® Green Supermix (BioRad; 1708884) were added and the reaction mix made up to a final reaction volume of 15 µL with nuclease-free H₂O. A Bio-Rad CFX384 RT-PCR machine was utilised using conditions as previously optimised for the selected primer pair (Section 2.9.5).

qPCR signals were then analysed using the Percent Input Method (Nagaki et al., 2003), where signals obtained from the three ChIP assay samples (histone, IgG and protein of interest) are divided by the signals obtained from the input sample, after which samples are presented as a percentage of the input value. This method is widely preferred as it includes normalisation for both background levels and input chromatin going into the ChIP. Significant differences in percent input were calculated by paired t-test using GraphPad Prism 8.

2.9.3 RNA Isolation

To extract RNA, first, cells of the desired cell line were pelleted as previously described (Section 2.4) and the resultant sample either used immediately or snap frozen in liquid nitrogen and stored at -80°C for later use. RNA was then extracted utilising the NucleoSpin® RNA Plus kit (Machery-Nagel) as per the manufacturer's instructions. The resultant RNA was either used immediately for downstream applications (Section 2.9.3.1) or transferred to -80°C for long-term storage.

2.9.3.1 Measuring RNA and DNA Concentration and Purity

RNA and DNA concentration and absorbance was assessed using a Nanodrop2000 spectrophotometer (Thermo Scientific). The ratio of absorbance at 260 nm and 280 nm was used to assess RNA/DNA purity, with a ratio of ~1.8 considered as “pure” for DNA and a ratio of ~2.0 considered as “pure” for RNA. A noticeably low ratio is indicative of contaminants such as protein and phenol. The ratio of absorbance at 260 nm and 230 nm was utilised as a secondary measure of nucleic acid purity. A 260/230 value of 2.0-2.2 usually indicates “pure” nucleic acid, while substantially lower values may indicate the presence of contaminants which absorb at 230 nm, notably EDTA and carbohydrates.

2.9.4 Complementary DNA (cDNA) Synthesis

cDNA synthesis was undertaken using RNA extracted as previously described (Section 2.9.3). To a sterile, nuclease-free tube, 2 µg RNA was added and made up to 11 µL in nuclease-free H₂O (Stratech Science; PCR-258L-JEN). 1 µL random primers (3 µg/µL; Invitrogen; 48190011) and 1 µL deoxynucleoside triphosphates (dNTPs; 25 mM; Thermo Scientific; R1121) were then added to each sample. Samples were incubated at 65°C for 5 minutes in order to remove RNA secondary structure. Following this, 1 µL dithiothreitol (DTT; 0.1M; Invitrogen; 1080-044), 4 µL 5x first strand buffer (Invitrogen; 1080-044), 1 µL RNaseOUT (Invitrogen; 10154652) and 1 µL superscript II reverse transcriptase (Invitrogen; 1080-044) was added to each tube to give a total volume of 20 µL and final RNA concentration of 100 ng/µL. The reaction mix was then incubated at 25°C for 5 min, 50°C for 45 min and 70°C for 15 min using a Techne TC-

512 Thermocycler. The resultant cDNA was either kept on ice for immediate use or stored at -20°C.

2.9.5 Temperature Gradient Optimisation of Primers

In order to improve the efficiency of qRT-PCR assays, temperature gradient PCR with a control cell line was employed to optimise primer annealing temperatures. For each sample, 7.5 µL iQ SYBR master mix, 1 µM of forward/reverse primer (Eurofins) and 50 ng cDNA template was added to PCR tubes and made up to a final volume of 15 µL with nuclease-free H₂O. The reaction was then run using a Techne TC-512 Thermocycler across a gradient of annealing temperatures, between the lowest and highest predicted for each primer pair. The PCR products were then electrophoresed on a 2% (w/v) agarose gel and analysed to identify the annealing temperature that provided the highest specificity and yield. To test the efficiency of primers, a qRT-PCR (Section 2.9.6) was set up with a dilution series of control RNA.

Table 2-11 Primers used for qRT-PCR/qPCR

Gene Target	Sequence	Optimised Annealing Temperature
<i>YBX1</i> (Forward)	AAG AAG GTC ATC GCA ACG AAG	62°C
<i>YBX1</i> (Reverse)	CTC CTA CAC TGC GAA GGT ACT	
<i>ABCB1</i> Exon 3 -189 (Forward)	CAT GCT GAA GAA AGA CCA CTG C	58°C
<i>ABCB1</i> Exon 3 -189 (Reverse)	CTC CGA CCT CTC CAA TTC TGT	
<i>ABCB1</i> Exon 3 +108 (Forward)	GTC ATC TGT GGT GAG GCT GA	60°C
<i>ABCB1</i> Exon 3 +108 (Reverse)	AGG CTT CCT GTG GCA AAG AG	
<i>GAPDH</i> (Forward)	ATG TTC GTC ATG GGT GTG AA	60°C
<i>GAPDH</i> (Reverse)	CTC TTC TGG GTG GCA GTG AT	
<i>ABCB1</i> (Forward)	CCC ATC ATT GCA ATA GCA GG	60°C
<i>ABCB1</i> (Reverse)	GTT CAA ACT TCT GCT CCT GA	

Primers in blue font highlight those used in CHIP qPCR.

2.9.6 qRT-PCR for Gene Expression Analysis

In order to assess relative gene expression levels across medulloblastoma cell lines, qRT-PCR was implemented using SYBR-green chemistry in order to detect DNA amplification. To each reaction 10 ng – 30 ng cDNA, 1 μ M forward and reverse primers and 5 μ L of iQ SYBR Green Supermix was added for a final reaction volume of 10 μ L. A list of primers used in this study can be found in Table 2-11. A Bio-Rad CFX384 RT-PCR machine was utilised using a standard qRT-PCR programme with annealing conditions as previously optimised (Section 2.9.5). To confirm the specificity of the product a melt curve was also added.

RT-PCR analysis was conducted using the ΔC_q (or $\Delta\Delta C_q$) method outlined below, in which mRNA expression was normalised to an endogenous reporter gene and (in the case of $\Delta\Delta C_q$) a control sample .

$$\Delta C_q = av. C_q (gene\ of\ interest) - av. C_q (reporter\ gene)$$

$$Relative\ Gene\ Expression = 2^{-\Delta C_q}$$

$$\Delta\Delta C_q = \Delta C_q (treated\ sample) - \Delta C_q (control\ sample)$$

$$Relative\ Fold\ Change\ Gene\ Expression = 2^{-\Delta\Delta C_q}$$

Where C_q represents the quantification cycle – the cycle in which fluorescence can be detected.

Significant differences in relative gene expression were calculated using ordinary one-way ANOVA analyses/unpaired t-test using GraphPad Prism 8.

2.9.7 Immunoblotting

2.9.7.1 Cell Lysis

2.9.7.1.1 Total Cell Lysate

To a washed cell pellet of $1 - 2 \times 10^6$ cells, 50 μL of NP-40 lysis buffer (Table 2-12) containing 1 x cComplete™ EDTA-free Protease Inhibitor Cocktail (11836170001, Roche) was added and the resulting cell suspension incubated on ice for 30 minutes with regular vortexing. Lysates were then centrifuged at $14,000 \times g$ for 15 minutes at 4°C and the resulting supernatants transferred to fresh Eppendorfs, stored on ice and used immediately for downstream applications.

2.9.7.1.2 Nuclear and Cytoplasmic Fractionation

Nuclear and cytoplasmic fractionation was undertaken using the Cell Fractionation Kit from Cell Signalling Technology (9038) as per manufacturer's instructions. Nuclear and cytoplasmic fractions were prepared from cell pellets of $1 - 2 \times 10^6$ cells as previously described (Section 2.5.4).

2.9.7.2 Preparation of Samples

Following a Bradford assay to determine protein concentration, protein lysates were diluted to a final concentration of $1 \mu\text{g}/\mu\text{L}$ in the appropriate lysis buffer and 4x SDS sample buffer (Table 2-12) and boiled for 10 minutes at 95°C . Samples were either used immediately or stored at -20°C .

2.9.7.3 Preparation of SDS gels

Gels were prepared according to target protein size – for the YB-1 (49 kDa), α -tubulin (50 kDa), GAPDH (36 kDa) and histone (18 kDa) proteins described in this report, a 12% gel was chosen. The separating gel was first prepared as described in Table 2-13,

pipetted into a gel casket set up with 1.5mm spacer plates and overlaid with ethanol to remove any air bubbles. After gel polymerisation, the ethanol was decanted and a stacking gel prepared and pipetted over the separating gel. A 1.5 mm comb was then slowly inserted into the gel. Following polymerisation the completed SDS-gel was either used directly or stored within running buffer-soaked towel (Table 2-12) and foil at 4°C for up to one week.

2.9.7.4 Electrophoresis

SDS-gels were prepared as previously outlined (Section 2.9.7.3) and 20 µg of sample loaded per well using a Hamilton syringe. In order to determine protein size, 5 µL of ECL rainbow ladder (Amersham; RPN800E) was also loaded. Gels were run in 1 x running buffer (Table 2-12) at 20 mA until samples reached the separating gel, at which point the current was increased to 40 mA. To transfer the gel, a Hybond® PVDF membrane (Amersham; 10600023) was first activated by incubation for 30 seconds in methanol, 3 minutes in water and 10 minutes in 1 x transfer buffer (Table 2-12). The blot was then assembled as follows: plastic grid; sponge; 3x filter paper; gel; activated membrane; 3x filter paper; sponge; plastic grid. The assembled blot was transferred for 1 hour at 4°C and 100V in 1 x transfer buffer. To increase the binding capacity of the membrane, it was washed in TBS-T and air-dried until opaque; following which the membrane was rehydrated in TBS-T until translucent.

2.9.7.5 Staining Target Proteins

Depending on the primary antibody, membranes were blocked in either 5% BSA (Sigma Aldrich; A3311) or 5% milk (Marvel) in TBS-T (Table 2-12) for 1 hour at room temperature. Following this, primary antibody was added (Table 2-14) and the

membrane incubated rolling overnight at 4°C. The membrane was then washed 3 x 10 minutes in TBS-T and the appropriate secondary antibody added (Table 2-14). After incubation for 1 hour at room temperature, the secondary antibody was decanted and the membrane washed as previously described.

In order to visualise protein bands, membranes were incubated with Pierce™ ECL Western Blotting Substrate (Thermo Fisher Scientific; 32106) for approximately 3 minutes as dictated by individual proteins. For proteins where detection was problematic, ECL Signal Fire solution (Cell Signalling; 68835) was utilised. Chemiluminescence was then measured using a LAS Mini 3000.

If further antibody staining was required, membranes were first washed briefly in TBS-T, following which ReBlot Plus Mild Antibody Stripping Solution (10x; Merck; 2502) was added and membranes incubated for 20 minutes at room temperature. After incubation, membranes were washed 2 x 2 minutes in TBS-T and the membrane blocked and stained again as described previously.

Table 2-12 Buffers used for immunoblotting

Buffer	Components	Storage
NP-40 Lysis Buffer	150 mM NaCl 0.5% NP-40 50 mM Tris pH 7.4 1mM EDTA	-20°C
4 x SDS Sample Buffer	40% Glycerol (Courtner and Warner) 240mM Tris/HCl pH 6.8 8% SDS 0.04% Bromophenol blue (Fisher) + 5% β -Mercaptoethanol (Sigma) added fresh.	-20°C
10 x Running Buffer	250 mM Tris base 1.9 M Glycine 4% SDS	RT
10 x Transfer Buffer	250 mM Tris base 1.9 M Glycine	RT
1 x Transfer Buffer	100 mL 10x transfer buffer 200 mL Methanol 700 mL ddH ₂ O	4°C
10 x TBS	20 mM Tris Base pH 7.6 1.5 M NaCl	RT
1 x TBS-T	100ml 10 x TBS 1ml Tween-20 (Sigma) 899ml ddH ₂ O	RT

Table 2-13 Preparation of SDS gels

Components	Separating Gel	Stacking Gel
1M Tris pH 8.8	3.9 mL	n/a
1M Tris pH 6.8	n/a	0.65 mL
ddH ₂ O	1.9 mL	3.58 mL
30% Acrylamide/Dis-acrylamide solution (Sigma)	4 mL	0.67 mL
10% SDS	0.1 mL	0.05 mL
10% Ammonium Persulphate (APS; Sigma)	0.1 mL	0.05 mL
N,N,N',N'-Tetramethylethylenediamine (TEMED; Sigma)	0.01 mL	0.005 mL

Table 2-14 Antibodies used for immunoblotting

Antibody	Primary/ Secondary	Host Species	Dilution	Source
YB-1	Primary	Rabbit (Polyclonal)	1:1000	Cell Signalling Technology (4202S)
Histone-XP	Primary	Rabbit (Monoclonal)	1:2000	Cell Signalling Technology (4499S)
α -Tubulin	Primary	Mouse (monoclonal)	1:1000	Abcam (DM1A)
GAPDH	Primary	Rabbit (Monoclonal)	1:1000	Cell Signalling Technology (2118S)
Anti-Rabbit IgG, HRP linked	Secondary	Goat	1:2000	Cell Signalling Technology (7074S)
Anti-Mouse IgG, HRP linked	Secondary	Goat	1:2000	Cell Signalling Technology (7076S)

2.9.7.5.1 Band Density Quantification

In order to accurately quantify band density and hence the amount of protein in each sample, the “Gels” analysis tool from Fiji (ImageJ) software was utilised. In brief, each

sample band in a blot was selected using the rectangular selection tool and histograms indicating the intensity of each band. The area of each histogram peak was then measured. This process was repeated to measure the band density for other samples and loading controls. In order to calculate relative density, the area of each sample peak was divided by the area of the appropriate loading control peak. Significant differences in relative density were then calculated by unpaired t-test/ordinary one-way ANOVA analyses using GraphPad Prism 8.

2.9.7.5.2 Calculation of Nuclear YB-1:Cytoplasmic YB-1

In order to calculate the ratio of nuclear to cytoplasmic YB-1 protein, band density was calculated using the histogram method as previously described (Section 2.9.7.5.1). Upon collection of peak areas for samples and loading controls, peak areas for each antibody were converted into a percentage of the total peak area for all peaks measured for that antibody. Next, relative density was calculated by dividing each percent value by the percent value for the standard (represented by the 0 hr sample). Relative densities were then scaled to the appropriate cytoplasmic/nuclear loading control to correct for variations in sample loading/fractionation. Next, for each sample, the nuclear scaled, relative densities were divided by the cytoplasmic scaled, relative densities to give a nuclear:cytoplasmic ratio. Significant differences in nuclear:cytoplasmic ratio were then calculated by ratio-paired t test using GraphPad Prism 8.

2.9.8 Immunofluorescence

For immunofluorescence (IF), cells were seeded in chamber slides and fixed as previously described (Section 2.5.4). To permeabilise cells, each slide was incubated

with PBX (PBS + 0.1% Triton X-100) for 30 minutes in a coplin jar. Slides were then rinsed briefly in PBS and blocked for one hour with 10% goat serum (Vector Laboratories; S1000) at room temperature in a humidity chamber. Following blocking, primary antibody diluted in blocking solution (Table 2-15) was added dropwise to slides and incubated in a humidity chamber either for one hour at room temperature or overnight at 4°C. Slides were then washed in PBT (PBS + 0.1% Tween-20) for 5, 10 and 15 minutes, after which secondary antibody was added dropwise to slides and incubated in a darkened humidity chamber for one hour at room temperature. Following secondary antibody incubation, slides were washed as previously described and equilibrated briefly in PBS. Following equilibration, samples were incubated in 300 nM 4',6-diamidino-2-phenylindole (DAPI) dihydrochloride (10 mg; Invitrogen; D1306) for 5 minutes in a darkened humidity chamber. Each slide was then rinsed 3 x 2 minutes in PBS, dried and mounted in Fluoromount Aqueous Mounting Medium (Sigma, F4680), following which a 24 x 50 mm coverslip (Fisher; 12-545F) was placed carefully over the sample. After the mounting medium had set, slides were sealed with nail polish and stored in a slide box at 4°C.

Table 2-15 Antibodies used for immunofluorescence

Antibody	Primary/ Secondary	Host Species	Dilution	Source
YB-1	Primary	Rabbit (Polyclonal)	1:50	Cell Signalling Technology (4202S)
α -Tubulin	Primary	Mouse (Monoclonal)	1:400	Abcam (DM1A)
Alexa-Fluor 488 Anti- Rabbit	Secondary	Goat	1:100	Invitrogen (A21244)
Alexa-Fluor 647 Anti- Mouse	Secondary	Goat	1:100	Invitrogen (A11029)

2.9.8.1 Image analysis

Slides were imaged using a Leica SPEII Confocal Microscope with a 20x air lens and 488 nm, 633 nm and 405 nm lasers. All images were taken at 1024 x 1024 pixel resolution. The resulting images were then viewed and analysed using Fiji (ImageJ) software.

2.9.8.1.1 Compartmental staining analysis

In order to quantify the nuclear and overall staining intensity of multi-channel immunofluorescence images, Fiji (ImageJ) software was employed. In both cases, staining intensity was measured through the generation of binary masks. First, multi-channel images were opened and the different fluorescence channels separated into mono-channel images. Next, either the 405 channel (DAPI nuclear staining) or the 488 channel (or channel of choice depending on conjugated secondary antibody used; overall staining) was selected and the fluorescent signal used to generate binary masks by using the “mean” Threshold function to isolate nuclei/GFP overall

staining. To avoid clumps of cells skewing measurements, the “Process > Binary > Watershed” function was utilised in order to separate cells. The following measurements were then selected for output: mean grey value, area, integrated density. Next, the “analyse particles” command was executed and parameters set as: size 50-infinity; pixel units; show outlines; add to manager; show results. The resulting image contained outlined and numbered nuclei marked as individual regions of interest (ROI). Using the ROI manager feature, ROIs of interest were then highlighted, the corresponding non-binary channel image selected and the measure command executed. The results window then displayed measurements for GFP signal in each ROI generated using the binary signal masks. An overview of this workflow is demonstrated in Figure 2.5. Integrated density was chosen as a measure to analyse staining intensity over mean grey value to account for the variability in cell size between drug-treated and vehicle-treated cells and in nuclei size between cell lines. On account of skewed number distributions, median integrated density (staining intensity) was calculated and processed relative to that in the appropriate control cells. Significant differences were calculated by unpaired t-test using GraphPad Prism 8.

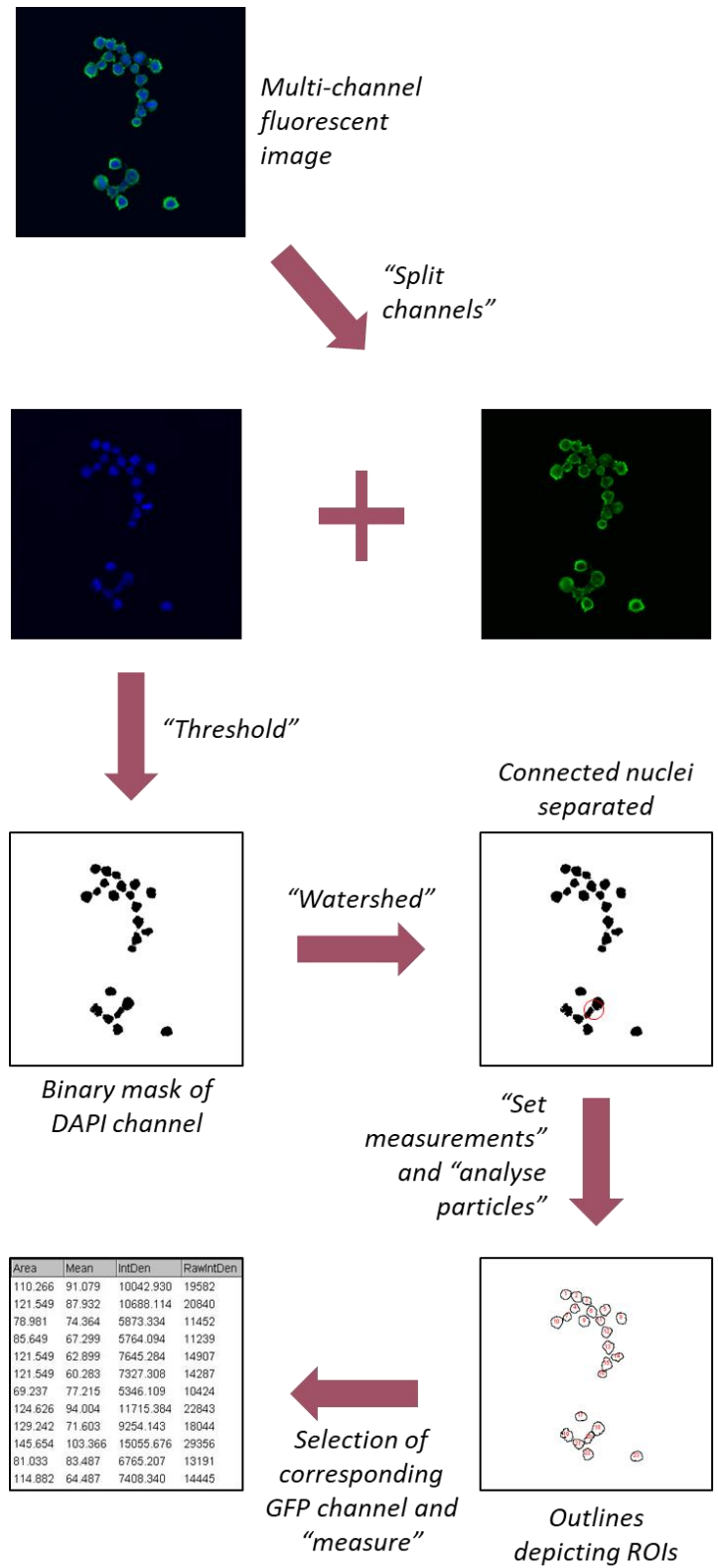


Figure 2.5 Simplified workflow depicting the calculation of nuclear staining intensity using binary masks in Fiji (ImageJ).

2.9.9 Immunohistochemistry

In order to detect the presence of proteins of interest in formalin-fixed paraffin embedded (FFPE) tissue, immunohistochemistry was undertaken using a Pierce™ Peroxidase IHC Detection Kit (Thermo Fisher; 36000) and an ABC Peroxidase Standard Staining Kit (Thermo Fisher; 32020) in order to improve staining sensitivity and specificity.

Prior to immunohistochemistry, samples were oven-dried at 60°C overnight. First, slides were deparaffinised in xylene for 15 minutes, rehydrated in ethanol (10 minutes in 100% ethanol followed by 10 minutes in 95% ethanol) and washed briefly in water. Heat-induced epitope retrieval was performed by steaming in sodium citrate buffer (pH 6.0) for 40 minutes. Slides were then washed in PBS in a Coplin jar for 2 minutes. To quench endogenous peroxidase activity, tissues were incubated for 30 minutes with Peroxidase Suppressor in a humidified box. Following this, slides were washed 2 x 3 minutes with TBS-T and incubated in Blocking Buffer for 30 minutes. Primary antibody (YB-1; 1:50; Cell Signalling 4202S) was then added dropwise to tissue and slides incubated at 4°C overnight.

Following overnight incubation, slides were washed as previously described and secondary biotinylated antibody (rabbit; Thermo Fisher; 65-6140) added for one hour at room temperature. During incubation, ABC Reagent was prepared in PBS as Reagent A:PBS:Reagent B in a ratio of 1.8 µL; 100 µL: 1.8 µL. The solution was mixed and incubated for 30 minutes to allow the formation of avidin-biotinylated horseradish peroxidase (HRP) complexes. Following secondary antibody incubation,

the slides were washed twice for 3 minutes in Wash Buffer, and the slides incubated with the pre-made ABC reagent for 30 minutes.

Following incubation, the slides were washed as previously described, meanwhile a 1x working solution of DAB/Metal Concentrate (10x; included in Pierce™ Peroxidase IHC Detection Kit) in Stable Peroxide Buffer was prepared. The 1x DAB was applied to each slide and incubated until the desired staining was achieved (10 minutes).

Slides were again washed in Wash Buffer and rinsed with distilled water. To counterstain, tissue was then covered with Harris Modified Haematoxylin (included in Pierce™ Peroxidase IHC Detection Kit) and incubated for 1 minute at room temperature. Slides were then washed several times in distilled water and rinsed under running water. After washing slides were dehydrated in ethanol (95% then 100%) followed by xylene and finally carefully dried. To mount, 1-3 drops of mounting medium (included in Pierce™ Peroxidase IHC Detection Kit) was applied and each slide covered with a 24 x 50 mm coverslip.

2.9.9.1 Image Analysis

Slides were imaged using a Brunell SP88 microscope using the brightfield channel and 4x magnification. The resultant images were then viewed using Fiji (Image J) software and analysed by way of the ImageJ IHC Profiler plugin.

2.9.9.1.1 IHC Profiler

The IHC Profiler plugin functions by converting DAB/haematoxylin counter-stained IHC images into a DAB and haematoxylin image by colour deconvolution. The DAB image can then be analysed separately to quantify staining intensity. To do this, IHC

profiler generates a histogram profile of the DAB image, which is a plot of pixel intensity values (X axis) against the number of pixels representing the intensity (Y axis). The plugin divides the histogram profile into 4 zones dependent on pixel intensity: high positive, positive, low positive and negative and assigns them a score of 4, 3, 2 and 1 respectively. Then, using the formula defined in Figure 2.6 A, an overall score of high positive, positive, low positive or negative is assigned to the image. For images in which $\geq 66\%$ pixels are contained within a zone, the images are directly assigned a score of that zone, eliminating the need to apply the formula.

In brief, IHC images taken of TMA cores were opened within ImageJ. Then, the IHC Profiler plugin was selected and nuclear or cytoplasmic mode chosen depending on the analysis required. The cytoplasmic mode selects only DAB cytoplasmic stain, while the nuclear mode utilises the threshold function of ImageJ to select nuclear-stained DAB. On application, it was found that the nuclear mode also selected other DAB immunoreaction not confined to the nucleus, however this effect could be minimised by changing the selection threshold. The image was deconvoluted generating a haematoxylin and DAB image. Upon thresholding and selection creation (nuclear measurements only), the IHC Profiler plugin automatically quantified the level of pixel intensity and plotted a histogram profile of the DAB image with the corresponding scoring log displayed (Figure 2.6 B – C).

To compile data and average the score attributed to each core to give a final score per patient, each IHC profiler score was assigned a numerical value. Negative was assigned 0, low positive was assigned 1, positive was assigned 2 and high positive assigned 3. This allowed the calculation of an average nuclear, cytoplasmic and

overall (the sum of nuclear and cytoplasmic scores) score for each patient. To simplify downstream analyses and allow for low sample numbers, patients were divided into three groups based upon average nuclear and overall scores: a negative group scoring 0, a low positive expression group scoring in the lower 50th percentile and a high positive group scoring in the upper 50th percentile.

A
$$Score = \frac{(Number\ of\ pixels\ in\ a\ zone) \times (Score\ of\ the\ zone)}{Total\ number\ of\ pixels\ in\ the\ image}$$

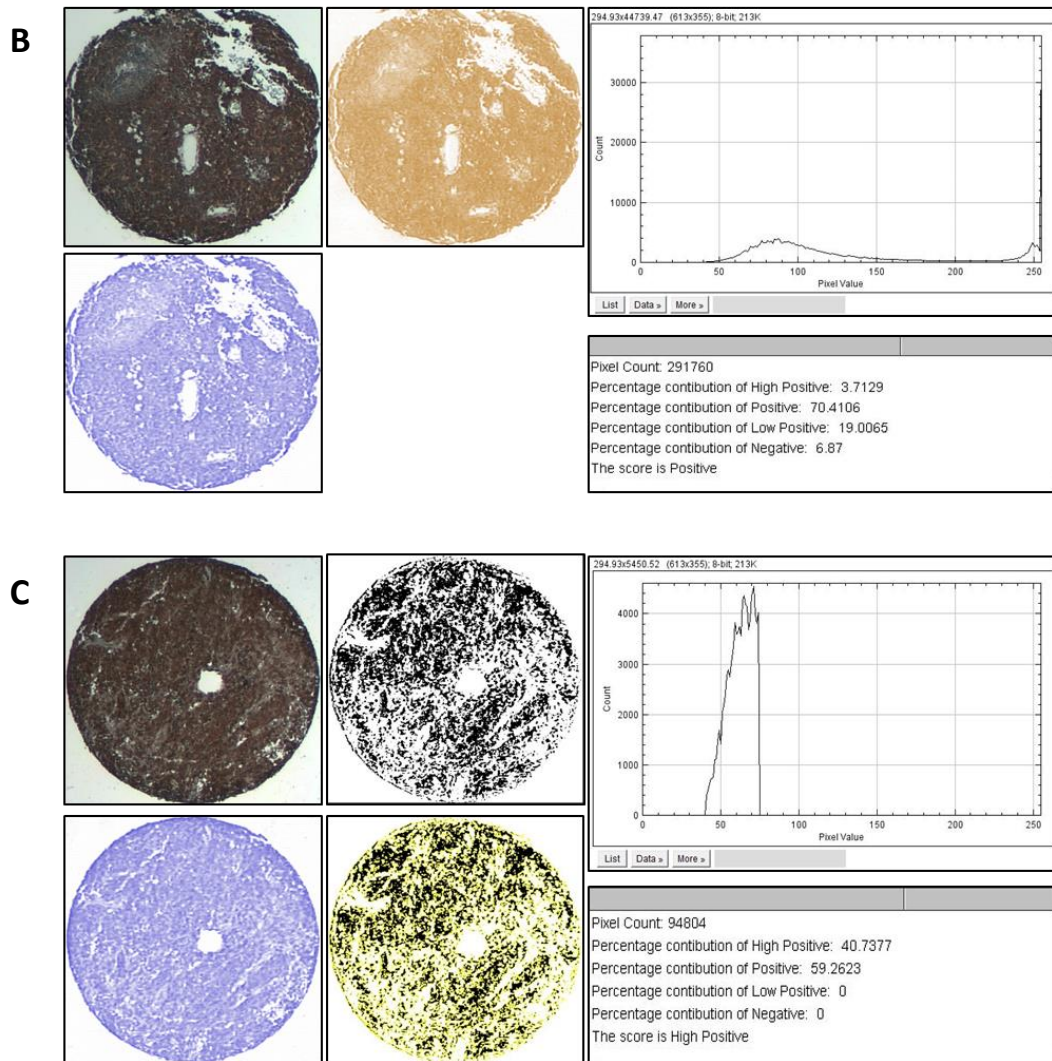


Figure 2.6 Colour deconvolution and quantification of cytoplasmic/nuclear staining intensity using IHC Profiler. A) Formula employed by the plugin for score assignment to IHC images where the score of the zone is assigned as 4 for the high positive zone, 3 for the positive zone, 2 for the low positive zone and 1 for the negative zone. B) IHC Profiler quantification using cytoplasmic mode including colour deconvolution and generation of a histogram profile of the DAB image/scoring log. C) IHC Profiler quantification using the nuclear mode including colour deconvolution, thresholding of the DAB image and selection creation and histogram profile/scoring log.

2.10 Next-generation sequencing

2.10.1 Whole Transcriptome Sequencing

2.10.1.1 Sample Preparation

RNA was isolated using the RNeasy Mini kit (Qiagen; 74104) according to manufacturer's instructions, with an elution volume of 30 μ L. Quality control was undertaken using an Agilent TapeStation to test RNA integrity levels and a Qubit Fluorometer to assess quantity. The TapeStation also provides a RINe (RNA integrity number) value for each RNA sample, where values higher than 7 are considered suitable quality for sequencing analysis.

2.10.1.1.1 Library Preparation

Library preparation was undertaken using the QIAseq Stranded Total RNA Library Kit (Qiagen; 180745) with QIAseq FastSelect rRNA/globin depletion and combinatorial indexes according to manufacturer's instructions. The library preparation workflow is described is displayed in Figure 2.7 A. In brief, RNA starting material was first fragmented in combination with QIAseq FastSelect rRNA HMR to reduce the amount of unwanted RNA species. Next, cleaved RNA fragments were copied into first-strand cDNA using RNase H- Reverse Transcriptase (RT) in combination with random primers (first-strand synthesis). Second-strand synthesis was then undertaken to remove the RNA template and synthesise a second cDNA strand. Following this, the cDNA was end-repaired and 3' adenylated. Sequencing adapters were then asymmetrically ligated to overhangs, after which adapted molecules were enriched by PCR. Amplified DNA was then purified by way of a bead-based clean-up.

The library fragment size distribution was validated and quality inspected using an Agilent 4200 TapeStation, following which libraries were pooled in equimolar concentrations. Library pools were quantified by qRT-PCR using the QIAseq Library Quant Assay kit (Qiagen; 333314) which specifically quantifies DNA molecules with adaptors at both ends (the only molecules that will be amplified during sequencing).

2.10.1.2 Whole Transcriptome Sequencing

Sequencing of previously generated libraries were performed on a NextSeq 500 instrument (Illumina; SY-415-1002) according to manufacturer's instructions in a dual index 1x75bp format at a sequencing depth of 30 M reads/sample.

2.10.1.3 Data Analysis

Raw sequencing data was first de-multiplexed and FASTQ files for each sample generated using bcl2fastq software (Illumina inc.). All following analyses were undertaken using the CLC Genomics Workbench (version 12.0.2) and CLC Genomics Server (version 11.0.2). An overview of the process is shown in Figure 2.7 B.

2.10.1.3.1 FASTQ Trimming

Adapter and quality trimming of FASTQ data was undertaken by the "Trim Reads" tool from CLC Genomics Workbench. Adapter trimming removes any adapter artefacts that remain following sequencing by identifying read-through adapter sequences - where the 3' end of one read includes the reverse complement of the adapter from the other read. Next, reads were trimmed based on quality scores and ambiguous nucleotides. A maximum of 2 ambiguous nucleotides were allowed in a read.

2.10.1.3.2 FASTQ Quality Control

Quality control reports were generated using “QC for Sequencing Reads” tool from CLC Genomics Workbench and provided an overview of any problems with the data prior to conducting further analyses. The following criteria were visualised and assessed prior to the progression of analyses: Sequence-read lengths and base coverages, nucleotide-contributions and base-ambiguities, quality scores as emitted by the base-caller, over-represented sequences and hints suggesting contamination events.

2.10.1.3.3 Alignment and Mapping

Read alignment, mapping and gene quantification were undertaken using the “RNA-Seq Analysis” tool from CLC Genomics Workbench. Reads were mapped to the reference genome (human genome version: hg38). This produced data including: the number of reads per sample and the average read length, the proportion of mapped reads, the distribution of paired-end distances, transcript length coverages and number of exons per transcript.

2.10.1.3.4 Differential Expression Analysis

Differential expression analysis was performed using the “Differential Expression for RNA-Seq” function from CLC Genomics Workbench. For normalization, the trimmed mean of M-values method (TMM normalization) was utilised, which uses a weighted trimmed mean of the log expression ratios between samples to facilitate gene count comparisons between and within samples.

2.10.1.3.5 Principal Component Analysis

Principal Component Analyses (PCA) were performed using the “PCA for RNA-seq” tool from CLC Genomic Workbench. PCA is a method used in unsupervised analysis to reduce the dimension of large data sets and is a useful tool to explore sample clusters arising naturally based on the gene expression profile.

2.10.1.3.6 Unsupervised Clustering and Heat Maps

Heatmaps that simultaneously cluster similarly-expressed genes and samples were generated by the “Create Heat Map for RNA-seq” tool from CLC Genomic Workbench. 50 genes with the highest variance across samples were selected for unsupervised clustering. Colours represented the difference of the count value to the row mean. The more similar the expression of the selected genes are between samples, the closer the samples will be related in the dendrogram.

2.10.1.3.7 Statistical Testing

Statistically differentially expressed (DE) transcripts were identified using the CLC Genomics Workbench algorithm Empirical analysis of Differential Gene Expression (EDGE), which is a re-implementation of the “Exact Test”, for two-group comparisons (Robinson & Smyth, 2008). A p-value was assigned to represent the significance of the observed fold change in normalised expression values for each gene. To avoid the identification of false positive genes arising from multiple testing, “false discovery rate (FDR) p-values” were also calculated using the Benjamini-Hochberg method.

2.10.1.3.8 Pathway Analysis

Pathway analysis was performed using Ingenuity Pathway Analysis (IPA) software (Qiagen). Prior to IPA core analyses significantly differentially expressed genes were

filtered according to mean expression (≥ 10 TPM), FDR p-values (≤ 0.01) and log fold change ratios (≥ 2 or ≤ -2). The following analyses were explored: canonical pathway analysis; upstream regulators analysis; diseases and function analysis, where the enrichment of a pathway or function was identified by the number of significantly differentially-expressed genes within a pathway or function. Fisher's exact t-test was used to assess whether the overlap between filtered genes and the genes within a biological attribute were statistically significant. Since multiple pathways were tested for each analysis, the Benjamini-Hochberg method was used to control the FDR.

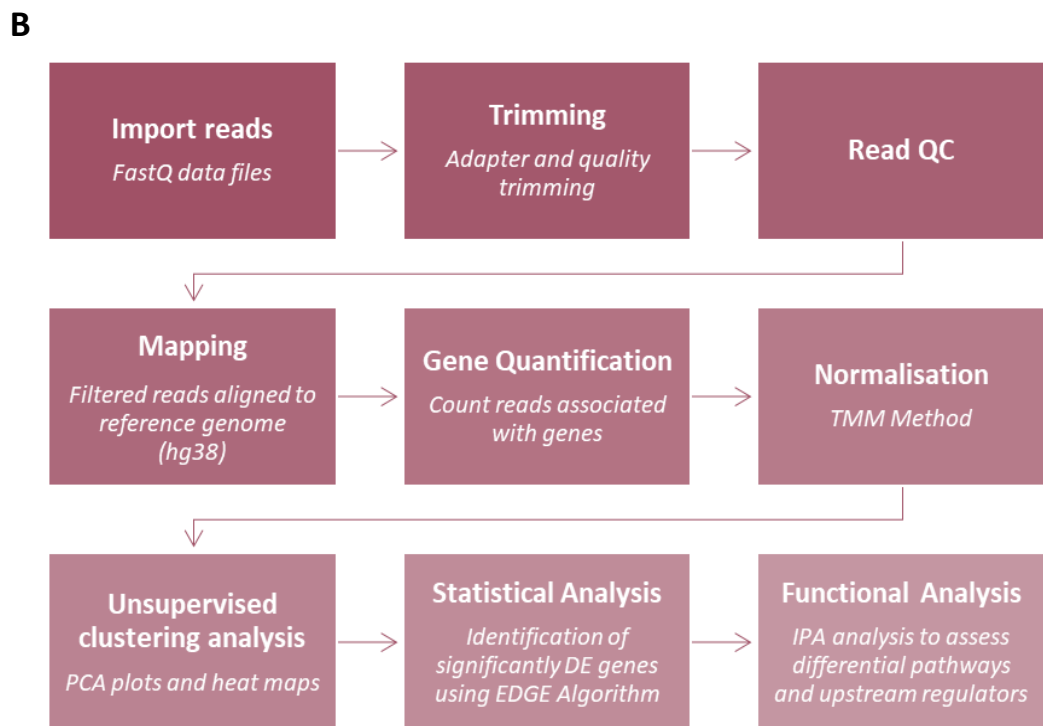
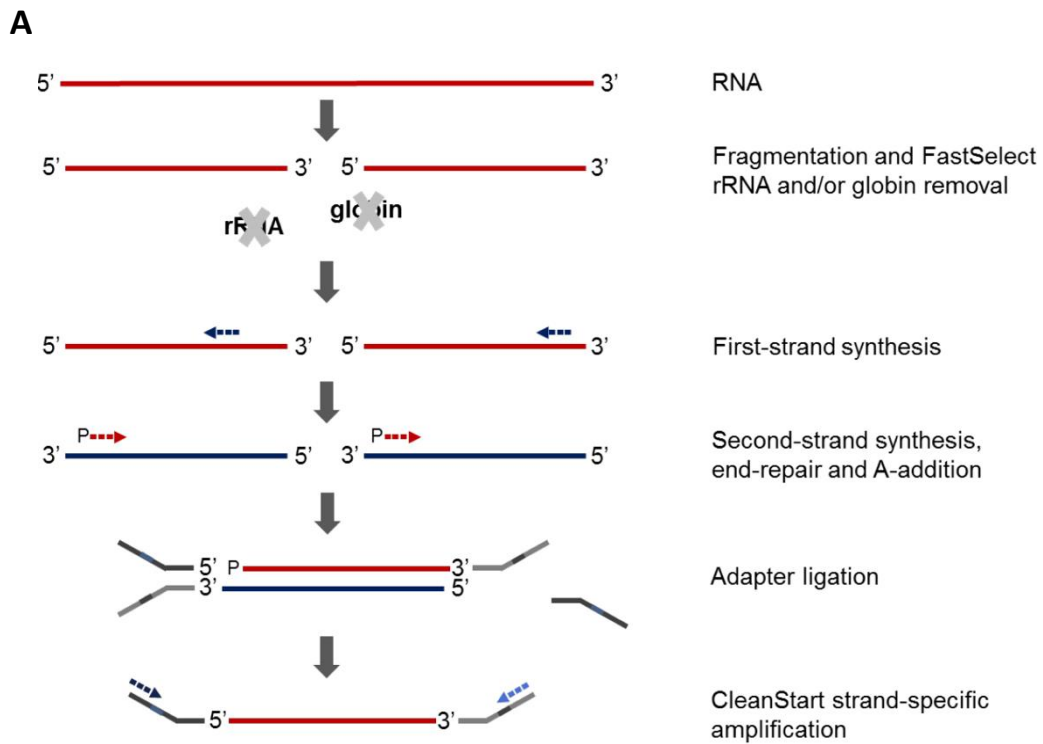


Figure 2.7 Whole transcriptome sequencing. A) Preparation of cDNA libraries for whole transcriptome sequencing. Libraries were generated using the QIAseq Stranded RNA Library kit. Figure adapted from the QIAseq Stranded protocol (Qiagen, 2021). B) Flow chart depicting whole transcriptome sequencing analysis. Analysis was undertaken using CLC Genomics Workbench and IPA software (Qiagen).

2.10.2 3'mRNA Sequencing

2.10.2.1 Sample Preparation

RNA was isolated as described in Section 2.9.3, with an elution volume of 40 μ L. RNA concentration and purity was analysed as described in Section 2.9.3.1 and only samples which met the following criteria were submitted for library preparation: RNA concentration > 100 ng/ μ L; 260/280 ratio 1.9 – 2.1; 260/230 ratio 1.8 – 2.2. Further quality control was undertaken using an Agilent TapeStation 4200 with the Agilent RNA ScreenTape Assay Kit (Agilent; 5067-5576 and 5067-5577) to test RNA integrity levels and a Qubit Fluorometer with the Qubit RNA BR Assay Kit (ThermoFisher Scientific; Q10211) to assess RNA quantity.

2.10.2.1.1 Library Preparation

3'mRNA sequencing (3'mRNA-Seq) libraries were prepared using the QuantSeq 3' mRNA-Seq library prep kit for Illumina in the forward read direction supplemented with unique molecular index (UMI) as per manufacturer's instructions (Lexogen; 015.96) as shown in Figure 2.8 and described in (Moll et al., 2014). The aforementioned kit uses total RNA as input, hence no prior poly(A) enrichment or rRNA depletion is needed. For each sample, cDNA was generated from 250 ng total RNA. First, total RNA was reverse transcribed using oligo-dT primers containing an Illumina-specific linker sequence. First-strand synthesis and RNA removal was followed by random-primed synthesis of the complementary strand (second-strand synthesis). The random primer contained another Illumina-specific linker sequence. The resulting double-stranded cDNA was purified with magnetic beads. Library PCR amplification then introduced the complete adapter sequences required for cluster

generation and UMIs which allow elimination of possible PCR duplicates in sequencing datasets (i7 6nt Index Set; 015.96; Lexogen). 14 PCR cycles were found to be optimal for library amplification (Moll et al., 2014).

Libraries were next quantified using the Qubit Fluorometer and the Qubit dsDNA HS Kit (ThermoFisher Scientific; Q32854), and library fragment-length distributions analysed using the Agilent TapeStation 4200 and the Agilent High Sensitivity D1000 ScreenTape Assay (Agilent; 5067-5584 and 5067-5585). Finally, libraries were pooled in equimolar amounts and final library quantification performed using the KAPA Library Quantification Kit for Illumina (Roche; KK4824).

2.10.2.2 3'mRNA Sequencing

Following library preparation and quality control as described in Section 2.10.2.1.1, the resultant library pool was sequenced on a NextSeq 500 High Output v2.5 75 cycle kit (Illumina; 20024906), to generate approximately 5 million 75bp single-end reads per sample.

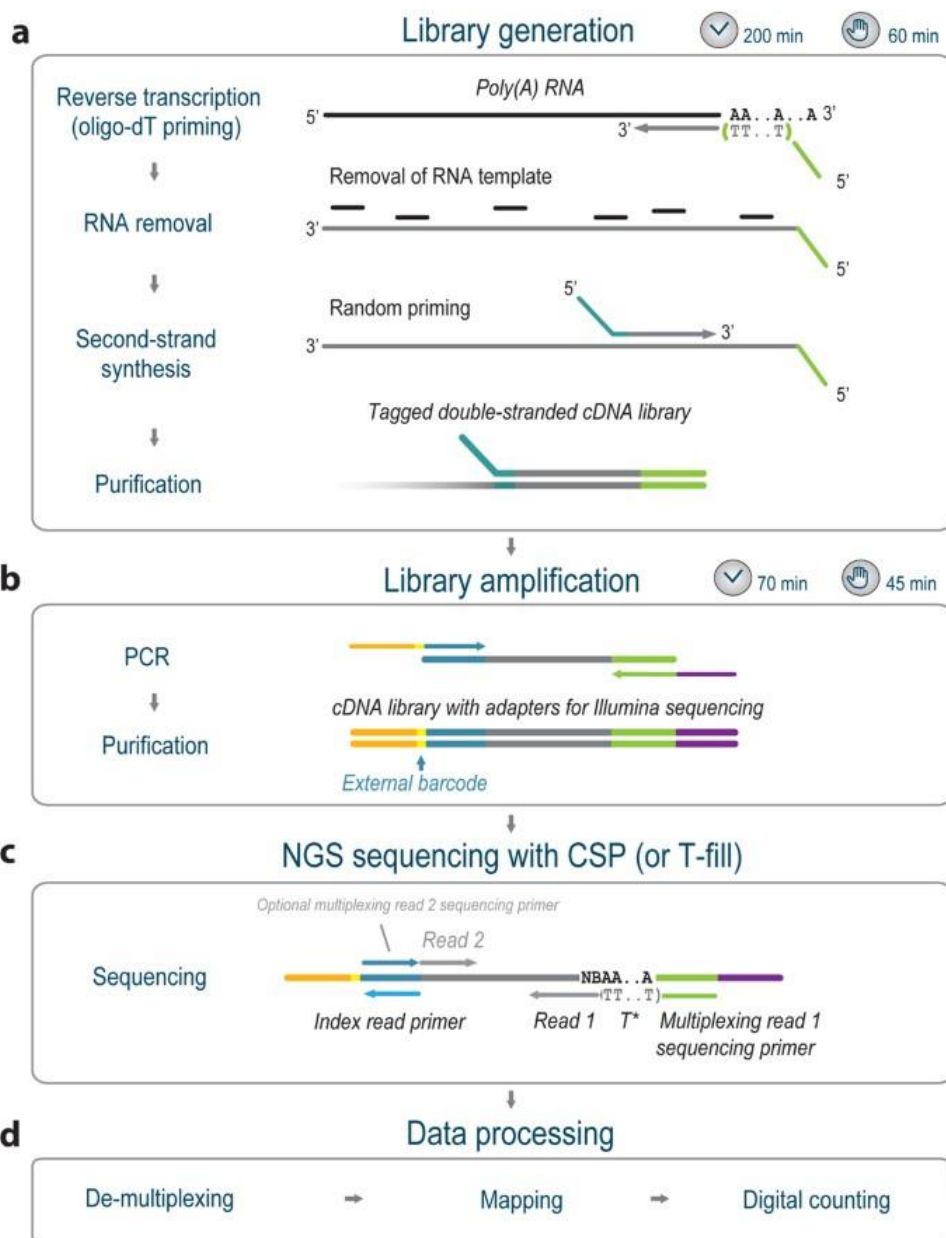


Figure 2.8 3'RNA-Seq workflow using Lexogen Quant-Seq sequencing library methodology. Libraries were generated using the QuantSeq 3' mRNA-Seq library prep kit for Illumina (A) and amplified with adapter sequences for Illumina sequencing and unique indices for multiplexing (B). Following quality control, the resultant library pool was sequenced on the Illumina NextSeq 500 (C) and analysed using R (D). Image from (Moll et al., 2014).

2.10.2.3 Data Analysis

Raw sequencing data was first de-multiplexed and FASTQ files for each sample generated. Data pre-analysis was performed by way of the Bluebee platform (Lexogen), following the workflow displayed in Figure 2.9. First, the *umi2index* tool was employed to add the 6 nucleotide UMI sequence to the identifier of each read and trim the UMI from the start of the read. Next, the *Bbduk* tool was used to trim low quality and poly(A) tails. Following quality control, reads were aligned to a reference genome (human genome version: hg38) using the *STAR Aligner* tool and reads with identical mapping co-ordinates and UMI sequences collapsed to remove duplicates, generating BAM files of uniquely and correctly mapped reads. Read counts for each gene were then calculated using the read count programme *featureCounts* (version 1.6.0).

2.10.2.3.1 Differential Expression Analysis

Differential gene expression analysis was undertaken using the R statistical environment package *DESeq2* (version 1.24.0) with default settings which facilitated read count normalisation and analysis of differential gene expression (Anders & Huber, 2010).

2.10.2.3.2 Gene Ontology Analysis

Gene ontology (GO) terms provide a standardised vocabulary to describe genes and allow the assignment of functionality. In order to conduct gene ontology enrichment analysis of differentially expressed genes, the R statistical environment package *GOSeq* (version 1.4.0) with default settings was employed (Young et al., 2010).

2.10.2.3.3 Statistical Testing

P-values were adjusted for multiple testing using the Benjamini and Hochberg method (Benjamini & Hochberg, 1995) and genes with an adjusted P-value of ≤ 0.05 considered differentially expressed.

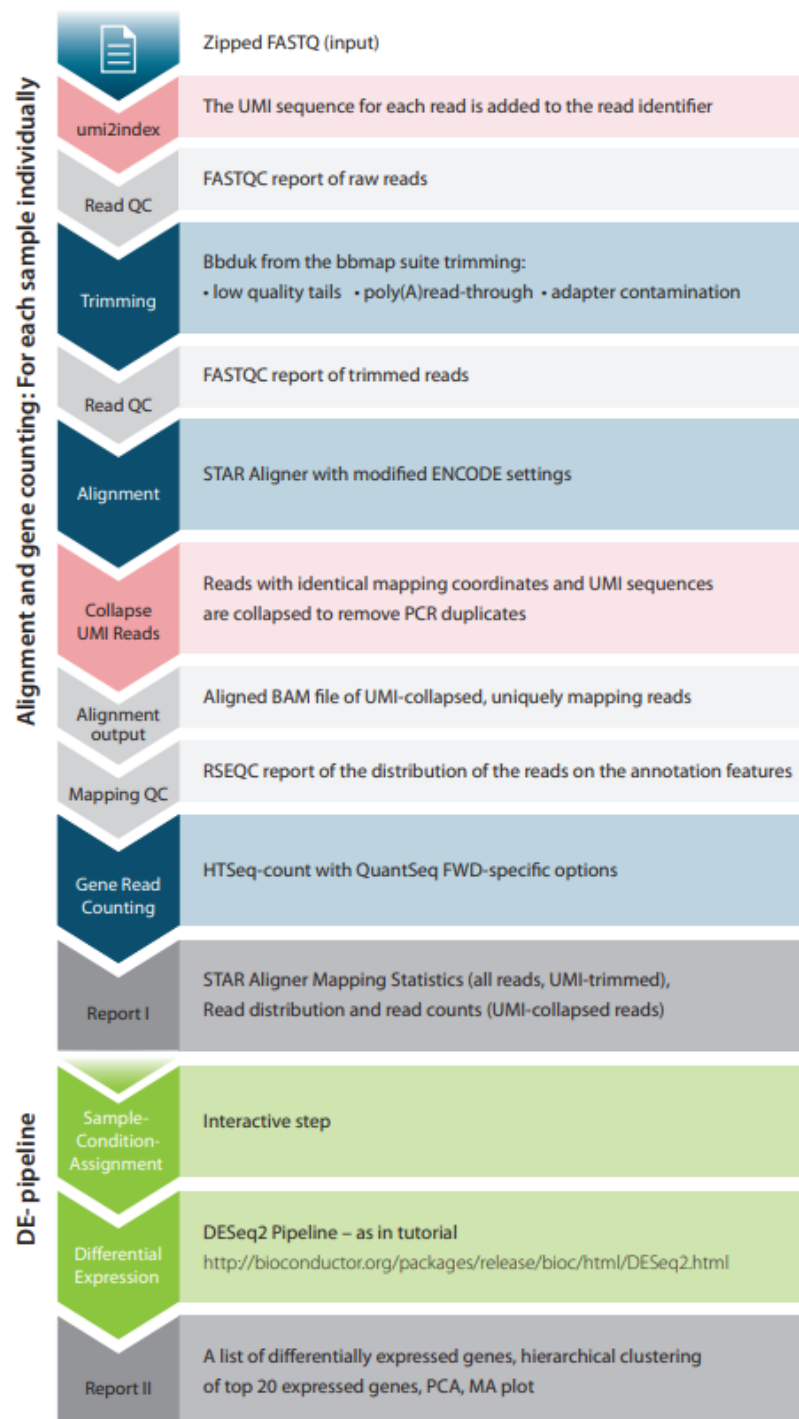


Figure 2.9 QuantSeq 3'mRNA-Seq data integrated data analysis pipeline using the BlueBee genomics platform. Pipeline demonstrating individual steps of data analysis using BlueBee (Lexogen). Steps in blue represent the data analysis processes, grey bars indicate the results and output files generated. Steps in green indicate differential gene expression data analysis. Figure from the QuantSeq BlueBee Genomics Platform Userguide (2021).

2.10.3 CHIP Sequencing

2.10.3.1 Sample Preparation

ChIP-Seq samples were prepared with the Active Motif ChIP-IT High Sensitivity kit according to manufacturer's instructions using the cross-linking parameters described in Section 2.9.2. For all samples, sonication was performed for 15 minutes using cycles of 30 seconds on/30 seconds off in a Bioruptor Pico water bath sonication device (B01060010; Diagenode). An overview of the ChIP assay process is described in Section 2.9.1 and Figure 2.4. Two biological replicates were collected for each cell line/treatment state sequenced, from which two immunoprecipitations (IPs) and one control sample (input) were submitted for library preparation and sequencing.

2.10.3.2 Library Preparation

Prior to library preparation, sample concentrations were measured using a Qubit Fluorometer and Qubit dsDNA HS Assay Kit (ThermoFisher Scientific; Q32854). For samples with concentrations over 1.5 ng/ μ l, 25 ng of DNA was used for library preparation, while for samples with lower concentrations, 12.5 μ l of DNA was used. ChIP-Seq libraries were prepared using a NEBNext Ultra II DNA library Prep Kit for Illumina (NEB; E7645) and NEBNext Multiplex Oligos for Illumina; 96 Unique Dual Index Primer Pairs (NEB; E6440). For PCR-enrichment of the adaptor-ligated libraries, samples with 25 ng of input underwent 4 cycles of amplification and samples with lower inputs underwent 9 cycles of amplification.

Prepared libraries were quantified using a Qubit Fluorometer with the Qubit dsDNA HS Assay Kit (ThermoFisher Scientific; Q32854) and library fragment-size

distributions were assessed using an Agilent Bioanalyzer with the High Sensitivity DNA Kit (Agilent; 5067-4626). Libraries were then pooled in ratios required to generate two times greater coverage of input libraries than of ChIP libraries and the final library pool was quantified using the KAPA Library Quantification Kit for Illumina Platforms (Roche; KK4824).

2.10.3.3 Sequencing

The final library pool was sequenced over one lane of an NovaSeq S4 flow cell on an Illumina NovaSeq 6000 System to generate 20 million pairs of 150-bp paired-end sequencing reads per IP sample and 30 million pairs of 150-bp paired-end sequencing reads per input control sample.

2.10.3.4 Mapping

An overview of Chip-Seq bioinformatic analysis can be found in Figure 2.10. Prior to read mapping, read quality was examined by *FastQC*. Raw reads with low sequencing scores, as well as reads aligned to adaptor sequences were trimmed by *skewer* with default settings (Jiang et al., 2014). Trimmed reads were then mapped onto the human genome (hg38, Ensembl Release 104) by mapping programme *hisat2* with the following options: `--no-spliced-alignment -fr` (Kim et al., 2015). Reads of input samples were then mapped by *hisat2* with the following, lower mapping stringency options: `--no-spliced-alignment --mp 1,0` (Kim et al., 2015). Uniquely and correctly aligned reads were extracted according to the mapping tags, and any duplicated reads were marked and filtered out by *picard-tools* data handling software (<https://broadinstitute.github.io/picard/>).

2.10.3.5 Peak Calling

Transcription factor binding sites (peaks) were identified by *Model-based analysis of ChIP-Seq (MACS2)* software, and the parameter `--keep-dup` was set to 1 (Zhang et al., 2008). Put simply, the *MACS2* algorithm estimates IP-DNA fragment size and uses this estimate to identify significantly enriched regions in each IP sample relative to the genome background (the input control sample). To identify if these sites of enrichment represent “real” binding sites, *MACS2* then undertakes statistical testing, calculating the FDR based on the number of peaks identified in input control samples divided by the number of peaks in IP samples that pass the same statistical threshold. As the input control sample should not exhibit substantial read enrichment, peaks that are identified in both the input control and IP samples likely represent false positives and should be discarded (Feng et al., 2012).

To avoid the identification of artificial peaks, arising from genomic regions with a high propensity for sequencing, “blacklisted” genomic regions, as outlined in <https://github.com/Boyle-Lab/Blacklist>, were applied (Amemiya et al., 2019).

To annotate transcription factor binding sites to specific genes and genomic regions, the *ChIPpeakAnno* package with the Ensembl R database (build version 104) was used. Shared transcription factor binding sites between biological replicates were determined by assessing the overlap regions of peaks using the *findOverlapsOfPeaks* function with the maximal 10 gaps allowed (Zhu et al., 2010).

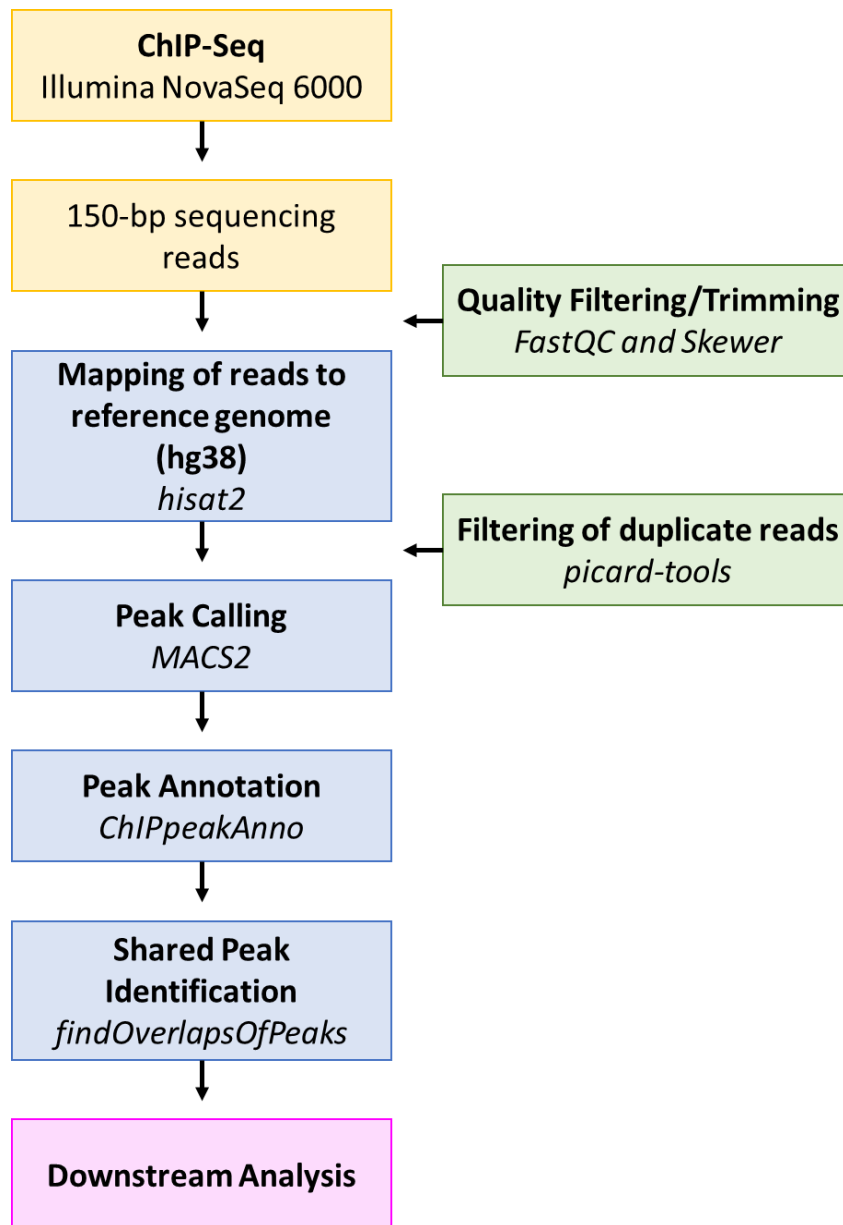


Figure 2.10 Overview of CHIP-Seq analysis process. Terms in *italics* denote the various software tools used in each stage of the analysis pipeline.

Chapter 3

The identification and
characterisation of a potential
regulator of *ABCB1* in
medulloblastoma.

Chapter 3 The identification and characterisation of a potential regulator of *ABCB1* in medulloblastoma.

3.1 Introduction

Numerous clinical studies have correlated ABC transporter gene expression with malignant progression and an aggressive phenotype. *ABCB1* is amongst the best characterised ABC transporters and along with *ABCG2* and *ABCC1*, is thought to contribute most to ABC transporter-mediated MDR in cancer (Robey et al., 2018). Widely distributed throughout the blood-brain barrier, placenta, kidneys and intestines, *ABCB1* protects organs by reducing the intracellular concentrations of a diverse range of toxins by efflux. However, the broad substrate specificity possessed by *ABCB1* also includes key anti-cancer drugs such as taxanes, anthracyclines and vinca alkaloids (Szakacs et al., 2006). This, combined with the over-expression of *ABCB1* observed in various cancers, frequently results in decreased intracellular levels of chemotherapeutic agents and hence reduced chemotherapy efficacy (Durrant et al., 2020; Eadie et al., 2016; Oba et al., 2016).

Disease relapse occurs in approximately 30% of medulloblastoma patients and is almost universally fatal. Over recent years, it has become evident that medulloblastomas display altered biology at relapse, indicative of the emergence and expansion of a minor, therapy resistant cancer cell population. In medulloblastoma, high *ABCB1* expression has been associated with chemoresistance and adverse prognosis (Chou et al., 1995; Othman et al., 2014). Notably, vincristine, a key

chemotherapeutic agent currently used in primary and recurrent medulloblastoma treatment protocols is a known ABCB1 substrate (Section 1.3). It has therefore been postulated that treatment with these drugs may select for the survival of a resistant, ABCB1-expressing sub-population of cells that over time may promote tumour relapse (Hussein et al., 2011; Othman et al., 2014).

Although some elements of *ABCB1* transcriptional control are known, there is the potential for other unknown sites of regulation. We believe that the identification and study of potential regulators of *ABCB1* is vital in order to better understand medulloblastoma cell mechanisms to therapy resistance, with the aim of reducing the risk of relapse for which outcome is so dire.

The aims of this chapter were to:

- A) Identify potential interactors of the *ABCB1* gene promoter.
- B) Analyse candidate transcription factor expression at protein and mRNA level across medulloblastoma cell lines and large-scale publicly available patient datasets.
- C) If deemed promising, assess expression and localisation of candidate transcription factor across medulloblastoma patient TMAs.

3.2 Identification of YB-1 and NFE2L2 as targets for further investigation

3.2.1 Search for potential regulators of the *ABCB1* gene

3.2.1.1 Genomatix MatInspector software analysis of promoter sequences

The first stage in the identification of potential regulators of *ABCB1* was to establish an appropriate method to A) identify the *ABCB1* promoter sequence and B) predict potential functional transcription factor binding sites within this sequence. The transcription factor binding site prediction software tool Genomatix MatInspector (software version 8.1; <http://www.genomatix.de/>) was chosen for this task (Cartharius et al., 2005; Quandt et al., 1995). MatInspector software uses a large library of weight matrices based on known *in vivo* binding sites to predict transcription factor binding sites in nucleotide sequences. The position weight matrix (PWM) model is the most frequently used mathematical model for binding motif prediction and holds certain advantages over alternative methods such as the consensus motif model, constructed using International Union of Pure and Applied Chemistry (IUPAC) codes. Where the PWM model contains information about the position-dependent frequency of each nucleotide in the motif, facilitating the distinction of strong binding sites to weak binding sites; consensus models assume that all valid bases occur with the same frequency. Thus, there exists a trade-off between the number of mismatches allowed, the ambiguity in the consensus sequence and the precision of the representation. For this reason, consensus models are better suited to model motifs with highly conserved consensus patterns.

MatInspector also allows quantification of the similarity between the weight matrix and a potential transcription factor binding site detected in the sequence, facilitating the assignment of quality ratings to matches and thus allowing quality-based filtering of matches.

A simplified workflow describing each stage of data processing by the MatInspector software and the data returned is displayed in Figure 3.1. In brief, a gene of interest is chosen. The Genomatix ELDorado Genome database is then used to extract all annotated promoter sequences and the transcripts that they control. Following the selection of one or more promoter sequences and the setting of search parameters, the software then searches for all matrices in the promoter. This returns a graphical view of matches, where each transcription factor binding site is displayed on the chosen promoter sequence. It also provides a detailed table containing match details such as sequence, matrix information, binding site position, matrix similarity and notably, additional lines of evidence, which includes literature citations and functional studies.

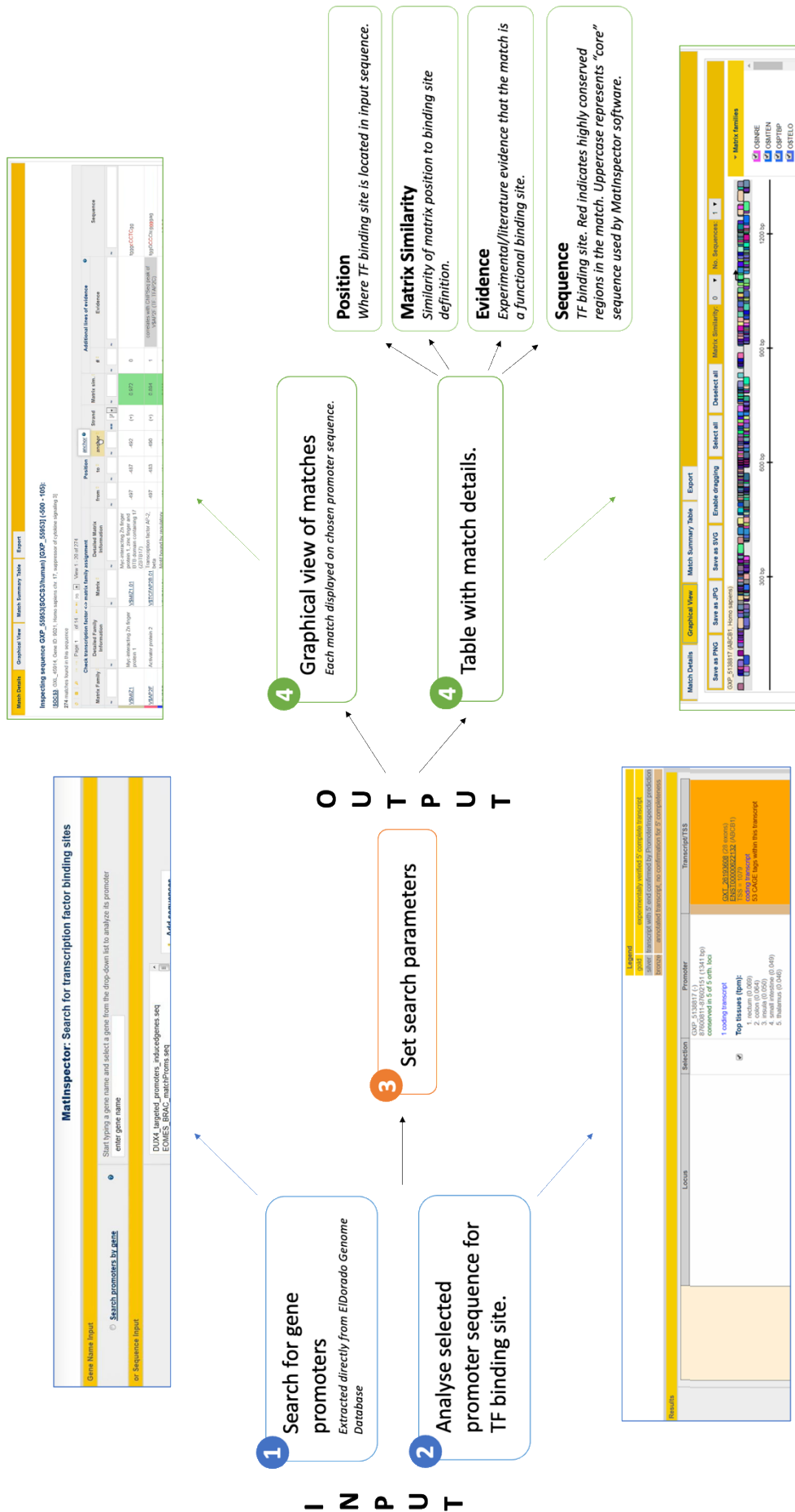


Figure 3.1 Workflow of Genomatix MatInspector Software. A simplified summary of the MatInspector transcription factor binding site prediction software employed in this study. Key information utilised from the table produced following promoter sequence analysis is described.

3.2.1.2 Candidate screening and selection

This process was followed for *ABCB1* as previously described (Figure 3.1). Following a MatInspector search of the *ABCB1* GXP_5138817 promoter (Section 2.1), the software returned over 450 matches representing potential *ABCB1* interactors and their binding sites within the *ABCB1* promoter (Figure 3.2). Screening for evidence to suggest binding site functionality and direct *ABCB1* regulation using the Genomatix “Evidence” function returned 21 candidates. A literature search of electronic database PubMed (January 2018) was next employed. Keywords “cancer”, “metastasis” and “drug resistance” alongside the candidate protein name and abbreviation were entered to search relevant articles. First abstracts and then full-text articles were screened and evidence of association between candidate proteins and tumorigenesis recorded. Following extensive research, four candidates were identified: nuclear factor, erythroid 2 like 2 (NFE2L2; also known as NRF-2), p53, nuclear factor kappa-light-chain-enhancer of activated B cells (NFκB) and Y-box binding protein 1 (YB-1).

P53 was discounted on account of its well-researched role in medulloblastoma, where patients with SHH tumours harbouring *TP53* mutations represent a very high risk subgroup (Ramaswamy et al., 2016; Zhukova et al., 2013). Indeed, *TP53*-mutant SHH medulloblastoma are frequently highly resistant to standard, high-intensity therapy, a factor largely attributed to disruption of p53-mediated apoptosis, although the relationship between p53 and *ABCB1* has also been studied (Bush & Li, 2002; Crowther et al., 2016). Likewise, NFκB signalling is thought to be implicated in medulloblastoma tumour growth (Spiller et al., 2011) and aberrant activation has

been widely reported to contribute to glioma and glioblastoma pathogenesis (Conti et al., 2018; Puliappadamba et al., 2013; Puliappadamba et al., 2014; Wang et al., 2004) with studies demonstrating a link between NFκB activation and the acquisition of radioresistance (Ahmed & Li, 2008). As a focus of this study was to identify novel regulators of chemoresistance in medulloblastoma, the widely researched role of NFκB in brain tumours including medulloblastoma led us to discount this protein.

Comparatively, although widely researched in cancer, both YB-1 and NFE2L2 appeared less frequently studied in medulloblastoma and indeed in brain tumours in general. Further to this, a number of studies show correlation between YB-1 and/or NFE2L2 expression and therapy resistance, tumour progression, metastasis and importantly *ABCB1* expression, suggesting that they may represent bona fide regulators of the *ABCB1* gene in medulloblastoma (Bargou et al., 1997; Lasham et al., 2013; Rojo de la Vega et al., 2018; Saji et al., 2003; Wang et al., 2014). Hence, YB-1 and NFE2L2 were selected to carry forward for initial analyses.

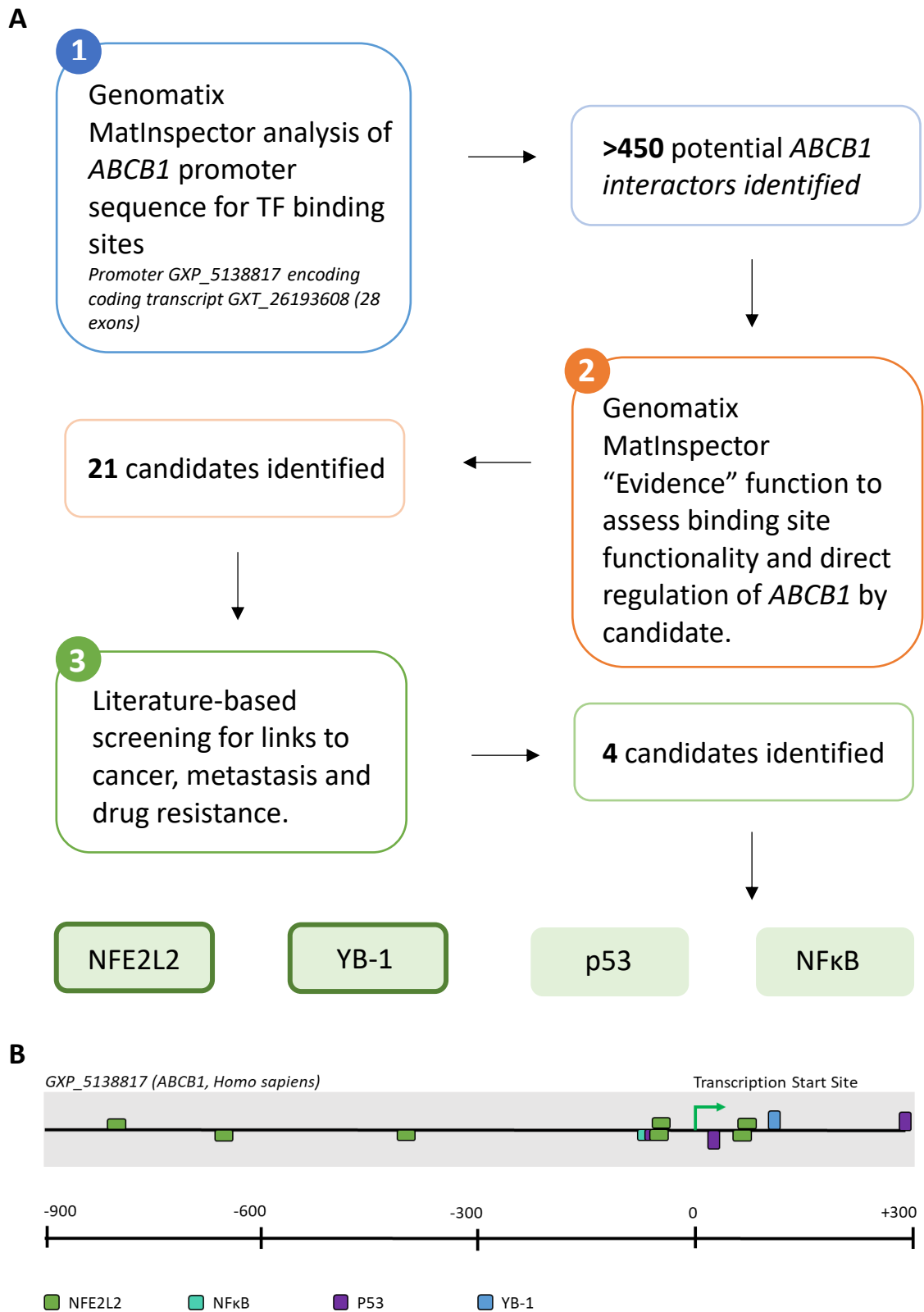


Figure 3.2 Identification of candidate regulators of the *ABCB1* promoter. Genomatix software was utilised to identify potential interactors of *ABCB1*. A) Workflow followed to identify candidate regulators of the *ABCB1* gene. NFE2L2, NFkB, p53 and YB-1 were identified as promising candidates. YB-1 and NFE2L2 were selected for further analysis. B) Position of candidate regulators at the *ABCB1* GXP_5138817 promoter with respect to the transcriptional start site (0).

3.2.1.2.1 Candidate binding sites in the *ABCB1* promoter

Genomatix MatInspector software identified the predicted YB-1 binding site at position +108 to +119 of the *ABCB1* GXP_5138817 input promoter sequence (Figure 3.2). The identified binding site (5' – CTGATTGGCTGGG – 3') was identified as a classic Y-Box of consensus sequence 5' – CTGATTGG(T/C)(T/C) – 3', containing an inverted CCAAT sequence (Table 3-1). It is the CCAAT/ATTGG pentanucleotide which is thought to be required for transcription factor binding and hence transcriptional activation (Dolfini & Mantovani, 2013).

MatInspector software identified five potential NFE2L2 binding sites within the *ABCB1* GXP_5138817 promoter. Of these five sites, two were identified near the transcription start site between positions -55 and +74 and are included in Table 3-1 for reference. The identified potential NFE2L2 binding sites were categorised as antioxidant response elements (ARE), also termed as electrophile response elements, the core motif of which was defined by MatInspector software as 5' – TGA CTCAGCA - 3', but is more commonly denoted as 5'-TGACNNNGC-3' (where N represents any nucleotide).

Table 3-1 YB-1 and NFE2L2 predicted binding sites in the *ABCB1* promoter

Protein	Binding Site Position(s)	Binding Site Sequence	Core Binding Motif	Effect
YB-1	+108 to +119	ctgatTGGCtgg	Y-Box consensus sequence: 5'-CTGATTGG(T/C)(T/C)-3'	Activating
NFE2L2	-55 to -31	gtcccaatgattCAGCt gatgcg	ARE consensus sequence: 5' – TGA CTCAGCA - 3	Activating
	+50 to +74	tttctcgaggaatcAGCAttcagtc		

Red font indicates highly conserved regions in the match and uppercase represents the “core” sequence used by MatInspector software.

3.3 Analysis of YB-1 and NFE2L2 expression across publicly available large-scale medulloblastoma datasets

3.3.1 *YBX1* and *NFE2L2* are highly expressed in paediatric brain tumours and across medulloblastoma subgroups

YB-1 (encoded for by the *YBX1* gene on chromosome 1p34.2) and NFE2L2 (encoded for by the *NFE2L2* gene on chromosome 2p31.2) have not been extensively studied in medulloblastoma. As such, we first wanted to assess candidate gene expression in medulloblastoma and study the association between gene expression and survival. First, *YBX1* and *NFE2L2* mRNA expression across large-scale publicly available patient datasets were analysed.

R2: Genomics Analysis and Visualisation Platform (<http://r2.amc.nl>) was used to assess *YBX1* and *NFE2L2* expression across a panel of the three most commonly occurring malignant paediatric brain tumours (Northcott et al., 2017; Pajtler et al., 2015; Paugh et al., 2010; Roth et al., 2006). *YBX1* expression was significantly elevated ($P < 0.0001$) in ependymoma, paediatric glioma (glioblastoma multiforme and high-grade glioma) and medulloblastoma when compared with normal cerebellum tissue (medulloblastoma) and normal brain tissue (prefrontal cortex; ependymoma and paediatric glioma; Figure 3.3 A). *YBX1* expression was also found to be significantly elevated in medulloblastoma compared with paediatric glioma ($P < 0.0001$). Analysis of *YBX1* expression across a human medulloblastoma cohort comprising over 200 samples revealed that *YBX1* expression was also elevated in all four molecular subgroups of medulloblastoma compared to normal cerebellum

controls. Differences in gene expression were tested by Brown-Forsythe and Welch ANOVA analysis and found to be significant ($P < 0.0001$; Figure 3.3 B). Interestingly, *YBX1* expression was most increased in Group 3 patients, a subgroup commonly associated with poor prognosis and a higher potential for metastatic dissemination. Indeed, Group 3 *YBX1* expression was found to be significantly higher than Group 4 *YBX1* expression ($P = 0.018$). Further analysis of *YBX1* expression across medulloblastoma subtypes is displayed in Appendix A1.

Likewise, *NFE2L2* expression was significantly elevated in ependymoma and paediatric glioma ($P < 0.0001$), as well as medulloblastoma ($P = 0.001$) when compared with normal tissue controls (Figure 3.4 A). *NFE2L2* expression was also found to be significantly higher in paediatric glioma than in medulloblastoma ($P < 0.0001$). Furthermore, *NFE2L2* expression was also found to be significantly elevated across WNT, SHH, Group 3 and Group 4 subgroups of medulloblastoma compared with normal cerebellum ($P = 0.0002, 0.0009, 0.0008$ and 0.0006 respectively; Figure 3.4 B). Further analysis of *YBX1* expression across medulloblastoma subtypes is displayed in Appendix A1.

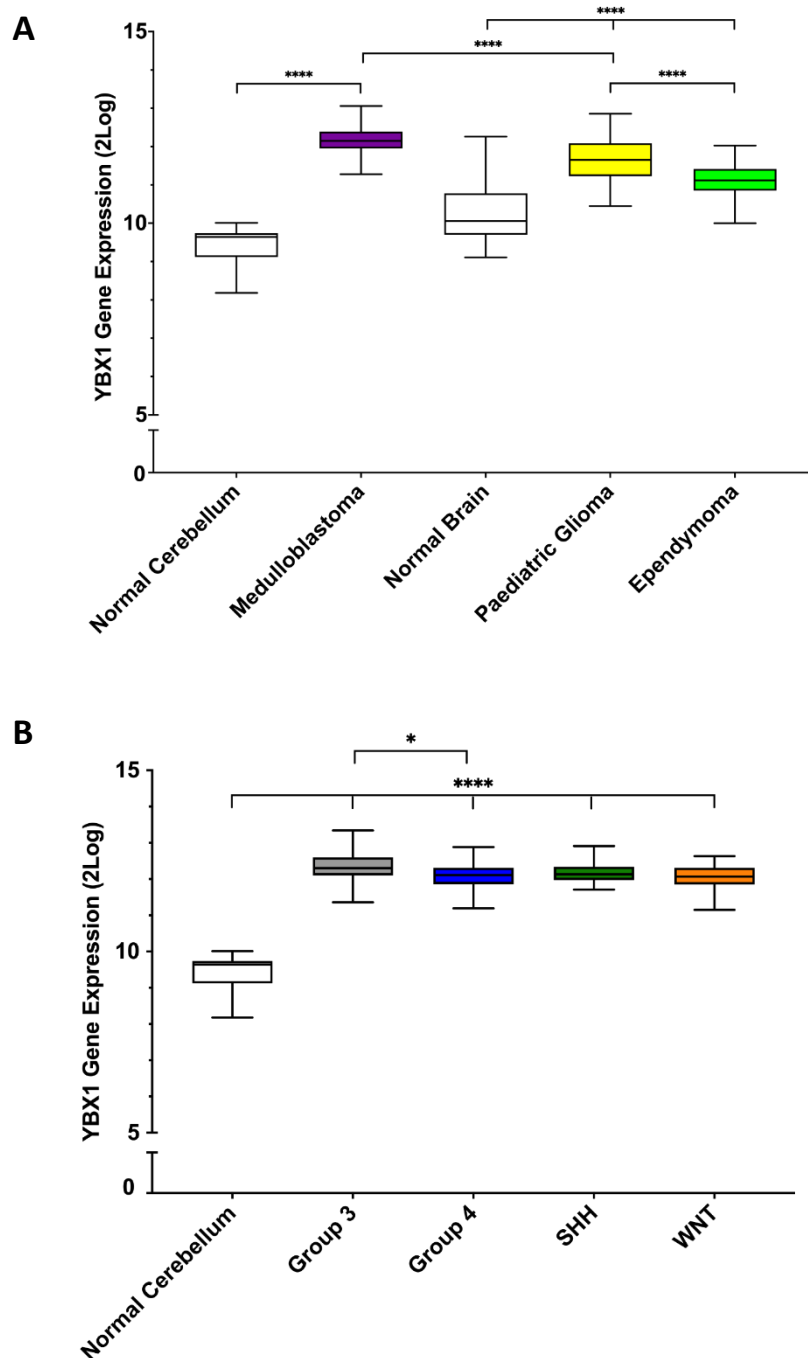


Figure 3.3 YBX1 expression is elevated in paediatric brain cancer and across all four subgroups of medulloblastoma. R2 Genomic Analysis was utilised to analyse differences in *YBX1* expression in paediatric brain cancers. A) *YBX1* expression levels are high in ependymoma, medulloblastoma and paediatric glioma compared to control tissue. Normal cerebellum (Roth dataset) n = 9; medulloblastoma (Pfister dataset) n = 223; normal brain (Harris dataset) n = 44; ependymoma (Pfister dataset) n = 209; paediatric glioma (Paugh dataset) n = 53. B) *YBX1* expression is elevated in all four medulloblastoma subgroups. Normal cerebellum (Roth dataset) n = 9; Group 3 n = 56, Group 4 n = 91 SHH, n = 59 WNT n = 17 (Pfister dataset). Expression displayed as box plots showing the sample minimum (lower line), lower quartile (bottom of box), median (line within box), upper quartile (top of box) and the sample maximum (upper line). *P < 0.05; ****P < 0.0001. Significance was assessed by Brown-Forsythe and Welch ANOVA analyses on account of unequal standard deviation with Dunnett's T3 multiple comparison test.

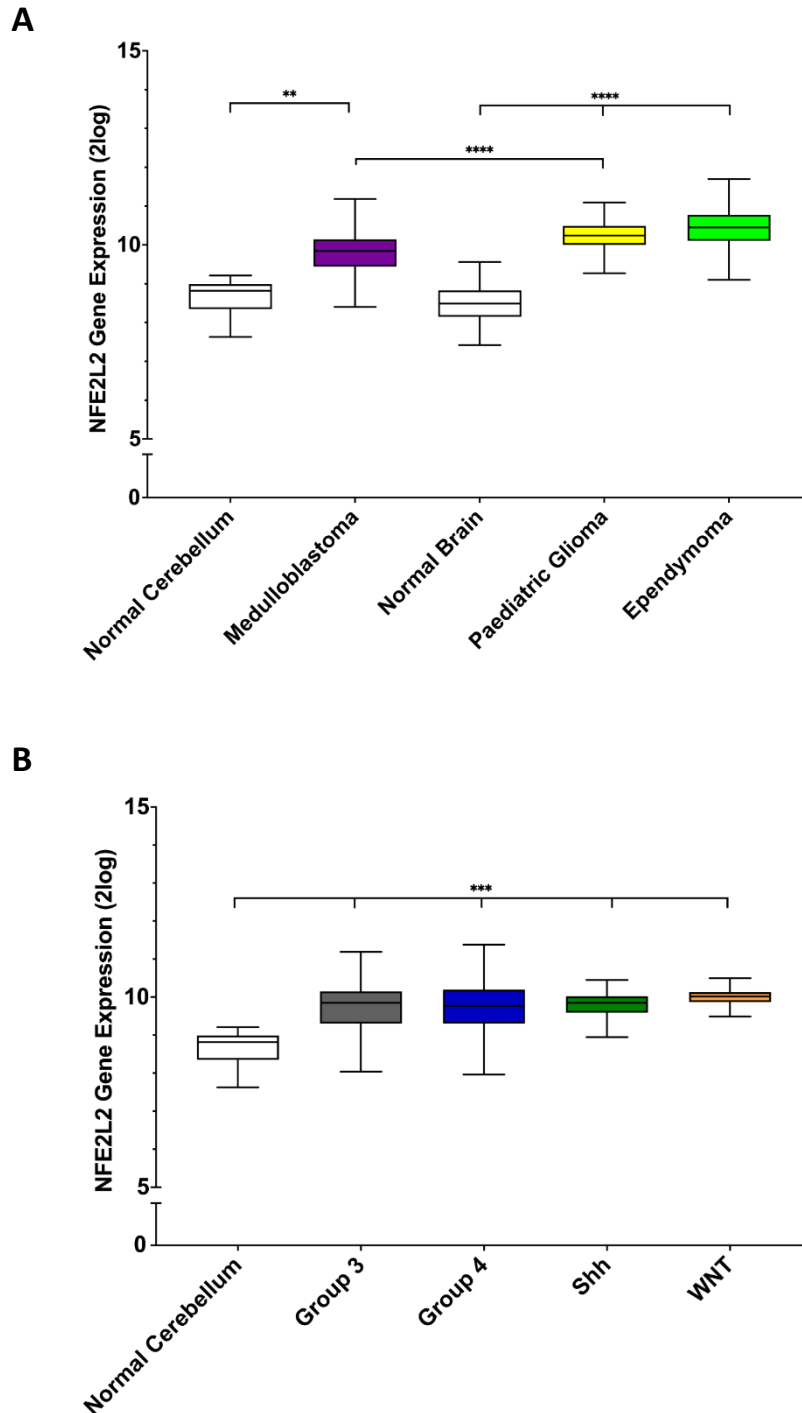


Figure 3.4 *NFE2L2* expression is elevated in paediatric brain cancer and across all four subgroups of medulloblastoma. R2 Genomic Analysis was utilised to analyse differences in *NFE2L2* expression in paediatric brain cancers. A) *NFE2L2* expression levels are high in ependymoma, medulloblastoma and paediatric glioma compared to control tissue. Normal cerebellum (Roth dataset) n = 9; medulloblastoma (Pfister dataset) n = 223; normal brain (Harris dataset) n = 44; ependymoma (Pfister dataset) n = 209; paediatric glioma (Paugh dataset) n = 53. B) *NFE2L2* expression is elevated in all four medulloblastoma subgroups. Normal cerebellum (Roth dataset) n = 9; Group 3 n = 56, Group 4 n = 91 SHH, n = 59 WNT n = 17 (Pfister dataset). **P < 0.01; ***P < 0.001; ****P < 0.0001. Significance was assessed by Brown-Forsythe and Welch ANOVA analyses with Dunnett's T3 multiple comparison test.

3.3.2 High *YBX1* expression correlates with poor overall survival and metastasis

Correlation between candidate gene expression and prognosis was then explored. The Cavalli dataset, obtained from R2: Genomics Analysis and Visualization Platform (<http://r2.amc.nl>), which comprises over 763 patient samples (of which 612 have survival data), was utilised to generate Kaplan-Meier survival curves (Cavalli et al., 2017). Patients with high expression levels of *YBX1* had significantly worse 5-year overall survival outcomes than those with low *YBX1* expression levels, suggesting that *YB-1* may represent a negative prognostic factor for overall survival in medulloblastoma patients ($P < 0.0001$; Figure 3.5 A). Separation by subgroup confirmed that this was maintained within Group 3, Group 4 and SHH patients, with high *YBX1* Group 3 and SHH patients presenting with the worst outcome ($P = 0.0159$ and < 0.0001 respectively; Figure 3.5 B). The same trend was not observed in WNT tumours alone, where no correlation between *YBX1* expression and survival was detected (Appendix A2). Comparatively, patients with elevated *NFE2L2* expression did not display significantly worse 5-year overall survival than patients with low *NFE2L2* expression (Figure 3.5 C). However, further division of patient data by molecular subgroup revealed that within Group 3, Group 4 and SHH groups, high *NFE2L2* does associate with significantly worse survival ($P = 0.0169$, 0.0315 and 0.0159 respectively; Figure 3.5 D). Like *YBX1*, *NFE2L2* did not associate with survival outcome in WNT medulloblastoma patients (Appendix A2). These findings clearly highlight the importance of considering the heterogeneity of medulloblastoma in analyses, rather than regarding the disease as a single entity.

In order to further measure the prognostic value of *YBX1*, various statistical methods were employed in order to determine the hazard ratio (HR) and 95% confidence interval (CI) between 5-year overall survival and *YBX1* expression. As displayed in Table 3-2, using data acquired from the Cavalli dataset and by way of the Mantel-Haenszel log-rank test, high *YBX1* expression was found to be significantly associated with a higher risk of death than low *YBX1* expression (HR = 1.42; 95% CI = 1.05 – 1.93; P = 0.024). A limiting factor of the Mantel-Haenszel log-rank test is the assumption that the risk of death is the same throughout the cohort. To account for confounding events, Cox's Proportional Hazard's Model (CPHM) was chosen. In addition to *YBX1* expression, continuous covariate age and categorical covariate metastatic status were included. The output of this multivariate model is displayed in Table 3-3. Compared with the Mantel-Haenszel log-rank model, the HR for *YBX1* expression increased from 1.42 to 1.47 following multivariate analysis (95% CI = 1.09 – 1.98; P = 0.012), demonstrating that after accounting for the confounding effect of age and metastatic status, the impact of *YBX1* expression on 5-year survival still holds. As such, *YBX1* expression can be considered an independent prognostic factor for 5-year overall survival.

The output also showed that the *YBX1*- and age-adjusted HR for metastatic status was just 1.072 and not significant. As metastatic disease represents a known risk factor in medulloblastoma, this result was unexpected. Analysis of Kaplan-Meier survival curves within this cohort using metastasis as a parameter revealed that the survival lines for M+ and M0 intersect (Appendix A3). This violates the assumption of proportional hazard rates which means that the CPHM will likely lose power,

indicating that a different statistical test would be better suited to assess the risk of metastatic status on survival probability within this cohort (Li et al., 2020). However, as the the variable metastatic status was only introduced to account for its confounding effect on the *YBX1*-survival relationship and censoring was independent of tested covariates in this cohort, it was accepted in this model.

Although both YB-1 and NFE2L2 represent potential *ABCB1* regulators and both display increased expression at an mRNA level in medulloblastoma when compared with control tissue, we wanted to select just one candidate transription factor for subsequent preliminary experiments. On account of the substantially elevated *YBX1* expression observed in medulloblastoma, together with the strong effect of *YBX1* level on patient outcome and status as an independent predictor of survival in medulloblastoma, it was decided that *YBX1* would be selected for further analyses.

Table 3-2 Output of the Mantel-Haenszel Log-rank Test for *YBX1* expression

Variable	HR	95% CI for HR		P Value
		Lower	Upper	
<i>YBX1</i> Expression (high/low)	1.42	1.05	1.93	0.02

An HR of 1.42 suggests that the rate of deaths in the high *YBX1* expression group is 1.42 times the rate in the low *YBX1* expression group. HR = hazard ratio. CI = confidence interval.

Table 3-3 Output of the Cox's Proportional Hazard's Model for *YBX1* expression, age and metastatic status

Variable	HR	95% CI for HR		P Value
		Lower	Upper	
<i>YBX1</i> Expression (high/low)	1.47	1.09	1.98	0.01
Age (continuous)	0.99	0.97	1.00	0.05
Metastatic Stage (M+/M0)	1.07	0.84	1.36	0.57

An HR of 1.47 suggests that the rate of deaths in the high *YBX1* expression group is 1.47 times the rate in the low *YBX1* expression group after adjustments for age and metastatic status.

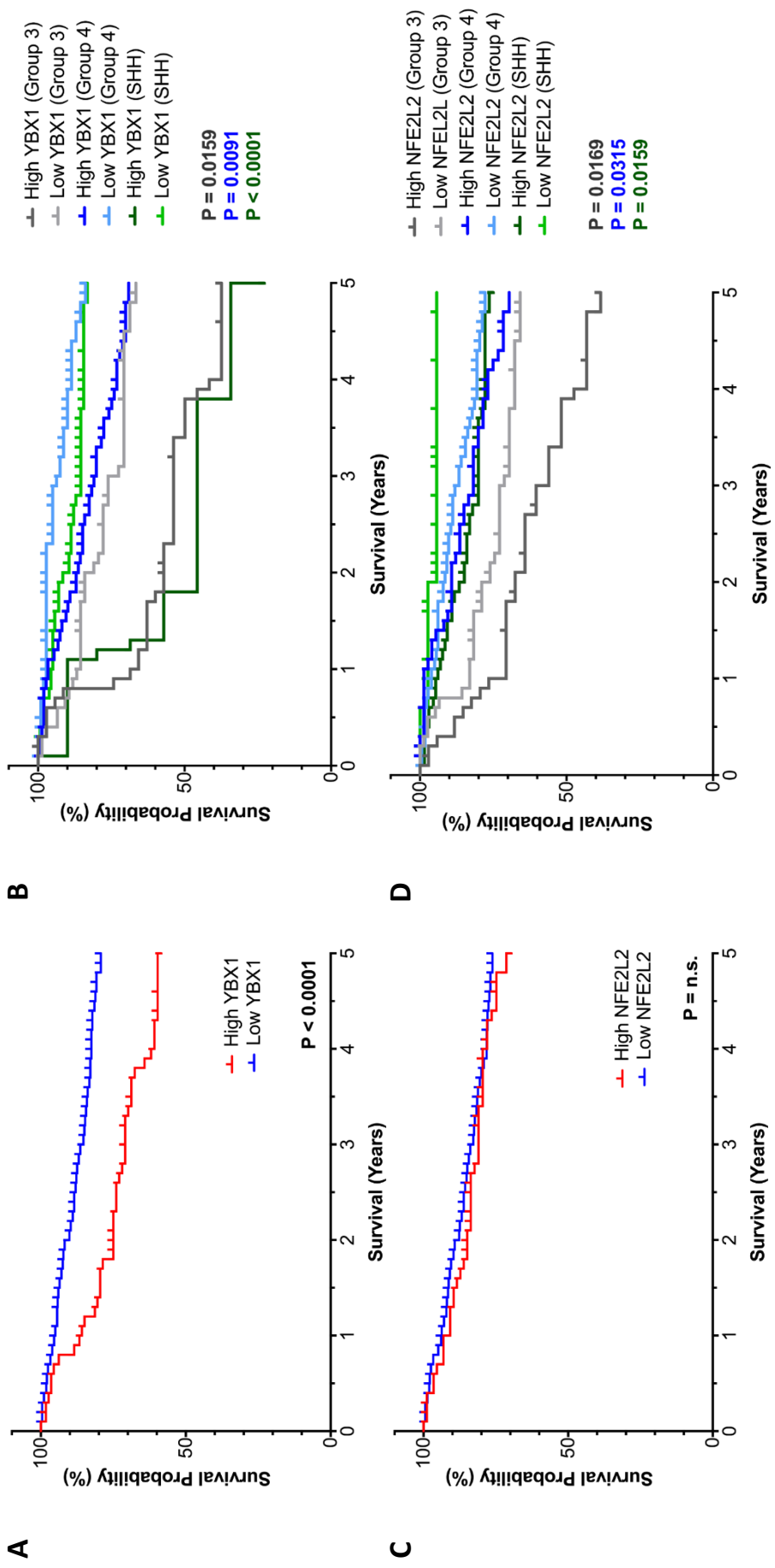
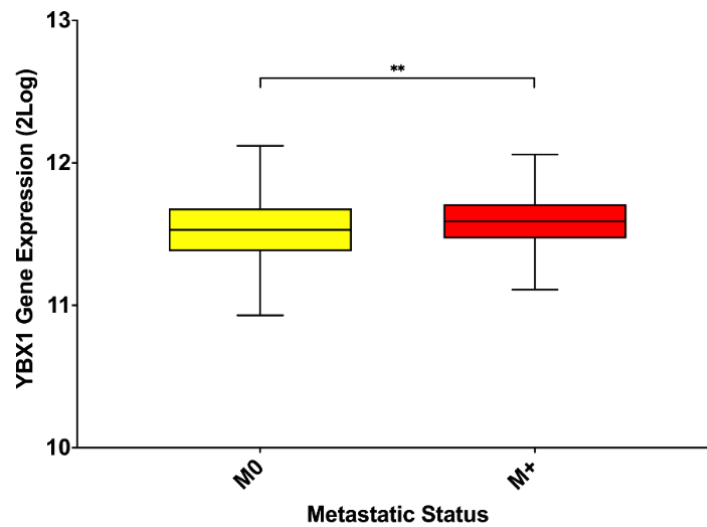


Figure 3.5 YBX1 expression correlates with poor survival in medulloblastoma. R2 genomics analysis was employed to explore correlation between YBX1/NFE2L2 expression and survival. A) Kaplan Meier analysis showed high YBX1 expression (red line) is associated with poor 5 year overall survival probability in patients with medulloblastoma over 5 years ($P < 0.0001$). B) Assessment of survival across subgroups revealed that survival is worst in SHH and Group 3 patients with high YBX1 expression ($P < 0.0001$ and $P = 0.0159$ respectively). C) NFE2L2 expression shows no correlation with overall survival probability over 5 years ($P = 0.0530$). D) Assessment of survival across subgroups revealed that survival is worst in Group 3 patients with high YBX1 expression ($P = 0.0169$). N = 612 (Cavalli dataset); Group 3 N = 144, Group 4 = 326, SHH = 223. Survival curves compared using the Log-rank (Mantel-Cox) test.

To further elucidate the association between *YBX1* expression and various aspects of medulloblastoma disease progression, *YBX1* expression was assessed in metastatic patients obtained from the Cavalli dataset (Cavalli et al., 2017). *YBX1* expression was found to be significantly higher in metastatic (M+) patients than non-metastatic (M0) patients ($P = 0.0077$; Figure 3.6 A). To explore the association between *YBX1* expression and metastasis further, expression was then analysed in matched primary and metastatic tumours using the Wang dataset (Appendix A4), obtained from the R2 database, which encompasses gene expression data for matched samples from 9 patients (Wang et al., 2015). Although statistical analysis could not be conducted on these samples, 7 out of 9 matched pairs displayed an increase in *YBX1* mRNA expression in the metastatic tumour(s) compared to the primary tumour (Figure 3.6 B). Interestingly, one of the patients that did not follow this trend (Patient 4), did display increased *YBX1* expression in the third metastasis (Mc), however not in the first metastatic tumour (Ma) or the second (Mb), in which *YBX1* expression was decreased.

A



B

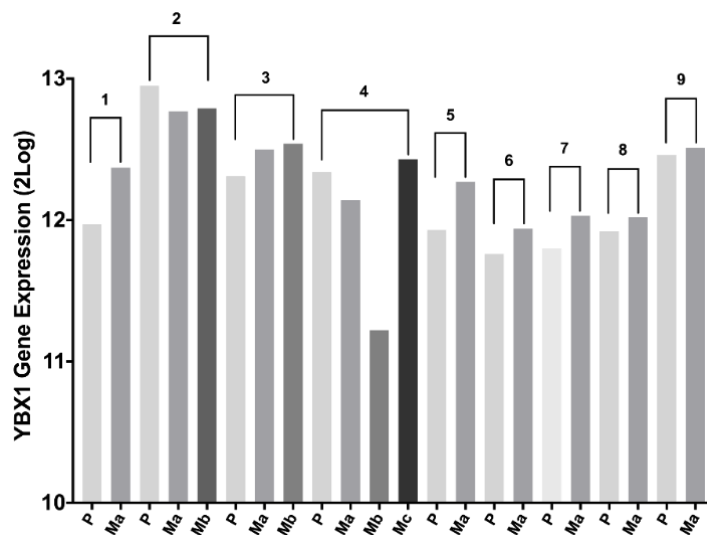


Figure 3.6 YBX1 gene expression is elevated in metastatic tumours. A) YBX1 gene expression was found to be significantly higher in metastatic tumours (M+; n = 176) compared to non-metastatic tumours (M0; n = 397). Cavalli dataset; **P < 0.01. Significance analysed by unpaired t-test with Welch's correction. B) YBX1 expression was frequently elevated in metastatic tumours when compared with the appropriate primary pair. N = 22 (Wang dataset). P represents primary tumour and Ma/b/c represent first/second/third metastases. Brackets define the samples attributed to each patient.

3.4 Analysis of YB-1 expression in a medulloblastoma cell line model

3.4.1 YB-1 is expressed across various medulloblastoma cell lines

Data obtained from the aforementioned genomic analysis showed *YBX1* to be highly expressed across large medulloblastoma patient cohorts and suggested it may represent a poor prognosis factor in medulloblastoma. In order to investigate this, it would be important to ensure that the medulloblastoma cell lines available represented an appropriate model for further study.

YBX1 expression across a range of medulloblastoma cell lines was analysed by qRT-PCR. Malignant glioma cell line U87 was utilised as a positive control, as confirmed by Protein Atlas online software (<http://www.proteinatlas.org>; (Uhlén et al., 2015)). At an mRNA level, *YBX1* was found to be expressed in all medulloblastoma cell lines analysed (Figure 3.7 A). Interestingly, expression was found to be highest in Group 3 and Group 4 cell lines. Both D283 and CHLA-01 lines were found to express significantly higher *YBX1* than DAOY and ONS-76 ($P = 0.025$ and 0.010) and DAOY, ONS-76, UW-228-3 and HDMB-03 ($P = 0.0091$, 0.0036 , 0.025 and 0.026) respectively.

Likewise, analysis of expression at a protein level yielded similar results, with YB-1 expressed across all medulloblastoma cell lines, again with expression highest in Group 3 and 4 cell lines (Figure 3.7 B-C). YB-1 protein expression was found to be significantly higher in D283 cells than SHH cell lines DAOY and UW-228-3 ($P = 0.033$ and 0.037). Surprisingly, YB-1 protein expression in HDMB-03 appeared markedly higher than *YBX1* expression detected at an mRNA level, perhaps indicative of differences in the translational regulation of YB-1 in this cell line.

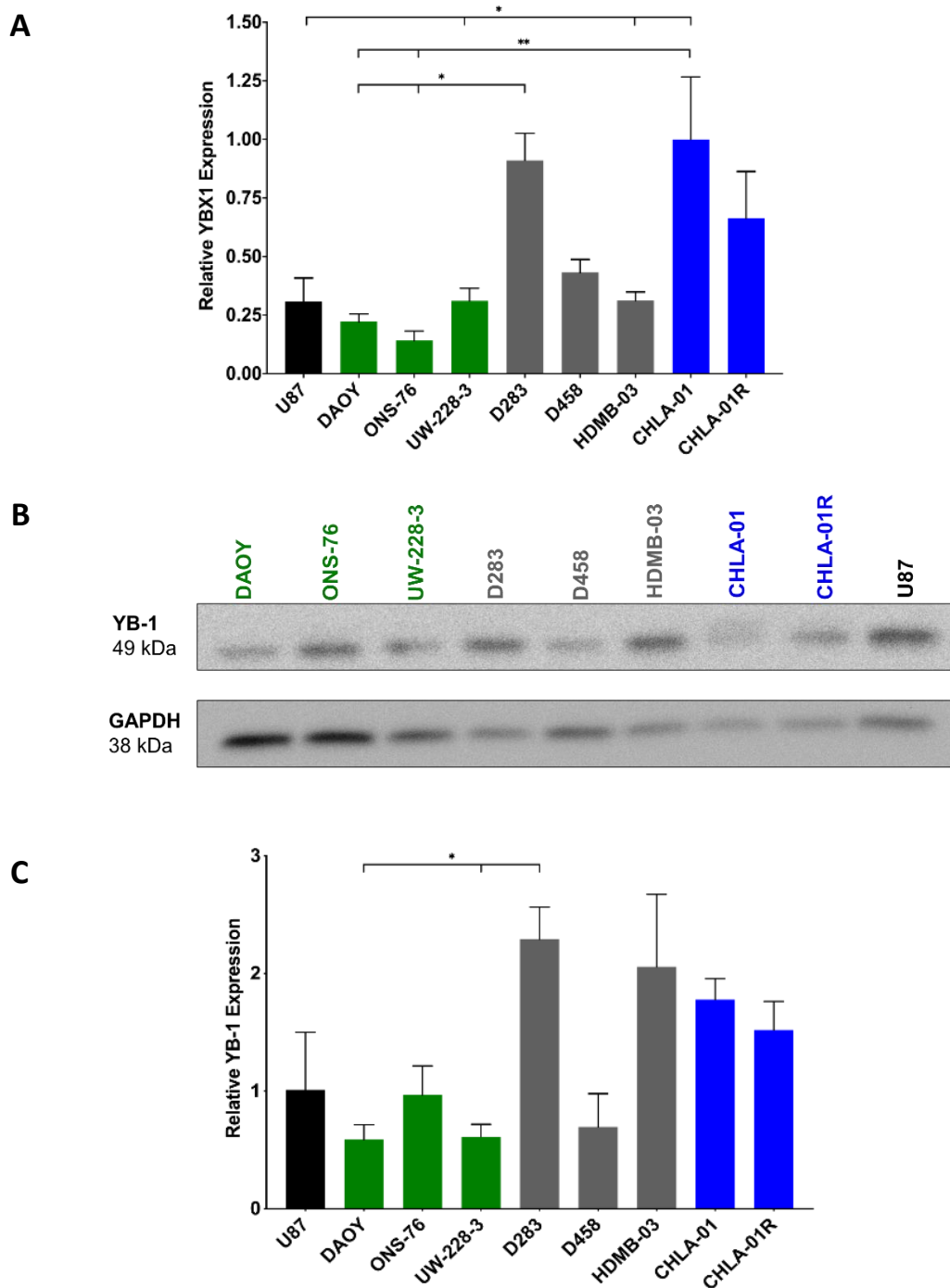


Figure 3.7 YBX1 and YB-1 are expressed in a range of medulloblastoma cell lines. A) Analysis of *YBX1* expression by qRT-PCR demonstrated that *YBX1* was expressed across all available medulloblastoma cell lines, with expression highest in Group 3 (grey) and Group 4 (blue) subgroups and lowest in SHH (green) subgroups. U87 glioblastoma cells were used as a positive control. Gene expression was calculated relative to housekeeping gene *GAPDH*. B) A representative western blot for total YB-1 expression. GAPDH served as a loading control. C) Densitometry analysis of YB-1 protein expression relative to GAPDH expression revealed that YB-1 was expressed in all medulloblastoma cell lines examined, with expression highest in Group 3 (grey) and Group 4 (blue) cell lines. Mean \pm SEM plotted; $n = 3$; * $P < 0.05$, ** $P < 0.01$. Significance was assessed by ordinary one-way ANOVA analyses with Tukey's multiple comparisons test. Full length western blots are presented in Appendix A4.

3.4.2 YB-1 localises predominantly to the cytoplasm in medulloblastoma cell lines

In Section 3.4.1, we showed that our cell lines exhibit high YB-1 and *YBX1* expression and hence represent an appropriate model to study YB-1. Previous research by other groups has suggested that YB-1 is localised to the cytoplasm in untreated cancer cell lines (Fujita et al., 2005). In order to inform future experiments, we wanted to analyse whether this was also true for medulloblastoma cell lines. SHH cell line DAOY and Group 3 cell lines HDMB-03, D458 and D283 were plated in chamber slides and immunostained for YB-1 when cells had reached approximately 70% confluency (Figure 3.8). As anticipated from RNA and protein expression analysis, all imaged cells were YB-1 positive. Furthermore, in all cell lines analysed, YB-1 was predominately cytoplasmic, although low level nuclear YB-1 staining was visible (as demonstrated in magnified cytoplasmic-nuclear-cytoplasmic cross-sections in Figure 3.8), consistent with the transcription factor/DNA repair functionality possessed by YB-1. The specificity of the YB-1 antibody, utilised in this report for western blot, immunofluorescence and immunohistochemistry methods, has been previously confirmed in medulloblastoma cells by way of peptide competition (Dey et al., 2016).

Immunofluorescence analysis also revealed clear differences in SHH and Group 3 cell line morphology. DAOY cells were visibly larger in diameter than the Group 3 cell lines imaged, with a greater cytoplasmic:nuclear ratio. Comparatively, HDMB-03, D283 and D458 possessed minimal cytoplasm and hence a smaller cytoplasmic:nuclear ratio, in accordance with the semi-adherent growth of these cell lines and also the large cell/anaplastic (LC/A) histological phenotype (Section 1.2.1.3) frequently observed in Group 3 tumours.

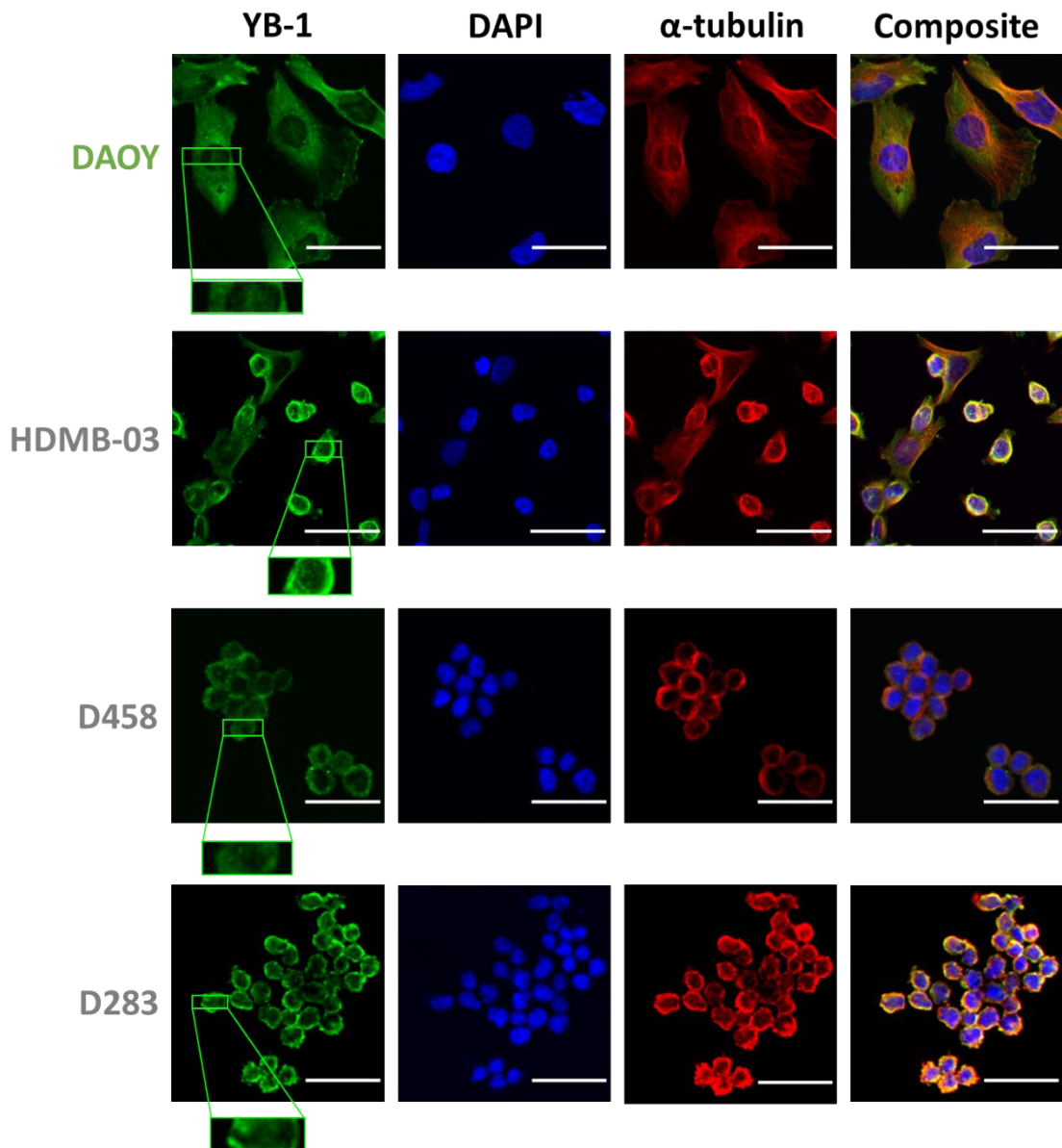


Figure 3.8 YB-1 localises mainly to the cytoplasm in untreated medulloblastoma cell lines. Immunofluorescence was employed to investigate YB-1 localisation in untreated medulloblastoma cell lines. Although nuclear YB-1 was visible in all cell lines analysed (as displayed in green magnified cross-sections), the majority of YB-1 was found localised to the cytoplasm. Cells were fixed and immunostained for YB-1 (green) and α -tubulin (red). DAPI (blue) was used to identify cell nuclei. All images are displayed as z-projections of cell mid-sections and all scale bars represent 50 μ m. Representative images shown; n = 3.

3.5 Investigation of YB-1 expression and localisation across patient medulloblastoma tumour microarrays

In order to analyse YB-1 expression and localisation in clinical samples, YB-1 protein expression was assessed on two patient tissue microarrays (TMAs). The first had been prepared from a retrospective cohort of 20 paediatric medulloblastoma patient samples diagnosed in Nottingham between 1985 and 2007 with a median age at diagnosis of 7.2 years. The second had been prepared from a retrospective cohort of 68 paediatric medulloblastoma patient samples diagnosed in Birmingham between 2004 and 2016 with a median age at diagnosis of 6 years (Section 2.3). In both cohorts, patients received non-standardised treatments and a number of patients had extremely limited clinical and survival data. All existing clinicopathological data has been previously published (Nasir et al., 2021; Othman et al., 2014). For both TMAs, three cores for each patient were analysed by immunohistochemistry (IHC) for YB-1. Prior to IHC of TMAs, the YB-1 antibody was optimised extensively on paediatric brain and small intestine formalin fixed paraffin embedded tissue (FFPE) slides to avoid wasting precious TMA samples (Appendix A5).

A total of 88 patient samples were stained by IHC. Out of the 87 patient samples successfully stained, a number of cores were depleted in both the Nottingham and Birmingham TMAs to an extent that they could not be scored. Of particular note, three patient samples had all three cores too depleted to accurately score. One of these patient sample sets was represented in duplicate and hence could still be scored, however the remaining two patients were removed from analysis.

Accordingly, 85 out of the total stained 87 samples, corresponding to 80 patients, were deemed adequate to score fairly.

In order to minimise issues arising from bias and inter-observer variation, samples were scored by automated IHC image analysis using ImageJ plugin IHC Profiler (Section 2.9.9). Prior to analysis commencement, a small scale test was undertaken to certify automated analysis results were comparable to manual analysis, hence ensuring reliability and confidence in the method (data not shown). The IHC Profiler software uses a spectral deconvolution method of DAB/hematoxylin colour spectra to assign a score to describe the level of nuclear and cytoplasmic staining in each core, which in this study ranged from 0 to 3. Each core was then averaged to reveal a final nuclear and cytoplasmic score, which were combined to give an overall score for that patient. The frequency of each score was plotted as a histogram and distribution and modality assessed (Appendix A6). Numerical scores were then used to assign the samples to high positive expression (upper 50th percentile) or low positive expression (lower 50th percentile) groups, with YB-1 negative samples (scoring 0) assigned to a third, YB-1 negative group.

Image analysis revealed that 98% of cores were positive for YB-1 expression. Tumour samples did, however, show different degrees of staining. The variances between low positive and high positive staining are displayed in Figure 3.9.

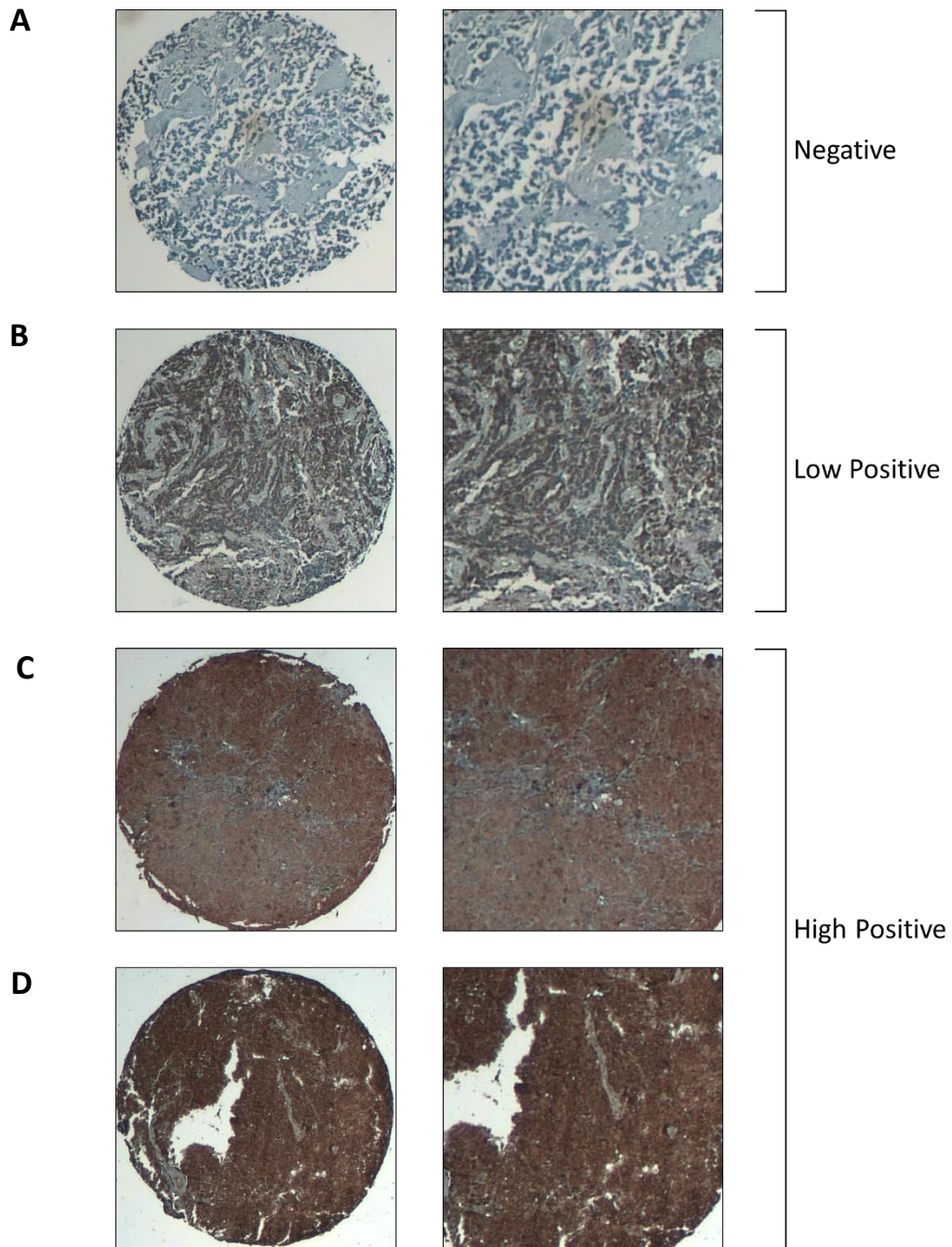


Figure 3.9 Medulloblastoma patient TMA display differential YB-1 protein expression. Samples were immunostained for YB-1 and scored automatically by way of the ImageJ IHC Profiler plugin resulting in a numerical score for each patient. An average was then taken for each patient and a final overall score calculated which was described as negative (A; no staining), low positive (B; staining intensity below the median score of 1.5 recorded across patients) or high positive (C and D; staining intensity above the median score of 1.5 recorded across patients). Representative images shown.

3.5.1 The majority of medulloblastoma patients exhibit high YB-1 protein levels and significant YB-1 nuclear accumulation.

Automated immunohistochemical analysis of overall YB-1 expression in patient TMAs revealed that 53% of patients exhibited low positive YB-1 expression (lower 50th percentile; scoring < 1.5), while 45% patients exhibited high positive YB-1 expression (upper 50th percentile; scoring > 1.5; Figure 3.10 B).

51 out of 80 patients had complete subgroup data, the Kaplan-Meier survival analysis of which can be found in Appendix A7. Unfortunately, this data did not include the two YB-1 negative patients. Notably, Group 3 patients displayed the greatest levels of overall YB-1 staining intensity, with 63% of samples scored as high positive, however this relationship was not found to be statistically significant (Figure 3.10 A and C). SHH patients exhibited equal levels of low positive and high positive YB-1 expression, while WNT and Group 4 patients both exhibited a smaller proportion of patients with high positive staining (43% and 33%, respectively) than patients with low positive staining (Figure 3.10 D – F). This observation is supported by R2: Genomics Analysis *YBX1* expression data (Figure 3.3), where Group 3 patients also exhibited the highest levels of *YBX1* expression.

As previously described (Section 2.9.9), both nuclear and cytoplasmic YB-1 staining was quantified during image analysis (Figure 3.11 A – B). The majority of cores exhibited cytoplasmic staining, as anticipated on account of the known cytoplasmic roles of YB-1 protein. However, automated scoring of nuclear YB-1 staining intensity also revealed that 98% of patients exhibited YB-1 nuclear expression, with 38% of

patients exhibiting high positive nuclear expression (Figure 3.11 C), indicative of elevated YB-1 nuclear activity in these patients. This observation is at difference with our previous immunofluorescence data (Figure 3.8) where YB-1 staining in untreated medulloblastoma cell lines revealed visible, but minimal YB-1 nuclear staining, a finding which perhaps highlights some of the differences between established cell lines and heterogeneous patient samples.

A

		Subgroup				Chi-Square Test
		Group 3	Group 4	SHH	WNT	
Total No. Patients		8	24	12	7	P = 0.50
Low Positive YB-1	No. Patients	3 (37%)	16 (67%)	6 (50%)	4 (57%)	
High Positive YB-1	No. Patients	5 (63%)	8 (33%)	6 (50%)	3 (43%)	

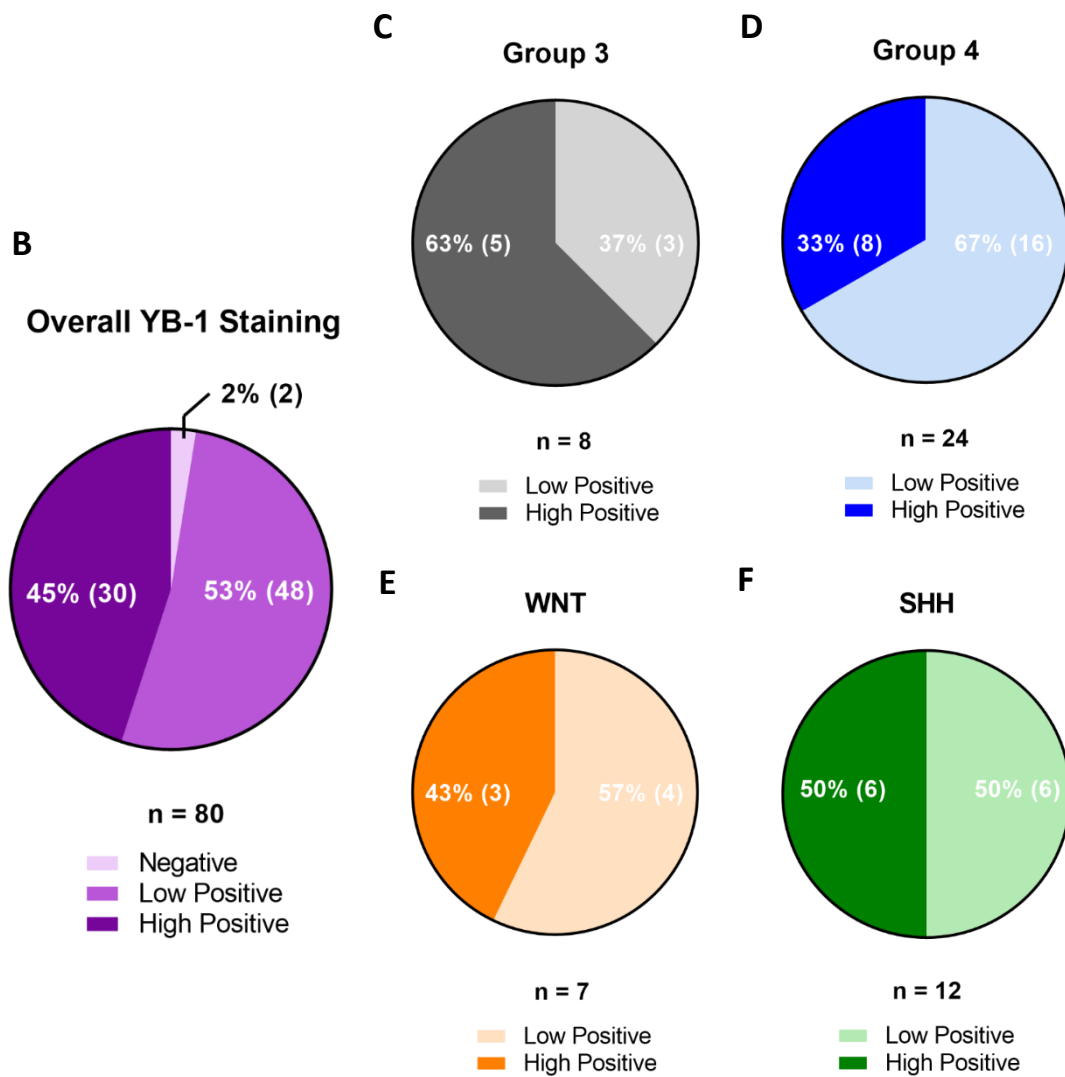


Figure 3.10 YB-1 is expressed in medulloblastoma patient tissue samples. A) A Chi-Square test revealed no association between YB-1 expression and molecular subgroup within a cohort of 51 medulloblastoma patients. B) Immunohistochemical analysis of YB-1 expression in patient TMAs revealed high positive (scoring > 1.5) YB-1 staining in 45% of patients and low positive (scoring < 1.5) YB-1 staining in 53% patients. 2% of patients were negative for YB-1 expression (n = 80). C) The majority of Group 3 patients displayed high positive YB-1 staining (63%; n = 8). D) The majority of Group 4 patients displayed low positive YB-1 staining (67%; n = 24). E) An equal proportion of SHH patients displayed high positive and positive staining (50%; n = 12). F) The majority of WNT patients displayed low positive YB-1 staining (57%; n = 7).

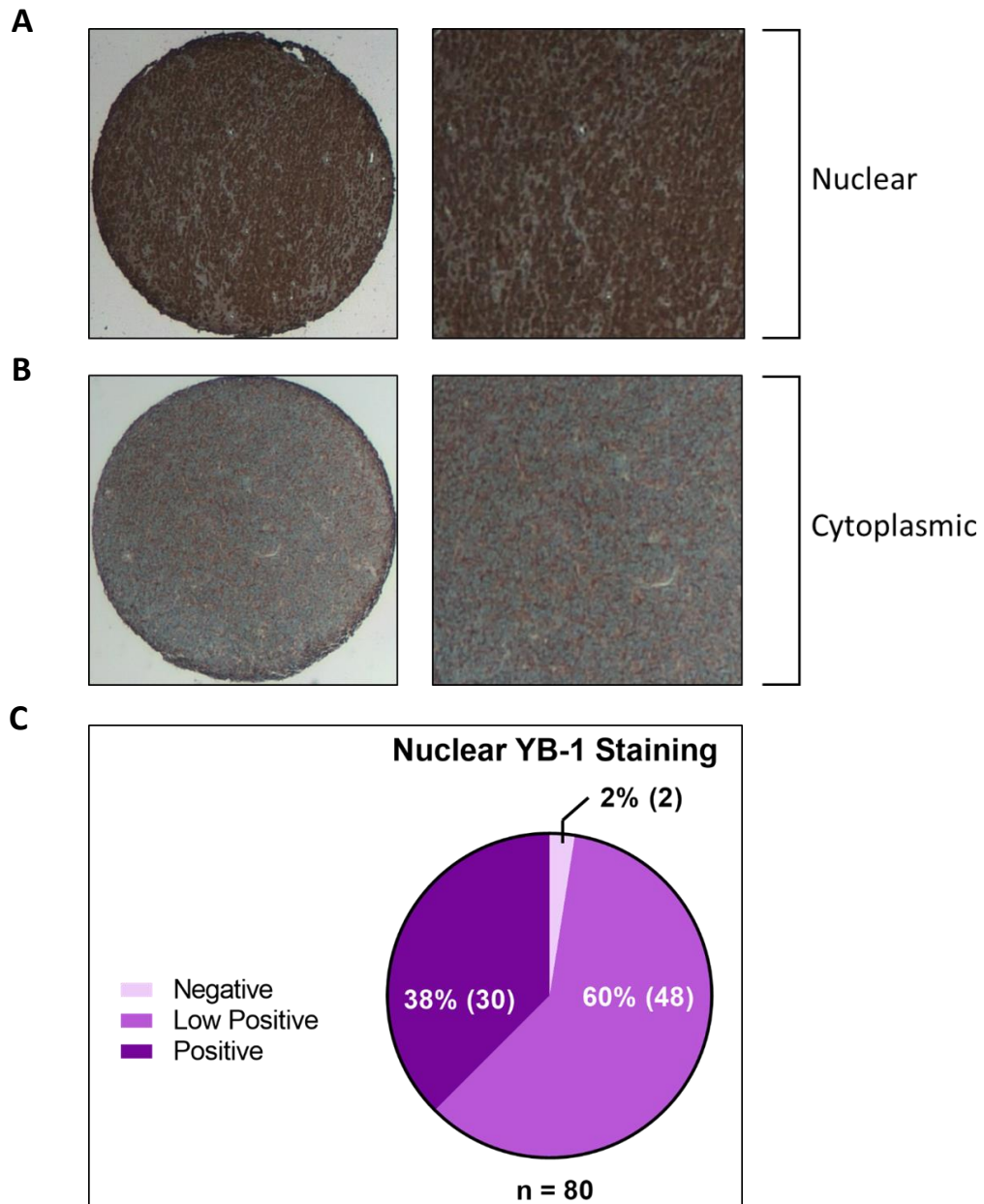


Figure 3.11 Medulloblastoma patients display significant YB-1 nuclear accumulation. A) Representative core demonstrating predominantly nuclear YB-1 expression. B) Representative core demonstrating predominantly cytoplasmic YB-1 staining. Almost all cores exhibited both staining patterns, although one pattern was occasionally more dominant than the other. C) Immunohistochemical analysis revealed nuclear staining in 98% of patients, with 38% patients displaying high positive (upper percentile; scoring > 1) YB-1 nuclear staining.

3.5.2 YB-1 expression does not appear to correlate with metastatic status at time of diagnosis in medulloblastoma

Metastatic status was known for 69 out of 80 samples scored for YB-1 expression. Analysis revealed that 62% of patients with high positive YB-1 expression were metastatic (M+) at diagnosis. Contrastingly, the majority (58%) of non-metastatic (M0) patients displayed low positive YB-1 expression. Despite of this, assessment with Pearson’s Exact Test did not detect non-random association between YB-1 expression and metastasis at diagnosis (P = 0.14; Table 3-4). However, it must be noted that although no significant correlation was found, these results do not discount a role for YB-1 in medulloblastoma metastatic dissemination. In this case, high YB-1 expression would likely precede the establishment of a metastatic site and hence the detection of a metastasis and thus would be challenging to analyse fully in a retrospective cohort such as this.

Table 3-4 YB-1 expression does not associate with metastatic status in medulloblastoma patients

		Metastatic Status		Fisher’s Exact Test
		M+	M0	
Total No. Patients		26	43	P = 0.14
Low Positive YB-1	No. Patients	10 (38%)	25 (58%)	
High Positive YB-1	No. Patients	16 (62%)	18 (42%)	

YB-1 overall expression was correlated with metastatic status. A Fisher’s Exact Test was used to assess non-random association between variables.

3.6 Summary

- Bioinformatic analysis of the *ABCB1* promoter by way of transcription factor binding site software Genomatix MatInspector revealed numerous candidate regulators of the *ABCB1* gene.
 - Extensive screening for functional-/literature-based evidence identified YB-1 and NFE2L2 as targets for further study.
- Investigation of *YBX1* and *NFE2L2* expression across large-scale medulloblastoma gene expression patient datasets demonstrated elevated candidate expression across all four medulloblastoma subgroups compared to normal cerebellar controls.
- High *YBX1* expression correlated with poor overall survival and was found to represent an independent indicator of 5-year overall survival. Accordingly, *YBX1* was selected for further analyses.
- Through analysis by qRT-PCR and immunoblotting, *YBX1*/YB-1 was found to be expressed across various medulloblastoma cell lines, with expression highest in Group 3 and 4 classified cell lines.
- Immunofluorescence revealed that YB-1 is predominantly localised in the cytoplasm in untreated SHH and Group 3 cell lines *in vitro*.
- Immunohistochemical analysis of Nottingham and Birmingham medulloblastoma TMAs revealed that patients exhibit YB-1 protein across all molecular subgroups and display significant YB-1 nuclear accumulation; a particularly important observation given the well documented association between nuclear YB-1 expression and drug resistance/cancer cell progression.

Chapter 4

Examination of YB-1 as a regulator of *ABCB1* in medulloblastoma

Chapter 4 Examination of YB-1 as a regulator of *ABCB1* in medulloblastoma

4.1 Introduction

In Chapter 3, YB-1 was identified as a potential transcriptional regulator of the *ABCB1* gene and shown to be highly expressed across medulloblastoma patient datasets and cell lines at protein and mRNA level. High YB-1 nuclear expression was also detected within two medulloblastoma TMA patient cohorts. In other cancers, YB-1 overexpression, and specifically nuclear expression, strongly correlates with disease progression, poor prognosis and metastatic potential (Lasham et al., 2013; Shibahara et al., 2001; Y. Wang et al., 2015). Crucially, nuclear YB-1 also plays a pivotal role in the acquisition of drug resistance, both via increased expression of a drug efflux-related gene *ABCB1* (Giménez-Bonafé et al., 2004), promotion of DNA repair mechanisms (Gaudreault et al., 2004) and the regulation of apoptotic response-related genes (Kloetgen et al., 2020). Indeed, in GBM patient-derived brain tumour-initiating cells (BTIC), YB-1 is localised to the nucleus in temozolomide-resistant lines, whereas it is predominately located in the cytoplasm in temozolomide-sensitive lines. Likewise, studies in other cancer cell lines have suggested that exposure to certain chemotherapeutics promotes YB-1 nuclear translocation (Fujita et al., 2005; Ohga et al., 1998), thus facilitating the oncogenic functions of YB-1.

Taken together, these data indicate that cancer cells may elevate nuclear YB-1 expression and/or promote nuclear YB-1 translocation as a protective measure in

response to extracellular stress. This led us to hypothesise that in medulloblastoma, nuclear YB-1 may also act as a regulator of chemoresistance and tumour progression.

Accordingly, the aims of this chapter were as follows:

- A) Investigate whether the YB-1 transcription factor represents a regulator of the *ABCB1* gene in medulloblastoma, by way of chromatin immunoprecipitation (ChIP) assays in Group 3 medulloblastoma cell lines.
- B) Analyse the effect of exposure to standard medulloblastoma chemotherapeutics cisplatin and vincristine on YB-1 expression and subcellular localisation in medulloblastoma cell lines.

4.2 Examination of the YB-1-*ABCB1* functional interaction

4.2.1 *ABCB1* expression is highest amongst SHH and Group 3 cell lines

We first wanted to assess *ABCB1* mRNA expression across a panel of un-treated medulloblastoma cell lines. This would allow us both to build a general picture of *ABCB1* expression across medulloblastoma subgroups *in vitro* and to ensure available cell lines would be suitable for downstream CHIP analysis (Figure 4.1). *ABCB1* expression was found to be highest in SHH cell lines DAOY and ONS-76 and was absent in SHH cell line UW-288-3. Indeed, ONS-76 was found to express significantly higher *ABCB1* than UW-288-3, D283, D458, HDMB-03 and CHLA-01 (P = 0.038; 0.043; 0.047; 0.0421 and 0.039 respectively). Comparatively, *ABCB1* was moderately expressed in Group 3 cell lines D283, D458 and HDMB-03, whilst expression was lowest in Group 4 cell lines CHLA-01 and CHLA-01R.

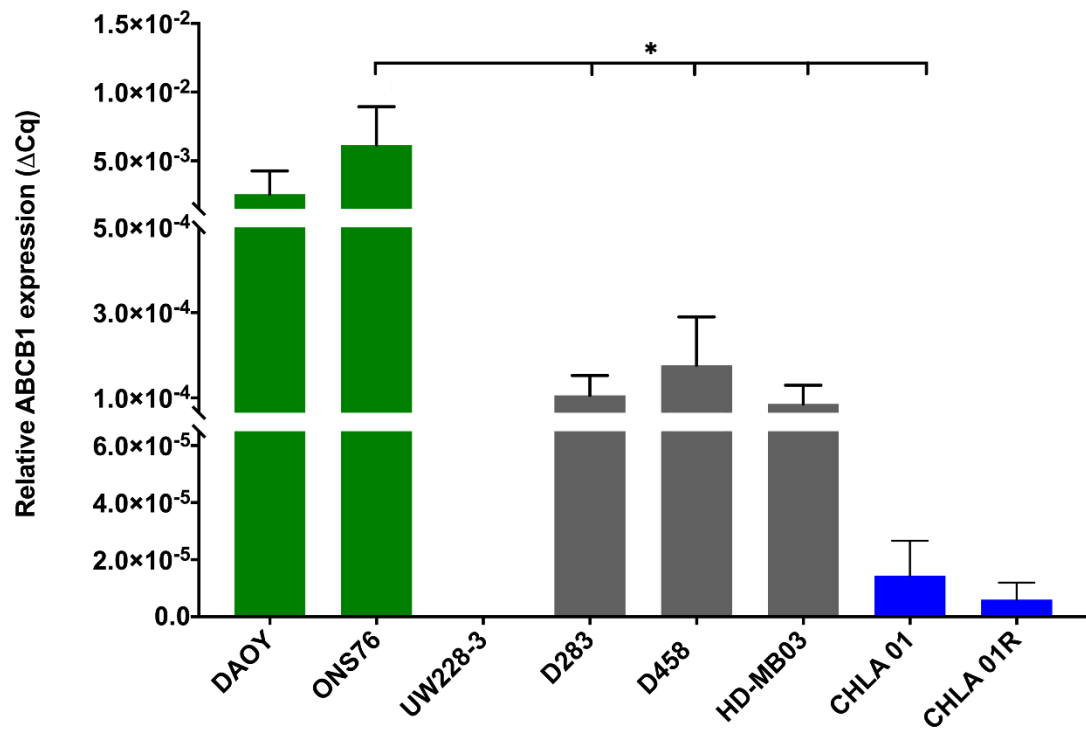


Figure 4.1 *ABCB1* expression is highest in SHH cell lines. Analysis of *ABCB1* expression by qRT-PCR demonstrated that *ABCB1* was expressed across all available medulloblastoma cell lines apart from UW-228-3, with expression highest in SHH (green) and Group 3 (grey) sub-groups and lowest in Group 4 (blue) subgroups. Relative *ABCB1* expression ($2^{-\Delta Cq}$) was calculated with respect to housekeeping gene *GAPDH*. $n = 3$; Mean \pm SEM; * $P < 0.05$. Significance was calculated by ordinary one-way ANOVA analysis with Tukey's multiple comparisons test.

4.2.2 YB-1 interacts directly with an inverted CCAAT box in the *ABCB1* promoter

In Chapter 3, it was observed that YB-1 expression was frequently elevated in Group 3 patients, both at mRNA level across large-scale patient datasets, and at protein level across TMA patient cohorts. Likewise, YB-1/*YBX1* expression was also high in Group 3 cell lines. This, in combination with the fact that Group 3 tumours are associated with the worst survival outcomes of any subgroup and are frequently metastatic at diagnosis (Juraschka & Taylor, 2019), led us to focus mainly on Group 3 cell lines for subsequent experiments.

Previously, Genomatix MatInspector software predicted that YB-1 binds to a Y-Box present at position +108 to +119 of the *ABCB1* promoter (Section 3.2.1.2.1). It is the CCAAT/ATTGG pentanucleotide at the core of a Y-Box that is thought to be required for transcriptional activation and as such, Y-Boxes and CCAAT/ATTGG boxes are considered functionally equivalent (Dolfini & Mantovani, 2013). A number of inverted CCAAT boxes are present throughout the *ABCB1* gene and a manual search of the *ABCB1* GXP_5138817 promoter revealed an inverted CCAAT box lying 297 bp upstream of the predicted Y-Box binding site at position -189 to -185 (Figure 4.2 A). In order to assess whether either predicted binding site represented a functional YB-1 interacting site, CHIP assays using the Group 3 cell line D283 were employed.

As previously described (Section 2.9.1), 5×10^6 cells were isolated and fixed with PFA using the Magna A/G Immunoprecipitation kit under optimised conditions (Appendix B1 and B2) to cross-link proteins onto DNA. Following this, cells were lysed and isolated chromatin sonicated. Chromatin was then added to magnetic beads coated with antibodies against YB-1, immunoglobulin G (IgG) or trimethylated histone H3

lysine 4 (H3K4Me3) in order to isolate protein/DNA complexes, after which these complexes were eluted from the magnetic beads. Finally, protein-DNA cross-links were reversed and the resultant DNA purified for use in qPCR analysis.

In order to assess whether YB-1 protein was enriched at either predicted binding site, primer pairs were designed to span both position -189 to -185 and position +108 to +119 of the *ABCB1* promoter. Following qPCR, the Percent Input Method (Nagaki et al., 2003) - where samples are presented as a percentage of the input sample - was utilised in order to determine the level of protein enrichment at the DNA sequence of interest.

Interestingly, YB-1 was found to be heavily enriched at the manually predicted inverted CCAAT box (Figure 4.2 B), suggestive of YB-1 interaction with the *ABCB1* gene in this region. Whereas, comparatively little YB-1 was detected at the software predicted Y-Box at position +108 to +119 (Figure 4.2 C), with the level of YB-1 at this region similar to that of IgG - a measure of non-specific binding. As such, it was concluded that YB-1 directly interacts with the inverted CCAAT box present at position -189 to -185 of the *ABCB1* gene, not with the Y-Box at position +108 to +119 as predicted by Genomatix MatInspector software.

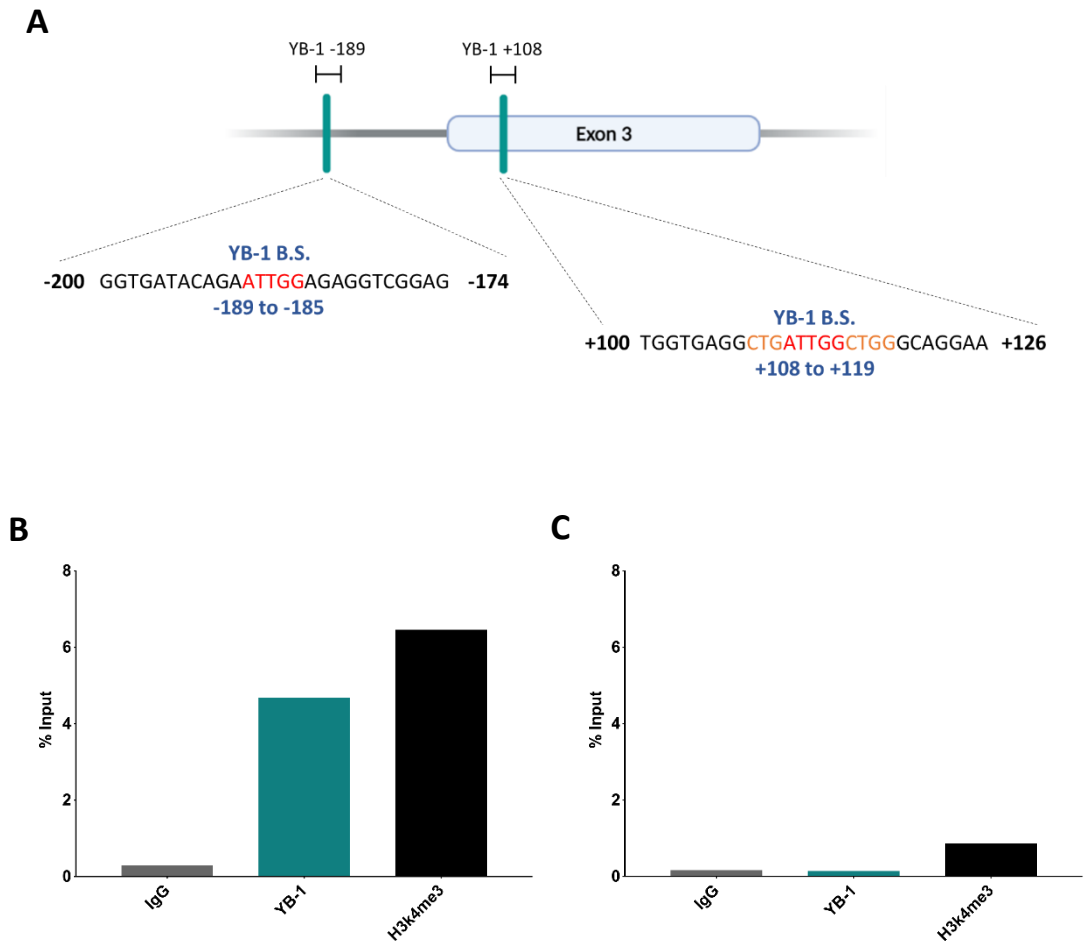


Figure 4.2 YB-1 binds to an inverted CCAAT box upstream of the Genomatix MatInspector predicted binding site in *ABCB1* promoter. A) Schematic displaying two potential YB-1 binding sites (B.S.) in the *ABCB1* promoter region, one (+108) predicted using Genomatix software, the other (-189) identified through a manual search of the *ABCB1* gene. The core inverted CCAAT pentanucleotide is highlighted in red, while flanking Y-Box residues are highlighted in orange. B) qPCR analysis of ChIP assay products revealed that YB-1 binds with high affinity at position -189 of the *ABCB1* promoter in the Group 3 cell line D283. Thus, this region was selected for further study. C) YB-1 does not accumulate at software-predicted position +108 in the D283 medulloblastoma cell line. Data normalised to input; n =1.

4.2.3 YB-1 represents a potential regulator of the *ABCB1* gene in medulloblastoma

The inverted CCAAT box within the *ABCB1* promoter was identified as an YB-1 binding site in preliminary experiments. To validate this finding, ChIP assays were repeated in Group 3 cell lines D283 and HDMB-03. As anticipated from preliminary data, analysis of YB-1 enrichment in D283 cells at the inverted CCAAT box confirmed significant accumulation of YB-1 in this region (Figure 4.3 A), compared with the IgG control ($P = 0.044$). Likewise, analysis of YB-1, IgG and H3K4Me3 accumulation at the same region in HDMB-03 (Figure 4.3 B) also revealed significant YB-1 enrichment ($P = 0.033$). Interestingly, the level of H3K4Me3 (trimethylated lysine 4 on histone H3) – a hallmark of active human promoters – is 12-fold greater in the HDMB-03 cell line *ABCB1* promoter region compared to the D283 cell line, perhaps indicative of increased promoter activity (Vermeulen et al., 2007). Taken together, these results identify YB-1 as a potential regulator of *ABCB1* - a gene whose expression is strongly associated with chemoresistance - in Group 3 medulloblastoma cell lines.

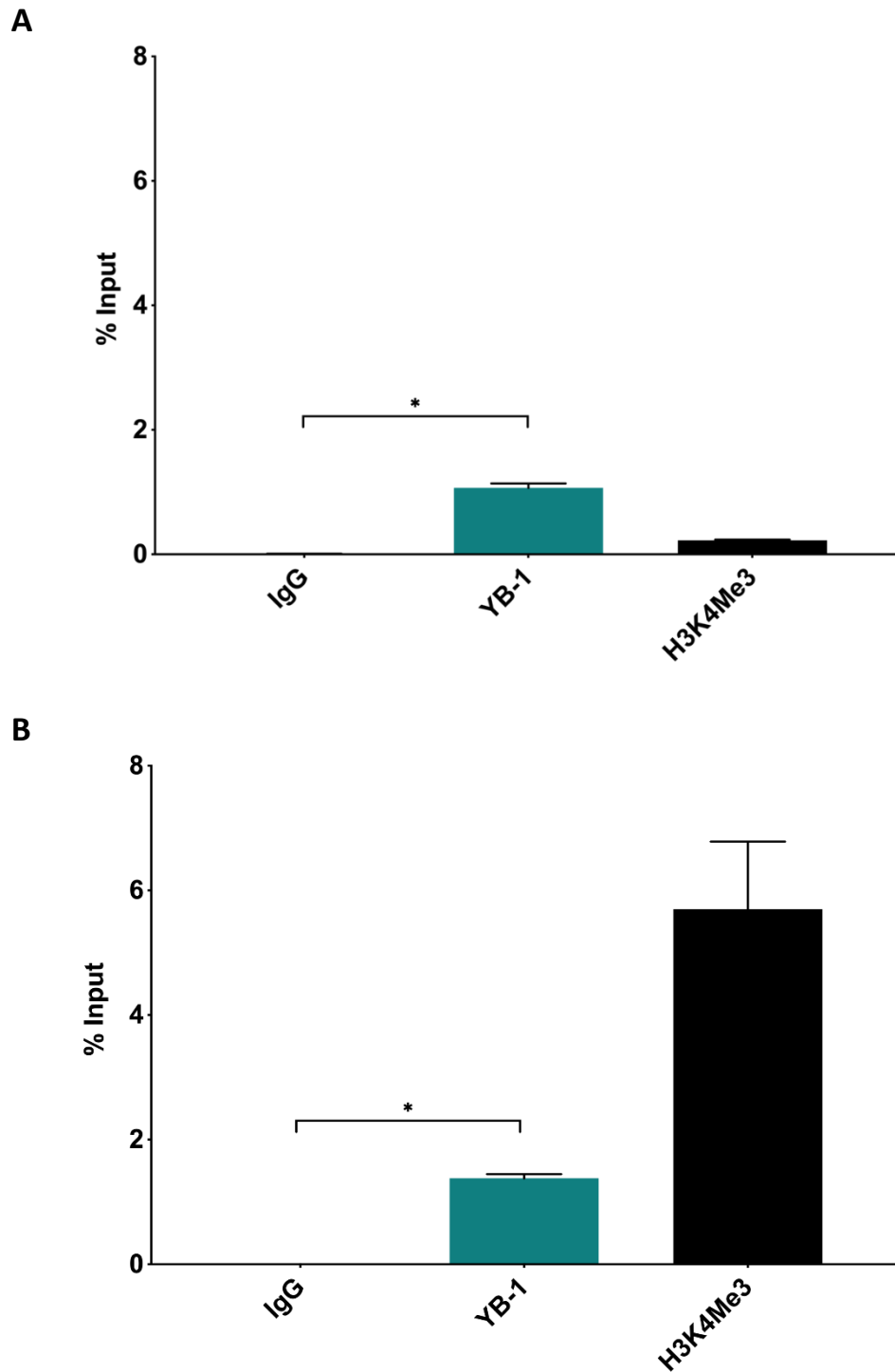


Figure 4.3 YB-1 is strongly enriched at an inverted CCAAT box in the *ABCB1* promoter in Group 3 medulloblastoma cell lines. qPCR analysis of CHIP assay products revealed that YB-1 binds strongly to an inverted CCAAT box in the *ABCB1* promoter of Group 3 cell lines A) D283 and B) HDMB-03. n = 3; data normalised to input; mean \pm SEM plotted; *P< 0.05 as assessed by paired t-test analysis.

4.3 Analysis of the effect of drug treatment on YB-1 subcellular localisation in medulloblastoma

4.3.1 Optimisation of chemotherapy drug concentration

Given that we have shown that YB-1 interacts strongly with the multi-drug transporter gene *ABCB1*, we next wanted to explore whether YB-1 is implicated in the cellular response to drug treatment and concurrent potentiation of drug tolerance.

First, we wanted to assess the effect of chemotherapy on cellular YB-1 expression and localisation. Two standard-of-care chemotherapy drugs - cisplatin and vincristine - were selected, both of which are currently used in standard and high-risk medulloblastoma treatment regimens (Section 1.2.1.7). Cisplatin has been previously demonstrated to trigger YB-1 nuclear translocation in breast cancer cell lines (Fujita et al., 2005). Comparatively, there are no records of vincristine triggering alterations in YB-1 localisation. However, as vincristine represents an *ABCB1* substrate, we were interested to see whether treatment could influence YB-1 expression/localisation within our cell lines.

First, an appropriate drug concentration with which to treat each cell line was determined. Fujita et al. promoted YB-1 nuclear translation using cisplatin at half-maximal inhibitory concentration (IC_{50}) (2005). Hence, drug response assays were employed in order to calculate IC_{50} values for cisplatin and vincristine in Group 3 cell lines HDMB-03, D283 and D458 and SHH cell line DAOY. Viability was calculated as a percentage of the vehicle-treated controls and non-linear regression analyses were

performed to normalise the data and produce dose-response curves, which ran from 100% to 0% viability.

Dose response curves and calculated IC_{50} values for each cell line are shown in Figure 4.4 and Figure 4.5 . The SHH cell line DAOY and the Group 3 cell line D458 were found to be more sensitive to cisplatin exposure (IC_{50} of 0.6 μ M and 0.4 μ M respectively) than the Group 3 cell lines HDMB-03 and D283 (IC_{50} of 1.5 μ M and 1.6 μ M respectively). Comparatively, DAOY and notably D283 were found to be more sensitive to vincristine exposure (IC_{50} of 1.3 nM and 1.0 nM respectively) than HDMB-03 and D458 (IC_{50} of 3.4 nM and 3.1 nM respectively). Interestingly, despite having the lowest vincristine IC_{50} compared to other lines tested, it was impossible to achieve a cell viability of less than 16% in D283 cells, even with a treatment dose of 500 nM vincristine (5x higher than the highest dose required in other cells) indicative of a resistant sub-population of cells in this cell line.

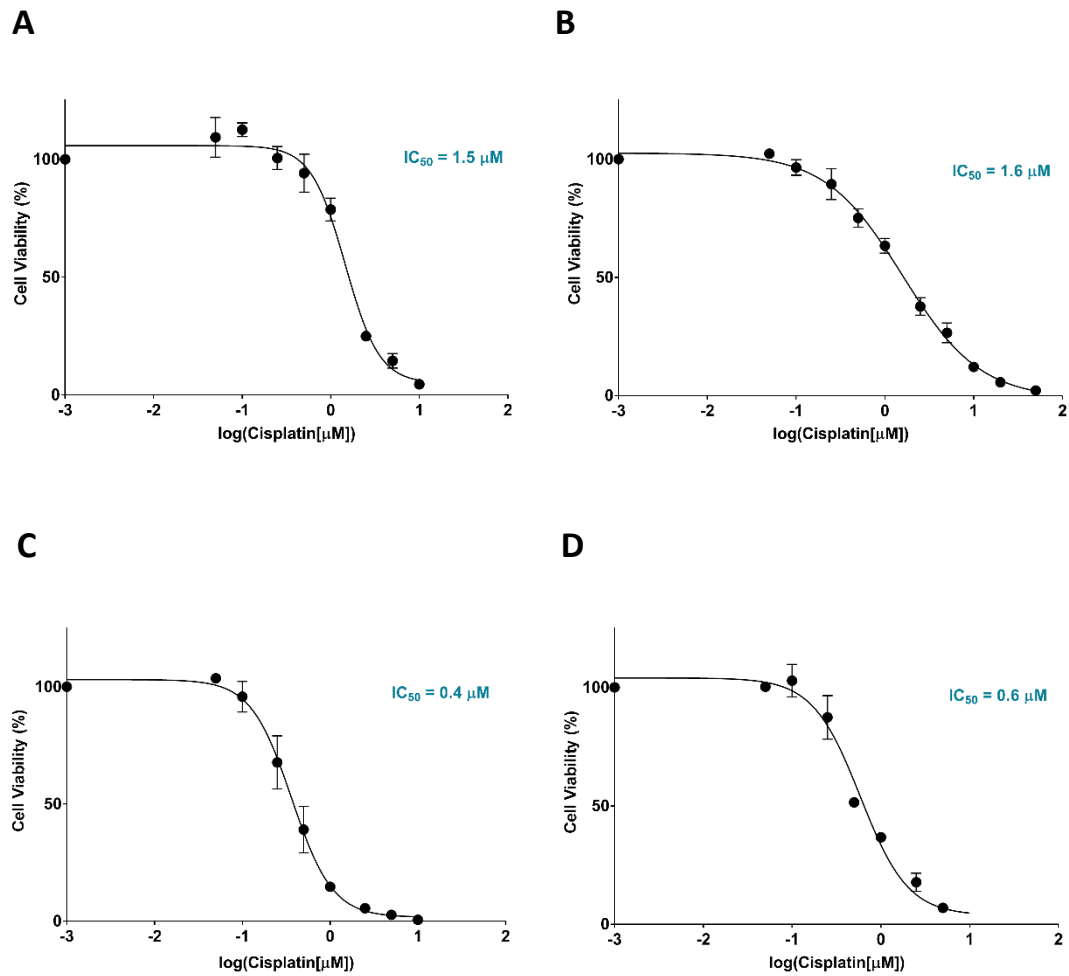


Figure 4.4 Cisplatin cytotoxicity in SHH and Group 3 cell lines. Cell lines were treated with increasing concentrations of cisplatin for 72 hours. PrestoBlue cell viability assays were performed to compare response and viability was calculated as a percentage of the vehicle-treated control. Group 3 cell lines HDMB-03 (A) and D283 (B) were more intrinsically resistant to cisplatin treatment than Group 3 cell line D458 (C) or SHH cell line DAOY (D). Mean \pm SEM plotted; $n = 3$. Dose response curves were generated using non-linear regression analyses and IC₅₀ values calculated accordingly.

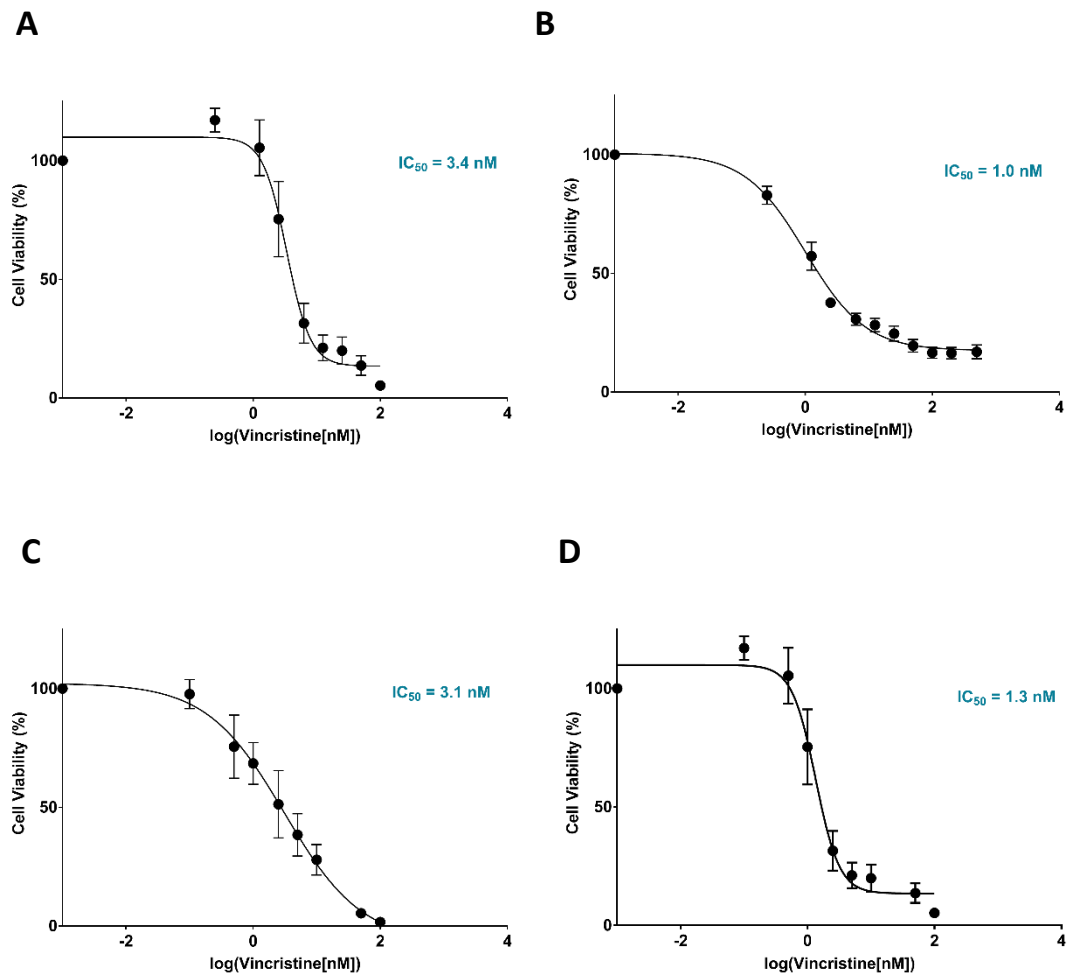


Figure 4.5 Vincristine cytotoxicity in SHH and Group 3 cell lines. Cell lines were treated with increasing concentrations of vincristine for 72 hours. PrestoBlue cell viability assays were performed to compare response and viability was calculated as a percentage of the vehicle-treated control. Although cell lines HDMB-03 (A) and D458 (C) and DAOY (D) displayed a higher IC_{50} than Group 3 cell line D283 (B), we were unable to achieve a cell viability of less than 16% in this cell line. Mean \pm SEM plotted; $n = 3$. Dose response curves were generated using non-linear regression analyses and IC_{50} values calculated accordingly.

4.3.2 Treatment of Group 3 medulloblastoma cell lines with cisplatin but not vincristine elevates levels of nuclear YB-1.

The effects of cisplatin and vincristine on cellular YB-1 distribution were examined using HDMB-03, D283 and D458 cell lines. We initially selected nuclear/ cytoplasmic fractionation (Section 2.9.7) with western blot analysis to analyse whether chemotherapeutic stimuli promoted YB-1 nuclear translocation. First, HDMB-03 cells were treated with 1.5 μM (IC_{50}) of cisplatin over a time course of 6 hours, during which cell pellets were harvested and nuclear and cytoplasmic fractions prepared. Samples were then analysed by immunoblotting and band density quantified. From this a ratio of nuclear YB-1:cytoplasmic YB-1 (relative to nuclear and cytoplasmic loading controls) was calculated in order to assess alterations in YB-1 subcellular localisation (Section 2.9.7.5).

An increase of approximately five-fold was observed in nuclear YB-1:cytoplasmic YB-1 in HDMB-03 cells after 1 hour treatment with cisplatin (Figure 4.6). Analysis by ratio paired t-test found this increase to be statistically significant ($P = 0.041$). This effect appeared to dissipate after the 1 hour time point, perhaps indicating that the alteration in YB-1 cellular localisation in response to acute cisplatin treatment is a short-term effect. Alterations in total YB-1 expression (non-fractionated samples) in response to cisplatin treatment were also examined over a 12-hour time course, however as shown in the representative blot in Figure 4.7, no changes in total YB-1 protein were observed at any time point relative to the 0 hour control sample.

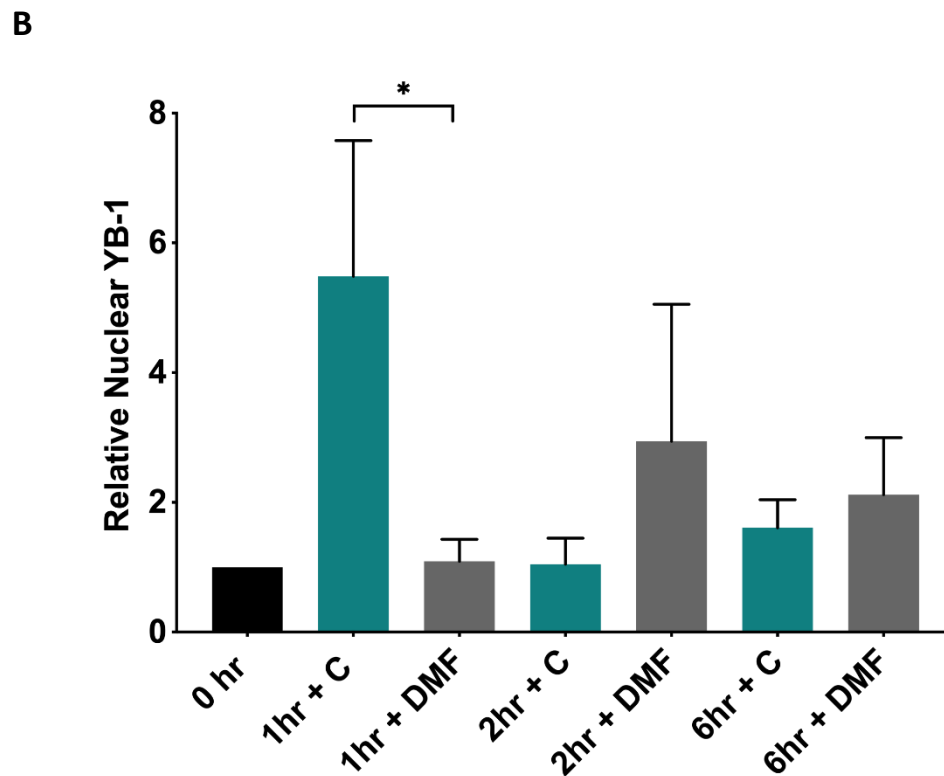
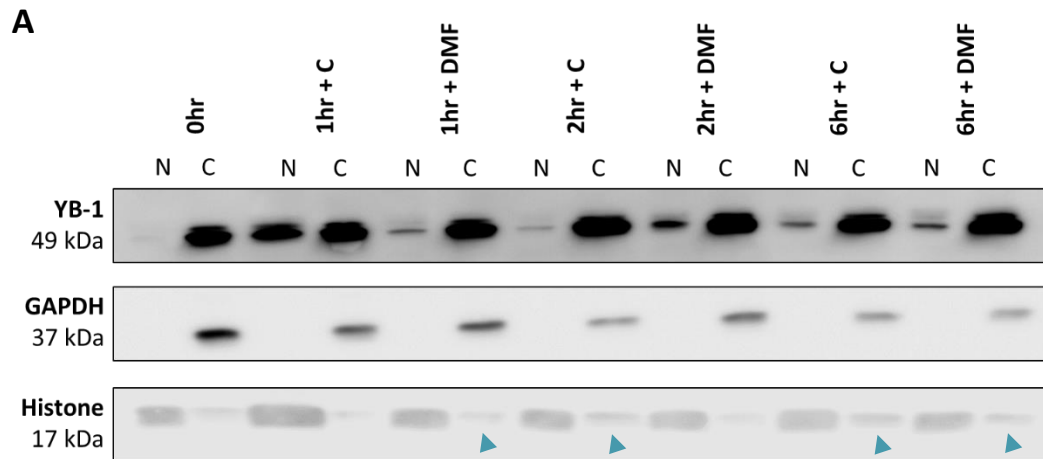


Figure 4.6 Treatment of Group 3 cell line HDMB-03 with cisplatin promotes YB-1 nuclear localisation. HDMB-03 cells were treated with 1.5 μ M cisplatin (IC_{50}) and harvested at the time points indicated. Nuclear/cytoplasmic fractionation followed by western blot served to analyse YB-1 cellular localisation. A) Western blot showing change in YB-1 protein levels in nuclear and cytoplasmic fractions following cisplatin treatment. Histone (nuclear) and GAPDH (cytoplasmic) verified successful fractionation and acted as loading controls. Arrowheads signify nuclear contamination detected in cytoplasmic fractions. B) Densitometry suggested that YB-1 protein levels increase in the nucleus 1 hr post-cisplatin treatment compared with the vehicle (DMF). Plots represent a ratio of nuclear YB-1:cytoplasmic YB-1. Data is presented relative to appropriate loading controls and normalised to the 0 hr control. Mean \pm SEM plotted. $n = 4$; statistically significant differences are indicated as * $P < 0.05$, where significance was assessed by ratio paired t test. Full length western blots are presented in Appendix B3.

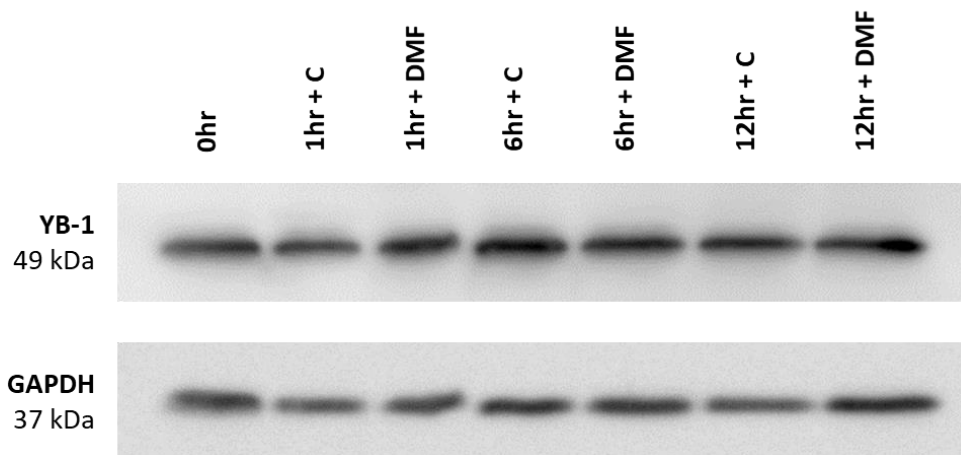


Figure 4.7 Cisplatin treatment does not alter total YB-1 protein level in HDMB-03 cells. HDMB-03 cells were treated with 1.5 μ M cisplatin (IC_{50}) and harvested at the time points indicated. Whole cell protein extraction followed by western blot served to analyse YB-1 expression. YB-1 level appeared to remain stable over the 12 hour time course following cisplatin treatment. GAPDH was utilised as a loading control. Representative blot shown; n = 2. Full length western blots are presented in Appendix B4.

Although these results were promising, there were difficulties in using nuclear/cytoplasmic fractionation as a method to assess YB-1 cellular localisation. Firstly, isolating clean cytoplasmic fractions was found to be challenging, with nuclear (histone) contamination frequently detected (see arrowheads in lower panel in Figure 4.6 A). This resulted in variation between repeats, raising concerns over the reproducibility of this method. For such reasons, an alternative method was sought to more reliably quantify YB-1 localisation across multiple cell lines. Immunofluorescence (IF) was selected as cell integrity is maintained in this method, therefore allowing greater consistency across experimental groups.

In order to assess changes in YB-1 cellular localisation by IF, HDMB-03, D283 and D458 cells were plated in chamber slides and treated with vincristine or cisplatin at previously calculated IC_{50} (Figure 4.4 and Figure 4.5). For D283 and D458 lines, samples were then fixed with 4% PFA over a 12-hour time course (1, 6 and 12 hours) and immunostained for YB-1, α -tubulin (to mark cell structure) and DAPI (to visualise cell nuclei). For cisplatin-treated HDMB-03 cells, samples were fixed at the previously optimised time point (1 hour) only prior to immunostaining as described. Confocal microscopy was then employed to visualise and record YB-1 distribution and resultant images were analysed in ImageJ. To quantify nuclear YB-1 staining, intensity masks based upon DAPI staining were used, whilst to quantify overall YB-1 staining levels intensity masks based upon Alexa Fluor 488 dye visualisation were used (Section 2.9.8.1).

Quantification of immunostained HDMB-03 revealed elevated nuclear YB-1 levels following treatment with cisplatin when compared with the vehicle-treated control at 1 hour post-cisplatin exposure (Figure 4.8 A; $P = 0.029$). Average overall YB-1 staining also appeared elevated upon image analysis; however variability in staining intensity between replicates meant this result was not statistically significant. Taken together, these results may indicate that the significant increase in nuclear YB-1 observed in HDMB-03 in response to cisplatin is largely a consequence of elevated YB-1 nuclear translocation, rather than simply increased expression of YB-1 protein throughout the cell (Figure 4.8 B). This is in agreement with results obtained from nuclear/cytoplasmic fractionation analyses (Figure 4.6) and total YB-1 protein analyses (Figure 4.7). Comparatively, no significant alteration in either nuclear or cellular YB-1 was observed post-vincristine exposure at 1, 6 or 12 hour time points, the 1 hour data being shown for reference (Figure 4.9; 6 and 12 hour time points displayed in Appendix B5).

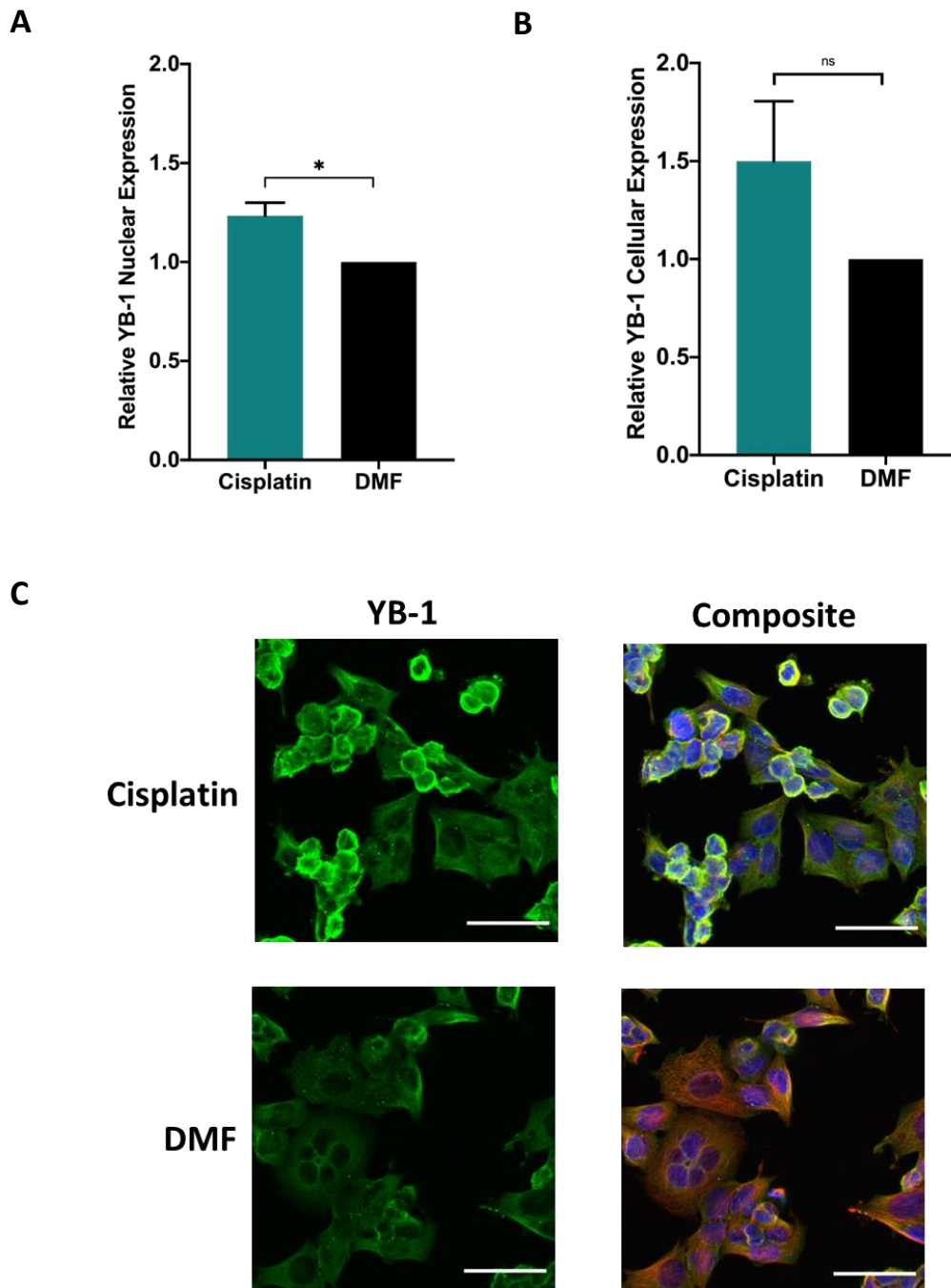


Figure 4.8 Treatment of Group 3 cell line HDMB-03 with standard-of-care medulloblastoma chemotherapeutic cisplatin results in elevated nuclear YB-1 expression. HDMB-03 cells were treated with 1.5 μ M cisplatin (IC_{50}) for 1 hour. Following drug treatment, cells were fixed with PFA and fluorescence detected by confocal microscopy. A) Automated quantification of cisplatin-treated cells revealed significant YB-1 nuclear import relative to the vehicle (DMF)-treated control. B) Image analysis did not reveal significant changes in total cellular YB-1 staining intensity. $n = 3$ (approx. 4000 cells). Mean \pm SEM; * $P < 0.05$, ns = not significant. Significance assessed by unpaired t-test analysis. C) Representative images of cisplatin-treated and DMF-treated cells. Cells were immunostained for YB-1 (green). α -tubulin (red) was used as a cytoplasmic marker and DAPI used to mark cell nuclei. All scale bars represent 50 μ m.

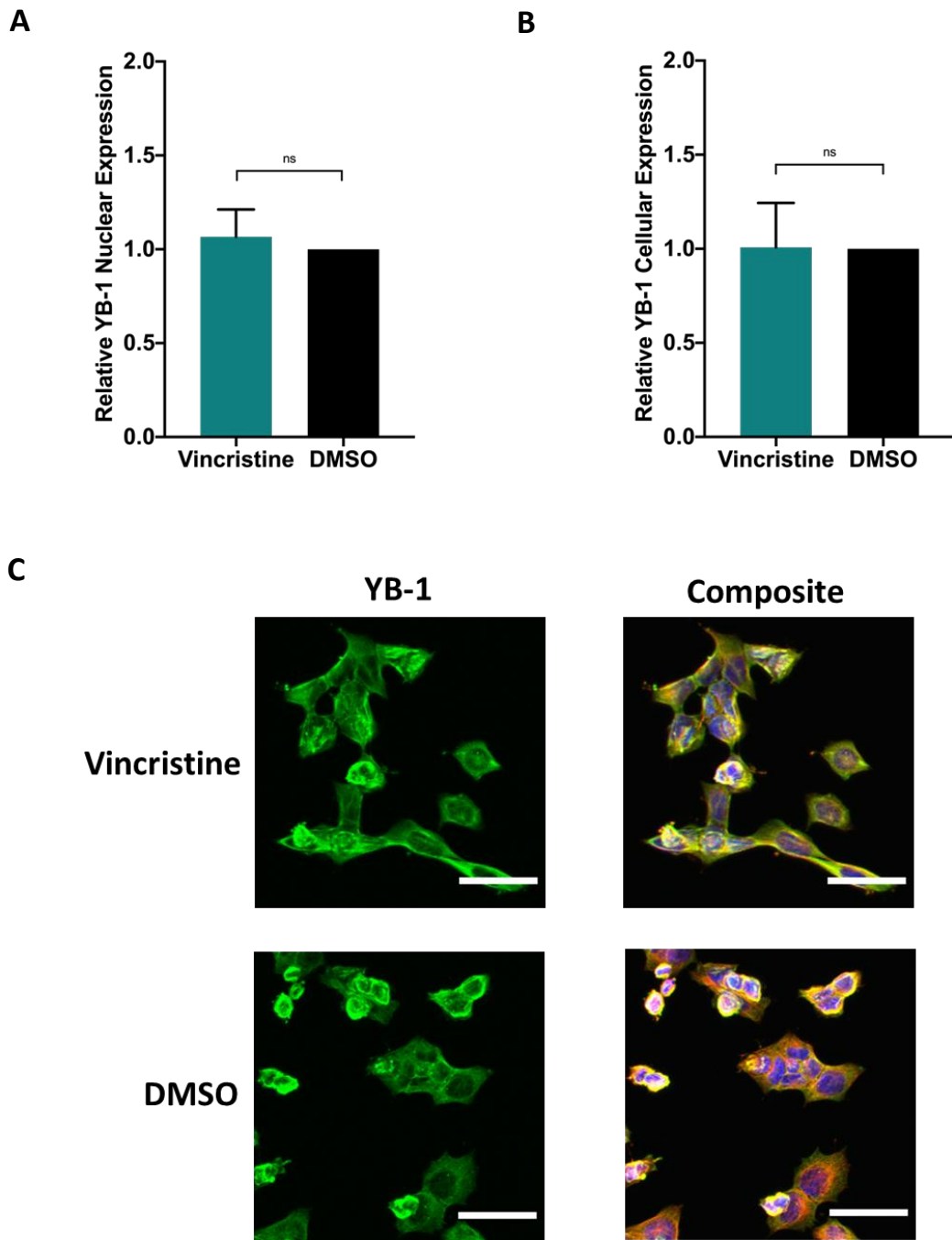


Figure 4.9 Treatment of Group 3 cell line HDMB-03 with standard-of-care medulloblastoma chemotherapeutic vincristine does not alter YB-1 expression or localisation. HDMB-03 cells were treated with 3.4 nM vincristine (IC_{50}) for 1 hour. Following drug treatment, cells were fixed with PFA and fluorescence detected by confocal microscopy. A) Automated quantification of vincristine-treated cells did not show significant alteration in nuclear YB-1 level relative to the vehicle (DMSO)-treated control. B) Image analysis also did not reveal significant changes in total cellular YB-1 staining intensity. $n = 3$ (approx. 2000 cells). Mean \pm SEM; ns = not significant. Significance assessed by unpaired t-test analysis. C) Representative images of vincristine-treated and DMSO-treated cells. Cells were immunostained for YB-1 (green). α -tubulin (red) was used as a cytoplasmic marker and DAPI used to mark cell nuclei. All scale bars represent 50 μ m.

The group 3 cell line D283 also exhibited significantly elevated levels of nuclear YB-1 following 1 hour exposure to cisplatin (Figure 4.10 A; $P = 0.0038$). Similar to observations in HDMB-03 cells, this increase was not associated with significant elevation of overall cellular YB-1 protein (Figure 4.10 B), although as in Figure 4.8 B, substantial variability between replicates was observed. Again, this observation may suggest that increased nuclear YB-1 levels at this time point are primarily due to increased YB-1 nuclear transport in response to cisplatin treatment. Unlike that observed in HDMB-03 cells (Figure 4.6), the nuclear YB-1 elevation effect appeared to be sustained until the 6 hour time point (Figure 4.10 C), after which it dissipated (Appendix B6). Interestingly, at 6 hours post-cisplatin treatment a significant increase in overall YB-1 expression was also observed (Figure 4.10 D). This result differs to our previous findings in the HDMB-03 line (Figure 4.7) and suggests that cisplatin treatment in D283 cells may also promote increased expression of YB-1 protein.

Like in the HDMB-03 line, vincristine did not promote increased nuclear or cellular YB-1 levels at any of the time points analysed. Again, the 1 hour time point is displayed for reference (Figure 4.11; 6 and 12 hour time points displayed in Appendix B7). As vincristine is a known substrate for ABCB1 whereas cisplatin is not, it is feasible that this observation may be linked to increased vincristine efflux from the cell, lessening intracellular drug concentration and thus minimising YB-1 nuclear translocation.

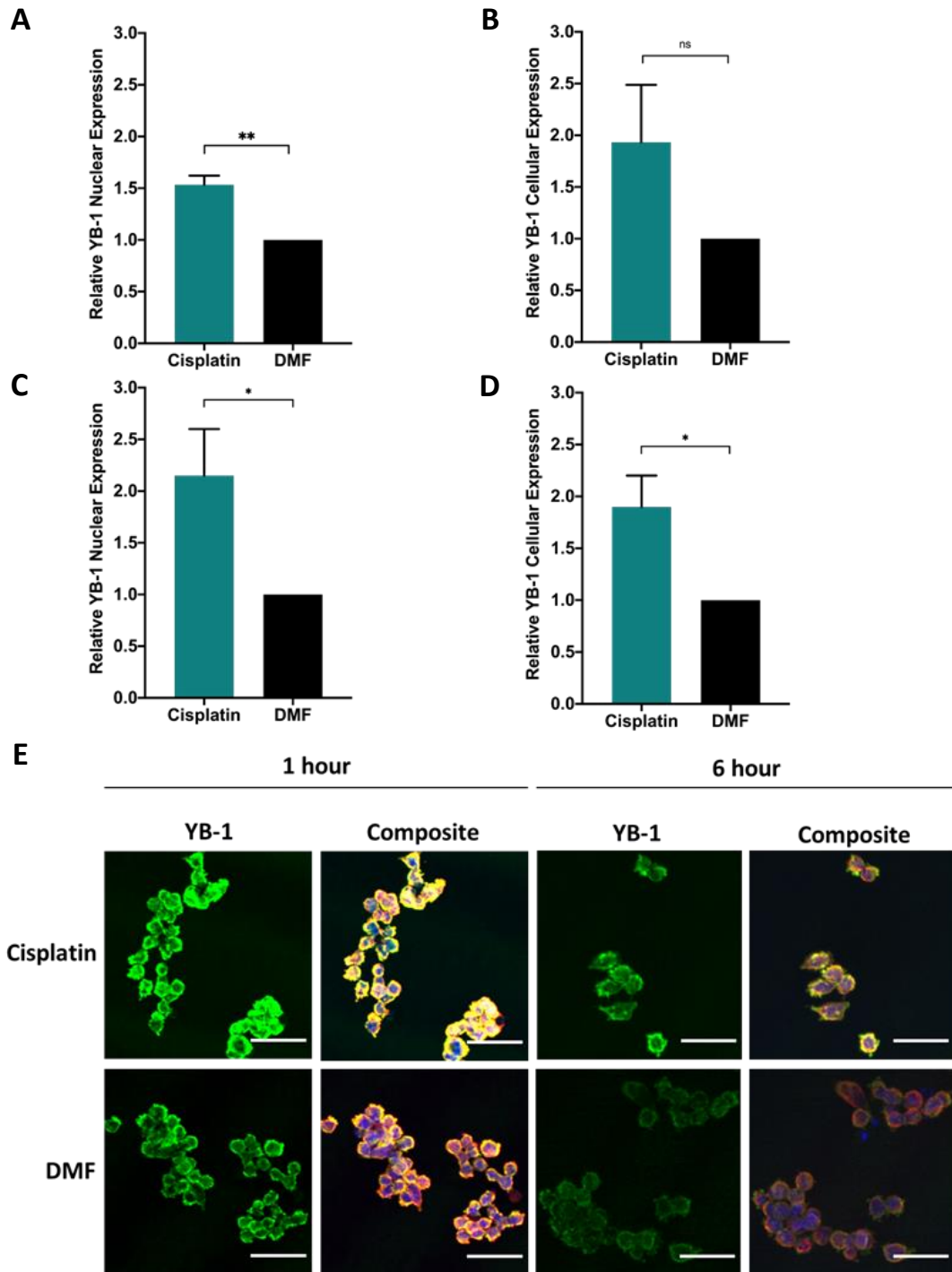


Figure 4.10 Treatment of Group 3 cell line D283 with cisplatin results in elevated nuclear YB-1 expression 1 and 6 hours post-cisplatin exposure. D283 cells were treated with 1.6 μ M cisplatin (IC_{50}) for 1 and 6 hour time points. Following drug treatment, cells were fixed with PFA and fluorescence detected by confocal microscopy. A) Automated quantification revealed increased YB-1 nuclear levels at 1 hour post-cisplatin treatment. B) Image analysis found no significant change in overall YB-1 staining intensity at 1 hour post-cisplatin treatment. C) Elevated nuclear YB-1 staining was detected at 6 hours post-cisplatin treatment. D) Image analysis revealed elevated overall YB-1 staining at 6 hours post-cisplatin treatment $n = 4$ (approx. 2500 cells). Mean \pm SEM; * $P < 0.05$, ** $P < 0.01$, ns = not significant. Significance assessed by unpaired t-test analysis. E) Representative images. Cells were immunostained for YB-1 (green). α -tubulin (red) was used as a cytoplasmic marker and DAPI used to mark cell nuclei. All scale bars represent 50 μ m.

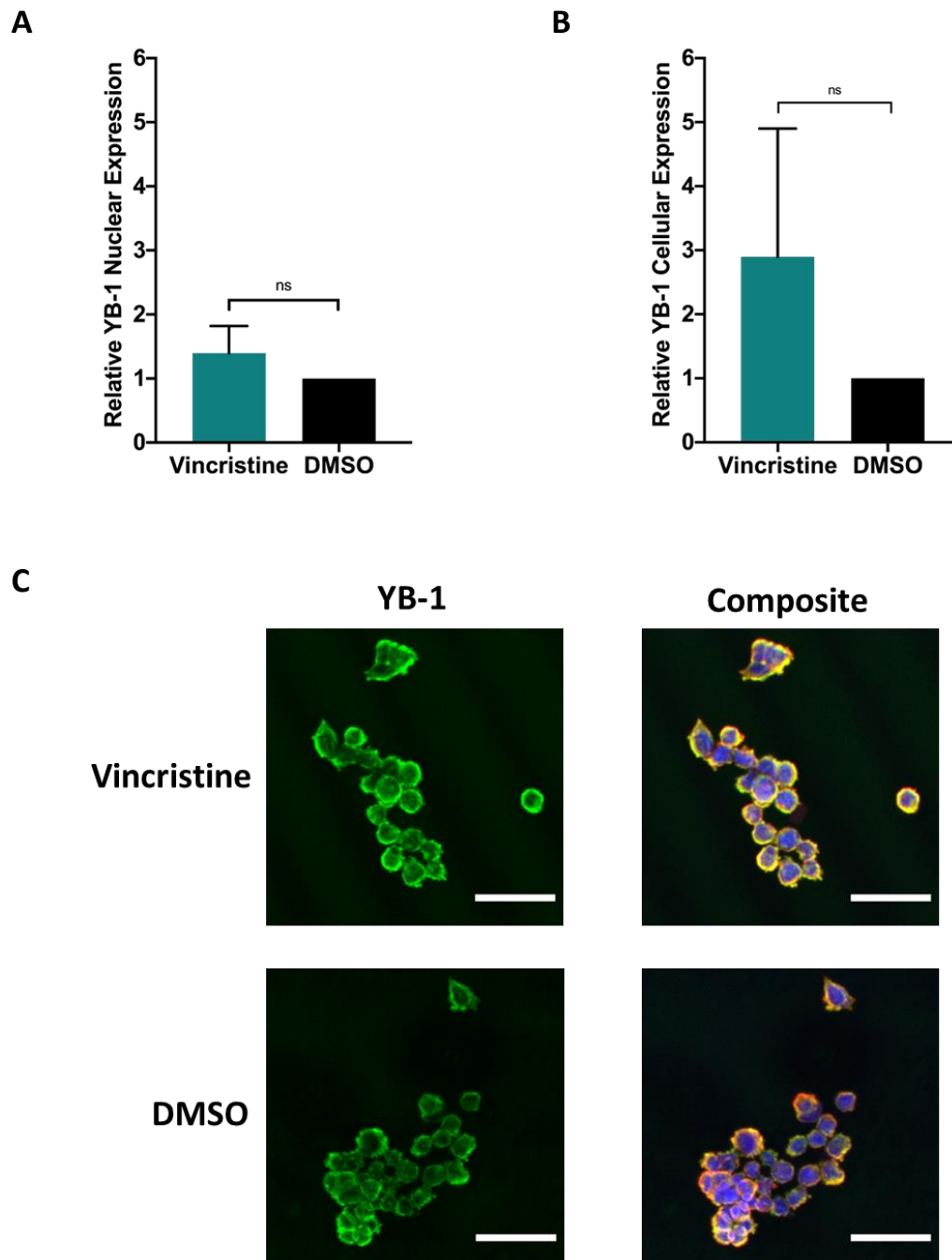


Figure 4.11 Treatment of Group 3 cell line D283 with standard-of-care medulloblastoma chemotherapeutic vincristine does not alter YB-1 expression or localisation. D283 cells were treated with 1 nM vincristine (IC_{50}) for 1 hour. Following drug treatment, cells were fixed with PFA and fluorescence detected by confocal microscopy. A) Automated quantification of vincristine-treated cells did not show significant alteration in nuclear YB-1 level relative to the vehicle (DMSO)-treated control. B) Image analysis also did not reveal significant changes in total cellular YB-1 staining intensity. $n = 3$ (approx. 2000 cells). Mean \pm SEM; ns = not significant. Significance assessed by unpaired t-test analysis. C) Representative images of vincristine-treated and DMSO-treated cells. Cells were immunostained for YB-1 (green). α -tubulin (red) was used as a cytoplasmic marker and DAPI used to mark cell nuclei. All scale bars represent 50 μ m.

A third Group 3 cell line, D458, was also subjected to the same cisplatin and vincristine time course. However, in comparison to both HDMB-03 and D283, cisplatin treatment did not trigger elevation of YB-1 at a nuclear or cellular level at any time point analysed in this cell line (Figure 4.12). Additionally, overall YB-1 staining intensity was found to significantly decrease following 12 hours of vincristine treatment (Figure 4.13 F), indicative of decreased YB-1 protein level at this time point. The D458 cell line was established from a secondary medulloblastoma metastasis, whereas both HDMB-03 and D283 cell lines were established from a primary medulloblastoma in a metastatic patient. Thus, perhaps the observed difference in YB-1 drug-induced subcellular localisation arises from the differential parental tumour stages of the cell lines.

As previously described, immunofluorescence was employed as an alternative technique to assess subcellular YB-1 expression. Although an improvement on our previous fractionation method, we did still observe variation between replicates, particularly when assessing overall cellular YB-1 expression. One advantage of immunofluorescence and confocal microscopy is the visualisation of protein on a cell-by-cell basis. In the examination of confocal microscopy images obtained from these experiments, clear heterogeneity in YB-1 expression within cell lines was observed, with some cells expressing much greater levels of YB-1 than others. It is possible that this intrinsic heterogeneity accounts for the large variation we observed between repeats in some cell lines using the immunofluorescence method.

Nevertheless, taken together the presented data does indicate that treatment of HDMB-03 and D283 Group 3 cell lines with cisplatin induces an acute elevation in YB-

1 expression within the nucleus. This result suggests that YB-1 may be implicated in the cellular stress response to cisplatin, however, what function YB-1 has in this response is yet to be explored.

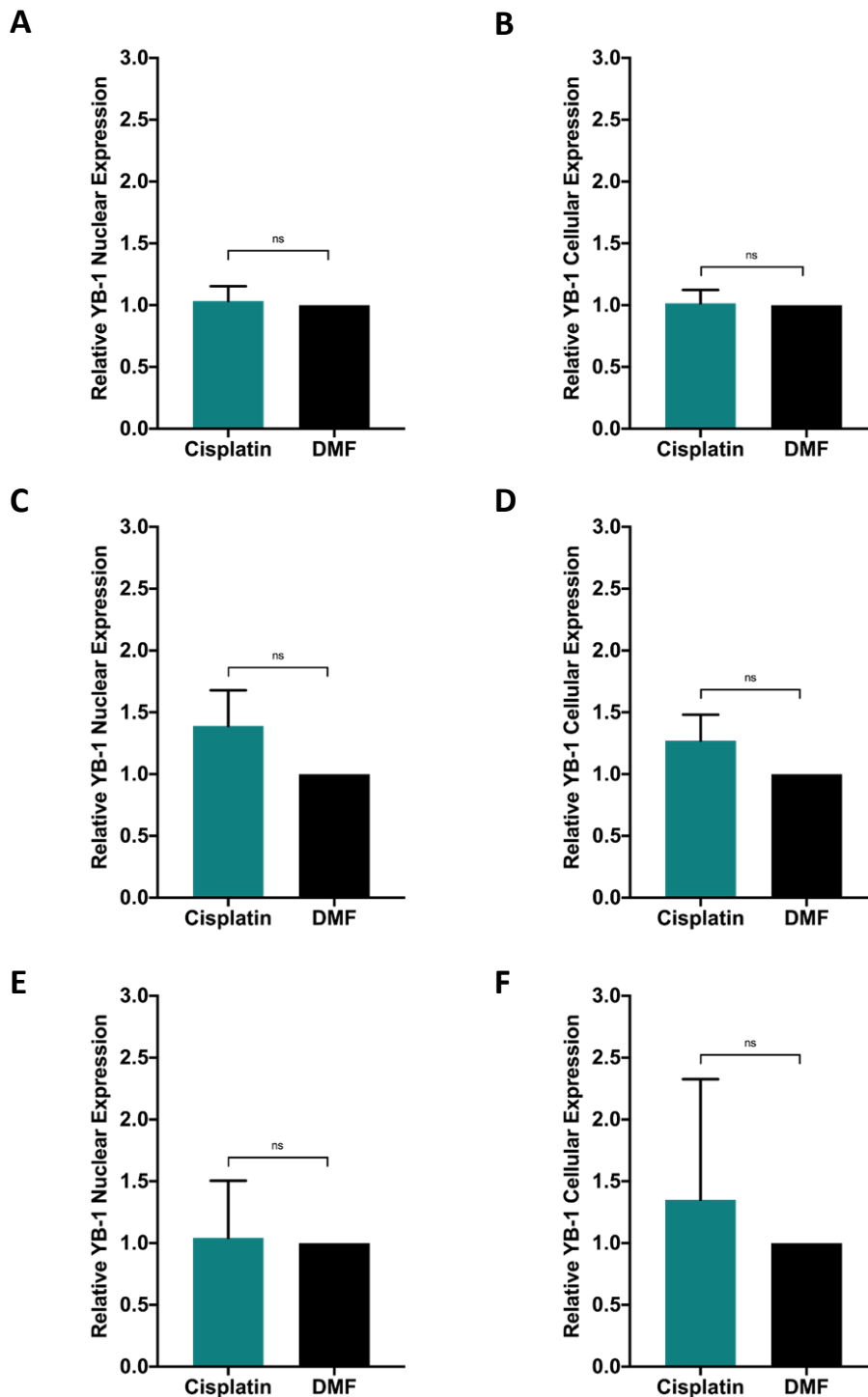


Figure 4.12 Treatment of Group 3 cell line D458 with cisplatin does not alter nuclear or cellular YB-1 expression. D458 cells were treated with 0.4 μ M cisplatin (IC_{50}) over a 12 hour time course. Following drug treatment, cells were fixed with PFA and fluorescence detected by confocal microscopy. Automated quantification of cisplatin-treated cells revealed no significant alteration in nuclear or cellular YB-1 staining intensity at 1, 6 and 12 hours post-cisplatin treatment (A – F). $n = 3$ (approx. 2000 – 3000 cells per time point). Mean \pm SEM; ns = not significant. Significance assessed by unpaired t-test analyses.

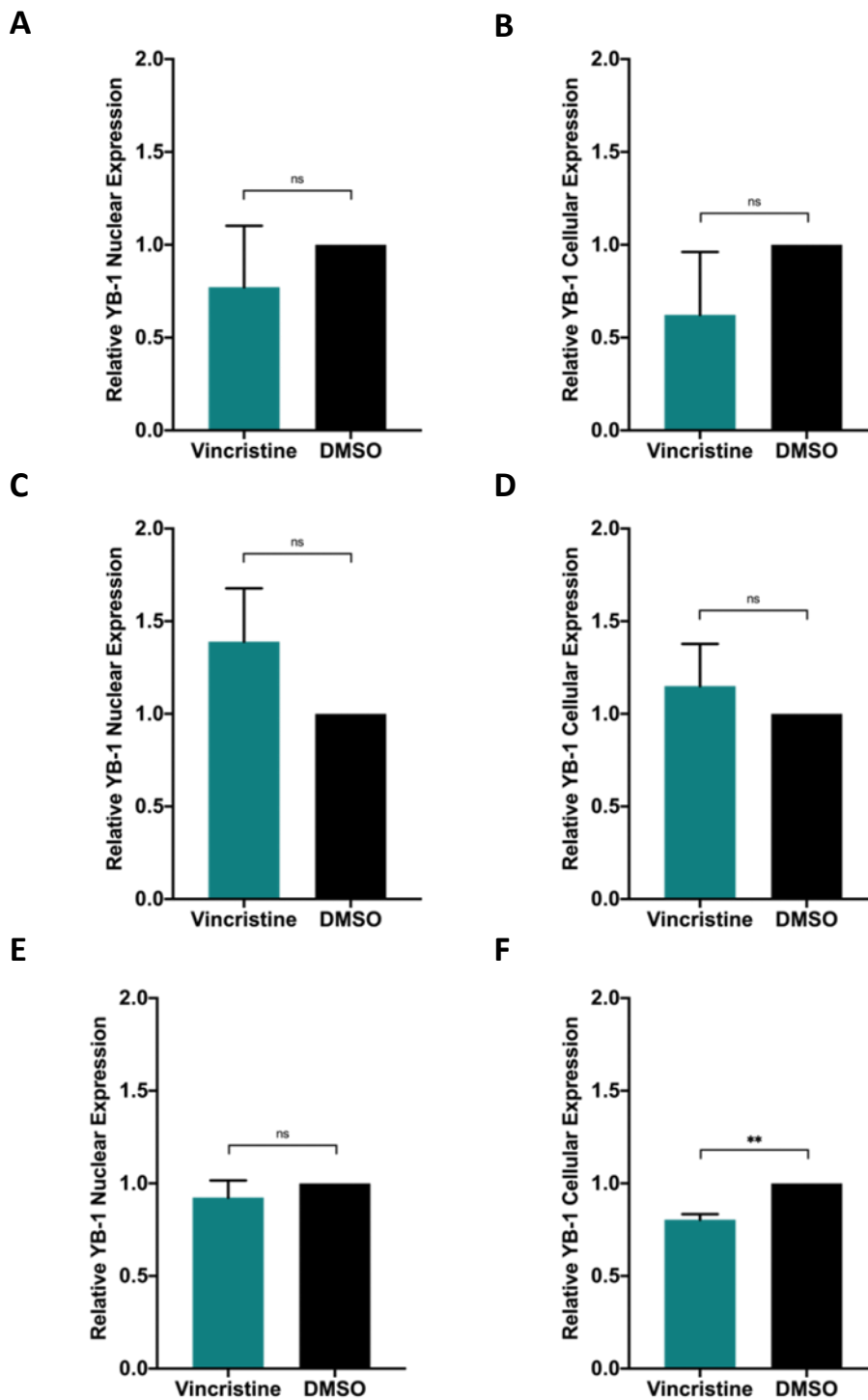


Figure 4.13 Treatment of D458 cells with vincristine decreases cellular YB-1 expression. D458 cells were treated with 3.1 nM vincristine (IC_{50}) over a 12 hour time course. Following drug treatment, cells were fixed with PFA and fluorescence detected by confocal microscopy. Automated quantification of vincristine-treated cells revealed a significant decrease in YB-1 cellular staining intensity relative to the vehicle (DMSO)-treated control at 12 hour post-vincristine treatment (F), whereas no significant alteration in nuclear YB-1 staining intensity was detected at 12 hour post-vincristine treatment (E) and no alteration in nuclear or cellular YB-1 staining intensity was detected at 1 and 6 hour post-vincristine treatment (A – D). $n = 3$ (approx. 2500-4000 cells per time point). Mean \pm SEM; ** $P < 0.01$; ns = not significant. Significance assessed by unpaired t-test analyses.

4.4 Study of *ABCB1* expression in response to drug treatment

4.4.1 *ABCB1* expression is elevated following treatment with vincristine, not cisplatin

So far, we have demonstrated that treatment of Group 3 cell lines HDMB-03 and D283 with cisplatin promotes increased levels of YB-1 protein in the nucleus; whereas treatment with vincristine does not alter YB-1 expression levels or cellular localisation in either cell line. We have also shown that YB-1 interacts with the *ABCB1* promoter and hence may represent a regulator of this gene. To further explore the association between chemotherapeutic treatment, *ABCB1* and drug resistance in these cell lines, we next wanted to deduce whether cisplatin or vincristine treatment had any effect on *ABCB1* expression.

HDMB-03 and D283 cells were treated with cisplatin or vincristine at IC_{50} over a time course of 48 hours, with samples harvested at 12 hour intervals. Interestingly, qRT-PCR analysis of collected samples relative to vehicle-treated controls suggested that *ABCB1* expression alters depending on the chemotherapeutic treatment employed (Figure 4.14 and Figure 4.15). Following cisplatin treatment, *ABCB1* expression remained unchanged in HDMB-03 cells (Figure 4.14 A). Likewise, no statistically significant alteration in *ABCB1* expression was detected in D283 cell line, despite the gradual decrease in *ABCB1* expression observed as the time course progressed (Figure 4.14 B). Comparatively, in vincristine-treated HDMB-03 cells a time-dependant increase in *ABCB1* expression was observed which was found to be significantly elevated at 48 hours post-treatment compared to cells collected at 12

hours ($P = 0.049$ respectively; Figure 4.15 A). Similarly, vincristine treatment in the D283 cell line resulted in elevated *ABCB1* expression, however this appeared to occur at a single time-point - 36 hours post-treatment - which was found to be significant when compared to samples collected at 12, 24 and 48 hours ($P = 0.025$, $P = 0.0093$ and $P = 0.013$, respectively; Figure 4.15 B).

These results suggest that treatment of Group 3 medulloblastoma cell lines with vincristine promotes the expression of *ABCB1* at an mRNA level. In contrast, cisplatin has no effect on *ABCB1* expression in either D283 or HDMB-03 cell lines. As mentioned previously, vincristine is a known *ABCB1* substrate and thus its increased expression could have a protective, pro-survival effect on a cancer cell undergoing vincristine treatment, promoting drug extrusion from the cell. Conversely, cisplatin is not a substrate for *ABCB1* and thus increased expression would likely have little effect on cellular survival in response to cisplatin treatment. Taken together, these data highlight that different chemotherapeutic treatments with different mechanisms of actions likely trigger different transcriptional responses within the cell, which may be associated with different mechanisms of cellular resistance.

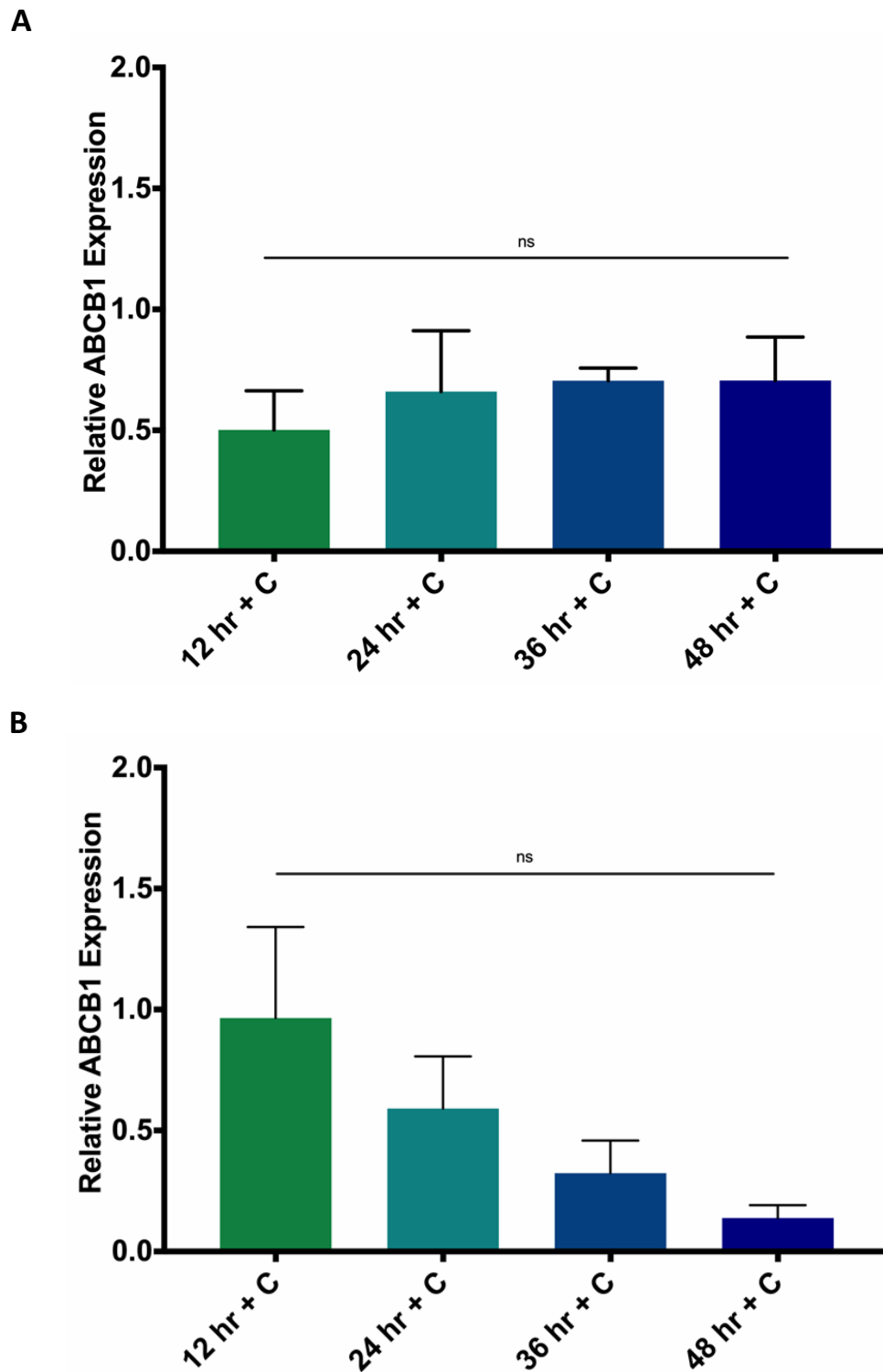


Figure 4.14 ABCB1 expression remains unchanged following cisplatin treatment. HDMB-03 and D283 cells were treated with 1.5 μ M and 1.6 μ M cisplatin (IC_{50}) respectively and samples collected at 12 hour intervals. ABCB1 expression was assayed using qRT-PCR. A) Cisplatin treatment did not alter ABCB1 expression in HDMB-03 cells over the 48 hour time course. B) Cisplatin treatment did not affect ABCB1 mRNA levels in D283 cells. Relative ABCB1 expression displayed as fold change ($2^{-\Delta\Delta Cq}$) relative to the vehicle-treated controls collected at each time point. $n = 3$; mean \pm SEM; ns = not significant as assessed by ordinary one-way ANOVA analysis with Tukey's multiple comparisons test.

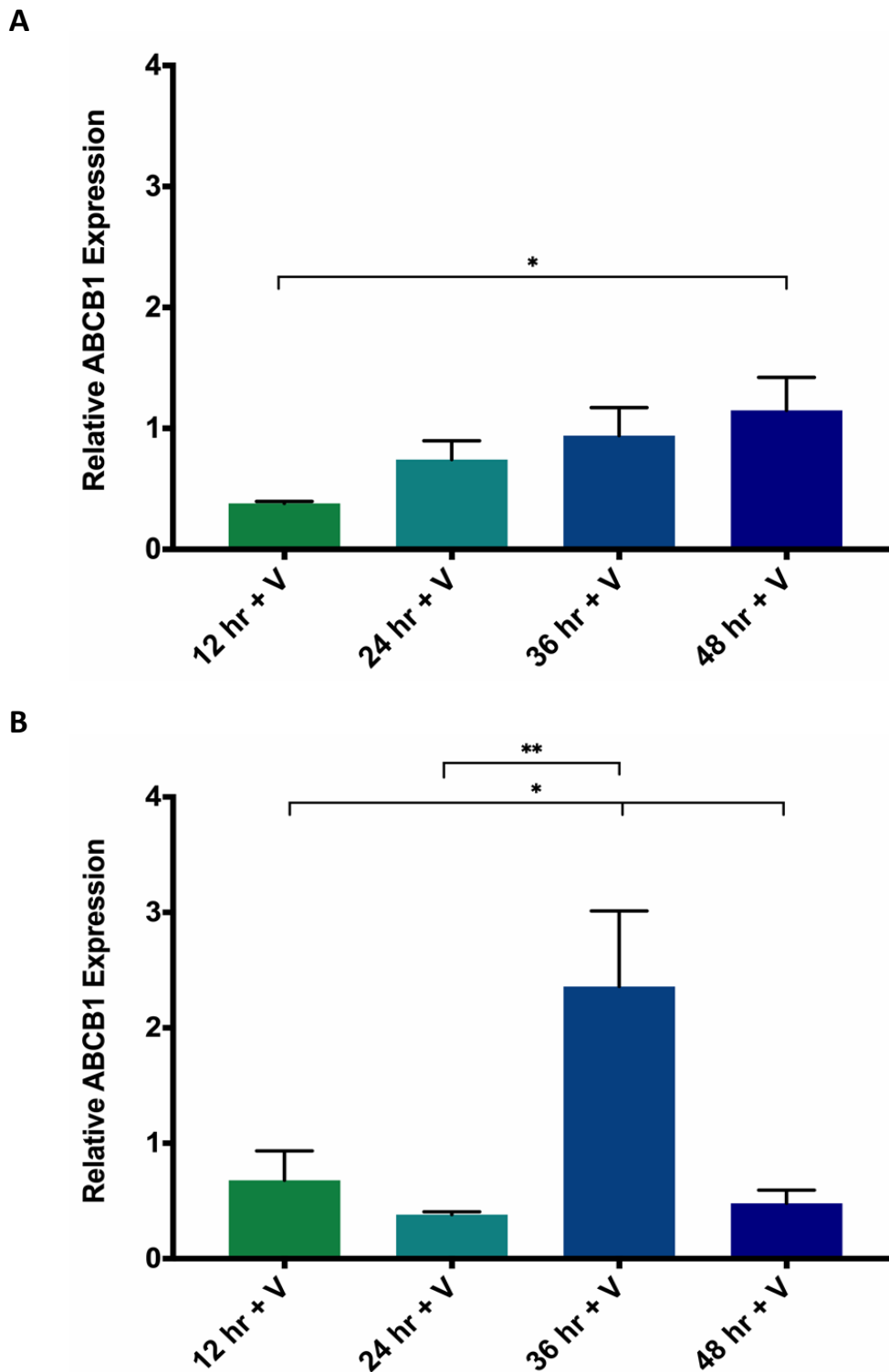


Figure 4.15 *ABCB1* expression increases following vincristine treatment. HDMB-03 and D283 cells were treated with 3.4 nM and 1.0 nM vincristine (IC_{50}) respectively and samples collected at 12 hour intervals. *ABCB1* expression was assayed using qRT-PCR. A) Vincristine resulted in significantly elevated *ABCB1* expression 48 hours post-treatment in the HDMB-03 cell line. B) Likewise, treatment with vincristine significantly increased *ABCB1* levels in D283 cells 36 hours post-treatment. Relative *ABCB1* expression displayed as fold change ($2^{-\Delta\Delta Cq}$) relative to the vehicle-treated controls collected at each time point. $n = 3$; mean \pm SEM; ** $P < 0.01$; * $P < 0.05$. Significance assessed by ordinary one-way ANOVA analysis with Tukey's multiple comparisons test.

4.4.2 YB-1 enrichment at the *ABCB1* promoter is likely altered dependent on the chemotherapeutic agent employed

To better understand the potential mechanisms underlying previously observed differential *ABCB1* expression levels in response to vincristine and cisplatin, we next employed ChIP assays to examine YB-1 enrichment at the *ABCB1* promoter following drug treatment. Accordingly, D283 and HDMB-03 Group 3 cell lines were treated with cisplatin and vincristine IC_{50} level. Following one hour of incubation (the time period where we observed maximal YB-1 translocation to the nucleus in response to cisplatin), cells were fixed and ChIP pull downs undertaken as previously described (Section 2.9.1).

Due to procurement issues severely affecting the supply of the consumables required for this experiment, we were only able to perform a single biological replicate of this assay. Nevertheless, the results appear interesting and support the resumption of further replicates when feasible. As displayed in Figure 4.16 A - B, our preliminary data indicates that treatment of both cell lines with cisplatin largely diminishes YB-1 enrichment at the *ABCB1* promoter, relative to the DMF-treated control. This finding may suggest that, although YB-1 levels in the nucleus increase following cisplatin treatment, YB-1 is diverted away from the *ABCB1* promoter toward an alternative transcriptional target, a finding intuitive given cisplatin is not a substrate of *ABCB1*. Comparatively, YB-1 enrichment is maintained and promoted at the *ABCB1* promoter relative to the DMSO-treated control following treatment with vincristine, perhaps indicative of the re-distribution of pre-existing nuclear YB-1 following vincristine-triggered cellular stress. This effect could then further stimulate transcriptional

activation of *ABCB1*; promoting the significantly increased levels of *ABCB1* expression we have previously demonstrated in response to vincristine (Figure 4.15). Of course, further repeats will be necessary to substantiate this theory.

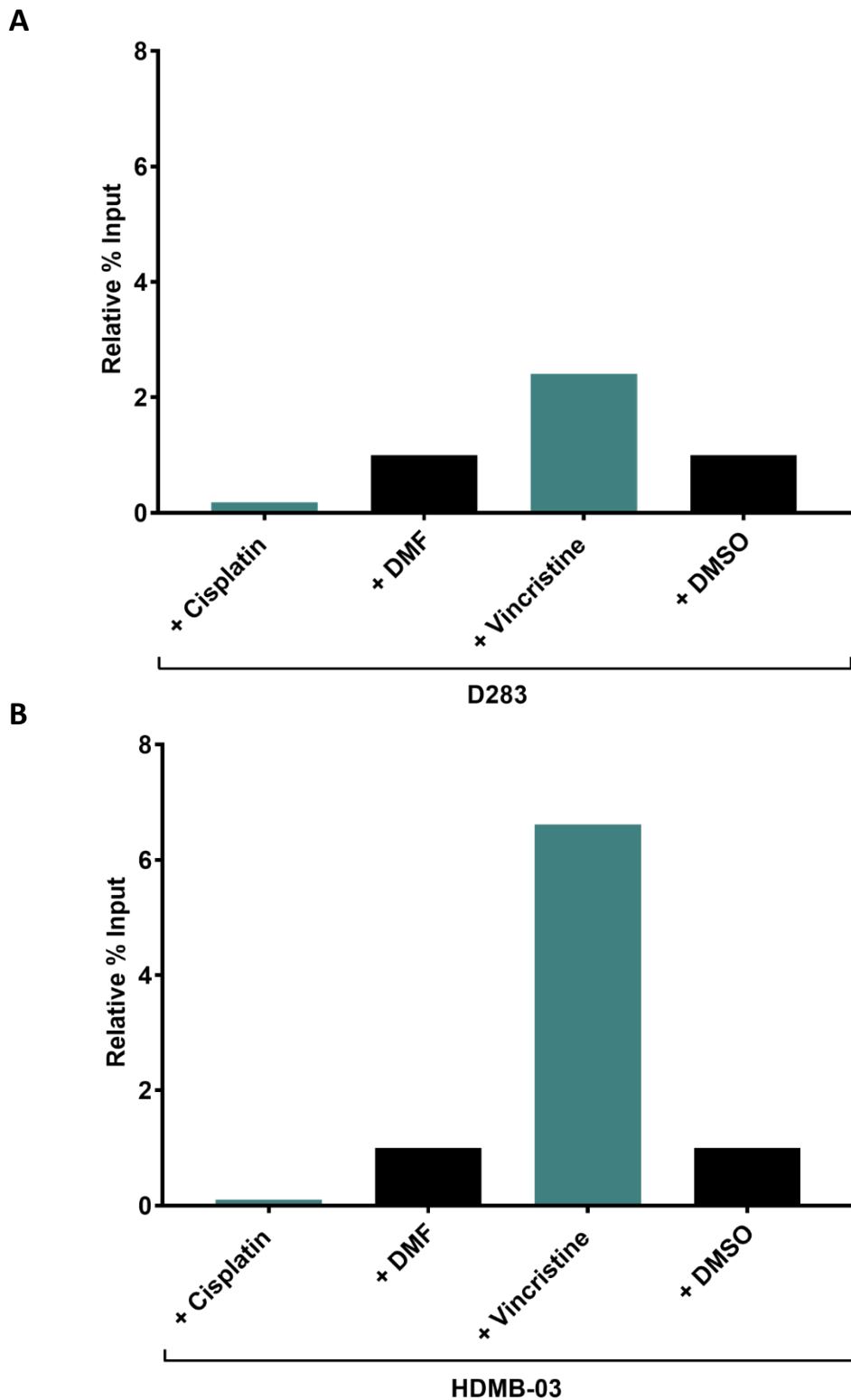


Figure 4.16 Cisplatin treatment may lessen YB-1 enrichment at the *ABCB1* promoter. D283 and HDMB-03 cells were treated with cisplatin and vincristine (or DMF and DMSO) at IC_{50} for 1 hr, following which ChIP assays were undertaken. ChIP assay products were analysed by qPCR. In D283 (A) and HDMB-03 (B) cells, YB-1 enrichment at the *ABCB1* promoter appeared reduced in response to cisplatin but maintained in response to vincristine, relative to vehicle treated controls. Preliminary data; n = 1. Data presented normalised to IgG control and relative to the vehicle-treated controls.

4.5 Summary

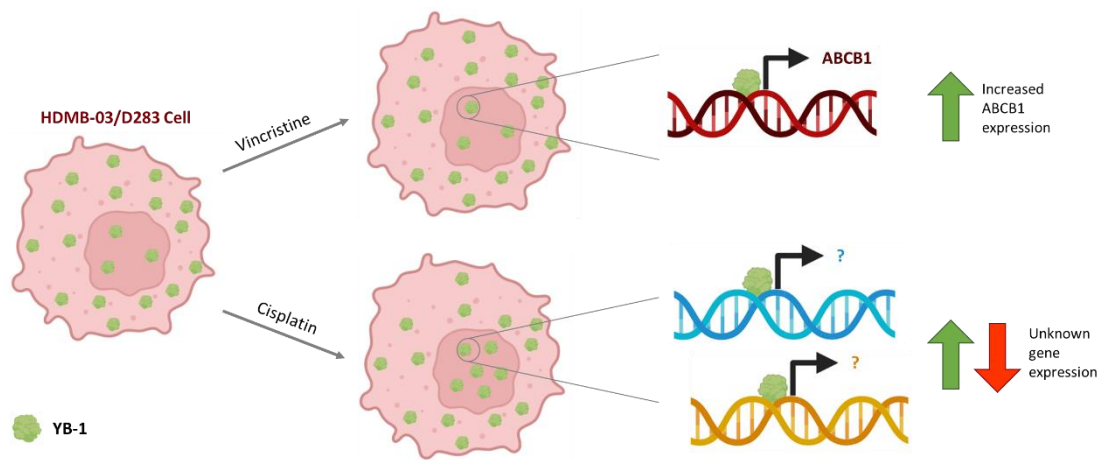


Figure 4.17 Graphical Summary. Treatment of HDMB-03 or D283 Group 3 medulloblastoma cell lines with vincristine does not significantly alter sub-cellular YB-1 expression or localisation, however does trigger increased expression of *ABCB1*, perhaps through re-distribution of pre-existing nuclear YB-1 to the *ABCB1* promoter and increased *ABCB1* transcription. Comparatively, cisplatin exposure does promote increased nuclear YB-1 levels, but without a significant alteration in *ABCB1* expression, likely indicative of a cellular stress response mediated by currently unknown YB-1 target genes.

- Comparison of YB-1 interaction at two predicted sequences within the *ABCB1* promoter by ChIP assay revealed that YB-1 interacts with a manually predicted inverted CCAAT box present at position -189 to -185, not with the Genomatix MatInspector predicted Y-Box present as position +108 to +119.
- YB-1 was found to be strongly enriched at the aforementioned inverted CCAAT box in HDMB-03 and D283 Group 3 cell lines.
- Treatment of HDMB-03 and D283 lines with cisplatin appears to promote significantly elevated levels of nuclear YB-1, perhaps indicative of increased YB-1 nuclear activity in response to this particular chemotherapeutic. In contrast, vincristine treatment did not significantly alter intracellular levels of YB-1 in either cell line.

- Chemotherapeutic treatment may alter the expression of drug-transporter *ABCB1*, with expression significantly elevated in HDMB-03 and D283 cell lines following treatment with vincristine, a known *ABCB1* substrate. Comparatively, cisplatin treatment did not have a significant effect on *ABCB1* expression in either cell line.
- Treatment of HDMB-03 and D283 Group 3 cell lines with different chemotherapeutic agents appears to differentially influence YB-1 enrichment at the *ABCB1* promoter. While vincristine treatment may maintain and promote YB-1 interaction at the CCAAT box site in both cell lines, cisplatin treatment may diminish such interaction.

Chapter 5

Functional analysis of the role
of YB-1 in drug resistance and
metastasis in
medulloblastoma

Chapter 5 Functional analysis of the role of YB-1 in drug resistance and metastasis in medulloblastoma

5.1 Introduction

In the previous chapter, we demonstrated that different chemotherapeutic treatments elicit different YB-1-related cellular responses, both in terms of YB-1 localisation/expression and YB-1 transcriptional regulation. Clearly, YB-1 has a varied and multi-functional role within medulloblastoma cells in response to different cellular stressors, all of which may promote cellular traits associated with chemoresistance. Indeed, silencing YB-1 has been demonstrated to increase cellular sensitivity to numerous cytotoxic drugs through a variety of suggested mechanisms. In paediatric and adult glioblastoma multiforme (GBM) models, depletion of YB-1 enhances temozolomide sensitivity, potentially through modulation of the MDM2/p53 pathway (Gao et al., 2009; Tong et al., 2019), whereas in neuroblastoma, silencing YB-1 *in vitro* sensitised cells to cisplatin, likely through disruption of NF- κ B signalling pathway (Wang et al., 2017). The effect of YB-1 depletion on medulloblastoma cells is, however, yet to be explored. Accordingly, we next wanted to examine the functional effect of YB-1 in cellular drug response and deduce whether it represents a novel driver of therapy tolerance in medulloblastoma.

Recent evidence has suggested that in addition to potential roles in drug tolerance, ABCB1 is also associated with metastasis in medulloblastoma patients (Nasir et al., 2021). Given our data indicating that YB-1 may act as a transcriptional regulator of *ABCB1*, combined with the strong association between *YB-1* and cancer cell invasion

in other cancer cell lines, we also wanted to deduce whether YB-1 is implicated in cancer cell invasion in medulloblastoma (Gao et al., 2009; Lasham et al., 2012; Lim et al., 2017; Lu et al., 2017).

As such, the aims of this chapter were as follows:

- A) Generate stable knockdown D283 and HDMB-03 Group 3 medulloblastoma cell lines exhibiting significantly reduced *YBX1* and YB-1 expression.
- B) Use the aforementioned *YBX1* knockdown lines to assess how diminished levels of YB-1 alter both the cellular response to various anti-cancer drugs and the invasive capacity of medulloblastoma cells.
- C) Analyse the *YBX1* knockdown cell lines by whole transcriptome RNA Sequencing in order to better understand the YB-1 transcriptome in Group 3 medulloblastoma.

5.2 shRNA-mediated knockdown of *YBX1* expression in medulloblastoma Group 3 cell lines

In order to generate stable *YBX1* knockdown cell lines, short hairpin RNA (shRNA) combined with the pGIPZ lentiviral system was selected (Horizon Discovery). The pGIPZ lentiviral vector uses a cytomegalovirus (CMV) promoter to drive transgene expression, encodes a TurboGFP reporter to facilitate monitoring of transduced cells, and encodes a puromycin drug resistance marker for selecting stable cell lines (see Appendix C1 for a lentiviral vector map). HDMB-03 and D283 cell lines were selected for transduction as both cell lines expressed YB-1 at protein and mRNA level, and both exhibited preliminary data to support a potential role for YB-1 in cellular stress response (Chapter 4). Prior to lentiviral transduction, both cell lines were subjected to treatment with increasing concentrations of puromycin in order to determine an appropriate concentration that would result in cell death. 2 µg/ml puromycin was deemed sufficient to kill D283 and HDMB-03 cell lines (Appendix C2).

5.2.1 Optimisation of shRNA knockdown

Prior to transduction with shRNA lentiviral particles (Section 2.6), relative transduction efficiency was first determined by ascertaining the functional titer of GIPZ non-silencing control virus particles in HDMB-03 and D283 lines (Figure 5.1). This was necessary as lentiviral titers provided with purchased GIPZ lentiviral particles are calculated by transducing HEK293T cells, not semi-adherent medulloblastoma cells, and transduction efficiency is known to vary significantly with cell type. By analysing the number of GFP-expressing colonies across a dilution series of non-silencing control shRNA viral stock, the relative transduction efficiency of

HDMB-03 cells was calculated to be 0.01 (Figure 5.1 C). This value was then used to calculate an extrapolated functional lentiviral titer for each virus particle, thus optimising the volume of virus particles required to achieve each multiplicity of infection (MOI) that would be employed in the HDMB-03 cell line. The aforementioned procedure was then repeated for D283 cells. The D283 line was found to have a relative transduction efficiency of 0.003 (Figure 5.1 C). This was deemed inefficient and further optimisation of the transduction protocol was undertaken in order to increase the efficiency of lentivirus-mediated gene transfer in this cell line. Common modifications to facilitate lentiviral transduction include: the addition of polybrene (hexadimethrine bromide) – a polycation that neutralizes the charge repulsion between the virus and cell target surface and/or spinoculation (“spinection”) - centrifugation to enhance viral infection. Both polybrene-alone, and polybrene plus spinoculation were trialled, in both cases using an adapted MOI (based upon the previously calculated relative transduction efficiency) of 0.05. As displayed in Figure 5.2, both methods proved similarly effective at this MOI, with a transduction efficiency of approximately 40% in both cases. Polybrene-alone was selected in order to avoid centrifugation.

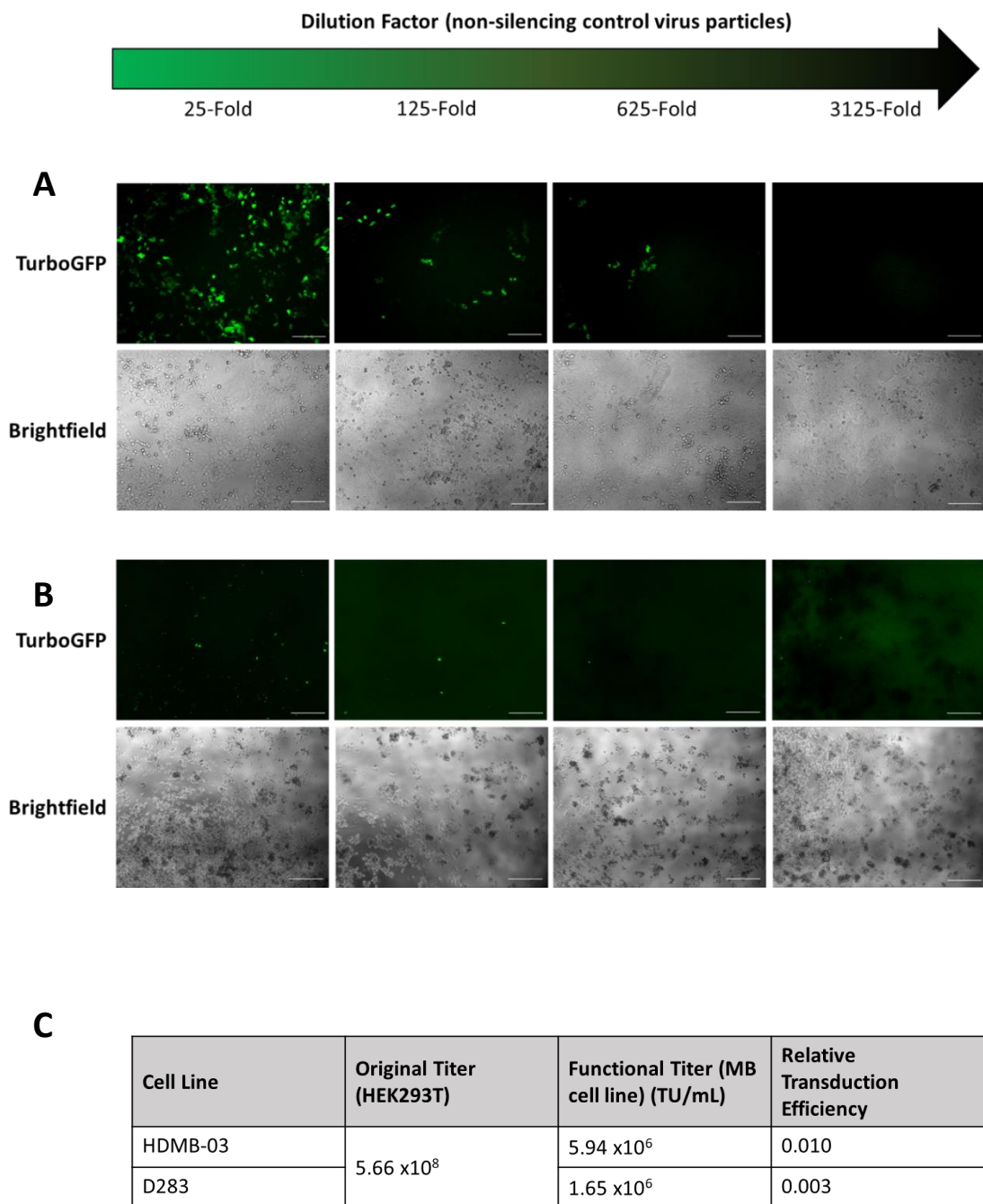


Figure 5.1 Calculation of lentiviral shRNA transduction efficiency in HDMB-03 and D283 cell lines. Relative transduction efficiency was determined by calculating the functional titer of GIPZ non-silencing control virus particles in each cell line of interest by analysing the number of GFP-expressing colonies across a dilution series of non-silencing control shRNA viral stock following a 72 hour incubation period. A) HDMB-03 cells displayed good levels of transduction at the lowest dilution of non-silencing shRNA particle (25x). B) D283 cells displayed very low levels of transduction at all four shRNA dilutions. All scale bars represent 500 μ m. C) Relative transduction efficiency was calculated by dividing the functional titer of non-silencing control shRNA virus stock in the cell line of interest by the titer of non-silencing control shRNA virus stock as calculated in HEK293T cells.

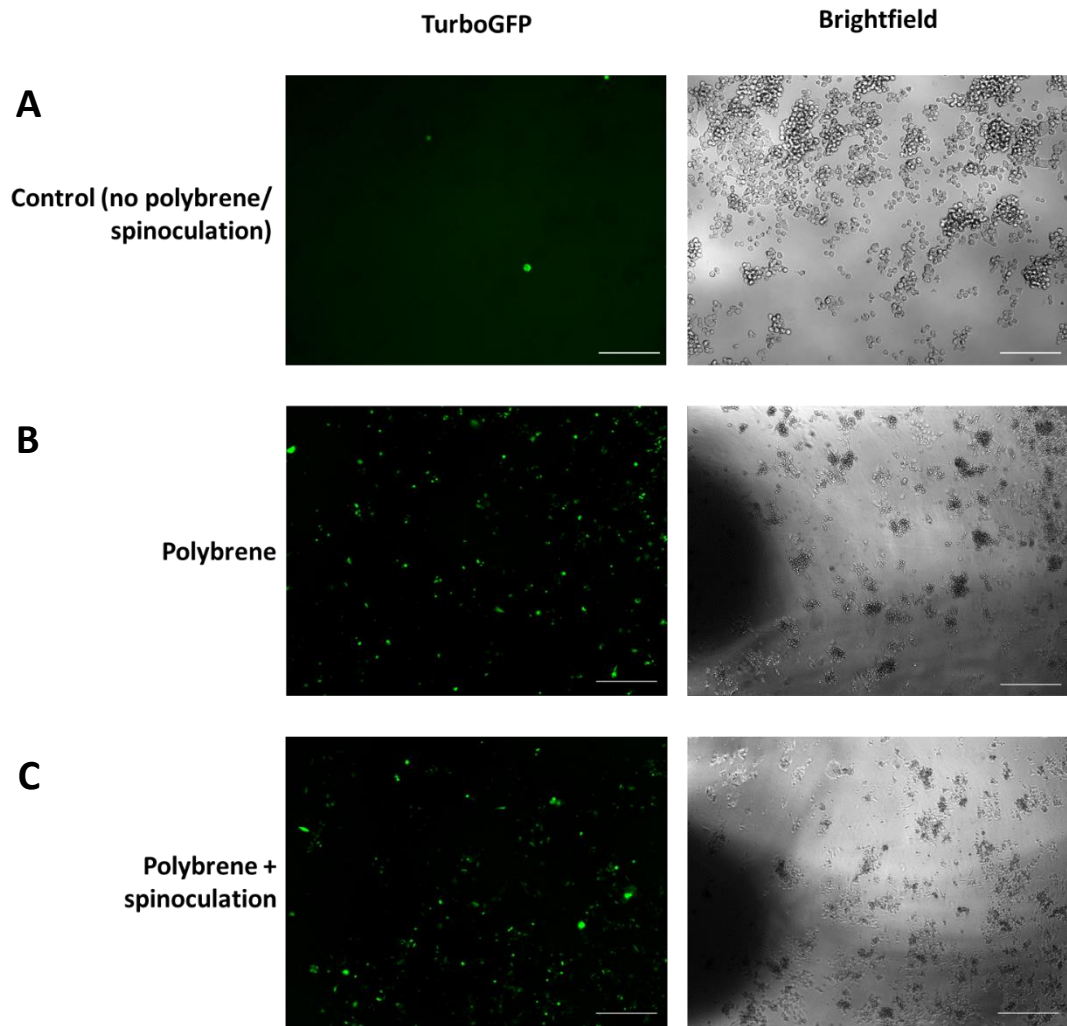


Figure 5.2 Incubation with polybrene enhances transduction efficiency in the D283 cell line. On account of very low transduction efficiency in the D283 cell line, modifications were made to the transduction protocol to enhance lentivirus-mediated gene transfer. A) D283 cells were transduced with non-silencing shRNA viral particles at an adjusted MOI of 0.05 alone and incubated for 72 hours to act as a control condition for protocol modification. B) D283 cells were transduced with non-silencing shRNA viral particles at an adjusted MOI of 0.05 and 8 $\mu\text{g}/\text{mL}$ polybrene and incubated for 72 hours. C) D283 cells were transduced with a 0.05 MOI of non-silencing shRNA viral particles and 8 $\mu\text{g}/\text{mL}$ polybrene, after which they were centrifuged at 2,000 rpm for 1 hour at room temperature and then incubated for 72 hours. All scale bars represent 500 μm .

5.2.2 Generation of stable *YBX1* knockdown cell lines

Using relative transduction efficiencies to calculate optimised MOIs (Section 5.2.1), HDMB-03 and D283 cells were infected with three *YBX1* shRNA constructs (*YBX1_A*; *YBX1_B*; *YBX1_C*) and one non-silencing shRNA control construct at MOIs ranging between of 0.1 and 0.5 (HDMB-03) and 0.03 and 0.1 (D283). *YBX1* shRNA construct sequences and target regions are described in detail in Section 2.6. The level of GFP expression was then analysed 72 hr after infection by immunofluorescence. This resulted in an infection efficiency of 30 – 70% in transduced HDMB-03 cells and 5 – 60% in transduced D283 cells, which in both cases increased with increasing MOI. Representative images of the lowest and highest MOIs tested are displayed in Figure 5.3 and Figure 5.4. For all MOIs tested, cells were then treated with puromycin at a previously optimised kill concentration of 2 µg/ml to select for transduced cells and lines expanded. Throughout the expansion process, cells were cultured in puromycin-containing media and GFP-expression monitored regularly to ensure 100% of cells possessed the required shRNA construct.

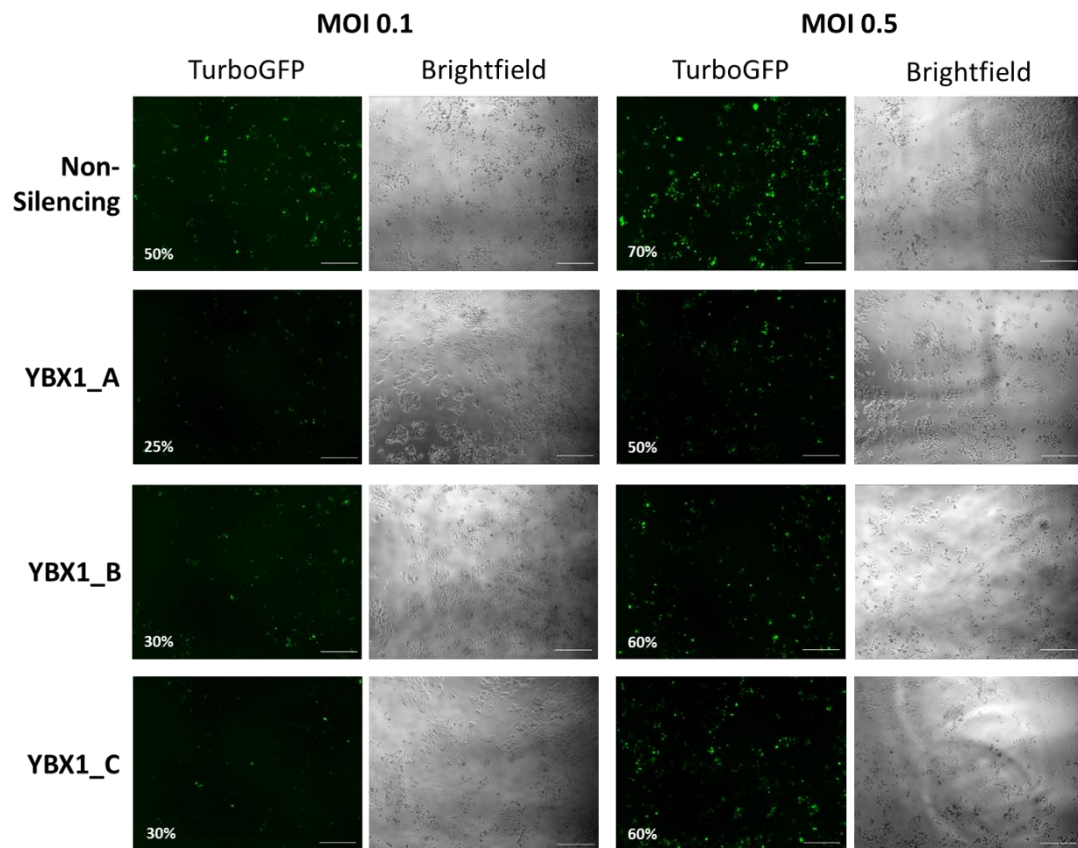


Figure 5.3 Comparison of lentiviral construct infection efficiencies within the HDMB-03 cell line. Group 3 cell line HDMB-03 was transduced with three different shRNA constructs targeting different regions of the *YBX1* gene at a range of MOIs. A non-silencing shRNA construct was also utilised in order to generate control cell lines. Infection efficiency was assessed 72 hours post-transduction via fluorescence microscopy where GFP-expressing cells indicate successful shRNA transduction. Approximate infection efficiencies are displayed in white. Scale bars represent 500 μ m.

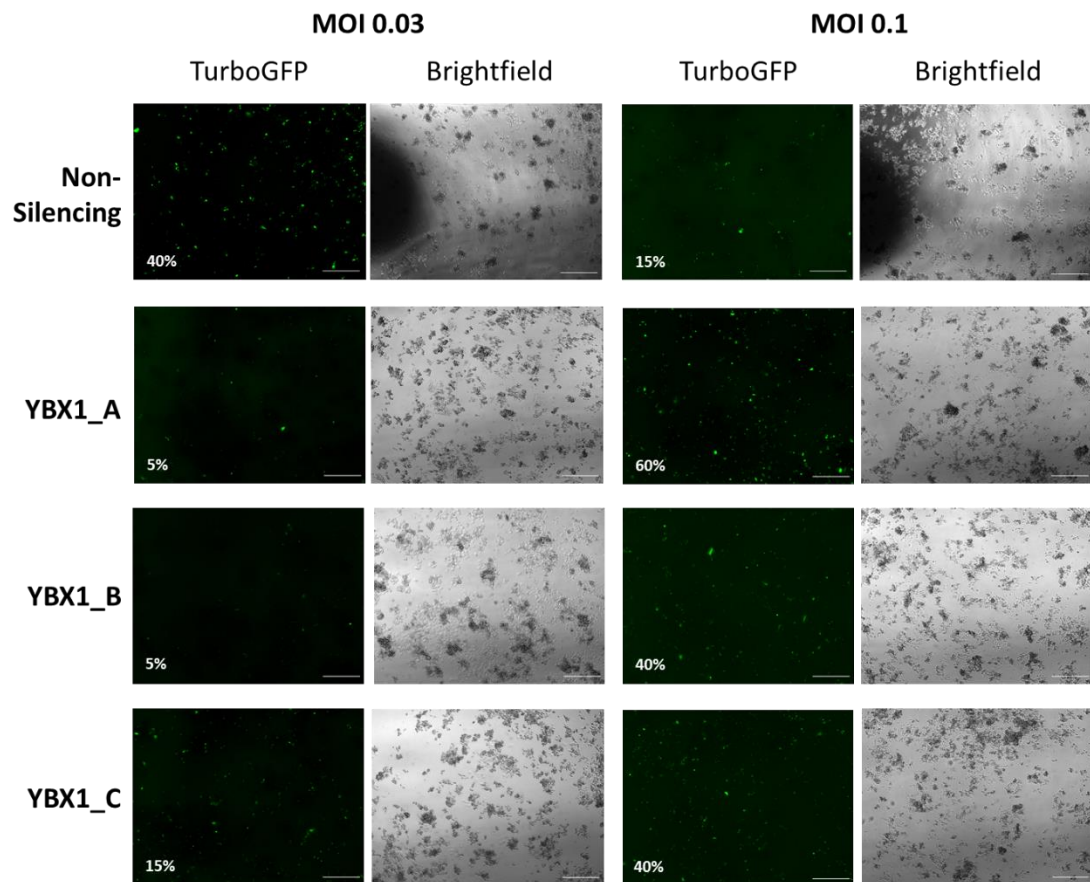


Figure 5.4 Comparison of lentiviral construct infection efficiencies within the D283 cell line. Group 3 cell line D283 was transduced with three different shRNA constructs targeting different regions of the *YBX1* gene at a range of MOIs. A non-silencing shRNA construct was also utilised in order to generate control cell lines. Infection efficiency was assessed 72 hours post-transduction via fluorescence microscopy where GFP-expressing cells indicate successful shRNA transduction. Approximate infection efficiencies are displayed in white. Scale bars represent 500 μ m.

5.2.3 Validation of Group 3 *YBX1* knockdown cell lines

To assess the efficiency of *YBX1* knockdown and determine which shRNA constructs and MOIs would be taken forward for functional analysis, *YB-1* expression was quantified at mRNA and protein level across D283 and HDMB-03 knockdown cell lines (KD-D283 and KD-HDMB-03). Accordingly, the effect of each *YBX1* shRNA construct (*YBX1_A* – *YBX1_C*) on *YBX1*/*YB-1* expression, at the highest and lowest MOIs tested was quantified relative to that detected in the matched non-silencing control cell line (KD-D283-N.S. and KD-HDMB-03-N.S.) across cell pellets from consecutive passages.

At mRNA level, only the *YBX1_A* shRNA construct resulted in significant *YBX1* depletion in both D283 and HDMB-03 cells (Figure 5.5). In both lines, an optimised MOI of 0.1 resulted in the greatest reduction in *YBX1* expression - 93% in the KD-HDMB-03-Y_A-0.1 cell line ($P = 0.011$) and by 73% in the KD-D283-Y-A_0.1 line ($P = 0.0052$). In HDMB-03 cells, the *YBX1_A* shRNA construct also caused a significant reduction in *YBX1* at an MOI of 0.5 ($P = 0.013$), as did the *YBX1_C* shRNA construct at an MOI of 0.5 ($P = 0.035$).

To ensure depletion in *YBX1* expression observed at an mRNA level was maintained at a protein level, the cell line with the highest level of *YBX1* knockdown was taken forward for western blot analysis. As anticipated, in both KD-HDMB-03-Y_A-0.1 and KD-D283-Y-A_0.1 lines a significant reduction in *YB-1* protein was observed (Figure 5.6). The KD-HDMB-03-Y_A-0.1 line exhibited an 83% reduction in *YB-1* expression ($P = 0.0011$), whilst the KD-D283-Y-A_0.1 exhibited a 50% reduction in protein expression ($P = 0.023$) compared to the appropriate non-silencing control line, replicating the trends seen at a transcriptional level.

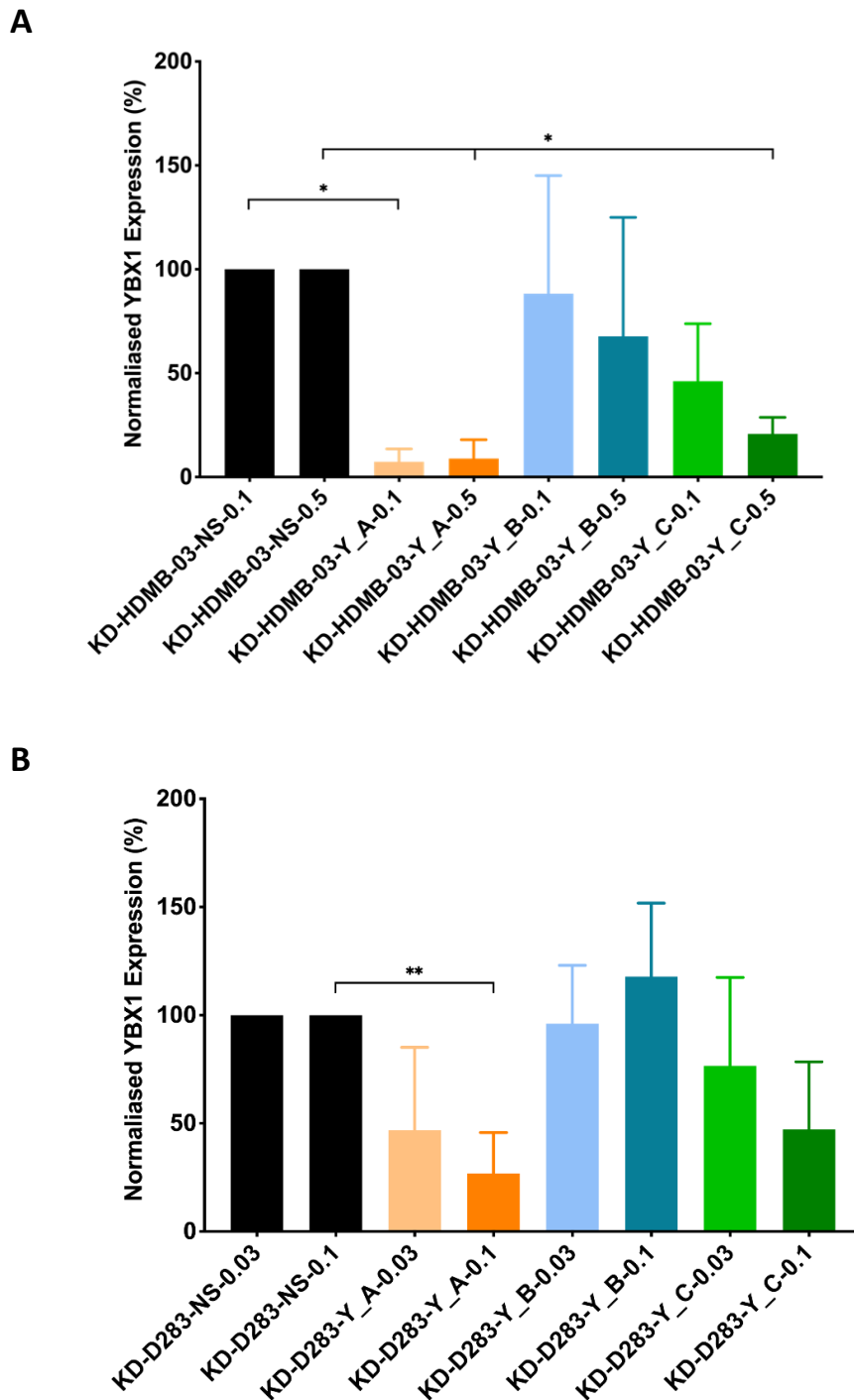


Figure 5.5 shRNA-mediated knockdown of *YBX1* effectively depletes *YBX1* mRNA expression in HDMB-03 and D283 Group 3 medulloblastoma cell lines. A) In HDMB-03 cells, *YBX1* was significantly depleted using the *YBX1_A* shRNA construct at an MOI of 0.1 and 0.5 (KD-HDMB-03-Y_A-0.1 and KD-HDMB-03-Y_A-0.5) and the *YBX1_C* construct at an MOI of 0.5 (KD-HDMB-03-Y_C-0.5), compared to the appropriate non-silencing control cell line (KD-HDMB-03-N.S.-0.1 and KD-HDMB-03-N.S.-0.5). B) In D283 cells, *YBX1* was significantly depleted using the *YBX1_A* shRNA construct at an MOI of 0.1 (KD-D283-Y_A-0.1) compared to the non-silencing control (KD-D283-N.S.-0.1). Relative *YBX1* expression displayed as fold change ($2^{-\Delta\Delta Cq}$) relative to the appropriate non-silencing control. n = 3; mean \pm SEM; **P < 0.01; *P < 0.05. Significance assessed by ordinary one-way ANOVA analysis with Sidak's multiple comparisons test.

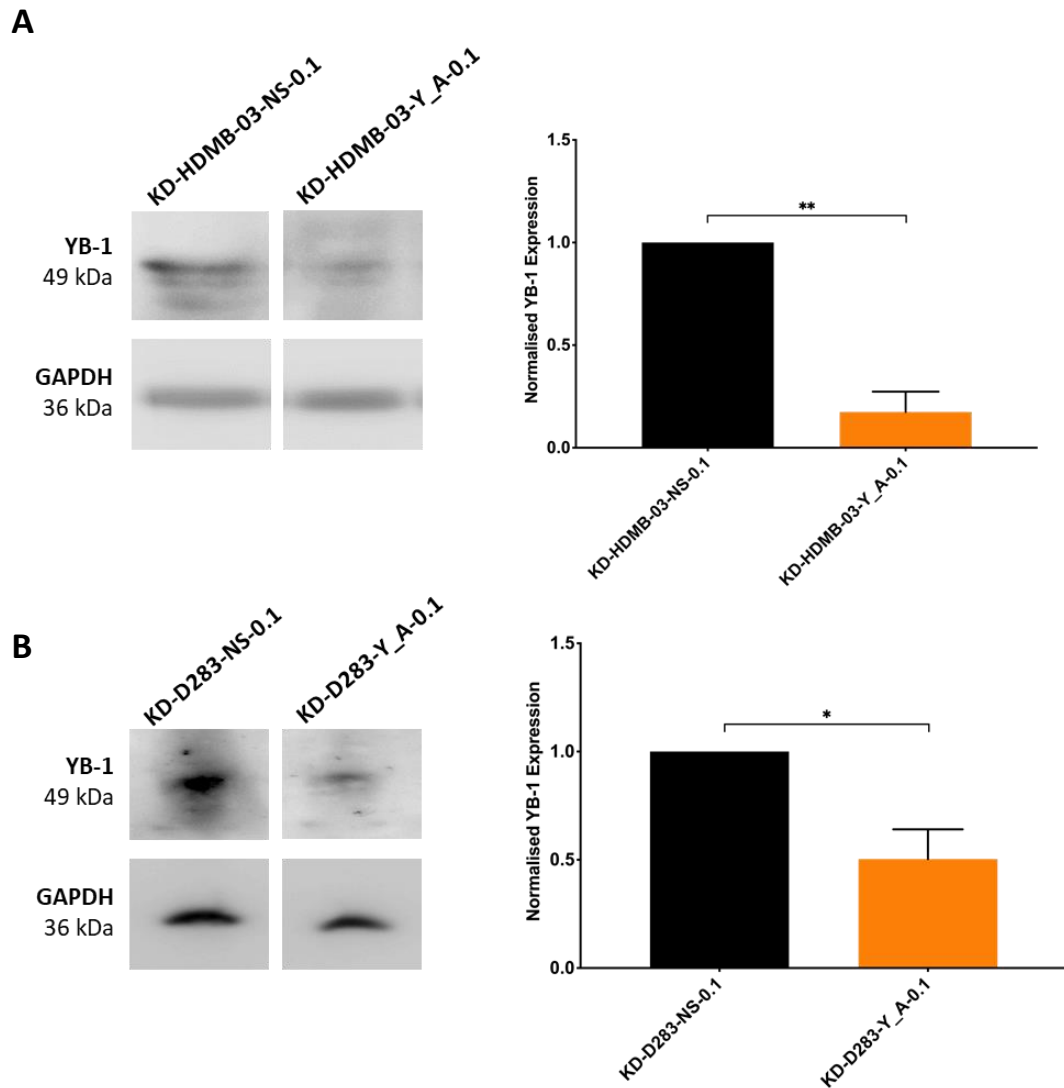
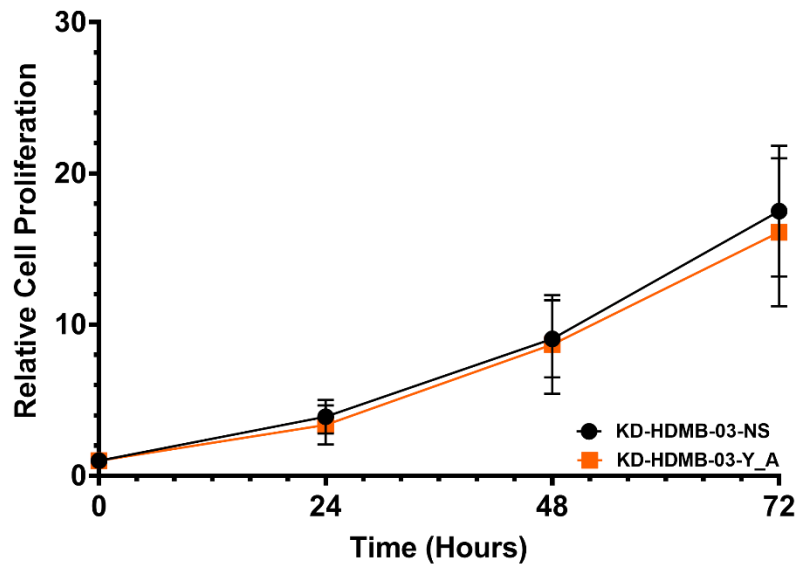


Figure 5.6 shRNA-mediated knockdown of *YBX1* effectively depletes **YB-1** protein expression in **HDMB-03** and **D283** Group 3 medulloblastoma cell lines. A) Western blot analysis and concurrent densitometry quantification revealed YB-1 expression to be significantly depleted in the KD-HDMB-03-Y_A-0.1 line compared to the non-silencing control line KD-HDMB-03-N.S.-0.1. B) Likewise, western blot analysis and densitometry quantification of KD-D283-Y_A-0.1 cells revealed reduced YB-1 expression compared to the non-silencing control line KD-D283-N.S.-0.1. Densitometry data are presented relative to the GAPDH loading control and normalised to the appropriate non-silencing control cell line. Mean \pm SEM plotted. $n = 3$; statistically significant differences are indicated as * $P < 0.05$ and ** $P < 0.01$, where significance was assessed by unpaired t-test. Full length western blots are presented in Appendix C3.

Prior to functional analysis of the consequence of YB-1 depletion in HDMB-03 and D283 cells on drug resistance, invasion and YB-1 transcriptional control, it was important to understand what effect, if any, reduction of YB-1 expression had on the proliferative capacity of both Group 3 cell lines. Cells were plated, following which a PrestoBlue metabolic activity assay was undertaken at 0, 24, 48 and 72 hour time points and cell proliferation calculated relative to the 0 hour cell viability fluorescence reading. As displayed in Figure 5.7, *YBX1* knockdown did not appear to alter the cell growth in the KD-HDMB-03-Y_A-0.1 cell line when compared to the KD-HDMB-03-N.S.-0.1 control line (henceforth described as KD-HDMB-03-Y_A and KD-HDMB-03-N.S. respectively). Similarly, no significant alteration in proliferative capacity was observed in the KD-D283-Y_A-0.1 cell line when compared to the KD-D283-N.S.-0.1 control line (henceforth described as KD-D283-Y_A and KD-D283-N.S. respectively), although the knockdown line did trend towards reduced proliferation. This finding was unexpected as silencing of the *YBX1* gene has been associated with the suppression of proliferation in other cancer cell lines (Fujiwara-Okada et al., 2013; Gong et al., 2020). This observation may further highlight the cancer- and cell-type dependent nature of YB-1 cellular functions.

A



B

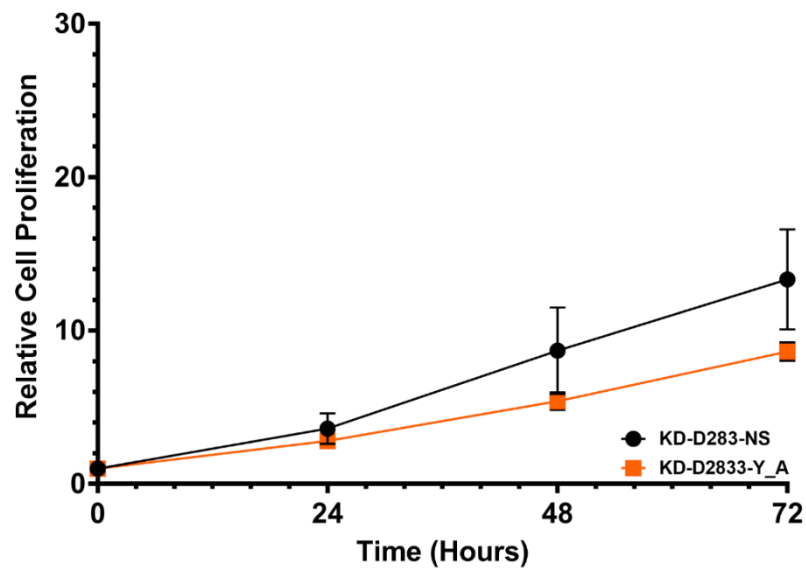


Figure 5.7 Depletion of YB-1 does not alter the proliferative capacity of HDMB-03 or D283 Group 3 medulloblastoma cell lines. In order to assess the effect of *YBX1* knockdown on proliferation, cell metabolic activity was assessed at 0, 24, 48 and 72 hour time points using an end-point PrestoBlue cell viability assay. A) No difference in relative cell proliferation was detected between KD-HDMB-03-N.S. and KD-HDMB-03-Y_A. $n = 3$. B) Similarly, no significant difference in proliferation was observed between KD-D283-N.S. and KD-D2833-Y_A at any time point tested. $n = 5$. Metabolic activity at each time point relative to metabolic activity at the 0 hour time point was used to calculate relative cell proliferation. Mean \pm SEM plotted. Significance was assessed by way of multiple t-tests with Holm-Sidak multiple comparisons testing.

5.3 Effect of YB-1 depletion on cellular sensitivity to anti-cancer agents

5.3.1 YB-1 depletion sensitises medulloblastoma Group 3 cell lines to vincristine

As previously described (Section 5.1), YB-1 expression has been linked to chemoresistance in a number of cancer cell lines. Therefore, we next wanted to investigate the effect of YB-1 depletion on chemoresistance in medulloblastoma. First, KD-HDMB-03 and KD-D283 cell lines were subjected to increasing doses of standard-of-care medulloblastoma chemotherapeutics cisplatin and vincristine and cell viability assessed following a 72 hour incubation period by way of PrestoBlue cell viability assays. As revealed in Figure 5.8 A and B, inhibition of YB-1 was found to significantly sensitise both HDMB-03 and D283 cells to vincristine, corresponding to a 36% and 58% reduction in IC_{50} , respectively. Interestingly, this effect was strongest at relatively low concentrations – 0.5 and 1 nM in the KD-HDMB-03-Y_A line and 0.5 nM, 1 nM and 5 nM in the KD-D283-Y_A line. Importantly, the measurable concentration of vincristine in the cerebrospinal fluid (CSF) is low, lying between 0.8 and 1.1 nM (Jackson et al., 1981). Thus, YB-1 depletion appears to potentiate vincristine treatment within a clinically achievable range in both cell lines.

Comparatively, cellular YB-1 reduction had little impact on cell sensitivity to cisplatin (Figure 5.8 C and D). In Section 4.3, we demonstrated a significant elevation in nuclear YB-1 level upon cisplatin treatment, which we hypothesised may indicate that YB-1 elicits some sort of protective cellular stress response consequent to cisplatin. Based upon these data, it appears YB-1 is either not implicated in the modulation of cisplatin resistance in these cell lines, or is insufficient to mediate

resistance alone. Alternatively, it is possible that the remaining YB-1 protein expression within HDMB-03 and D283 cells following *YBX1* knockdown (20 – 50%) is ample to trigger YB-1-mediated cisplatin resistance associated events. In order to better understand these findings, further experiments investigating YB-1 targets within the nucleus in response to cisplatin treatment will be crucial.

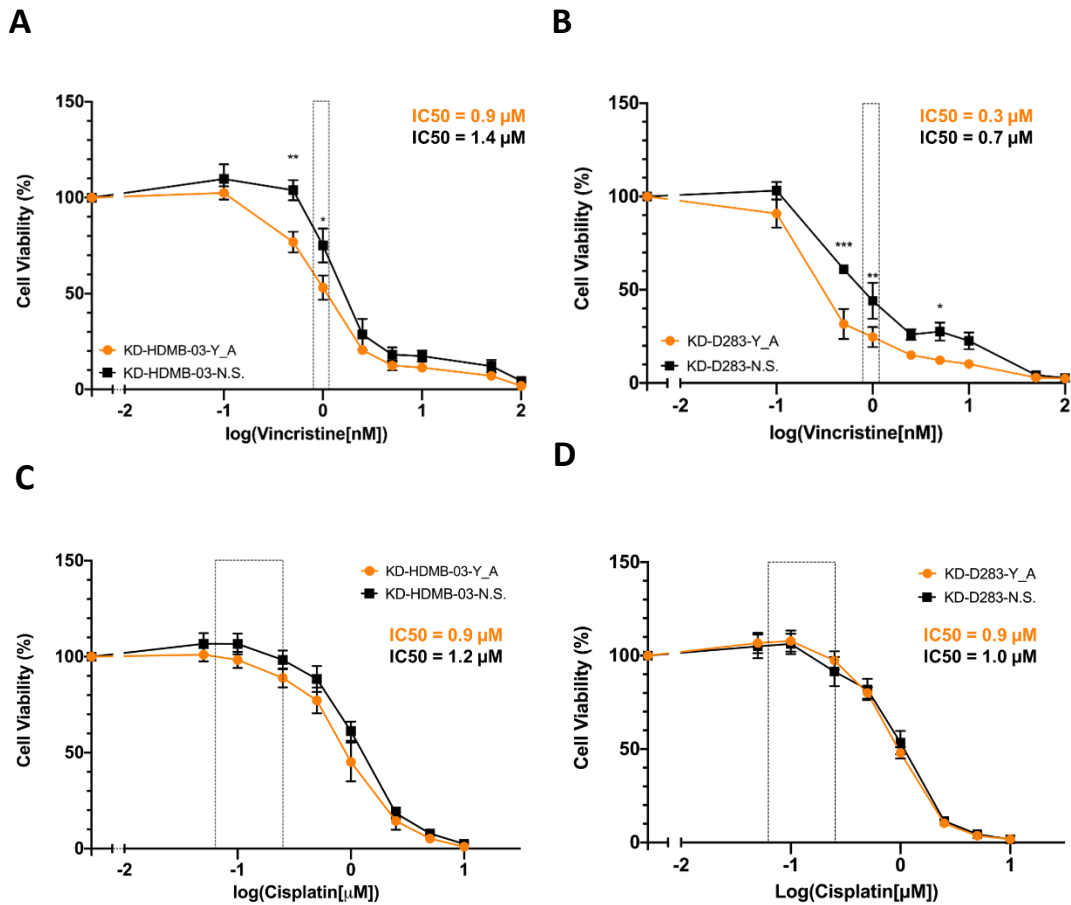


Figure 5.8 YB-1 depletion sensitises HDMB-03 and D283 cells to vincristine but not cisplatin treatment. KD-D283 and KD-HDMB-03 cells were treated with various doses of vincristine (0.1, 0.5, 1.0, 2.5, 5.0, 10, 50 and 100 nM) and cisplatin (0.05, 0.1, 0.25, 0.5, 1.0, 2.5, 5.0 and 10 μ M) for 72 hours, after which cell viability was assessed by PrestoBlue cell viability assays. A) KD-HDMB-03-Y_A cells showed a significant reduction in cell viability compared to the KD-HDMB-03-N.S. control line at 0.5 and 1 nM vincristine treatment. B) KD-D283-Y_A cells showed a significant reduction in cell viability compared to the KD-D283-N.S. control line at 0.5 nM, 1 nM and 5 nM vincristine treatment. C) No change in cell viability was detected in KD-HDMB-03-Y_A cells compared to the KD-HDMB-03-N.S. control line in response to cisplatin. D) No change in cell viability was detected in KD-D283-Y_A cells compared to the KD-D283-N.S. control line in response to cisplatin. Grey boxes depict clinically achievable drug CSF concentrations. Mean \pm SEM plotted; n = 4; statistically significant differences are indicated as *P < 0.05, **P < 0.01 and ***P < 0.001. Significance was assessed by way of Two-Way ANOVA with Sidak's multiple comparisons test.

5.3.2 YB-1 depletion results in significantly reduced expression of drug-efflux pump *ABCB1*

In Section 4.2 we demonstrated that YB-1 interacts with the *ABCB1* promoter in both HDMB-03 and D283 cell lines. We have also shown that *YBX1* knockdown sensitises both D283 and HDMB-03 cell lines to vincristine, which is an *ABCB1* substrate (Section 5.3.1). Accordingly, we hypothesised that the increased sensitivity to vincristine exhibited by YB-1 depleted cell lines may arise from decreased expression of *ABCB1*. Using qRT-PCR, we investigated the expression levels of *ABCB1* in *YBX1* knockdown cell lines relative to that in non-silencing control lines (Figure 5.9). As anticipated, genetic disruption of *YBX1* significantly reduced the expression of *ABCB1* by ~40% in KD-HDMB-03-Y_A (P = 0.012) and ~50% KD-D283-Y_A (P = 0.029) Group 3 cell lines, a finding which further supports the notion that YB-1 transcriptionally regulates *ABCB1* and importantly, suggests that YB-1 may mediate cellular resistance to vincristine through the expression of drug efflux pump *ABCB1*.

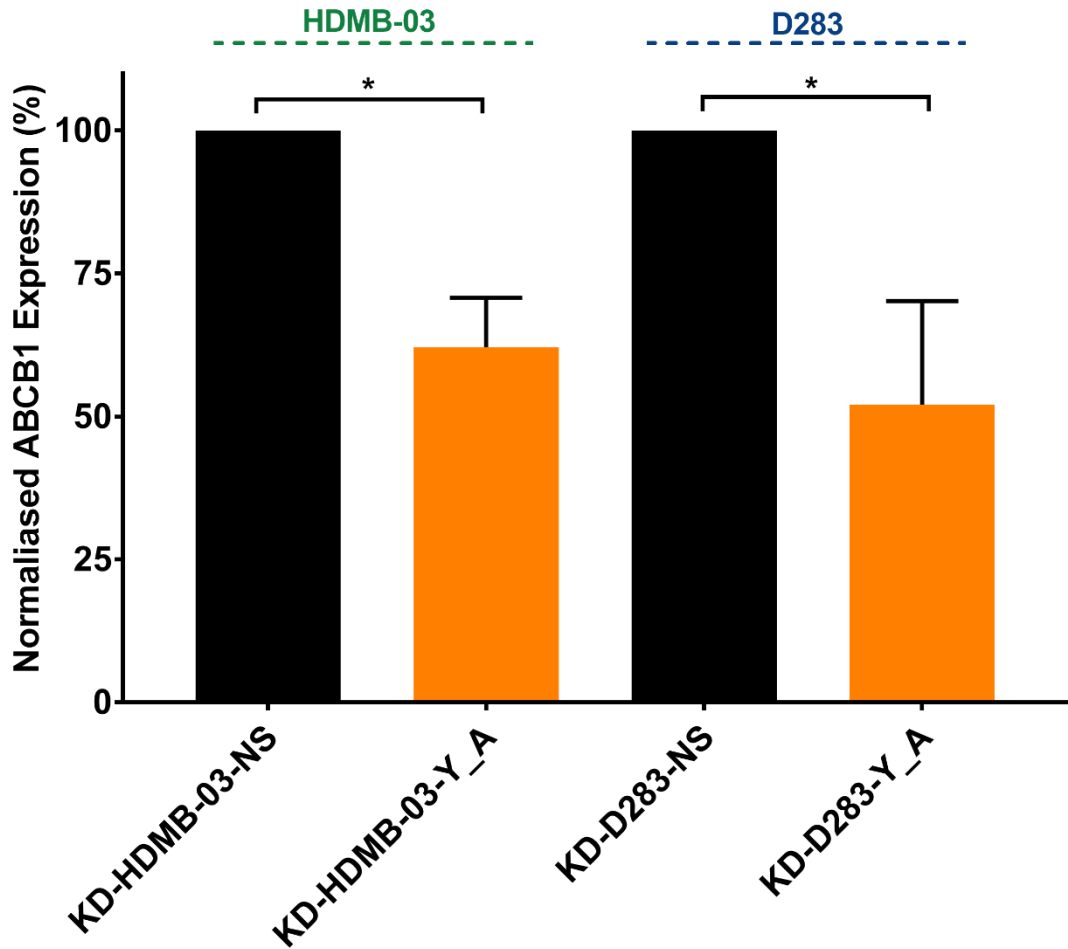


Figure 5.9 *YBX1* knockdown reduces *ABCB1* expression in Group 3 medulloblastoma cell lines. *ABCB1* expression in KD-D283 and KD-HDMB-03 cell lines was analysed by qRT-PCR and quantified relative to non-silencing controls. KD-HDMB-03-Y_A (n = 3) and KD-D283-Y_A cells (n = 5) exhibited a significant reduction in *ABCB1* expression relative to the non-silencing control line. Mean \pm SEM plotted; statistically significant differences are indicated as *P < 0.05 and ***P < 0.001. Significance was assessed using an unpaired t-test.

5.3.3 YB-1 depletion sensitises medulloblastoma Group 3 cell line HDMB-03 to HDAC inhibitor panobinostat and BET bromodomain inhibitor JQ1

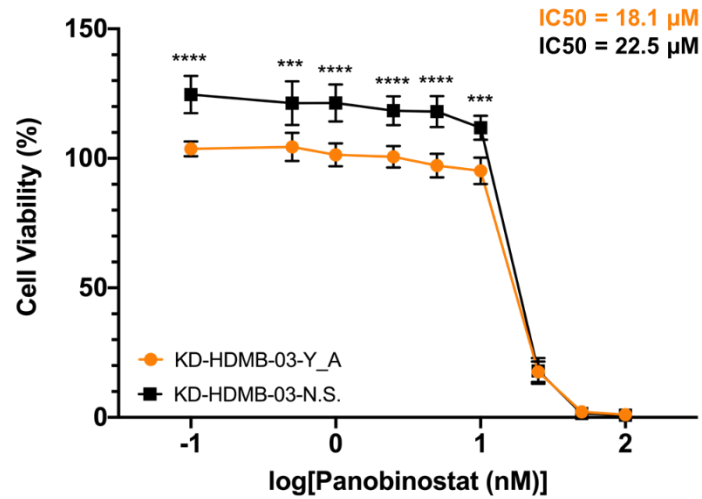
In addition to assessing how YB-1 depletion alters cellular response to current, standard-of-care medulloblastoma therapies, we also wanted to assess if loss of YB-1 function had any effect on cell sensitivity to novel medulloblastoma therapies. Panobinostat is a histone deacetylase (HDAC) inhibitor which has proven to be effective in the inhibition of *in vivo* models of *MYC*-driven Group 3 medulloblastoma, likely through the induction of *FOXO1* expression, a tumour suppressor gene (Pei et al., 2016). It is currently being examined in an Early Phase 1 clinical trial (NCT04315064) designed to examine the safety and antitumor activity of panobinostat infusions in patients with recurrent medulloblastoma. JQ1 is a BET bromodomain inhibitor which has shown promising anti-proliferative and pro-survival effects in *MYC*-amplified medulloblastoma in *in vitro* and *in vivo* models (Bandopadhyay et al., 2014; Bandopadhyay et al., 2019). Cell viability curves for both parental cell lines in response to JQ1 and panobinostat can be found in Appendix C4.

To assess the consequence of YB-1 reduction on cell viability to both anti-cancer agents, KD-HDMB-03 and KD-D283 cell lines were subjected to increasing doses of panobinostat and JQ1 and cell viability assessed relative to a vehicle (DMSO)-treated control following a 72 hour incubation period by way of PrestoBlue cell viability assays. As displayed in Figure 5.10 A, YB-1 depletion in the KD-HDMB-03-Y_A line resulted in a 20% reduction in IC_{50} in response to panobinostat when compared with the KD-HDMB-03-N.S. line. This reduction in survival was significant in the range of 0.1 – 10 nM panobinostat, however at doses greater than this YB-1 depletion did not

impact cell survival. This finding suggests that YB-1 may play a function in the mediation of cell survival and tolerance to panobinostat treatment. Conversely, YB-1 depletion in the KD-D283-Y_A line had no effect on cell viability in response to panobinostat, with the KD-D283-Y_A and KD-D283-N.S. cell lines exhibiting almost identical responses to the drug (Figure 5.10 B).

YBX1 knockdown had a similar effect in the KD-HDMB-03-Y_A cell line in response to JQ1, where a significant reduction in cell viability was recorded at 0.05, 0.1, 0.5, 1.0 and 5 μ M JQ1, corresponding to a 50% reduction in IC_{50} (Figure 5.11 A), compared to the non-silencing control cell line. Comparatively, no significant difference in cell viability was recorded between the KD-D283-Y_A line and KD-D283-N.S. line in response to JQ1 treatment (Figure 5.11 B), suggesting that YB-1 does not have a functional role in cell survival and/or the maintenance of drug tolerance in response to JQ1 in the D283 cell line. The cellular sensitivity displayed by the KD-D283-Y_A line in response to JQ1 and panobinostat compared to that in response to vincristine may also indicate that the mechanisms of tolerance to these drugs in medulloblastoma cell lines do not involve ABCB1. Further investigations, such as sequencing and pathway analysis, will be required to better understand YB-1-mediated mechanisms of resistance to these novel anti-cancer therapies.

A



B

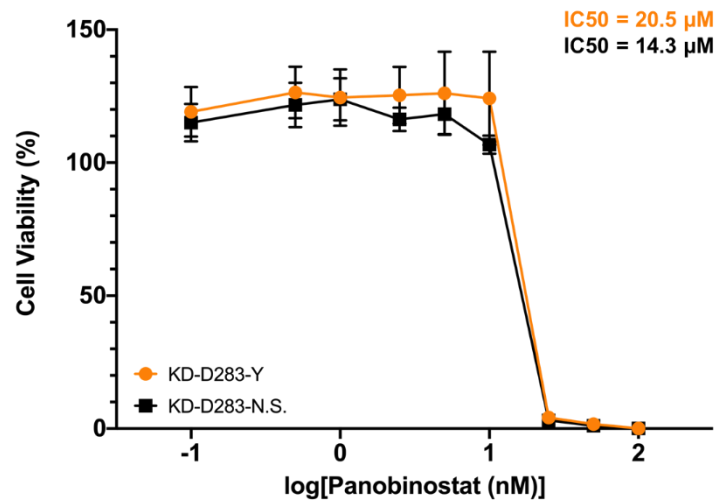


Figure 5.10 YB-1 depletion sensitises HDMB-03 cells to HDAC inhibitor panobinostat. KD-HDMB-03 and KD-D283 cells were treated with increasing doses of panobinostat (0.1, 0.5, 1.0, 2.5, 5.0, 10, 50 and 100 nM) for 72 hours, after which cell viability was assessed by PrestoBlue and presented as a percentage relative to the vehicle (DMSO). A) Treatment of KD-HDMB-03-Y_A cells with panobinostat resulted in a significant reduction in cell viability compared to the non-silencing control line KD-HDMB-03-N.S. $n = 4$. B) Treatment of KD-D283-Y_A cells with panobinostat did not significantly alter cell viability compared to the relevant non-silencing control line. $n = 3$; mean \pm SEM plotted; statistically significant differences are indicated as *** $P < 0.001$ and **** $P < 0.0001$. Significance was assessed by way of Two-Way ANOVA with Sidak's multiple comparisons test.

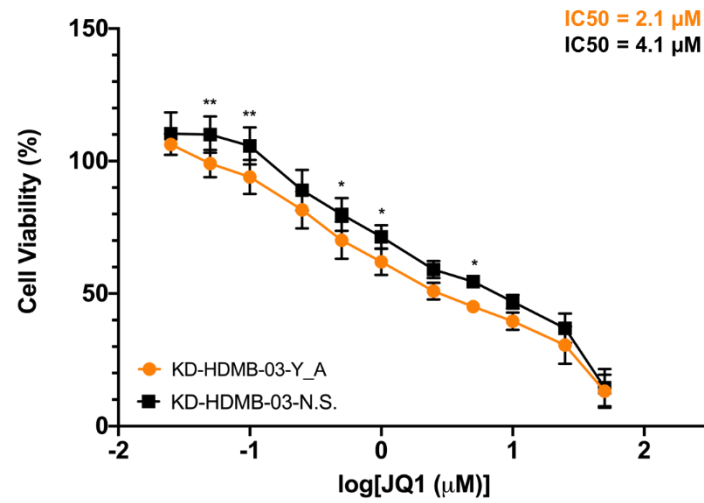
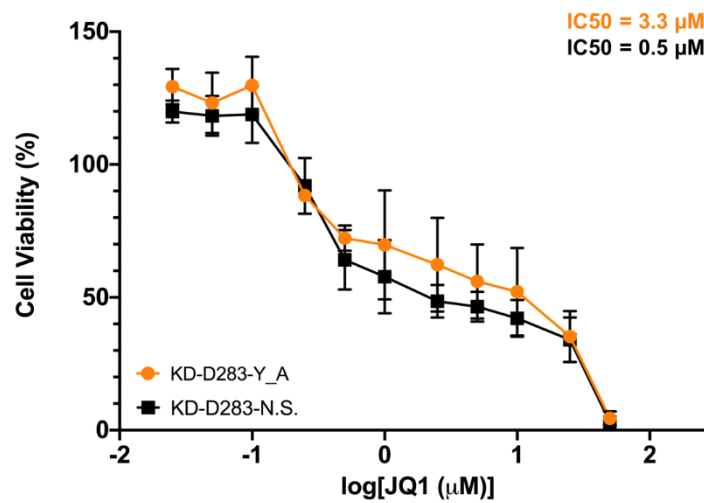
A**B**

Figure 5.11 YB-1 depletion sensitises HDMB-03 cells to BET bromodomain inhibitor JQ1. KD-HDMB-03 and KD-D283 cells were treated with increasing doses of JQ1 (0.025, 0.05, 0.1, 0.25, 0.5, 1.0, 2.5, 5, 10, 25 and 50 µM) for 72 hours, after which cell viability was assessed by PrestoBlue and presented as a percentage relative to the vehicle (DMSO). A) Treatment of KD-HDMB-03-Y_A cells with JQ1 resulted in a significant reduction in cell viability compared to the non-silencing control line KD-HDMB-03-NS. $n = 4$. B) Treatment of KD-D283-Y_A cells with JQ1 did not significantly alter cell viability compared to the relevant non-silencing control line. $n = 3$; mean \pm SEM plotted; statistically significant differences are indicated as * $P < 0.05$ and ** $P < 0.01$. Significance was assessed by way of Two-Way ANOVA with Sidak's multiple comparisons test.

We were curious to investigate whether the differing responses of each *YBX1*-knockdown cell line to panobinostat and particularly JQ1 could be in any way linked to the *MYC* status of each cell line. In their 2014 paper, Bandopadhyay et al. showed that JQ1 was only efficacious in reducing cell viability in cell lines driven by *MYC*, with a minimal effect found in non-*MYC* amplified lines. Additionally, YB-1 appears to function as translational regulator of *MYC* in multiple myeloma, with YB-1 knockdown associated with reduced c-*MYC* expression (Bommert et al., 2013). Whilst the parental HDMB-03 cell line is widely considered *MYC*-amplified, the *MYC* status of the D283 cell line is less clear, with some groups categorising it as *MYC*-amplified (Bandopadhyay et al., 2014) and others recording no *MYC* amplification (Bigner et al., 1990). Thus, to assess c-*MYC* protein expression, western blots using whole-cell protein lysates extracted from KD-HDMB-03 and KD-D283 cell lines were undertaken (Section 2.9.7). Initial analysis of c-*MYC* protein expression revealed a slight reduction in c-*MYC* in both KD-D283-Y_A cell lines and KD-HDMB-03-Y_A cell lines compared to the appropriate non-silencing control line (Figure 5.12). However, statistical analysis by unpaired t-test did not find this alteration to be statistically significant. There was also no significant difference found in c-*MYC* expression between either *YBX1* knockdown cell line.

Taken together, it appears that *YBX1* knockdown in the HDMB-03 cell line results in a significant reduction in cell viability to novel anti-cancer therapies JQ1 and panobinostat at low-intermediate drug concentrations, which may be clinically relevant depending on achievable CSF concentrations for these drugs (currently unknown). Conversely, YB-1 depletion has little effect on cellular survival in response to either JQ1 or panobinostat in the D283 cell line. It is currently unclear why the two

Group 3 cell lines respond differently to each drug upon YB-1 knockdown. We cannot rule out the possibility that these results may simply reflect a higher retention of YB-1 expression, arising from lower levels of *YBX1* knockdown, in the D283 cell line, resulting in less pronounced phenotypic effects. Nevertheless, the observed results appear unlikely to arise from differences in the c-MYC expression status of each line.

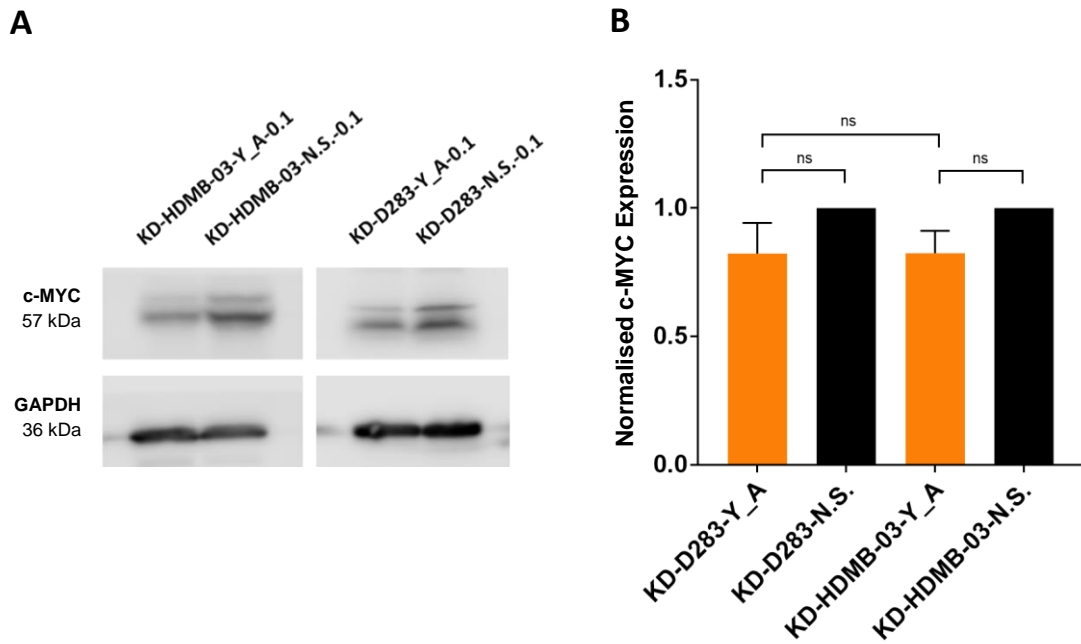


Figure 5.12 *YBX1* knockdown has little effect on c-MYC expression in HDMB-03 and D283 Group 3 cell lines. A) Western blot analysis of c-MYC expression revealed a small reduction in c-MYC expression in both KD-HDMB-03-Y_A and KD-D283-Y-A cell lines when compared to the appropriate non-silencing control line. Representative Western blot shown. B) Densitometry analysis did not find the observed reduction in c-MYC expression to be significant in either *YBX1* knockdown cell line. Densitometry data are presented relative to the GAPDH loading control and normalised to the appropriate non-silencing control cell line. Mean \pm SEM plotted. $n = 4$; ns = not significant, where significance was assessed by unpaired t-test. Full length western blots are presented in Appendix C5.

5.3.4 YB-1 depletion impedes the invasive capacity of medulloblastoma cells

As described extensively in Section 1.4.3.2, a number of studies have demonstrated a role for YB-1 in the regulation of cellular invasion, with YB-1 depletion associated with significantly reduced invasive capability in a number of different cancer cell lines (Gao et al., 2009; Lim et al., 2017; Lu et al., 2017). As such, we next wanted to understand if loss of YB-1 expression affected the invasive ability of Group 3 medulloblastoma cells. A modified Boyden chamber assay was utilised, designed to recapitulate invasion through a simplified brain extra-cellular matrix (ECM)-like barrier, a schematic of which can be found in Figure 5.13 A (Aldighieri, 2020). Cells were seeded in serum-free media in the upper chamber of the assay and incubated for 48 hours to facilitate migration (uncoated membrane), or invasion (coated membrane), towards the complete media-containing lower chamber (Section 2.8). ECM proteins collagen IV and laminin 111 were selected to form the membrane coating as both represent abundant components of the brain ECM and readily form networks *in vitro* (Sasaki et al., 2004; Xu et al., 2019).

All cell lines were found to invade and migrate in the transwell assay (Figure 5.13). *YBX1* knockdown resulted in a significantly decreased number of invaded cells in both knockdown cell lines compared to non-silencing control lines. KD-HDMB-03-Y_A cells exhibited a 36% reduction in invasion compared to the KD-HDMB-03-N.S. line ($P = 0.049$), while KD-D283-Y_A cells exhibited a 46% reduction in invasion compared to the KD-D283-N.S. line ($P = 0.032$). Given that *YBX1* knockdown does not significantly impede proliferation in either the KD-HDMB-03-Y_A or KD-D283-Y_A line at 12, 48 or 72 hours (Figure 5.7), one can assume that the observed reduction in invaded cells arises from decreased invasive capability following YB-1 depletion and not simply

reduced proliferation. Comparatively, no alteration in migration was observed upon YB-1 depletion in either cell line, indicating that YB-1 predominantly regulates cellular traits associated with invasion through the laminin 111/collagen IV ECM-like coating, rather than subsequent migration through the transwell insert.

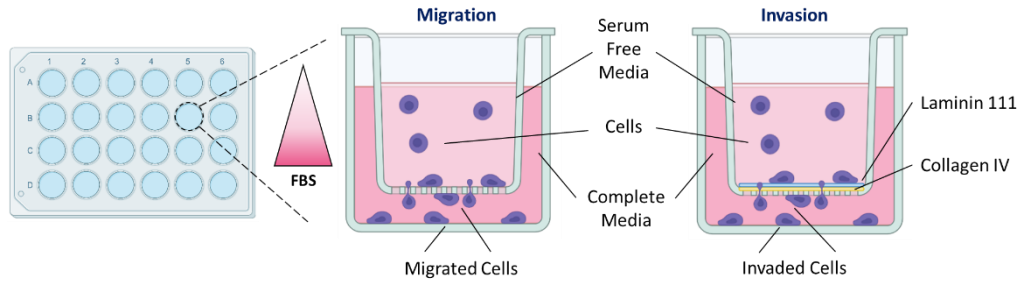
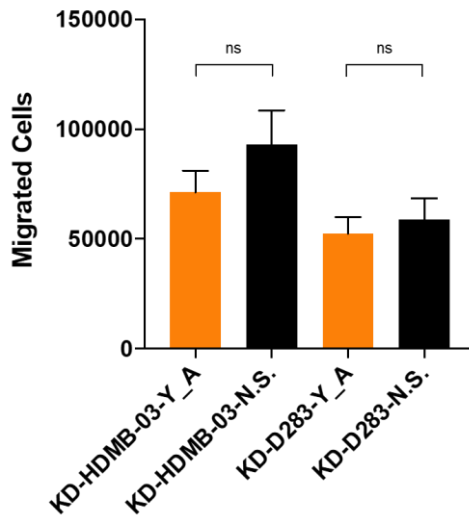
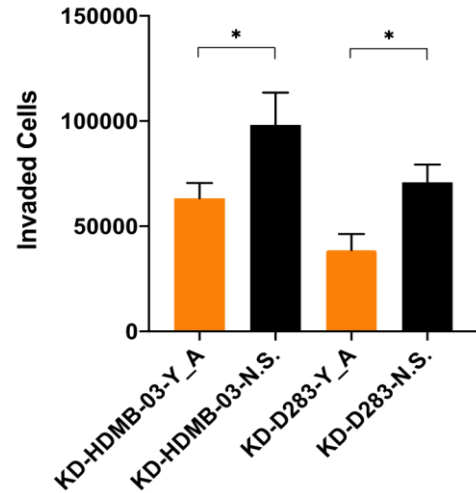
A**B****C**

Figure 5.13 YBX1 knockdown significantly impedes the invasive capacity of Group 3 medulloblastoma cell lines. Following seeding, KD-HDMB-03 and KD-D283 cell lines migrated/invaded for 48 hours through uncoated/coated transwell inserts, facilitated by a FBS gradient. Cells were collected from the underside of the transwell and from the lower chamber and cell numbers were quantified using PrestoBlue metabolic activity assays. A) A schematic representation of the transwell migration and invasion assays utilised in this experiment. Invasion assays involved an identical experimental set-up to migration assays, with the addition of a laminin 111/collagen IV membrane to model the brain ECM. B) YB-1 depletion did not have a significant effect on the migratory capacity of either KD-HDMB-03_Y_A or KD-D283_Y_A compared to the appropriate non-silencing control cell line. C) YB-1 depletion resulted in a significant reduction in the number of invading cells detected in both KD-HDMB-03_Y_A and KD-D283_Y_A compared to the appropriate non-silencing control cell line. Mean \pm SEM plotted; n = 3; *P < 0.05, ns = not significant; significance assessed by unpaired t-test.

5.4 Whole transcriptome sequencing of *YBX1*-knockdown medulloblastoma Group 3 cell lines

In order to better understand the YB-1 transcriptome and, for the first time, build a picture of global YB-1 transcriptional control in Group 3 medulloblastoma, whole transcriptome sequencing was undertaken using previously generated KD-D283 and KD-HDMB-03 cell lines (Section 5.2.2).

5.4.1 Sample preparation and sequencing

Samples from four cell lines (KD-HDMB-03-Y_A, KD-HDMB-03-N.S., KD-D283-Y_A and KD-D283-N.S.) were collected in triplicate and shipped to QIAGEN Genomic Services (Hilden, Germany) for RNA extraction and subsequent sequencing and analysis. In order to ensure RNA quality and yield was sufficient for sequencing, all samples underwent preliminary quality control using an Agilent TapeStation. As demonstrated in Table 5-1, all RNA samples had excellent RINe (RNA integrity number) values of 9.7 - 10 and hence were considered suitable for downstream sequencing. Likewise, all samples had an adequate concentration for downstream sequencing (>200 ng/ μ L).

Libraries were then prepared and sequenced, as described in detail in Section 2.10.1.2. Library preparation was carried out using the QIAseq Stranded Total RNA Library Kit with QIAseq FastSelect rRNA/globin depletion. All prepared libraries successfully passed Qiagen's internal quality control checks (capillary electrophoresis) and hence were pooled in equimolar concentrations and quantified by way of qPCR. Library pools were subsequently sequenced using an Illumina NextSeq 500 instrument in a dual index 1x75bp format at a sequencing depth of 30

M reads/sample. Following sequencing and adapter/quality trimming of resultant FASTQ files (Section 2.10.1.4), quality control reports were generated to provide an overview of any potential data issues prior to further analysis. All samples achieved very high quality scores, indicating good technical performance of the sequencing and passing all samples for downstream primary and secondary data analysis.

Table 5-1 Quantification of RNA concentration and integrity in whole transcriptome sequencing samples

Sample	Sample ID	Concentration (ng/ μ l)	RINe Value
KD-HDMB-03-Y_A (N = 1)	30394-001	874	9.8
KD-HDMB-03-Y_A (N = 2)	30394-002	790	10.0
KD-HDMB-03-Y_A (N = 3)	30394-003	780	10.0
KD-HDMB-03-NS (N = 1)	30394-004	500	10.0
KD-HDMB-03-NS (N = 2)	30394-005	666	9.7
KD-HDMB-03-NS (N = 3)	30394-006	582	9.9
KD-D283-Y_A (N = 1)	30394-007	698	10.0
KD-D283-Y_A (N = 2)	30394-008	898	9.9
KD-D283-Y_A (N = 3)	30394-009	534	9.8
KD-D283-NS (N = 1)	30394-010	872	10.0
KD-D283-NS (N = 2)	30394-011	544	9.9
KD-D283-NS (N = 3)	30394-012	652	10.0

RNA was extracted from 12 samples and concentration and RNA integrity (RINe) quantified using an Agilent Tapestation. A RINe value >7 is considered acceptable for downstream sequencing analysis.

5.4.2 Mapping of sequencing data

The alignment (mapping) of sequencing data is a fundamental step in next-generation sequencing analysis and involves mapping reads generated from sequencing to a reference genome, in this case human genome assembly GRCh38 (hg38). An important mapping parameter is the percentage of mapped reads, which

is a global indicator of the overall sequencing accuracy and the presence of contaminating DNA. Generally, 70-90% of standard RNA sequencing reads are expected to map to the human genome, with a significant amount of reads mapping to two or more identical regions equally well (non-specifically mapped reads) (Conesa et al., 2016). As displayed in Table 5-2, an average of 57,304,959 reads were obtained for each sample, with >95% of reads mapping to the human genome. Furthermore, across all samples analysed ~80% of reads mapped uniquely. Taken together, these data are indicative of high mapping quality and sequencing accuracy.

Table 5-2 Mapping of whole transcriptome sequencing data

Sample	Sample ID	Total Reads	Mapped Reads (%)	- Uniquely (%)	- non-specifically (%)	Unmapped Reads (%)
KD-HDMB-03-Y_A (N = 1)	30394-001	62,897,190	95.52	80.62	14.90	4.48
KD-HDMB-03-Y_A (N = 2)	30394-002	59,257,231	95.88	79.53	16.34	4.12
KD-HDMB-03-Y_A (N = 3)	30394-003	62,103,565	95.79	79.65	16.14	4.21
KD-HDMB-03-NS (N = 1)	30394-004	60,588,519	95.36	80.14	15.22	4.64
KD-HDMB-03-NS (N = 2)	30394-005	60,897,410	95.45	79.95	15.50	4.55
KD-HDMB-03-NS (N = 3)	30394-006	58,843,636	95.67	80.60	15.07	4.33
KD-D283-Y_A (N = 1)	30394-007	56,187,993	96.08	82.29	13.79	3.92
KD-D283-Y_A (N = 2)	30394-008	60,811,121	96.15	83.03	13.12	3.85
KD-D283-Y_A (N = 3)	30394-009	56,147,325	95.23	79.57	15.66	4.77
KD-D283-NS (N = 1)	30394-010	47,046,408	95.85	81.92	13.93	4.15
KD-D283-NS (N = 2)	30394-011	52,533,027	95.76	81.05	14.71	4.24
KD-D283-NS (N = 3)	30394-012	50,076,081	96.01	82.81	13.20	3.99

Percentages of mapped, uniquely mapped, non-specifically mapped and unmapped reads are displayed.

5.4.3 Differential gene expression analysis

Quantification of the number of reads that map to each transcript sequence allowed an estimate of gene expression in transcripts per million (TPM), which was further normalised using the trimmed mean of M values (TMM) normalisation technique to allow for comparison between samples (Robinson & Oshlack, 2010).

Prior to statistical analysis, unsupervised analysis in the form of Principal Component Analyses (PCA) was first undertaken to explore sample clusters and variation between samples (Section 2.10.1.3.5). On a PCA plot, the data points representing individual replicates are projected onto the 2D plane such that they spread out in the two directions that demonstrate the greatest variance in the data. As illustrated in Figure 5.14 A, the PCA plot for all samples shows a clear separation between KD-D283 and KD-HDMB-03 samples. The D283 knockdown vs. non-silencing comparison is also well separated by PCA analysis (Figure 5.14 B). Comparatively, expression levels in KD-HDMB-03 samples showed the least distinctive clustering patterns of the comparisons performed (Figure 5.14 C). The interspersed nature of KD-HDMB-03-N.S. replicates with KD-HDMB-03-Y_A replicates suggests that, in the HDMB-03 line, *YBX1* knockdown has a restricted effect on gene expression profile. The lack of clustering between KD-HDMB-03-N.S. samples may also highlight some variability between biological repeats, however as this experiment was conducted in triplicate only and no quality issues were recorded in any of the samples during sample preparation, sequencing or analysis, all three replicates were retained.

Next, unsupervised hierarchical clustering was undertaken using the top 50 most altered genes across paired sample types (Figure 5.15 and Figure 5.16). These are

presented as heatmaps generated using an online heatmap generation tool (heatmapper.ca/expression/) using the average linkage method for hierarchical clustering calculations (Babicki et al., 2016). Lowly expressed genes were filtered out of normalised gene expression datasets prior to heatmap generation as described by (Chen et al., 2016). Each heatmap row represents one gene and each column represents one sample. The heatmap colour represents the difference in normalised gene expression compared to the row mean, represented as Z-scores⁴. Supporting observations from PCA, differences in gene expression were clearly visible between KD-D283-Y_A and KD-D283-N.S. samples, with each triplicate clustering together (Figure 5.15). KD-HDMB-03-Y_A and KD-HDMB-03-N.S. samples had a less distinctive gene expression pattern, as expected from PCA analysis, however samples did cluster together according to *YBX1* knockdown status (Figure 5.16).

⁴ Z-scores are calculated for each gene (i.e. each row) by subtracting the mean and then dividing by the standard deviation. Z-scores are calculated after clustering and are plotted instead of normalised expression values in order to improve the visualisation of expression patterns.

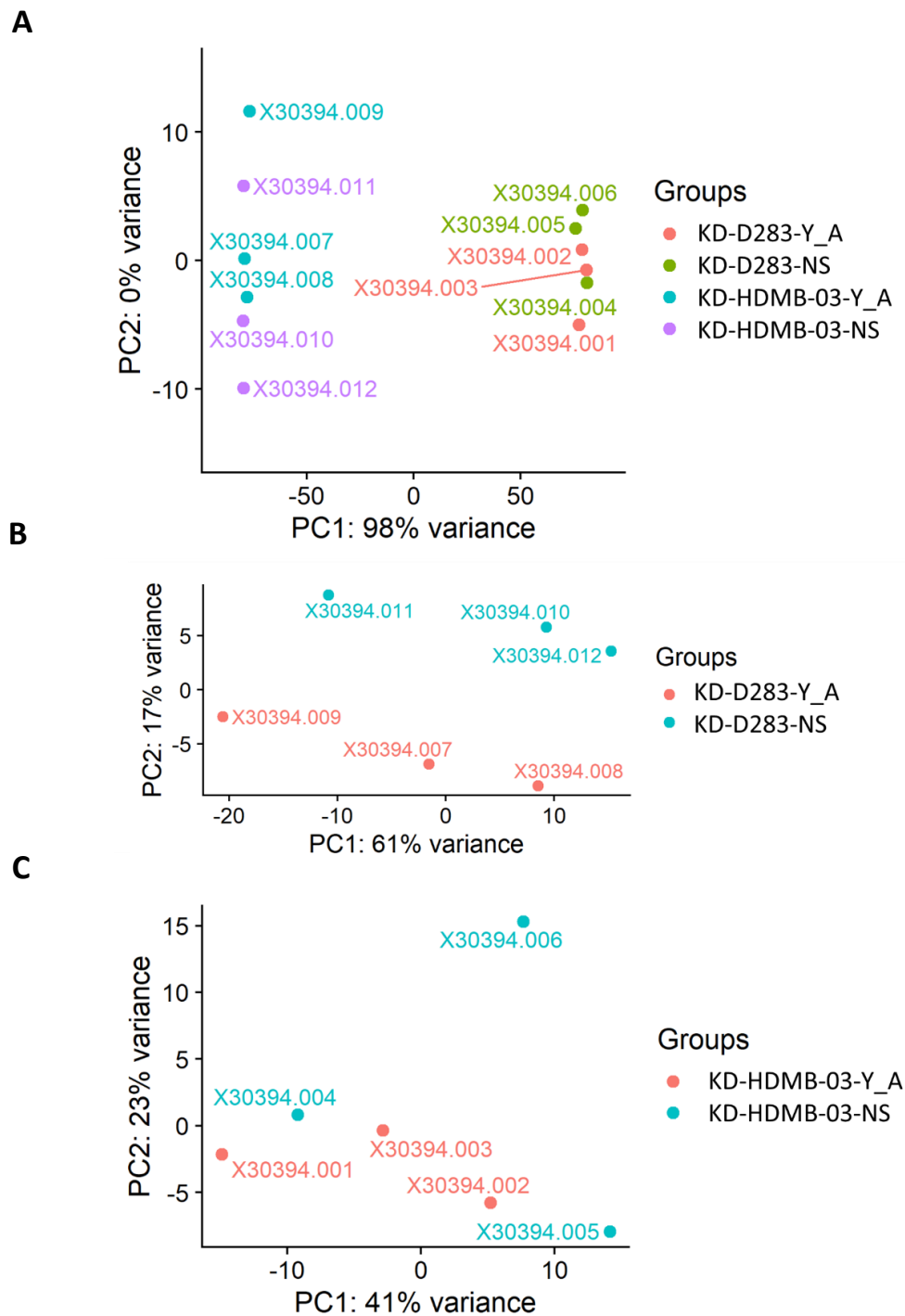


Figure 5.14 Principle component (PC) analysis of *YBX1* knockdown whole transcriptome sequencing samples. PCA analysis was performed on all samples submitted to sequencing using normalised gene expression values in order to visualise sample clustering. A) PCA plot of all samples showed clear separation between KD-D283 and KD-HDMB-03 cell lines. B) PCA plot of KD-D283 samples showed clustering of KD-D283-Y_A samples separate from KD-D283-N.S. samples. C) PCA plot of KD-HDMB-03 samples showed some clustering within KD-HDMB-03-Y_A samples, however less distinctive clustering within KD-HDMB-03-N.S. replicates.

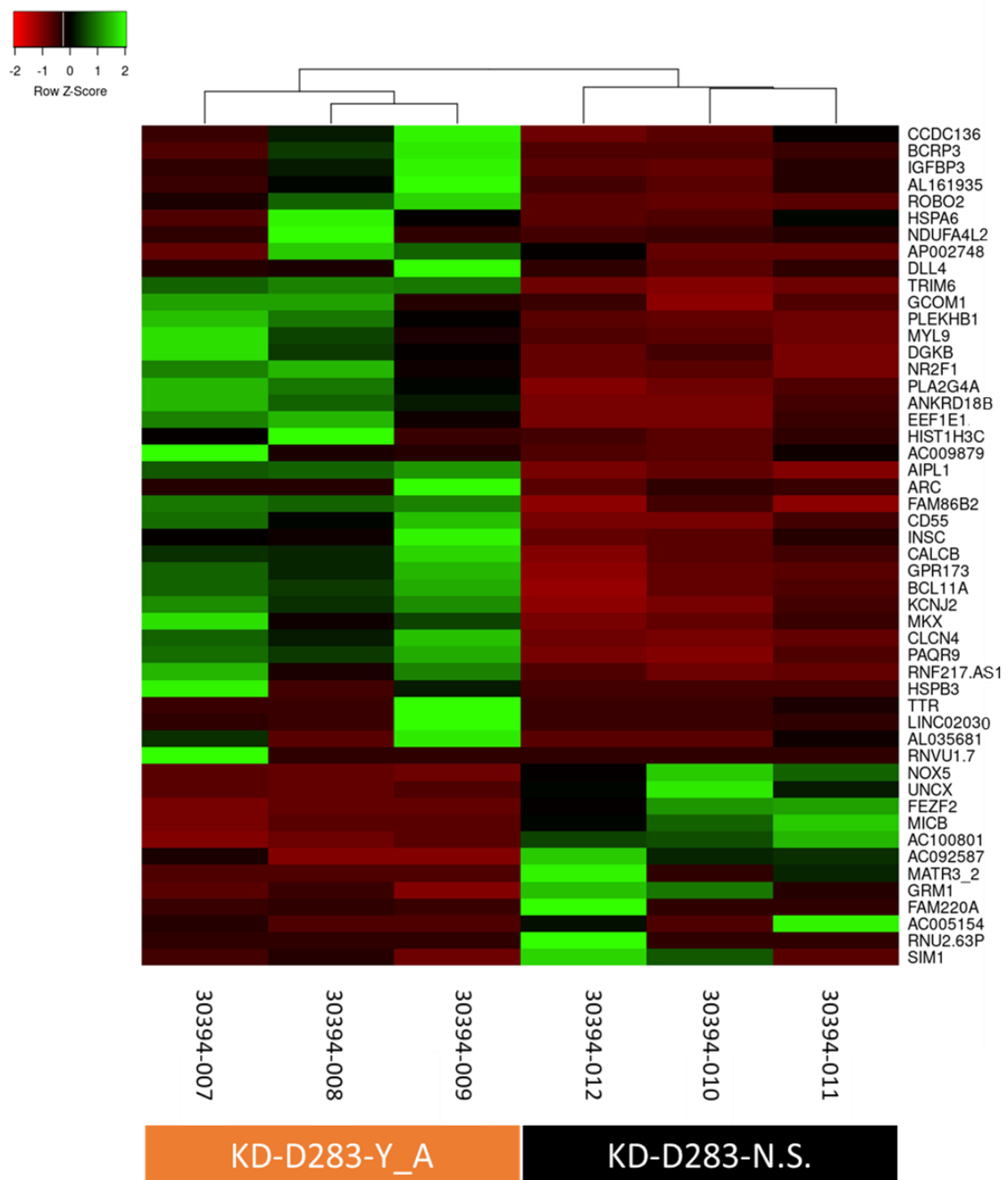


Figure 5.15 Unsupervised clustering of *YBX1*-knockdown and non-silencing control D283 cell lines. Unsupervised transformed gene counts were used to create a heatmap representing the top 50 most altered genes across all knockdown and non-silencing samples. The colour scale signifies the relative expression level of a gene across all samples. Expression levels above the mean are shown as green and below the mean are red. Differences in gene expression between non-silencing and knockdown cell lines were clear, with triplicates from each sample set clustering together.

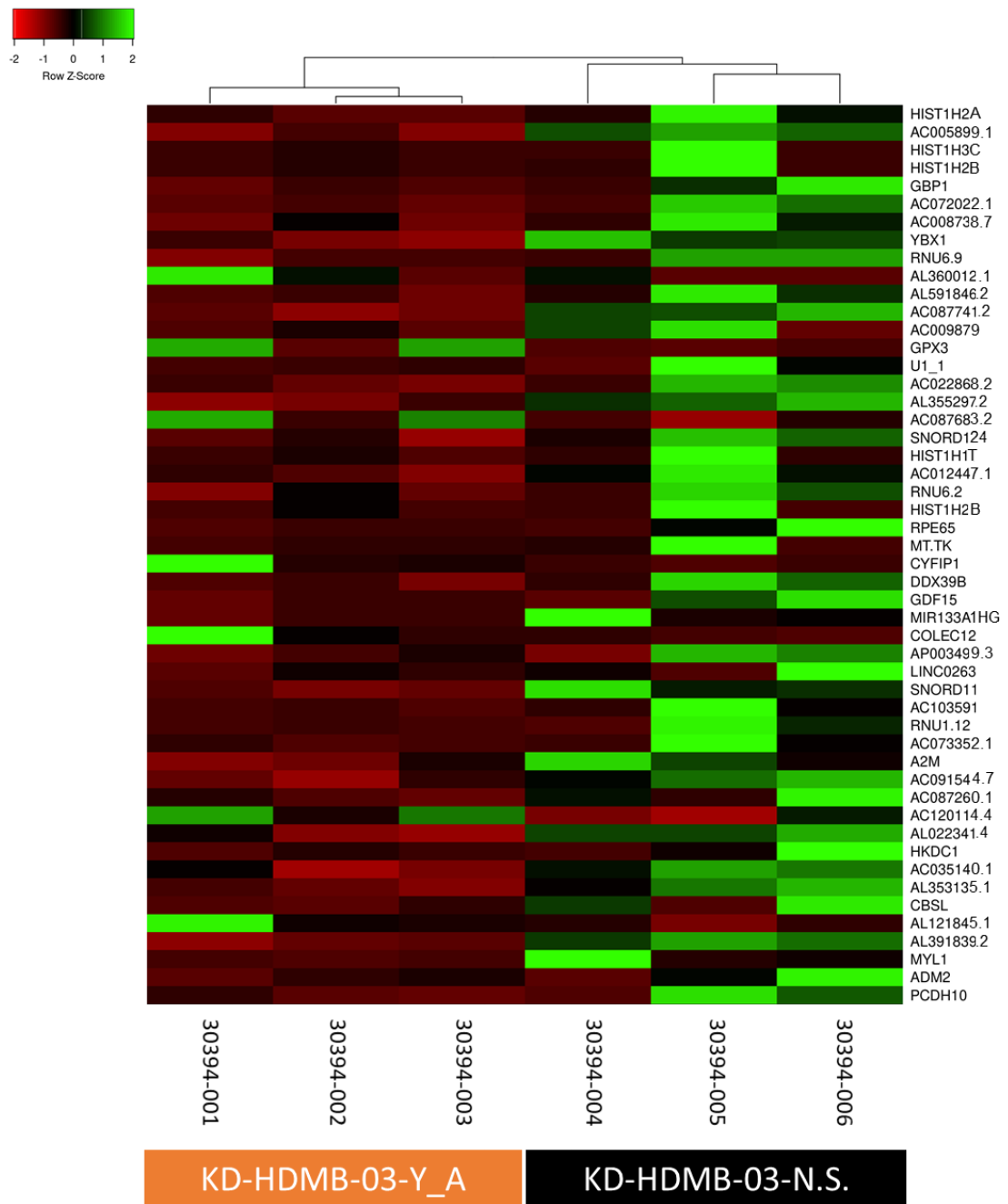


Figure 5.16 Unsupervised clustering of *YBX1*-knockdown and non-silencing control HDMB-03 cell lines. Unsupervised transformed gene counts were used to create a heatmap representing the top 50 most altered genes across all knockdown and non-silencing samples. The colour scale signifies the relative expression level of a gene across all samples. Expression levels above the mean are shown as green and below the mean are red. Triplicates from each sample set were found to cluster according to *YBX1* knockdown status.

5.4.4 Analysis of significantly differentially expressed genes arising from *YBX1* knockdown

Normalised read count data was next taken forward for statistical analysis to elucidate quantitative changes in expression levels between groups (Section 2.10.1.4). Analysis was conducted within cell lines i.e. KD-D283-Y_A versus KD-D283-N.S. and KD-HDMB-03-Y_A versus KD-HDMB-03-N.S. Significantly differentially expressed genes were filtered based upon the following criteria, as described in (Bandopadhyay et al., 2019):

- 1) Fold Change Threshold – $\text{Log}_2 \geq 0.5$ or ≤ -0.5
- 2) P-value – ≤ 0.05
- 3) False Discovery Rate (FDR) P-value – ≤ 0.1
- 4) Mean Expression – ≥ 0.1 TPM

This resulted in a list of significantly differentially up- and down-regulated genes for each cell line, the top 10 of which are displayed in Figure 5.17 and Figure 5.18, respectively. The shortest list of low FDR values was identified in the comparison of HDMB-03 samples, with significantly fewer up-regulated and down-regulated genes present compared to D283 samples. Interestingly, there was no overlap in significantly up-regulated genes upon *YBX1* knockdown between both D283 and HDMB-03 cell lines (Figure 5.17 C). Likewise, only one down-regulated gene, *YBX1*, overlapped between cell lines (Figure 5.18 C), indicative of differential YB-1-mediated transcriptional control between D283 and HDMB-03 Group 3 cells. Importantly, the *YBX1* changes revealed in Figure 5.18 A and B by whole transcriptome sequencing mirror those detected by qRT-PCR in Figure 5.5, further validating the success and stability of the *YBX1* knockdown cell lines.

A

Gene	TPM Value (Non-Silencing)	TPM Value (YBX1 Knockdown)	Log2 Fold Change	P-Value
<i>LINC02030</i>	0.12	1.65	3.91	6.33E-05
<i>ANKRD18B</i>	0.011	0.13	3.43	5.12E-05
<i>FAM86B2</i>	0.048	0.53	3.39	0.00038
<i>TTR</i>	2.99	26.27	3.28	0.00026
<i>TRIM6</i>	0.054	0.50	3.21	5.05E-09
<i>MYL9</i>	0.25	2.23	3.13	2.14E-08
<i>PLEKHB1</i>	0.051	0.36	2.79	1.97E-07
<i>ROBO2</i>	0.089	0.58	2.74	4.00E-08
<i>INSC</i>	0.35	2.14	2.71	3.70E-05
<i>NDUFA4L2</i>	0.60	3.71	2.61	0.00036

B

Gene	TPM Value (Non-Silencing)	TPM Value (YBX1 Knockdown)	Log2 Fold Change	P-Value
<i>NPIPA3</i>	0.023	2.01	6.33	1.13E-05
<i>APO01781.2</i>	0.036	0.37	3.33	3.31E-05
<i>CADM3</i>	0.060	0.39	2.67	8.87E-05
<i>GPX3</i>	1.28	4.76	1.97	5.49E-06
<i>LDLRAD4</i>	0.075	0.26	1.94	3.53E-06
<i>CYFIP1</i>	0.53	1.83	1.79	4.51E-08
<i>WT1</i>	0.22	0.70	1.78	9.86E-07
<i>COLEC12</i>	0.48	1.60	1.75	2.85E-05
<i>RASSF2</i>	5.88	15.19	1.47	3.63E-06
<i>PTPRZ1</i>	4.13	10.22	1.41	4.81E-11

C

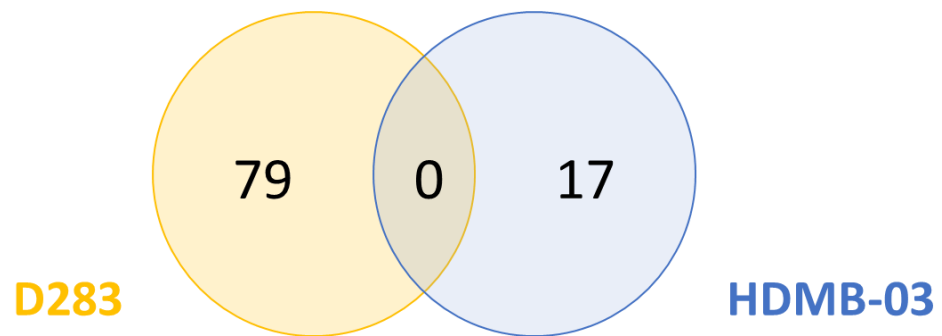


Figure 5.17 Significantly up-regulated genes upon YBX1 knockdown in Group 3 medulloblastoma cell lines. A) Top 10 genes most significantly up-regulated upon YBX1 knockdown in the D283 cell line. B) Top 10 genes most significantly up-regulated upon YBX1 knockdown in the HDMB-03 cell line. Genes were ordered based upon Log2 fold change. Significance was determined using an uncorrected P-value (≤ 0.05) and an FDR P-value (≤ 0.1). P-Values were adjusted using the Benjamini-Hochberg False Discovery Rate (FDR) approach to correct for multiple testing. C) A Venn diagram depicting the number of shared and non-shared genes for each comparison.

A

Gene	TPM Value (Non-Silencing)	TPM Value (YBX1 Knockdown)	Log2 Fold Change	P-Value
<i>FAM220A</i>	1.87	0.15	-3.64	1.12E-05
<i>AC100801.1</i>	0.27	0.025	-3.28	8.28E-06
<i>AC005154.5</i>	2.38	0.25	-3.22	0.00034
<i>UNCX</i>	0.40	0.051	-2.87	0.00010
<i>NOX5</i>	0.71	0.10	-2.77	1.48E-10
<i>FEZF2</i>	1.94	0.37	-2.34	5.45E-06
<i>GRM1</i>	1.36	0.34	-2.01	0.00035
<i>COL8A1</i>	0.23	0.056	-1.98	0.00055
<i>OLFM1</i>	2.23	0.62	-1.83	1.76E-09
<i>YBX1</i>	786.99	228.79	-1.78	2.68E-11

B

Gene	TPM Value (Non-Silencing)	TPM Value (YBX1 Knockdown)	Log2 Fold Change	P-Value
<i>HIST1H2AJ</i>	5.00	0.46	-3.52	5.07E-08
<i>NIBAN1</i>	0.81	0.074	-3.29	1.67E-05
<i>AC005899.4</i>	8.45	0.77	-3.25	9.72E-07
<i>GBP1</i>	1.89	0.34	-2.34	9.78E-06
<i>YBX1</i>	465.10	101.89	-2.15	8.94E-16
<i>TTN</i>	4.33	1.41	-1.49	6.16E-09
<i>AC083843.2</i>	70.32	26.02	-1.34	0.00013
<i>TNC</i>	39.95	15.30	-1.28	2.84E-05
<i>FYTTD1</i>	0.56	0.25	-1.11	8.22E-05
<i>DLEU7</i>	8.30	4.29	-0.85	0.00014

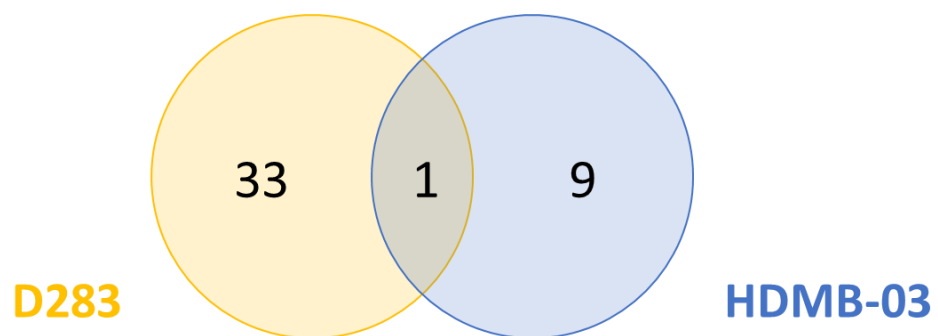
C

Figure 5.18 Significantly down-regulated genes upon YBX1 knockdown in Group 3 medulloblastoma cell lines. A) Top 10 genes most significantly down-regulated upon YBX1 knockdown in the D283 cell line. B) Top 10 genes most significantly down-regulated upon YBX1 knockdown in the HDMB-03 cell line. Genes were ordered based upon Log2 fold change. Significance was determined using an uncorrected P-value (≤ 0.05) and an FDR P-value (≤ 0.1) to correct for multiple testing. C) A Venn diagram depicting the number of shared and non-shared genes for each comparison.

5.4.5 Ingenuity Pathway Analysis (IPA) of gene expression profiles following in *YBX1* knockdown

Given that any gene is likely to be part of a more complex biological process, it was next of interest to see if any cellular functions or pathways were commonly disrupted following *YBX1* knockdown in D283 and HDMB-03 cell lines. As such, differential gene expression patterns (Section 5.4.4) were utilised to predict affected cellular biology using Qiagen's Ingenuity Pathway Analysis (IPA) software as previously described (Section 2.10.1.4.5). Put simply, IPA software is a gene expression functional annotation tool which utilises a scientific literature-based database (the Ingenuity Pathway Knowledge Base) to identify disease/cellular functions and canonical pathways that are most significant to gene expression outcomes, and to categorise differentially expressed genes in specific pathways/functions. For all IPA, Fisher's exact test was performed to assess which pathways and biological functions were significantly associated with analysis-ready gene lists, with the Benjamini-Hochberg method employed to control the false discovery rate.

5.4.5.1 Metabolic, cell death and survival functions are dysregulated upon *YBX1* depletion in both D283 and HDMB-03 cell lines.

First, we wanted to explore molecular and cellular functions that appeared altered upon *YBX1* knockdown, using the IPA software package. For each knockdown vs. non-silencing comparison, the five most significantly altered molecular and cellular functions are listed alongside involved representative genes (Figure 5.19). Metabolic functions were frequently dysregulated across both HDMB-03 and D283 cell line

comparisons. “Lipid metabolism” was found to be highly affected across both cell lines, with alterations in “carbohydrate metabolism” specific to the HDMB-03 knockdown vs. non-silencing comparison and “vitamin and mineral metabolism” specific to the D283 knockdown vs. non-silencing comparison. In addition, cell maintenance functions were also frequently altered, with “cell death and survival” dysregulated upon *YBX1* knockdown in both cell lines. Furthermore, “cellular development” and “cellular growth and proliferation” functions were specific to the HDMB-03 comparison, while “cellular function and maintenance” was observed in the D283 comparison alone. The overlap of certain cellular processes (“cell death and survival” and “lipid metabolism”) observed upon *YBX1* knockdown in both cell lines indicates that, although the YB-1 transcriptome differs between HDMB-03 and D283 lines at a gene level, at a broader functional level, similarities exist between both Group 3 cell lines.

A

Molecular/Cellular Function	P-Value Range	Number of Genes	Gene Name(s)
Lipid Metabolism	9.82E-03 - 1.14E-05	13	<i>CALB1,CEBPB,DBI,DDIT4,DHCR24,EDIL3,EIF2AK3,EPAS1,HMGCR,IDI1,RARB,S1PR1,SLC44A2</i>
Small Molecule Biochemistry	1.16E-02 - 1.14E-05	15	<i>CALB1,CEBPB,DBI,DDIT4,DHCR24,EDIL3,EIF2AK3,EPAS1,HMGCR,IDI1,LOX,PPP2R5A,RARB,S1PR1,SLC44A2</i>
Cell Death and Survival	9.17E-03 - 2.18E-05	19	<i>ARHGEF2,CALB1,CDK6,CEBPB,DDIT4,DHCR24,EDIL3,EIF2AK3,EPAS1,GADD45A,HMGCR,LOX,MALAT1,MGP,NEFM,PPP2R5A,RARB,RFK,S1PR1</i>
Vitamin and Mineral Metabolism	1.16E-02 - 3.42E-05	8	<i>CALB1,DBI,DHCR24,EIF2AK3,HMGCR,IDI1,PPP2R5A,S1PR1</i>
Cellular Function and Maintenance	1.12E-02 - 4.68E-05	10	<i>CALB1,CEBPB,DDIT4,EDIL3,EIF2AK3,EPAS1,MGP,NEFM,PCDH8,S1PR1</i>

B

Molecular/Cellular Function	P-Value Range	Number of Genes	Gene Name(s)
Cell Death and Survival	1.46E-02 - 5.30E-07	29	<i>ARHGEF2,ATP5MC1,CA4,DHCR24,FABP5,FASN,GAPDH,GDF15,GPX1,GSTP1,H1-O,LDHA,LPCAT1,MIF,MT1X,MT2A,MYBL2,NRL,PPIF,PRDX1,PSMB3,SEC61G,SESN2,SMYD1,TK1,TMSB10/TMSB4X,TNC,UNG,VCL</i>
Cellular Development	1.46E-02 - 1.42E-05	24	<i>ARHGEF2,DHCR24,DLX5,FABP5,FASN,GAPDH,GDF15,GPX1,GSTP1,KLHL41,LDHA,MIF,MT2,AMYBL2,NEB,PPIF,PSMB3,RNF187,SEC61G,SMYD1,TMSB10/TMSB4X,TNC,UNG,VCL</i>
Cellular Growth and Proliferation	1.46E-02 - 1.42E-05	23	<i>ARHGEF2,DHCR24,DLX5,FABP5,FASN,GAPDH,GDF15,GPX1,GSTP1,KLHL41,LDHA,MIF,MT2,AMYBL2,NEB,PPIF,PSMB3,RNF187,SEC61G,TMSB10/TMSB4X,TNC,UNG,VCL</i>
Carbohydrate Metabolism	1.46E-02 - 1.33E-04	11	<i>DBI,FABP5,FASN,GAPDH,GDF15,GPX1,GSTP1,LDHA,LPCAT1,MIF,SESN2</i>
Lipid Metabolism	1.46E-02 - 1.33E-04	10	<i>DBI,DHCR24,FABP5,FASN,GDF15,GPX1,GSTP1,LPCAT1,MIF,TNC</i>

C

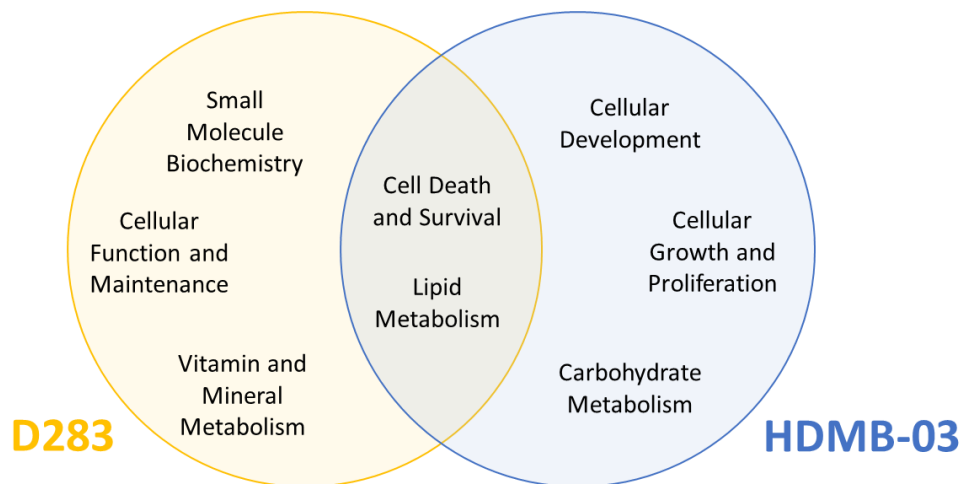


Figure 5.19 Significantly altered molecular and cellular functions upon *YBX1* knockdown in medulloblastoma Group 3 cell lines. A) The 5 most significantly altered functions following *YBX1*-knockdown in D283 cells. B) The 5 most significantly altered functions following *YBX1*-knockdown in HDMB-03 cells. Significance was calculated using Fisher's exact test. Genes driving altered cellular functions are shown. Highlighted rows are functions shared between both cell line comparisons. C) A Venn diagram displaying shared functions following *YB-1* depletion in HDMB-03 and D283 lines.

5.4.5.2 Lipid metabolism pathways are dysregulated following *YBX1* depletion in medulloblastoma Group 3 cell lines.

In order to build upon findings from Section 5.4.5.1 and to investigate predicted affected biology based on differential gene expression in more depth, known canonical pathways significantly affected by *YBX1* knockdown in HDMB-03 and D283 cell lines were categorised using IPA software. By utilising data from the Ingenuity Pathway Knowledge Base, dysregulated genes in each canonical pathway and where possible, the change in direction of the pathway were revealed.

The top dysregulated canonical pathways and percentage overlap of differentially expressed genes for knockdown vs. non-silencing comparisons are shown in Figure 5.20. In agreement with molecular and cellular function analysis (Section 5.4.5.1), a number of canonical pathways associated with lipid metabolism were dysregulated following loss of YB-1 across both lines. In the HDMB-03 knockdown vs. non-silencing comparison, Palmitate Biosynthesis I, Fatty Acid Biosynthesis Initiation II and Stearate Biosynthesis I were significantly altered, while Superpathway of Cholesterol Biosynthesis, Mevalonate Pathway I and Superpathway of Geranylgeranyl Diphosphate (GGPP) were significantly altered in the D283 comparison. A schematic overview of lipid metabolism within human cells is depicted in Figure 5.21, with affected pathways highlighted. These data indicate that YB-1 is implicated in multiple aspects of lipid biosynthesis, a finding novel in the context of brain tumours. Indeed, only two studies have associated YB-1 with lipid metabolism, both in renal cell carcinoma where YB-1 was found to negatively regulate *SCD1* – a gene that encodes stearoyl-CoA desaturase, an enzyme implicated in the biosynthesis of monounsaturated fatty acids (Jeffords et al., 2020; McCauley et al., 2020).

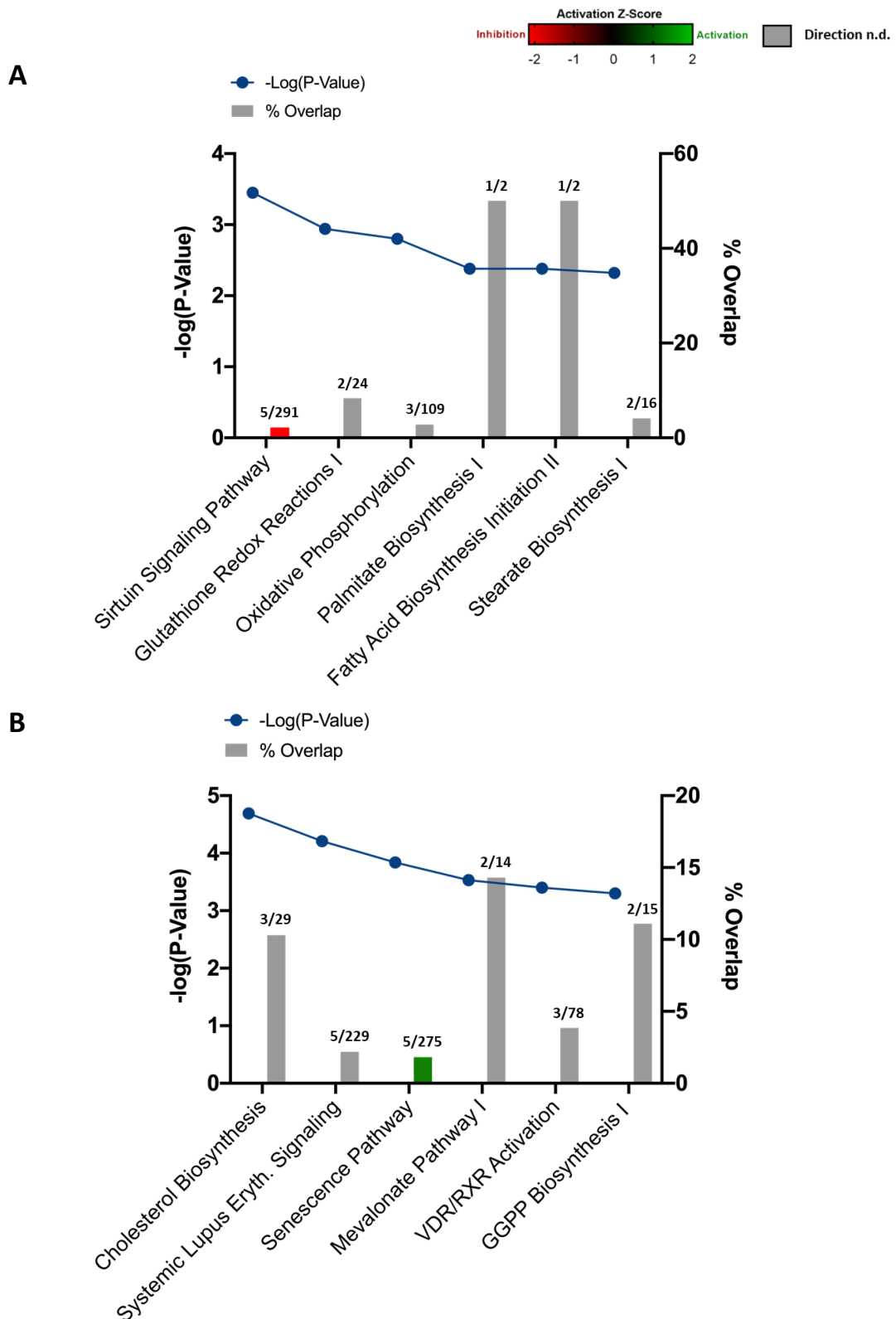


Figure 5.20 Significantly altered canonical pathways upon YB-1 depletion in HDMB-03 and D283 cells. Top significantly altered canonical pathways following *YBX1*-knockdown in HDMB-03 (A) and D283 (B) cells are displayed. $-\log(P\text{-Value})$ and % overlap (the percentage of differentially regulated genes in each canonical pathway) are shown. The number of affected genes/ total number of genes in each pathway are indicated. A number of biosynthetic and metabolic pathways were altered. Where possible, an activation Z-score was determined, red indicates an inhibitory effect while green indicates an activational effect. Grey bars represent pathways for which a Z-score could not be determined (n.d.). Significance calculated using Fisher's exact test.

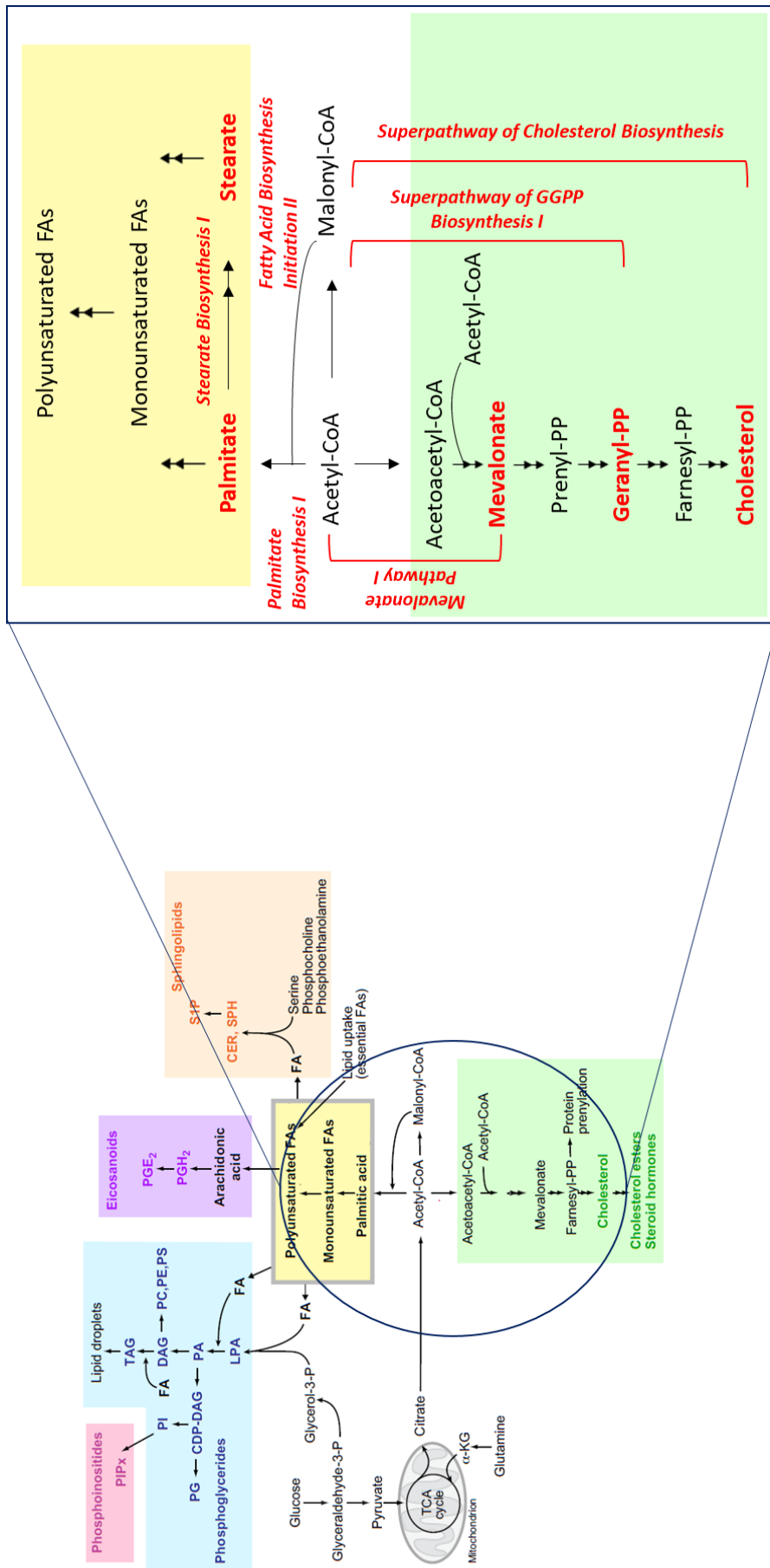


Figure 5.21 YB-1 may play a role in the regulation of a number of pathways implicated in lipid metabolism in paediatric brain tumours. Schematic overview of the pathways involved in the synthesis of fatty acids (FAs), cholesterol, phosphoglycerides, eicosanoids and sphingolipids. YB-1-regulated pathways (and products) are indicated in red within the magnified section. YB-1 appears to regulate canonical pathways within fatty acid (yellow) and cholesterol (green) biosynthetic processes. Figure adapted from (Baenke et al., 2013).

For many of the significantly altered canonical pathways identified, directional Z-scores could not be determined (portrayed by grey bars in Figure 5.20). This was expected on account of the relatively small number of filtered DEGs within both datasets. Nevertheless, Z-scores could be generated for two pathways – the Sirtuin Pathway in the HDMB-03 knockdown vs. non-silencing comparison and the Senescence Pathway in the D283 knockdown vs. non-silencing comparison. Activation Z-scores describe the activation state of the identified biological function (in this case canonical pathways), with scores > 0 and < 0 signifying increased or decreased activity. In practice, Z-scores ≥ 2 or ≤ -2 are considered significant, however pathways falling outside these criteria may still hold interest and should not be ignored (Qiagen, 2016).

The Sirtuin Signalling Pathway was found to have an activation Z-score of -2, indicative of significant pathway inactivation upon YB-1 depletion within the HDMB-03 cell line. DEGs identified within the pathway include: *ATP5MC1* (encodes a subunit of mitochondrial ATP synthase ($ATP5\beta$); \log_2 fold change (LFC) = 0.6), *LDHA* (encodes A chain of lactate dehydrogenase (LDH); LFC = 0.7), *PPIF* (encodes a major component of the mitochondrial permeability transition pore (mPTP); LFC = 0.6); *H1-0* (encodes Histone H1.0; LFC = -0.7) and *HC3C* (encodes Histone H3.1; LFC = -3.2). The Sirtuin Signalling Pathway is displayed in Figure 5.22 with differentially expressed genes highlighted. The Sirtuin Signalling Pathway is driven by sirtuins – NAD^+ -dependent histone deacetylases which are implicated in the detection and response to cellular stress (Bosch-Presegué & Vaquero, 2011). Interestingly, perturbation of the Sirtuin Pathway, both by inhibition (Cea et al., 2011), and activation (Scuto et al., 2013) of SIRT1 has previously been shown to potentiate the effect of HDAC inhibitors on

cancer cell lines. Further to this, two downstream targets of SIRT1 that are differentially expressed in the dataset, Histone H1 and Histone H3 (Figure 5.22), are known to be important upstream regulators of panobinostat treatment (Yan-Fang et al., 2015). Taken together, this canonical pathway analysis suggests that YB-1 may positively regulate the Sirtuin Signalling pathway. I hypothesise therefore that depletion of YB-1 and the concurrent inactivation of Sirtuin Signalling that follows may render medulloblastoma cells more sensitive to HDAC inhibitor treatment, perhaps providing an explanation for the increased sensitivity to panobinostat exhibited by HDMB-03 cells upon *YBX1*-knockdown observed in Section 5.3.3.

The Senescence Pathway was found to have an activation Z-score of 1.3, indicative of pathway activation upon YB-1 depletion within the D283 cell line. As this score falls under the Z-score threshold of ≥ 2 , it should not be considered significantly predictive, however could still represent an interesting finding, with a number of dysregulated genes detected upon *YBX1* knockdown. Differentially expressed genes detected within the Senescence Pathway are depicted in Figure 5.23 and include: *CDK6* (encodes cyclin-dependent kinase 6 (CDK6); LFC = -0.6), *CEBPB* (encodes CCAAT/enhancer-binding protein beta (cEBP β); LFC = 1.1), *DHCR24* (encodes delta(24)-sterol reductase (DHRC24); LFC = -0.9), *GADD45* (encodes growth arrest and DNA damage-inducible protein (GADD45); LFC = 0.8) and *PPP2R5A* (encodes a subunit of Serine/threonine-protein phosphatase 2A (Pp2A); LFC = 0.7). This analysis indicates that YB-1 is implicated in the regulation of the senescence pathway in the D283 line. This finding was unexpected given that we observe no significant difference in the proliferative capacity of D283 cells following YB-1 depletion (Section 5.2.3). Further functional assays will be required to explore and validate this finding,

including longer-term proliferation assays and screening for biomarkers of senescence such as senescence-associated beta-galactosidase (SA-beta-gal).

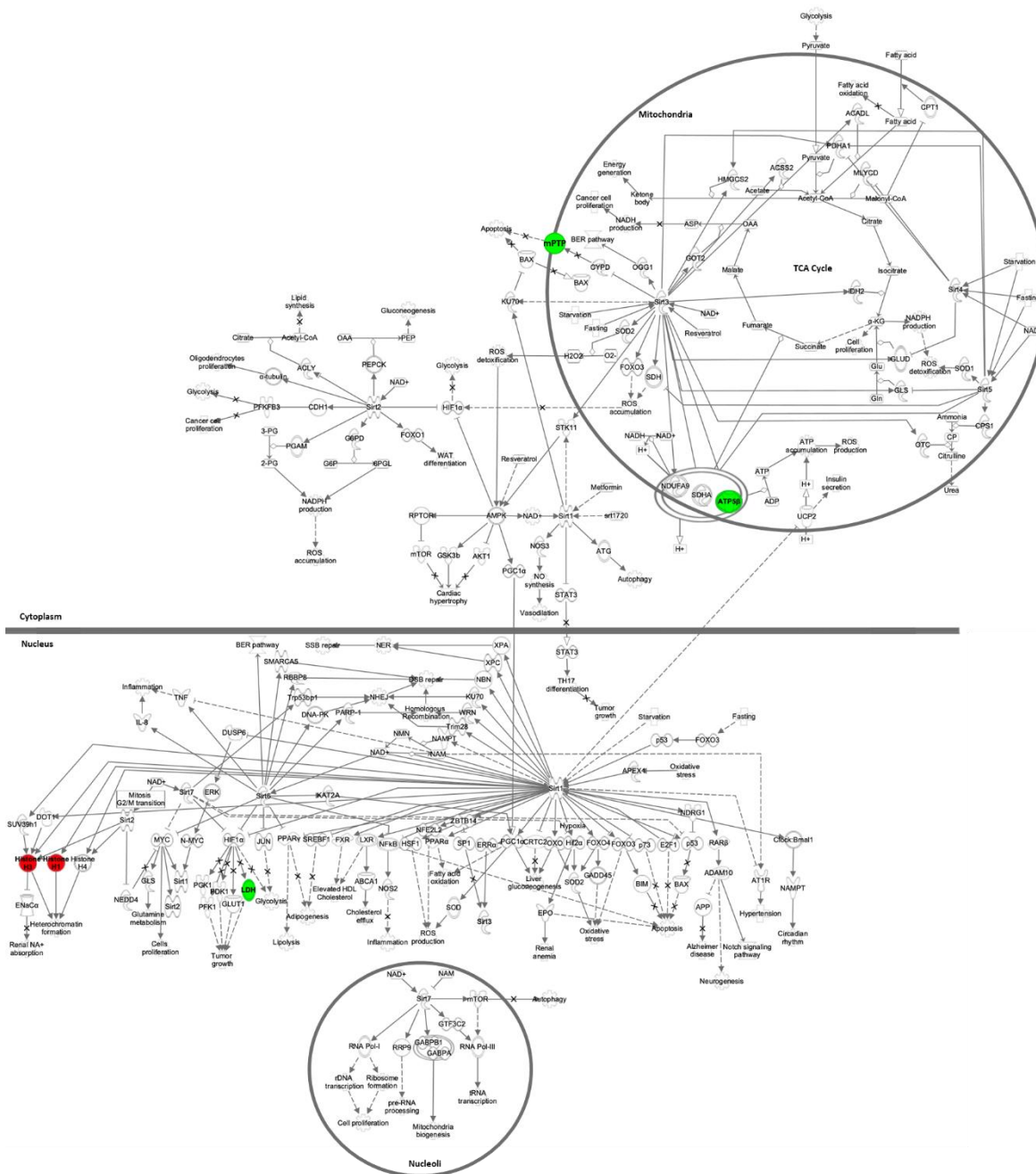


Figure 5.22 *YBX1*-knockdown results in inactivation of the Sirtuin Signaling Pathway in HDMB-03 cells. *YB-1* depletion significantly disrupts the Sirtuin Signaling Pathway in HDMB-03 cells. Activation Z-score analysis found this dysregulation to result in pathway inactivation (Z-score = -2). Genes differentially expressed upon *YBX1* knockdown in HDMB-03 cell lines are indicated as green (up-regulated in the dataset) or red (down-regulated in the dataset). Pathway constructed using the IPA programme (Qiagen).

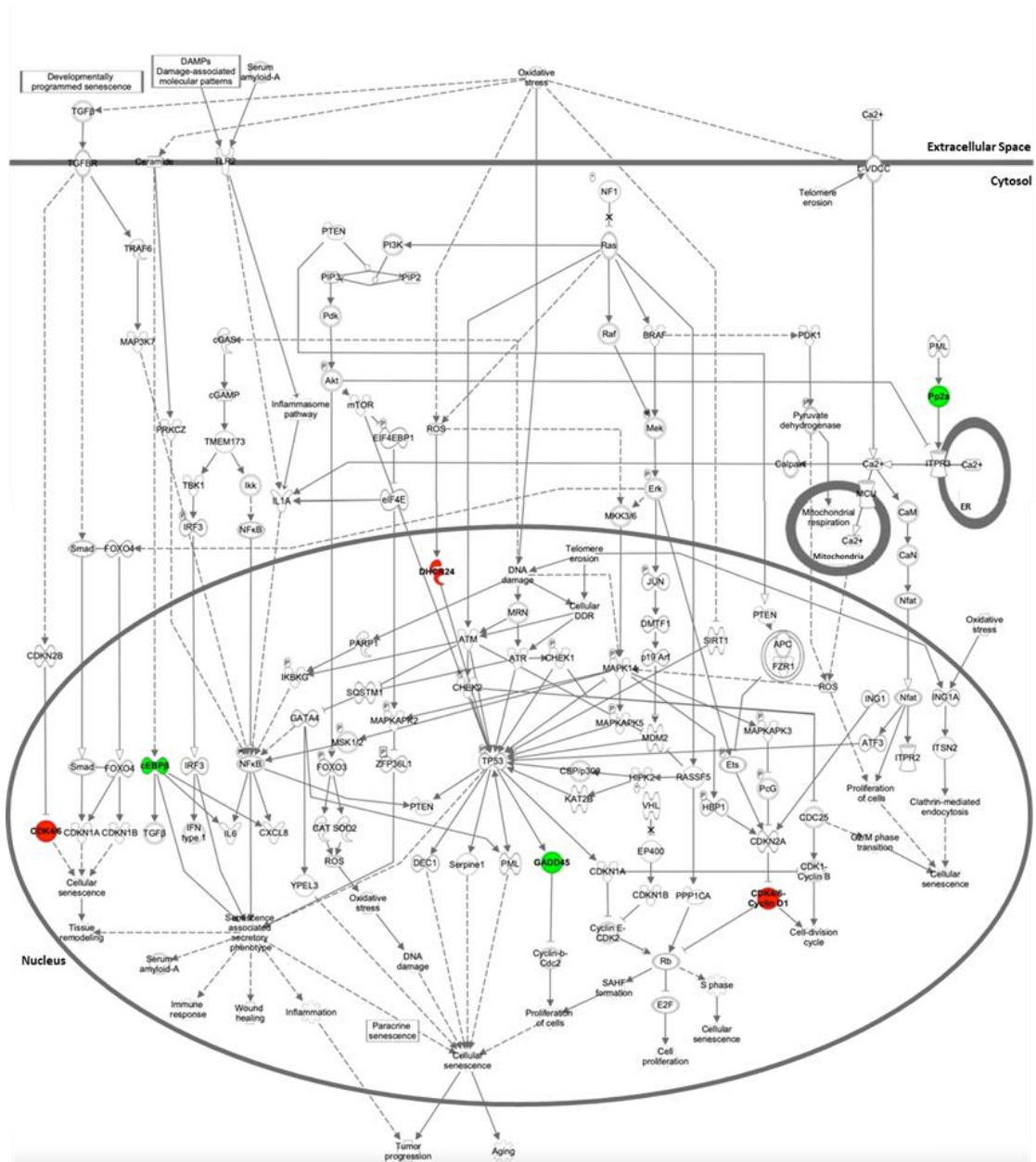


Figure 5.23 *YBX1*-knockdown has an activational effect on the Senescence Pathway in D283 cells. *YB-1* depletion significantly disrupts the Senescence Pathway in D283 cells. Activation Z-score analysis found this dysregulation to result in slight pathway activation (Z-score = 1.3), however as the activation Z-score is < 2, this was not considered significantly predictive. Genes differentially expressed upon *YBX1* knockdown are indicated as green (up-regulated in the dataset) or red (down-regulated in the dataset). Pathway constructed using the IPA programme (Qiagen).

5.4.5.3 Upstream regulator analysis indicates altered MYC activity levels in D283 cells upon *YBX1* knockdown

IPA software (Qiagen) was also used to conduct upstream regulator analysis, a process which identifies upstream regulators that may be responsible for the gene expression changes observed in a dataset based on information from the Ingenuity Knowledge Base. Activation Z-scores are generated based on gene expression patterns of target genes within the dataset, which predict the activation state of the upstream regulator. An upstream regulator is considered as activated if the Z-score is ≥ 2 and inhibited if the Z-score ≤ -2 . Importantly, IPA upstream regulator analysis does not simply assess the expression of various regulators, but instead the expression of the regulator's targets to provide an approximation of the regulator's functional state. For this analysis, upstream regulators included transcription factors, growth factors, cytokines, phosphatases, kinases and other complexes. The top significant (P-value and Z-score) upstream regulators for both HDMB-03 and D283 knockdown vs. non-silencing comparisons are displayed in the heatmap in Figure 5.24.

Importantly, MYC was found to be significantly inhibited in D283 cells following *YBX1* knockdown (Z-score = - 2.1). No significant change in MYC activity was identified in HDMB-03 cells following *YBX1* knockdown, indicating that this observation is unique to the D283 line. As previously discussed, no alteration in MYC expression level was observed in either knockdown cell line at a protein level (Section 5.2.3), nor was any alteration of expression at an mRNA level detected (LFC = 0.11; P-value = 0.62). Thus, this result suggests that, rather than simply causing reduced MYC expression, YB-1 depletion in D283 cells inhibits the activity of the MYC. This result

may implicate YB-1 in the maintenance of MYC pathway activity in the D283 cell line, a finding with potential therapeutic implications given the association of *MYC/MYCN* amplification and/or overexpression with aggressive disease and relapse in medulloblastoma (Hill et al., 2015; R. Tao et al., 2019). Furthermore, it is possible that reduced MYC pathway activity may also render D283 cells less susceptible to treatment with BET-bromodomain inhibitors, such as JQ1. Previous medulloblastoma studies have demonstrated that JQ1 was efficacious in reducing cell viability in lines driven by active MYC signalling only, with a minimal effect found in non-*MYC* amplified lines (Bandopadhyay et al., 2014; Bolin et al., 2018). In Section 5.3.3, we demonstrated that YB-1 depletion resulted in increased sensitivity to JQ1 in HDMB-03 cells but not in D283 cells. Thus, I hypothesise that this observed difference in response to JQ1 upon YB-1 knockdown in D283 and HDMB-03 cells may arise from alterations in MYC pathway activity between D283 and HDMB-03 knockdown lines.

Interestingly, upstream regulator analysis also revealed inhibition of components of the mechanistic target of rapamycin (mTOR) signalling pathway were common to both *YBX1* knockdown cell lines (Figure 5.24). In HDMB-03 cells, rapamycin-insensitive companion of mTOR (RICTOR), a component of the mTOR complex 2 (mTORC2) complex, was identified as a significantly inhibited upstream regulator following YB-1 depletion (Z-score = -2.2). In the D283 knockdown vs. non-silencing comparison, regulatory-associated protein of mTOR (RPTOR), a component of the mTORC1 complex, was identified as a significantly inhibited upstream regulator (Z-score = -2.0). Both RICTOR and RPTOR did not exhibit any alteration in mRNA expression following *YBX1* knockdown (LFC = -0.07 and P = 0.71; LFC = -0.10 and P =

0.57 respectively), indicative again of an alteration in the functional state of the upstream regulator following YB-1 depletion, rather than decreased expression. Previous studies have demonstrated clear communication between YB-1 and the PI3K/AKT/mTOR pathway, with YB-1 translation thought to be regulated by mTOR signalling (Section 1.4.2.1) and mTOR activity and expression associated with YB-1 expression (Fujii et al., 2009; Gong et al., 2020; Lee et al., 2008). This finding may indicate a similar association between YB-1 and mTOR signalling within paediatric brain tumours, however functional assays will be required to validate this interesting finding.

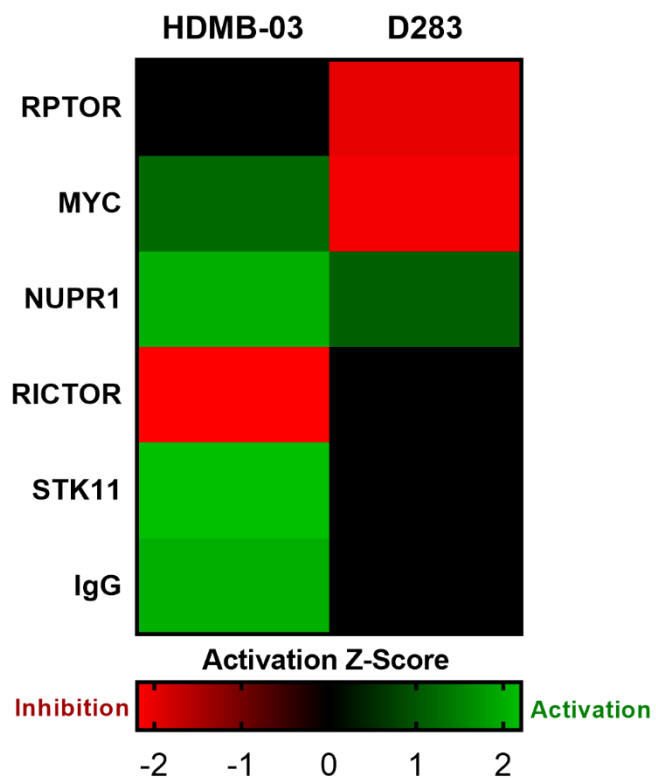


Figure 5.24 YB-1 depletion results in functional inhibition of MYC-, RPTOR- and RICTOR-associated pathways in medulloblastoma Group 3 cell lines. Heatmap presenting results of Upstream Regulator Analysis, conducted using IPA software. mTOR binding protein RICTOR was found to be significantly inhibited following *YBX1* knockdown in HDMB-03 cells (Z-score = -2.2), while MYC and mTOR binding protein RPTOR were found to be significantly inhibited in D283 cells (Z-scores = -2.1 and -2.0 respectively).

5.5 Summary

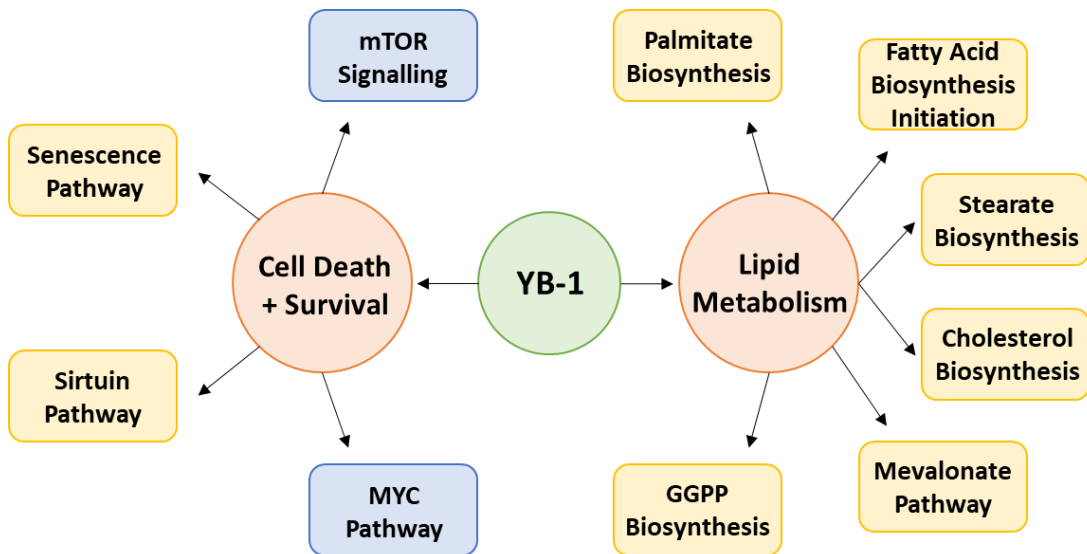


Figure 5.25 Graphical Summary of the YB-1 transcriptome in Group 3 medulloblastoma. YB-1 appears to regulate the function of a number of pathways and upstream regulators within lipid metabolism and cell death and survival cellular functions. The major, most significant cellular functions (orange), canonical pathways (yellow) and upstream regulators (blue) influenced by diminished YB-1 expression are shown.

- shRNA-mediated knockdown of *YBX1* in medulloblastoma Group 3 cell lines D283 and HDMB-03 resulted in the production of stable knockdown lines – KD-D283-Y_A and KD-HDMB-03-Y_A – with significantly reduced *YBX1* and YB-1 expression.
- YB-1 depletion does not alter the proliferative capacity of either KD-HDMB-03-Y_A or KD-D283-Y_A cell lines relative to the appropriate non-silencing control line.
- YB-1 depletion sensitizes KD-HDMB-03-Y_A and KD-D283-Y_A cells to low concentrations of vincristine, an effect likely mediated by the reduced expression of vincristine efflux pump *ABCB1* in both *YBX1* knockdown cell lines.

- YB-1 depletion sensitizes KD-HDMB-03-Y_A, not KD-D283-Y_A, cells to low-intermediate concentrations of HDAC inhibitor panobinostat and BET bromodomain inhibitor JQ1, indicating that YB-1 may play a role in the cellular stress response of this cell line to both anti-cancer therapies.
 - Increased sensitivity of the KD-HDMB-03-Y_A line to panobinostat may arise from the dysregulation of the Sirtuin Pathway (a stress response pathway regulated by HDACs called SIRTs), which was found to be inhibited following *YBX1* knockdown in HDMB-03 cells.
 - Lack of sensitivity of the KD-D283-Y_A line to JQ1 may arise from the functional inhibition of upstream regulator MYC, which may result in decreased MYC pathway activity and a subsequent lack of response to BET-bromodomain inhibitors.
- Loss of YB-1 expression impedes the invasive, not migratory, capabilities of both KD-HDMB-03-Y_A and KD-D283-Y_A cell lines, although the functional mechanism by which this occurs, and whether *ABCB1* is implicated, is currently unclear.
- Whole transcriptome sequencing reveals lipid metabolism and cell death and survival functions are frequently dysregulated upon *YBX1* knockdown in D283 and HDMB-03 cell lines (Figure 5.25).
 - Canonical pathway analysis revealed various pathways of lipid/cholesterol biosynthesis were dysregulated in both cell lines following YB-1 depletion, highlighting a possible novel function of YB-1 in the regulation of lipid metabolism in brain tumours.

Chapter 6

Examination of the route to drug tolerance in medulloblastoma

Chapter 6 Examination of the route to drug tolerance in medulloblastoma

6.1 Introduction

As discussed throughout this study, there is an urgent unmet need for the development of novel therapeutic strategies for relapsed medulloblastoma. In spite of this, biopsy at relapse is rare and few genetic drivers or markers of medulloblastoma relapse have thus far been identified. One of the only large-scale genetic characterisation studies of relapsed medulloblastoma, published in 2021, revealed that although some genetic events are selectively maintained between diagnosis and relapse, a large proportion of novel genetic events emerge at relapse (Richardson et al., 2021). Such genetic divergence following therapy likely arises through the expansion of a sub-population of cells that are either intrinsically resistant to standard medulloblastoma therapy, or have acquired resistance to therapy. Thus, the identification of targets that either mark therapy resistant cancer cell populations, or drive the survival and proliferation of resistant medulloblastoma cells, will provide a basis for improved clinical management of relapsed disease.

In Chapter 4 and Chapter 5, we provided evidence to indicate a potential function for YB-1 in cellular stress response and drug resistance. However, our data thus far is complex and, particularly in relation to cisplatin and vincristine, at times paradoxical. We have demonstrated that *YBX1* knockdown promotes increased sensitivity to vincristine (likely through altered *ABCB1* expression), despite no alteration in YB-1 sub-cellular localisation upon acute vincristine treatment. Conversely, YB-1

translocates to the nucleus following acute cisplatin treatment and yet YB-1 depletion does not alter cellular sensitivity to cisplatin. Investigation of YB-1 nuclear targets following cisplatin and vincristine treatment, as well as an improved understanding of global gene changes surrounding the acquisition of drug resistance in medulloblastoma, will provide further clarity on the role played by YB-1 in stress response and drug resistance in medulloblastoma.

Accordingly, the aims of the present chapter were as follows:

- A) Develop stable *in vitro* models of acquired medulloblastoma resistance, using standard-of-care chemotherapeutics cisplatin and vincristine.
- B) Submit the aforementioned stable drug-tolerant cell lines for 3'mRNA sequencing to analyse transcriptomic changes that occur upon the acquisition of cisplatin and vincristine resistance in medulloblastoma.
- C) Prepare CHIP assay samples from medulloblastoma cell lines subjected to either acute or chronic cisplatin/vincristine treatment and submit for CHIP sequencing to identify YB-1 targets associated with different treatment states.

6.2 Generation of drug-tolerant medulloblastoma cell lines

In order to identify drug-specific YB-1 transcriptional targets in response to cisplatin and vincristine treatment and investigate how the transcriptome is altered upon the acquisition of drug tolerance *in vitro*, we required cisplatin- and vincristine-tolerant medulloblastoma cell lines. Drug-tolerant cell lines are developed by repeatedly exposing cells to the drug of interest. At the end of the process, the surviving resistant daughter cells are compared to the parental sensitive cells by way of cell viability assays. The IC₅₀ for these paired cell lines can be used to determine the increase in resistance known as fold resistance (McDermott et al., 2014). Drug tolerance is considered acquired when the IC₅₀ of the tolerant cell line exceeds its treatment dose and an increase in fold resistance is observed. In the present study, we also wished to see a significant elevation of the IC₅₀ of the drug-tolerant line compared to the parental/vehicle-treated control line. To establish a reliable, long-term model of drug-tolerance, the resistant phenotype should also be stable following freeze/thaw.

6.2.1 Long-term drug treatment with continuous selection promotes increased tolerance to cisplatin in medulloblastoma Group 3 cell lines

Cisplatin dose response assays undertaken in Section 4.3.1 revealed that D283 and D458 Group 3 cell lines have an IC₅₀ of 1.6 μ M and 0.4 μ M respectively. As previously described, a selection strategy of continuous exposure was utilised to generate cisplatin-tolerant Group 3 cell lines (Section 2.7). D283 and D458 lines were exposed to cisplatin at an initial concentration of 1/100 IC₅₀, following which drug concentration was increased incrementally upon cell proliferation, with

chemotherapeutic-containing media replenished every 3-4 days. Vehicle (DMF)-treated controls were passaged alongside the treated cells to account for alterations in cellular characteristics arising from long-term cell culture and vehicle treatment. To monitor cell resistance, cell viability assays were undertaken once the 1/5 IC_{50} dose was reached.

After three months of treatment, cisplatin-treated D458 cells (DT-D458-CIS) had reached a treatment dose of 1.5 fold IC_{50} (0.6 μ M). Both DT-D458-CIS and the DMF-treated control cell line (DT-D458-DMF) were cultured in drug-free media for five days, following which cisplatin dose response assays were undertaken (Figure 6.1 A). The cisplatin IC_{50} value for the DT-D458-DMF cells was 0.9 μ M, increased slightly from that of the parental line (0.4 μ M). Comparatively, the cisplatin IC_{50} for the DT-D458-CIS cells was found to be 18.5-fold increased from that of the parental D458 line at 7.4 μ M. As the DT-D458-CIS cisplatin IC_{50} value both exceeded the treatment dose (0.6 μ M) and was found to be significantly greater than the IC_{50} values of the parental line ($P < 0.0001$) and DT-D458-DMF line ($P < 0.0001$), it was deemed drug-tolerant. The resistance phenotype was also maintained following freeze/thaw, confirming stable cisplatin-tolerance.

After five months of treatment, cisplatin-treated D283 cells (DT-D283-CIS) had reached a treatment dose of 1/1 IC_{50} , equivalent to 1.6 μ M. As before, dose response assays were undertaken to assess the development of a resistance phenotype (Figure 6.1 B). The cisplatin IC_{50} value for the DMF-treated control line (DT-D283-DMF) was found to be 0.8 μ M, half of that observed in the parental D283 line. In comparison, the DT-D283-CIS line developed a cisplatin IC_{50} value of 4.0 μ M, indicative of a 2.5-

fold increase in resistance. Again, the DT-line IC_{50} value both exceeded the treatment dose (1.6 μ M) and was significantly increased when compared to both the DT-D283-DMF line ($P = 0.0032$) and the parental line ($P = 0.023$), hence was considered drug-tolerant. The resistance phenotype was again maintained following freeze/thaw, inferring stable resistance.

Throughout continuous selection, the morphology of both DT-lines was monitored (Appendix D1). Interestingly, DT-D283-CIS cells exhibited distinct morphological changes compared to the paired DT-D283-DMF line. Cells appeared more adherent, with fewer large clumps of cells – characteristic of the D283 line – visible in suspension. Adhered cells also appeared flatter and grew in larger adherent clusters than that observed in the DT-D283-DMF line. Although less marked, similar observations were made for the DT-D458-CIS line, which also appeared to grow more adherently than either the parental D458 line or the paired DT-D458-DMF line.

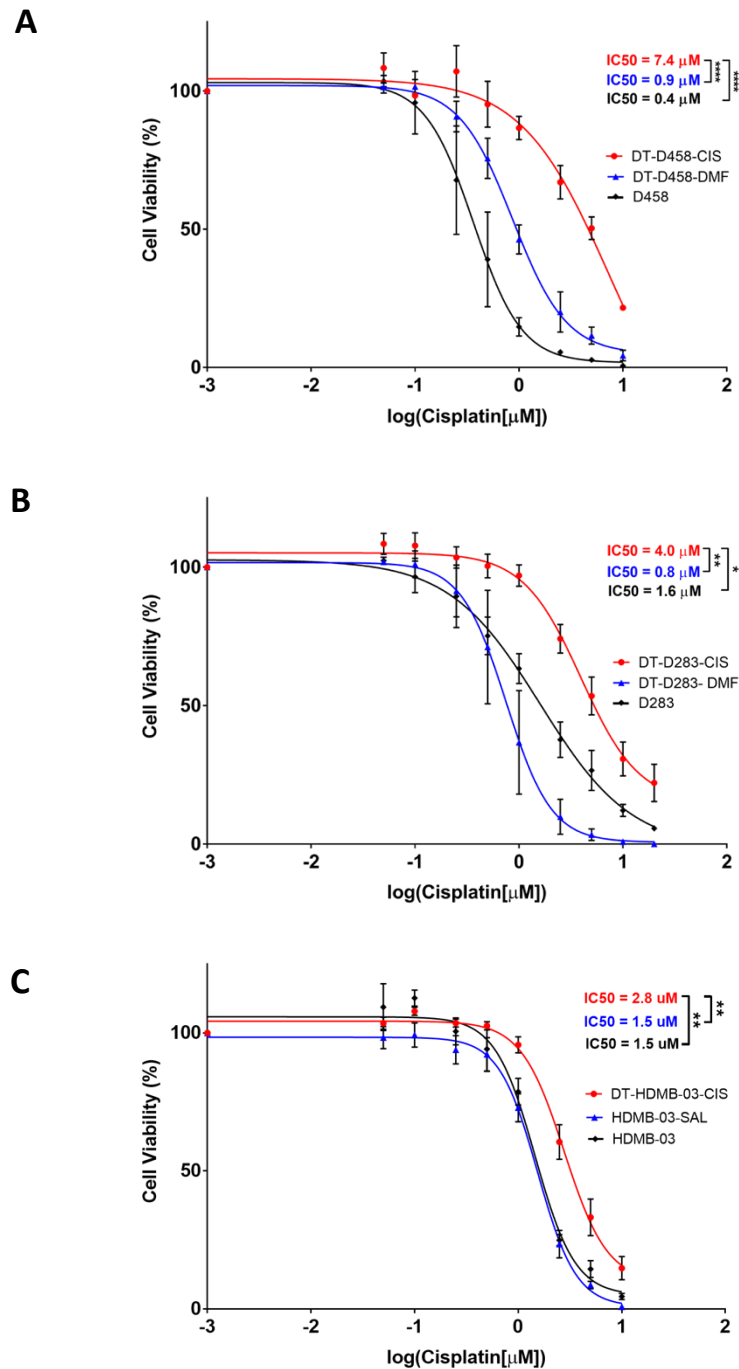


Figure 6.1 Continuous selection of D458, D283 and HDMB-03 Group 3 cell lines with cisplatin. D458, D283 and HDMB-03 cell lines were cultured continuously in the presence of cisplatin. Cell viability assays (PrestoBlue) allowed monitoring of cellular resistance compared to a vehicle-treated control line and/or the parental line. A) DT-D458-CIS cells exhibited an 18.5-fold increase in IC₅₀ value compared to the parental cell line following continuous treatment in 0.6 μM cisplatin. B) DT-D283-CIS cells exhibited a 2.5-fold increase in IC₅₀ value compared to the parental cell line following continuous treatment in 1.6 μM cisplatin. C) HDMB-03 cells exhibited a 1.6-fold increase in IC₅₀ value compared to the parental cell line following continuous treatment in 0.5 μM cisplatin. Mean ± SEM plotted; n = 3. Dose response curves were generated using non-linear regression analyses and IC₅₀ values calculated accordingly. Significance of IC₅₀ values was assessed by ordinary one-way ANOVA analyses with Tukey's multiple comparisons test. *P < 0.05, **P < 0.01, ***P < 0.0001.

We were kindly given a third Group 3 drug-tolerant cell line, DT-HDMB-03-CIS, generated at the University of Salford courtesy of Dr Gianpiero Di Leva. The DT-HDMB-03-CIS line had been cultured continuously in 0.5 μM cisplatin (equivalent to 1/3 cisplatin IC_{50} value) prior to assessment and validation of drug tolerance. Upon receiving this line, we repeated cisplatin dose response assays to ensure resistance had been maintained following freeze/thaw (Figure 6.1 C). The parental line from which the DT-HDMB-03-CIS cells were derived (HDMB-03-SAL) was also tested to facilitate comparison between it and our own HDMB-03 cell line. As anticipated, both HDMB-03 and HDMB-03-SAL cell lines produced near identical dose response curves and hence both had a cisplatin IC_{50} value of 1.5 μM . Comparatively, the DT-HDMB-03-CIS line exhibited a cisplatin IC_{50} value of 2.8 μM , representative of a 1.6-fold increase in resistance compared to the parental line. This was both significantly elevated compared to the IC_{50} value observed in parental line ($P = 0.0069$) and exceeded the treatment dose, hence the DT-HDMB-03-CIS line was also considered cisplatin-tolerant.

6.2.2 Group 3 cell lines are unable to develop tolerance to vincristine following continuous selection and dose escalation.

Generation of vincristine-tolerant D283 and D458 cell lines was also attempted by continuous selection with vincristine and dose escalation upon proliferation. As with cisplatin-tolerant lines, vincristine dosing was initiated at a concentration of 1/100 of the previously calculated parental cell line IC_{50} (Section 4.3.1).

Surprisingly, in comparison to cisplatin-tolerant cell line generation, Group 3 cell lines appeared unable to develop vincristine tolerance. Although proliferation was observed in both cell lines in the presence of vincristine up to a concentration of 1/3 IC_{50} , any further increase in vincristine dose resulted in significant cell death and senescence of any surviving cells. Despite maintaining 1/2 IC_{50} -treated flasks in culture for 2 months with bi-weekly media changes, no further proliferation was observed and any remaining cells eventually died. Nevertheless, we wished to evaluate if the D283 and D458 vincristine-treated cell lines (DT-D283-VIN and DT-D458-VIN) had developed a resistant phenotype from their culture in 1/3 IC_{50} maintaining media. Vincristine dose response assays showed the DT-D458-VIN line to exhibit an IC_{50} of 4.3 nM and DT-D283-VIN line an IC_{50} of 2.3 nM (Appendix D2), which were not found to be statistically different when compared to the appropriate vehicle (DMSO)-treated control lines or parental lines. As such, DT-D458-VIN and DT-D283-VIN lines were not considered resistant to vincristine and thus were not taken forward for further study.

6.2.3 Continuous vincristine selection facilitates tolerance in SHH cell line DAOY

In comparison to D283 and D458 Group 3 cell lines (Section 6.2.2), the SHH cell line DAOY did develop tolerance to vincristine treatment. The DT-DAOY-VIN cell line was a gift from Dr Gianpiero Di Leva at the University of Salford. As with previously described drug-tolerant lines, the DT-DAOY-VIN line was generated through a model of continuous selection with vincristine up to a concentration of 2 nM (equivalent to 1.5-fold vincristine IC_{50}). Upon receiving the DT-DAOY-VIN line, dose response assays were undertaken to ensure resistance had been maintained following freeze/thaw (Figure 6.2). The parental line from which the DT-DAOY-VIN line was derived (DAOY-SAL) was also tested, as was our own DAOY line (DAOY) for comparison. The DAOY-SAL cell line exhibited a higher sensitivity to vincristine than the Nottingham DAOY line, with an IC_{50} of 0.9 nM compared to 1.3 nM. The DT-DAOY-VIN line exhibited an IC_{50} of 3.7 nM, equivalent to a 4-fold increase in resistance. This was significantly elevated compared to the parental line ($P = 0.0030$) and higher than the treatment dose (2 nM) and as such, the DT-DAOY-VIN line was considered vincristine tolerant. It is unclear why Group 3 cell lines D283 and D458 were unable to acquire vincristine resistance, while the SHH cell line DAOY developed significant tolerance. One explanation could perhaps lie in the differences in *ABCB1* expression between cell lines from different sub-groups (Section 4.2.1). DAOY cells express approximately 15-fold greater quantities of *ABCB1* mRNA than D283 and D458 lines. It is feasible that this high-level expression may facilitate the survival of DAOY cells following vincristine treatment, promoting a resistant phenotype. Additional experiments such as loss-of-function studies would be required to explore this further.

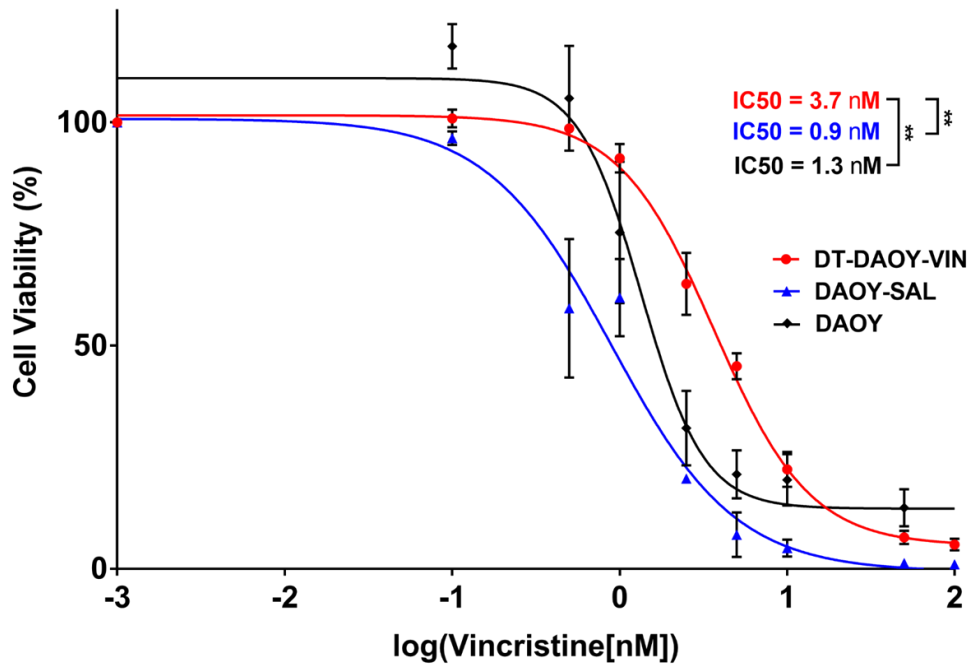


Figure 6.2 Continuous selection of SHH cell line DAOY with vincristine. DT-DAOY-VIN cells were cultured continuously in the presence of vincristine. Cells exhibited a 4-fold increase in IC₅₀ value compared to the parental cell line following continuous treatment in 2 nM vincristine (~1.5 IC₅₀). Mean ± SEM plotted; n = 3. Dose response curves were generated using non-linear regression analyses and IC₅₀ values calculated accordingly. Significance of IC₅₀ values was assessed by ordinary one-way ANOVA analyses with Tukey's multiple comparisons test. **P < 0.01.

6.2.4 Drug-tolerant cell lines express altered levels of ABC transporters

Prior to the study of global changes in gene expression following the acquisition of drug tolerance, expression levels of ABC transporters, known mediators of chemoresistance (Section 1.3), were first investigated in drug-tolerant cell lines (Figure 6.3).

qRT-PCR analysis was undertaken for genes encoding the three most commonly reported multi-drug resistance ABC transporters – *ABCB1*, *ABCC1* and *ABCG2*. In the vincristine-tolerant cell line DT-DAOY-VIN line, both *ABCB1* and *ABCC1* showed significant up-regulation ($P \leq 0.0001$), concomitant with vincristine representing a substrate of both transporters. Interestingly, elevated *ABCC1* expression was also recorded in the DT-D458-CIS line ($P = 0.0002$) and DT-D283-CIS line ($P = 0.028$), despite cisplatin not being a substrate of *ABCC1*. This finding is in agreement with previous studies where platinum compound resistant cell lines have demonstrated increased *ABCC1* expression, and may suggest that *ABCC1* has a function in therapy resistance and/or cell survival independent of its role in cytotoxic drug efflux (Beretta et al., 2010).

Comparatively, no alteration in *ABCG2* expression was recorded across any drug-tolerant cell line tested (Figure 6.3 C). This finding was, however, anticipated on account of neither compounds representing *ABCG2* substrates.

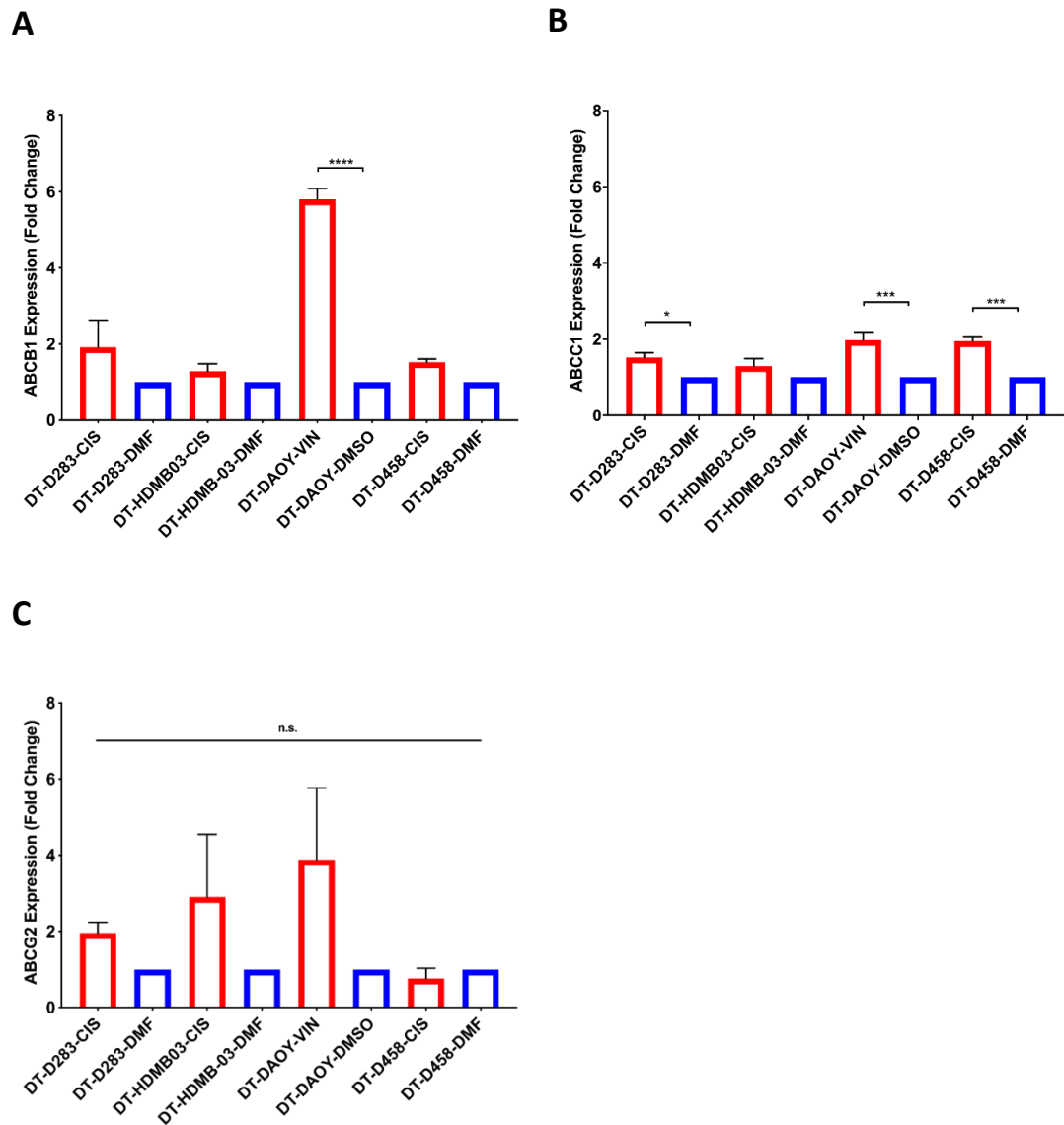


Figure 6.3 ABC transporter expression is altered in drug-tolerant medulloblastoma cell lines. A) Assessment of *ABCB1* expression across drug-tolerant cell lines revealed elevated expression in DT-DAOY-VIN cells compared to the DT-DAOY-DMSO line. B) Expression of *ABCC1* was found to be significantly increased in DT-DAOY-VIN, DT-D458-CIS and DT-D283-CIS lines relative to appropriate vehicle treated controls. C) *ABCG2* expression remained unchanged across all drug-tolerant cell lines tested. Fold change in ABC transporter gene expression was calculated relative to the *GAPDH* housekeeping gene and vehicle-treated control cell line ($2^{-\Delta\Delta Cq}$). N = 3. Mean \pm SEM; *P < 0.05, ****P < 0.0001. Significance was assessed using ordinary one-way ANOVA analyses with Sidak's multiple comparisons test.

6.2.5 Drug-tolerant cell lines display reduced levels of *YBX1*

We next wanted to assess whether long-term exposure to cisplatin/vincristine had any effect on *YBX1* mRNA levels. As before, qRT-PCR analysis was used to examine *YBX1* expression in each drug-tolerant cell line, relative to the appropriate vehicle treated control line. *YBX1* expression was found to be significantly decreased in DT-DAOY-VIN ($P = 0.046$) and DT-D283-CIS ($P = 0.0004$) cells, while expression in DT-HDMB-03-CIS and DT-D458-CIS cell lines remained unchanged (Figure 6.4 A).

To ensure that this trend was maintained at a protein level, all four drug-tolerant cell lines were plated and immunofluorescence employed as previously described (Section 2.9.8). Similar to that observed at an mRNA level, little difference in cellular YB-1 expression was detected between most drug-tolerant and vehicle-treated control cell lines. However, replicating the result shown in Figure 6.4 A, the DT-D283-CIS line did display reduced YB-1 expression at an overall level. Representative confocal microscopy images and concurrent quantification for DT-HDMB-03-CIS and DT-HDMB-03-DMF cell lines is presented in Figure 6.4 B – D for reference, while confocal images and quantification for all other cell lines is displayed in Appendix D3.

Interestingly, a selection of cells in the drug-tolerant lines did exhibit punctate, “speckled” YB-1 nuclear staining which was more frequent than that observed in their vehicle-treated control counterparts, as indicated by the arrowheads in Figure 6.4 D. This was particularly evident in the DT-DAOY-VIN and DT-HDMB-03-CIS lines. However, analysis of all cells in each image did not find any significant alteration in YB-1 nuclear expression between drug-tolerant and vehicle-treated control cell lines,

other than the DT-D283-CIS cell line, where a significant decrease in nuclear YB-1 expression was observed (Appendix D3).

Together, these findings were unexpected. In a glioma patient cohort, high YB-1 expression was associated with patients with a history of drug resistance (Tong et al., 2019). Likewise, in other cancer types such as renal cell carcinoma, both YB-1 and ABCB1 were found to be up-regulated in sunitinib-resistant *in vitro*, *in vivo* and *ex vivo* models (D'Costa et al., 2020). This is, however, the first study that has examined YB-1 expression in medulloblastoma models of drug-tolerance. Thus, this finding led us to speculate that YB-1 may be associated with an acute, short-term cell stress response and perhaps its function differs in medulloblastoma cells undergoing chronic cisplatin/vincristine exposure which have become tolerant to the drug treatment dose.

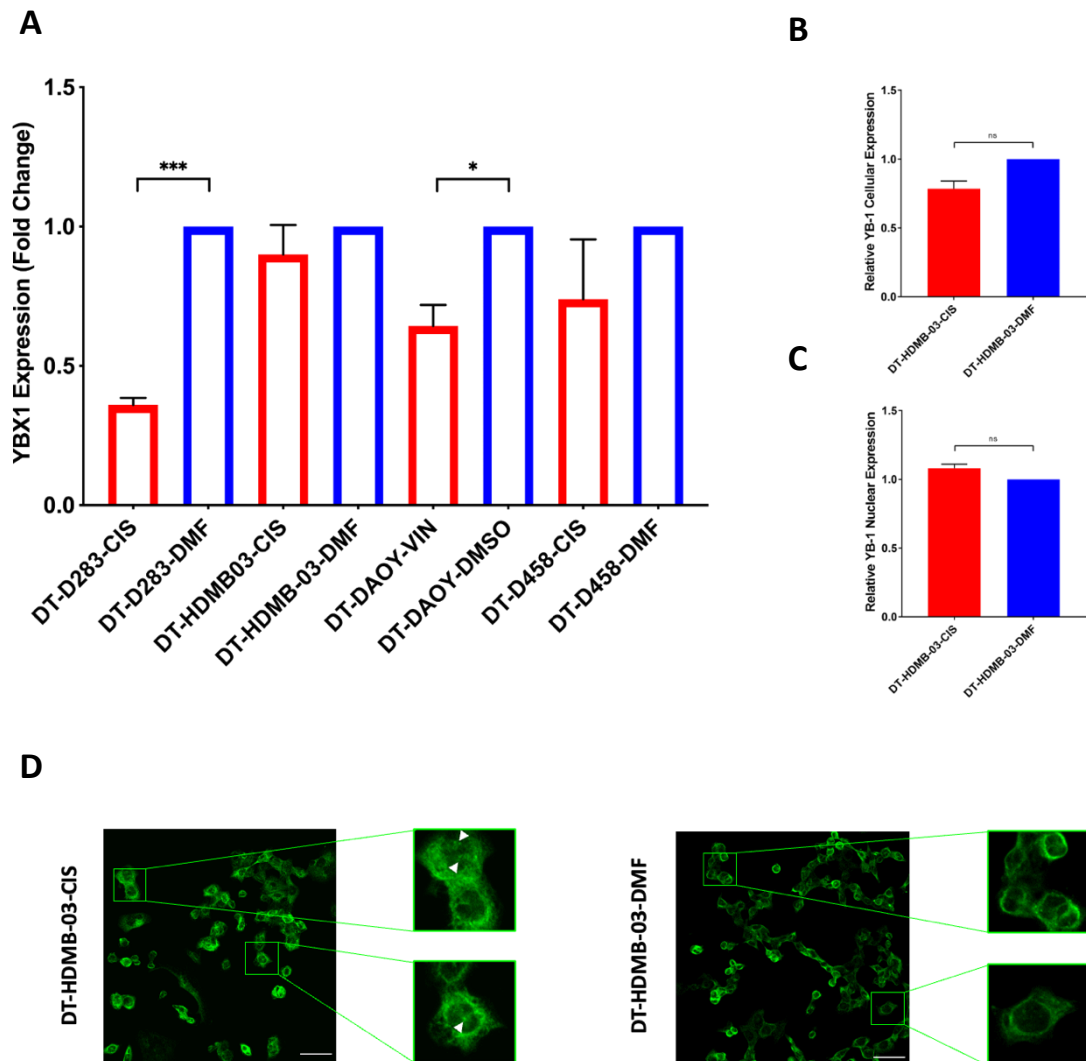


Figure 6.4 *YBX1* and *YB-1* expression is either reduced or unaltered in drug tolerant medulloblastoma cell lines. A) Assessment of *YBX1* expression across drug-tolerant cell lines revealed decreased expression in DT-D283-CIS and DT-DAOY-VIN lines. Fold change in *YBX1* expression was calculated relative to the *GAPDH* housekeeping gene and vehicle-treated control cell line ($2^{-\Delta\Delta Cq}$ method). $N = 3$. Mean \pm SEM; * $P < 0.05$, *** $P < 0.001$. Significance was assessed using ordinary one-way ANOVA analyses with Sidak's multiple comparisons test. B) Automated quantification of confocal microscopy images revealed no difference in overall staining intensity between DT-HDMB-03-CIS and the vehicle-treated control line. C) Automated quantification of confocal microscopy images revealed no difference in nuclear staining intensity between DT-HDMB-03-CIS and the vehicle-treated control line. $n = 2$ (approx. 700 cells per cell line); ns = not significant. Significance assessed by unpaired t-test. D) Representative confocal images. Cells were immunostained for *YB-1* (green). All scale bars represent 50 μm .

6.3 Analysis of the transcriptomic changes that occur upon the acquisition of drug tolerance in medulloblastoma Group 3 and SHH cell lines

As described previously (Section 6.1), the development of tolerance to chemotherapeutic agents in medulloblastoma is likely associated with tumour relapse, for which there are currently no effective therapies. Thus, understanding how cells acquire and maintain resistance to current, standard-of-care therapies is of vital importance. To begin to elucidate potential mechanisms of drug tolerance to cisplatin and vincristine in an *in vitro* model, and see how these mechanisms differ between cell lines and drugs, we employed 3'mRNA sequencing (3'mRNA-Seq) using the aforementioned drug-tolerant cell lines (DT-D283-CIS, DT-D548-CIS, DT-HDMB-03-CIS and DT-DAOY-VIN).

3'mRNA-Seq offers an alternative method to the whole transcriptome sequencing described in Section 5.4. In the 3'mRNA-Seq method, mRNAs are not fragmented before reverse transcription. Instead, cDNA is reverse transcribed from the 3' polyadenylated end of mRNA. Only one copy of cDNA is generated for each transcript, thus directly linking the number of reads mapping to a gene to its expression. Although a 3'-end, coding region focused approach cannot provide information regarding non-coding RNA like whole transcriptome sequencing, its main benefit is that, due to the focus on poly(A)-enriched RNA molecules only, it requires much less sequencing data (25-50 million reads per sample compared to 100-200 million reads per sample), facilitating a greater read depth at a lower cost.

6.3.1 Sample preparation and sequencing

Samples from eight cell lines (DT-D283-CIS/DMF, DT-D548-CIS/DMF, DT-HDMB-03-CIS/DMF and DT-DAOY-VIN/DMSO) were collected in triplicate and RNA extracted as described in Section 2.9.3. In order to ensure RNA quality and yield was sufficient for sequencing, all samples underwent preliminary quality control using an Agilent TapeStation 4200 to assess RNA integrity and a Qubit Fluorometer to assess RNA concentration. All samples displayed excellent RINe values ranging between 9.8 and 10 (Appendix D4) and hence were considered suitable for downstream sequencing.

Libraries were then prepared and sequenced, as described previously in Section 2.10.2.1 – 2.10.2.2 by Matthew Carlile at the University of Nottingham's DEEP-SEQ sequencing facility. PolyA-selected libraries were made from 250 ng of total RNA input using QuantSeq 3'mRNA-Seq Library Prep Kit FWD for Illumina and external multiplexing barcodes for Illumina with 14 PCR cycles for library amplification. The fragment size and quality of the libraries were assessed by Agilent TapeStation 4200 before sequencing on an Illumina NextSeq 500 to generate approximately 5 million 75bp single-end reads per sample.

6.3.2 Mapping of sequencing data

Following sequencing, pre-analysis was performed using the BlueBee platform (Lexogen) as described extensively in Section 2.10.2.3. Following index processing and read trimming, quality controlled reads were mapped against human genome assembly GRCh38 (hg38). Overall, the quality of reads was excellent. Total mapped reads ranged between 97.3% and 99.3%, while uniquely mapped reads ranged

between 72.7% and 80.9%, representing ~17,000 genes per sample (Appendix D5). Taken together, these data are indicative of high mapping quality and sequencing accuracy.

6.3.3 Differential Gene Expression Analysis

Uniquely mapped reads were then used to generate counts for each gene using the programme “featureCounts” which determines the number of uniquely and correctly aligned reads per gene. Following this, differential gene expression analysis was undertaken using the R statistical environment package “DESeq2” which facilitated read count normalisation and analysis of differential gene expression (Anders & Huber, 2010).

Prior to the analysis of significantly differentially expressed genes, unsupervised analysis in the form of Principal Component Analyses (PCA) was first undertaken to explore sample clusters and variation between samples. As displayed in Figure 6.5 A-D, each drug tolerant (DT)-vehicle control comparison clustered separately on a PCA plot, indicative of variation in gene expression profile upon the acquisition of drug-tolerance in each cell line. Additionally, clustering was observed within biological replicates, indicative of similar gene expression profiles within sample groups.

Next, unsupervised clustering was undertaken using the 50 genes with the largest variance between biological replicates for each DT-vehicle comparison. Following the filtering out of lowly expressed genes (Chen et al., 2016), heatmaps were generated using an online heatmap generation tool (heatmapper.ca/expression/) using the average linkage method for hierarchical clustering calculations (Babicki et al., 2016). As displayed in Figure 6.6 - Figure 6.9, and replicating trends observed from PCA

plots, biological replicates from DT or vehicle-treated samples were found to cluster together. For all cell lines, DT and vehicle-treated samples clustered separately, indicative of clear differences between treatment conditions.

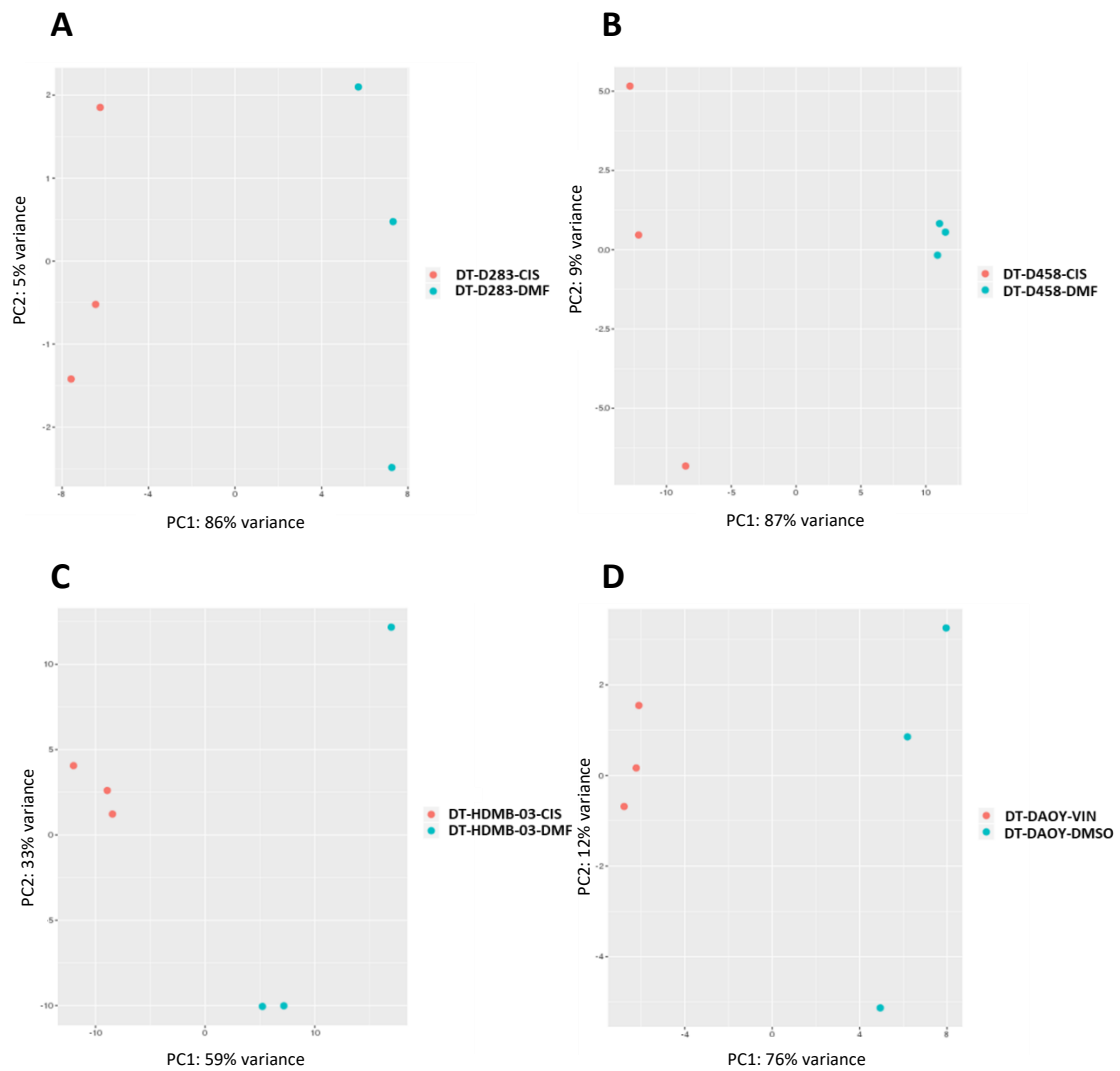


Figure 6.5 Principal component (PC) analysis of drug-tolerant cell line 3'mRNA sequencing samples. PCA was performed on all samples submitted to sequencing using normalised gene expression values in order to visualise sample clustering. For each drug-tolerant (DT)-vehicle control pair, clustering was observed between replicates, while clear separation was observed between sample type. A) PCA plot of DT-D283-CIS and DT-D283-DMF samples. B) PCA plot of DT-D458-CIS and DT-D458-DMF samples. C) PCA plot of DT-HDMB-03-CIS and DT-HDMB-03-DMF samples. D) PCA plot of DT-DAOY-VIN and DT-DAOY-DMSO samples.



Figure 6.6 Unsupervised clustering of DT-D283-CIS and DT-D283-DMF cell lines. Unsupervised transformed gene counts were used to create a heatmap representing the top 50 genes with the largest variance across all D283 drug-tolerant and vehicle-treated samples. The colour scale signifies the relative expression level of a gene across all samples. Expression levels above the mean are shown as green and below the mean are red. Differences in gene expression between drug-tolerant and vehicle-treated cell lines were clear, with triplicates from each sample set clustering together.

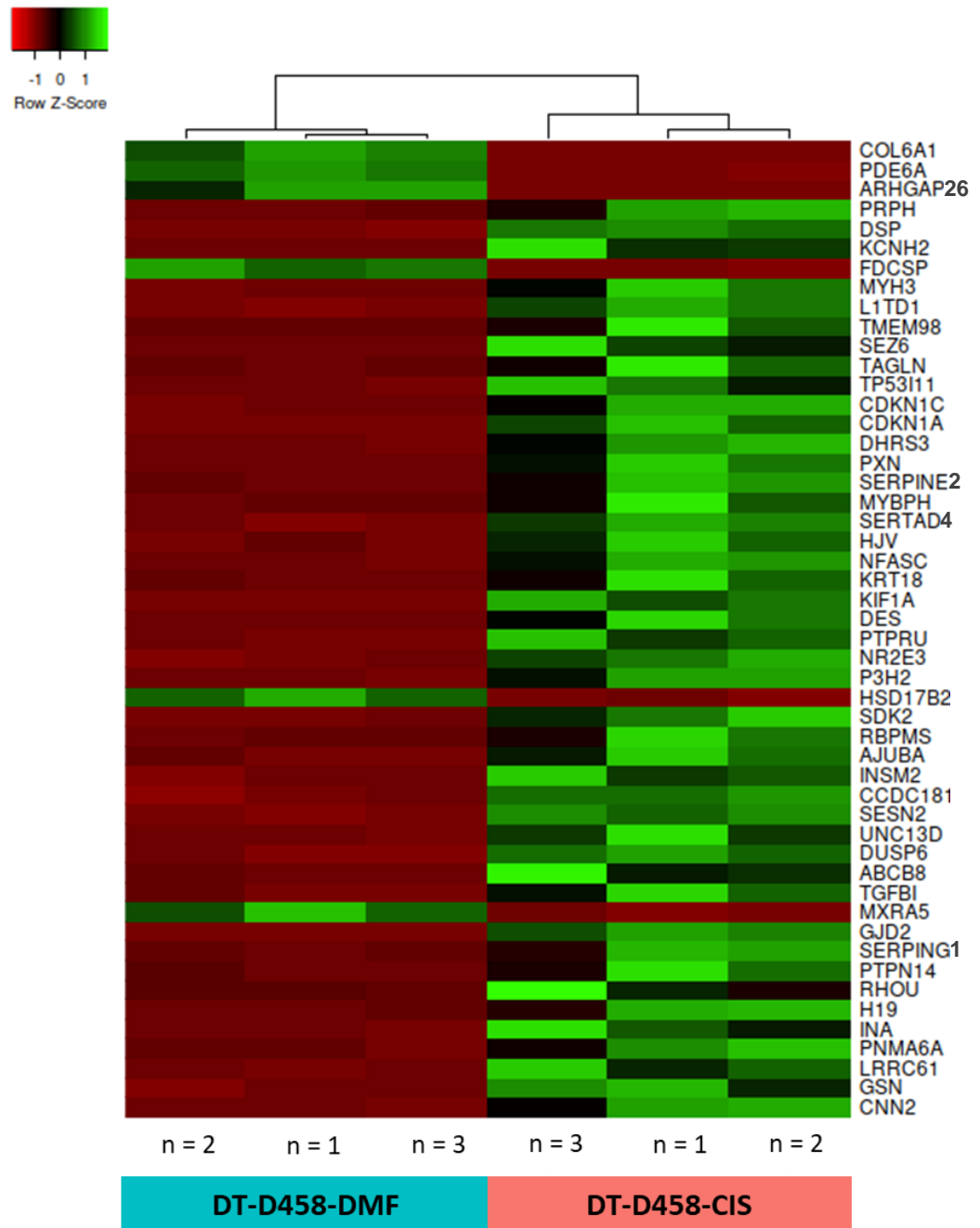


Figure 6.7 Unsupervised clustering of DT-D458-CIS and DT-D458-DMF cell lines. Unsupervised transformed gene counts were used to create a heatmap representing the top 50 genes with the largest variance across all D458 drug-tolerant and vehicle-treated samples. The colour scale signifies the relative expression level of a gene across all samples. Expression levels above the mean are shown as green and below the mean are red. Differences in gene expression between drug-tolerant and vehicle-treated cell lines were clear, with triplicates from each sample set clustering together.

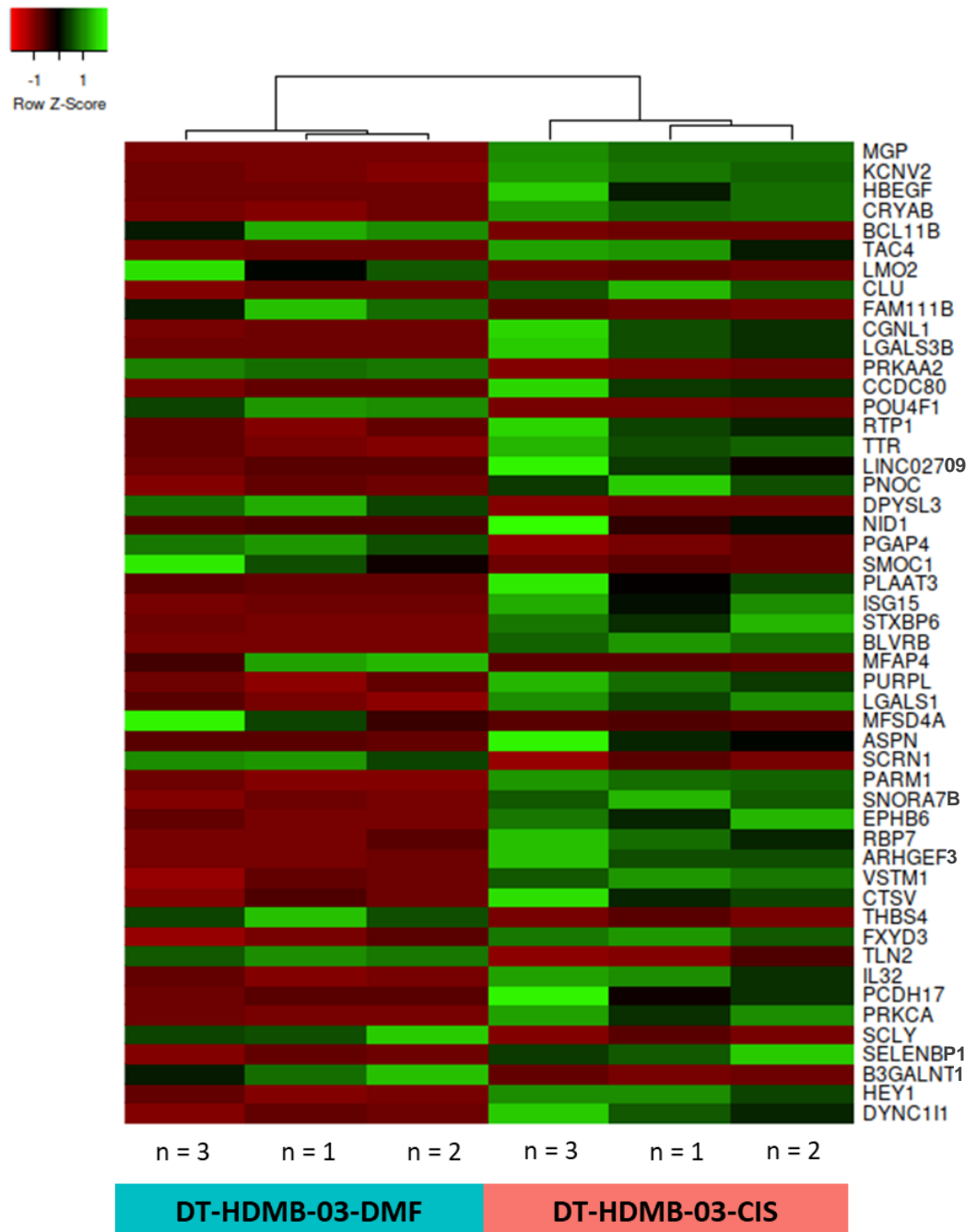


Figure 6.8 Unsupervised clustering of DT-HDMB-03-CIS and DT-HDMB-03-DMF cell lines. Unsupervised transformed gene counts were used to create a heatmap representing the top 50 genes with the largest variance across all HDMB-03 drug-tolerant and vehicle-treated samples. The colour scale signifies the relative expression level of a gene across all samples. Expression levels above the mean are shown as green and below the mean are red. Differences in gene expression between drug-tolerant and vehicle-treated cell lines were clear, with triplicates from each sample set clustering together.

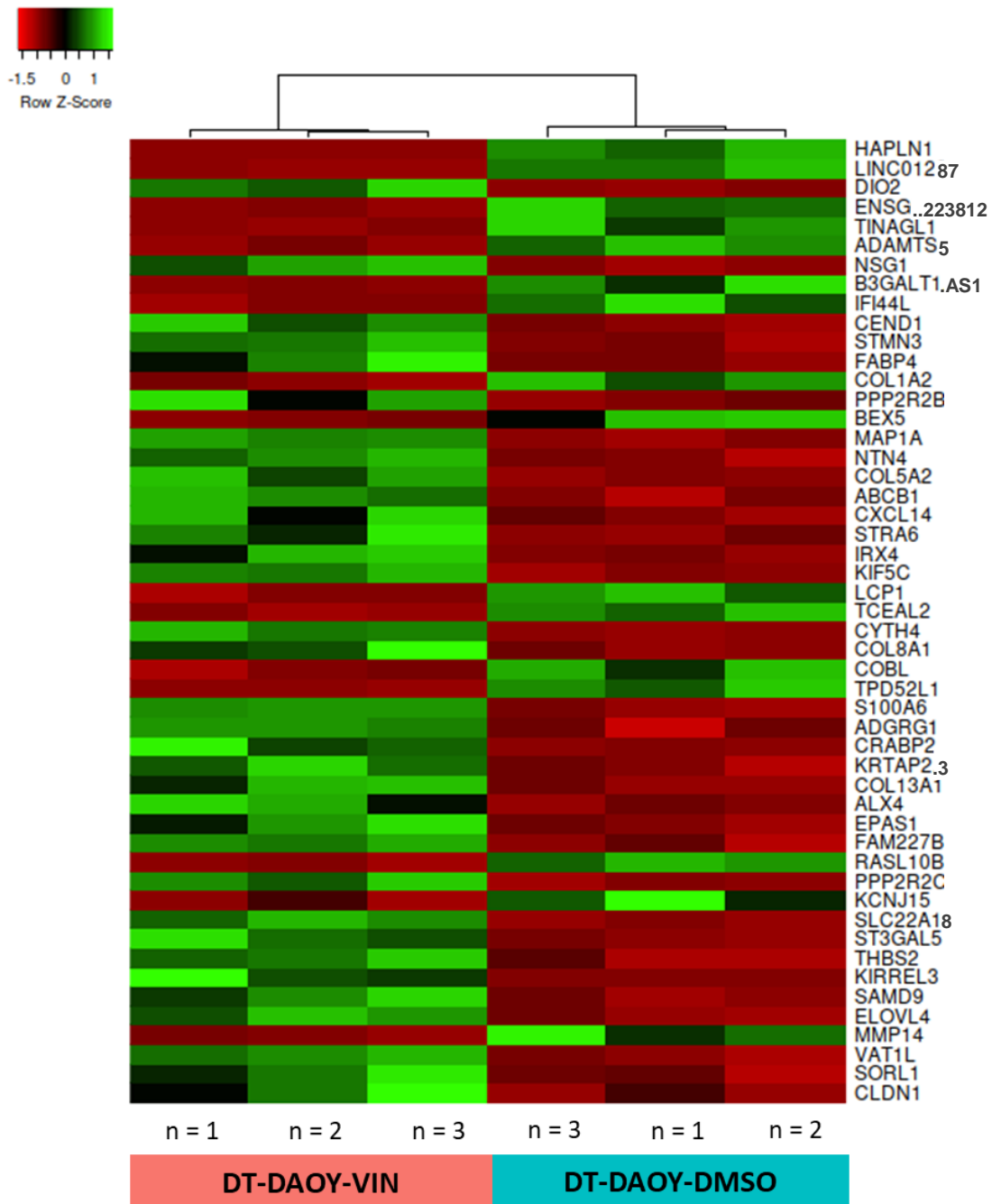


Figure 6.9 Unsupervised clustering of DT-DAOY-VIN and DT-DAOY-DMSO cell lines. Unsupervised transformed gene counts were used to create a heatmap representing the top 50 genes with the largest variance across all DAOY drug-tolerant and vehicle-treated samples. The colour scale signifies the relative expression level of a gene across all samples. Expression levels above the mean are shown as green and below the mean are red. Differences in gene expression between drug-tolerant and vehicle-treated cell lines were clear, with triplicates from each sample set clustering together.

6.3.4 Analysis of significantly differentially expressed genes arising from the development of drug-tolerance

Statistical analysis of differentially expressed genes was undertaken using DT-vehicle comparisons for each cell line. For all comparisons, significantly differentially expressed genes (DEGs) were filtered based upon the following criteria:

- 1) Fold Change Threshold – $\text{Log}_2 \geq 0.5$ or ≤ -0.5 .
- 2) Adjusted P-value (Benjamini-Hochberg; BH) – ≤ 0.05
- 3) Mean Expression – ≥ 2 normalised counts

Filtering in this way generated a list of significantly differentially up- and down-regulated genes for each cell line. The level of differential gene expression upon the acquisition of drug tolerance appeared to correlate approximately with the level of resistance possessed by each drug-tolerant cell line (Table 6-1). The greatest number of DEGs was detected in the DT-D458-CIS/DT-D458-DMF comparison, which exhibited an 18.5-fold increase in cisplatin resistance compared to its vehicle-treated control line, whereas the lowest number of DEGs was detected in the DT-HDMB-03-CIS/DT-HDMB-03-DMF comparison, which exhibited a 1.6-fold increase in cisplatin resistance compared to its vehicle-treated control line.

Table 6-1 Differential gene expression profiles of drug-tolerant cell lines

Comparison	Fold-Resistance of DT cell line	Significantly up-regulated genes	Significantly down-regulated genes	Total Significantly DEGs
DT-D283-CIS v. DT-D283-DMF	2.5	694	600	1294
DT-D458-CIS v. DT-D458-DMF	18.5	1238	910	2148
DT-HDMB-03-CIS v. DT-HDMB-03-DMF	1.6	515	395	910
DT-DAOY-VIN v. DT-DAOY-DMSO	4	606	662	1268

6.3.4.1 Drug tolerant cell lines of different subgroups and treatment states share common up-regulated genes

Interestingly, assessment of shared DEGs identified almost 60 genes that were commonly up-regulated in at least three of the four drug-tolerant cell lines compared to their vehicle-treated control. Furthermore, a seven gene “signature” of significantly up-regulated genes was present across all four drug-tolerant cell lines (DT-D283-CIS, DT-D458-CIS, DT-HDMB-03 and DT-DAOY-VIN), despite these lines arising from different subgroups and chemotherapeutic treatments (Figure 6.10). The signature 7 genes were: *Latent Transforming Growth Factor Beta Binding Protein 1 (LTBP1)*, *Microtubule Associated Protein 1A (MAP1A)*, *Muscleblind Like Splicing Regulator 2 (MBNL2)*, *Galectin 1 (LGALS1)*, *Proline Rich Nuclear Receptor Coactivator 1 (PNRC1)*, *DAB Adaptor Protein 2 (DAB2)* and *Phospholipase A And Acyltransferase 3 (PLAAT3)*. Only one of these genes, *LGALS1*, had previously been researched in the context of medulloblastoma, where it was shown to be expressed highly in SHH subgroup patients (Susanto et al., 2020). As displayed in Table 6-2, a literature search

revealed that all other identified shared up-regulated genes have been associated with tumourigenesis and in some cases drug resistance, in other solid tumours.

In addition to the 7 genes common to all drug-tolerant cell lines (Table 6-2), a further 27 genes were shared between the three cisplatin-tolerant vs. vehicle-control Group 3 cell line comparisons, listed in Figure 6.10. Of particular note, *Collagen Type I Alpha 1 Chain (COL1A1)*; (Jia & Wang, 2020), *Lysine Demethylase 5B (KDM5B)*; (Xu et al., 2018), *LIM Domain Containing Preferred Translocation Partner In Lipoma (LPP)*; (Chen et al., 2021), *Potassium Voltage-Gated Channel Subfamily H Member 2 (KCNH2)*; (Pillozzi et al., 2018) and *Actin Alpha 2 (ACTA2)*; (M. Li et al., 2018) have all been reported to be either associated with cisplatin resistance or up-regulated in cisplatin-resistant cell lines in previous studies performed in other cancer types.

It is feasible that these common up-regulated genes may, either together as a drug-tolerant gene signature or separately, represent markers of drug tolerance in medulloblastoma. Especially intriguing are the 7 genes shared between cisplatin- and vincristine-treated lines, which may be associated with global mechanisms of drug tolerance, common to multiple treatment types. Further studies to explore whether these genes represent direct mediators of drug resistance or simply markers of a drug tolerant state would be highly beneficial. RNAi methodology or treatment with drugs known to target each shared up-regulated gene/gene product (Table 6-2) would allow exploration of how target inhibition affects cell metabolic activity and cell sensitivity to cisplatin/vincristine.

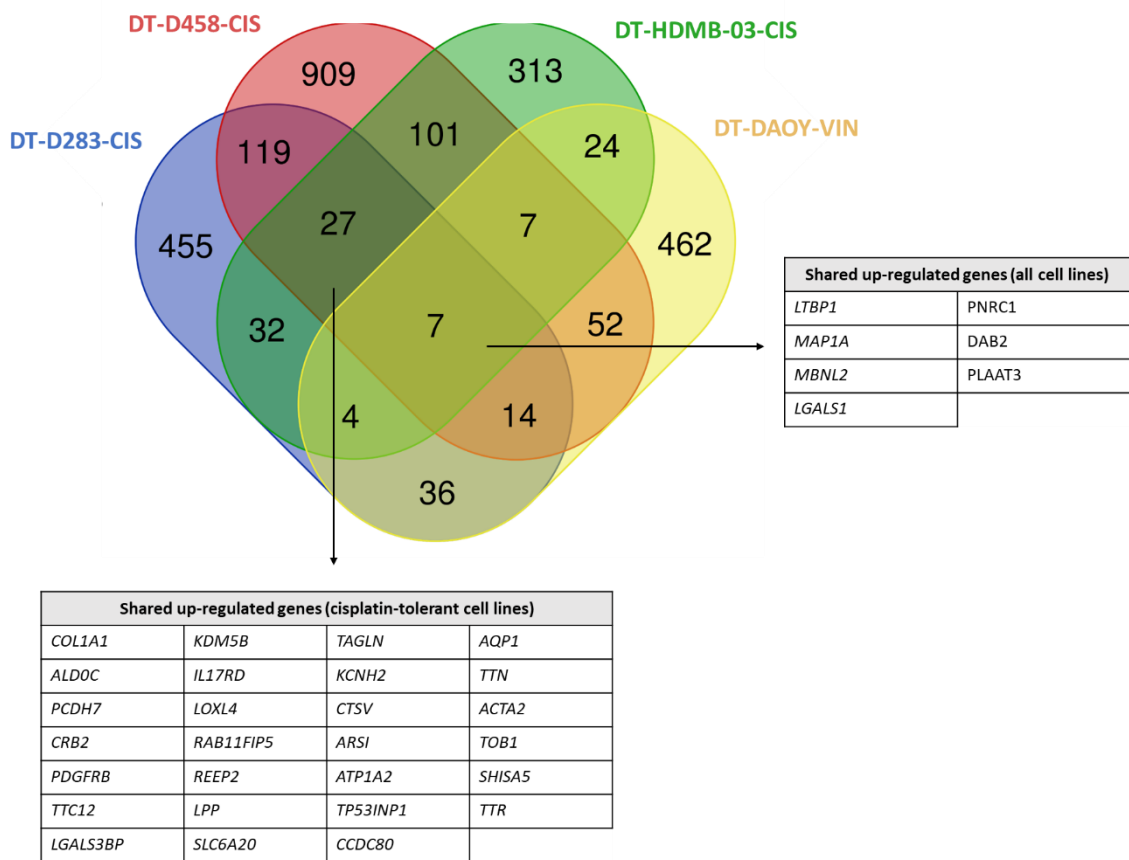


Figure 6.10 Significantly up-regulated genes detected in drug-tolerant cell lines compared to vehicle-treated control cell lines. Significantly up-regulated genes were those found to be up-regulated in DT cell lines compared to vehicle-treated control lines, with a Log2 fold change of $\geq +0.5$, a BH-adjusted P-value of ≤ 0.05 and expression of ≥ 2 normalised counts. 7 genes were identified as commonly up-regulated between all four DT cell lines.

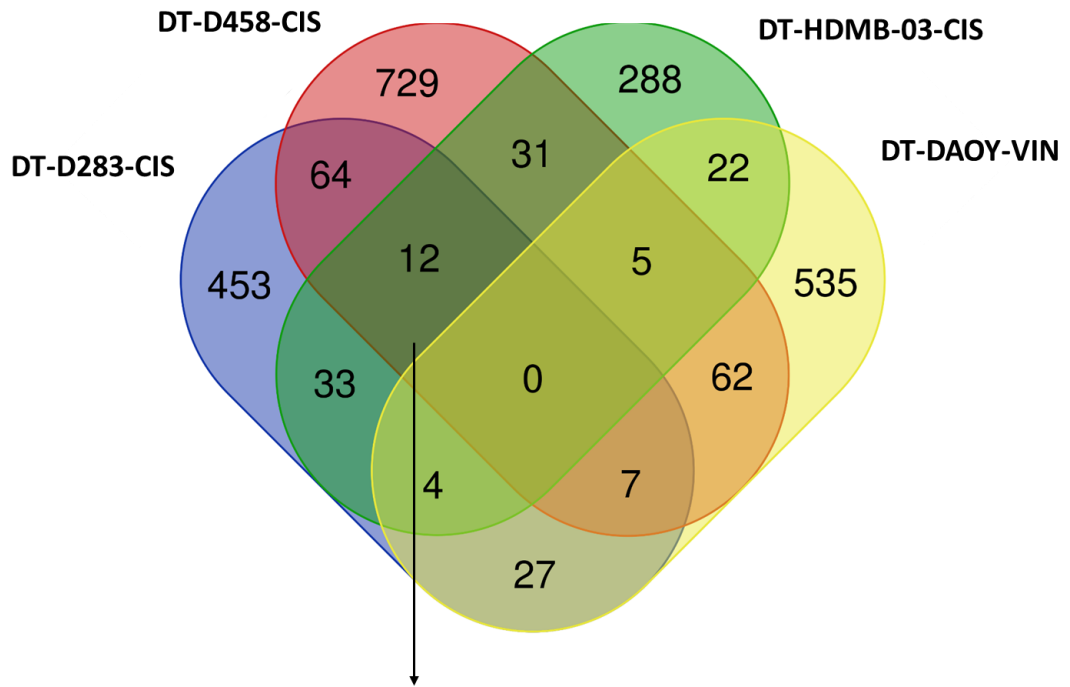
Table 6-2 Association between shared up-regulated genes and recorded roles in tumour progression and drug resistance

Gene	Function	Link to cancer?	Link to drug resistance?	Inhibitors	Key references
LTBP1	Encodes an extracellular multi-domain protein crucial for the correct folding, secretion, extracellular matrix deposition, and activation of TGF- β .	Yes. LTBP1 is associated with tumour progression, metastasis and cancer cell proliferation in squamous cell carcinoma and lymphoma via TGF- β signalling. Linked to malignancy grade and poor prognosis in glioma, likely associated with TGF- β activation status.	N/A	None recorded	Lin et al., 2021 Cai et al., 2020 Tritschler et al., 2009
MAP1A	Encodes a precursor polypeptide which undergoes proteolytic processing to produce microtubule associated protein 1A heavy chain and LC2 light chain.	Yes. MAP1A expression is associated with poor overall survival in lung cancer and has been identified as an autophagy-related gene in bladder cancer where high expression correlates with poor survival.	Partial. No direct link, however MAP1LC3B (encodes part of MAP1A quaternary structure), is associated with increased autophagy in response to cisplatin treatment which facilitates cisplatin resistance in lung cancer.	Estramustine	Wu et al., 2015 Yan et al., 2021 Luo et al., 2021
MBNL2	Encodes a multi-functional RNA-binding protein with key roles in neuronal differentiation and the differentiation of embryonic stem cells.	Yes. MBNL2 is up-regulated in metastatic renal cell carcinoma, where silencing promotes inhibition of proliferation and activation of apoptosis. Induced by hypoxia in lung/breast cancer cell lines where it regulates transcript abundance of hypoxia response genes and gene deletion reduces cell proliferation/migration.	N/A	None recorded	Perron et al., 2018 Fischer et al., 2020
LGALS1	Encodes a β -galactoside binding protein implicated in a wide range of cellular processes including cell adhesion, proliferation, apoptosis, mRNA splicing and immune response.	Yes. LGALS1 expression associated with poor overall and progression free survival in ovarian cancer via NF- κ B pathway activation. Over-expression linked to increased proliferation, migration and fibrosis by TGF- β 1/Smad pathway modulation in pancreatic cancer. Expression up-regulated in medulloblastoma patients where LGALS1 appears to be a target of SHH signalling.	Yes. Links to chemotherapy and radiotherapy resistance. In neuroblastoma, LGALS1 knockdown associated with increased sensitivity to cisplatin through the inhibition of cisplatin-induced autophagy.	Thiodigalactoside 1,4-Dithiothreitol Mercaptoethanol Artenimol	Gao et al., 2019 Chen et al., 2017 Tang et al., 2018 Susanto et al., 2020
PNRC1	Encodes a co-activator for several nuclear receptors including AR, ER α , ERR α , ERR γ , GR, SF1, PR, TR, RAR and RXR.	Yes. Suggested TSG. PNRC1 expression is often decreased in cancer patient samples compared to normal tissue. Low expression correlates with decreased proliferation, likely through negative regulation of RAS/MAPK pathway.	N/A	None recorded	Zhou et al., 2004 Gaviraghi et al., 2018
DAB2	Encodes a diathrin and cargo binding endocytic adaptor protein implicated in signalling pathways involved in cellular differentiation, proliferation and migration.	Yes. Tumour suppressive and pro-tumorigenic functions. Expression frequently lost in breast cancer. In cervical cancer, DAB2 expression is down-regulated by miR-106b which correlates with decreased EMT. Conversely, DAB2 is expressed in some cancer cell lines where it is associated with TGF- β -mediated VEGF expression and endothelial cell migration.	N/A	None recorded	Bagadi et al., 2007 Piao et al., 2017 Cheong et al., 2012
PLAAT3	Encodes a phospholipase that metabolizes phospholipids. Removes a fatty acyl chain from phosphatidic acid to generate lysophosphatidic acid (LPA) and free fatty acid (FFA).	Yes. Phospholipase activity associated with tumorigenesis through generation of LPA. PLAAT3 is overexpressed in osteosarcoma where it promotes poor prognosis and MAPK pathway activation. Expression required for proliferation and anchorage independent growth of lung cancer cells via Ras-GTPase activation. Associated with poor prognosis, proliferation and aerobic glycolysis in pancreatic cancer.	Yes. Overexpression of PLAAT3 in osteosarcoma cell lines causes decreased sensitivity to cisplatin, doxorubicin and etoposide.	None recorded	Li et al., 2016 Liang et al., 2015 Nazarenko et al., 2006 Xia et al., 2020

FDA approved inhibitors are shown in blue.

6.3.4.2 Down-regulated genes are common to cisplatin-tolerant Group 3 cell lines

Unlike that observed in the assessment of shared up-regulated genes, no common down-regulated genes were found following comparison of DT-D283-CIS/-DMF, DT-D458-CIS/-DMF, DT-HDMB-03/-DMF and DT-DAOY-VIN/-DMSO cell lines (Figure 6.11). However, 12 genes were found to be significantly shared between the three cisplatin-tolerant cell lines, perhaps indicative of shared mechanisms of cisplatin resistance. Interestingly, 8 of the 12 shared down-regulated genes have been linked with cisplatin resistance in previous studies in non-CNS tumour types. However, in contrast to the findings presented here, *Nucleolin (NCL)*; (Ke et al., 2021), *PCNA Clamp Associated Factor (PCLAF)*; (Cheng et al., 2013), *Pre-mRNA Processing Factor 19 (PRPF19)*; (He et al., 2021), *P53 And DNA Damage Regulated 1 (PDRG1)*; (Z. Tao et al., 2019), *Prothymosin Alpha (PTMA)*; (Lin et al., 2016), *High Mobility Group Nucleosome Binding Domain 5 (HMG5)*; (X. Liu et al., 2017) and *Flap Structure-Specific Endonuclease 1 (FEN1)*; (Mesquita et al., 2021) are often over-expressed in other cancer cell lines, with gene depletion frequently associated with enhanced sensitivity to cisplatin. All of the aforementioned studies were conducted following gene over-expression/knockdown and thus differ to the experimental set-up in the present investigation where chronic cisplatin-tolerant cell lines utilised. Further, many cancer-related genes frequently display altered roles in different cancer types. Indeed, one of the 12 shared down-regulated genes *High Mobility Group Box 2 (HMGB2)* has been associated with both promoting and inhibiting cellular resistance to cisplatin in head and neck cancer and lung cancer, respectively (Arioka et al., 1999; Syed et al., 2015). Validation of gene expression by qRT-PCR will be important to confirm these results.



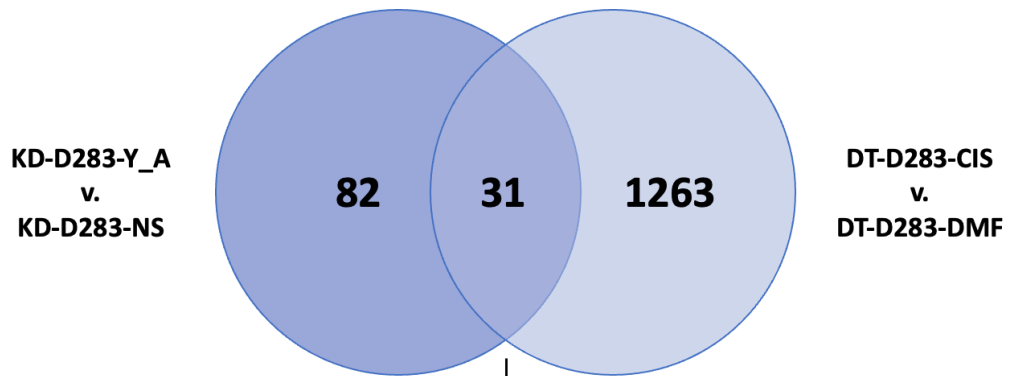
Shared down-regulated genes (cisplatin-tolerant cell lines)			
<i>PCLAF</i>	<i>MAGOH</i>	<i>PDRG1</i>	<i>PTMA</i>
<i>PTPRF</i>	<i>UPF3B</i>	<i>PRPF38B</i>	<i>HMG5</i>
<i>NCL</i>	<i>PRPF19</i>	<i>HMGB2</i>	<i>FEN1</i>

Figure 6.11 Significantly down-regulated genes detected in drug-tolerant cell lines compared to vehicle-treated control cell lines. Significantly down-regulated genes were those found to be down-regulated in DT cell lines compared to vehicle-treated control lines, with a Log2 fold change of ≥ -0.5 , a BH-adjusted P-value of ≤ 0.05 and expression of ≥ 2 normalised counts. 12 genes were identified as commonly down-regulated between cisplatin-tolerant Group 3 medulloblastoma cell lines, while no common down-regulated genes were identified between all four DT cell lines.

6.3.4.3 Differentially expressed genes are shared between drug-tolerant cell lines and *YBX1* knockdown cell lines

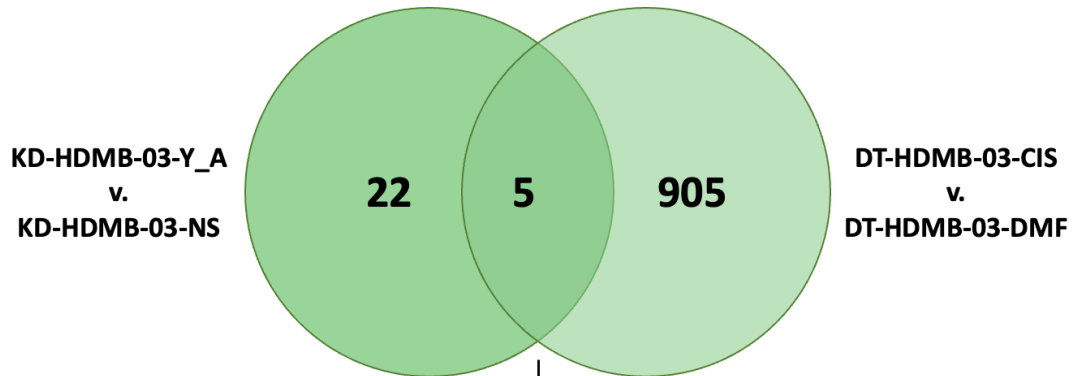
We also looked to integrate DEGs identified in the whole transcriptome sequencing of *YBX1* knockdown HDMB-03 and D283 cell lines (KD-D283-Y_A/-N.S. and KD-HDMB-03-Y-A/-N.S.) presented in Section 5.4 with DEGs identified in cisplatin-tolerant HDMB-03 and D283 cell lines (DT-D283-CIS/-DMF and DT-HDMB-03/-DMF) in the current sequencing study. Importantly, a number of genes were shared between *YBX1* knockdown cell lines and cisplatin-tolerant cell lines: 31 genes in the D283 comparison and 5 genes in the HDMB-03 comparison (Figure 6.12). This correlated with the number of DEGs observed within each cell line, with the D283 line presenting with a higher number of up- and down-regulated genes in both knockdown and drug-tolerant sequencing studies. This finding was unexpected - in Section 5.3, YB-1 knockdown was found to have little effect on the sensitivity of D283 and HDMB-03 cell lines to cisplatin and in the current chapter, cisplatin-tolerant cell lines were shown to display either reduced, or unchanged *YBX1* expression (Section 6.2.5). This led us to hypothesise that YB-1 is not implicated in the direct acquisition of resistance to cisplatin, nor the maintenance of chronic cisplatin tolerance. The current finding suggests that YB-1 may indeed, either directly or indirectly, regulate the expression of numerous genes differentially expressed upon the acquisition of cisplatin tolerance in Group 3 medulloblastoma, potentially highlighting a function for existing cellular YB-1 in the maintenance of a chronic, cisplatin-tolerant state. In order to better understand this and identify target genes directly regulated by YB-1 in response to cisplatin treatment, CHIP sequencing of cisplatin-tolerant cell lines will be an important next step (Section 6.4).

A



Shared DEGs between whole transcriptome sequencing and 3'mRNA-Seq (D283 cell line)						
<i>UNC5B</i>	<i>CD55</i>	<i>OLFM1</i>	<i>EDIL3</i>	<i>CALCB</i>	<i>NAV1</i>	<i>VCAN</i>
<i>NFIA</i>	<i>AIPL1</i>	<i>TLCD4</i>	<i>UNCX</i>	<i>GSPT2</i>	<i>SHISA9</i>	<i>LOX</i>
<i>NR2F1</i>	<i>CLCN4</i>	<i>RFK</i>	<i>TTR</i>	<i>S1PR1</i>	<i>FEZF2</i>	<i>MYL9</i>
<i>GPNMB</i>	<i>SPX</i>	<i>FLT1</i>	<i>NUDT11</i>	<i>PHACTR2</i>	<i>PEG3</i>	<i>FAM111B</i>
<i>INSIG1</i>	<i>APP</i>	<i>RPRML</i>				

B



Shared DEGs between whole transcriptome sequencing and 3'mRNA-Seq (HDMB-03 cell line)		
<i>UTRN</i>	<i>GPX3</i>	<i>COLEC12</i>
<i>TTN</i>	<i>RBP7</i>	

Figure 6.12 Significantly DEGs are shared between cisplatin-tolerant and *YBX1* knockdown Group 3 medulloblastoma cell lines. Numerous up- and down-regulated genes were found to be common between *YBX1* knockdown and cisplatin-tolerant D283 and HDMB-03 cell lines. A) 31 DEGs were identified as common between the KD-D283-Y_A/-N.S. comparison and the DT-D283-CIS/-DMF comparison. B) 5 DEGs were identified as common between the KD-HDMB-03-Y_A/-N.S. comparison and the DT-HDMB-03-CIS/-DMF comparison.

6.3.5 Gene ontology analysis of gene expression profiles in drug-tolerant cell lines

We next wanted to better understand the functional significance of the DEGs identified from each DT-vehicle cell line comparison, and what affect the altered gene expression had on biological processes in the cell. To investigate this, gene ontology (GO) enrichment analysis of differentially expressed genes was undertaken using the R statistical environment package (Young et al., 2010). A consistent number of significantly ($P \leq 0.05$) enriched GO terms was observed within each comparison, with 324 significantly enriched in the DT-D283-CIS/-DMF dataset, 342 in the DT-D458-CIS/-DMF dataset, 346 in the DT-HDMB-03-CIS/-DMF dataset and 361 in the DT-DAOY-VIN/-DMSO dataset.

The top ten significantly altered GO terms from each DT-vehicle cell line comparison are displayed in Figure 6.13. For ease, individual GO terms have been grouped into wider colour-coded categories based upon parental processes as defined by The Gene Ontology knowledgebase (geneontology.org). Interestingly, different cell lines displayed a predominance for different biological processes, even if the treatment type was the same. For example, the DT-D283-CIS cell line exhibited mainly altered RNA processing and translation processes while the DT-D458-CIS cell line exhibited a predominance for altered mitochondrial and oxidative phosphorylation processes, and the DT-HDMB-03-CIS cell line a predominance for migration processes. Despite arising from a different subgroup and chronic treatment type, the DT-DAOY-VIN cell line displayed a similar GO term signature to that of the DT-D283-CIS cell line, with RNA processing and translation processes frequently altered.

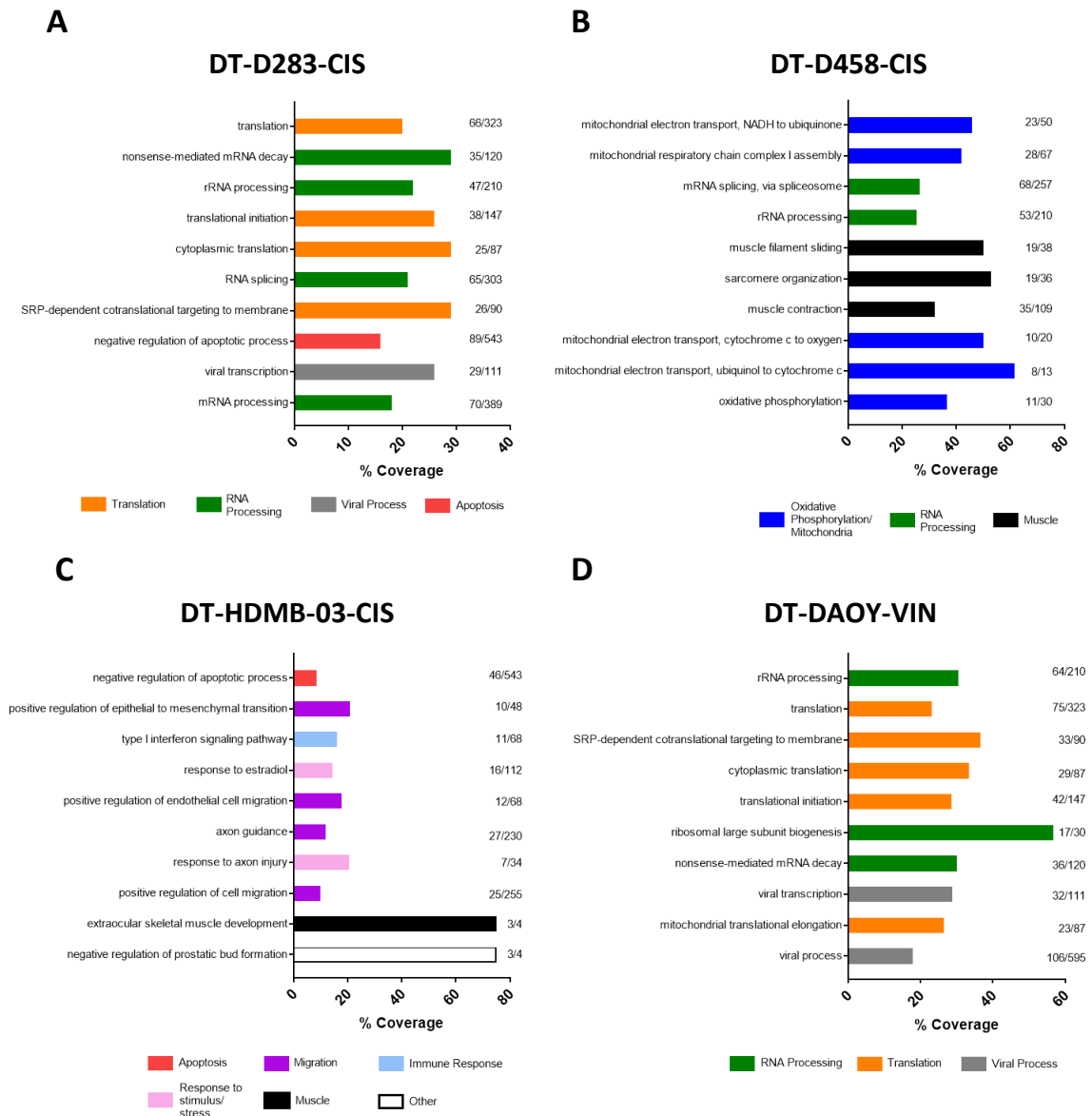
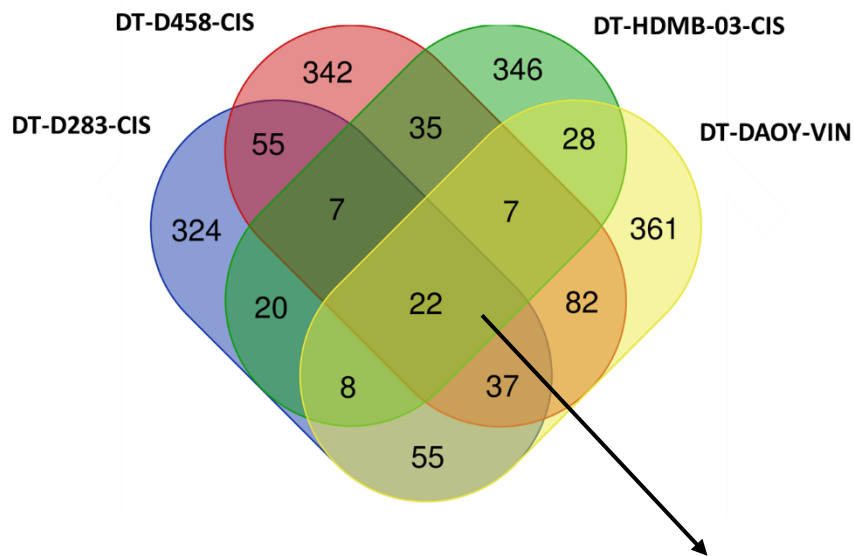


Figure 6.13 Different cell lines exhibit different altered biological processes upon the acquisition of drug-tolerance. GO enrichment analysis was undertaken on each drug-tolerant-vehicle control cell line comparison. % coverage defines the percentage of gene products identified in the current study functioning within a specific GO term. A) The DT-D283-CIS/-DMF cell line comparison showed a predominance of genes involved in translation and RNA processing. B) The DT-D458-CIS/-DMF cell line comparison indicated a predominance of genes involved in oxidative phosphorylation/mitochondrial processes. C) The DT-HDMB-03-CIS/-DMF cell line comparison showed a predominance of genes involved in cell migration. D) The DT-DAOY-VIN/-DMSO cell line comparison revealed a predominance of genes involved in translation and RNA processing.

To identify GO terms common to cellular resistance to cisplatin or to both cisplatin and vincristine, overlapping analysis of GO terms enriched across drug-tolerant cell lines was performed. Despite some differences in the pattern of top enriched GO terms in each drug-tolerant cell line (Figure 6.13), comparison of all significantly altered GO terms across lines revealed overlapping functions. 22 biological processes were found to be common between DT-D283-CIS, DT-D458-CIS, DT-HDMB-03 and DT-DAOY-VIN cell lines and a further seven were common between the Group 3 cisplatin-tolerant cell lines alone Figure 6.14. As in Figure 6.13, individual GO terms were grouped into parental processes, with six terms associated with “response to stimulus/stress”, five terms associated with “RNA processing”, four terms associated with “apoptosis” and two terms associated with “translation”. Other common terms were linked to “transcription”, “viral process” or could not be grouped and hence were termed “other”. Together, the overlapping biological processes described in Figure 6.14 may represent major processes involved in the acquisition and/or maintenance of a drug-tolerant cellular state, regardless of treatment parental cell line, molecular subgroup or treatment type.

Taken together, the 3' mRNA-Seq analysis of stable, drug-tolerant cell lines described here provides new insights into the genes and cellular functions altered upon the acquisition of drug tolerance in medulloblastoma cells. Surprisingly, a number of genes and biological processes were found to be shared, not only between cell lines of the same subgroup and treatment type (DT-D283-CIS/-DMF, DT-D458-CIS/-DMF and DT-HDMB-03/-DMF) but also with a cell line where these parameters differ (DT-DAOY-VIN/-DMSO), indicating that these genes and processes may represent major and global mediators of drug resistance in medulloblastoma.



GO Term	Parental Process
nonsense-mediated mRNA decay	RNA Processing
Ribosomal small subunit biogenesis	
rRNA processing	
RNA splicing	
Regulation of alternative mRNA splicing, via spliceosome	
Release of cytochrome c from mitochondria	Apoptosis
Positive regulation of apoptotic process	
Apoptotic process	
Negative regulation of apoptotic process	
Response to estradiol	Response to stimulus/stress
Response to copper ion	
Response to organic cyclic compound	
Response to hyperoxia	
Cellular response to organic cyclic compound	
Response to hormone	
Negative regulation of transcription, DNA-template	Transcription
Cytoplasmic translation	Translation
SRP-dependent co-translational targeting to membrane	
Cell cycle	Other
Negative regulation of amyloid fibril formation	
Positive regulation of erythrocyte aggregation	
Viral process	Viral process

Figure 6.14 Significantly enriched GO terms overlap between drug-tolerant medulloblastoma cell lines of different subgroups and treatment types. A Venn diagram of overlapping GO terms enriched in DT-D283-CIS/-DMF, DT-D458-CIS/-DMF, DT-HDMB-03-CIS/-DMF and DT-DAOY-VIN/-DMSO datasets. The 22 overlapping terms are listed and grouped by parental biological process.

6.4 Identification of YB-1 downstream targets upon acute and chronic drug exposure

Thus far, we have demonstrated that short-term treatment with cisplatin triggers increased levels of nuclear YB-1. We have also shown that YB-1 may contribute to cellular resistance to vincristine, likely through the regulation of *ABCB1* expression. Finally, we have observed that in cell lines tolerant to cisplatin and vincristine, YB-1 cellular and nuclear levels appear either stable or reduced compared to non-drug-tolerant cell lines, however shared DEGs exist between *YBX1* knockdown cell lines and cisplatin-tolerant cell lines, indicative of a role for YB-1 in the transcriptional regulation of drug-tolerance associated genes. Clearly, the functional role of YB-1 in short-term drug response and long-term drug tolerance is complex and context dependent. To fully understand how YB-1 modulates cellular drug response and resistance in medulloblastoma, YB-1 response to various treatment types/states must be investigated. Thus, in addition to investigating global mechanisms of drug tolerance in medulloblastoma cell lines using 3'UPX-sequencing, we also wanted to identify transcriptional targets regulated by YB-1 in response to cisplatin and vincristine under two treatment states, acute and chronic, by way of CHIP Sequencing (CHIP-Seq).

In the acute treatment state, D283 and HDMB-03 cell lines would be exposed to short-term treatment with cisplatin or vincristine. CHIP assays and concurrent sequencing of these samples would then allow us to identify targets regulated by YB-1 that are involved in the acute cellular response to cisplatin and vincristine and see how these targets differ between two drugs with different mechanisms of action. In

the chronic treatment state, DT-D283-CIS and DT-HDMB-03-CIS cell lines would undergo ChIP sequencing, with the aim to identify direct YB-1 targets required for the maintenance of a cisplatin-tolerant state.

6.4.1 ChIP sample preparation

6.4.1.1 Obstacles to ChIP sequencing sample preparation

An overview of the ChIP assay process is depicted in Figure 2.4 and described in Section 2.9.1. ChIP sample preparation was initially undertaken using the “Magna A/G Immunoprecipitation kit” utilised in Section 4.2.2. Unfortunately, this kit was discontinued and replaced with the “Magna G ChIP kit” during sample preparation, which led to re-optimisation of ChIP assay parameters (Section 2.9.2). Agarose gels displaying optimised conditions using the “Magna G ChIP kit” can be found in Appendix D6. The optimised kit was found to produce ChIP samples of optimal fragment length for ChIP sequencing (100 – 300 bp), which were confirmed by high sensitivity DNA Tapestation analysis (Appendix D7).

Unfortunately, the remaining “Magna G ChIP” kits ordered were significantly delayed on account of quality control issues. This led to the purchase and testing of a third kit, the “Active Motif ChIP-IT High Sensitivity kit” (Section 2.9.2). Cell lysis, sonication and fixation parameters were again optimised using D283 and HDMB-03 cell lines until appropriate fragment size was achieved (Appendix D8). Fragments produced using the “Active Motif ChIP-IT High Sensitivity kit” were found to be larger than those produced with previous kits. This may partly be due to the requirement of a high-temperature, high-salt denaturation step prior to agarose gel electrophoresis, which resulted in chromatin samples running differently on a gel when compared to

chromatin prepared using traditional CHIP methods. Accordingly, a fragment distribution of 200 – 1000 bp on an agarose gel is recommended by Active Motif as representative of adequate chromatin shearing. As test samples yielded fragments lying predominantly between 200 and 600 bp (Appendix D8), sample preparation utilising this kit was commenced.

6.4.1.2 CHIP sample preparation using the Active Motif ChIP-IT High Sensitivity Kit

For acute sample generation, D283 and HDMB-03 cells were treated with cisplatin or vincristine (or an equivalent DMF or DMSO vehicle respectively) for 1 hour at IC_{50} (Section 4.3.1), following which samples were fixed in PFA to cross-link proteins to DNA (Section 2.9.2). For chronic samples, DT-D283-CIS and DT-HDMB-03-CIS cell lines were cultured in drug-free media for 5 days prior to sample collection, after which samples were treated with cisplatin at IC_{50} for 1 hour, fixed and stored. DT-D283-DMF and DT-HDMB-03-DMF lines were also sampled for comparison and treated with the appropriate vehicle as previously described. Two biological replicates were collected for each cell line/treatment state.

To ensure chromatin fragment size remained consistent between samples, and remained in the required size range for CHIP Sequencing, every sample was run on an agarose gel prior to sample submission (Appendix D9). Any samples in which average fragment size appeared > 200 – 600 bp, with smearing > 1000 bp were re-synthesised. Following CHIP assay completion, two biological replicates (YB-1 Immunoprecipitations (IPs)) and one control (input), were submitted per cell line/treatment state, totalling 36 samples (24 IPs, 12 inputs).

6.4.1.3 ChIP Library Preparation and Sequencing

Library preparation was undertaken by Dr Nadine Holmes at the University of Nottingham's DEEP-SEQ sequencing facility using the NEBNext Ultra II DNA library Prep Kit for Illumina as described in Section 2.10.3.2. Sample concentrations were first measured using a Qubit Fluorometer, the results of which can be found in Appendix D10. Input sample concentrations ranged from 6.3 to 27.4 ng/ μ L and ChIP (IP) sample concentrations ranged from below the limit of detection up to 20.4 ng/ μ L. For samples with adequate concentrations, 25 ng of DNA was used for library preparation, while for samples with lower concentrations a total volume of 12.5 μ L of DNA was used.

On account of fragment size appearing larger than optimal using the "Active Motif ChIP-IT High Sensitivity kit", we first wanted to assess library fragment size distribution across a set of test libraries prior to full-scale library preparation. As displayed in Figure 6.15, test libraries had an average fragment size of 460 – 630 bp (including a ligated NEBNext adaptor of 120 bp). Although this is slightly longer than optimal for ChIP sequencing (100 – 300 bp), it fell between 200 – 1500 bp which is the suitable size range for sequencing and thus full-scale library preparation was continued.

Due to differences in the input concentrations of the ChIP samples, no size selection was included in library preparation protocol clean-up steps. To minimise the amount of PCR duplicates in the final sequencing data, different numbers of PCR cycles were employed for PCR-enrichment of the adaptor-ligated libraries, depending on ChIP/input sample concentration. Accordingly, samples with 25 ng of starting

material had 4 cycles of amplification, while samples with lower yields had 9 cycles of amplification.

Libraries were quantified using a Qubit Fluorometer and library fragment-size distributions assessed using an Agilent Bioanalyzer. As displayed in Appendix D11, mean library fragment-length distributions varied between ~440-660 bp. A number of libraries exhibited fragment distributions over 1000 bp (see Figure 6.15 – Bioanalyzer traces rightward of red line). As shorter fragments sequence more efficiently than larger fragments (illumina, 2020), Bioanalyzer region analysis (200-1000 bp) concentrations were used to normalize and pool libraries in an attempt to correct for this. Libraries were pooled in ratios required to generate two times greater coverage of input libraries than ChIP libraries and the final library pool quantified using the KAPA Library Quantification Kit for Illumina Platforms.

The library pool was sent to Source Biosciences (Cambridge, UK) for sequencing over one lane of a NovaSeq S4 flow cell on an Illumina NovaSeq 6000 System, to generate 20 million pairs of 150-bp paired-end sequencing reads per IP sample and 30 million pairs of 150-bp paired-end sequencing reads per input control sample.

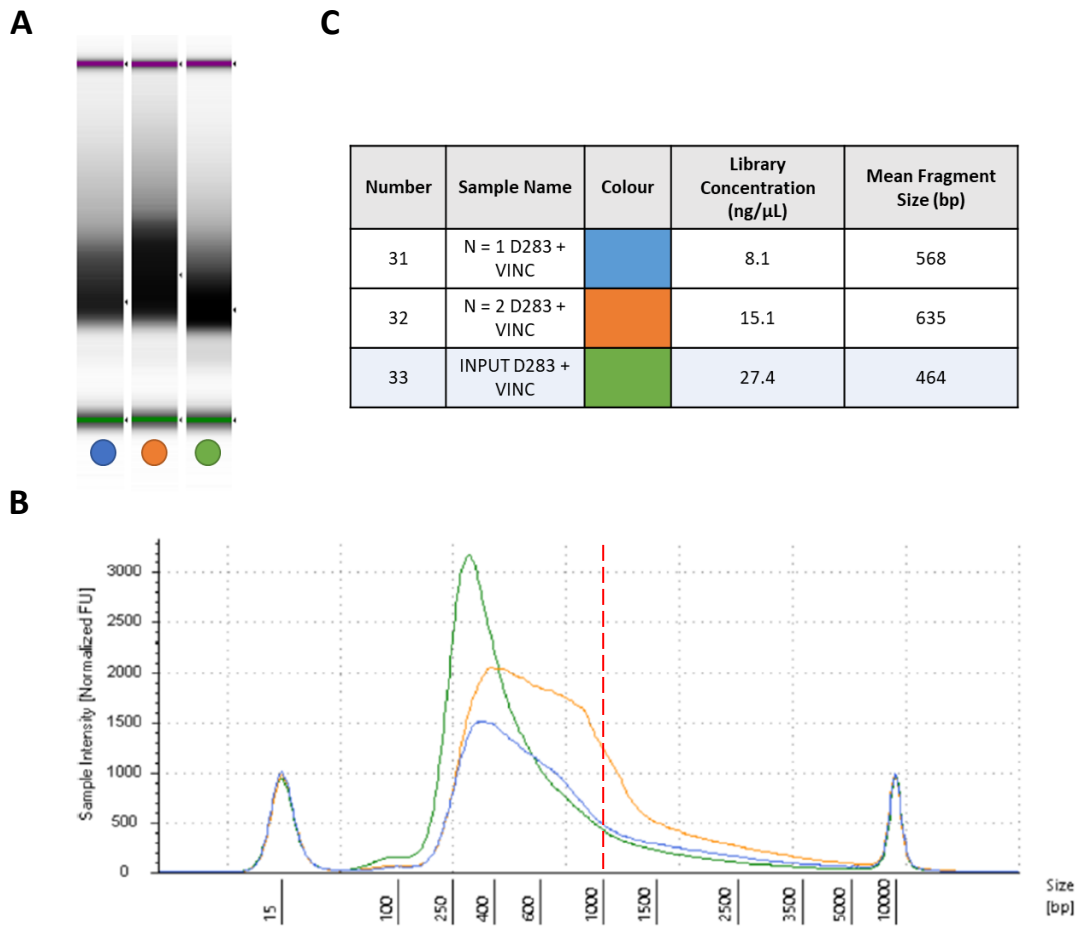


Figure 6.15 DNA fragment profiles of test libraries. In order to ensure prepared libraries would be of appropriate fragment-size distribution (bp) for sequencing, three small-scale test libraries were prepared using the NEB Next Ultra II DNA Library Preparation Kit. Resultant libraries were assessed using an Agilent TapeStation with the High Sensitivity D5000 assay. A) Gel image of test libraries. The lower marker (15 bp) is highlighted with a green line. The upper marker (10000 bp) is highlighted with a purple line. B) Electropherogram of test libraries. Small peaks depict upper and lower size markers. C) Table showing average fragment-size distribution of test libraries with the input sample row highlighted.

6.4.2 Mapping of ChIP-Seq Samples

ChIP-Seq bioinformatic analysis was undertaken by Dr Fei Sang at the University of Nottingham's DEEP-SEQ sequencing facility. Prior to mapping sequencing reads to the reference genome, read quality was examined by *FastQC* – a quality control analysis tool for raw sequencing data. Raw reads were trimmed, filtering out reads aligned to adaptor sequences and reads with low quality scores, as determined by *skewer* adaptor trimming tool (Jiang et al., 2014). Trimmed reads were next mapped onto the human genome (hg38, Ensembl Release 104) using mapping programme *hisat2*, following which duplicated reads were marked and filtered out using *picard-tools* data handling software (Kim et al., 2019; www.broadinstitute.github.io/picard).

As displayed in Table 6-3, all IP samples were found to align well to the human genome, with 70-80% of reads mapping uniquely. Following the removal of duplicate reads, which frequently arise from PCR amplification of a single fragment and thus represent experimental artefacts, read alignment was still very good in most samples, with 60-70% reads mapping. For one IP sample (Sample 28), the number of mapped reads post-duplicate removal was found to be very low. Analysing duplicate reads of all samples in more detail (Appendix D12) revealed very high occurrence of duplicate reads in Sample 28, thus it was decided to exclude this sample for downstream analysis.

Unfortunately, upon initial read mapping, reads from input samples appeared to align poorly with the human genome, with only 40-50% of reads found to map uniquely across all input samples (data not shown). In general, > 70% of ChIP-Seq reads should map to the genome, with mapping of < 50% considered cause for

concern (Bailey et al., 2013). Typically, low read mapping is associated with excessive amplification in the PCR step, inadequate read length, or problems with the sequencing platform (Bailey et al., 2013). However, in the current study, input sample concentration pre-library preparation was very good, requiring a low number of PCR cycles during library preparation. Furthermore, input samples were sequenced alongside IP samples and passed quality control checks and thus sequencing-related problems seem unlikely. Accordingly, the reason for such sub-optimal read mapping is unclear.

In order to facilitate downstream analysis, it was decided to re-run read mapping of input samples, this time using less stringent mismatch criteria. Adjusting the stringency in this way improved read mapping significantly, increasing uniquely mapped reads to 70 – 85% and reads post-duplicate removal to 65-78%. However, it must be noted that reducing mapping stringency in this way may introduce error in downstream peak calling analyses, raising the importance of validating any identified hits with additional sequencing datasets and further ChIP assays.

6.4.2.1 Fingerprint plots highlight further anomalies within input control samples.

To further investigate input sample quality and to assess how well signals in the IP sample can be differentiated from the background distribution of reads in the input control sample, fingerprint plots were generated. deepTOOLS fingerprint plot tool randomly samples genome regions and sums the read coverage in indexed BAM files (converted from fastq files during read mapping) that overlap with those regions (Diaz et al., 2012). Values are then sorted and the cumulative sum of read counts is plotted. A perfect input control with uniform distribution of reads along the genome

will generate a straight, diagonal line on the plot, as displayed in the model fingerprint plot in Figure 6.16 A. Specific and strong IP sample enrichments will present with deep curves with a large difference between input and ChIP signal, whereas IP samples with lower/broader levels of enrichment will present with curves closer to that of the input signal. Replicate IP samples should follow similar traces to one another.

Analysis of samples from the present study frequently resulted in plots resembling that in Figure 6.16 B. The input line for all samples appeared down-shifted, highlighting the existence of unexpected enrichment in the input samples. Some regions of highly enriched signal are expected in input samples and are mostly just artefacts arising from genomic regions with a high propensity for sequencing. However, these sites are known and are typically filtered, as was done in the present study (<https://github.com/Boyle-Lab/Blacklist>). It is therefore currently unclear why the input samples appear more “peaky” than expected. Unfortunately, this anomaly may also affect downstream peak calling, as fewer genomic regions are likely to be detected as enriched in IP samples when the input control presents with non-uniform, high-level peaks across the genome. To assess if this would be the case, peak calling and annotation was undertaken with all samples, as described in Section 6.4.3.

Table 6-3 Mapping of ChIP-Seq data

Number	Sample Name	Trimmed Reads (pairs)	Mapped Reads	Uniquely Mapped Reads	Reads Post-Duplicate Removal
1	DT-HDMB-03-CIS N = 1	34758215	93.6%	76.2%	68.0%
2	DT-HDMB-03-CIS N = 2	23926817	93.0%	73.4%	67.3%
3	INPUT DT-HDMB-03-CIS	49827755	99.8%	80.1%	72.5%
4	DT-HDMB-03-DMF N = 1	32643467	93.6%	77.2%	67.3%
5	DT-HDMB-03-DMF N = 2	26478190	93.4%	73.8%	67.1%
6	INPUT DT-HDMB-03-DMF	38410446	99.8%	83.6%	77.0%
7	DT-D283-CIS N = 1	30489099	93.5%	71.0%	62.9%
8	DT-D283-CIS N = 2	22885510	94.3%	78.5%	72.2%
9	INPUT DT-D283-CIS	37087370	99.8%	69.9%	64.5%
10	DT-D283-DMF N = 1	21158110	94.5%	77.1%	71.4%
11	DT-D283-DMF N = 2	27511576	93.5%	71.8%	65.0%
12	INPUT DT-D283-DMF	37336128	99.8%	73.7%	68.6%
13	HDMB-03 + CIS N = 1	42741027	93.3%	74.7%	63.7%
14	HDMB-03 + CIS N = 2	35431045	93.8%	76.3%	64.6%
15	INPUT HDMB-03 CIS	32970113	99.7%	75.6%	70.0%
16	HDMB-03 + DMF N = 1	30387498	92.4%	69.0%	61.5%
17	HDMB-03 + DMF N = 2	17322656	93.1%	75.4%	70.3%
18	INPUT HDMB-03 DMF	35228095	99.9%	80.8%	74.5%
19	HDMB-03 + VIN N = 1	34200500	93.8%	78.2%	67.1%
20	HDMB-03 + VIN N = 2	23496383	94.4%	79.3%	73.0%
21	INPUT HDMB-03 VIN	44466761	99.8%	84.0%	78.2%
22	HDMB-03 + DMSO N = 1	33464987	92.5%	72.7%	62.5%
23	HDMB-03 + DMSO N = 2	28381538	92.6%	70.7%	65.6%
24	INPUT HDMB-03 DMSO	47119040	99.9%	72.7%	65.0%
25	D283 + CIS N = 1	31131560	93.5%	77.5%	68.8%
26	D283 + CIS N = 2	32990591	93.3%	73.9%	67.4%
27	INPUT D283 CIS	41135937	99.8%	80.7%	74.6%
28	D283 + DMF N = 1	30211926	89.7%	75.0%	27.7%
29	D283 + DMF N = 2	21809674	93.9%	73.7%	68.8%
30	INPUT D283 DMF	41138010	99.7%	83.5%	78.6%
31	D283 + VIN N = 1	34184594	94.5%	81.0%	73.8%
32	D283 + VIN N = 2	21217621	94.4%	76.7%	71.6%
33	INPUT D283 VIN	49023027	99.9%	78.9%	72.8%
34	D283 + DMSO N = 1	32475757	94.6%	77.2%	70.6%
35	D283 + DMSO N = 2	16166722	93.8%	77.3%	71.4%
36	INPUT D283 DMSO	44325899	99.8%	84.9%	78.0%

Mapping stringency was lowered in input samples (blue) to increase read mapping. Sample 28 (red) was found to have a high occurrence of duplicate reads and would be excluded from peak calling.

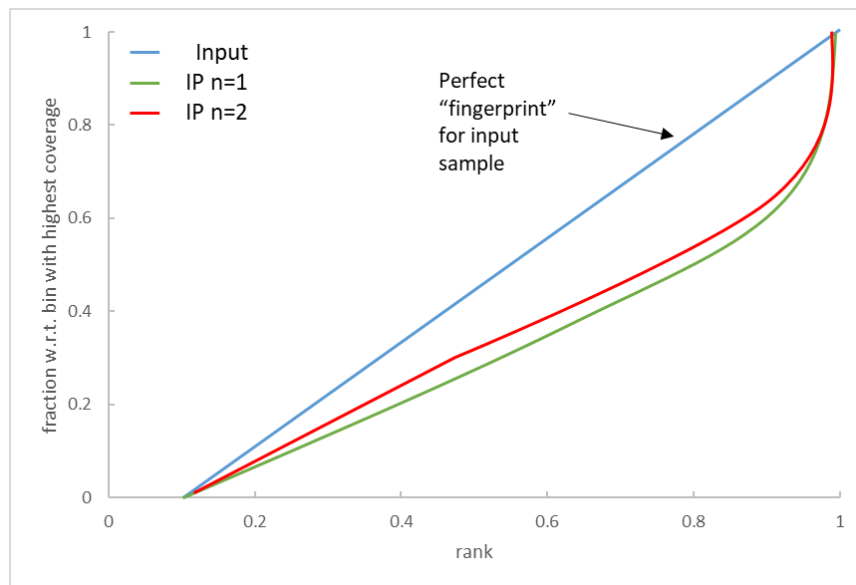
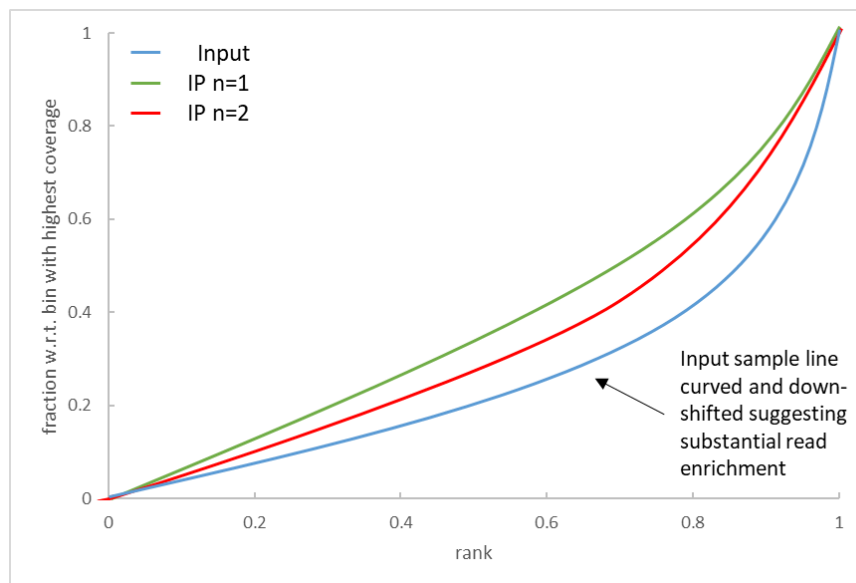
A**B**

Figure 6.16 Fingerprint plots revealed unexpected enrichment in input control samples. Fingerprint plots provide an additional quality control step when undertaking ChIP-Seq, facilitating assessment of IP sample enrichment compared to background enrichment in input controls. A) Example of “perfect” input sample fingerprint (blue line), demonstrating uniform and low-level distribution of reads across the genome. B) Representative plot of input and IP replicates from the present study, revealing a down-shifted and curved input sample fingerprint, representing more peaks than anticipated in input control. Replicate IP lines lie close to input line, indicative of less difference between input and ChIP signal.

6.4.3 Peak Calling

Peak calling represents the most pivotal stage of ChIP-Seq analysis and predicts regions of the genome bound by YB-1 by identifying sites with a significant number of mapped reads (peaks). Peaks were identified using *MACS2* peak calling software, as described extensively in Section 2.10.3.5. Put simply, the *MACS2* algorithm estimates IP-DNA fragment size and uses this estimate to identify significantly enriched regions in each IP sample relative to the genome background (the input control sample). As the input control sample should not exhibit substantial read enrichment, peaks that are identified in both the input control and IP samples likely represent false positives and should be discarded (Feng et al., 2012). The annotations of binding sites were then conducted by the *ChIPpeakAnno* package using the Ensembl R database (Zhu et al., 2010).

Following the identification and annotation of peaks in each sample, the number of common peaks between biological replicates was studied to assess the similarity of YB-1 binding patterns across replicate samples, using the Ensembl R database *findOverlapsOfPeaks* function. Only shared peaks would be taken forward to identify potential YB-1 binding sites. In undertaking this analysis, we first noticed the low number of peaks within individual biological replicates, resulting in a very low number of shared peaks between samples (Table 6-4). One would commonly expect to observe approximately 4,000 – 5,000 shared peaks in a human transcription factor IP sample (Dr Fei Sang; personal communication), however in the present study, shared peaks ranged from just 22 – 746. As suggested in Section 6.4.2.1 and displayed in Figure 6.16, the low number of peaks identified here likely arises from “peaky”

input samples with substantial levels of read enrichment, which may act to mask real YB-1 binding sites in IP samples.

Table 6-4 Number of individual and shared peaks within IP biological replicates

Number	Sample Name	Number of Peaks			Number of Shared Genes
		N = 1	N = 2	Shared	
1 - 2	DT-HDMB-03-CIS	1451	2330	477	77
4 - 5	DT-HDMB-03-DMF	1690	928	582	74
7 - 8	DT-D283-CIS	755	557	72	45
10 - 11	DT-D283-DMF	393	1109	78	40
13 - 14	HDMB-03 + CIS	1732	1587	746	91
16 - 17	HDMB-03 + DMF	1881	830	533	65
19 - 20	HDMB-03 + VIN	1731	862	632	55
22 - 23	HDMB-03 + DMSO	1882	1519	731	76
25 - 26	D283 + CIS	2847	4702	635	276
28 - 29	D283 + DMF	393	1109	22	15
31 - 32	D283 + VIN	2203	199	63	44
34 - 35	D283 + DMSO	1674	134	36	26

Sample 28 (red) is included for reference however would be excluded from downstream analysis on account of a high occurrence of duplicate reads (Table 6-3).

This finding raises concerns over the reliability of the present ChIP-Seq dataset. The problematic input control samples in this study, alongside the low stringency mapping employed to facilitate peak calling, is expected to lower the sensitivity of calling “true” peaks during the peak calling pipeline. Furthermore, low numbers of shared peaks makes downstream analysis, such as differential binding analysis and motif searching impossible. As such, it was decided that only ChIP samples with matching 3’RNA-Seq data (Section 6.3) would be taken forward for downstream analysis for the identification of YB-1 target genes implicated in drug resistance. The logic being that integration of both datasets will provide validation that any hits

identified as YB-1 targets in ChIP-Seq are true YB-1 transcriptional targets, which correlate with gene expression changes in 3'mRNA-Seq.

6.4.3.1 Peak annotation of drug-tolerant cell lines

As previously described, it was decided that integration of ChIP-Seq and 3'mRNA-Seq datasets would be vital in order to increase confidence and reliability of identified YB-1 targets. Unfortunately, as only drug-tolerant cell lines underwent 3'mRNA-Seq (Section 6.3), only ChIP-Seq samples 1 – 12 (DT-HDMB-03-CIS/DMF and DT-D283-CIS/DMF), would be further analysed at present.

Peak annotation allows the association of ChIP-Seq peaks with functionally relevant genomic regions such as promoters, transcription start sites (TSS) and intergenic regions. Such analyses can reveal to which genomic sites transcription factors preferentially bind, and if this binding pattern changes under certain conditions. Of YB-1 binding sites in DT-HDMB-03-CIS IP samples, 6% were present in the promoter region, with 3.6% of promoter sites within 500 bp of a TSS. The majority of binding sites were found in the gene body (50%) or distal intergenic regions (40%). Binding in exon regions accounted for 12.6% of sites, whereas binding in intron regions accounted for 43.8% (Figure 6.17 A). An almost identical pattern of YB-1 binding was detected in DT-HDMB-03-DMF samples (Figure 6.17 B). Although such a low frequency of promoter binding may seem unexpected for a transcription factor like YB-1, this binding distribution is in line with a recent large-scale transcription factor binding site study, which estimated that 70% of transcription factor binding sites lie in enhancer-containing intron and intergenic regions, whereas only 12% lie in promoters (Yu et al., 2021).

Comparatively, analyses of YB-1 binding in DT-D283-CIS and DT-D283-DMF IP samples reveals differences between treatment states. Whereas 5.2% of YB-1 binding in DT-D283-DMF IP samples were present in the promoter region, with 3.9% of promoter binding sites within 500 bp of a TSS, only 2.8% of YB-1 binding was detected in the promoter region of DT-D283-CIS IP samples, with 1.4% of sites within 500 bp of a TSS (Figure 6.17 C – D). It is tempting to speculate that such data is suggestive of an alteration in YB-1 transcriptional regulation following chronic cisplatin treatment. Indeed Yu et al. suggest transcription factor promoter binding is indicative of “core” transcription factor functionality, whereas intergenic region binding suggests interaction with distal enhancers. Unfortunately, due to previously described reliability issues within this study, it is difficult to draw definite conclusions from these datasets.

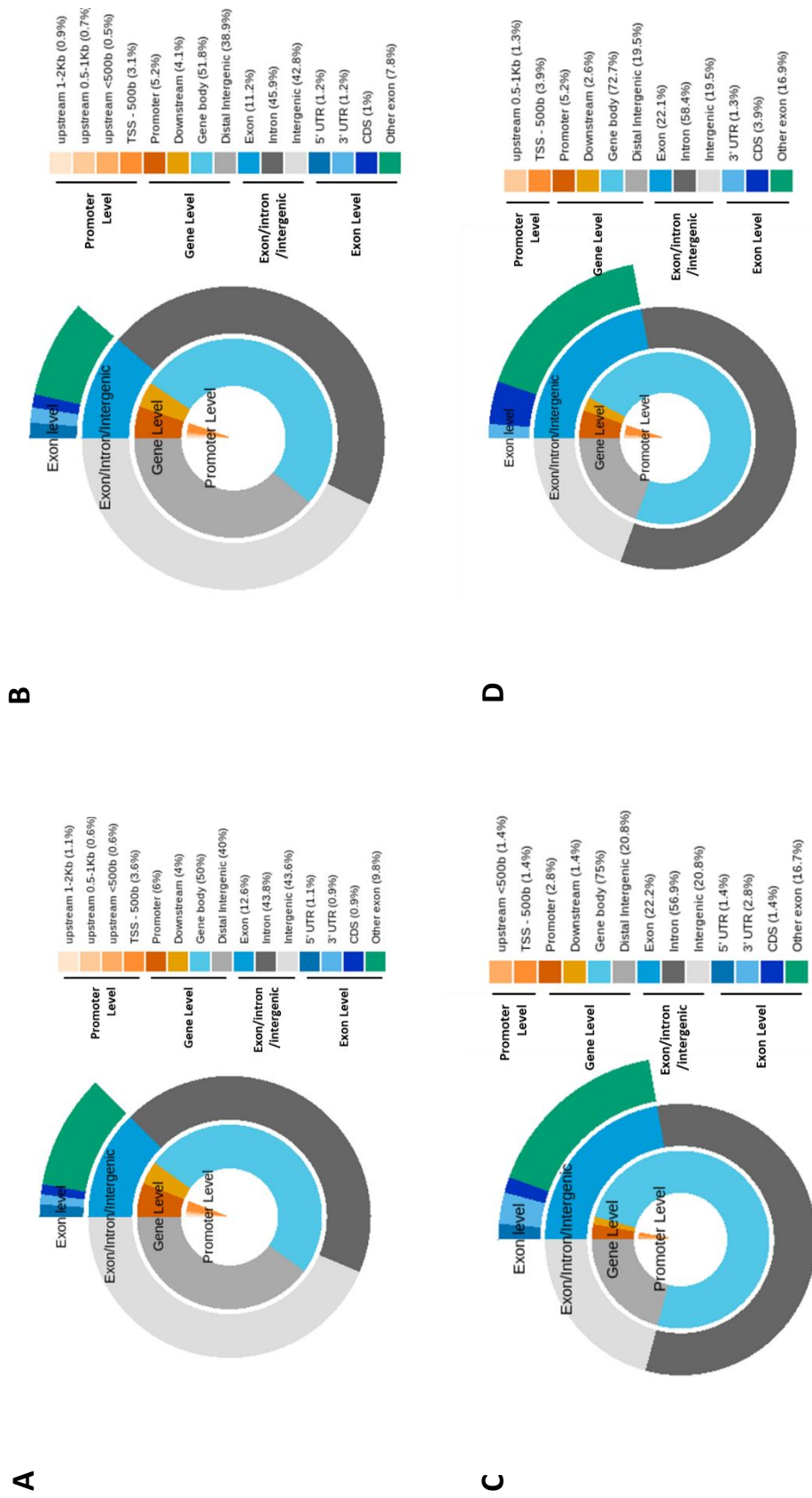


Figure 6.17 Peak annotation of YB-1 binding regions in drug-tolerant medulloblastoma cell lines. The distribution of YB-1 binding across different genomic regions at a promoter, gene, exon/intron/intergenic and exon level is shown. A) Analysis of YB-1 binding regions in DT-HDMB-03-CIS cell lines. B) Analysis of YB-1 binding regions in DT-HDMB-03-DMF cell lines. C) Analysis of YB-1 binding regions in DT-D283-CIS cell lines. D) Analysis of YB-1 binding regions in DT-D283-DMF cell lines.

6.4.4 Integration of ChIP-Seq and 3'mRNA-Seq datasets reveals potential YB-1 targets implicated in drug resistance in medulloblastoma cell lines

In order to increase confidence in YB-1 target genes identified following annotation of significant peaks, DT-HDMB-03-CIS and DT-D283-CIS IP samples were compared with DEGs detected upon 3'mRNA-Seq of drug-tolerant cell lines.

477 shared peaks were identified in DT-HDMB-03-CIS IP samples (Table 6-4), corresponding to 77 unique genes. Similarly, 582 shared peaks were identified in DT-HDMB-03-DMF IP samples (Table 6-4), corresponding to 74 unique genes. Comparatively, substantially fewer peaks were identified in DT-D283-CIS and DT-D283-DMF samples. 72 shared peaks were detected in DT-D283-CIS IPs, corresponding to 45 unique genes. Likewise, 78 shared peaks were detected in DT-D283-DMF IPs, corresponding to 40 unique genes. Interestingly a total of 20 and 32 possible YB-1 target genes were found to be unique to the drug-tolerant DT-HDMB-03-CIS and DT-D283-CIS lines, respectively, displayed in Appendix D13 and D14. Unfortunately, these unique genes did not overlap with identified genes in the comparable 3'mRNA-Seq datasets, suggesting either that these genes represent false positive hits or that although YB-1 binds with each gene, it does not have a direct, measurable transcriptional effect.

In a standard ChIP-Seq dataset, differential binding analysis can be performed between samples. Differential binding analysis allows comparison of the level of protein binding at a gene identified in sample and control datasets, for example to assess how the level of binding at a gene in a drug-tolerant cell line compares to that in a vehicle-control cell line. Unfortunately, due to the low number of shared peaks

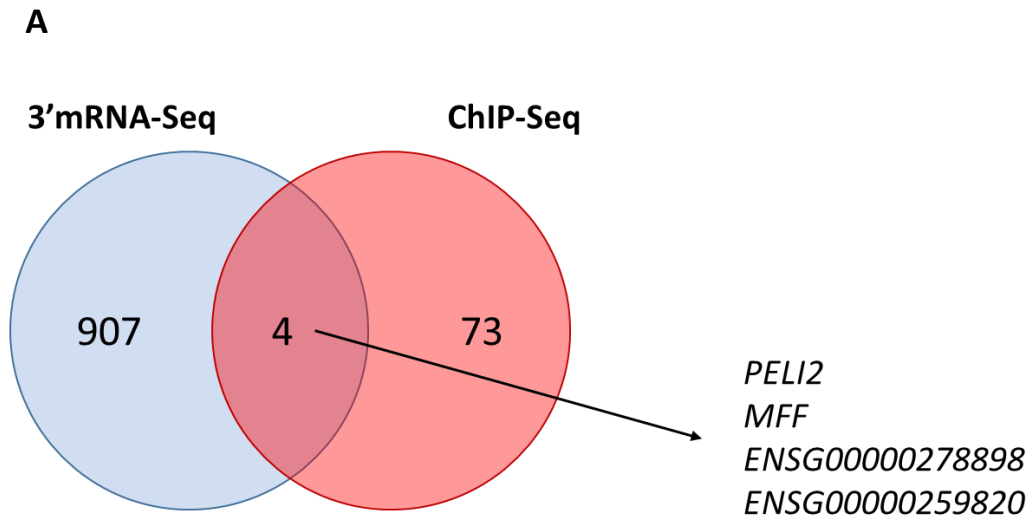
and thus low number of identified gene targets in the current dataset, differential binding analysis was not possible. As such, it was decided to compare all YB-1 targets identified in drug-tolerant cell line IP samples (DT-HDMB-03-CIS and DT-D283-CIS) with DEGs identified from 3'mRNA-Seq upon comparison of drug-tolerant and vehicle-treated control cell lines. Any genes which overlap between datasets are strong candidates for transcriptional regulation by YB-1.

Analysis of the DT-HDMB-03-CIS line in this way revealed four genes that were both identified as YB-1 binding targets in ChIP-Seq and were significantly differentially expressed in 3'mRNA-Seq. These genes were *Pellino E3 Ubiquitin Protein Ligase Family Member 2 (PELI2)*, *Mitochondrial Fission Factor (MFF)* and novel genes *ENSG00000278898* and *ENSG00000259820* (Figure 6.18). Although little is known about *ENSG00000278898* and *ENSG00000259820*, more studies have been conducted on *PELI2*, which encodes an E3 ubiquitin ligase and *MFF*, which encodes a protein involved in the regulation of mitochondrial size and shape. Importantly, both gene products have been associated with oncogenic cellular traits and thus may represent interesting targets to research further in the context of medulloblastoma cisplatin resistance (B. Y. Cheng et al., 2018; Ma et al., 2020; Seo et al., 2019).

Integration of 3'mRNA-Seq and ChIP-Seq datasets to identify possible targets of YB-1 in cisplatin-tolerant D283 cell lines revealed a single common hit – *Solute Carrier Family 26 Member 7 (SLC26A7)*; Figure 6.19). *SLC26A7* encodes an anion exchange transporter associated with bicarbonate, chloride and sulphate transport and was up-regulated in DT-D283-CIS cells compared with DT-D283-DMF control cells. Although little has been published to date regarding the functional role of *SLC26A7*

in tumour progression, other members of the Solute Carrier (SLC) family have been associated with the transport of and resistance to cisplatin, perhaps indicative of a potential role for SLC26A7 in drug transport (Girardi et al., 2020; Rodrigo et al., 2019).

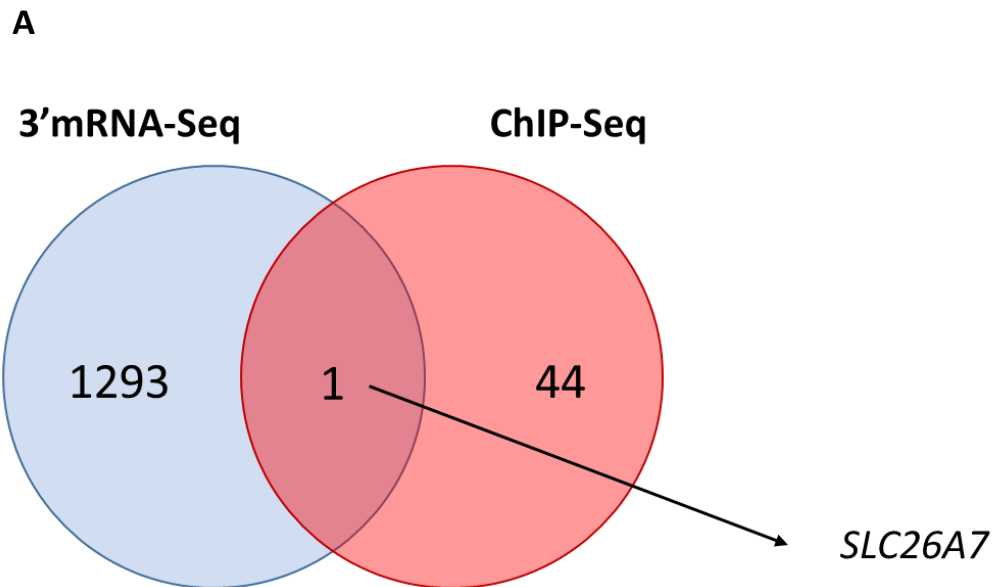
Although the YB-1 targets identified here will require further ChIP assay validation, it is highly plausible that all five genes identified in Figure 6.18 and Figure 6.19 represent direct transcriptional targets of YB-1 and are associated with long-term cisplatin resistance in HDMB-03/D283 Group 3 cell lines. Thus, taken together, the integration of ChIP-Seq and 3'mRNA-Seq datasets described here has successfully identified YB-1 targets implicated in chronic cisplatin resistance, both providing further insight into the diverse transcriptional role played by YB-1 in medulloblastoma drug resistance and identifying novel YB-1 downstream hits, which may hold greater therapeutic benefit than simply targeting YB-1 alone.



B

Gene Name	3'mRNA-Seq		
	Direction of gene expression	Log ₂ Fold Change	P-Value
<i>PELI2</i>	Down-regulated	-1.13	2.81E-04
<i>MFF</i>	Up-regulated	0.91	1.18E-05
<i>ENSG00000278898</i>	Up-regulated	1.17	0.034
<i>ENSG00000259820</i>	Down-Regulated	-1.68	6.35E-07

Figure 6.18 Integration of DT-HDMB-03-CIS CHIP-Seq and 3'mRNA-Seq datasets reveals common genes. Integration of YB-1 target genes identified from CHIP-Seq and DEGs identified from 3'mRNA-Seq reveals four genes common to both datasets that may represent direct YB-1 transcriptional targets implicated in drug resistance. A) Venn diagram showing genes common to both datasets – *PELI2*, *MFF*, *ENSG00000278898* and *ENSG00000259820*. B) Table displaying 3'mRNA-Seq Log₂ Fold Changes and P-Values of identified CHIP-Seq targets.



B

Gene Name	3'mRNA-Seq		
	Direction of gene expression	Log ₂ Fold Change	P-Value
<i>SLC26A7</i>	Up-regulated	0.75	0.0076

Figure 6.19 Integration of DT-D283-CIS CHIP-Seq and 3'mRNA-Seq datasets reveals a common gene. Integration of YB-1 target genes identified from CHIP-Seq and DEGs identified from 3'mRNA-Seq reveals one gene common to both datasets that may represent a direct YB-1 transcriptional target implicated in drug resistance. A) Venn diagram showing common gene *SLC26A7*. B) Table displaying 3'mRNA-Seq Log₂ Fold Changes and P-Values of the identified CHIP-Seq target.

6.5 Summary

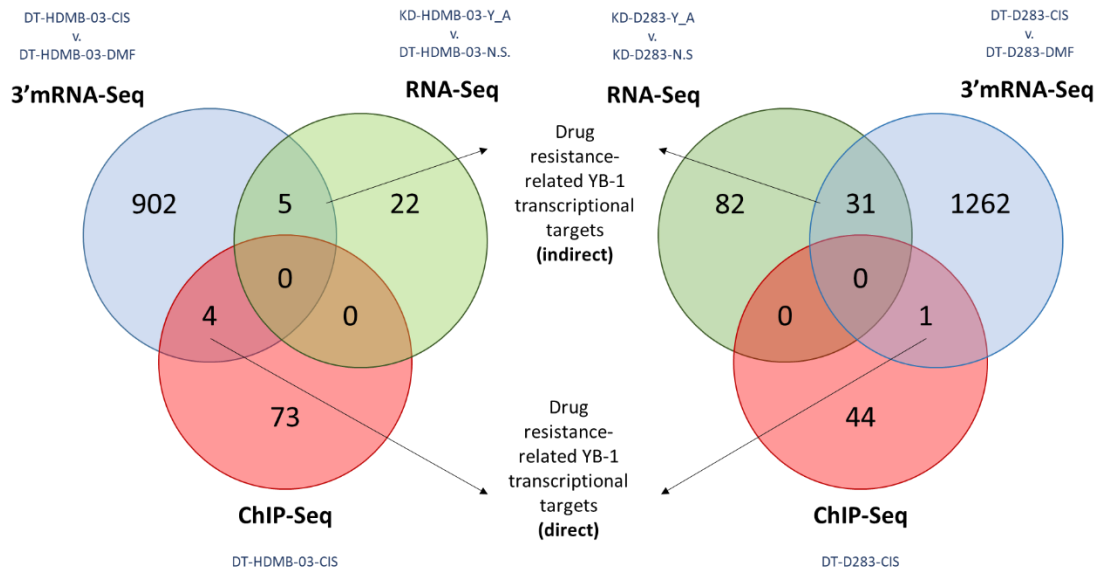


Figure 6.20 Summary Venn diagrams displaying overlapping genes identified upon integration of RNA-Seq, 3'mRNA-Seq and ChIP-Seq datasets. Common genes identified between independent sequencing methods are shown. Genes which overlap between ChIP-Seq and 3'mRNA-Seq datasets likely represent drug resistance-related genes directly regulated by YB-1, while genes which are common between RNA-Seq (Chapter 5) and 3'mRNA-Seq datasets may still represent YB-1 transcriptional targets, but are either indirectly regulated by YB-1 or not detected in the present ChIP-Seq study.

- Long-term cisplatin treatment with continuous selection resulted in the generation of stable, cisplatin-tolerant Group 3 cell lines.
- Long-term vincristine treatment with continuous selection facilitated production of a stable, vincristine-tolerant SHH cell line (DT-DAOY-VIN), however this selection strategy was not successful in the generation of vincristine-tolerant Group 3 medulloblastoma cell lines, likely arising from the reduced *ABCB1* expression possessed by cell lines of this subgroup.
- Cisplatin- and vincristine-tolerant cell lines displayed altered ABC transporter expression, with DT-DAOY-VIN cells exhibiting significantly elevated *ABCB1*

expression and DT-DAOY-VIN, DT-D283-CIS and DT-D458-CIS exhibiting significantly increased levels of *ABCC1*.

- 3'mRNA-Seq revealed numerous DEGs and biological processes common to all four DT-cell lines, despite different parental cell lines, treatment types and subgroups, indicating that these genes and processes may represent major and global mediators of drug resistance in medulloblastoma.
- DEGs are shared between DT-cell lines and *YBX1* knockdown cell lines, suggesting YB-1 may regulate the expression of numerous genes implicated in the acquisition/maintenance of cisplatin tolerance in Group 3 medulloblastoma.
- ChIP-Seq of acute cisplatin- and vincristine-treated and chronic cisplatin-treated medulloblastoma cell lines was hindered due to unexpected read enrichment across input samples, which caused significant issues when calling and annotating peaks.
 - Downstream analysis was conducted on chronic DT-HDMB-03-CIS and DT-D283-CIS ChIP samples only, as these datasets could be supported with pre-existing 3'mRNA-Seq data.
- Integration of ChIP-Seq and 3'mRNA-Seq datasets identified possible novel YB-1 target genes implicated in long-term cisplatin resistance in Group 3 medulloblastoma. These include *PELI2*, *MFF* and *SLC26A7*.

Chapter 7

Discussion

Chapter 7 Discussion

This thesis functionally characterised the role of multi-functional oncoprotein YB-1 in medulloblastoma and explored its function in the regulation of drug resistance-related gene *ABCB1*. Through a combination of *in vitro* assays and next-generation sequencing methodologies, YB-1 was shown to represent a transcriptional regulator of the *ABCB1* gene in medulloblastoma, with YB-1 interaction identified at a previously unknown site. Next, evidence was presented to indicate YB-1 involvement in numerous aspects of medulloblastoma tumourigenesis including cellular invasion, lipid metabolism and MYC oncoprotein activity. Importantly, a clear function for YB-1 in the cellular response to acute drug treatment and the acquisition of a drug-tolerant cellular state was demonstrated, both independent from and related to its aforementioned association with the *ABCB1* gene.

7.1 *YBX1* expression has oncogenic implications in medulloblastoma patients

Despite considerable research in solid tumours, there is a significant lack of studies exploring the role of YB-1 in brain and CNS tumours (Taylor et al., 2021). Elevated *YBX1* expression has been reported in glioblastoma, where it has been associated with the generation of brain-tumour initiating cells, temozolomide resistance, high-grade disease and tumour cell invasion (Faury et al., 2007; Fotovati et al., 2011; Gao et al., 2009; Zheng et al., 2016). Less is known regarding the functional role of YB-1 in medulloblastoma, with only two papers published to-date. One describes a

function for YB-1 in driving the proliferation of both SHH medulloblastoma cells and cerebellar granule neural precursors (CGNPs; the cell of origin of SHH medulloblastoma) through the SHH-IGF2 signalling axis (Dey et al., 2016). The other, through *YBX1* knockdown and subsequent next-generation sequencing (NGS) studies, demonstrated a role for YB-1 in post-transcriptional regulation of the inflammatory response (Kloetgen et al., 2020). Further investigations are required to build upon this interesting preliminary data and better understand the functional significance of YB-1 in medulloblastoma.

7.1.1 High *YBX1* expression correlates with poor overall survival in medulloblastoma patients

R2 genomic analysis found *YBX1* expression to be significantly higher both in paediatric brain tumour patient datasets and across all four core molecular subgroups of medulloblastoma compared to normal cerebellum controls (Section 3.3.1). Group 3 patients possessed the highest levels of *YBX1* expression, which is interesting on account of the aggressive nature of this subgroup and its high propensity for relapse. This is in agreement with similar R2 genomic analysis obtained by Dey *et al.* and analysis of RNA-binding protein microarray data undertaken by Kloetgen *et al.*, who also demonstrate high and ubiquitous *YBX1* expression across all medulloblastoma subgroups (Dey et al., 2016; Kloetgen et al., 2020). In the present study, universal *YBX1* and YB-1 expression was also found across established SHH, Group 3 and Group 4 medulloblastoma cell lines, indicative that these lines are adequately representative of medulloblastoma subgroups (Section 3.4).

In Section 3.3.2 it was demonstrated, for the first time, that high *YBX1* expression correlates with poor prognosis in medulloblastoma, identifying *YBX1* as an independent predictor of survival. At a subgroup level, high *YBX1* expression correlated with poor overall survival across SHH, Group 3 and Group 4 patients. Interestingly, *YBX1* expression levels did not influence patient survival in the WNT subgroup, perhaps indicative that *YBX1* has a lesser role in disease progression in low-risk tumours. These findings are in agreement with numerous other studies where, in alternate cancers, *YBX1* expression correlates with poor prognosis (Fujiwara-Okada et al., 2013; Liu et al., 2020; X. Wang et al., 2015; Y. Wang et al., 2015) and high-risk disease (Gluz et al., 2009; Janz et al., 2002; Zhao et al., 2016).

7.1.2 YB-1 exhibits substantial nuclear accumulation in a medulloblastoma patient cohort

In addition to analysis of large-scale gene expression datasets, the investigation of clinical samples at a protein level can provide valuable insights into protein localisation and expression, which may be more predictive of biological function. Thus, in this thesis, a novel analysis of YB-1 expression in primary medulloblastoma TMAs was performed (Section 3.5).

In agreement with the ubiquitous expression of *YBX1* observed across all subgroups at a gene level, 98% of patients were positive for both overall and nuclear YB-1 expression (Section 3.5.1). Such a high proportion of nuclear YB-1 positive patients differs to studies conducted in other cancer types, where positive nuclear YB-1 expression commonly appears to account for between 30% and 60% of patients (Basaki et al., 2007; Gessner et al., 2004; Heumann et al., 2017; Xu et al., 2009).

However, it is possible that YB-1 nuclear expression is particularly evident in paediatric brain tumours. Indeed, in their 2007 study, Faury et al., demonstrated that in paediatric glioblastoma patients positive for YB-1 expression, 88% of tumours displayed nuclear YB-1 staining (Faury et al., 2007).

Unfortunately, it was impossible to infer clinical significance from these findings, likely on account of the low number of patients for whom full clinicopathological data was provided in our TMA cohorts. Additionally, disparity in YB-1 cellular localisation was observed between patient tissue samples, where 38% of tumours exhibited high nuclear YB-1 expression and medulloblastoma cell lines, where YB-1 localised predominantly cytoplasmically (Section 3.4.2); highlighting differences between patient tissue samples and established *in vitro* cell models.

7.2 YB-1 may represent a novel regulator of metastasis in medulloblastoma

At the point of diagnosis, up to 40% of medulloblastoma patients display clinically detectable metastatic disease (Wu et al., 2012). In epithelial tumours, YB-1 has been associated with invasion *in vitro* (Lim et al., 2017; Lu et al., 2017) and *in vivo* (Lasham et al., 2012) and appears to regulate multiple aspects of the metastatic cascade (Section 1.4.3.2). To date, YB-1 had not been investigated in the context of medulloblastoma cell invasion.

7.2.1 YBX1 expression correlates with metastatic disease

R2 genomic analysis was employed to assess if high YBX1 expression correlated with

metastatic disease in medulloblastoma patient datasets. Of note, in a large-scale medulloblastoma cohort (Cavalli et al., 2017), patients who presented with metastatic disease exhibited significantly higher *YBX1* levels than non-metastatic patients (Section 3.3.2). In support of this, in a smaller cohort comprising matched primary and metastatic tumour samples (Wang et al., 2015), approximately 88% of patients had elevated *YBX1* expression in a metastatic tumour compared to the matched primary tumour (Section 3.3.2).

The demonstration of correlation between *YBX1* expression and metastatic disease in two separate patient datasets indicated a potential role for YB-1 in medulloblastoma cell invasion. However, in contrast to mRNA studies, assessment of medulloblastoma patient TMAs did not reveal a significant association between YB-1 protein level and metastatic disease (Section 3.5.2). This result may indicate that YB-1 protein and mRNA expression are not directly correlative in medulloblastoma patients. Alternatively, metastatic dissemination in medulloblastoma is a complex process which may differ between medulloblastoma subgroups (Van Ommeren et al., 2020; Zapotocky et al., 2018). YB-1/*YBX1* expression may be differentially regulated at various steps within the process and thus it is challenging to analyse YB-1 involvement based on single samples from primary tumours alone. Larger cohorts and matched primary and metastatic samples would aid a more direct understanding of the association of YB-1 protein expression and medulloblastoma metastasis.

7.2.2 *YBX1* knockdown impedes Group 3 medulloblastoma cell invasion

Another method to assess the role of a protein in invasion and metastasis is to stably deplete its expression and then test the function of the resultant cells in an

appropriate model of cellular invasion. We stably inhibited *YBX1* expression in HDMB-03 and D283 cell lines by way of shRNA (Section 5.2.1 - 5.2.3).

The ability of the knockdown cell lines to migrate and invade was tested in a modified transwell invasion assay (Section 5.3.4). To migrate, cells had to change shape, squeezing through 8 μm pores present in the transwell insert, driven by an FBS gradient. To invade, cells also had to break through a simplified brain extra-cellular matrix (ECM)-like barrier, degrading key ECM proteins collagen IV and laminin 111. Notably, both D283 and HDMB-03 cell lines exhibited a marked reduction in their ability to invade through the collagen IV/laminin 111 coating following *YBX1* knockdown. Comparatively, no alteration in migration was observed in either cell line. These findings indicate that in medulloblastoma cells, YB-1 predominantly regulates traits associated with invasion through an ECM-like barrier, rather than the chemotactic capability of cells towards a chemo-attractant (Figure 7.1). With this in mind, future worthwhile investigations will include the assessment of protease expression and activity in the *YBX1* knockdown cell lines. Studies in epithelial tumours have suggested that YB-1 can regulate the expression or enhance the activity of various matrix metalloproteinases (MMPs) including MMP-11, MMP-14, MMP-2, MMP9 and (MT1)-MMP (Ghatak et al., 2021; Lovett et al., 2010; Lu et al., 2017; Schitteck et al., 2007). In medulloblastoma, MMP2 and MMP9 have been shown to be highly expressed (Bodey et al., 2000; Vince et al., 2001) and thus assessment of MMP2 and MMP9 activity by way of zymography in *YBX1* knockdown cell lines would be of interest.

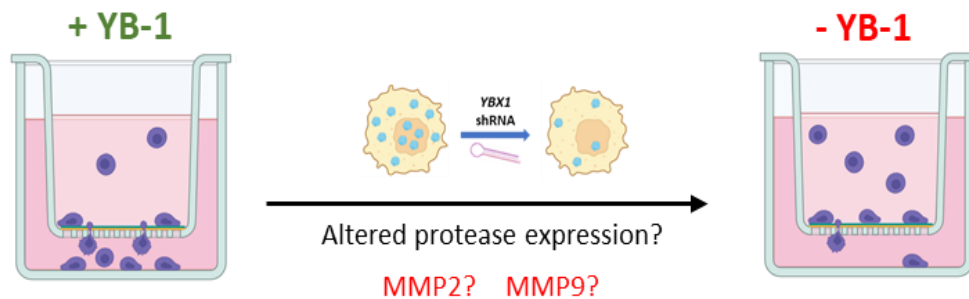


Figure 7.1 Graphical summary of YB-1 function in medulloblastoma cell invasion. Modified transwell invasion assays were conducted with *YBX1* knockdown Group 3 medulloblastoma cell lines. YB-1 depletion diminished the invasive capacity of medulloblastoma cells, potentially via reduced protease expression.

7.3 Whole transcriptome sequencing reveals a function for *YBX1* in numerous key cellular pathways in Group 3 medulloblastoma

In order to build a picture of the global YB-1 transcriptome in Group 3 medulloblastoma, whole transcriptome sequencing using *YBX1* knockdown D283 and HDMB-03 cell lines (KD-D283-Y_A/N.S. and KD-HDMB-03-Y_A/N.S.; Section 5.4) was employed. Only one current study has undertaken NGS to understand the YB-1 regulatory landscape in medulloblastoma (Kloetgen et al., 2020). In the forenamed study, RNA-Seq analysis of two SHH cell lines (DAOY and UW-228-3) and one Group 3 cell line (Med8a) revealed that inflammation response-associated genes were differentially expressed following *YBX1* knockdown, with interferon signalling a canonical pathway activated across all three cell lines.

Whole transcriptome sequencing of *YBX1* knockdown medulloblastoma cell identified 113 DEGs in the KD-D283-Y_A vs. KD-D283-N.S. comparison and 27 in the KD-HDMB-03-Y_A vs. KD-HDMB-03-N.S. comparison (Section 5.4.4). This is in agreement with Kloetgen et al., who find similar numbers of DEGs following *YBX1*

knockdown in DAOY and Med8a lines. Accordingly, no shared DEGs were detected between both Group 3 lines. However, as different genes may converge on common or related pathways, assessment of cellular processes altered following YB-1 depletion was also conducted, revealing common cellular functions and related canonical pathways (Section 5.4.5).

7.3.1 *YBX1* knockdown dysregulates various aspects of lipid metabolism, highlighting a novel function of YB-1 in medulloblastoma

Interestingly, assessment of dysregulated cellular functions revealed “Lipid metabolism” to be significantly altered following *YBX1* knockdown in both D283 and HDMB-03 cell lines (Section 5.4.5.1). Analysis of dysregulated canonical pathways further supported this, with three of the top six affected canonical pathways in each cell line implicated in lipid or cholesterol biosynthesis (Section 5.4.5.2). Lipid biosynthesis processes palmitate biosynthesis I, fatty acid biosynthesis initiation II and stearate biosynthesis I were found to be altered in the KD-HDMB-03-Y_A/-N.S comparison, while cholesterol biosynthesis processes cholesterol biosynthesis, mevalonate pathway I and GGPP biosynthesis I were dysregulated in the KD-D283-Y_A/-N.S comparison. Taken together, these data provide evidence to suggest YB-1 regulates multiple aspects of lipid metabolism in medulloblastoma, an exciting and novel finding which may hold therapeutic potential.

The function of YB-1 in lipid metabolism is relatively under-researched, with a single study reporting association between YB-1 and lipid biosynthesis (Jeffords et al., 2020). The aforementioned study reports YB-1 negatively regulates *stearoyl-CoA desaturase (SCID1)*, which encodes a major enzyme in the biosynthesis of mono-

unsaturated fatty acids. Low SCID1 protein was associated with poor overall survival in renal cell carcinoma patients, providing evidence for interplay between YB-1, unsaturated fatty acid levels and oncogenic capacity in cancer cell lines (Jeffords et al., 2020).

Indeed, the re-programming of lipid metabolism represents a newly recognised hallmark of cancer, with lipid and cholesterol biosynthesis frequently exploited in cancer cells to meet energy demands for rapid growth (C. Cheng et al., 2018). *In vivo* models of SHH-driven medulloblastoma display exaggerated lipogenesis, driven by SHH signalling which stimulates fatty acid synthase (FASN), the key enzyme in the biosynthesis of long chain fatty acids (Bhatia et al., 2011). Importantly, targeting lipid biosynthesis pharmacologically in this system inhibited tumour cell growth and afforded a survival advantage to SHH medulloblastoma-bearing mice (Bhatia et al., 2011). More recently, lipidome alterations between *in vivo* models of non-metastatic and metastatic SHH medulloblastoma have been demonstrated, further supporting the theory that lipid metabolism is associated with medulloblastoma tumour progression (Huang et al., 2020).

The likely role for YB-1 in the regulation of various components of medulloblastoma lipid and cholesterol biosynthesis, as revealed by this whole transcriptome sequencing study represents an interesting finding. However, these data are preliminary and represent a starting point for further investigations. As previous studies have focused on SHH subgroup medulloblastoma, it is currently unclear if and how lipid metabolism is dysregulated in Group 3 tumours. Immunohistochemical analysis of lipid and cholesterol accumulation by way of Oil Red O and filipin staining

in Group 3 medulloblastoma patient samples compared to normal brain tissue may yield interesting data regarding the contribution of lipid metabolism to Group 3 medulloblastoma progression. Further important analyses will include lipidomics of *YBX1* knockdown cells compared to non-silencing control cells, as described by (Zhang et al., 2021), which will allow more accurate study of how lipid metabolism is affected by YB-1 depletion.

7.3.2 *YBX1* knockdown alters cell death and survival pathways in Group 3 medulloblastoma

In addition to “Lipid Metabolism”, a collection of genes dysregulated in both *YBX1* knockdown D283 and HDMB-03 cell lines were related to the cellular function “Cell Death and Survival” (Section 5.4.5.1). This finding was perhaps anticipated. YB-1 exerts pleiotropic cellular functions in processes such as proliferation, DNA repair, RNA splicing and cellular stress response (Figure 1.7). Accordingly, in cancer cells, YB-1 has been demonstrated to perform a number pro-survival and anti-apoptotic functions, as detailed in Section 1.4.3.

7.3.2.1 YB-1 depletion inactivates the Sirtuin signalling pathway, which may potentiate HDAC inhibitor treatment

The Sirtuin signalling pathway was found to be significantly inactivated following *YBX1* knockdown in HDMB-03 cells, suggesting YB-1 may positively regulate the pathway under normal conditions (Section 5.4.5.2). Sirtuins (SIRT) are class III HDACs which mediate processes involved in cell stress response, chromatin regulation, metabolic homeostasis regulation, and cell differentiation (Bosch-Presegué &

Vaquero, 2011). We find downstream targets of SIRT1, SIRT2, SIRT3 and SIRT7 to be differentially expressed in our dataset (Figure 5.22).

Of particular interest, disruption of the Sirtuin signalling pathway by SIRT1 inhibition appears to potentiate the effect of HDAC inhibitor treatment in leukaemia cell lines (Cea et al., 2011). In the aforementioned study, HDAC inhibition up-regulates the expression of pro-apoptotic protein Bax, whose translocation to the mitochondria is usually prevented by SIRT1. The synergistic use of SIRT1 inhibition therefore permits cellular apoptosis. In the current study we found KD-HDMB-03-Y_A cells to exhibit significant sensitivity to HDAC inhibitor panobinostat compared to the KD-HDMB-03-N.S. control line (Section 5.3.3). KD-HDMB-03-Y_A cells also display reduced expression of SIRT1 targets Histone H1 and H3, both of which represent important regulators of the cellular response to panobinostat treatment (Yan-Fang et al., 2015). Thus, YB-1 depletion in HDMB-03 cells may act to potentiate the effect of panobinostat treatment by inactivating components of the Sirtuin signalling pathway.

A growing body of evidence suggests that Sirtuin signalling deregulation is implicated in tumorigenesis. Thus, upon further validation, this finding may both contribute to our understanding of Sirtuin pathway regulation in medulloblastoma, and provide further mechanisms by which to perturb Sirtuin signalling. The study of whether SIRT1 inhibition synergises with panobinostat treatment in medulloblastoma cell lines, and assessment of whether *YBX1* knockdown potentiates this, would be an interesting starting point.

7.3.2.2 YB-1 depletion may promote a senescence-associated phenotype in medulloblastoma cell lines

Senescence can be induced by multiple mechanisms in the cell, including DNA damage and oncogene expression (Figure 7.2). Accordingly, senescence likely represents an anti-cancer mechanism designed to suppress proliferation of damaged or neoplastic cells (Childs et al., 2014). Canonical pathway analysis demonstrated that the senescence pathway is significantly dysregulated in D283 cells following *YBX1* knockdown, likely in a positive direction (Section 5.4.5.2). Although the activation Z-score for this analysis fell below the threshold to be considered significantly predictive, it may still hold biological interest given the recorded function of YB-1 in the transcriptional and translational repression of various senescence-promoting proteins in other cell types (Kotake et al., 2013; Kwon et al., 2018; Lu et al., 2005). To investigate the association between YB-1 and senescence functionally, repeating the proliferation assays conducted in Section 5.2.3 – which found no significant alteration in proliferative capacity upon *YBX1* knockdown – over a longer time course may be beneficial. Furthermore, staining of KD-D283-Y_A and KD-D283-N.S. for senescence-associated beta-galactosidase would facilitate the identification and quantification of senescent cells. It will be interesting to see if such studies reveal a role for YB-1 in senescence, as our whole transcriptome sequencing data appears to suggest.

7.3.2.3 Upstream regulator analysis identifies important pathway regulators altered by *YBX1* knockdown in medulloblastoma cells

Upstream regulator analysis allows identification of upstream regulators that may be responsible for the gene expression changes in a particular dataset and uses these gene expression changes to estimate the regulator's activation state (Section 5.4.5.3).

Interestingly, we identified the MYC oncoprotein to be significantly inactivated in D283 cells following *YBX1* knockdown. MYC protein expression was unaltered in both *YBX1* knockdown cell lines (Section 5.3.3), indicating that this effect occurs at an activity level, rather than from the alteration of MYC expression. This is in contrast to previously published work which has demonstrated a role for YB-1 in both the translational and transcriptional control of MYC (Bommert et al., 2013; Liu et al., 2018). In turn, MYC can modulate YB-1 transcription via E-Box sequences within the *YBX1* promoter, hence forming a co-regulatory feed-forward loop (Bommert et al., 2013).

Numerous studies support a model in which MYC interacts differentially with various co-factors in dynamic complexes to control target gene selection and downstream pathways (Hann, 2014). It is feasible that YB-1 represents one such co-factor in D283 medulloblastoma cells. In fact, proteomic profiling to identify abundant proteins associated with MYC in human cells identified YB-1 as a novel MYC interacting protein, supporting this theory (Agrawal et al., 2010). In this case, *YBX1* knockdown could inhibit the YB-1-MYC interaction and thus impede the ability of MYC to engage in downstream cellular functions. Further studies to examine MYC-YB-1 protein-protein interactions would support the investigation of this hypothesis (Rao et al., 2014).

mTOR signalling pathway components RICTOR and RPTOR were also identified as upstream regulators, down-regulated following *YBX1* knockdown in HDMB-03 and D283 cell lines, respectively. RICTOR represents a component of the mTORC2 complex, which primarily controls cell proliferation and survival. Comparatively,

RPTOR is part of the mTORC1 complex, which regulates cell growth and metabolism (Saxton & Sabatini, 2017). Both RICTOR and RPTOR did not exhibit any alteration in mRNA expression following *YBX1* knockdown, again implying an activational role for YB-1 in the regulation of these proteins. In agreement with the results presented here, a number of studies have found associations between YB-1 expression and mTOR pathway activity, with *YBX1* knockdown causing decreased phosphorylation and expression of mTOR signalling pathway members (Gong et al., 2020; Lee et al., 2008). The mTOR signalling pathway also represents one of the signalling cascades responsible for YB-1 synthesis regulation (Lyabin et al., 2012), raising the possibility of some sort of feed-forward mechanism governing YB-1 and mTOR pathway activity as previously discussed with respect to YB-1 and MYC. In recent years, targeting mTOR signalling has been explored as a therapeutic approach for SHH medulloblastoma treatment (Aldaregia et al., 2018) and thus, better understanding the association between YB-1, a protein highly expressed in SHH subgroup medulloblastoma, and mTOR pathway activity may hold therapeutic benefit.

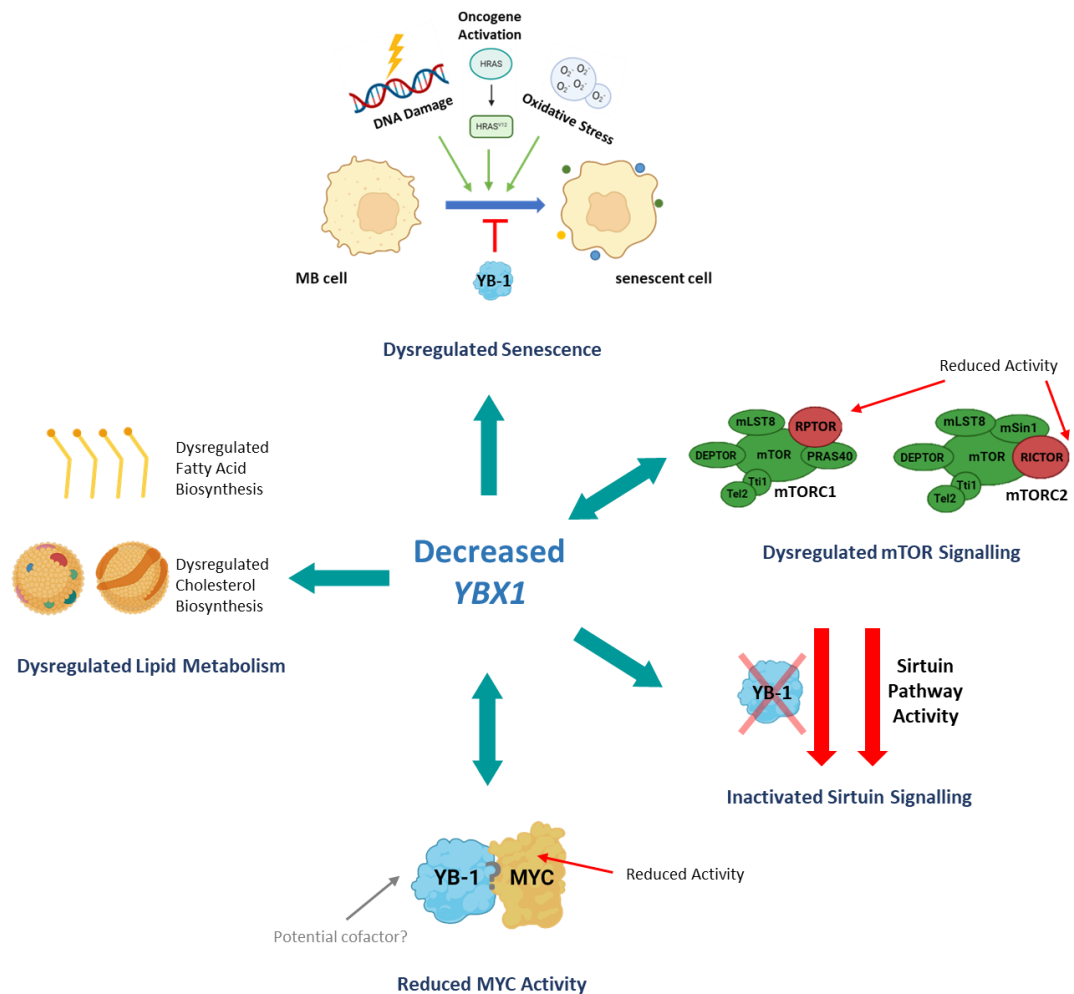


Figure 7.2 Graphical summary of YB-1 cellular functions in medulloblastoma, as identified by whole-transcriptome sequencing. Whole transcriptome sequencing of *YBX1* knockdown cell lines identified lipid and cholesterol metabolism, senescence and sirtuin signalling as significantly altered pathways and MYC, RPTOR and RICTOR as significantly inactivated upstream regulators. Further functional assays will be important to validate these findings. Double-headed arrows dictate a scenario in which the dysregulated function also has an experimentally proven regulatory role in YB-1 expression.

7.4 3'mRNA-Seq of medulloblastoma drug-tolerant cell lines identifies novel drug-tolerant gene signatures

In order to contribute to our understanding of medulloblastoma cell resistance and how it may be targeted therapeutically, 3'mRNA-Seq of cisplatin- and vincristine-tolerant medulloblastoma cell lines (DT-D283-CIS, DT-D548-CIS, DT-HDMB-03-CIS and DT-DAOY-VIN) was undertaken (Section 6.2 and 6.3). To the best of our

knowledge this is the first study in which the cisplatin-/vincristine-resistant transcriptome has been investigated in medulloblastoma cell lines.

Differential gene expression analysis revealed drug-tolerant cells display markedly different gene expression profiles than matched vehicle-control cells (Section 6.3.3). Interestingly, the number of DEGs detected in each drug-tolerant vs. vehicle-control comparison appeared to correlate with the fold resistance possessed by each cell line (Section 6.3.4). As such, cell lines with a greater fold resistance exhibited enhanced gene expression dysregulation, suggesting the more resistant medulloblastoma cells become, the more their transcriptome is altered to maintain this phenotype.

7.4.1 A seven gene signature defines all drug-tolerant cell lines sequenced, regardless of parental line or treatment type

One of the most striking observations in the data analysis of drug-tolerant 3'mRNA-Seq datasets was the high occurrence of common genes identified between different drug-tolerant cell lines. 59 genes were commonly up-regulated and 28 genes commonly down-regulated in at least three of the four drug-tolerant cell lines compared to vehicle-treated controls (Section 6.3.4.1 and 6.3.4.2). The most significant finding from this experiment was the existence of a seven gene drug-tolerant signature in all four drug-tolerant cell lines irrespective of parental cell line, subgroup or chemotherapeutic treatment - *LTBP1*, *MAP1A*, *MBNL2*, *LGALS1*, *PNRC1*, *DAB2*, and *PLAAT3* (Section 6.3.4.1). Only one of these genes, *LGALS1*, had been researched previously in relation to medulloblastoma, where it is up-regulated in SHH medulloblastoma patients and activated by the SHH signalling pathway (Susanto et al., 2020). Thus, there exists here the potential to uncover and characterise novel

therapeutic targets implicated in the acquisition of resistance to cisplatin and vincristine in medulloblastoma.

The remaining common genes were predominantly shared between the cisplatin-tolerant Group 3 lines, indicative of additional shared mechanisms of cisplatin resistance in Group 3 medulloblastoma cells. Accordingly, a number of these genes had been previously associated with cisplatin resistance in non-CNS tumour cell types, supporting the theory that these genes represent bona fide, global mediators of cisplatin tolerance. Only two genes identified as common between cisplatin-tolerant cell lines have been previously researched in medulloblastoma – *platelet-derived growth factor receptor beta (PDGFRB)* and *ATPase Na⁺/K⁺ transporting subunit alpha (ATP1A2)* – both with regards to metastasis (das Chagas et al., 2021; Gilbertson & Clifford, 2003). Interestingly, in the present study there does appear to be association between drug tolerance and metastasis, with GO enrichment analysis of the DT-HDMB-03-CIS cell line revealing a predominance for significantly altered migratory processes including epithelial to mesenchymal transition and cell migration (Section 6.3.5). *In vitro* invasion assays (Section 7.2) would be beneficial to explore this association further.

The next steps in this research are two-fold. First, it would be of interest to establish whether the seven gene drug-tolerant signature is present in relapsed medulloblastoma patient samples. The access and study of recently published matched diagnostic-relapse patient sample next-generation sequencing datasets would aid this (Richardson et al., 2021). The investigation of how perturbation of the drug-tolerant signature impacts medulloblastoma cell viability and response to

chemotherapy will also be vital. Rather than targeting individual genes, it may be of benefit to target the drug-tolerant signature as a whole. In line with this, various studies have utilised drug screening approaches to target whole gene expression profiles associated with cancer cell therapy resistance (Leshchenko et al., 2014; Samuels et al., 2014; Wei et al., 2020). A screening approach which may prove valuable here is publically available software Connectivity Map (CMAP). CMAP allows the input of a gene expression signature associated with a disease-associated phenotype (such as drug resistance), which is then compared with established gene signatures of therapeutic compounds to identify agents likely to reverse the disease-associated gene signature (Musa et al., 2018; Qu & Rajpal, 2012). This method has proved successful in repurposing therapeutic agents to target a drug-resistant signature in leukaemia and lymphoma models (Leshchenko et al., 2014; Samuels et al., 2014). Importantly, it allows identification of agents beyond known inhibitors of target genes, advantageous here where only two identified genes have commercially available inhibitors (Table 6-2).

Supplementary to this data, current work in the group has indicated that exosomes are secreted by the aforementioned drug-tolerant cell lines in higher quantities than that secreted by matched vehicle control cells (Wade et al., unpublished data). Exosomes are nanovesicles secreted by cells, which in recent years have been implicated in cancer progression and metastasis by facilitating intercellular cross-talk (Mashouri et al., 2019). Interestingly, studies have suggested that drug-resistant cell-derived exosomes can confer a resistant phenotype in sensitive cells (Samuel et al., 2018; Tang et al., 2021). One mechanism by which this occurs may be through the uptake and expulsion of anti-cancer drugs such as cisplatin (Safaei et al., 2005).

Ongoing studies will investigate if exosomes and exosome-mediate drug uptake represent additional mechanisms for the acquisition of cisplatin resistance in medulloblastoma cell lines, beyond the gene expression changes discussed here.

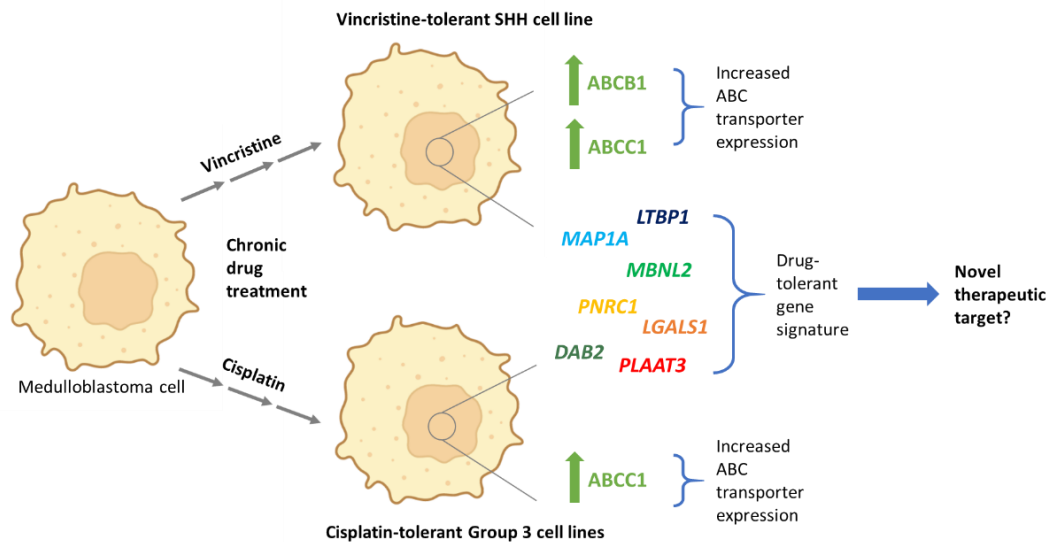


Figure 7.3 Graphical summary of 3'mRNA-Seq data analysis. 3'mRNA-Seq of drug-tolerant cell lines revealed a drug-tolerant gene expression signature common to all drug-tolerant lines regardless of subgroup or treatment type, which may hold therapeutic promise.

7.5 YB-1 mediates intrinsic vincristine tolerance in Group 3 medulloblastoma cells by the transcriptional regulation of the *ABCB1* gene

ABCB1 has oncogenic implications in medulloblastoma (Chou et al., 1995; Nasir et al., 2021; Othman et al., 2014), thus a better understanding of how *ABCB1* is regulated may both provide novel therapeutic routes and aid our understanding of the mechanisms surrounding medulloblastoma drug resistance. Certain aspects of *ABCB1* transcriptional regulation are known, for example the *ABCB1* promoter contains a TCF/LEF consensus binding site targeted by β -catenin (Corrêa et al., 2012) and a

cluster of E-box elements targeted by BMI1 (Banerjee Mustafi et al., 2016). However, there is potential for other sites of *ABCB1* transcriptional regulation, and this was investigated in the present study.

7.5.1 Binding site prediction software identified a Y-Box binding site within the *ABCB1* promoter region

Transcription factor binding site prediction tool Genomatix MatInspector identified YB-1 as a potential regulator of the *ABCB1* gene, predicting interaction at a Y-box site of consensus sequence 5' – CTGATTGG(T/C)(T/C) – 3' within the exon 3 promoter region (Section 3.2). Y-boxes represent the most commonly studied site of YB-1 transcriptional regulation, with functional assays demonstrating binding site enrichment at *EGFR* (Stratford et al., 2007), *GADD45* (Wang et al., 2021) and MHC Class II *DRA* (MacDonald et al., 1995) promoter regions.

Concerning the YB-1-*ABCB1* axis, a number of studies show correlation between YB-1 expression and *ABCB1* expression (Bargou et al., 1997; Basaki et al., 2007; S. Li et al., 2018; Oda et al., 2003; Xu & Hu, 2016). Less evidence exists demonstrating transcriptional regulation at a molecular level, with just two papers displaying functional evidence of YB-1 interaction with *ABCB1*, both at different YB-1-interacting regions, one in the exon 1 *ABCB1* promoter region and one in the exon 3 *ABCB1* promoter region (Ghatak et al., 2021; Shen et al., 2011). Interestingly, the Y-box site identified by Shen et al., corresponds to the Y-box identified in this study using MatInspector software.

7.5.2 YB-1 represents a novel transcriptional regulator of *ABCB1* in medulloblastoma

In order to investigate YB-1 interaction with the *ABCB1* Exon 3 promoter region, ChIP assays were undertaken. Substantial YB-1 enrichment was detected at an inverted CCAAT box site lying approximately 300 bp upstream from the MatInspector-predicted site, with little YB-1 detected at the predicted Y-box (Section 4.2.2 and 4.2.3). Although surprising, studies have suggested that it is the CCAAT/ATTGG pentanucleotide at the core of the Y-Box sequence that is required for transcriptional activation, suggesting Y-boxes and inverted CCAAT boxes may be functionally equivalent (Dolfini & Mantovani, 2013; Ghatak et al., 2021). To the best of our knowledge, this is the first report of YB-1 interaction at this site in the *ABCB1* gene.

In the above text, two transcription start regions were mentioned, a promoter in exon 1 and a promoter in exon 3. Interestingly, *ABCB1* contains two promoters, both of which transcribe the same protein product. The exon 1 promoter is the proximal promoter, required for constitutive expression, whereas the exon 3 promoter likely represents a distal promoter, active in drug-selected cell lines and cancer patient samples for overexpression of the protein product (Hodges et al., 2011). Both this study and a B-cell lymphoma study find YB-1 interaction at the distal promoter, perhaps suggestive that YB-1 has a preference for distal promoter binding in cancer cell lines (Shen et al., 2011).

Of course, protein interaction at a gene promoter region is not necessarily synonymous with transcriptional regulation. One must also validate if the protein in question is capable of altering the transcription of a particular gene. Using previously

mentioned stable *YBX1* knockdown HDMB-03 and D283 cell lines, YB-1 depletion was found to be associated with significantly reduced *ABCB1* expression, providing convincing evidence that YB-1 represents a true transcriptional regulator of the *ABCB1* gene (Section 5.3.2).

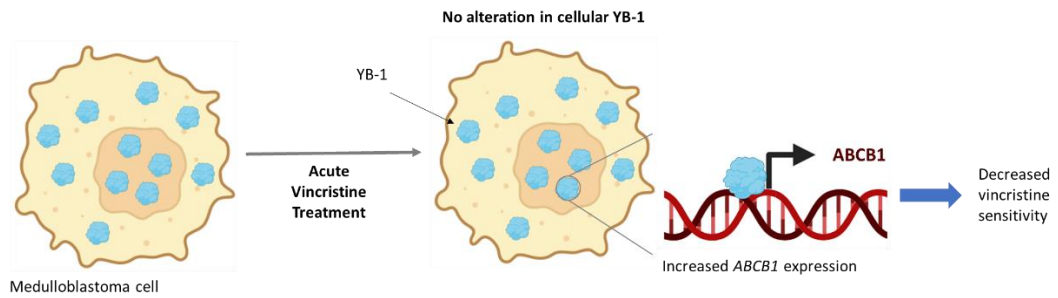


Figure 7.4 Graphical summary of proposed YB-1 function in response to vincristine treatment. Following acute vincristine treatment, we hypothesise that pre-existing nuclear YB-1 is re-distributed to the *ABCB1* gene promoter, resulting in increased *ABCB1* expression and decreased cellular sensitivity to vincristine.

7.5.3 YB-1 depletion increases cellular sensitivity to vincristine in medulloblastoma Group 3 cell lines

Vincristine is highly toxic, likely owing to the high serum concentrations required for sufficient entry to the brain. Indeed, it is estimated that the concentration of vincristine in the CSF is just 5% of that in the plasma, likely attributed to its large size (~825 daltons) and susceptibility to ABCB1 transport (Wang et al., 2010), which hinders blood-brain-barrier infiltration. Thus, mechanisms to decrease ABCB1-mediated vincristine efflux from the brain may facilitate the administration of lower vincristine doses and therefore lessen side effects associated with vincristine toxicity.

In this study, *YBX1* knockdown in both HDMB-03 and D283 Group 3 medulloblastoma cell lines was found to be associated with a 1.4- and 2.5-fold increase in cellular sensitivity to vincristine respectively, at low-intermediate vincristine concentrations

(0.5 - 5 nM; Section 5.3.1). We hypothesised that this arises through down-regulation of *ABCB1* expression following YB-1 depletion, resulting in elevated intracellular concentrations of vincristine. Comparison of intracellular vincristine concentration between *YBX1* knockdown and non-silencing cells following drug exposure by way of cell lysis and high-performance liquid chromatography would confirm this. At concentrations greater than the low-intermediate range, *ABCB1* saturation may account for similarities in vincristine response between both knockdown and control lines. Although observed increases in cellular sensitivity were modest, they lie within a clinically relevant range of measurable vincristine concentration within the CSF (Jackson et al., 1981). Thus, recapitulation *in vivo* could hold clinical benefit.

A limitation of this study was our focus on 2D cell culture techniques. In order to further examine the mechanism of YB-1 depletion on vincristine sensitivity in a more clinically relevant setting, 3D spheroid and/or hydrogel models – known to more accurately mimic drug response, would be of value (Linke et al., 2021; Roper et al., 2021). Notably, the spheroid model described by Roper et al. revealed significant differences in drug response between genetically modified and wild-type medulloblastoma cell lines grown as spheroids which were not observed in 2D, indicating that 3D cell culture can identify key alterations in drug response which are not evident in 2D culture.

7.5.4 Vincristine treatment promotes elevated *ABCB1* expression, likely mediated by pre-existing nuclear YB-1

To further explore the association between the YB-1-*ABCB1* axis and vincristine, *ABCB1* expression was quantified at 12 hour intervals following vincristine treatment.

In both D283 and HDMB-03 Group 3 cell lines, *ABCB1* expression was found to increase significantly following vincristine exposure (Section 4.4.1). As vincristine represents a substrate of *ABCB1*, elevated expression likely acts as a cell-protective, pro-survival mechanism, promoting the extrusion of highly toxic vincristine from medulloblastoma cells. In support of this rationale, vincristine-resistant colon carcinoma cell lines display increased *ABCB1*-mediated drug efflux which correlates with significantly elevated levels of *ABCB1* (Y. R. Liu et al., 2017). Indeed, in the present study the vincristine-tolerant SHH subgroup cell line DT-DAOY-VIN, which demonstrated a four-fold increase in vincristine tolerance compared to its parental line, displayed significantly elevated *ABCB1* expression when compared to the vehicle-treated control cell line.

The results discussed in Section 7.5.2 – Section 7.5.4 provide convincing evidence that increased *ABCB1* expression in medulloblastoma cells, which is likely mediated by YB-1 transcriptional regulation, facilitates cell survival and drug tolerance in response to vincristine treatment. In support of this, preliminary ChIP data revealed that, following short-term vincristine treatment, YB-1 accumulation at the *ABCB1* promoter is both maintained and promoted in HDMB-03 and D283 Group 3 cell lines, compared to vehicle-treated control lines (Section 4.4.2). Interesting however, is that these observations do not appear to be occur through increased nuclear or cellular levels of YB-1. Indeed, in Section 4.3.2, short-term vincristine treatment did not trigger elevated YB-1 levels in D283 or HDMB-03 cell lines, as quantified by immunofluorescence. Likewise, in Section 6.2.5 the DT-DAOY-VIN chronic vincristine-treated cell line displayed reduced *YBX1* levels and unchanged YB-1 protein levels, despite exhibiting elevated levels of *ABCB1*.

Taken together, these results have led us to speculate that instead of triggering nuclear import or elevated cellular YB-1 expression, acute and chronic vincristine treatment instead promotes re-distribution of pre-existing nuclear YB-1, resulting in YB-1 enrichment at the *ABCB1* distal promoter and elevated *ABCB1* expression, providing cells with a protective measure against vincristine therapy (Figure 7.4). Mutation of the identified inverted CCAAT box site in the *ABCB1* promoter by way of site-directed mutagenesis and assessment of how this impacts YB-1 binding and cell sensitivity to vincristine, would be beneficial to substantiate this theory.

7.6 YB-1 may regulate multiple genes implicated in acquired cisplatin resistance in Group 3 medulloblastoma

YB-1 has been described as a mediator of cisplatin resistance in several non-CNS cancer models (Section 1.4.3.3). Accordingly, in the present study, YB-1 response to cisplatin treatment was investigated in order to assess if YB-1 is implicated in the acquisition of cellular cisplatin resistance in medulloblastoma.

7.6.1 Acute cisplatin treatment triggers elevated YB-1 nuclear levels in Group 3 medulloblastoma cell lines

In comparison to vincristine, treatment of D283 and HDMB-03 medulloblastoma cells with cisplatin triggers increased nuclear levels of YB-1 (Section 4.3.2). This appears to occur over a short time-period, just 1 hour in the HDMB-03 cell line and 1 and 6 hours in the D283 cell line, after which the effect appears to dissipate, indicative that YB-1 mediates a short-term cellular cisplatin response. This is supported by a breast cancer study where a clear increase in nuclear YB-1 expression was detected at 6 and 12

hours following treatment with cisplatin at IC₅₀ level, by both immunofluorescence and nuclear fractionation analysis (Fujita et al., 2005). In the aforementioned study, alterations in nuclear YB-1 expression appeared to arise from increased YB-1 nuclear import, rather than elevated total YB-1 expression. In the present study, elevated nuclear YB-1 expression may occur both from increased nuclear translocation alone (HDMB-03 cells) and a combination of increased nuclear YB-1 import and increased YB-1 cellular expression (D283 cells) (Section 4.3.2).

However, a clear limitation in this study was the high variability in YB-1 cellular expression detected by quantitative immunofluorescence. Thus, definite conclusions surrounding whether increased nuclear YB-1 expression arises from elevated total expression or solely nuclear translocation should be made with caution. Observation of individual cells within the immunofluorescence images presented in Section 4.3.2 highlights that this likely arises from heterogeneity in YB-1 staining localisation and intensity, both in vehicle-treated control cells and drug-treated cells. In their 2010 study, Cohen et al. also investigated genotoxic stress-induced YB-1 nuclear translocation; displaying increased levels of cellular and nuclear YB-1 following cisplatin exposure. Similar to observations here, analysis of the immunofluorescence images provided in the Cohen *et al.* paper highlight variation in nuclear and cellular YB-1 levels post-cisplatin treatment, both in staining intensity and also YB-1 distribution, with diffuse and punctate patterns visible. The authors suggest that such variability may highlight a complexity of the YB-1 activation process that remains to be explored following genotoxic stress, which may involve other proteins and/or post-translational modifications such as phosphorylation (Cohen et al., 2010). Moving forwards, a combinatorial method approach may yield more robust data. For

example, immunofluorescence was found to be more reliable for the detection of the nuclear YB-1 levels within medulloblastoma cells in this study than our alternative method – fractionation followed by Western blot, which was associated with frequently contaminated nuclear and cytoplasmic fractions. However, due to variation observed in cellular YB-1 as quantified by immunofluorescence, Western blot using whole cell lysates may represent a more reliable method for assessing total YB-1 levels in response to drug treatment.

7.6.1.1 Alteration in YB-1 expression does not impact medulloblastoma cell sensitivity to acute cisplatin treatment

Due to increases in YB-1 nuclear expression following acute cisplatin treatment, it was hypothesised that YB-1 must play a role in the acute cisplatin stress response. Interesting then, was the finding that *YBX1* knockdown does not alter cisplatin sensitivity in D283 or HDMB-03 cells (Section 5.3.1). This is in contrast to previous studies, where *YBX1* knockdown has been demonstrated to sensitise cancer cell lines to cisplatin treatment (Ohga et al., 1996; Schitteck et al., 2007; Wang et al., 2017). Based upon these data, it was hypothesised that YB-1 either remains too highly expressed in medulloblastoma *YBX1* knockdown cell lines to elicit a measurable effect on cisplatin sensitivity (Figure 5.6), or is not implicated in the direct modulation of cisplatin sensitivity in medulloblastoma. If the latter is true, it asks the question – what is YB-1 interacting with in the nucleus in response to acute cisplatin treatment?

One feasible explanation could be associated with the known function of YB-1 in DNA repair (Section 1.4.3.3). Previous studies have revealed that YB-1 preferentially binds cisplatin-modified DNA and is capable of exerting strand separation and nuclease

activity (Gaudreault et al., 2004; Ise et al., 1999). Furthermore, YB-1 interacts with proteins involved in nucleotide excision repair, mismatch repair (MMR) and non-homologous end-joining, all of which are involved in repairing cisplatin-induced DNA damage (Chang et al., 2014; Fomina et al., 2015; Gaudreault et al., 2004; Rocha et al., 2018). Notably, a 2008 study by Guay et al. revealed that the DNA repair activity possessed by YB-1 is not required for, or associated with, cellular sensitivity to cisplatin (Guay et al., 2008). With these studies in mind, our findings may describe a system where short-term treatment with cisplatin generates cisplatin-modified DNA which triggers YB-1 nuclear import. Although YB-1 knockdown would impede its DNA repair functionality and interaction with DNA repair proteins in the nucleus, this may not affect cellular sensitivity to acute cisplatin treatment. In order to study this, affinity purification pull-down assays and immunofluorescence co-localisation studies could be employed to assess whether YB-1 interacts with DNA repair-associated proteins in medulloblastoma, as it appears to do in other cancers.

In contrast to the studies described above, assessment of *YBX1* expression across three cisplatin-tolerant cell lines subjected to chronic cisplatin treatment revealed either unchanged (DT-HDMB-03-CIS and DT-D458-CIS) or decreased (DT-D283-CIS) *YBX1* mRNA and YB-1 protein expression (Section 6.2.5). Again, these results differed to similar studies in bladder and prostate cancer cells, where cisplatin-tolerant lines exhibited substantially elevated levels of *YBX1*/YB-1 compared to cisplatin-sensitive cells (Ohga et al., 1996; Shiota et al., 2010). Fortunately, subsequent 3'mRNA- and ChIP sequencing studies (Sections 7.6.2 and 7.6.3) facilitated further examination of the association between YB-1 and chronic cisplatin exposure, revealing a number of notable and interesting data.

7.6.2 YB-1 may represent a transcriptional regulator of numerous genes implicated in chronic cisplatin tolerance in Group 3 medulloblastoma

Earlier in this study, 3'mRNA-Seq of stable generated drug-tolerant medulloblastoma cell lines (DT-D283-CIS/-DMF, DT-D458-CIS/-DMF, DT-HDMB-03-CIS/-DMF and DT-DAOY-VIN/-DMSO) was employed in order to better understand general mechanisms of drug tolerance to cisplatin and vincristine in an *in vitro* medulloblastoma model (Section 6.3). As well as allowing the investigation of global transcriptomic changes that occur upon the acquisition of drug tolerance (Section 7.4), this study also facilitated integration of differentially expressed genes identified following 3'mRNA-Seq of drug-tolerant lines DT-D283-CIS/-DMF and DT-HDMB-03-CIS/-DMF with those identified in matched *YBX1* knockdown cell lines KD-D283-Y_A/-N.S. and KD-HDMB-03-Y_A/-N.S. that had previously undergone whole transcriptome sequencing (Section 5.4; Section 7.3).

To our surprise, a number of genes were identified as common between *YBX1* knockdown cell lines and matched cisplatin-tolerant cell lines. Of particular note, known cisplatin resistance-related genes such as *Sphingosine-1-Phosphate Receptor 1 (S1RP1)*, *Riboflavin Kinase (RFK)* and *CD55* (Gong et al., 2020; Hirano et al., 2011; Saygin, 2017) and apoptosis-related gene *Unc-5 Netrin Receptor B (UNC5B)*, which has also been implicated in cisplatin resistance (Yu et al., 2020), were identified in the DT-D283-CIS/-DMF and KD-D283-Y_A/-N.S. comparison. Pro-survival factor *Nuclear Factor I A (NFIA)*, which encodes a protein product implicated in temozolomide resistance in glioblastoma was also recorded (Lee et al., 2017; Yu et al., 2019). In the DT-HDMB-03-CIS/-DMF and KD-HDMB-03-Y_A/-N.S. comparison, *Glutathione*

Peroxidase 3 (GPX3) was identified, a gene associated with cisplatin sensitivity in clear cell adenocarcinoma (Saga et al., 2008).

The occurrence of overlapping genes between datasets, combined with the proven association between many of the identified genes with cisplatin resistance in other cancer cell lines, suggests that YB-1 may regulate the expression of genes associated with cisplatin tolerance in medulloblastoma. Rather than cellular YB-1 levels increasing, it is plausible that pre-existing nuclear YB-1, re-distributed to appropriate target genes, is adequate for the acquisition of a drug tolerant state. In support of this, *YBX1* expression in medulloblastoma patients is significantly higher than *YBX1* expression in patients of cancer types (prostate and bladder cancer; (Ohga et al., 1996; Shiota et al., 2010)), in which the association between YB-1 and cisplatin resistance has previously been investigated (Appendix E1). Furthermore, medulloblastoma patient samples exhibit substantially higher levels of nuclear YB-1 accumulation than patient samples derived from non-CNS tumours, as previously discussed in Section 7.1.2. Thus, it is possible that in medulloblastoma cells, elevated YB-1 levels are not required to promote the expression of drug resistance-related genes because nuclear YB-1 expression is already sufficiently high.

7.6.3 ChIP-Seq identifies direct transcriptional targets of YB-1 implicated in the acquisition and maintenance of a chronic cisplatin-tolerant state

A key aim of this study was to better understand how YB-1 modulates cellular drug response and resistance in medulloblastoma cells. To achieve this, YB-1 transcriptional response to different treatment types (cisplatin and vincristine) and states (acute and chronic) would be investigated by way of ChIP-Seq (Mundade et al.,

2014). Analysis of YB-1 targets in response to acute drug-treatment would allow identification of YB-1-regulated genes implicated in the short-term cellular stress response to cisplatin or vincristine in Group 3 medulloblastoma. Alternatively, ChIP-Seq of chronic-treated, cisplatin-tolerant cell lines would facilitate identification of direct YB-1 targets required for the acquisition and/or maintenance of a drug-tolerant cellular state (Section 6.4).

7.6.3.1 Input control sample quality issues raises concerns over the reliability of ChIP-Seq datasets

Unfortunately, as described extensively throughout Section 6.4, significant concerns regarding the quality of input control samples were identified during ChIP-Seq sample analysis. All input samples generated, regardless of cell line/treatment state, exhibited unexpected peak enrichment, appearing more akin to IP samples than control samples. This resulted in poor alignment to the human genome and problematic peak calling analysis, with substantially fewer binding sites identified than anticipated for a transcription factor such as YB-1. Thus, in order to increase confidence in identified YB-1 target genes, it was decided that only ChIP samples with matched 3'RNA-Seq datasets (DT-HDMB-03-CIS/DMF and DT-D283-CIS/DMF) would be taken forward for downstream analysis (Section 7.4).

It is currently unclear as to why all input samples exhibited high-level peak enrichment. As discussed in Section 6.4.2, known causes for poor mapping and low peak calling such as PCR mistakes, sequencing miscalls and the inclusion of blacklisted genomic regions in data analysis seem unlikely in the present study (Amemiya et al., 2019; Bailey et al., 2013). It is possible that the aforementioned sequencing issues

could be attributed to mutagenic DNA damage, namely either artefactual or intrinsic DNA oxidation. In a previous sequencing study undertaken by the University of Nottingham DEEP-SEQ facility, a type of DNA damage known as 8-oxoGuanine(G) was detected in a dataset which aligned poorly to its reference genome (Dr Fei Sang and Victoria Wright; personal communication). G > 8-oxoG represents the most frequent lesion in DNA and is triggered by oxidation. The resultant 8-oxoG can pair with both cytosine (C) and adenine (A), resulting in C > A/G > T transversions. A 2013 study by Costello *et al.* revealed that the 8-oxoG product can be introduced at abnormally high levels in sequencing studies during sample preparation if a high-powered sonication step (as was used for chromatin shearing in the present ChIP-Seq study) is required. This effect is particularly evident in sequencing methods where relatively low DNA starting quantities are utilised (Costello *et al.*, 2013), an example of which is ChIP-Seq. Such artefactual DNA oxidation during sample preparation may then promote sequencing bias during PCR amplification/adaptor ligation steps, resulting in the generation of false positive signals during sequencing (Mingard *et al.*, 2020). It is perhaps possible that such false positive signals, produced as a result of oxygen species-induced DNA damage, could generate the unexpected enrichment observed in input control samples in the current study.

In mammals, 8-oxoG damage is repaired by base excision repair (BER), with evidence to suggest MMR systems also play a role (Colussi *et al.*, 2002; David *et al.*, 2007; Macpherson *et al.*, 2005; Russo *et al.*, 2007). Of note here, both BER and MMR pathway defects have been recorded in patients with medulloblastoma (Amayiri *et al.*, 2016; Bagchi *et al.*, 2021; Kline *et al.*, 2016). In addition, a number of medulloblastoma cell lines, including the D283 line utilised in the present study,

appear to be MMR deficient, arising from hypermethylation of the *MutL Homolog 1* (*MLH1*) MMR pathway gene promoter (Dong et al., 1999; von Bueren et al., 2012). It seems feasible to hypothesise that MMR/BER repair deficiency pre-existing within the medulloblastoma cell lines utilised in this study could further contribute to a high frequency of C > A/G > T transversions (as has been shown recently in neuroblastoma (van den Boogaard et al., 2021)), resulting in the introduction of sequencing bias as previously described. Of course, at present this theory is simply speculation. In order to investigate this further, assessment of the abundance of 8-oxoG damage in ChIP-Seq data files (by alignment of BAM files to the human genome and assessment for G > T and C > A conversions) will be necessary. If such a mutational signature is detected, assessment of whether this arises from the input sample preparation method or simply from the use of paediatric medulloblastoma cell lines would provide further important clarification.

7.6.3.2 Integration of ChIP-Seq and 3'mRNA-Seq datasets facilitates identification of YB-1 target genes implicated in cisplatin resistance

The data discussed in Section 7.6.2 suggested that, although YB-1 expression is not elevated in cisplatin-tolerant Group 3 medulloblastoma cell lines, pre-existing cellular YB-1 may still be sufficient for the regulation of target genes implicated in acquired cisplatin resistance. Although concerns arose regarding the reliability of the ChIP-Seq datasets produced in this study, the existence of cisplatin-tolerant D283 and HDMB-03 3'mRNA-Seq datasets facilitated a form of cross-validation for the ChIP-Seq data acquired for these line (Section 6.3), allowing downstream data analysis to take place. Consequently, YB-1 target genes identified in drug-tolerant cell line IP samples (DT-HDMB-03-CIS and DT-D283-CIS) were integrated with DEGs identified from matched

3'mRNA-Seq datasets with the rationale that any common genes likely represent direct, active transcriptional targets of YB-1.

Analysis revealed shared YB-1 target genes between ChIP-Seq and 3'mRNA-Seq datasets in both cisplatin-tolerant Group 3 medulloblastoma cell lines (DT-HDMB-03-CIS and DT-D283-CIS). Four genes were identified both as YB-1 binding targets in ChIP-Seq and as differentially expressed in 3'mRNA-Seq in the DT-HDMB-03-CIS line – *PELI2*, *MFF* and novel genes *ENSG00000278898* and *ENSG00000259820*. *MFF* encodes a regulator of mitochondrial fission and was found to be over-expressed in the DT-HDMB-03-CIS line compared to the DT-HDMB-03-DMF control line. Its product, MFF, is over-expressed in lung cancer cells where it forms complexes with Voltage-Dependent Anion Channel 1 (VDAC1) at the outer mitochondrial membrane, blocking channel conductance and thus decreasing membrane permeability (Seo et al., 2019). Interestingly, mitochondrial membrane permeability is frequently altered in cancer, where decreased permeability promotes tumour cell survival and confers treatment resistance (Adams & Cory, 2018; Hanahan & Weinberg, 2011). Accordingly, inhibition of MFF in drug-resistant melanoma, glioblastoma, breast cancer and lung cancer pre-clinical models promotes significant tumour cell death, with no measurable effect on healthy cells (Seo et al., 2019).

PELI2, encodes an E3 ubiquitin ligase which is involved in the ubiquitination and activation state regulation of IRAK1, a protein implicated in MAPK/JNK signalling (Ma et al., 2020). *PELI2* was found to be down-regulated in the DT-HDMB-03-CIS line compared to the DT-HDMB-03-DMF control line. Of note, previous studies have demonstrated that down-regulation of *PELI2* disrupts the balance of IRAK1

ubiquitination resulting in increased IRAK1 activity, which has been linked to proliferation, stemness and drug resistance in hepatocellular carcinoma cells (B. Y. Cheng et al., 2018; Ma et al., 2020).

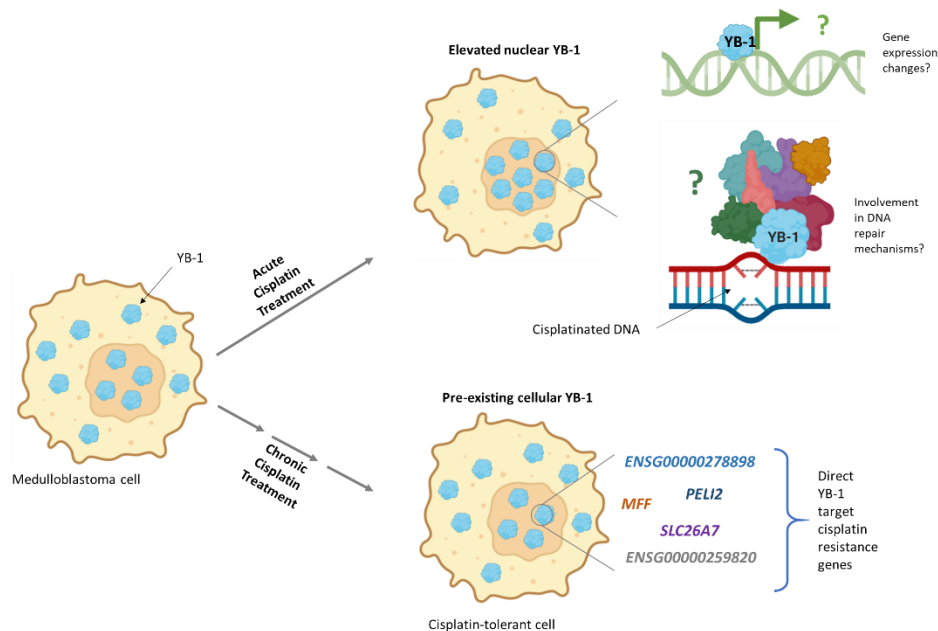


Figure 7.5 Graphical summary of the function of YB-1 in the response to acute and chronic treatment with cisplatin. Following acute treatment, YB-1 nuclear expression is elevated, perhaps due to YB-1 involvement in the repair of damaged, cisplatinated DNA. Alternatively, pre-existing cellular YB-1 in cisplatin-tolerant cell lines likely regulates the transcription of several genes implicated in the acquisition of cisplatin resistance in Group 3 medulloblastoma.

Integration of 3'mRNA-Seq and ChIP-Seq datasets in the DT-D283-CIS cell line revealed a single common hit – *SLC26A7*. *SLC26A7* encodes an anion exchange transporter of the SLC family associated with bicarbonate, chloride and sulphate transport and was found to up-regulated in DT-D283-CIS cells compared with DT-D283-DMF control cells. Much like the ABC transporters discussed throughout this report, the wider SLC family has been associated with the transport of numerous anticancer drugs, affecting drug potency and activity (Pizzagalli et al., 2021). Findings regarding whether these transporters have drug import or export roles in tumours

are conflicting and likely depend on tumour type and the SLC transporter in question. A recent study in which cisplatin-resistant cell lines were generated from parental neuroblastoma cells revealed up-regulation of numerous SLC transporter genes, which the authors concluded may represent a mechanism of acquired chemoresistance to cisplatin, where transporter up-regulation results in the binding and export of cisplatin from the intracellular region (Rodrigo et al., 2019). Contrastingly, SLC35A2 and SLC38A5 are required for cisplatin sensitivity in human *HAP1* cells, with their depletion associated with cisplatin resistance (Girardi et al., 2020). Less is known regarding the role of *SLC26A7* in tumour progression. However, the few studies that describe an association between *SLC26A7* and cancer, most of which focus on subtypes of thyroid carcinoma, show that despite being frequently down-regulated in thyroid carcinoma patients (Dai et al., 2020; Weinberger et al., 2017), high *SLC26A7* expression is associated with poor survival and high-risk disease (Dai et al., 2020; Lv et al., 2020).

In conclusion, we discuss here five novel potential transcriptional targets of YB-1, identified through the integration of ChIP-Seq and 3'mRNA-Seq datasets. The previously published data regarding *PELI2*, *SLC26A7* and *MFF* described above, combined with their dysregulated expression in Group 3 cisplatin-tolerant cell lines highlights a likely role for these potential YB-1 target genes in drug resistance and tumour progression in medulloblastoma and thus may identify novel therapeutic targets in Group 3 medulloblastoma cells. Further investigations both confirming YB-1 interaction with each target gene and assessing the effect of *PELI2*, *MFF* and *SLC26A7* inhibition, either by RNA interference or small molecule inhibition will be important to confirm these findings and investigate potential therapeutic benefit.

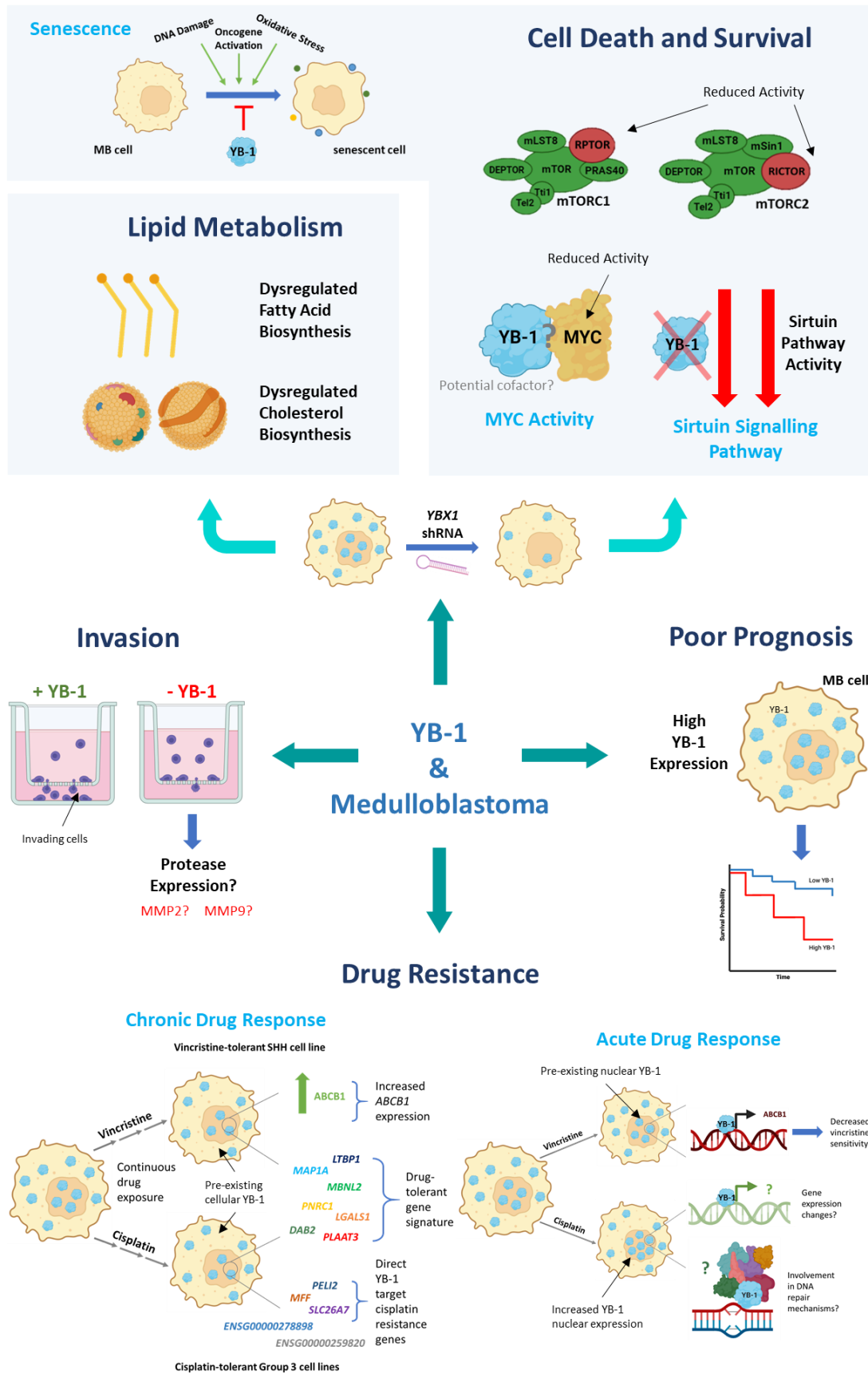


Figure 7.6 Graphical summary of YB-1 functions in medulloblastoma as elucidated by this study. Blue shading highlights functions inferred from sequencing data analysis which will require functional validation. MB = medulloblastoma.

7.7 Concluding Statement

This thesis has functionally characterised the role of oncogene *YBX1*, and its protein product YB-1, in various aspects of medulloblastoma tumourigenesis. We demonstrate that YB-1 likely plays an important function in numerous tumour-associated mechanisms within medulloblastoma cells, including cell invasion, drug resistance, lipid metabolism and MYC oncoprotein activity. We also identify YB-1 as a transcriptional regulator of drug resistance-related gene *ABCB1*. Accordingly, we find *YBX1* expression to serve as a poor prognosis factor in medulloblastoma. Independent of YB-1, we also investigated global mechanisms of acquired drug-tolerance in medulloblastoma cell lines and importantly identify a gene expression signature associated with cisplatin and vincristine resistance.

The wealth of next-generation sequencing data provided by this study has generated numerous research avenues to follow. The analysis of the function of YB-1 in lipid metabolism (whole transcriptome sequencing), the validation of YB-1 transcriptional target genes implicated in cisplatin resistance (ChIP-Seq) and the characterisation of the drug-tolerant gene expression signature in cisplatin and vincristine medulloblastoma cell resistance (3'mRNA-Seq) will be particularly intriguing.

Through a combination of *in vitro* assays, bioinformatic techniques and next-generation sequencing methodologies, this thesis provides convincing evidence to support a function for YB-1 in driving tumour progression in medulloblastoma and investigates the mechanisms by which this occurs. Above all, the identification of therapeutically targetable hits implicated in the acquisition of drug-tolerance, both directly regulated by YB-1 and globally, may inform future pre-clinical investigations, with a focus on hindering the development of medulloblastoma therapy resistance.

References

- Abubakar, D. S., & Traunecker, H. C. (2014). Current perspectives on childhood brain tumours: a review. *Paediatrics and Child Health*, 24(4), 155-160. <https://doi.org/doi:10.1016/j.paed.2014.01.002>
- Adams, J. M., & Cory, S. (2018). The BCL-2 arbiters of apoptosis and their growing role as cancer targets. *Cell Death Differ*, 25(1), 27-36. <https://doi.org/10.1038/cdd.2017.161>
- Agrawal, P., Yu, K., Salomon, A. R., & Sedivy, J. M. (2010). Proteomic profiling of Myc-associated proteins. *Cell Cycle*, 9(24), 4908-4921. <https://doi.org/10.4161/cc.9.24.14199>
- Ahmed, K. M., & Li, J. J. (2008). NF-kappa B-mediated adaptive resistance to ionizing radiation. *Free radical biology & medicine*, 44(1), 1-13. <https://doi.org/10.1016/j.freeradbiomed.2007.09.022>
- Akan, I., Akan, S., Akca, H., Savas, B., & Ozben, T. (2005). Multidrug resistance-associated protein 1 (MRP1) mediated vincristine resistance: effects of N-acetylcysteine and Buthionine sulfoximine. *Cancer Cell Int*, 5(1), 22. <https://doi.org/10.1186/1475-2867-5-22>
- Aldaregia, J., Odriozola, A., Matheu, A., & Garcia, I. (2018). Targeting mTOR as a Therapeutic Approach in Medulloblastoma. *Int J Mol Sci*, 19(7). <https://doi.org/10.3390/ijms19071838>
- Aldighieri, M. (2020). *Identifying factors that control medulloblastoma cell migration using a model of brain-CSF dissemination*. University of Nottingham].
- Amayiri, N., Al-Hussaini, M., Swaidan, M., Jaradat, I., Qandeel, M., Tabori, U., . . . Bouffet, E. (2016). Synchronous glioblastoma and medulloblastoma in a child with mismatch repair mutation. *Childs Nerv Syst*, 32(3), 553-557. <https://doi.org/10.1007/s00381-015-2883-3>
- Ambudkar, S. V., Dey, S., Hrycyna, C. A., Ramachandra, M., Pastan, I., & Gottesman, M. M. (1999). Biochemical, cellular, and pharmacological aspects of the multidrug transporter. *Annu Rev Pharmacol Toxicol*, 39, 361-398. <https://doi.org/10.1146/annurev.pharmtox.39.1.361>
- Amemiya, H. M., Kundaje, A., & Boyle, A. P. (2019). The ENCODE Blacklist: Identification of Problematic Regions of the Genome. *Sci Rep*, 9(1), 9354. <https://doi.org/10.1038/s41598-019-45839-z>
- Anders, S., & Huber, W. (2010). Differential expression analysis for sequence count data. *Genome Biol*, 11(10), R106. <https://doi.org/10.1186/gb-2010-11-10-r106>
- Arioka, H., Nishio, K., Ishida, T., Fukumoto, H., Fukuoka, K., Nomoto, T., . . . Saijo, N. (1999). Enhancement of cisplatin sensitivity in high mobility group 2 cDNA-transfected human lung cancer cells. *Jpn J Cancer Res*, 90(1), 108-115. <https://doi.org/10.1111/j.1349-7006.1999.tb00673.x>
- Babicki, S., Arndt, D., Marcu, A., Liang, Y., Grant, J. R., Maciejewski, A., & Wishart, D. S. (2016). Heatmapper: web-enabled heat mapping for all. *Nucleic Acids Res*, 44(W1), W147-153. <https://doi.org/10.1093/nar/gkw419>

- Bader, A. G., & Vogt, P. K. (2005). Inhibition of protein synthesis by Y box-binding protein 1 blocks oncogenic cell transformation. *Mol Cell Biol*, 25(6), 2095-2106. <https://doi.org/10.1128/MCB.25.6.2095-2106.2005>
- Bader, A. G., & Vogt, P. K. (2008). Phosphorylation by Akt disables the anti-oncogenic activity of YB-1. *Oncogene*, 27(8), 1179-1182. <https://doi.org/10.1038/sj.onc.1210719>
- Baenke, F., Peck, B., Miess, H., & Schulze, A. (2013). Hooked on fat: the role of lipid synthesis in cancer metabolism and tumour development. *Dis Model Mech*, 6(6), 1353-1363. <https://doi.org/10.1242/dmm.011338>
- Bagadi, S. A., Prasad, C. P., Srivastava, A., Prashad, R., Gupta, S. D., & Ralhan, R. (2007). Frequent loss of Dab2 protein and infrequent promoter hypermethylation in breast cancer. *Breast Cancer Res Treat*, 104(3), 277-286. <https://doi.org/10.1007/s10549-006-9422-6>
- Bagchi, A., Beddows, I., Cornelius, A., Robinson, G. W., & Jewell, S. D. (2021). Rare cases of medulloblastoma with hypermutation. *Cancer Rep (Hoboken)*, e1521. <https://doi.org/10.1002/cnr2.1521>
- Bailey, T., Krajewski, P., Ladunga, I., Lefebvre, C., Li, Q., Liu, T., . . . Zhang, J. (2013). Practical guidelines for the comprehensive analysis of ChIP-seq data. *PLoS Comput Biol*, 9(11), e1003326. <https://doi.org/10.1371/journal.pcbi.1003326>
- Balayssac, D., Cayre, A., Authier, N., Bourdu, S., Penault-Llorca, F., Gillet, J. P., . . . Coudore, F. (2005). Patterns of P-glycoprotein activity in the nervous system during vincristine-induced neuropathy in rats. *J Peripher Nerv Syst*, 10(3), 301-310. <https://doi.org/10.1111/j.1085-9489.2005.10308.x>
- Bandopadhyay, P., Bergthold, G., Nguyen, B., Schubert, S., Gholamin, S., Tang, Y., . . . Cho, Y. J. (2014). BET bromodomain inhibition of MYC-amplified medulloblastoma. *Clin Cancer Res*, 20(4), 912-925. <https://doi.org/10.1158/1078-0432.CCR-13-2281>
- Bandopadhyay, P., Piccioni, F., O'Rourke, R., Ho, P., Gonzalez, E. M., Buchan, G., . . . Beroukhim, R. (2019). Neuronal differentiation and cell-cycle programs mediate response to BET-bromodomain inhibition in MYC-driven medulloblastoma. *Nat Commun*, 10(1), 2400. <https://doi.org/10.1038/s41467-019-10307-9>
- Banerjee Mustafi, S., Chakraborty, P. K., Naz, S., Dwivedi, S. K., Street, M., Basak, R., . . . Bhattacharya, R. (2016). MDR1 mediated chemoresistance: BMI1 and TIP60 in action. *Biochim Biophys Acta*, 1859(8), 983-993. <https://doi.org/10.1016/j.bbagr.2016.06.002>
- Bargou, R. C., Jürchott, K., Wagener, C., Bergmann, S., Metzner, S., Bommert, K., . . . Royer, H. D. (1997). Nuclear localization and increased levels of transcription factor YB-1 in primary human breast cancers are associated with intrinsic MDR1 gene expression. *Nat Med*, 3(4), 447-450. <https://doi.org/10.1038/nm0497-447>
- Bartsevich, V., & Juliano, R. (2000). Regulation of the MDR1 Gene by Transcriptional Repressors Selected Using Peptide Combinatorial Libraries. *Molecular Pharmacology*, 58(1), 1 - 10. <https://doi.org/https://doi.org/10.1124/mol.58.1.1>

- Basaki, Y., Hosoi, F., Oda, Y., Fotovati, A., Maruyama, Y., Oie, S., . . . Kuwano, M. (2007). Akt-dependent nuclear localization of Y-box-binding protein 1 in acquisition of malignant characteristics by human ovarian cancer cells. *Oncogene*, 26(19), 2736-2746. <https://doi.org/10.1038/sj.onc.1210084>
- Benjamini, Y., & Hochberg, Y. (1995). Controlling the False Discovery Rate: A Practical and Powerful Approach to Multiple Testing. *J R Stat Soc Series B Stat Methodol*, 57, 289-300. <https://doi.org/10.1111/j.2517-6161.1995.tb02031.x>
- Beretta, G. L., Benedetti, V., Cossa, G., Assaraf, Y. G., Bram, E., Gatti, L., . . . Perego, P. (2010). Increased levels and defective glycosylation of MRPs in ovarian carcinoma cells resistant to oxaliplatin. *Biochem Pharmacol*, 79(8), 1108-1117. <https://doi.org/10.1016/j.bcp.2009.12.002>
- Bhatia, B., Hsieh, M., Kenney, A. M., & Nahlé, Z. (2011). Mitogenic Sonic hedgehog signaling drives E2F1-dependent lipogenesis in progenitor cells and medulloblastoma. *Oncogene*, 30(4), 410-422. <https://doi.org/10.1038/onc.2010.454>
- Bigner, S. H., Friedman, H. S., Vogelstein, B., Oakes, W. J., & Bigner, D. D. (1990). Amplification of the c-myc gene in human medulloblastoma cell lines and xenografts. *Cancer Res*, 50(8), 2347-2350.
- Birzu, C., Tran, S., Bielle, F., Touat, M., Mokhtari, K., Younan, N., . . . Idbaih, A. (2020). Leptomeningeal Spread in Glioblastoma: Diagnostic and Therapeutic Challenges. *Oncologist*, 25(11), e1763-e1776. <https://doi.org/10.1634/theoncologist.2020-0258>
- Bledzka, K., Schiemann, B., Schiemann, W. P., Fox, P., Plow, E. F., & Sossey-Alaoui, K. (2017). The WAVE3-YB1 interaction regulates cancer stem cells activity in breast cancer. *Oncotarget*, 8(61), 104072-104089. <https://doi.org/10.18632/oncotarget.22009>
- Bodey, B., Siegel, S. E., & Kaiser, H. E. (2000). Matrix metalloproteinase expression in childhood medulloblastomas/primitive neuroectodermal tumors. *In Vivo*, 14(5), 667-673.
- Bolin, S., Borgenvik, A., Persson, C. U., Sundström, A., Qi, J., Bradner, J. E., . . . Swartling, F. J. (2018). Combined BET bromodomain and CDK2 inhibition in MYC-driven medulloblastoma. *Oncogene*, 37(21), 2850-2862. <https://doi.org/10.1038/s41388-018-0135-1>
- Bommert, K. S., Effenberger, M., Leich, E., Küspert, M., Murphy, D., Langer, C., . . . Bommert, K. (2013). The feed-forward loop between YB-1 and MYC is essential for multiple myeloma cell survival. *Leukemia*, 27(2), 441-450. <https://doi.org/10.1038/leu.2012.185>
- Bortolozzi, R., Luraghi, A., Mattiuzzo, E., Sacchetti, A., Silvani, A., & Viola, G. (2020). Ecdysteroid Derivatives that Reverse P-Glycoprotein-Mediated Drug Resistance. *J Nat Prod*, 83(8), 2434-2446. <https://doi.org/10.1021/acs.jnatprod.0c00334>
- Bosch-Presegué, L., & Vaquero, A. (2011). The dual role of sirtuins in cancer. *Genes Cancer*, 2(6), 648-662. <https://doi.org/10.1177/1947601911417862>
- Bush, J. A., & Li, G. (2002). Cancer chemoresistance: the relationship between p53 and multidrug transporters. *Int J Cancer*, 98(3), 323-330. <https://doi.org/10.1002/ijc.10226>

- Cai, R., Wang, P., Zhao, X., Lu, X., Deng, R., Wang, X., . . . Lin, J. (2020). LTBP1 promotes esophageal squamous cell carcinoma progression through epithelial-mesenchymal transition and cancer-associated fibroblasts transformation. *J Transl Med*, *18*(1), 139. <https://doi.org/10.1186/s12967-020-02310-2>
- Cancer Research UK. (2020). *Children's Cancer Statistics*. Retrieved 14/04/2020 from <https://www.cancerresearchuk.org/health-professional/cancer-statistics/childrens-cancers>
- Cartharius, K., Frech, K., Grote, K., Klocke, B., Haltmeier, M., Klingenhoff, A., . . . Werner, T. (2005). MatInspector and beyond: promoter analysis based on transcription factor binding sites. *Bioinformatics*, *21*(13), 2933-2942. <https://doi.org/10.1093/bioinformatics/bti473>
- Cavalli, F. M. G., Remke, M., Rampasek, L., Peacock, J., Shih, D. J. H., Luu, B., . . . Taylor, M. D. (2017). Intertumoral Heterogeneity within Medulloblastoma Subgroups. *Cancer Cell*, *31*(6), 737-754.e736. <https://doi.org/https://doi.org/10.1016/j.ccell.2017.05.005>
- Cea, M., Soncini, D., Fruscione, F., Raffaghello, L., Garuti, A., Emionite, L., . . . Nencioni, A. (2011). Synergistic interactions between HDAC and sirtuin inhibitors in human leukemia cells. *PLoS One*, *6*(7), e22739. <https://doi.org/10.1371/journal.pone.0022739>
- Chang, Y. W., Mai, R. T., Fang, W. H., Lin, C. C., Chiu, C. C., & Wu Lee, Y. H. (2014). YB-1 disrupts mismatch repair complex formation, interferes with MutS α recruitment on mismatch and inhibits mismatch repair through interacting with PCNA. *Oncogene*, *33*(43), 5065-5077. <https://doi.org/10.1038/onc.2013.450>
- Chen, L., Yao, Y., Sun, L., & Tang, J. (2017). Galectin-1 promotes tumor progression via NF- κ B signaling pathway in epithelial ovarian cancer. *J Cancer*, *8*(18), 3733-3741. <https://doi.org/10.7150/jca.20814>
- Chen, S., Yang, M., Wang, C., Ouyang, Y., Chen, X., Bai, J., . . . Zhang, Q. (2021). Forkhead box D1 promotes EMT and chemoresistance by upregulating lncRNA CYTOR in oral squamous cell carcinoma. *Cancer Lett*, *503*, 43-53. <https://doi.org/10.1016/j.canlet.2020.11.046>
- Chen, Y., Lun, A. T., & Smyth, G. K. (2016). From reads to genes to pathways: differential expression analysis of RNA-Seq experiments using Rsubread and the edgeR quasi-likelihood pipeline. *F1000Res*, *5*, 1438. <https://doi.org/10.12688/f1000research.8987.2>
- Cheng, B. Y., Lau, E. Y., Leung, H. W., Leung, C. O., Ho, N. P., Gurung, S., . . . Lee, T. K. (2018). IRAK1 Augments Cancer Stemness and Drug Resistance via the AP-1/AKR1B10 Signaling Cascade in Hepatocellular Carcinoma. *Cancer Res*, *78*(9), 2332-2342. <https://doi.org/10.1158/0008-5472.CAN-17-2445>
- Cheng, C., Geng, F., Cheng, X., & Guo, D. (2018). Lipid metabolism reprogramming and its potential targets in cancer. *Cancer Commun (Lond)*, *38*(1), 27. <https://doi.org/10.1186/s40880-018-0301-4>
- Cheng, Y., Li, K., Diao, D., Zhu, K., Shi, L., Zhang, H., . . . Dang, C. (2013). Expression of KIAA0101 protein is associated with poor survival of esophageal cancer patients and resistance to cisplatin treatment in vitro. *Lab Invest*, *93*(12), 1276-1287. <https://doi.org/10.1038/labinvest.2013.124>

- Cheong, S. M., Choi, H., Hong, B. S., Gho, Y. S., & Han, J. K. (2012). Dab2 is pivotal for endothelial cell migration by mediating VEGF expression in cancer cells. *Exp Cell Res*, 318(5), 550-557. <https://doi.org/10.1016/j.yexcr.2012.01.013>
- Childs, B. G., Baker, D. J., Kirkland, J. L., Campisi, J., & van Deursen, J. M. (2014). Senescence and apoptosis: dueling or complementary cell fates? *EMBO Rep*, 15(11), 1139-1153. <https://doi.org/10.15252/embr.201439245>
- Chou, P. M., Reyes-Mugica, M., Barquin, N., Yasuda, T., Tan, X., & Tomita, T. (1995). Multidrug resistance gene expression in childhood medulloblastoma: correlation with clinical outcome and DNA ploidy in 29 patients. *Pediatr Neurosurg*, 23(6), 283-291; discussion 291-282. <https://doi.org/10.1159/000120984>
- Cohen, S. B., Ma, W., Valova, V. A., Algie, M., Harfoot, R., Woolley, A. G., . . . Braithwaite, A. W. (2010). Genotoxic stress-induced nuclear localization of oncoprotein YB-1 in the absence of proteolytic processing. *Oncogene*, 29(3), 403-410. <https://doi.org/10.1038/onc.2009.321>
- Colussi, C., Parlanti, E., Degan, P., Aquilina, G., Barnes, D., Macpherson, P., . . . Bignami, M. (2002). The mammalian mismatch repair pathway removes DNA 8-oxodGMP incorporated from the oxidized dNTP pool. *Curr Biol*, 12(11), 912-918. [https://doi.org/10.1016/s0960-9822\(02\)00863-1](https://doi.org/10.1016/s0960-9822(02)00863-1)
- Conesa, A., Madrigal, P., Tarazona, S., Gomez-Cabrero, D., Cervera, A., McPherson, A., . . . Mortazavi, A. (2016). A survey of best practices for RNA-seq data analysis. *Genome Biol*, 17, 13. <https://doi.org/10.1186/s13059-016-0881-8>
- Conti, S., Vexler, A., Edry-Botzer, L., Kalich-Philosoph, L., Corn, B. W., Shtraus, N., . . . Lev-Ari, S. (2018). Combined acetyl-11-keto- β -boswellic acid and radiation treatment inhibited glioblastoma tumor cells. *PLoS One*, 13(7), e0198627. <https://doi.org/10.1371/journal.pone.0198627>
- Corrêa, S., Binato, R., Du Rocher, B., Castelo-Branco, M. T., Pizzatti, L., & Abdelhay, E. (2012). Wnt/ β -catenin pathway regulates ABCB1 transcription in chronic myeloid leukemia. *BMC Cancer*, 12, 303. <https://doi.org/10.1186/1471-2407-12-303>
- Costello, M., Pugh, T. J., Fennell, T. J., Stewart, C., Lichtenstein, L., Meldrim, J. C., . . . Getz, G. (2013). Discovery and characterization of artifactual mutations in deep coverage targeted capture sequencing data due to oxidative DNA damage during sample preparation. *Nucleic Acids Res*, 41(6), e67. <https://doi.org/10.1093/nar/gks1443>
- Crowther, A. J., Ocasio, J. K., Fang, F., Meidinger, J., Wu, J., Deal, A. M., . . . Gershon, T. R. (2016). Radiation Sensitivity in a Preclinical Mouse Model of Medulloblastoma Relies on the Function of the Intrinsic Apoptotic Pathway. *Cancer Res*, 76(11), 3211-3223. <https://doi.org/10.1158/0008-5472.CAN-15-0025>
- D'Costa, N. M., Lowerison, M. R., Raven, P. A., Tan, Z., Roberts, M. E., Shrestha, R., . . . So, A. I. (2020). Y-box binding protein-1 is crucial in acquired drug resistance development in metastatic clear-cell renal cell carcinoma. *J Exp Clin Cancer Res*, 39(1), 33. <https://doi.org/10.1186/s13046-020-1527-y>
- Daggubati, V., Hochstelter, J., Bommireddy, A., Choudhury, A., Krup, A. L., Kaur, P., . . . Raleigh, D. R. (2021). Smoothened-activating lipids drive resistance to

- CDK4/6 inhibition in Hedgehog-associated medulloblastoma cells and preclinical models. *J Clin Invest*, 131(6). <https://doi.org/10.1172/JCI141171>
- Dai, J., Yu, X., Han, Y., Chai, L., Liao, Y., Zhong, P., . . . Jia, C. (2020). TMT-labeling Proteomics of Papillary Thyroid Carcinoma Reveal Invasive Biomarkers. *J Cancer*, 11(20), 6122-6132. <https://doi.org/10.7150/jca.47290>
- das Chagas, P. F., de Sousa, G. R., Veronez, L. C., Martins-da-Silva, A., Corrêa, C. A. P., Cruzeiro, G. A. V., . . . Valera, E. T. (2021). Identification of ITPR1 as a Hub Gene of Group 3 Medulloblastoma and Coregulated Genes with Potential Prognostic Values. *J Mol Neurosci*. <https://doi.org/10.1007/s12031-021-01942-3>
- Das, K. K., & Kumar, R. (2017). Pediatric Glioblastoma. In S. De Vleeschouwer (Ed.), *Glioblastoma* (pp. 297-213). Codon Publications. <https://doi.org/10.15586/codon.glioblastoma.2017>
- Das, S., Chattopadhyay, R., Bhakat, K. K., Boldogh, I., Kohno, K., Prasad, R., . . . Hazra, T. K. (2007). Stimulation of NEIL2-mediated oxidized base excision repair via YB-1 interaction during oxidative stress. *J Biol Chem*, 282(39), 28474-28484. <https://doi.org/10.1074/jbc.M704672200>
- David, S. S., O'Shea, V. L., & Kundu, S. (2007). Base-excision repair of oxidative DNA damage. *Nature*, 447(7147), 941-950. <https://doi.org/10.1038/nature05978>
- Dean, M. (2005). The genetics of ATP-binding cassette transporters. *Methods Enzymol*, 400, 409-429. [https://doi.org/10.1016/S0076-6879\(05\)00024-8](https://doi.org/10.1016/S0076-6879(05)00024-8)
- Dey, A., Robitaille, M., Remke, M., Maier, C., Malhotra, A., Gregorieff, A., . . . Kenney, A. M. (2016). YB-1 is elevated in medulloblastoma and drives proliferation in Sonic hedgehog-dependent cerebellar granule neuron progenitor cells and medulloblastoma cells. *Oncogene*, 35(32), 4256-4268. <https://doi.org/10.1038/onc.2015.491>
- Diaz, A., Park, K., Lim, D. A., & Song, J. S. (2012). Normalization, bias correction, and peak calling for CHIP-seq. *Stat Appl Genet Mol Biol*, 11(3), Article 9. <https://doi.org/10.1515/1544-6115.1750>
- Ding, P. R., Tiwari, A. K., Ohnuma, S., Lee, J. W., An, X., Dai, C. L., . . . Chen, Z. S. (2011). The phosphodiesterase-5 inhibitor vardenafil is a potent inhibitor of ABCB1/P-glycoprotein transporter. *PLoS One*, 6(4), e19329. <https://doi.org/10.1371/journal.pone.0019329>
- Dolfini, D., & Mantovani, R. (2013). Targeting the Y/CCAAT box in cancer: YB-1 (YBX1) or NF-Y? *Cell Death Differ*, 20(5), 676-685. <https://doi.org/10.1038/cdd.2013.13>
- Dong, Q., Johnson, S. P., Colvin, O. M., Bullock, N., Kilborn, C., Runyon, G., . . . Friedman, H. S. (1999). Multiple DNA repair mechanisms and alkylator resistance in the human medulloblastoma cell line D-283 Med (4-HCR). *Cancer Chemother Pharmacol*, 43(1), 73-79. <https://doi.org/10.1007/s002800050865>
- Durrant, D. E., Das, A., Dyer, S., & Kukreja, R. C. (2020). A dual PI3 kinase/mTOR inhibitor BEZ235 reverses doxorubicin resistance in ABCB1 overexpressing ovarian and pancreatic cancer cell lines. *Biochim Biophys Acta Gen Subj*, 1864(6), 129556. <https://doi.org/10.1016/j.bbagen.2020.129556>

- Eadie, L. N., Hughes, T. P., & White, D. L. (2016). ABCB1 Overexpression Is a Key Initiator of Resistance to Tyrosine Kinase Inhibitors in CML Cell Lines. *PLoS One*, 11(8), e0161470. <https://doi.org/10.1371/journal.pone.0161470>
- Eliseeva, I. A., Kim, E. R., Guryanov, S. G., Ovchinnikov, L. P., & Lyabin, D. N. (2011). Y-box-binding protein 1 (YB-1) and its functions. *Biochemistry (Mosc)*, 76(13), 1402-1433. <https://doi.org/10.1134/S0006297911130049>
- Evdokimova, V., Ruzanov, P., Anglesio, M. S., Sorokin, A. V., Ovchinnikov, L. P., Buckley, J., . . . Sorensen, P. H. (2006). Akt-mediated YB-1 phosphorylation activates translation of silent mRNA species. *Mol Cell Biol*, 26(1), 277-292. <https://doi.org/10.1128/MCB.26.1.277-292.2006>
- Evdokimova, V., Tognon, C., Ng, T., Ruzanov, P., Melnyk, N., Fink, D., . . . Sorensen, P. H. (2009). Translational activation of snail1 and other developmentally regulated transcription factors by YB-1 promotes an epithelial-mesenchymal transition. *Cancer Cell*, 15(5), 402-415. <https://doi.org/10.1016/j.ccr.2009.03.017>
- Faury, D., Nantel, A., Dunn, S. E., Guiot, M. C., Haque, T., Hauser, P., . . . Jabado, N. (2007). Molecular profiling identifies prognostic subgroups of pediatric glioblastoma and shows increased YB-1 expression in tumors. *J Clin Oncol*, 25(10), 1196-1208. <https://doi.org/10.1200/JCO.2006.07.8626>
- Feng, J., Liu, T., Qin, B., Zhang, Y., & Liu, X. S. (2012). Identifying ChIP-seq enrichment using MACS. *Nat Protoc*, 7(9), 1728-1740. <https://doi.org/10.1038/nprot.2012.101>
- Fischer, S., Di Liddo, A., Taylor, K., Gerhardus, J. S., Sobczak, K., Zarnack, K., & Weigand, J. E. (2020). Muscleblind-like 2 controls the hypoxia response of cancer cells. *RNA*, 26(5), 648-663. <https://doi.org/10.1261/rna.073353.119>
- Fletcher, J. I., Williams, R. T., Henderson, M. J., Norris, M. D., & Haber, M. (2016). ABC transporters as mediators of drug resistance and contributors to cancer cell biology. *Drug Resist Updat*, 26, 1-9. <https://doi.org/10.1016/j.drug.2016.03.001>
- Fomina, E. E., Pestryakov, P. E., Maltseva, E. A., Petrusheva, I. O., Kretov, D. A., Ovchinnikov, L. P., & Lavrik, O. I. (2015). Y-box binding protein 1 (YB-1) promotes detection of DNA bulky lesions by XPC-HR23B factor. *Biochemistry (Mosc)*, 80(2), 219-227. <https://doi.org/10.1134/S000629791502008X>
- Fotovati, A., Abu-Ali, S., Wang, P. S., Deleyrolle, L. P., Lee, C., Triscott, J., . . . Dunn, S. E. (2011). YB-1 bridges neural stem cells and brain tumor-initiating cells via its roles in differentiation and cell growth. *Cancer Res*, 71(16), 5569-5578. <https://doi.org/10.1158/0008-5472.CAN-10-2805>
- Fox, E., Widemann, B. C., Pastakia, D., Chen, C. C., Yang, S. X., Cole, D., & Balis, F. M. (2015). Pharmacokinetic and pharmacodynamic study of tariquidar (XR9576), a P-glycoprotein inhibitor, in combination with doxorubicin, vinorelbine, or docetaxel in children and adolescents with refractory solid tumors. *Cancer Chemother Pharmacol*, 76(6), 1273-1283. <https://doi.org/10.1007/s00280-015-2845-1>
- Friedman, H. S., Burger, P. C., Bigner, S. H., Trojanowski, J. Q., Wikstrand, C. J., Halperin, E. C., & Bigner, D. D. (1985). Establishment and characterization of the human medulloblastoma cell line and transplantable xenograft D283

- Med. *J Neuropathol Exp Neurol*, 44(6), 592-605. <https://doi.org/10.1097/00005072-198511000-00005>
- Frye, B. C., Halfter, S., Djudjaj, S., Muehlenberg, P., Weber, S., Raffetseder, U., . . . Mertens, P. R. (2009). Y-box protein-1 is actively secreted through a non-classical pathway and acts as an extracellular mitogen. *EMBO Rep*, 10(7), 783-789. <https://doi.org/10.1038/embor.2009.81>
- Fujii, T., Seki, N., Namoto-Matsubayashi, R., Takahashi, H., Inoue, Y., Toh, U., . . . Shirouzu, K. (2009). YB-1 prevents apoptosis via the mTOR/STAT3 pathway in HER-2-overexpressing breast cancer cells. *Future Oncol*, 5(2), 153-156. <https://doi.org/10.2217/14796694.5.2.153>
- Fujita, T., Ito, K., Izumi, H., Kimura, M., Sano, M., Nakagomi, H., . . . Fujimori, M. (2005). Increased nuclear localization of transcription factor Y-box binding protein 1 accompanied by up-regulation of P-glycoprotein in breast cancer pretreated with paclitaxel. *Clin Cancer Res*, 11(24 Pt 1), 8837-8844. <https://doi.org/10.1158/1078-0432.CCR-05-0945>
- Fujiwara-Okada, Y., Matsumoto, Y., Fukushi, J., Setsu, N., Matsuura, S., Kamura, S., . . . Iwamoto, Y. (2013). Y-box binding protein-1 regulates cell proliferation and is associated with clinical outcomes of osteosarcoma. *Br J Cancer*, 108(4), 836-847. <https://doi.org/10.1038/bjc.2012.579>
- Gao, J., & Wang, W. (2019). Knockdown of galectin-1 facilitated cisplatin sensitivity by inhibiting autophagy in neuroblastoma cells. *Chem Biol Interact*, 297, 50-56. <https://doi.org/10.1016/j.cbi.2018.10.014>
- Gao, Y., Fotovati, A., Lee, C., Wang, M., Cote, G., Guns, E., . . . Dunn, S. E. (2009). Inhibition of Y-box binding protein-1 slows the growth of glioblastoma multiforme and sensitizes to temozolomide independent O6-methylguanine-DNA methyltransferase. *Mol Cancer Ther*, 8(12), 3276-3284. <https://doi.org/10.1158/1535-7163.MCT-09-0478>
- Gaudreault, I., Guay, D., & Lebel, M. (2004). YB-1 promotes strand separation in vitro of duplex DNA containing either mispaired bases or cisplatin modifications, exhibits endonucleolytic activities and binds several DNA repair proteins. *Nucleic Acids Res*, 32(1), 316-327. <https://doi.org/10.1093/nar/gkh170>
- Gaviraghi, M., Vivori, C., Pareja Sanchez, Y., Invernizzi, F., Cattaneo, A., Santoliquido, B. M., . . . Tonon, G. (2018). Tumor suppressor PNR1 blocks rRNA maturation by recruiting the decapping complex to the nucleolus. *EMBO J*, 37(23). <https://doi.org/10.15252/emboj.201899179>
- Gerber, N. U., Mynarek, M., von Hoff, K., Friedrich, C., Resch, A., & Rutkowski, S. (2014). Recent developments and current concepts in medulloblastoma. *Cancer Treat Rev*, 40(3), 356-365. <https://doi.org/10.1016/j.ctrv.2013.11.010>
- Ghatak, S., Hascall, V. C., Markwald, R. R., & Misra, S. (2021). FOLFOX Therapy Induces Feedback Upregulation of CD44v6 through YB-1 to Maintain Stemness in Colon Initiating Cells. *Int J Mol Sci*, 22(2). <https://doi.org/10.3390/ijms22020753>
- Gilbertson, R. J., & Clifford, S. C. (2003). PDGFRB is overexpressed in metastatic medulloblastoma. *Nat Genet*, 35(3), 197-198. <https://doi.org/10.1038/ng1103-197>

- Giménez-Bonafé, P., Fedoruk, M. N., Whitmore, T. G., Akbari, M., Ralph, J. L., Ettinger, S., . . . Nelson, C. C. (2004). YB-1 is upregulated during prostate cancer tumor progression and increases P-glycoprotein activity. *Prostate*, *59*(3), 337-349. <https://doi.org/10.1002/pros.20023>
- Girardi, E., César-Razquin, A., Lindinger, S., Papakostas, K., Konecka, J., Hemmerich, J., . . . Superti-Furga, G. (2020). A widespread role for SLC transmembrane transporters in resistance to cytotoxic drugs. *Nat Chem Biol*, *16*(4), 469-478. <https://doi.org/10.1038/s41589-020-0483-3>
- Goda, K., Fenyvesi, F., Bacsó, Z., Nagy, H., Márián, T., Megyeri, A., . . . Szabó, G. (2007). Complete inhibition of P-glycoprotein by simultaneous treatment with a distinct class of modulators and the UIC2 monoclonal antibody. *J Pharmacol Exp Ther*, *320*(1), 81-88. <https://doi.org/10.1124/jpet.106.110155>
- Gomez-Zepeda, D. A.-O., Taghi, M., Scherrmann, J. M., Decleves, X., & Menet, M. A.-O. (2020). ABC Transporters at the Blood-Brain Interfaces, Their Study Models, and Drug Delivery Implications in Gliomas. *Pharmaceutics*, *12*(1999-4923 (Print)).
- Gong, H., Gao, S., Yu, C., Li, M., Liu, P., Zhang, G., . . . Zheng, J. (2020). Effect and mechanism of YB-1 knockdown on glioma cell growth, migration, and apoptosis. *Acta Biochim Biophys Sin (Shanghai)*, *52*(2), 168-179. <https://doi.org/10.1093/abbs/gmz161>
- Gottesman, M. M., Fojo, T., & Bates, S. E. (2002). Multidrug resistance in cancer: role of ATP-dependent transporters. *Nat Rev Cancer*, *2*(1), 48-58. <https://doi.org/10.1038/nrc706>
- Gu, J., Zhang, C., Chen, R., Pan, J., Wang, Y., Ming, M., . . . Wang, D. (2009). Clinical implications and prognostic value of EMMPRIN/CD147 and MMP2 expression in pediatric gliomas. *Eur J Pediatr*, *168*(6), 705-710. <https://doi.org/10.1007/s00431-008-0828-5>
- Guay, D., Evoy, A. A., Paquet, E., Garand, C., Bachvarova, M., Bachvarov, D., & Lebel, M. (2008). The strand separation and nuclease activities associated with YB-1 are dispensable for cisplatin resistance but overexpression of YB-1 in MCF7 and MDA-MB-231 breast tumor cells generates several chemoresistance signatures. *Int J Biochem Cell Biol*, *40*(11), 2492-2507. <https://doi.org/10.1016/j.biocel.2008.04.011>
- Guay, D., Gaudreault, I., Massip, L., & Lebel, M. (2006). Formation of a nuclear complex containing the p53 tumor suppressor, YB-1, and the Werner syndrome gene product in cells treated with UV light. *Int J Biochem Cell Biol*, *38*(8), 1300-1313. <https://doi.org/10.1016/j.biocel.2006.01.008>
- Guryanov, S. G., Selivanova, O. M., Nikulin, A. D., Enin, G. A., Melnik, B. S., Kretov, D. A., . . . Ovchinnikov, L. P. (2012). Formation of amyloid-like fibrils by Y-box binding protein 1 (YB-1) is mediated by its cold shock domain and modulated by disordered terminal domains. *PLoS One*, *7*(5), e36969. <https://doi.org/10.1371/journal.pone.0036969>
- Hanahan, D., & Weinberg, R. A. (2011). Hallmarks of cancer: the next generation. *Cell*, *144*(5), 646-674. <https://doi.org/10.1016/j.cell.2011.02.013>
- Hann, S. R. (2014). MYC cofactors: molecular switches controlling diverse biological outcomes. *Cold Spring Harb Perspect Med*, *4*(9), a014399. <https://doi.org/10.1101/cshperspect.a014399>

- Harada, M., Kotake, Y., Ohhata, T., Kitagawa, K., Niida, H., Matsuura, S., . . . Kitagawa, M. (2014). YB-1 promotes transcription of cyclin D1 in human non-small-cell lung cancers. *Genes Cells*, 19(6), 504-516. <https://doi.org/10.1111/gtc.12150>
- Hartmann, W., Koch, A., Brune, H., Waha, A., Schüller, U., Dani, I., . . . Pietsch, T. (2005). Insulin-like growth factor II is involved in the proliferation control of medulloblastoma and its cerebellar precursor cells. *Am J Pathol*, 166(4), 1153-1162. [https://doi.org/10.1016/S0002-9440\(10\)62335-8](https://doi.org/10.1016/S0002-9440(10)62335-8)
- Hasegawa, S. L., Doetsch, P. W., Hamilton, K. K., Martin, A. M., Okenquist, S. A., Lenz, J., & Boss, J. M. (1991). DNA binding properties of YB-1 and dbpA: binding to double-stranded, single-stranded, and abasic site containing DNAs. *Nucleic Acids Res*, 19(18), 4915-4920. <https://doi.org/10.1093/nar/19.18.4915>
- He, Y., Huang, C., Cai, K., Liu, P., Chen, X., Xu, Y. I., . . . Wei, R. (2021). PRPF19 promotes tongue cancer growth and chemoradiotherapy resistance. *Acta Biochim Biophys Sin (Shanghai)*, 53(7), 893-902. <https://doi.org/10.1093/abbs/gmab059>
- Hicks, D., Rafiee, G., Schwalbe, E. C., Howell, C. I., Lindsey, J. C., Hill, R. M., . . . Clifford, S. C. (2021). The molecular landscape and associated clinical experience in infant medulloblastoma: prognostic significance of second-generation subtypes. *Neuropathol Appl Neurobiol*, 47(2), 236-250. <https://doi.org/10.1111/nan.12656>
- Hill, R. M., Kuijper, S., Lindsey, J. C., Petrie, K., Schwalbe, E. C., Barker, K., . . . Clifford, S. C. (2015). Combined MYC and P53 defects emerge at medulloblastoma relapse and define rapidly progressive, therapeutically targetable disease. *Cancer Cell*, 27(1), 72-84. <https://doi.org/10.1016/j.ccell.2014.11.002>
- Hill, R. M., Richardson, S., Schwalbe, E. C., Hicks, D., Lindsey, J. C., Crosier, S., . . . Clifford, S. C. (2020). Time, pattern, and outcome of medulloblastoma relapse and their association with tumour biology at diagnosis and therapy: a multicentre cohort study. *Lancet Child Adolesc Health*, 4(12), 865-874. [https://doi.org/10.1016/S2352-4642\(20\)30246-7](https://doi.org/10.1016/S2352-4642(20)30246-7)
- Hirano, G., Izumi H Fau - Yasuniwa, Y., Yasuniwa Y Fau - Shimajiri, S., Shimajiri S Fau - Ke-Yong, W., Ke-Yong W Fau - Sasagiri, Y., Sasagiri Y Fau - Kusaba, H., . . . Kohno, K. (2011). Involvement of riboflavin kinase expression in cellular sensitivity against cisplatin. *Int J Oncol*, 38(1791-2423), 893-902. <https://doi.org/10.3892/ijo.2011.938>
- Hodges, L. M., Markova, S. M., Chinn, L. W., Gow, J. M., Kroetz, D. L., Klein, T. E., & Altman, R. B. (2011). Very important pharmacogene summary: ABCB1 (MDR1, P-glycoprotein). *Pharmacogenet Genomics*, 21(3), 152-161. <https://doi.org/10.1097/FPC.0b013e3283385a1c>
- Holm, P. S., Bergmann, S., Jurchott, K., Lage, H., Brand, K., Ladhoff, A., . . . Royer, H. D. (2002). YB-1 relocates to the nucleus in adenovirus-infected cells and facilitates viral replication by inducing E2 gene expression through the E2 late promoter. *J Biol Chem*, 277(12), 10427-10434. <https://doi.org/10.1074/jbc.M106955200>
- Holzmüller, R., Mantwill, K., Haczek, C., Rognoni, E., Anton, M., Kasajima, A., . . . Holm, P. S. (2011). YB-1 dependent virotherapy in combination with temozolomide

- as a multimodal therapy approach to eradicate malignant glioma. *Int J Cancer*, 129(5), 1265-1276. <https://doi.org/10.1002/ijc.25783>
- Homer, C., Knight, D. A., Hananeia, L., Sheard, P., Risk, J., Lasham, A., . . . Braithwaite, A. W. (2005). Y-box factor YB1 controls p53 apoptotic function. *Oncogene*, 24(56), 8314-8325. <https://doi.org/10.1038/sj.onc.1208998>
- Huang, D., Liu, J., Eldridge, R. C., Gaul, D. A., Paine, M. R. L., Uppal, K., . . . Fernández, F. M. (2020). Lipidome signatures of metastasis in a transgenic mouse model of sonic hedgehog medulloblastoma. *Anal Bioanal Chem*, 412(25), 7017-7027. <https://doi.org/10.1007/s00216-020-02837-9>
- Hussein, D., Punjaruk, W., Storer, L. C., Shaw, L., Othman, R., Ottoman, R., . . . Coyle, B. (2011). Pediatric brain tumor cancer stem cells: cell cycle dynamics, DNA repair, and etoposide extrusion. *Neuro Oncol*, 13(1), 70-83. <https://doi.org/10.1093/neuonc/noq144>
- Hyogotani, A., Ito, K., Yoshida, K., Izumi, H., Kohno, K., & Amano, J. (2012). Association of nuclear YB-1 localization with lung resistance-related protein and epidermal growth factor receptor expression in lung cancer. *Clin Lung Cancer*, 13(5), 375-384. <https://doi.org/10.1016/j.clcc.2011.11.006>
- illumina. (2020). *How short inserts affect sequencing performance*. Retrieved 13/01/2022 from <https://emea.support.illumina.com/bulletins/2020/12/how-short-inserts-affect-sequencing-performance.html>
- Ise, T., Nagatani, G., Imamura, T., Kato, K., Takano, H., Nomoto, M., . . . Kohno, K. (1999). Transcription factor Y-box binding protein 1 binds preferentially to cisplatin-modified DNA and interacts with proliferating cell nuclear antigen. *Cancer Res*, 59(2), 342-346.
- Izumi, H., Imamura, T., Nagatani, G., Ise, T., Murakami, T., Uramoto, H., . . . Kohno, K. (2001). Y box-binding protein-1 binds preferentially to single-stranded nucleic acids and exhibits 3'→5' exonuclease activity. *Nucleic Acids Res*, 29(5), 1200-1207. <https://doi.org/10.1093/nar/29.5.1200>
- Jackson, D. V., Sethi, V. S., Spurr, C. L., & McWhorter, J. M. (1981). Pharmacokinetics of vincristine in the cerebrospinal fluid of humans. *Cancer Res*, 41(4), 1466-1468.
- Jacobsen, P. F., Jenkyn, D. J., & Papadimitriou, J. M. (1985). Establishment of a human medulloblastoma cell line and its heterotransplantation into nude mice. *J Neuropathol Exp Neurol*, 44(5), 472-485. <https://doi.org/10.1097/00005072-198509000-00003>
- Janz, M., Harbeck, N., Dettmar, P., Berger, U., Schmidt, A., Jürchott, K., . . . Royer, H.-D. (2002). Y-box factor YB-1 predicts drug resistance and patient outcome in breast cancer independent of clinically relevant tumor biologic factors HER2, uPA and PAI-1. *International Journal of Cancer*, 97(3), 278-282. <https://doi.org/10.1002/ijc.1610>
- Jeffords, E., Freeman, S., Cole, B., Root, K., Chekouo, T., Melvin, R. G., . . . Simmons, G. E. (2020). Y-box binding protein 1 acts as a negative regulator of stearoyl CoA desaturase 1 in clear cell renal cell carcinoma. *Oncol Lett*, 20(5), 165. <https://doi.org/10.3892/ol.2020.12026>

- Jia, R., & Wang, C. (2020). MiR-29b-3p Reverses Cisplatin Resistance by Targeting COL1A1 in Non-Small-Cell Lung Cancer A549/DDP Cells. *Cancer Manag Res*, 12, 2559-2566. <https://doi.org/10.2147/CMAR.S246625>
- Jiang, H., Lei, R., Ding, S. W., & Zhu, S. (2014). Skewer: a fast and accurate adapter trimmer for next-generation sequencing paired-end reads. *BMC Bioinformatics*, 15, 182. <https://doi.org/10.1186/1471-2105-15-182>
- Johnson, T. G., Schelch, K., Mehta, S., Burgess, A., & Reid, G. (2019). Why Be One Protein When You Can Affect Many? The Multiple Roles of YB-1 in Lung Cancer and Mesothelioma. *Front Cell Dev Biol*, 7, 221. <https://doi.org/10.3389/fcell.2019.00221>
- Jones, D. T., Jäger, N., Kool, M., Zichner, T., Hutter, B., Sultan, M., . . . Lichter, P. (2012). Dissecting the genomic complexity underlying medulloblastoma. *Nature*, 488(7409), 100-105. <https://doi.org/10.1038/nature11284>
- Juliano, R. L., & Ling, V. (1976). A surface glycoprotein modulating drug permeability in Chinese hamster ovary cell mutants. *Biochim Biophys Acta*, 455(1), 152-162. [https://doi.org/10.1016/0005-2736\(76\)90160-7](https://doi.org/10.1016/0005-2736(76)90160-7)
- Juraschka, K., & Taylor, M. D. (2019). Medulloblastoma in the age of molecular subgroups: a review. *J Neurosurg Pediatr*, 24(4), 353-363. <https://doi.org/10.3171/2019.5.PEDS18381>
- Jurchott, K., Bergmann, S., Stein, U., Walther, W., Janz, M., Manni, I., . . . Royer, H. D. (2003). YB-1 as a cell cycle-regulated transcription factor facilitating cyclin A and cyclin B1 gene expression. *J Biol Chem*, 278(30), 27988-27996. <https://doi.org/10.1074/jbc.M212966200>
- Kamura, T., Yahata, H., Amada, S., Ogawa, S., Sonoda, T., Kobayashi, H., . . . Nakano, H. (1999). Is nuclear expression of Y box-binding protein-1 a new prognostic factor in ovarian serous adenocarcinoma? *Cancer*, 85(11), 2450-2454. [https://doi.org/10.1002/\(sici\)1097-0142\(19990601\)85:11<2450::aid-cncr21>3.0.co;2-u](https://doi.org/10.1002/(sici)1097-0142(19990601)85:11<2450::aid-cncr21>3.0.co;2-u)
- Kariyawasam, D. S. M., T. (2015). Brain tumours in paediatrics: when should they be suspected? *Archives of Disease in Childhood*, 100(2), 1102-1103. <https://doi.org/10.1136/archdischild-2015-308729>
- Karlsson, J., Rui, Y., Kozielski, K. L., Placone, A. L., Choi, O., Tzeng, S. Y., . . . Green, J. J. (2019). Engineered nanoparticles for systemic siRNA delivery to malignant brain tumours. *Nanoscale*, 11(42), 20045-20057. <https://doi.org/10.1039/c9nr04795f>
- Ke, J., Gu, C., Zhang, H., Liu, Y., Zhang, W., Rao, H., . . . Wu, F. (2021). Nucleolin Promotes Cisplatin Resistance in Cervical Cancer by the YB1-MDR1 Pathway. *J Oncol*, 2021, 9992218. <https://doi.org/10.1155/2021/9992218>
- Keles, G. E., Berger, M. S., Srinivasan, J., Kolstoe, D. D., Bobola, M. S., & Silber, J. R. (1995). Establishment and characterization of four human medulloblastoma-derived cell lines. *Oncol Res*, 7(10-11), 493-503.
- Kelly, R. J., Robey, R. W., Chen, C. C., Draper, D., Luchenko, V., Barnett, D., . . . Bates, S. E. (2012). A pharmacodynamic study of the P-glycoprotein antagonist CBT-1® in combination with paclitaxel in solid tumors. *Oncologist*, 17(4), 512. <https://doi.org/10.1634/theoncologist.2012-0080>

- Khandelwal, P., Padala, M., Cox, J., & Guntaka, V. (2009). The N-Terminal Domain of Y-Box Binding Protein-1 Induces Cell Cycle Arrest in G2/M Phase by Binding to Cyclin D1. *Int J Cell Biol*. <https://doi.org/doi:10.1155/2009/243532>
- Kim, D., Langmead, B., & Salzberg, S. L. (2015). HISAT: a fast spliced aligner with low memory requirements. *Nat Methods*, 12(4), 357-360. <https://doi.org/10.1038/nmeth.3317>
- Kline, C. N., Joseph, N. M., Grenert, J. P., van Ziffle, J., Yeh, I., Bastian, B. C., . . . Solomon, D. A. (2016). Inactivating MUTYH germline mutations in pediatric patients with high-grade midline gliomas. *Neuro Oncol*, 18(5), 752-753. <https://doi.org/10.1093/neuonc/now013>
- Kloetgen, A., Duggimpudi, S., Schuschel, K., Hezaveh, K., Picard, D., Schaal, H., . . . Hoell, J. I. (2020). YBX1 Indirectly Targets Heterochromatin-Repressed Inflammatory Response-Related Apoptosis Genes through Regulating CBX5 mRNA. *Int J Mol Sci*, 21(12). <https://doi.org/10.3390/ijms21124453>
- Kloks, C. P., Spronk, C. A., Lasonder, E., Hoffmann, A., Vuister, G. W., Grzesiek, S., & Hilbers, C. W. (2002). The solution structure and DNA-binding properties of the cold-shock domain of the human Y-box protein YB-1. *J Mol Biol*, 316(2), 317-326. <https://doi.org/10.1006/jmbi.2001.5334>
- Koike, K., Uchiumi, T., Ohga, T., Toh, S., Wada, M., Kohno, K., & Kuwano, M. (1997). Nuclear translocation of the Y-box binding protein by ultraviolet irradiation. *FEBS Lett*, 417(3), 390-394. [https://doi.org/10.1016/s0014-5793\(97\)01296-9](https://doi.org/10.1016/s0014-5793(97)01296-9)
- Kolk, A., Jubitz, N., Mengele, K., Mantwill, K., Bissinger, O., Schmitt, M., . . . Holm, P. S. (2011). Expression of Y-box-binding protein YB-1 allows stratification into long- and short-term survivors of head and neck cancer patients. *Br J Cancer*, 105(12), 1864-1873. <https://doi.org/10.1038/bjc.2011.491>
- Kool, M., Jones, D. T., Jäger, N., Northcott, P. A., Pugh, T. J., Hovestadt, V., . . . Project, I. P. T. (2014). Genome sequencing of SHH medulloblastoma predicts genotype-related response to smoothed inhibition. *Cancer Cell*, 25(3), 393-405. <https://doi.org/10.1016/j.ccr.2014.02.004>
- Kool, M., Korshunov, A., Remke, M., Jones, D. T., Schlanstein, M., Northcott, P. A., . . . Pfister, S. M. (2012). Molecular subgroups of medulloblastoma: an international meta-analysis of transcriptome, genetic aberrations, and clinical data of WNT, SHH, Group 3, and Group 4 medulloblastomas. *Acta Neuropathol*, 123(4), 473-484. <https://doi.org/10.1007/s00401-012-0958-8>
- Kortmann, R. D., Kühl, J., Timmermann, B., Mittler, U., Urban, C., Budach, V., . . . Bamberg, M. (2000). Postoperative neoadjuvant chemotherapy before radiotherapy as compared to immediate radiotherapy followed by maintenance chemotherapy in the treatment of medulloblastoma in childhood: results of the German prospective randomized trial HIT '91. *Int J Radiat Oncol Biol Phys*, 46(2), 269-279. [https://doi.org/10.1016/s0360-3016\(99\)00369-7](https://doi.org/10.1016/s0360-3016(99)00369-7)
- Kotake, Y., Ozawa, Y., Harada, M., Kitagawa, K., Niida, H., Morita, Y., . . . Kitagawa, M. (2013). YB1 binds to and represses the p16 tumor suppressor gene. *Genes Cells*, 18(11), 999-1006. <https://doi.org/10.1111/gtc.12093>

- Kwon, E., Todorova, K., Wang, J., Horos, R., Lee, K. K., Neel, V. A., . . . Mandinova, A. (2018). The RNA-binding protein YBX1 regulates epidermal progenitors at a posttranscriptional level. *Nat Commun*, 9(1), 1734. <https://doi.org/10.1038/s41467-018-04092-0>
- Lasham, A., Mehta, S. Y., Fitzgerald, S. J., Woolley, A. G., Hearn, J. I., Hurley, D. G., . . . Print, C. G. (2016). A novel EGR-1 dependent mechanism for YB-1 modulation of paclitaxel response in a triple negative breast cancer cell line. *Int J Cancer*, 139(5), 1157-1170. <https://doi.org/10.1002/ijc.30137>
- Lasham, A., Moloney, S., Hale, T., Homer, C., Zhang, Y. F., Murison, J. G., . . . Watson, J. (2003). The Y-box-binding protein, YB1, is a potential negative regulator of the p53 tumor suppressor. *J Biol Chem*, 278(37), 35516-35523. <https://doi.org/10.1074/jbc.M303920200>
- Lasham, A., Print, C. G., Woolley, A. G., Dunn, S. E., & Braithwaite, A. W. (2013). YB-1: oncoprotein, prognostic marker and therapeutic target? *Biochem J*, 449(1), 11-23. <https://doi.org/10.1042/BJ20121323>
- Lasham, A., Samuel, W., Cao, H., Patel, R., Mehta, R., Stern, J. L., . . . Braithwaite, A. W. (2012). YB-1, the E2F pathway, and regulation of tumor cell growth. *J Natl Cancer Inst*, 104(2), 133-146. <https://doi.org/10.1093/jnci/djr512>
- Law, J. H., Li, Y., To, K., Wang, M., Astanehe, A., Lambie, K., . . . Dunn, S. E. (2010). Molecular decoy to the Y-box binding protein-1 suppresses the growth of breast and prostate cancer cells whilst sparing normal cell viability. *PLoS One*, 5(9). <https://doi.org/10.1371/journal.pone.0012661>
- Lee, C., Dhillon, J., Wang, M. Y., Gao, Y., Hu, K., Park, E., . . . Dunn, S. E. (2008). Targeting YB-1 in HER-2 overexpressing breast cancer cells induces apoptosis via the mTOR/STAT3 pathway and suppresses tumor growth in mice. *Cancer Res*, 68(21), 8661-8666. <https://doi.org/10.1158/0008-5472.CAN-08-1082>
- Lee, J., Hoxha, E., & Song, H. R. (2017). A novel NFIA-NFκB feed-forward loop contributes to glioblastoma cell survival. *Neuro Oncol*, 19(4), 524-534. <https://doi.org/10.1093/neuonc/now233>
- Leonard, G., Polgar, O., & Bates, S. (2002). ABC transporters and inhibitors: new targets, new agents. 3, 1652-1659.
- Leshchenko, V. V., Kuo, P. Y., Jiang, Z., Thirukonda, V. K., & Parekh, S. (2014). Integrative genomic analysis of temozolomide resistance in diffuse large B-cell lymphoma. *Clin Cancer Res*, 20(2), 382-392. <https://doi.org/10.1158/1078-0432.CCR-13-0669>
- Li, L., Liang, S., Wasylshen, A. R., Zhang, Y., Yang, X., Zhou, B., . . . Xiong, S. (2016). PLA2G16 promotes osteosarcoma metastasis and drug resistance via the MAPK pathway. *Oncotarget*, 7(14), 18021-18035. <https://doi.org/10.18632/oncotarget.7694>
- Li, L., Yang, Z., Hou, Y., & Chen, Z. (2020). Moving beyond the Cox proportional hazards model in survival data analysis: a cervical cancer study. *BMJ Open*, 10(7), e033965. <https://doi.org/10.1136/bmjopen-2019-033965>
- Li, M., Zhai, G., Gu, X., & Sun, K. (2018). ATF3 and PRAP1 play important roles in cisplatin-induced damages in microvascular endothelial cells. *Gene*, 672, 93-105. <https://doi.org/10.1016/j.gene.2018.06.017>

- Li, S., Zhao, Q., Wang, B., Yuan, S., Wang, X., & Li, K. (2018). Quercetin reversed MDR in breast cancer cells through down-regulating P-gp expression and eliminating cancer stem cells mediated by YB-1 nuclear translocation. *Phytother Res*, 32(8), 1530-1536. <https://doi.org/10.1002/ptr.6081>
- Liang, S., Ren, Z., Han, X., Yang, J., Shan, L., Li, L., . . . Wang, G. (2015). PLA2G16 Expression in Human Osteosarcoma Is Associated with Pulmonary Metastasis and Poor Prognosis. *PLoS One*, 10(5), e0127236. <https://doi.org/10.1371/journal.pone.0127236>
- Lim, J. P., Shyamasundar, S., Gunaratne, J., Scully, O. J., Matsumoto, K., & Bay, B. H. (2017). YBX1 gene silencing inhibits migratory and invasive potential via CORO1C in breast cancer in vitro. *BMC Cancer*, 17(1), 201. <https://doi.org/10.1186/s12885-017-3187-7>
- Lin, R., Li, X., Wu, S., Qian, S., Hou, H., Dong, M., . . . Zhang, M. (2021). Suppression of latent transforming growth factor- β (TGF- β)-binding protein 1 (LTBP1) inhibits natural killer/ T cell lymphoma progression by inactivating the TGF- β /Smad and p38. *Exp Cell Res*, 407(1), 112790. <https://doi.org/10.1016/j.yexcr.2021.112790>
- Lin, Y. T., Liu, Y. C., & Chao, C. C. (2016). Inhibition of JNK and prothymosin-alpha sensitizes hepatocellular carcinoma cells to cisplatin. *Biochem Pharmacol*, 122, 80-89. <https://doi.org/10.1016/j.bcp.2016.10.003>
- Lindsey, J. C., Schwalbe, E. C., Potluri, S., Bailey, S., Williamson, D., & Clifford, S. C. (2014). TERT promoter mutation and aberrant hypermethylation are associated with elevated expression in medulloblastoma and characterise the majority of non-infant SHH subgroup tumours. *Acta Neuropathol*, 127(2), 307-309. <https://doi.org/10.1007/s00401-013-1225-3>
- Linke, F., Aldighieri, M., Lourdasamy, A., Grabowska, A. M., Stolnik, S., Kerr, I. D., . . . Coyle, B. (2021). 3D hydrogels reveal medulloblastoma subgroup differences and identify extracellular matrix subtypes that predict patient outcome. *J Pathol*, 253(3), 326-338. <https://doi.org/10.1002/path.5591>
- List, A. F., Kopecky, K. J., Willman, C. L., Head, D. R., Persons, D. L., Slovak, M. L., . . . Appelbaum, F. R. (2001). Benefit of cyclosporine modulation of drug resistance in patients with poor-risk acute myeloid leukemia: a Southwest Oncology Group study. *Blood*, 98(12), 3212-3220. <https://doi.org/10.1182/blood.v98.12.3212>
- Liu, S., Marneth, A. E., Alexe, G., Walker, S. R., Gandler, H. I., Ye, D. Q., . . . Frank, D. A. (2018). The kinases IKBKE and TBK1 regulate MYC-dependent survival pathways through YB-1 in AML and are targets for therapy. *Blood Adv*, 2(23), 3428-3442. <https://doi.org/10.1182/bloodadvances.2018016733>
- Liu, X., Ma, W., Yan, Y., & Wu, S. (2017). Silencing HMGN5 suppresses cell growth and promotes chemosensitivity in esophageal squamous cell carcinoma. *J Biochem Mol Toxicol*, 31(12). <https://doi.org/10.1002/jbt.21996>
- Liu, Y. R., Liang, L., Zhao, J. M., Zhang, Y., Zhang, M., Zhong, W. L., . . . Yang, C. (2017). Twist1 confers multidrug resistance in colon cancer through upregulation of ATP-binding cassette transporters. *Oncotarget*, 8(32), 52901-52912. <https://doi.org/10.18632/oncotarget.17548>
- Louis, D. N., Ohgaki, H., Wiestler, O. D., Cavenee, W. K., Burger, P. C., Jouvett, A., . . . Kleihues, P. (2007). The 2007 WHO classification of tumours of the central

- nervous system. *Acta neuropathologica*, 114(2), 97-109. <https://doi.org/10.1007/s00401-007-0243-4>
- Louis, D. N., Perry, A., Reifenberger, G., von Deimling, A., Figarella-Branger, D., Cavenee, W. K., . . . Ellison, D. W. (2016). The 2016 World Health Organization Classification of Tumors of the Central Nervous System: a summary. *Acta Neuropathol*, 131(6), 803-820. <https://doi.org/10.1007/s00401-016-1545-1>
- Louis, D. N., Perry, A., Wesseling, P., Brat, D. J., Cree, I. A., Figarella-Branger, D., . . . Ellison, D. W. (2021). The 2021 WHO Classification of Tumors of the Central Nervous System: a summary. *Neuro Oncol*, 23(8), 1231-1251. <https://doi.org/10.1093/neuonc/noab106>
- Lovett, D. H., Cheng, S., Cape, L., Pollock, A. S., & Mertens, P. R. (2010). YB-1 alters MT1-MMP trafficking and stimulates MCF-7 breast tumor invasion and metastasis. *Biochem Biophys Res Commun*, 398(3), 482-488. <https://doi.org/10.1016/j.bbrc.2010.06.104>
- Low, S. Y. Y., Bte Syed Sulaiman, N., Tan, E. E. K., Ng, L. P., Kuick, C. H., Chang, K. T. E., . . . Seow, W. T. (2020). Cerebrospinal fluid cytokines in metastatic group 3 and 4 medulloblastoma. *BMC Cancer*, 20(1), 554. <https://doi.org/10.1186/s12885-020-07048-0>
- Lu, J., Li, X., Wang, F., Guo, Y., Huang, Y., Zhu, H., . . . Wang, Z. (2017). YB-1 expression promotes pancreatic cancer metastasis that is inhibited by microRNA-216a. *Exp Cell Res*, 359(2), 319-326. <https://doi.org/10.1016/j.yexcr.2017.07.039>
- Lu, Z. H., Books, J. T., & Ley, T. J. (2005). YB-1 is important for late-stage embryonic development, optimal cellular stress responses, and the prevention of premature senescence. *Mol Cell Biol*, 25(11), 4625-4637. <https://doi.org/10.1128/MCB.25.11.4625-4637.2005>
- Luo, J., Hu, Q., Gou, M., Liu, X., Qin, Y., Zhu, J., . . . Deng, H. (2021). Expression of Microtubule-Associated Proteins in Relation to Prognosis and Efficacy of Immunotherapy in Non-Small Cell Lung Cancer. *Front Oncol*, 11, 680402. <https://doi.org/10.3389/fonc.2021.680402>
- Luo, X., Teng, Q. X., Dong, J. Y., Yang, D. H., Wang, M., Dessie, W., . . . Chen, Z. S. (2020). Antimicrobial Peptide Reverses ABCB1-Mediated Chemotherapeutic Drug Resistance. *Front Pharmacol*, 11, 1208. <https://doi.org/10.3389/fphar.2020.01208>
- Lv, L., Cao, L., Hu, G., Shen, Q., & Wu, J. (2020). Methylation-Driven Genes Identified as Novel Prognostic Indicators for Thyroid Carcinoma. *Front Genet*, 11, 294. <https://doi.org/10.3389/fgene.2020.00294>
- Lyabin, D. N., Eliseeva, I. A., & Ovchinnikov, L. P. (2012). YB-1 synthesis is regulated by mTOR signaling pathway. *PLoS One*, 7(12), e52527. <https://doi.org/10.1371/journal.pone.0052527>
- Lyabin, D. N., Eliseeva, I. A., & Ovchinnikov, L. P. (2014). YB-1 protein: functions and regulation. *Wiley Interdiscip Rev RNA*, 5(1), 95-110. <https://doi.org/10.1002/wrna.1200>
- Ma, T., Hou, J., Zhou, Y., Chen, Y., Qiu, J., Wu, J., . . . Li, D. (2020). Dibutyl phthalate promotes juvenile Sertoli cell proliferation by decreasing the levels of the E3

- ubiquitin ligase Pellino 2. *Environ Health*, 19(1), 87. <https://doi.org/10.1186/s12940-020-00639-1>
- MacDonald, G. H., Itoh-Lindstrom, Y., & Ting, J. P. (1995). The transcriptional regulatory protein, YB-1, promotes single-stranded regions in the DRA promoter. *J Biol Chem*, 270(8), 3527-3533. <https://doi.org/10.1074/jbc.270.8.3527>
- Macpherson, P., Barone, F., Maga, G., Mazzei, F., Karran, P., & Bignami, M. (2005). 8-oxoguanine incorporation into DNA repeats in vitro and mismatch recognition by MutSalpha. *Nucleic Acids Res*, 33(16), 5094-5105. <https://doi.org/10.1093/nar/gki813>
- Malbari, F., & Lindsay, H. (2020). Genetics of Common Pediatric Brain Tumors. *Pediatr Neurol*, 104, 3-12. <https://doi.org/10.1016/j.pediatrneurol.2019.08.004>
- Malek, R., Matta, J., Taylor, N., Perry, M. E., & Mendrysa, S. M. (2011). The p53 inhibitor MDM2 facilitates Sonic Hedgehog-mediated tumorigenesis and influences cerebellar foliation. *PLoS One*, 6(3), e17884. <https://doi.org/10.1371/journal.pone.0017884>
- Mantwill, K., Naumann, U., Seznec, J., Girbinger, V., Lage, H., Surowiak, P., . . . Holm, P. S. (2013). YB-1 dependent oncolytic adenovirus efficiently inhibits tumor growth of glioma cancer stem like cells. *J Transl Med*, 11, 216. <https://doi.org/10.1186/1479-5876-11-216>
- Martínez-Vélez, N., Garcia-Moure, M., Marigil, M., González-Huarriz, M., Puigdelloses, M., Gallego Pérez-Larraya, J., . . . Alonso, M. M. (2019). The oncolytic virus Delta-24-RGD elicits an antitumor effect in pediatric glioma and DIPG mouse models. *Nat Commun*, 10(1), 2235. <https://doi.org/10.1038/s41467-019-10043-0>
- Mashouri, L., Yousefi, H., Aref, A. R., Ahadi, A. M., Molaei, F., & Alahari, S. K. (2019). Exosomes: composition, biogenesis, and mechanisms in cancer metastasis and drug resistance. *Mol Cancer*, 18(1), 75. <https://doi.org/10.1186/s12943-019-0991-5>
- Massimino, M., Biassoni, V., Gandola, L., Garrè, M. L., Gatta, G., Giangaspero, F., . . . Rutkowski, S. (2016). Childhood medulloblastoma. *Crit Rev Oncol Hematol*, 105, 35-51. <https://doi.org/10.1016/j.critrevonc.2016.05.012>
- McCauley, C., Anang, V., Cole, B., & Simmons, G. E. (2020). Potential Links between YB-1 and Fatty Acid Synthesis in Clear Cell Renal Carcinoma. *Med Res Arch*, 8(10). <https://doi.org/10.18103/mra.v8i10.2273>
- McDermott, M., Eustace, A. J., Busschots, S., Breen, L., Crown, J., Clynes, M., . . . Stordal, B. (2014). In vitro Development of Chemotherapy and Targeted Therapy Drug-Resistant Cancer Cell Lines: A Practical Guide with Case Studies. *Front Oncol*, 4, 40. <https://doi.org/10.3389/fonc.2014.00040>
- Mesquita, K. A., Ali, R., Doherty, R., Toss, M. S., Miligy, I., Alblihy, A., . . . Madhusudan, S. (2021). FEN1 Blockade for Platinum Chemo-Sensitization and Synthetic Lethality in Epithelial Ovarian Cancers. *Cancers (Basel)*, 13(8). <https://doi.org/10.3390/cancers13081866>
- Milde, T., Lodrini, M., Savelyeva, L., Korshunov, A., Kool, M., Brueckner, L. M., . . . Deubzer, H. E. (2012). HD-MB03 is a novel Group 3 medulloblastoma model demonstrating sensitivity to histone deacetylase inhibitor treatment. *J*

Neurooncol, 110(3), 335-348. <https://doi.org/10.1007/s11060-012-0978-1>

- Minderman, H., O'Loughlin, K. L., Pendyala, L., & Baer, M. R. (2004). VX-710 (biricodar) increases drug retention and enhances chemosensitivity in resistant cells overexpressing P-glycoprotein, multidrug resistance protein, and breast cancer resistance protein. *Clin Cancer Res*, 10(5), 1826-1834. <https://doi.org/10.1158/1078-0432.ccr-0914-3>
- Mingard, C., Wu, J., McKeague, M., & Sturla, S. J. (2020). Next-generation DNA damage sequencing. *Chem Soc Rev*, 49(20), 7354-7377. <https://doi.org/10.1039/d0cs00647e>
- Mo, J., Liu, F., Sun, X., Huang, H., Tan, K., Zhao, X., . . . Tang, Y. (2021). Inhibition of the FACT Complex Targets Aberrant Hedgehog Signaling and Overcomes Resistance to Smoothed Antagonists. *Cancer Res*, 81(11), 3105-3120. <https://doi.org/10.1158/0008-5472.CAN-20-3186>
- Moll, P., Ante, M., Seitz, A., & Reda, T. (2014). QuantSeq 3' mRNA sequencing for RNA quantification. *Nature Methods*, 11(12), i-iii. <https://doi.org/10.1038/nmeth.f.376>
- Mordovkina, D. A., Kim, E. R., Buldakov, I. A., Sorokin, A. V., Eliseeva, I. A., Lyabin, D. N., & Ovchinnikov, L. P. (2016). Transportin-1-dependent YB-1 nuclear import. *Biochem Biophys Res Commun*, 480(4), 629-634. <https://doi.org/10.1016/j.bbrc.2016.10.107>
- Motta, F. J., Valera, E. T., Lucio-Eterovic, A. K., Queiroz, R. G., Neder, L., Scrideli, C. A., . . . Tone, L. G. (2008). Differential expression of E-cadherin gene in human neuroepithelial tumors. *Genet Mol Res*, 7(2), 295-304. <https://doi.org/10.4238/vol7-2gmr424>
- Mundade, R., Ozer, H. G., Wei, H., Prabhu, L., & Lu, T. (2014). Role of ChIP-seq in the discovery of transcription factor binding sites, differential gene regulation mechanism, epigenetic marks and beyond. *Cell Cycle*, 13(18), 2847-2852. <https://doi.org/10.4161/15384101.2014.949201>
- Musa, A., Ghorai, L. S., Zhang, S. D., Glazko, G., Yli-Harja, O., Dehmer, M., . . . Emmert-Streib, F. (2018). A review of connectivity map and computational approaches in pharmacogenomics. *Brief Bioinform*, 19(3), 506-523. <https://doi.org/10.1093/bib/bbw112>
- Myung, J. K., Choi, S. A., Kim, S. K., Wang, K. C., & Park, S. H. (2014). Snail plays an oncogenic role in glioblastoma by promoting epithelial mesenchymal transition. *Int J Clin Exp Pathol*, 7(5), 1977-1987.
- Nagaki, K., Talbert, P. B., Zhong, C. X., Dawe, R. K., Henikoff, S., & Jiang, J. (2003). Chromatin immunoprecipitation reveals that the 180-bp satellite repeat is the key functional DNA element of Arabidopsis thaliana centromeres. *Genetics*, 163(3), 1221-1225.
- Nasir, A., Cardall, A., Othman, R. T., Nicolaou, N., Lourdasamy, A., Linke, F., . . . Coyle, B. (2021). ABCB1 inhibition provides a novel therapeutic target to block TWIST1-induced migration in medulloblastoma. *Neurooncol Adv*, 3(1), vdab030. <https://doi.org/10.1093/noainj/vdab030>
- National Cancer Intelligence Network. (2012). *National Registry of Childhood Tumours Progress Report*.

- Nazarenko, I., Kristiansen, G., Fonfara, S., Guenther, R., Gieseler, C., Kemmner, W., . . . Sers, C. (2006). H-REV107-1 stimulates growth in non-small cell lung carcinomas via the activation of mitogenic signaling. *Am J Pathol*, *169*(4), 1427-1439. <https://doi.org/10.2353/ajpath.2006.051341>
- NCRAS. (2018). Childhood Cancer Statistics, England Annual Report 2018. In.
- Neglia, J. P. a. R. L. L. a. S. M. a. L. Y. a. P. R. J. a. H. S. a. Y. Y. a. K. C. E. a. M. (2006). New Primary Neoplasms of the Central Nervous System in Survivors of Childhood Cancer: a Report From the Childhood Cancer Survivor Study. *JNCI: Journal of the National Cancer Institute*, *98*(21), 1528-1537. <https://doi.org/10.1093/jnci/djj411>
- Nobili, S., Lapucci, A., Landini, I., Coronello, M., Roviello, G., & Mini, E. (2020). Role of ATP-binding cassette transporters in cancer initiation and progression. *Seminars in Cancer Biology*, *60*(1096-3650 (Electronic)), 72-95.
- Northcott, P., Buchhalter, I., Morrissy, A. S., Hovestadt, V., Weischenfeldt, J., Ehrenberger, T., . . . Lichter, P. (2017). The whole-genome landscape of medulloblastoma subtypes. *Nature*, *547*(7663), 311-317. <https://doi.org/10.1038/nature22973>
- Northcott, P., Jones, D., Kool, M., Robinson, G., Gilbertson, R., Cho, Y., . . . Pfister, S. (2012). Medulloblastomics: the end of the beginning. *Nature Rev Can*, *12*(12), 818-834. <https://doi.org/10.1038/nrc3410>
- Northcott, P., Robinson, G. W., Kratz, C. P., Mabbott, D. J., Pomeroy, S. L., Clifford, S. C., . . . Pfister, S. M. (2019). Medulloblastoma. *Nat Rev Dis Primers*, *5*(1), 11. <https://doi.org/10.1038/s41572-019-0063-6>
- Northcott, P., Rutka, J. T., & Taylor, M. D. (2010). Genomics of medulloblastoma: from Giemsa-banding to next-generation sequencing in 20 years. *Neurosurg Focus*, *28*(1), E6. <https://doi.org/10.3171/2009.10.FOCUS09218>
- Northcott, P., Shih, D. J., Peacock, J., Garzia, L., Morrissy, A. S., Zichner, T., . . . Taylor, M. D. (2012). Subgroup-specific structural variation across 1,000 medulloblastoma genomes. *Nature*, *488*(7409), 49-56. <https://doi.org/10.1038/nature11327>
- Oba, T., Izumi, H., & Ito, K. I. (2016). ABCB1 and ABCC11 confer resistance to eribulin in breast cancer cell lines. *Oncotarget*, *7*(43), 70011-70027. <https://doi.org/10.18632/oncotarget.11727>
- Oda, Y., Ohishi, Y., Saito, T., Hinoshita, E., Uchiumi, T., Kinukawa, N., . . . Tsuneyoshi, M. (2003). Nuclear expression of Y-box-binding protein-1 correlates with P-glycoprotein and topoisomerase II alpha expression, and with poor prognosis in synovial sarcoma. *J Pathol*, *199*(2), 251-258. <https://doi.org/10.1002/path.1282>
- Oda, Y., Sakamoto, A., Shinohara, N., Ohga, T., Uchiumi, T., Kohno, K., . . . Iwamoto, Y. (1998). Nuclear expression of YB-1 protein correlates with P-glycoprotein expression in human osteosarcoma. *Clin Cancer Res*, *4*(9), 2273-2277.
- Ohga, T., Koike, K., Ono, M., Makino, Y., Itagaki, Y., Tanimoto, M., . . . Kohno, K. (1996). Role of the human Y box-binding protein YB-1 in cellular sensitivity to the DNA-damaging agents cisplatin, mitomycin C, and ultraviolet light. *Cancer Res*, *56*(18), 4224-4228.
- Ohga, T., Uchiumi, T., Makino, Y., Koike, K., Wada, M., Kuwano, M., & Kohno, K. (1998). Direct involvement of the Y-box binding protein YB-1 in genotoxic

- stress-induced activation of the human multidrug resistance 1 gene. *J Biol Chem*, 273(11), 5997-6000. <https://doi.org/10.1074/jbc.273.11.5997>
- Okamoto, T., Izumi, H., Imamura, T., Takano, H., Ise, T., Uchiumi, T., . . . Kohno, K. (2000). Direct interaction of p53 with the Y-box binding protein, YB-1: a mechanism for regulation of human gene expression. *Oncogene*, 19(54), 6194-6202. <https://doi.org/10.1038/sj.onc.1204029>
- Orr, B. A. (2020). Pathology, diagnostics, and classification of medulloblastoma. *Brain Pathol*, 30(3), 664-678. <https://doi.org/10.1111/bpa.12837>
- Othman, R. T., Kimishi, I., Bradshaw, T. D., Storer, L. C. D., Korshunov, A., Pfister, S. M., . . . Coyle, B. (2014). Overcoming multiple drug resistance mechanisms in medulloblastoma. *Acta neuropathologica communications*, 2, 57-57. <https://doi.org/10.1186/2051-5960-2-57>
- Ozen, O., Krebs, B., Hemmerlein, B., Pekrun, A., Kretschmar, H., & Herms, J. (2004). Expression of matrix metalloproteinases and their inhibitors in medulloblastomas and their prognostic relevance. *Clin Cancer Res*, 10(14), 4746-4753. <https://doi.org/10.1158/1078-0432.CCR-0625-03>
- Packer, R. J., Gajjar, A., Vezina, G., Rorke-Adams, L., Burger, P. C., Robertson, P. L., . . . Spoto, R. (2006). Phase III study of craniospinal radiation therapy followed by adjuvant chemotherapy for newly diagnosed average-risk medulloblastoma. *J Clin Oncol*, 24(25), 4202-4208. <https://doi.org/10.1200/JCO.2006.06.4980>
- Packer, R. J., Zhou, T., Holmes, E., Vezina, G., & Gajjar, A. (2013). Survival and secondary tumors in children with medulloblastoma receiving radiotherapy and adjuvant chemotherapy: results of Children's Oncology Group trial A9961. *Neuro Oncol*, 15(1), 97-103. <https://doi.org/10.1093/neuonc/nos267>
- Pajtler, K. W., Witt, H., Sill, M., Jones, D. T., Hovestadt, V., Kratochwil, F., . . . Pfister, S. M. (2015). Molecular Classification of Ependymal Tumors across All CNS Compartments, Histopathological Grades, and Age Groups. *Cancer Cell*, 27(5), 728-743. <https://doi.org/10.1016/j.ccell.2015.04.002>
- Pang, T., Li, M., Zhang, Y., Yong, W., Kang, H., Yao, Y., & Hu, X. (2017). Y Box-Binding Protein 1 Promotes Epithelial-Mesenchymal Transition, Invasion, and Metastasis of Cervical Cancer via Enhancing the Expressions of Snail. *Int J Gynecol Cancer*, 27(8), 1753-1760. <https://doi.org/10.1097/IGC.0000000000001066>
- Patutina, O. A., Mironova, N. L., Logashenko, E. B., Popova, N. A., Nikolin, V. P., Vasil'ev, G. V., . . . Vlasov, V. V. (2012). Cyclophosphamide metabolite inducing apoptosis in RLS mouse lymphosarcoma cells is a substrate for P-glycoprotein. *Bull Exp Biol Med*, 152(3), 348-352. <https://doi.org/10.1007/s10517-012-1525-y>
- Paugh, B. S., Qu, C., Jones, C., Liu, Z., Adamowicz-Brice, M., Zhang, J., . . . Baker, S. J. (2010). Integrated molecular genetic profiling of pediatric high-grade gliomas reveals key differences with the adult disease. *J Clin Oncol*, 28(18), 3061-3068. <https://doi.org/10.1200/JCO.2009.26.7252>
- PDQ® Pediatric Treatment Editorial Board. (2020). *PDQ Childhood Medulloblastoma and Other Central Nervous System Embryonal Tumors Treatment*. National Cancer Institute. .

- Pei, Y., Liu, K. W., Wang, J., Garancher, A., Tao, R., Esparza, L. A., . . . Wechsler-Reya, R. J. (2016). HDAC and PI3K Antagonists Cooperate to Inhibit Growth of MYC-Driven Medulloblastoma. *Cancer Cell*, 29(3), 311-323. <https://doi.org/10.1016/j.ccell.2016.02.011>
- Perron, G., Jandaghi, P., Solanki, S., Safisamghabadi, M., Storoz, C., Karimzadeh, M., . . . Riazalhosseini, Y. (2018). A General Framework for Interrogation of mRNA Stability Programs Identifies RNA-Binding Proteins that Govern Cancer Transcriptomes. *Cell Rep*, 23(6), 1639-1650. <https://doi.org/10.1016/j.celrep.2018.04.031>
- Phillips, H. S., Kharbanda, S., Chen, R., Forrest, W. F., Soriano, R. H., Wu, T. D., . . . Aldape, K. (2006). Molecular subclasses of high-grade glioma predict prognosis, delineate a pattern of disease progression, and resemble stages in neurogenesis. *Cancer Cell*, 9(3), 157-173. <https://doi.org/10.1016/j.ccr.2006.02.019>
- Phoenix, T. N., Patmore, D. M., Boop, S., Boulos, N., Jacus, M. O., Patel, Y. T., . . . Gilbertson, R. J. (2016). Medulloblastoma Genotype Dictates Blood Brain Barrier Phenotype. *Cancer Cell*, 29(4), 508-522. <https://doi.org/10.1016/j.ccell.2016.03.002>
- Piao, J., You, K., Guo, Y., Zhang, Y., Li, Z., & Geng, L. (2017). Substrate stiffness affects epithelial-mesenchymal transition of cervical cancer cells through miR-106b and its target protein DAB2. *Int J Oncol*, 50(6), 2033-2042. <https://doi.org/10.3892/ijo.2017.3978>
- Pillozzi, S., D'Amico, M., Bartoli, G., Gasparoli, L., Petroni, G., Crociani, O., . . . Arcangeli, A. (2018). The combined activation of K. *Br J Cancer*, 118(2), 200-212. <https://doi.org/10.1038/bjc.2017.392>
- Pizer, B. L., & Clifford, S. C. (2009). The potential impact of tumour biology on improved clinical practice for medulloblastoma: progress towards biologically driven clinical trials. *Br J Neurosurg*, 23(4), 364-375. <https://doi.org/10.1080/02688690903121807>
- Pizzagalli, M. D., Bensimon, A., & Superti-Furga, G. (2021). A guide to plasma membrane solute carrier proteins. *FEBS J*, 288(9), 2784-2835. <https://doi.org/10.1111/febs.15531>
- Prabhu, L., Hartley, A. V., Martin, M., Warsame, F., Sun, E., & Lu, T. (2015). Role of post-translational modification of the Y box binding protein 1 in human cancers. *Genes Dis*, 2(3), 240-246. <https://doi.org/10.1016/j.gendis.2015.05.001>
- Public Health England. (2018). *Childhood Cancer Statistics, England Annual report 2018*.
- Puliyappadamba, V. T., Chakraborty, S., Chauncey, S. S., Li, L., Hatanpaa, K. J., Mickey, B., . . . Habib, A. A. (2013). Opposing effect of EGFRWT on EGFRvIII-mediated NF-κB activation with RIP1 as a cell death switch. *Cell Rep*, 4(4), 764-775. <https://doi.org/10.1016/j.celrep.2013.07.025>
- Puliyappadamba, V. T., Hatanpaa, K. J., Chakraborty, S., & Habib, A. A. (2014). The role of NF-κB in the pathogenesis of glioma. *Mol Cell Oncol*, 1(3), e963478. <https://doi.org/10.4161/23723548.2014.963478>
- Qi, S., Song, Y., Peng, Y., Wang, H., Long, H., Yu, X., . . . Fang, W. (2012). ZEB2 mediates multiple pathways regulating cell proliferation, migration, invasion, and

- apoptosis in glioma. *PLoS One*, 7(6), e38842. <https://doi.org/10.1371/journal.pone.0038842>
- Qiagen. (2016). *IPA Training: Maximizing the Biological Interpretation of Gene, Transcript & Protein Expression Data with IPA*. Retrieved 01/11/2021 from <https://www.stat.purdue.edu/bigtap/docs/IPA%20training.pdf>
- Qu, X. A., & Rajpal, D. K. (2012). Applications of Connectivity Map in drug discovery and development. *Drug Discov Today*, 17(23-24), 1289-1298. <https://doi.org/10.1016/j.drudis.2012.07.017>
- Quandt, K., Frech, K., Karas, H., Wingender, E., & Werner, T. (1995). MatInd and MatInspector: new fast and versatile tools for detection of consensus matches in nucleotide sequence data. *Nucleic Acids Res*, 23(23), 4878-4884. <https://doi.org/10.1093/nar/23.23.4878>
- Raffetseder, U., Frye, B., Rauen, T., Jürchott, K., Royer, H. D., Jansen, P. L., & Mertens, P. R. (2003). Splicing factor SRp30c interaction with Y-box protein-1 confers nuclear YB-1 shuttling and alternative splice site selection. *J Biol Chem*, 278(20), 18241-18248. <https://doi.org/10.1074/jbc.M212518200>
- Ramaswamy, V., Remke, M., Bouffet, E., Bailey, S., Clifford, S. C., Doz, F., . . . Pomeroy, S. L. (2016). Risk stratification of childhood medulloblastoma in the molecular era: the current consensus. *Acta Neuropathol*, 131(6), 821-831. <https://doi.org/10.1007/s00401-016-1569-6>
- Rao, V. S., Srinivas, K., Sujini, G. N., & Kumar, G. N. (2014). Protein-protein interaction detection: methods and analysis. *Int J Proteomics*, 2014, 147648. <https://doi.org/10.1155/2014/147648>
- Remke, M., Ramaswamy, V., Peacock, J., Shih, D. J., Koelsche, C., Northcott, P. A., . . . Taylor, M. D. (2013). TERT promoter mutations are highly recurrent in SHH subgroup medulloblastoma. *Acta Neuropathol*, 126(6), 917-929. <https://doi.org/10.1007/s00401-013-1198-2>
- Richardson, S., Hill, R. M., Kui, C., Lindsey, J. C., Grabovksa, Y., Keeling, C., . . . Clifford, S. C. (2021). Emergence and maintenance of actionable genetic drivers at medulloblastoma relapse. *Neuro Oncol*. <https://doi.org/10.1093/neuonc/noab178>
- Robey, R. W., Pluchino, K. M., Hall, M. D., Fojo, A. T., Bates, S. E., & Gottesman, M. M. (2018). Revisiting the role of ABC transporters in multidrug-resistant cancer. *Nat Rev Cancer*, 18(7), 452-464. <https://doi.org/10.1038/s41568-018-0005-8>
- Robinson, G. W., Rudneva, V. A., Buchhalter, I., Billups, C. A., Waszak, S. M., Smith, K. S., . . . Northcott, P. A. (2018). Risk-adapted therapy for young children with medulloblastoma (SJYC07): therapeutic and molecular outcomes from a multicentre, phase 2 trial. *Lancet Oncol*, 19(6), 768-784. [https://doi.org/10.1016/S1470-2045\(18\)30204-3](https://doi.org/10.1016/S1470-2045(18)30204-3)
- Robinson, M. D., & Oshlack, A. (2010). A scaling normalization method for differential expression analysis of RNA-seq data. *Genome Biol*, 11(3), R25. <https://doi.org/10.1186/gb-2010-11-3-r25>

- Robinson, M. D., & Smyth, G. K. (2008). Small-sample estimation of negative binomial dispersion, with applications to SAGE data. *Biostatistics*, *9*(2), 321-332. <https://doi.org/10.1093/biostatistics/kxm030>
- Rocha, C. R. R., Silva, M. M., Quinet, A., Cabral-Neto, J. B., & Menck, C. F. M. (2018). DNA repair pathways and cisplatin resistance: an intimate relationship. *Clinics (Sao Paulo)*, *73*(suppl 1), e478s. <https://doi.org/10.6061/clinics/2018/e478s>
- Rodrigo, M. A. M., Buchtelova, H., Jimenez, A. M. J., Adam, P., Babula, P., Heger, Z., & Adam, V. (2019). Transcriptomic Landscape of Cisplatin-Resistant Neuroblastoma Cells. *Cells*, *8*(3). <https://doi.org/10.3390/cells8030235>
- Rojo de la Vega, M., Chapman, E., & Zhang, D. D. (2018). NRF2 and the Hallmarks of Cancer. *Cancer Cell*, *34*(1), 21-43. <https://doi.org/10.1016/j.ccell.2018.03.022>
- Roper, S. J., Linke, F., Scotting, P. J., & Coyle, B. (2021). 3D spheroid models of paediatric SHH medulloblastoma mimic tumour biology, drug response and metastatic dissemination. *Sci Rep*, *11*(1), 4259. <https://doi.org/10.1038/s41598-021-83809-6>
- Roth, R. B., Hevezi, P., Lee, J., Willhite, D., Lechner, S. M., Foster, A. C., & Zlotnik, A. (2006). Gene expression analyses reveal molecular relationships among 20 regions of the human CNS. *Neurogenetics*, *7*(2), 67-80. <https://doi.org/10.1007/s10048-006-0032-6>
- Russo, M. T., De Luca, G., Degan, P., & Bignami, M. (2007). Different DNA repair strategies to combat the threat from 8-oxoguanine. *Mutat Res*, *614*(1-2), 69-76. <https://doi.org/10.1016/j.mrfmmm.2006.03.007>
- Ruzanov, P. V., Evdokimova, V. M., Korneeva, N. L., Hershey, J. W., & Ovchinnikov, L. P. (1999). Interaction of the universal mRNA-binding protein, p50, with actin: a possible link between mRNA and microfilaments. *J Cell Sci*, *112* (Pt 20), 3487-3496.
- Sabnis, D. H., Storer, L. C. D., Liu, J. F., Jackson, H. K., Kilday, J. P., Grundy, R. G., . . . Coyle, B. (2019). A role for ABCB1 in prognosis, invasion and drug resistance in ependymoma. *Sci Rep*, *9*(1), 10290. <https://doi.org/10.1038/s41598-019-46700-z>
- Safaei, R., Larson, B. J., Cheng, T. C., Gibson, M. A., Otani, S., Naerdemann, W., & Howell, S. B. (2005). Abnormal lysosomal trafficking and enhanced exosomal export of cisplatin in drug-resistant human ovarian carcinoma cells. *Mol Cancer Ther*, *4*(10), 1595-1604. <https://doi.org/10.1158/1535-7163.MCT-05-0102>
- Saga, Y., Ohwada, M., Suzuki, M., Konno, R., Kigawa, J., Ueno, S., & Mano, H. (2008). Glutathione peroxidase 3 is a candidate mechanism of anticancer drug resistance of ovarian clear cell adenocarcinoma. *Oncol Rep*, *20*(6), 1299-1303.
- Saji, H., Toi, M., Saji, S., Koike, M., Kohno, K., & Kuwano, M. (2003). Nuclear expression of YB-1 protein correlates with P-glycoprotein expression in human breast carcinoma. *Cancer Lett*, *190*(2), 191-197. [https://doi.org/10.1016/s0304-3835\(02\)00590-6](https://doi.org/10.1016/s0304-3835(02)00590-6)
- Samuel, P., Mulcahy, L. A., Furlong, F., McCarthy, H. O., Brooks, S. A., Fabbri, M., . . . Carter, D. R. F. (2018). Cisplatin induces the release of extracellular vesicles

- from ovarian cancer cells that can induce invasiveness and drug resistance in bystander cells. *Philos Trans R Soc Lond B Biol Sci*, 373(1737). <https://doi.org/10.1098/rstb.2017.0065>
- Samuels, A. L., Beesley, A. H., Yadav, B. D., Papa, R. A., Sutton, R., Anderson, D., . . . Lock, R. B. (2014). A pre-clinical model of resistance to induction therapy in pediatric acute lymphoblastic leukemia. *Blood Cancer J*, 4, e232. <https://doi.org/10.1038/bcj.2014.52>
- Sasaki, T., Fässler, R., & Hohenester, E. (2004). Laminin: the crux of basement membrane assembly. *J Cell Biol*, 164(7), 959-963. <https://doi.org/10.1083/jcb.200401058>
- Saxton, R. A., & Sabatini, D. M. (2017). mTOR Signaling in Growth, Metabolism, and Disease. *Cell*, 168(6), 960-976. <https://doi.org/10.1016/j.cell.2017.02.004>
- Saygin, C., Wiechert, A., Rao, V. S., Alluri, R., Connor, E., Thiagarajan, P. S., Hale, J. S., Li, Y., Chumakova, A., Jarrar, A., Parker, Y., Lindner, D. J., Nagaraj, A. B., Kim, J. J., DiFeo, A., Abdul-Karim, F. W., Michener, C., Rose, P. G., DeBernardo, R., Mahdi, H., ... Reizes, O. (2017). CD55 regulates self-renewal and cisplatin resistance in endometrioid tumors. *The Journal of experimental medicine*, 214(9), 2715–2732. <https://doi.org/10.1084/jem.20170438>
- Schinkel, A. H. (1999). P-Glycoprotein, a gatekeeper in the blood-brain barrier. *Adv Drug Deliv Rev*, 36(2-3), 179-194. [https://doi.org/10.1016/s0169-409x\(98\)00085-4](https://doi.org/10.1016/s0169-409x(98)00085-4)
- Schittek, B., Psenner, K., Sauer, B., Meier, F., Iftner, T., & Garbe, C. (2007). The increased expression of Y box-binding protein 1 in melanoma stimulates proliferation and tumor invasion, antagonizes apoptosis and enhances chemoresistance. *Int J Cancer*, 120(10), 2110-2118. <https://doi.org/10.1002/ijc.22512>
- Schwalbe, E. C., Lindsey, J. C., Nakjang, S., Crosier, S., Smith, A. J., Hicks, D., . . . Clifford, S. C. (2017). Novel molecular subgroups for clinical classification and outcome prediction in childhood medulloblastoma: a cohort study. *Lancet Oncol*, 18(7), 958-971. [https://doi.org/10.1016/S1470-2045\(17\)30243-7](https://doi.org/10.1016/S1470-2045(17)30243-7)
- Scuto, A., Kirschbaum, M., Buettner, R., Kujawski, M., Cermak, J. M., Atadja, P., & Jove, R. (2013). SIRT1 activation enhances HDAC inhibition-mediated upregulation of GADD45G by repressing the binding of NF-κB/STAT3 complex to its promoter in malignant lymphoid cells. *Cell Death Dis*, 4, e635. <https://doi.org/10.1038/cddis.2013.159>
- Sechi, M., Lall, R. K., Afolabi, S. O., Singh, A., Joshi, D. C., Chiu, S. Y., . . . Syed, D. N. (2018). Fisetin targets YB-1/RSK axis independent of its effect on ERK signaling: insights from in vitro and in vivo melanoma models. *Sci Rep*, 8(1), 15726. <https://doi.org/10.1038/s41598-018-33879-w>
- Seo, J. H., Chae, Y. C., Kossenkov, A. V., Lee, Y. G., Tang, H. Y., Agarwal, E., . . . Altieri, D. C. (2019). MFF Regulation of Mitochondrial Cell Death Is a Therapeutic Target in Cancer. *Cancer Res*, 79(24), 6215-6226. <https://doi.org/10.1158/0008-5472.CAN-19-1982>
- Shanmugavadivel, D., Liu, J. F., Murphy, L., Wilne, S., Walker, D., & HeadSmart. (2020). Accelerating diagnosis for childhood brain tumours: an analysis of the HeadSmart UK population data. *Arch Dis Child*, 105(4), 355-362. <https://doi.org/10.1136/archdischild-2018-315962>

- Sharma, T., Schwalbe, E. C., Williamson, D., Sill, M., Hovestadt, V., Mynarek, M., . . . Clifford, S. C. (2019). Second-generation molecular subgrouping of medulloblastoma: an international meta-analysis of Group 3 and Group 4 subtypes. *Acta Neuropathol*, 138(2), 309-326. <https://doi.org/10.1007/s00401-019-02020-0>
- Shen, H., Xu, W., Luo, W., Zhou, L., Yong, W., Chen, F., . . . Han, X. (2011). Upregulation of *mdr1* gene is related to activation of the MAPK/ERK signal transduction pathway and YB-1 nuclear translocation in B-cell lymphoma. *Exp Hematol*, 39(5), 558-569. <https://doi.org/10.1016/j.exphem.2011.01.013>
- Shi, Z., Tiwari, A. K., Patel, A. S., Fu, L. W., & Chen, Z. S. (2011). Roles of sildenafil in enhancing drug sensitivity in cancer. *Cancer Res*, 71(11), 3735-3738. <https://doi.org/10.1158/0008-5472.CAN-11-0375>
- Shibahara, K., Sugio, K., Osaki, T., Uchiyama, T., Maehara, Y., Kohno, K., . . . Kuwano, K. (2001). Nuclear Expression of the Y-Box Binding Protein, YB-1, as a Novel Marker of Disease Progression in Non-Small Cell Lung Cancer. *Clin Cancer Res*, 7(10), 3151-3155.
- Shibao, K., Takano, H., Nakayama, Y., Okazaki, K., Nagata, N., Izumi, H., . . . Itoh, H. (1999). Enhanced coexpression of YB-1 and DNA topoisomerase II α genes in human colorectal carcinomas. *Int J Cancer*, 83(6), 732.
- Shih, D. J. H., Northcott, P., Remke, M., Korshunov, A., Ramaswamy, V., Kool, M., . . . Garzia, L. a. P. J. a. M. S. C. a. W. X. a. R. A. a. M. A. S. a. C. F. M. G. a. J. D. T. (2014). Cytogenetic Prognostication Within Medulloblastoma Subgroups. *Journal of Clinical Oncology*, 32(9), 886-896. <https://doi.org/10.1200/JCO.2013.50.9539>
- Shiota, M., Izumi, H., Onitsuka, T., Miyamoto, N., Kashiwagi, E., Kidani, A., . . . Kohno, K. (2008). Twist promotes tumor cell growth through YB-1 expression. *Cancer Res*, 68(1), 98-105. <https://doi.org/10.1158/0008-5472.CAN-07-2981>
- Shiota, M., Izumi, H., Tanimoto, A., Takahashi, M., Miyamoto, N., Kashiwagi, E., . . . Kohno, K. (2009). Programmed cell death protein 4 down-regulates Y-box binding protein-1 expression via a direct interaction with Twist1 to suppress cancer cell growth. *Cancer Res*, 69(7), 3148-3156. <https://doi.org/10.1158/0008-5472.CAN-08-2334>
- Shiota, M., Yokomizo, A., Tada, Y., Uchiyama, T., Inokuchi, J., Tatsugami, K., . . . Naito, S. (2010). P300/CBP-associated factor regulates Y-box binding protein-1 expression and promotes cancer cell growth, cancer invasion and drug resistance. *Cancer Sci*, 101(8), 1797-1806. <https://doi.org/10.1111/j.1349-7006.2010.01598.x>
- Skabkin, M. A., Kiselyova, O. I., Chernov, K. G., Sorokin, A. V., Dubrovin, E. V., Yaminsky, I. V., . . . Ovchinnikov, L. P. (2004). Structural organization of mRNA complexes with major core mRNP protein YB-1. *Nucleic Acids Res*, 32(18), 5621-5635. <https://doi.org/10.1093/nar/gkh889>
- Skabkina, O., Skabkin, M., Popova, N., Lyabin, D., Penalva, L., & Ovchinnikov, L. (2003). Poly(A)-binding protein positively affects YB-1 mRNA translation through specific interaction with YB-1 mRNA. *J Biol Chem*, 278, 18191-18198.
- Skabkina, O. V., Lyabin, D. N., Skabkin, M. A., & Ovchinnikov, L. P. (2005). YB-1 autoregulates translation of its own mRNA at or prior to the step of 40S

- ribosomal subunit joining. *Mol Cell Biol*, 25(8), 3317-3323. <https://doi.org/10.1128/MCB.25.8.3317-3323.2005>
- Smolinski, M. P., Uргаonkar, S., Pitzonka, L., Cutler, M., Lee, G., Suh, K. H., & Lau, J. Y. N. (2021). Discovery of Encequidar, First-in-Class Intestine Specific P-glycoprotein Inhibitor. *J Med Chem*, 64(7), 3677-3693. <https://doi.org/10.1021/acs.jmedchem.0c01826>
- Sorokin, A., Selyutina, A., Skabkin, M., Guryanov, S., Nazimov, I., Richard, C., . . . Evdokimova, V. (2005). Proteasome-mediated cleavage of the Y-box-binding protein 1 is linked to DNA-damage stress response. *EMBO J*, 24(20), 3602-3612.
- Spiller, S. E., Logsdon, N. J., Deckard, L. A., & Sontheimer, H. (2011). Inhibition of nuclear factor kappa-B signaling reduces growth in medulloblastoma in vivo. *BMC Cancer*, 11, 136. <https://doi.org/10.1186/1471-2407-11-136>
- Sreenivasan, L., Wang, H., Yap, S. Q., Leclair, P., Tam, A., & Lim, C. J. (2020). Autocrine IL-6/STAT3 signaling aids development of acquired drug resistance in Group 3 medulloblastoma. *Cell Death Dis*, 11(12), 1035. <https://doi.org/10.1038/s41419-020-03241-y>
- Stein, U., Jurchott, K., Walther, W., Bergmann, S., Schlag, P., & Royer, H. (2001). Hyperthermia-induced nuclear translocation of transcription factor YB-1 leads to enhanced expression of multidrug resistance-related ABC transporters. *J Biol Chem*, 276, 28562–28569
- Stratford, A., Fry, C., Desilets, C., Davies, A., Cho, Y., Li, Y., . . . Dunn, S. (2008). Y-box binding protein-1 serine 102 is a downstream target of p90 ribosomal S6 kinase in basal-like breast cancer cells. *Breast Cancer Res*, 10, 99.
- Stratford, A. L., Habibi, G., Astanehe, A., Jiang, H., Hu, K., Park, E., . . . Dunn, S. E. (2007). Epidermal growth factor receptor (EGFR) is transcriptionally induced by the Y-box binding protein-1 (YB-1) and can be inhibited with Iressa in basal-like breast cancer, providing a potential target for therapy. *Breast Cancer Res*, 9(5), R61. <https://doi.org/10.1186/bcr1767>
- Sun, S., Cai, J., Yang, Q., Zhu, Y., Zhao, S., & Wang, Z. (2016). Prognostic Value and Implication for Chemotherapy Treatment of ABCB1 in Epithelial Ovarian Cancer: A Meta-Analysis. *PLoS One*, 11(11), e0166058. <https://doi.org/10.1371/journal.pone.0166058>
- Sun, X., Chen, Y., Zhao, H., Qiao, G., Liu, M., Zhang, C., . . . Ma, L. (2018). Dual-modified cationic liposomes loaded with paclitaxel and survivin siRNA for targeted imaging and therapy of cancer stem cells in brain glioma. *Drug Deliv*, 25(1), 1718-1727. <https://doi.org/10.1080/10717544.2018.1494225>
- Sung, T., Miller, D. C., Hayes, R. L., Alonso, M., Yee, H., & Newcomb, E. W. (2000). Preferential inactivation of the p53 tumor suppressor pathway and lack of EGFR amplification distinguish de novo high grade pediatric astrocytomas from de novo adult astrocytomas. *Brain Pathol*, 10(2), 249-259. <https://doi.org/10.1111/j.1750-3639.2000.tb00258.x>
- Susa, M., Iyer, A. K., Ryu, K., Choy, E., Hornicek, F. J., Mankin, H., . . . Duan, Z. (2010). Inhibition of ABCB1 (MDR1) expression by an siRNA nanoparticulate delivery system to overcome drug resistance in osteosarcoma. *PLoS One*, 5(5), e10764. <https://doi.org/10.1371/journal.pone.0010764>

- Susanto, E., Marin Navarro, A., Zhou, L., Sundström, A., van Bree, N., Stantic, M., . . . Wilhelm, M. (2020). Modeling SHH-driven medulloblastoma with patient iPSC cell-derived neural stem cells. *Proc Natl Acad Sci U S A*, *117*(33), 20127-20138. <https://doi.org/10.1073/pnas.1920521117>
- Sutherland, B. W., Kucab, J., Wu, J., Lee, C., Cheang, M. C., Yorida, E., . . . Dunn, S. E. (2005). Akt phosphorylates the Y-box binding protein 1 at Ser102 located in the cold shock domain and affects the anchorage-independent growth of breast cancer cells. *Oncogene*, *24*(26), 4281-4292. <https://doi.org/10.1038/sj.onc.1208590>
- Syed, N., Chavan, S., Sahasrabudde, N. A., Renuse, S., Sathe, G., Nanjappa, V., . . . Chatterjee, A. (2015). Silencing of high-mobility group box 2 (HMGB2) modulates cisplatin and 5-fluorouracil sensitivity in head and neck squamous cell carcinoma. *Proteomics*, *15*(2-3), 383-393. <https://doi.org/10.1002/pmic.201400338>
- Szakacs, G., Paterson, J. K., Ludwig, J. A., Booth-Genthe, C., & Gottesman, M. (2006). Targeting multidrug resistance in cancer. *Nat Rev Drug Discov*, *5*, 219-234.
- Tanabe, Y., Nagatoishi, S., & Tsumoto, K. (2015). Thermodynamic characterization of the interaction between the human Y-box binding protein YB-1 and nucleic acids. *Mol Biosyst*, *11*(9), 2441-2448. <https://doi.org/10.1039/c5mb00184f>
- Tanaka, T., Saito, H., Miyairi, S., & Kobayashi, S. (2021). 7-Hydroxyindirubin is capable of specifically inhibiting anticancer drug-induced YB-1 nuclear translocation without showing cytotoxicity in HepG2 hepatocellular carcinoma cells. *Biochem Biophys Res Commun*, *544*, 15-21. <https://doi.org/10.1016/j.bbrc.2021.01.048>
- Tang, D., Wu, Q., Zhang, J., Zhang, H., Yuan, Z., Xu, J., . . . Wang, D. (2018). Galectin-1 expression in activated pancreatic satellite cells promotes fibrosis in chronic pancreatitis/pancreatic cancer via the TGF- β 1/Smad pathway. *Oncol Rep*, *39*(3), 1347-1355. <https://doi.org/10.3892/or.2018.6202>
- Tang, Z., He, J., Zou, J., Yu, S., Sun, X., & Qin, L. (2021). Cisplatin-resistant HepG2 cell-derived exosomes transfer cisplatin resistance to cisplatin-sensitive cells in HCC. *PeerJ*, *9*, e11200. <https://doi.org/10.7717/peerj.11200>
- Tao, R., Murad, N., Xu, Z., Zhang, P., Okonechnikov, K., Kool, M., . . . Pei, Y. (2019). Drives Group 3 Medulloblastoma through Transformation of Sox2. *Cancer Res*, *79*(8), 1967-1980. <https://doi.org/10.1158/0008-5472.CAN-18-1787>
- Tao, Z., Zhang, Y., Zhu, S., Ni, Z., You, Q., Sun, X., & Xu, D. (2019). Knockdown of PDRG1 Could Inhibit the Wnt Signaling Pathway in Esophageal Cancer Cells. *Ann Clin Lab Sci*, *49*(6), 794-803.
- Taylor, L., Kerr, I. D., & Coyle, B. (2021). Y-Box Binding Protein-1: A Neglected Target in Pediatric Brain Tumors? *Mol Cancer Res*, *19*(3), 375-387. <https://doi.org/10.1158/1541-7786.MCR-20-0655>
- Taylor, M. D., Northcott, P. A., Korshunov, A., Remke, M., Cho, Y. J., Clifford, S. C., . . . Pfister, S. M. (2012). Molecular subgroups of medulloblastoma: the current consensus. *Acta Neuropathol*, *123*(4), 465-472. <https://doi.org/10.1007/s00401-011-0922-z>

- Taylor, R. E., Bailey Cc Fau - Robinson, K., Robinson K Fau - Weston, C. L., Weston Cl Fau - Ellison, D., Ellison D Fau - Ironside, J., Ironside J Fau - Lucraft, H., . . . Lashford, L. S. (2003). Results of a randomized study of preradiation chemotherapy versus radiotherapy alone for nonmetastatic medulloblastoma: The International Society of Paediatric Oncology/United Kingdom Children's Cancer Study Group PNET-3 Study. (0732-183X).
- Theodoulou, F. L., & Kerr, I. D. (2015). ABC transporter research: going strong 40 years on. *Biochem Soc Trans*, 43(5), 1033-1040. <https://doi.org/10.1042/BST20150139>
- Thompson, E. M., Ashley, D., & Landi, D. (2020). Current medulloblastoma subgroup specific clinical trials. *Transl Pediatr*, 9(2), 157-162. <https://doi.org/10.21037/tp.2020.03.03>
- Thompson, E. M., Hielscher, T., Bouffet, E., Remke, M., Luu, B., Gururangan, S., . . . Taylor, M. D. (2016). Prognostic value of medulloblastoma extent of resection after accounting for molecular subgroup: a retrospective integrated clinical and molecular analysis. *Lancet Oncol*, 17(4), 484-495. [https://doi.org/10.1016/S1470-2045\(15\)00581-1](https://doi.org/10.1016/S1470-2045(15)00581-1)
- Tiwari, A., Rebholz, S., Maier, E., Dehghan Harati, M., Zips, D., Sers, C., . . . Toulany, M. (2018). Stress-Induced Phosphorylation of Nuclear YB-1 Depends on Nuclear Trafficking of p90 Ribosomal S6 Kinase. *Int J Mol Sci*, 19(8). <https://doi.org/10.3390/ijms19082441>
- To, K., Fotovati, A., Reipas, K. M., Law, J. H., Hu, K., Wang, J., . . . Dunn, S. E. (2010). Y-box binding protein-1 induces the expression of CD44 and CD49f leading to enhanced self-renewal, mammosphere growth, and drug resistance. *Cancer Res*, 70(7), 2840-2851. <https://doi.org/10.1158/0008-5472.CAN-09-3155>
- Tong, H., Zhao, K., Zhang, J., Zhu, J., & Xiao, J. (2019). YB-1 modulates the drug resistance of glioma cells by activation of MDM2/p53 pathway. *Drug Des Devel Ther*, 13, 317-326. <https://doi.org/10.2147/DDDT.S185514>
- Triller, N., Korosec, P., Kern, I., Kosnik, M., & Debeljak, A. (2006). Multidrug resistance in small cell lung cancer: expression of P-glycoprotein, multidrug resistance protein 1 and lung resistance protein in chemo-naive patients and in relapsed disease. *Lung Cancer*, 54(2), 235-240. <https://doi.org/10.1016/j.lungcan.2006.06.019>
- Tritschler, I., Gramatzki, D., Capper, D., Mittelbronn, M., Meyermann, R., Saharinen, J., . . . Weller, M. (2009). Modulation of TGF-beta activity by latent TGF-beta-binding protein 1 in human malignant glioma cells. *Int J Cancer*, 125(3), 530-540. <https://doi.org/10.1002/ijc.24443>
- Uhlén, M., Fagerberg, L., Hallström, B. M., Lindskog, C., Oksvold, P., Mardinoglu, A., . . . Pontén, F. (2015). Proteomics. Tissue-based map of the human proteome. *Science*, 347(6220), 1260419. <https://doi.org/10.1126/science.1260419>
- Uramoto, H., Izumi, H., Ise, T., Tada, M., Uchiumi, T., Kuwano, M., . . . Kohno, K. (2002). p73 Interacts with c-Myc to regulate Y-box-binding protein-1 expression. *J Biol Chem*, 277(35), 31694-31702. <https://doi.org/10.1074/jbc.M200266200>
- van den Boogaard, M. L., Oka, R., Hakkert, A., Schild, L., Ebus, M. E., van Gerven, M. R., . . . Molenaar, J. J. (2021). Defects in 8-oxo-guanine repair pathway cause high frequency of C > A substitutions in neuroblastoma. *Proc Natl Acad Sci U S A*, 118(36). <https://doi.org/10.1073/pnas.2007898118>

- Van Ommeren, R., Garzia, L., Holgado, B. L., Ramaswamy, V., & Taylor, M. D. (2020). The molecular biology of medulloblastoma metastasis. *Brain Pathol*, 30(3), 691-702. <https://doi.org/10.1111/bpa.12811>
- van Roeyen, C. R., Scurt, F. G., Brandt, S., Kuhl, V. A., Martinkus, S., Djudjaj, S., . . . Mertens, P. R. (2013). Cold shock Y-box protein-1 proteolysis autoregulates its transcriptional activities. *Cell Commun Signal*, 11, 63. <https://doi.org/10.1186/1478-811X-11-63>
- Vermeulen, M., Mulder, K. W., Denissov, S., Pijnappel, W. W., van Schaik, F. M., Varier, R. A., . . . Timmers, H. T. (2007). Selective anchoring of TFIIID to nucleosomes by trimethylation of histone H3 lysine 4. *Cell*, 131(1), 58-69. <https://doi.org/10.1016/j.cell.2007.08.016>
- Vince, G. H., Herbold, C., Klein, R., Kühl, J., Pietsch, T., Franz, S., . . . Tonn, J. C. (2001). Medulloblastoma displays distinct regional matrix metalloprotease expression. *J Neurooncol*, 53(2), 99-106. <https://doi.org/10.1023/a:1012241031138>
- von Bueren, A. O., Bacolod, M. D., Hagel, C., Heinemann, K., Fedier, A., Kordes, U., . . . Rutkowski, S. (2012). Mismatch repair deficiency: a temozolomide resistance factor in medulloblastoma cell lines that is uncommon in primary medulloblastoma tumours. *Br J Cancer*, 107(8), 1399-1408. <https://doi.org/10.1038/bjc.2012.403>
- Wang, F., Zhou, F., Kruh, G. D., & Gallo, J. M. (2010). Influence of blood-brain barrier efflux pumps on the distribution of vincristine in brain and brain tumors. *Neuro Oncol*, 12(10), 1043-1049. <https://doi.org/10.1093/neuonc/noq056>
- Wang, H., Sun, R., Chi, Z., Li, S., & Hao, L. (2017). Silencing of Y-box binding protein-1 by RNA interference inhibits proliferation, invasion, and metastasis, and enhances sensitivity to cisplatin through NF- κ B signaling pathway in human neuroblastoma SH-SY5Y cells. *Molecular and Cellular Biochemistry*, 433(1-2), 1-12. <https://doi.org/https://doi.org/10.1007/s11010-017-3011-3>
- Wang, H., Zhang, W., Huang, H. J., Liao, W. S., & Fuller, G. N. (2004). Analysis of the activation status of Akt, NF κ B, and Stat3 in human diffuse gliomas. *Lab Invest*, 84(8), 941-951. <https://doi.org/10.1038/labinvest.3700123>
- Wang, L., Zhu, N., Jia, J., Gu, L., Du, Y., Tang, G., . . . Yuan, W. (2021). Trimethylamine N-oxide mediated Y-box binding protein-1 nuclear translocation promotes cell cycle progression by directly downregulating Gadd45a expression in a cellular model of chronic kidney disease. *Life Sci*, 271, 119173. <https://doi.org/10.1016/j.lfs.2021.119173>
- Wang, X., Campos, C. R., Peart, J. C., Smith, L. K., Boni, J. L., Cannon, R. E., & Miller, D. S. (2014). Nrf2 Upregulates ATP Binding Cassette Transporter Expression and Activity at the Blood–Brain and Blood–Spinal Cord Barriers. *The Journal of Neuroscience*, 34(25), 8585. <https://doi.org/10.1523/JNEUROSCI.2935-13.2014>
- Wang, X., Dubuc, A. M., Ramaswamy, V., Mack, S., Gendoo, D. M., Remke, M., . . . Taylor, M. D. (2015). Medulloblastoma subgroups remain stable across primary and metastatic compartments. *Acta Neuropathol*, 129(3), 449-457. <https://doi.org/10.1007/s00401-015-1389-0>

- Wang, X., Guo, X. B., Shen, X. C., Zhou, H., Wan, D. W., Xue, X. F., . . . Kuang, Y. T. (2015). Prognostic role of YB-1 expression in breast cancer: a meta-analysis. *Int J Clin Exp Med*, *8*(2), 1780-1791.
- Wang, Y., Chen, Y., Geng, H., Qi, C., Liu, Y., & Yue, D. (2015). Overexpression of YB1 and EZH2 are associated with cancer metastasis and poor prognosis in renal cell carcinomas. *Tumour Biol*, *36*(9), 7159-7166. <https://doi.org/10.1007/s13277-015-3417-z>
- Ward, E., DeSantis, C., Robbins, A., Kohler, B., & Jemal, A. (2014). Childhood and adolescent cancer statistics. *CA: A Cancer Journal for Clinicians*, *64*(2), 83-103. <https://doi.org/10.3322/caac.21219>
- Waszak, S., Northcott, P., Buchhalter, I., Robinson, G., Sutter, C., Groebner, S., & et al. (2018). Spectrum and prevalence of genetic predisposition in medulloblastoma: a retrospective genetic study and prospective validation in a clinical trial cohort. *The Lancet Oncology*, *19*(6), 785-798. [https://doi.org/https://doi.org/10.1016/S1470-2045\(18\)30242-0](https://doi.org/https://doi.org/10.1016/S1470-2045(18)30242-0)
- Watanabe, S., Hayashi, K., Toh, K., Kim, H. J., Liu, X., Chaya, H., . . . Kataoka, K. (2019). In vivo rendezvous of small nucleic acid drugs with charge-matched block cationomers to target cancers. *Nat Commun*, *10*(1), 1894. <https://doi.org/10.1038/s41467-019-09856-w>
- Wei, N., Song, Y., Zhang, F., Sun, Z., & Zhang, X. (2020). Transcriptome Profiling of Acquired Gefitinib Resistant Lung Cancer Cells Reveals Dramatically Changed Transcription Programs and New Treatment Targets. *Front Oncol*, *10*, 1424. <https://doi.org/10.3389/fonc.2020.01424>
- Weinberg, R. (2014). *The Biology of Cancer* (Second ed.). Garland Science, Taylor & Francis Group, LLC.
- Weinberger, P., Ponny, S. R., Xu, H., Bai, S., Smallridge, R., Copland, J., & Sharma, A. (2017). Cell Cycle M-Phase Genes Are Highly Upregulated in Anaplastic Thyroid Carcinoma. *Thyroid*, *27*(2), 236-252. <https://doi.org/10.1089/thy.2016.0285>
- Wilne, S., Collier, J., Kennedy, C., Koller, K., Grundy, R., & Walker, D. (2007). Presentation of childhood CNS tumours: a systematic review and meta-analysis. *The Lancet Oncology*, *8*(8), 685 - 695. [https://doi.org/https://doi.org/10.1016/S1470-2045\(07\)70207-3](https://doi.org/https://doi.org/10.1016/S1470-2045(07)70207-3)
- Woolley, A. G., Algie, M., Samuel, W., Harfoot, R., Wiles, A., Hung, N. A., . . . Braithwaite, A. W. (2011). Prognostic association of YB-1 expression in breast cancers: a matter of antibody. *PLoS One*, *6*(6), e20603. <https://doi.org/10.1371/journal.pone.0020603>
- Wu, T., Wang, M. C., Jing, L., Liu, Z. Y., Guo, H., Liu, Y., . . . Liang, X. (2015). Autophagy facilitates lung adenocarcinoma resistance to cisplatin treatment by activation of AMPK/mTOR signaling pathway. *Drug Des Devel Ther*, *9*, 6421-6431. <https://doi.org/10.2147/DDDT.S95606>
- Wu, X., Northcott, P. A., Dubuc, A., Dupuy, A. J., Shih, D. J., Witt, H., . . . Taylor, M. D. (2012). Clonal selection drives genetic divergence of metastatic medulloblastoma. *Nature*, *482*(7386), 529-533. <https://doi.org/10.1038/nature10825>

- Xia, W., Bai, H., Deng, Y., & Yang, Y. (2020). PLA2G16 is a mutant p53/KLF5 transcriptional target and promotes glycolysis of pancreatic cancer. *J Cell Mol Med*, 24(21), 12642-12655. <https://doi.org/10.1111/jcmm.15832>
- Xu, D., Ye, D., Fisher, M., & Juliano, R. L. (2002). Selective inhibition of P-glycoprotein expression in multidrug-resistant tumor cells by a designed transcriptional regulator. *J Pharmacol Exp Ther*, 302(3), 963-971. <https://doi.org/10.1124/jpet.102.033639>
- Xu, J., & Hu, Z. (2016). Y-box-binding protein 1 promotes tumor progression and inhibits cisplatin chemosensitivity in esophageal squamous cell carcinoma. *Biomed Pharmacother*, 79, 17-22. <https://doi.org/10.1016/j.biopha.2016.01.037>
- Xu, J., Margol, A. S., Shukla, A., Ren, X., Finlay, J. L., Krieger, M. D., . . . Erdreich-Epstein, A. (2015). Disseminated Medulloblastoma in a Child with Germline BRCA2 6174delT Mutation and without Fanconi Anemia. *Front Oncol*, 5, 191. <https://doi.org/10.3389/fonc.2015.00191>
- Xu, L., Nirwane, A., & Yao, Y. (2019). Basement membrane and blood-brain barrier. *Stroke Vasc Neurol*, 4(2), 78-82. <https://doi.org/10.1136/svn-2018-000198>
- Xu, W., Zhou, B., Zhao, X., Zhu, L., Xu, J., Jiang, Z., . . . Jin, H. (2018). KDM5B demethylates H3K4 to recruit XRCC1 and promote chemoresistance. *Int J Biol Sci*, 14(9), 1122-1132. <https://doi.org/10.7150/ijbs.25881>
- Yamada, M., Shimizu, K., Tamura, K., Okamoto, Y., Matsui, Y., Moriuchi, S., . . . Hayakawa, T. (1989). [Establishment and biological characterization of human medulloblastoma cell lines]. *No To Shinkei*, 41(7), 695-702.
- Yan, X., Wu, H. H., Chen, Z., Du, G. W., Bai, X. J., Tuoheti, K., & Liu, T. Z. (2021). Construction and Validation of an Autophagy-Related Prognostic Signature and a Nomogram for Bladder Cancer. *Front Oncol*, 11, 632387. <https://doi.org/10.3389/fonc.2021.632387>
- Yan-Fang, T., Zhi-Heng, L., Li-Xiao, X., Fang, F., Jun, L., Gang, L., . . . Jian, P. (2015). Molecular Mechanism of the Cell Death Induced by the Histone Deacetylase Pan Inhibitor LBH589 (Panobinostat) in Wilms Tumor Cells. *PLoS One*, 10(7), e0126566. <https://doi.org/10.1371/journal.pone.0126566>
- Yang, X. J., Zhu, H., Mu, S. R., Wei, W. J., Yuan, X., Wang, M., . . . Huang, Y. (2019). Crystal structure of a Y-box binding protein 1 (YB-1)-RNA complex reveals key features and residues interacting with RNA. *J Biol Chem*, 294(28), 10998-11010. <https://doi.org/10.1074/jbc.RA119.007545>
- Yeo, K. K., Margol, A. S., Kennedy, R. J., Hung, L., Robison, N. J., Dhall, G., & Asgharzadeh, S. (2019). Prognostic significance of molecular subgroups of medulloblastoma in young children receiving irradiation-sparing regimens. *J Neurooncol*, 145(2), 375-383. <https://doi.org/10.1007/s11060-019-03307-8>
- Yokoyama, H., Harigae, H., Takahashi, S., Furuyama, K., Kaku, M., Yamamoto, M., & Sasaki, T. (2003). Regulation of YB-1 gene expression by GATA transcription factors. *Biochem Biophys Res Commun*, 303(1), 140-145. [https://doi.org/10.1016/s0006-291x\(03\)00296-1](https://doi.org/10.1016/s0006-291x(03)00296-1)

- Young, M. D., Wakefield, M. J., Smyth, G. K., & Oshlack, A. (2010). Gene ontology analysis for RNA-seq: accounting for selection bias. *Genome Biol*, *11*(2), R14. <https://doi.org/10.1186/gb-2010-11-2-r14>
- Yu, C. P., Kuo, C. H., Nelson, C. W., Chen, C. A., Soh, Z. T., Lin, J. J., . . . Li, W. H. (2021). Discovering unknown human and mouse transcription factor binding sites and their characteristics from ChIP-seq data. *Proc Natl Acad Sci U S A*, *118*(20). <https://doi.org/10.1073/pnas.2026754118>
- Yu, M., Ozaki, T., Sun, D., Xing, H., Wei, B., An, J., . . . Zhu, Y. (2020). HIF-1 α -dependent miR-424 induction confers cisplatin resistance on bladder cancer cells through down-regulation of pro-apoptotic UNC5B and SIRT4. *J Exp Clin Cancer Res*, *39*(1), 108. <https://doi.org/10.1186/s13046-020-01613-y>
- Yu, X., Wang, M., Zuo, J., Wahafu, A., Mao, P., Li, R., . . . Wang, J. (2019). Nuclear factor I A promotes temozolomide resistance in glioblastoma via activation of nuclear factor κ B pathway. *Life Sci*, *236*, 116917. <https://doi.org/10.1016/j.lfs.2019.116917>
- Yuan, L., Zhang, H., Liu, J., Malhotra, A., Dey, A., Yu, B., . . . MacDonald, T. J. (2021). STAT3 is required for Smo-dependent signaling and mediates Smo-targeted treatment resistance and tumorigenesis in Shh medulloblastoma. *Mol Oncol*. <https://doi.org/10.1002/1878-0261.13097>
- Zapotocky, M., Mata-Mbemba, D., Sumerauer, D., Liby, P., Lassaletta, A., Zamecnik, J., . . . Ramaswamy, V. (2018). Differential patterns of metastatic dissemination across medulloblastoma subgroups. *J Neurosurg Pediatr*, *21*(2), 145-152. <https://doi.org/10.3171/2017.8.PEDS17264>
- Zhang, H., Wang, Y., Guan, L., Chen, Y., Chen, P., Sun, J., . . . Bi, H. (2021). Lipidomics reveals carnitine palmitoyltransferase 1C protects cancer cells from lipotoxicity and senescence. *J Pharm Anal*, *11*(3), 340-350. <https://doi.org/10.1016/j.jpha.2020.04.004>
- Zhang, Y., Liu, T., Meyer, C. A., Eeckhoutte, J., Johnson, D. S., Bernstein, B. E., . . . Liu, X. S. (2008). Model-based analysis of ChIP-Seq (MACS). *Genome Biol*, *9*(9), R137. <https://doi.org/10.1186/gb-2008-9-9-r137>
- Zheng, J., Dong, W., Zhang, J., Li, G., & Gong, H. (2016). YB-1, a new biomarker of glioma progression, is associated with the prognosis of glioma patients. *Acta Biochim Biophys Sin (Shanghai)*, *48*(4), 318-325. <https://doi.org/10.1093/abbs/gmw012>
- Zhou, D., Chen, B., Ye, J. J., & Chen, S. (2004). A novel crosstalk mechanism between nuclear receptor-mediated and growth factor/Ras-mediated pathways through PNC-Grb2 interaction. *Oncogene*, *23*(31), 5394-5404. <https://doi.org/10.1038/sj.onc.1207695>
- Zhu, L. J., Gazin, C., Lawson, N. D., Pagès, H., Lin, S. M., Lapointe, D. S., & Green, M. R. (2010). ChIPpeakAnno: a Bioconductor package to annotate ChIP-seq and ChIP-chip data. *BMC Bioinformatics*, *11*, 237. <https://doi.org/10.1186/1471-2105-11-237>
- Zhu, Y., Liu, C., Nadiminty, N., Lou, W., Tummala, R., Evans, C. P., & Gao, A. C. (2013). Inhibition of ABCB1 expression overcomes acquired docetaxel resistance in prostate cancer. *Mol Cancer Ther*, *12*(9), 1829-1836. <https://doi.org/10.1158/1535-7163.MCT-13-0208>

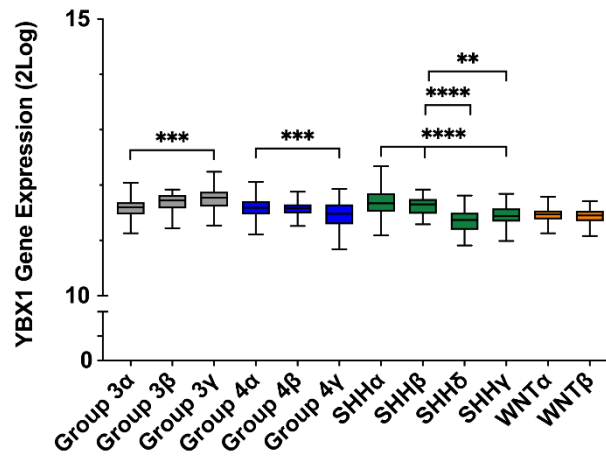
Zhukova, N., Ramaswamy, V., Remke, M., Pfaff, E., Shih, D. J., Martin, D. C., . . . Tabori, U. (2013). Subgroup-specific prognostic implications of TP53 mutation in medulloblastoma. *J Clin Oncol*, 31(23), 2927-2935. <https://doi.org/10.1200/JCO.2012.48.5052>

Appendix

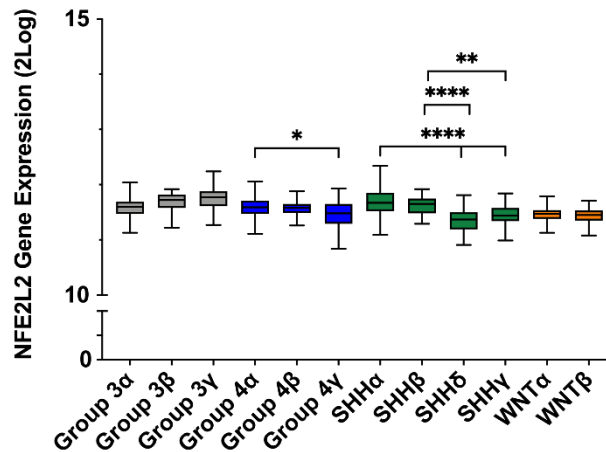
Appendix A: Chapter 3 – The identification and characterisation of a potential regulator of *ABCB1* in medulloblastoma.

Appendix A1

A

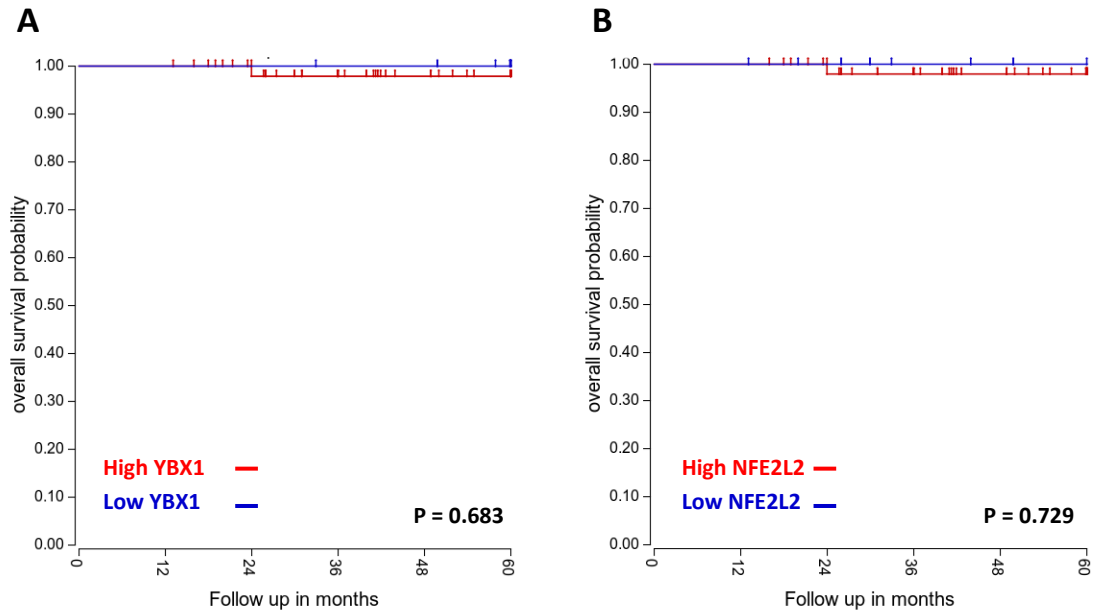


B



Appendix A1. *YBX1* and *NFE2L2* across medulloblastoma subtypes. A) *YBX1* expression across medulloblastoma subtypes, as assessed by R2 Genomic Analysis. B) *NFE2L2* expression across medulloblastoma subtypes, as assessed by R2 Genomic Analysis. Group 3α n = 67, Group 3β n = 37, Group 3γ n = 40, Group 4α n = 98, Group 4β n = 109, Group 4γ n = 119, SHHα n = 65, SHHβ n = 35, SHHδ n = 76, SHHy n = 47, WNTα n = 49 and WNTβ n = 21 (Cavalli dataset). Expression displayed as box plots showing the sample minimum (lower line), lower quartile (bottom of box), median (line within box), upper quartile (top of box) and the sample maximum (upper line). *P < 0.05; **P < 0.01, ***P < 0.001, ****P < 0.0001. Significance was assessed by One-Way ANOVA analyses with Tukey's multiple comparison test.

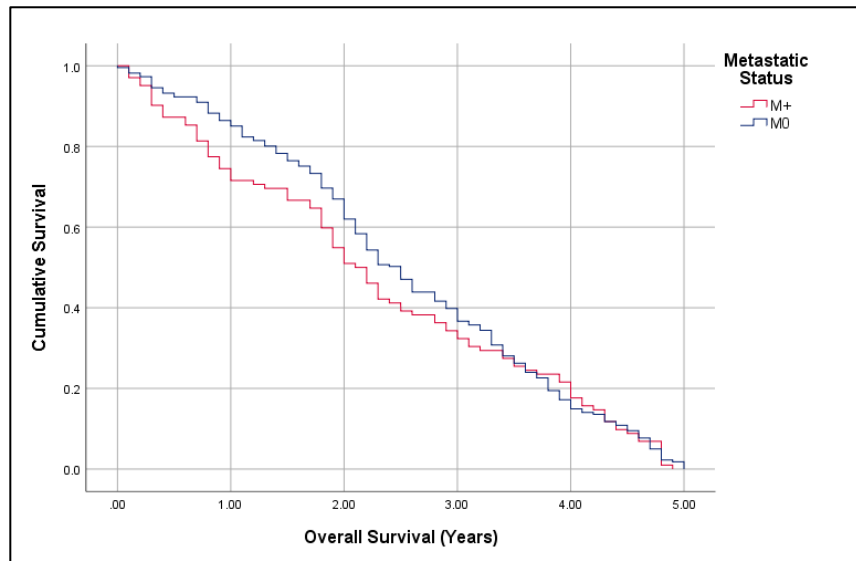
Appendix A2



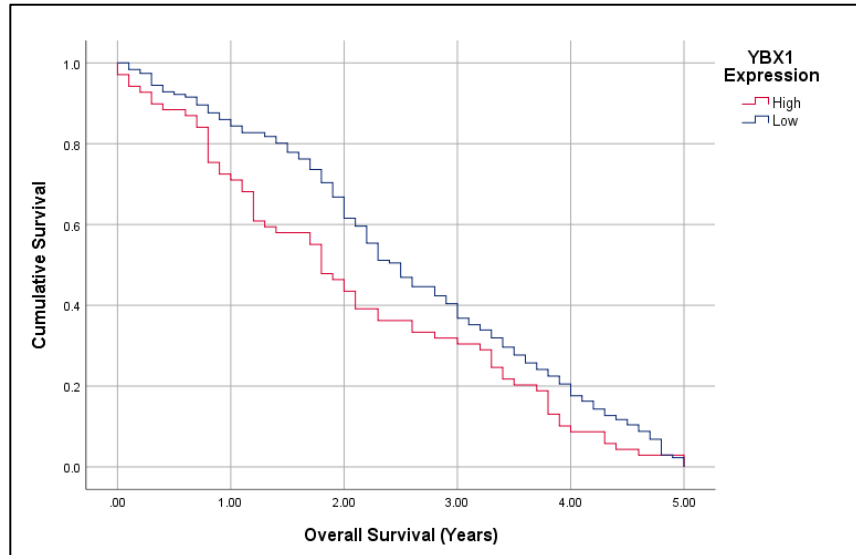
Appendix A2. *YBX1* and *NFE2L2* expression does not correlate with survival outcomes in WNT medulloblastoma. R2 genomics analysis was employed to explore correlation between *YBX1/NFE2L2* expression and survival in WNT subgroup medulloblastoma. A) Kaplan Meier analysis showed no association between *YBX1* expression and 5 year overall survival probability in patients with WNT medulloblastoma ($P = 0.683$). B) No association was also found between *NFE2L2* expression and 5 year overall survival probability in patients with WNT medulloblastoma ($P = 0.729$). $N = 70$ (Cavalli dataset). Survival curves compared using the Log-rank (Mantel-Cox) test.

Appendix A3

A



B



Appendix A3. Kaplan-Meier survival analysis demonstrates association between *YBX1* expression and survival. Kaplan Meier curves were used to analyse the associated of various parameters with clinical outcomes. A) Metastasis was not found to be significantly associated with 5-year survival, $P = 0.42$. B) *YBX1* expression was found to correlate significantly with poor overall 5-year survival, $P = 0.017$). Association was assessed using the log-rank test.

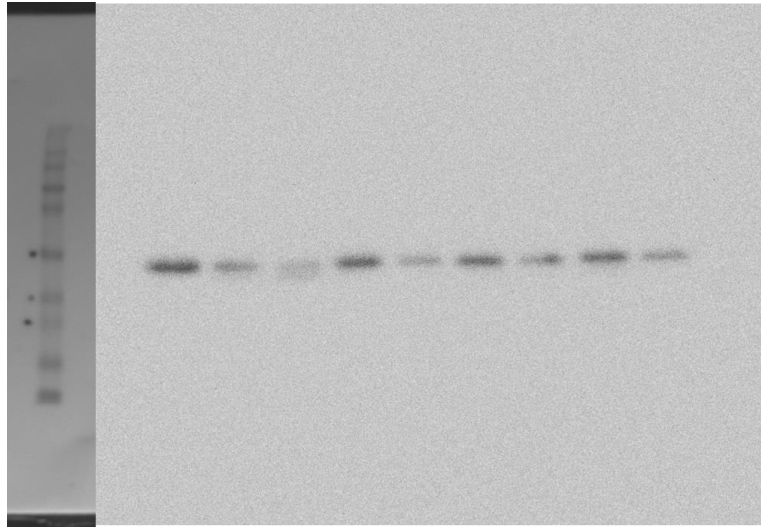
Appendix A4

Patient	Compartment	Age	Gender	Subgroup	Histology	Metastases	Dead of Dx
1	Primary	9	F	4	Classic		1
1	Metastasis					N/A	
2	Primary	N/A	N/A	3	N/A		N/A
2	Metastasis					N/A	
2	Metastasis					N/A	
3	Primary	8	M	4	N/A		1
3	Metastasis					supratentorial	
3	Metastasis					spinal	
4	Primary	4.5	M	3	LCA		1
4	Metastasis					N/A	
4	Metastasis					N/A	
4	Metastasis					N/A	
5	Primary	9	M	4	Classic		0
5	Metastasis					N/A	
6	Primary	21	F	4	N/A		N/A
6	Metastasis					N/A	
7	Primary	6	F	4	Classic		1
7	Metastasis					supratentorial leptomeninges	
8	Primary	9	F	4	N/A		N/A
8	Metastasis					N/A	
9	Primary	N/A	N/A	2	N/A		N/A
9	Metastasis					N/A	

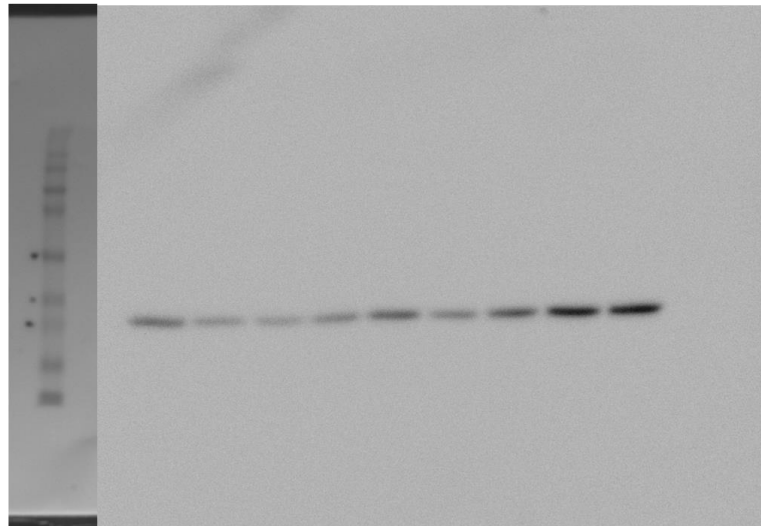
Appendix A4. Clinicopathological information of patients from the Wang dataset

Appendix A5

A



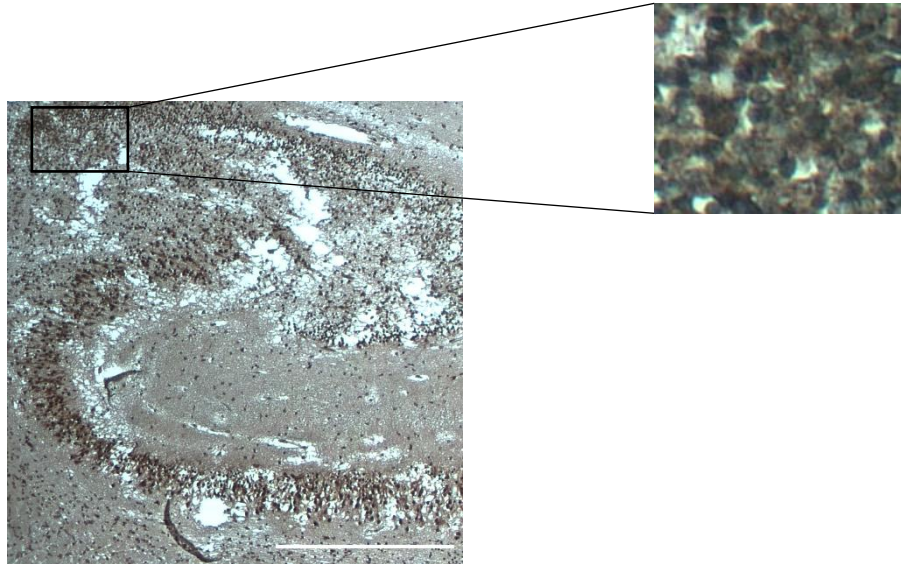
B



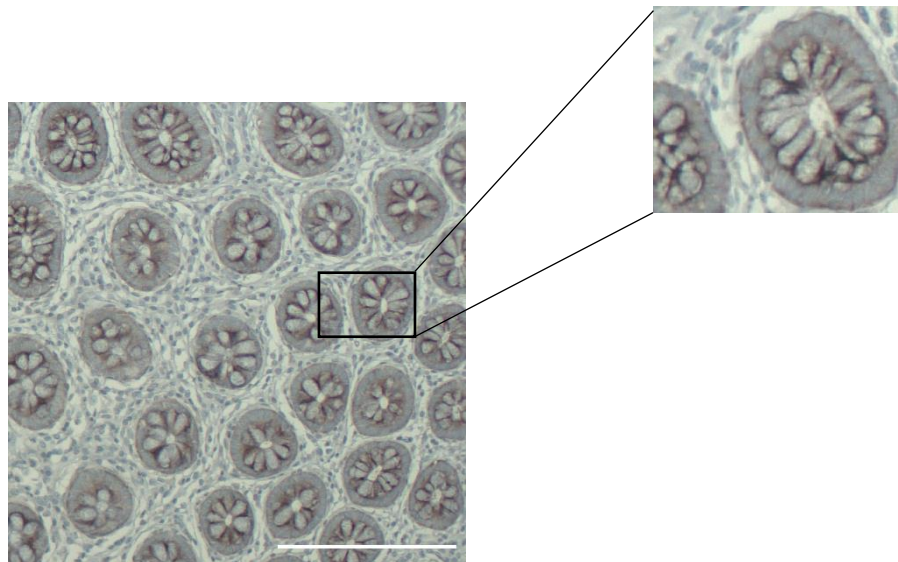
Appendix A5. Full length western blots version of Figure 3.7. Authentication blots are presented throughout this thesis to provide confidence that any identified bands are representative of the stated protein. A) YB-1 protein expression (approximately 49 kDa). B) GAPDH protein expression (approximately 37 kDa).

Appendix A6

A



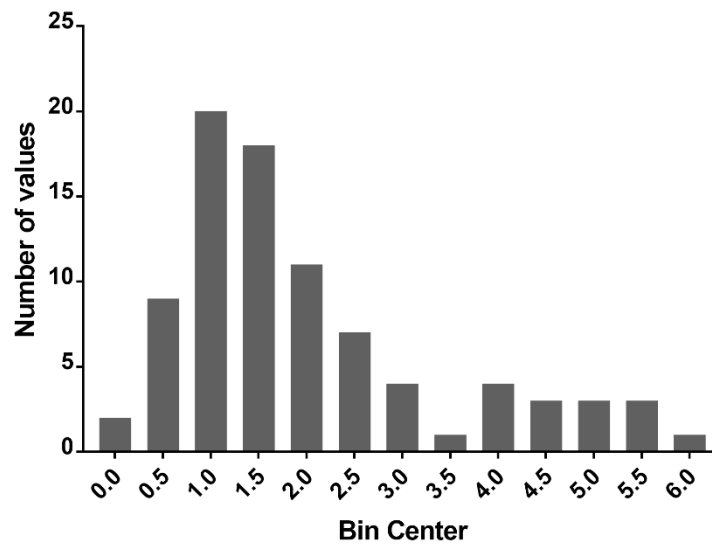
B



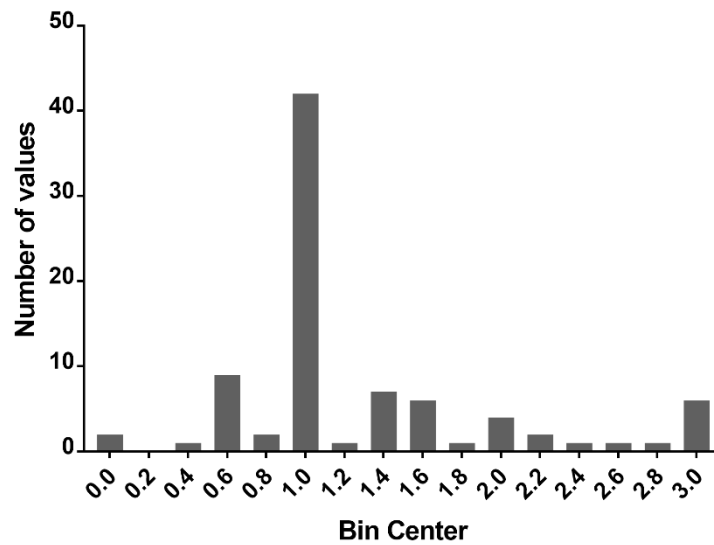
Appendix A6. Optimisation of YB-1 Antibody for IHC. The polyclonal YB-1 antibody employed in this study was optimised extensively on paediatric brain (A) and small intestine (B) prior to use on TMAs. Representative images shown. All scale bars represent 500 μm .

Appendix A7

A

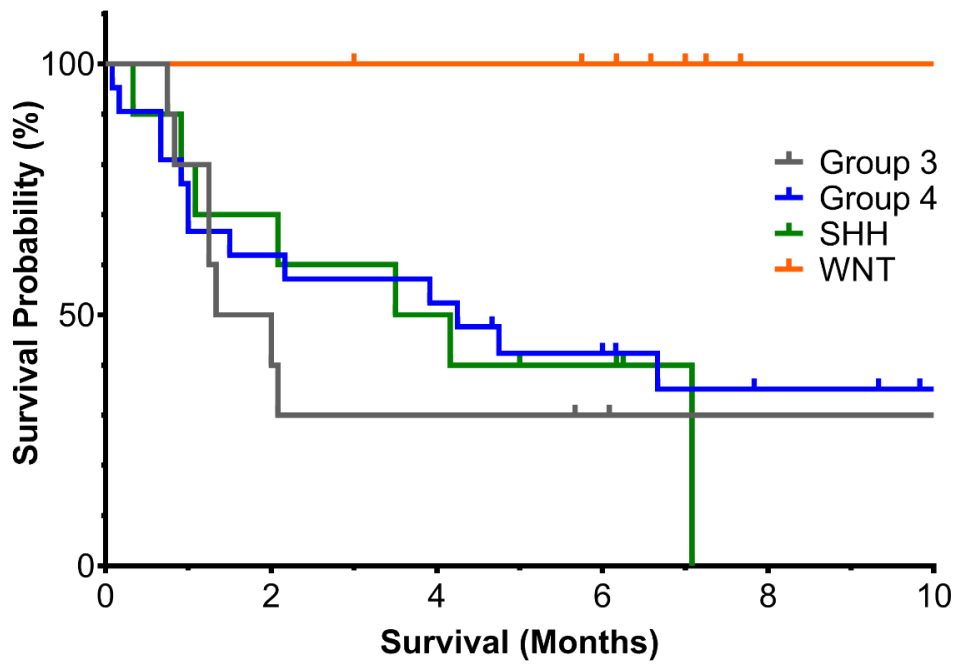


B



Appendix A7. Frequency distribution of YB-1 immunohistochemical scoring. A histogram displaying frequency of patients against immunohistochemical score of YB-1 staining. A) Histogram of overall YB-1 staining. Samples demonstrated a positive skew with unimodal distribution. 25th percentile = 1; median (50th percentile) = 1.5; 75th percentile = 2.6. B) Histogram of nuclear YB-1 staining. Again, samples exhibited a positive skew with unimodal distribution. 25th percentile = 1; median (50th percentile) = 1; 75th percentile = 1.5.

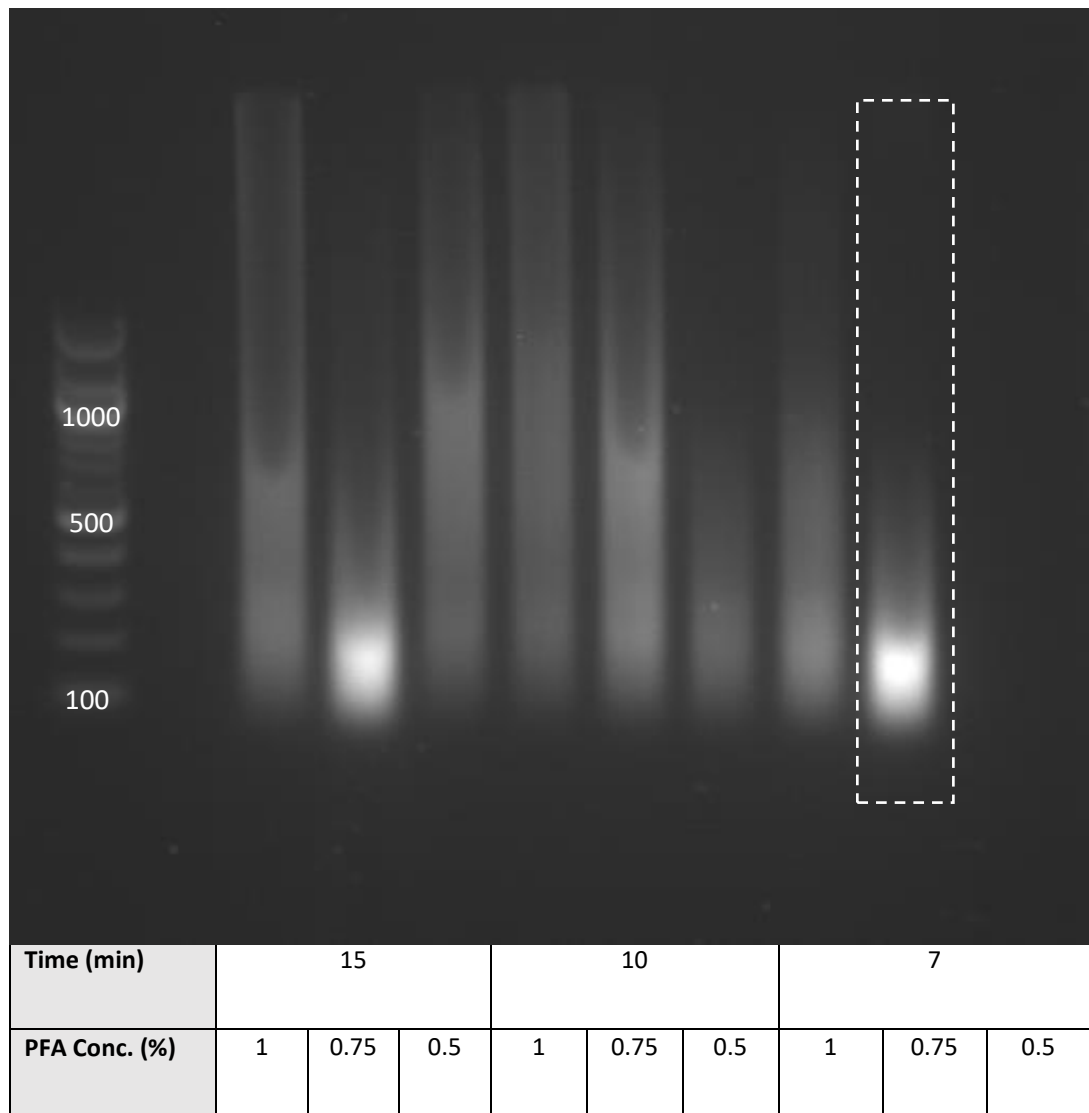
Appendix A8



Appendix A8. Kaplan Meier survival analysis of medulloblastoma patients included in the Nottingham and Birmingham TMAs. Survival curves depict overall survival probability of patients within each medulloblastoma molecular subgroup. N = 51.

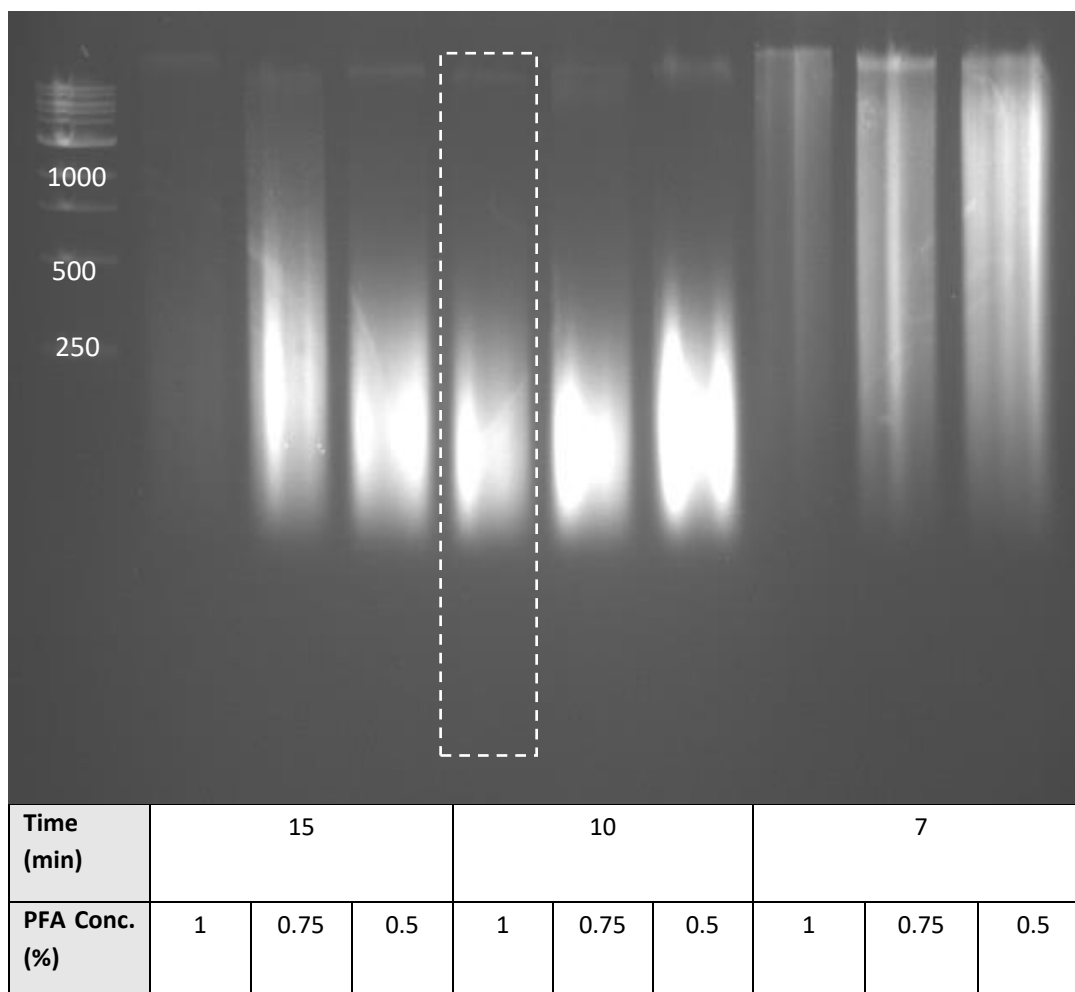
Appendix B: Chapter 4 – Examination of YB-1 as a regulator of *ABCB1* in medulloblastoma

Appendix B1



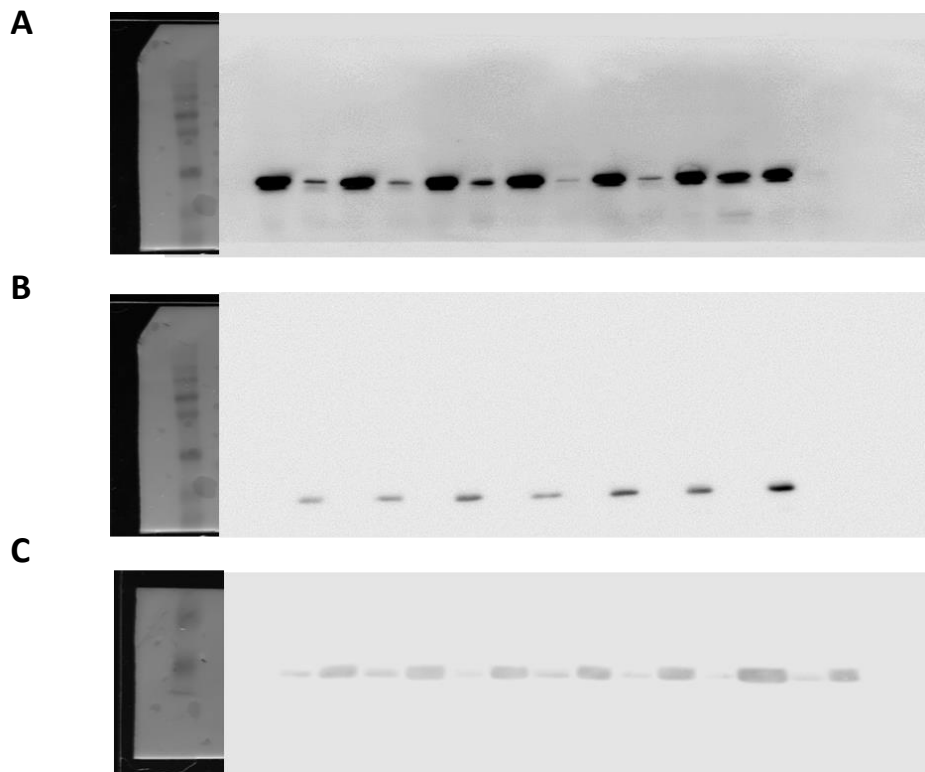
Appendix B1. Optimisation of cross-linking conditions for D283 ChIP assays. Purified, sheared chromatin isolated from fixed D283 cells was loaded onto a 1.5% agarose gel and electrophoresed at 120V. Cross-linking times and concentrations are displayed below the gel. The condition which gave the cleanest band between 200 – 500 bp, with the least smearing above 1000 bp was selected for future ChIP assays, in this case 7 minutes in 0.75% PFA. D283 cross-linking conditions were optimised by previous CBTRC PhD student, Dr Alice Cardall using the Magna A/G Immunoprecipitation kit.

Appendix B2



Appendix B2. Optimisation of shearing cross-linking conditions for HDMB-03 ChIP assays. Purified, sheared chromatin isolated from fixed D283 cells was loaded onto a 1.5% agarose gel and electrophoresed at 120V. Cross-linking times and concentrations are displayed below the gel. The condition which gave the cleanest band between 200 – 500 bp, with the least smearing above 1000 bp was selected for future ChIP assays, in this case 10 minutes in 1% PFA. Optimisation was carried out using the Magna A/G Immunoprecipitation kit.

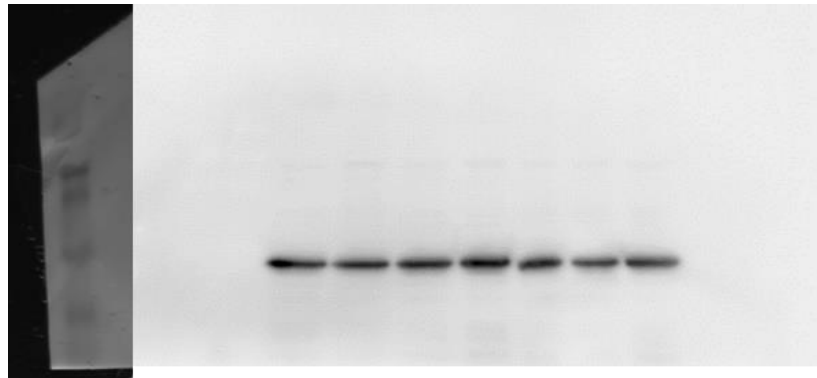
Appendix B3



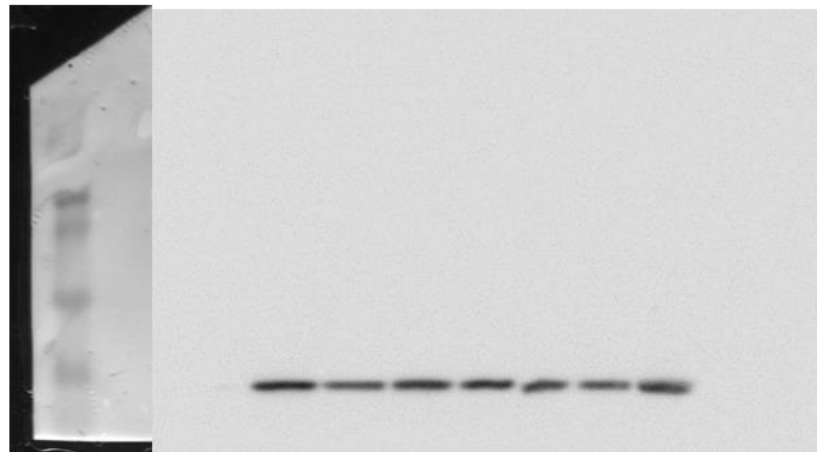
Appendix B3. Full length western blots of Figure 4.6. Authentication blots are presented throughout this thesis to provide confidence that any identified bands are representative of the stated protein. A) YB-1 protein expression (approximately 49 kDa). B) GAPDH protein expression (approximately 37 kDa). C) Histone protein expression (approximately 17 kDa).

Appendix B4

A

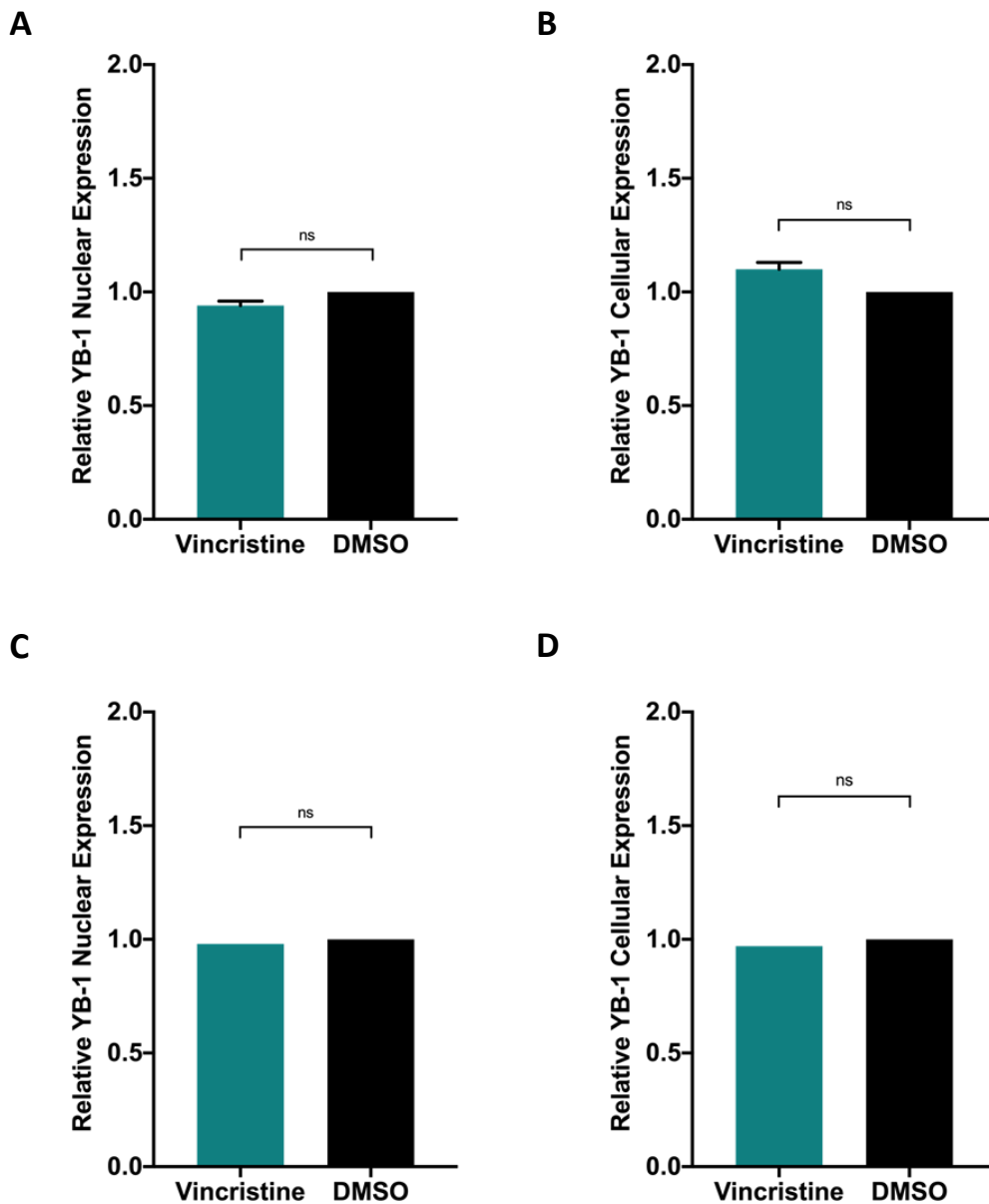


B



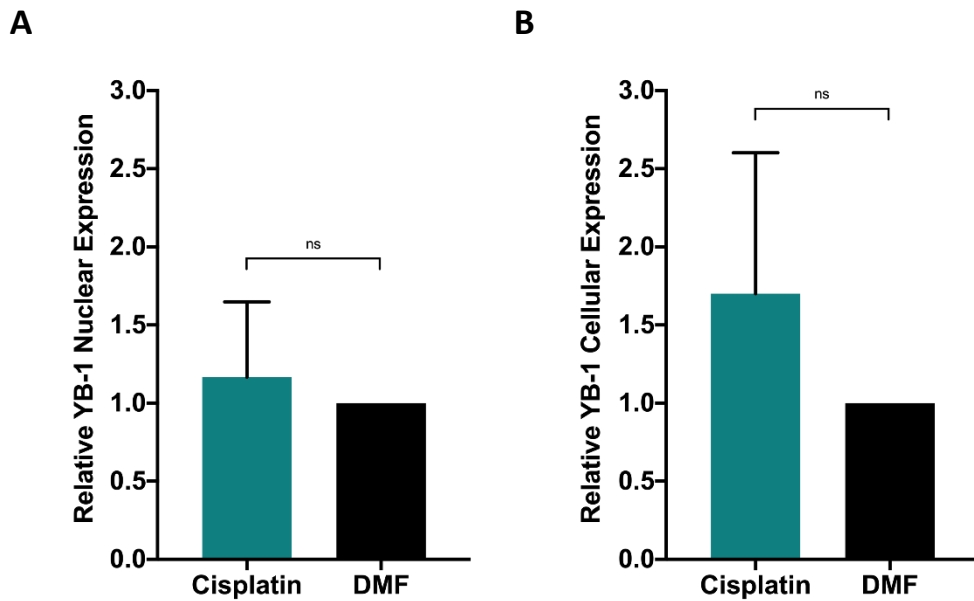
Appendix B4. Full length western blot of Figure 4.7. Authentication blots are presented throughout this thesis to provide confidence that any identified bands are representative of the stated protein. A) YB-1 protein expression (approximately 49 kDa). B) GAPDH protein expression (approximately 37 kDa).

Appendix B5



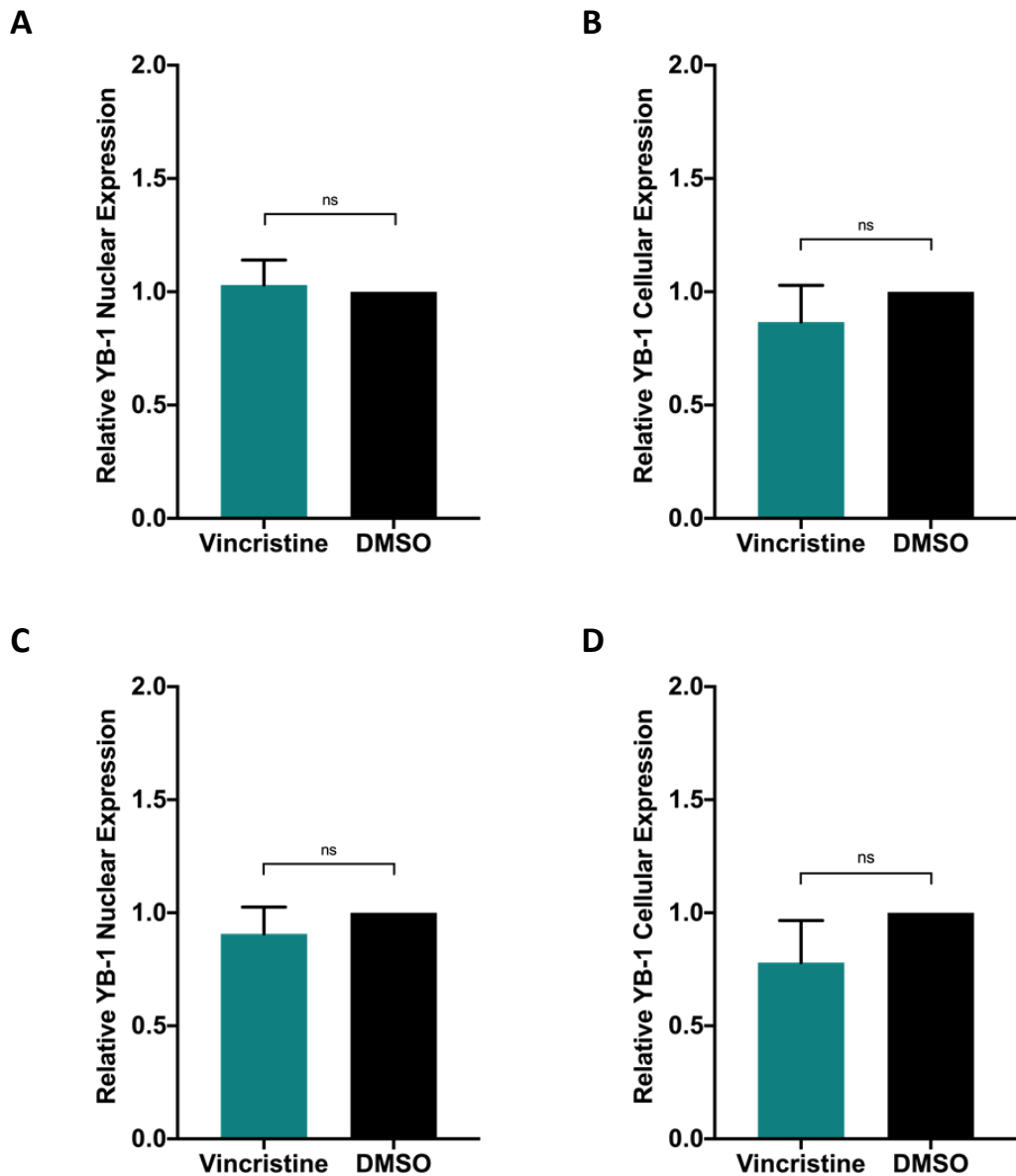
Appendix B5. Treatment of HDMB-03 cells with chemotherapeutic vincristine over 6 and 12 hours does not elevate nuclear or cellular YB-1 expression. HDMB-03 cells were treated with 3.4 nM vincristine (IC_{50}) over a 12 hour time course. Following drug treatment, cells were fixed with PFA and fluorescence detected by confocal microscopy. Automated quantification of vincristine-treated cells 6 hours-post treatment revealed no alteration in YB-1 nuclear expression (A) or overall expression (B) relative to the vehicle (DMSO)-treated control. $n = 2$ (approx. 1000 cells). Automated quantification of HDMB-03 cells 12 hours post-treatment also revealed no alteration YB-1 nuclear expression (C) or overall expression (D) relative to the vehicle (DMSO)-treated control. $n = 1$ (approx. 500 cells).

Appendix B6



Appendix B6. Treatment of D283 cells with medulloblastoma chemotherapeutic cisplatin over 12 hours does not elevate nuclear or cellular YB-1 expression. D283 cells were treated with 1.6 μ M cisplatin (IC_{50}) for 6 hours. Following drug treatment, cells were fixed with PFA and fluorescence detected by confocal microscopy. A) Automated quantification of cisplatin-treated cells revealed no alteration in YB-1 nuclear expression relative to the vehicle (DMF)-treated control. B) Automated quantification of cisplatin-treated cells revealed no alteration in YB-1 overall expression relative to the vehicle (DMF)-treated control. $n = 3$ (approx. 2000 cells).

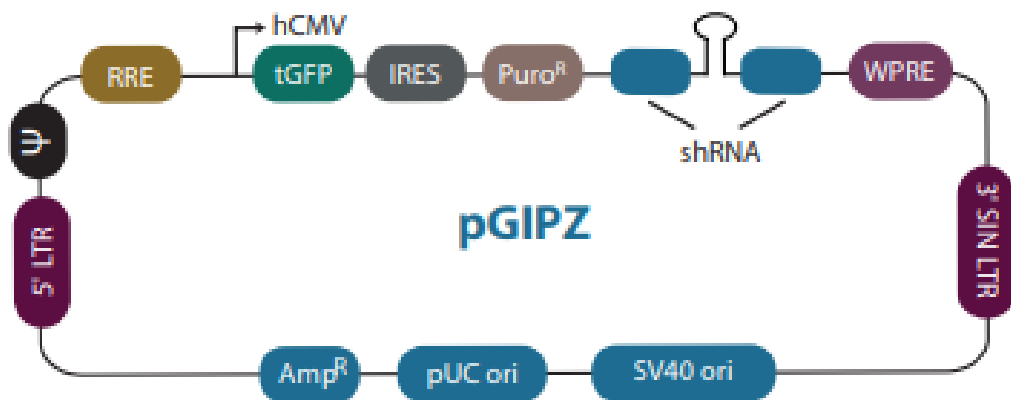
Appendix B7



Appendix B7. Treatment of D283 cells with vincristine over 6 and 12 hours does not elevate nuclear or cellular YB-1 expression. D283 cells were treated with 3.1 nM vincristine (IC_{50}) over a 12 hour time course. Following drug treatment, cells were fixed with PFA and fluorescence detected by confocal microscopy. Automated quantification of vincristine-treated cells 6 hours-post treatment revealed no alteration in YB-1 nuclear expression (A) or overall expression (B) relative to the vehicle (DMSO)-treated control. $n = 3$ (approx. 2000 cells). Automated quantification of D283 cells 12 hours post-treatment also revealed no alteration YB-1 nuclear expression (C) or overall expression (D) relative to the vehicle (DMSO)-treated control. $n = 3$ (approx. 2000 cells).

Appendix C: Chapter 5 – Functional analysis of the role of YB-1 in drug resistance and metastasis in medulloblastoma

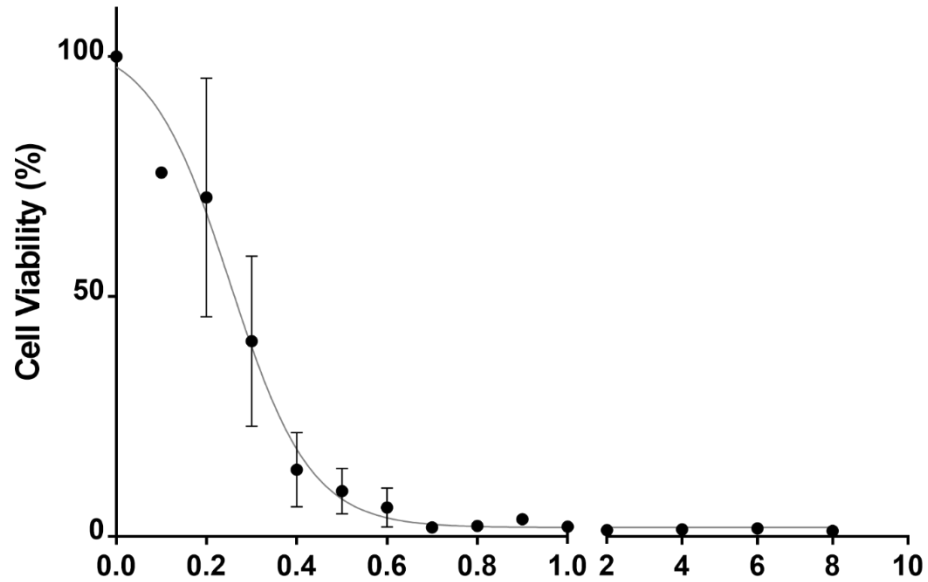
Appendix C1



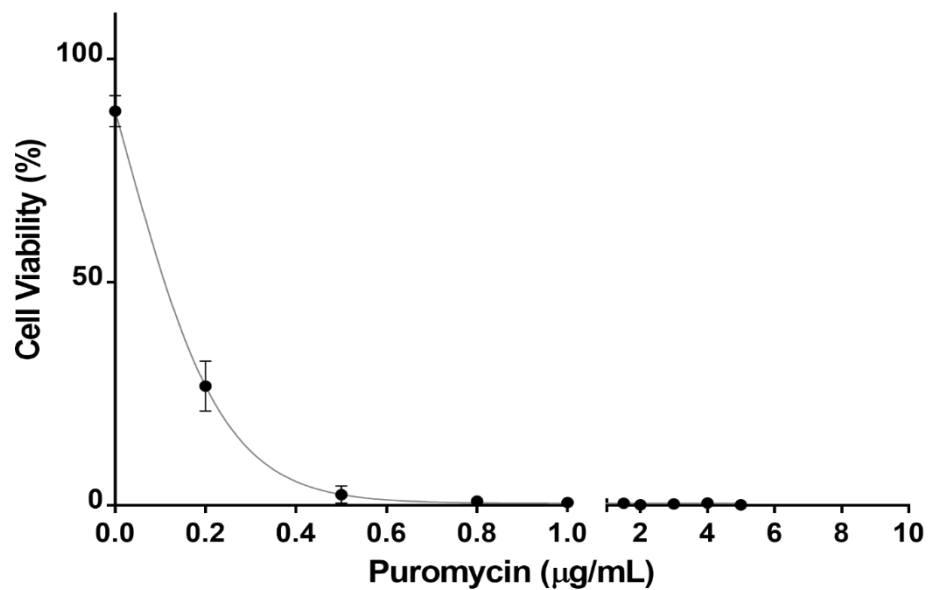
Appendix C1. pGIPZ lentiviral vector. Simplified map of the pGIPZ lentiviral vector showing important vector elements including: human cytomegalovirus promoter (hCMV); turboGFP reporter (tGFP); puromycin resistance marker (Puro^R); internal ribosome entry site (IRES); microRNA-adapted shRNA (shRNA); psi (Ψ) packaging sequence; Rev response element (RRE); woodchuck hepatitis post-transcriptional regulatory element (WPRE). Diagram taken from Horizon GIPZ Lentiviral shRNA Technical Manual.

Appendix C2

A



B



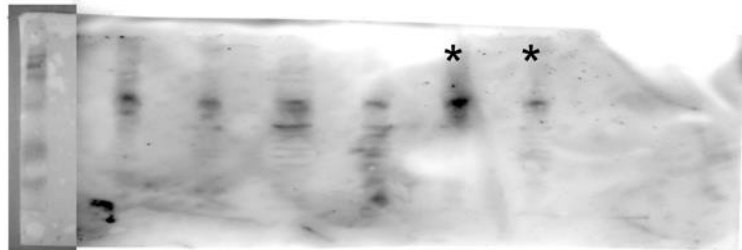
Appendix C2. Puromycin kill curves. In order to calculate a puromycin kill concentration for non-transduced cells, cells were treated with puromycin at increasing concentrations (0 – 8 µg/mL) for 48 hours and cell viability assessed after this time by PrestoBlue™ assay. A) The HDMB-03 cell line was calculated to have a puromycin kill concentration of 2 µg/mL. B) The D283 cell line was also calculated to have a puromycin kill concentration of 2 µg/mL.

Appendix C3

A



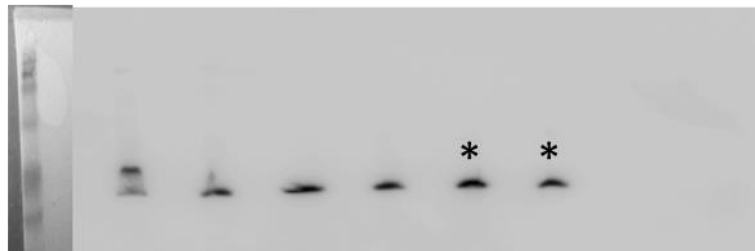
B



C

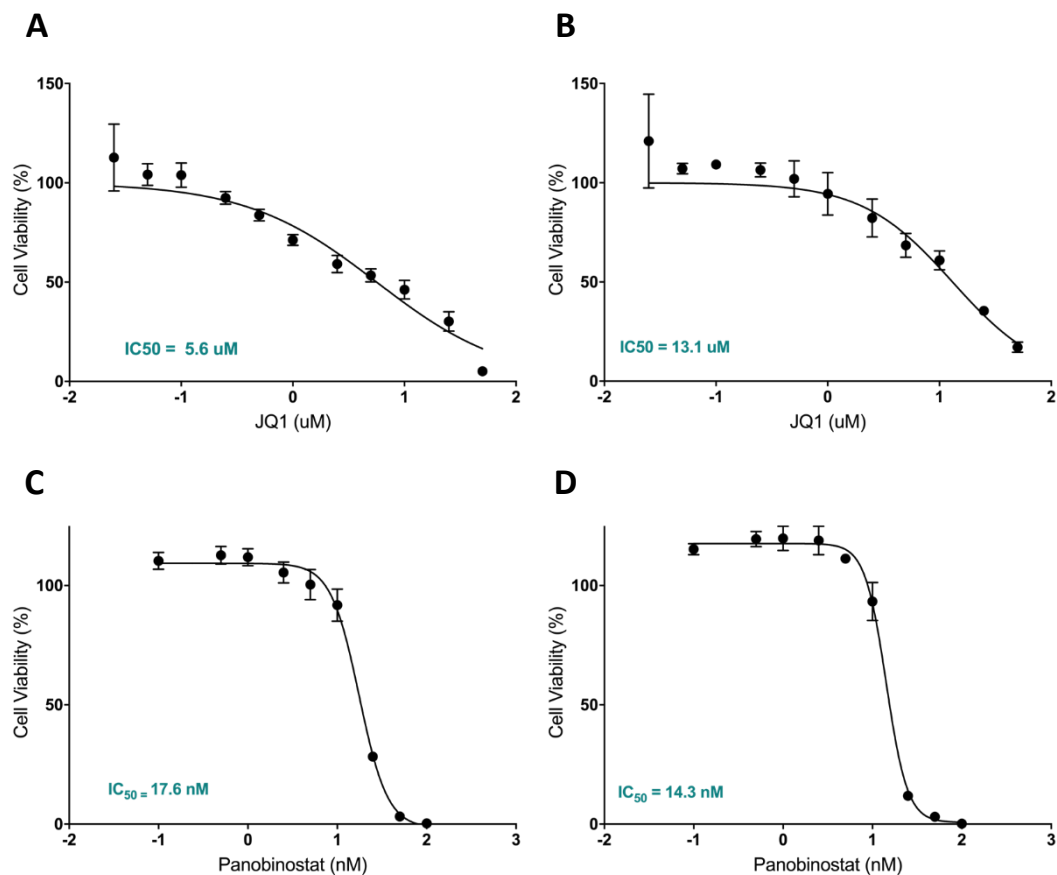


D



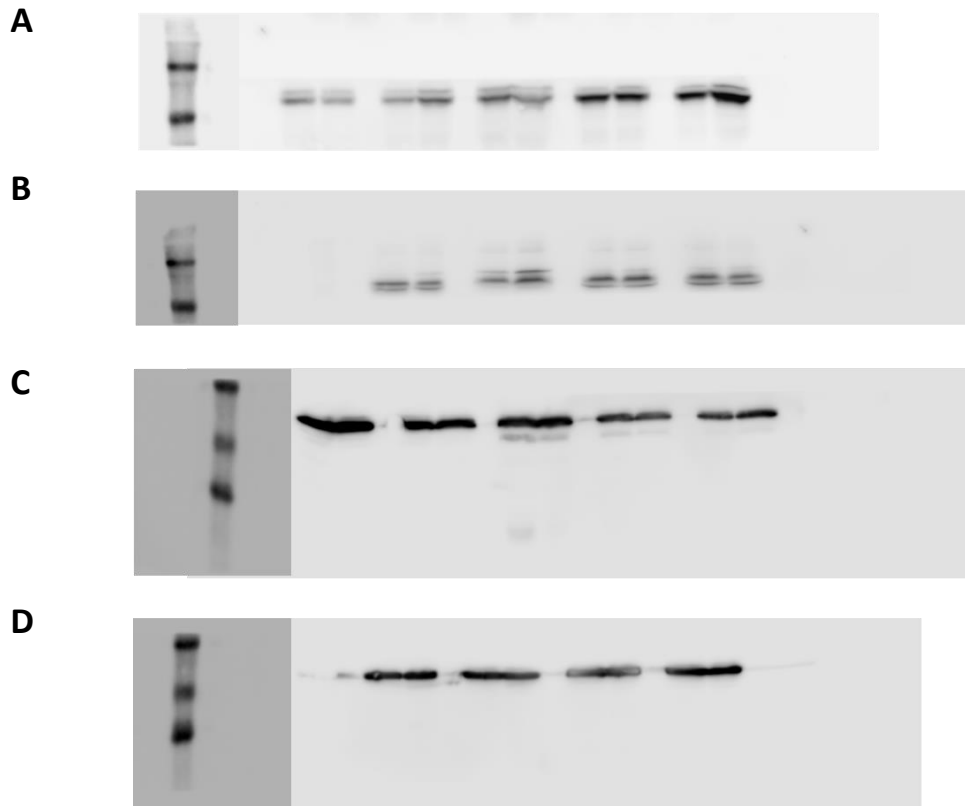
Appendix C3. Full length western blots of Figure 5.6. Authentication blots are presented throughout this thesis to provide confidence that any identified bands are representative of the stated protein. A) YB-1 protein expression (approximately 49 kDa) in KD-HDMB-03 cells. B) YB-1 protein expression (approximately 49 kDa) in KD-D283 cells. C) GAPDH protein expression (approximately 37 kDa) in KD-HDMB-03 cells. D) GAPDH protein expression (approximately 37 kDa) in KD-D283 cells. Asterisks denote bands which were cropped and used in the current thesis.

Appendix C4



Appendix C4. Panobinostat and JQ1 cell viability in Group 3 cell lines. Cell lines were treated with increasing concentrations of JQ1 (A - B) or panobinostat (C - D) for 72 hours. PrestoBlue cell viability assays were performed to compare response and viability was calculated as a percentage of the vehicle-treated control. D283 cells (B) were more intrinsically resistant to JQ1 treatment than HDMB-03 cells (A), while HDMB-03 cells (C) exhibited a greater tolerance to panobinostat than D283 (D). Mean \pm SEM plotted; n = 3. Dose response curves were generated using non-linear regression analyses and IC₅₀ values calculated accordingly.

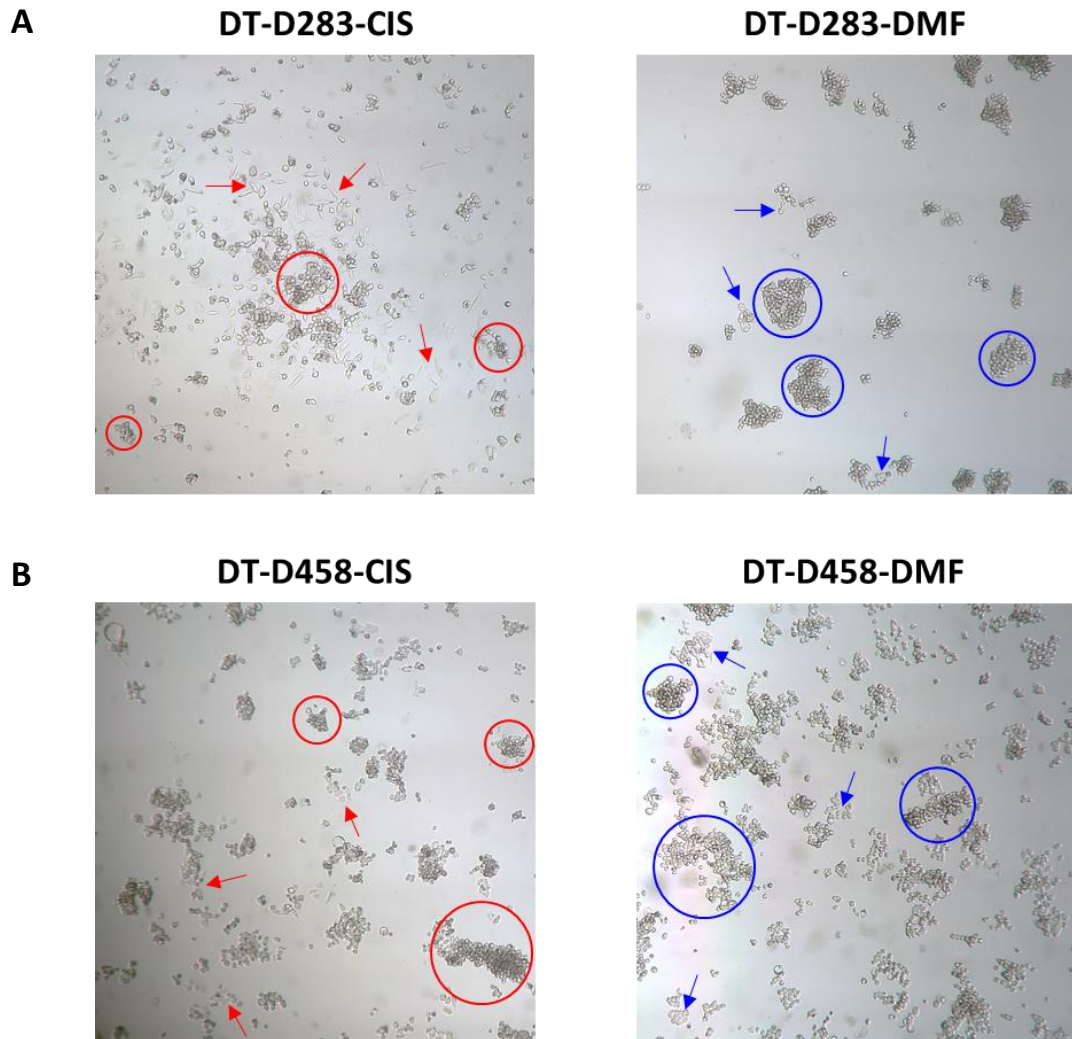
Appendix C5



Appendix C5. Full length western blots of Figure 5.12. Authentication blots are presented throughout this thesis to provide confidence that any identified bands are representative of the stated protein. A) MYC protein expression (approximately 57 kDa) in KD-HDMB-03 cells. B) MYC protein expression (approximately 57 kDa) in KD-D283 cells. C) GAPDH protein expression (approximately 37 kDa) in KD-HDMB-03 cells. D) GAPDH protein expression (approximately 37 kDa) in KD-D283 cells.

Appendix D: Chapter 6 - Examination of the route to drug tolerance in medulloblastoma.

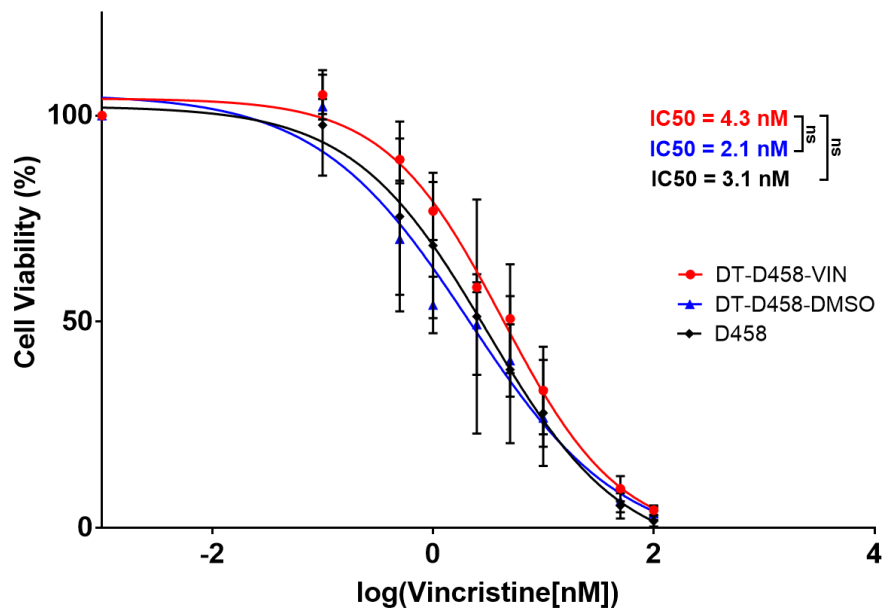
Appendix D1



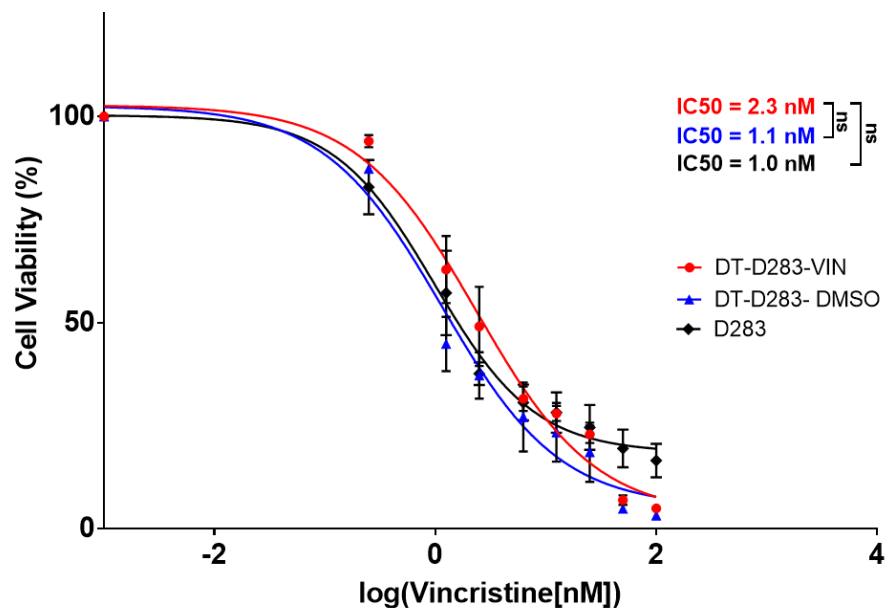
Appendix D1. Drug-tolerant cell lines undergo morphological alterations following continuous selection. A) DT-D283-CIS cells were more adherent than the paired DT-D283-DMF line and adherent cells were frequently larger and flatter, growing in large clusters. B) DT-D458-CIS cells were also found to be more adherent than the DT-D458-DMF line, with large clumps of suspension cells visible. Circles highlight examples of cells in suspension, whereas arrows identify examples of adherent cells.

Appendix D2

A

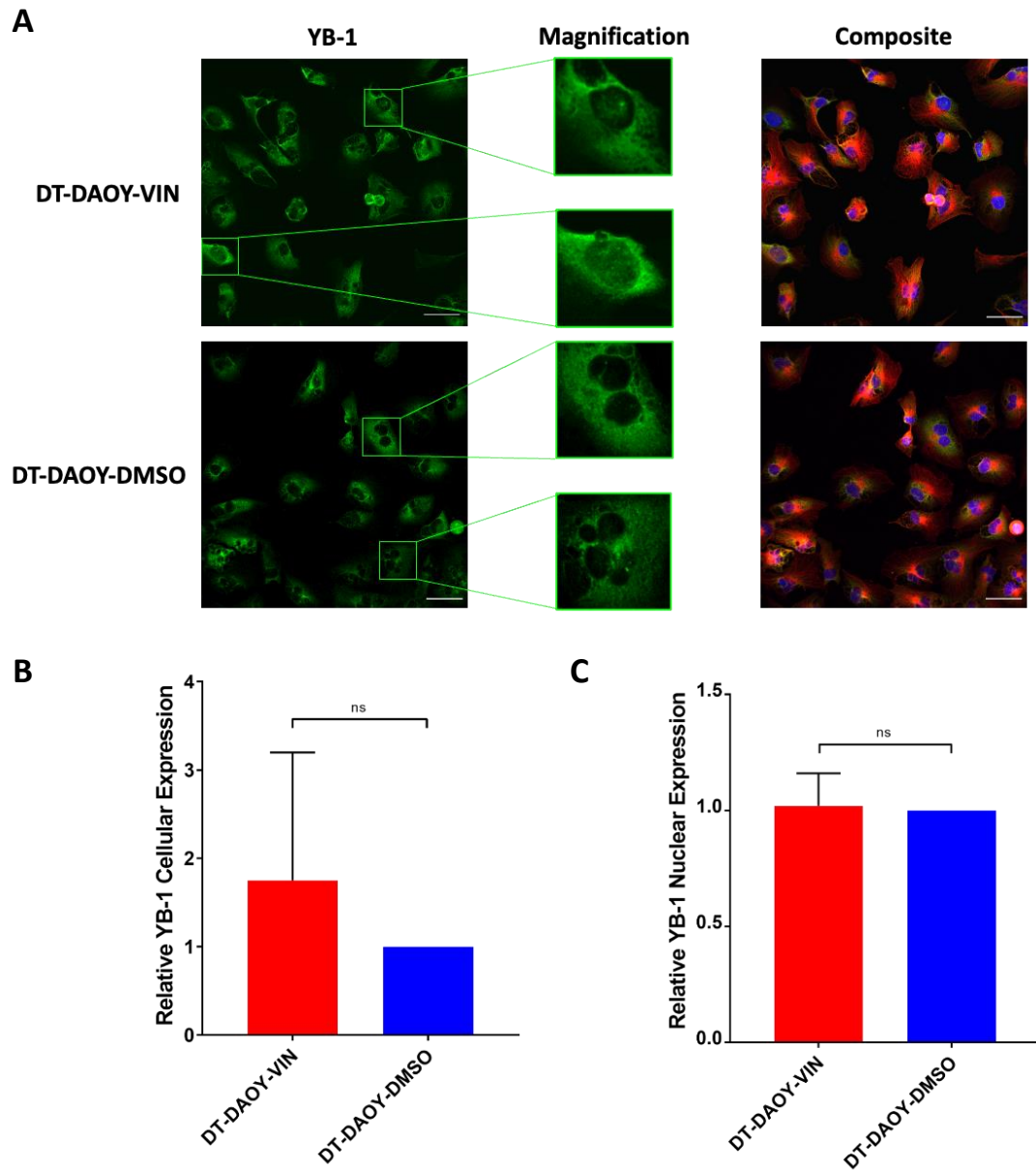


B

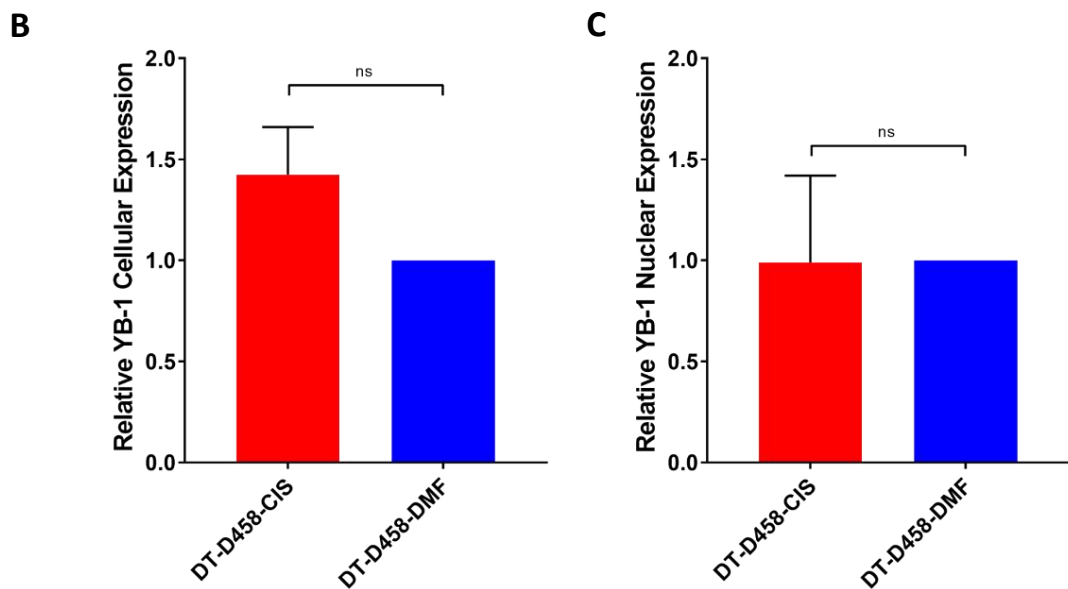
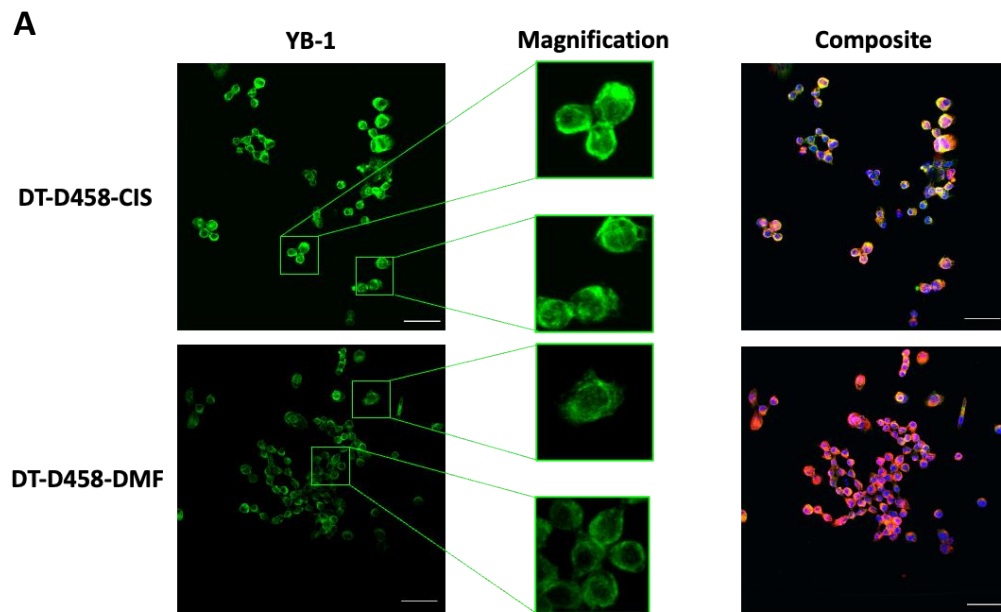


Appendix D2. Continuous selection of D458 and D283 cells with vincristine did not yield drug-tolerant cell lines. D458 and D283 cell lines were cultured continuously in the presence of vincristine. Dose escalation was halted at 1/3 vincristine IC₅₀ value for each cell line, above which no proliferation was observed. A) DT-D458-VIN cells exhibited a 1.4-fold increase in resistance compared to the parental cell line following continuous treatment in 1.0 nM vincristine, however this was not found to be significant when compared to parental or vehicle-treated control cell lines. B) DT-D283-VIN cells exhibited a 2.3-fold increase in resistance compared to the parental cell line following continuous treatment in 0.33 nM vincristine, however again this was not found to be significant. Mean \pm SEM plotted; n = 3. Dose response curves were generated using non-linear regression analyses and IC₅₀ values calculated accordingly. Significance was assessed by ordinary one-way ANOVA analyses with Tukey's multiple comparisons test. ns = not significant.

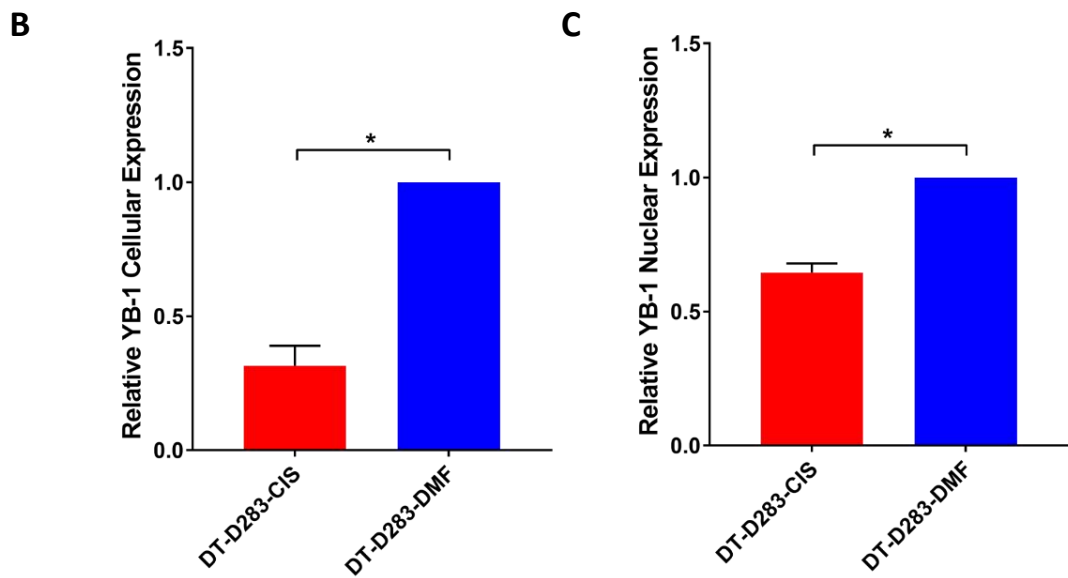
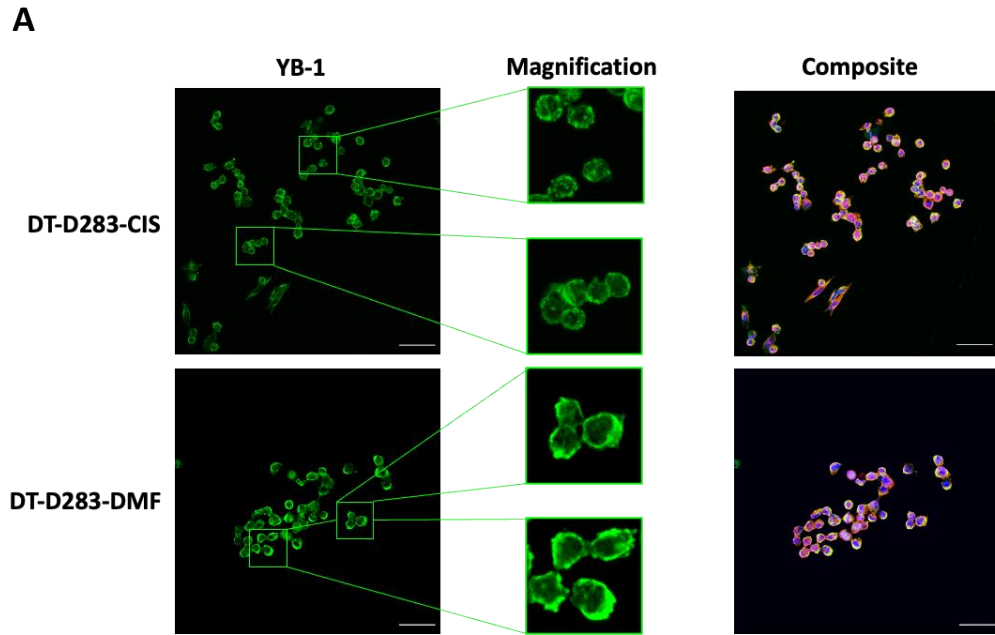
Appendix D3



Appendix D3.1. Immunofluorescence of drug-tolerant cell lines reveals little alteration in overall cellular YB-1 expression between drug-tolerant and vehicle-treated control lines. DT-DAOY-VIN/-DMSO cells were fixed with PFA and fluorescence detected by confocal microscopy. A) Representative confocal images. B) Automated quantification of confocal microscopy images revealed no difference in overall staining intensity between DT-DAOY-VIN and the vehicle-treated control line. C) Automated quantification of confocal microscopy images revealed no difference in nuclear staining intensity between DT-DAOY-VIN and the vehicle-treated control line. $n = 2$ (approx. 700 cells per cell line); * $P < 0.05$. Significance assessed by unpaired t-test.



Appendix D3.2. Immunofluorescence of drug-tolerant cell lines reveals little alteration in overall cellular YB-1 expression between drug-tolerant and vehicle-treated control lines. DT-D458-CIS/-DMF cells were fixed with PFA and fluorescence detected by confocal microscopy. A) Representative confocal images. B) Automated quantification of confocal microscopy images revealed no difference in overall staining intensity between DT-D458-CIS and the vehicle-treated control line. C) Automated quantification of confocal microscopy images revealed no difference in nuclear staining intensity between DT-D458-CIS and the vehicle-treated control line. $n = 2$ (approx. 700 cells per cell line); $*P < 0.05$. Significance assessed by unpaired t-test.



Appendix D3.3. Immunofluorescence of drug-tolerant cell lines reveals little alteration in overall cellular YB-1 expression between drug-tolerant and vehicle-treated control lines. DT-D283-CIS/-DMF cells were fixed with PFA and fluorescence detected by confocal microscopy. A) Representative confocal images. B) Automated quantification of confocal microscopy images revealed a reduction in overall staining intensity between DT-D283-CIS and the vehicle-treated control line. C) Automated quantification of confocal microscopy images revealed a reduction in nuclear staining intensity between DT-D283-CIS and the vehicle-treated control line. $n = 2$ (approx. 700 cells per cell line); * $P < 0.05$. Significance assessed by unpaired t-test.

Appendix D4

Sample	Concentration (ng/ μ l)	RINe Value
DT-D283-CIS (n = 1)	170	10
DT-D283-CIS (n = 2)	266	10
DT-D283-CIS (n = 3)	342	10
DT-D283-DMF (n = 1)	722	10
DT-D283-DMF (n = 2)	940	10
DT-D283-DMF (n = 3)	1040	10
DT-D458-CIS (n = 1)	236	10
DT-D458-CIS (n = 2)	49	10
DT-D458-CIS (n = 3)	57.4	10
DT-D458-DMF (n = 1)	1200	10
DT-D458-DMF (n = 2)	814	10
DT-D458-DMF (n = 3)	440	10
DT-HDMB-03-CIS (n = 1)	682	10
DT-HDMB-03-CIS (n = 2)	794	10
DT-HDMB-03-CIS (n = 3)	340	9.9
DT-HDMB-03-DMF (n = 1)	1080	10
DT-HDMB-03-DMF (n = 2)	856	10
DT-HDMB-03-DMF (n = 3)	1120	9.8
DT-DAOY-VIN (n = 1)	328	10
DT-DAOY-VIN (n = 2)	352	10
DT-DAOY-VIN (n = 3)	492	10
DT-DAOY-DMSO (n = 1)	328	10
DT-DAOY-DMSO (n = 2)	282	10
DT-DAOY-DMSO (n = 3)	862	10

Appendix D4. Quantification of RNA concentration and integrity in 3' mRNA sequencing samples. RNA was extracted from 24 samples and RNA integrity quantified using an Agilent TapeStation. A RINe value >7 is considered acceptable for downstream sequencing analysis.

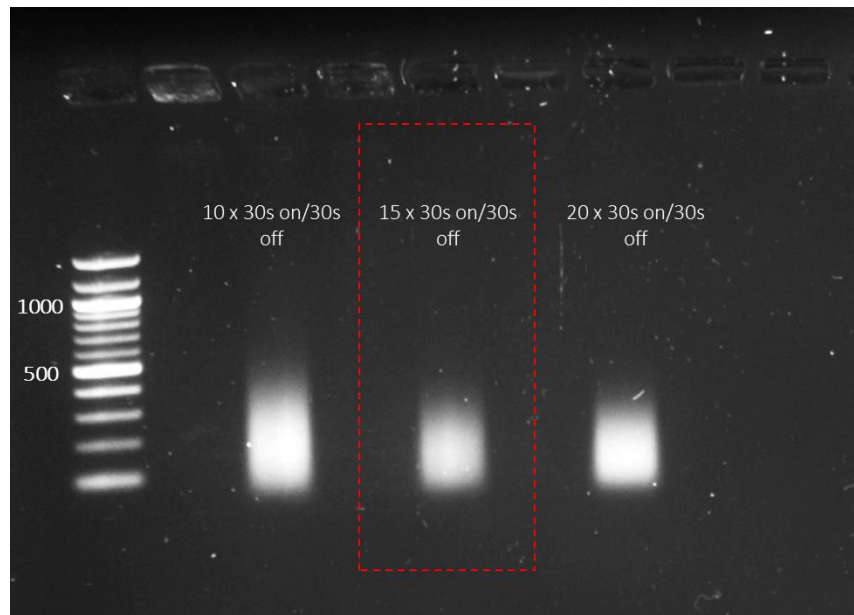
Appendix D5

Sample	Total Reads	Mapped Reads (%)	- Uniquely (%)	No. Detected Genes
DT-D283-CIS (n = 1)	8,064,074	98.36%	74.23	17,188
DT-D283-CIS (n = 2)	8,751,511	98.74%	76.50	17,357
DT-D283-CIS (n = 3)	7,745,935	98.92%	75.58	16,976
DT-D283-DMF (n = 1)	8,697,467	99.11%	77.78	17,064
DT-D283-DMF (n = 2)	8,438,028	98.79%	79.59	17,002
DT-D283-DMF (n = 3)	8,847,718	98.83%	79.28	16,990
DT-D458-CIS (n = 1)	7,175,053	98.96%	77.93	16,899
DT-D458-CIS (n = 2)	7,367,199	99.28%	75.59	16,469
DT-D458-CIS (n = 3)	8,197,631	98.42%	73.94	17,165
DT-D458-DMF (n = 1)	9,039,463	98.42%	79.96	17,200
DT-D458-DMF (n = 2)	8,515,634	98.60%	80.29	16,939
DT-D458-DMF (n = 3)	8,183,452	98.53%	77.19	16,373
DT-HDMB-03-CIS (n = 1)	7,418,811	98.00%	77.81	17,193
DT-HDMB-03-CIS (n = 2)	7,999,532	98.85%	77.71	17,207
DT-HDMB-03-CIS (n = 3)	7,625,802	97.32%	74.26	16,463
DT-HDMB-03-DMF (n = 1)	8,311,589	98.01%	78.88	16,870
DT-HDMB-03-DMF (n = 2)	8,248,097	97.82%	77.89	16,680
DT-HDMB-03-DMF (n = 3)	8,017,356	98.44%	78.04	16,434
DT-DAOY-VIN (n = 1)	7,151,168	99.15%	74.31	17,574
DT-DAOY-VIN (n = 2)	6,500,640	99.32%	76.15	17,473
DT-DAOY-VIN (n = 3)	8,737,744	99.11%	80.86	18,419
DT-DAOY-DMSO (n = 1)	6,595,509	99.05%	72.72	17,891
DT-DAOY-DMSO (n = 2)	9,740,902	98.99%	73.45	19,258
DT-DAOY-DMSO (n = 3)	11,303,156	99.30%	73.27	19,122

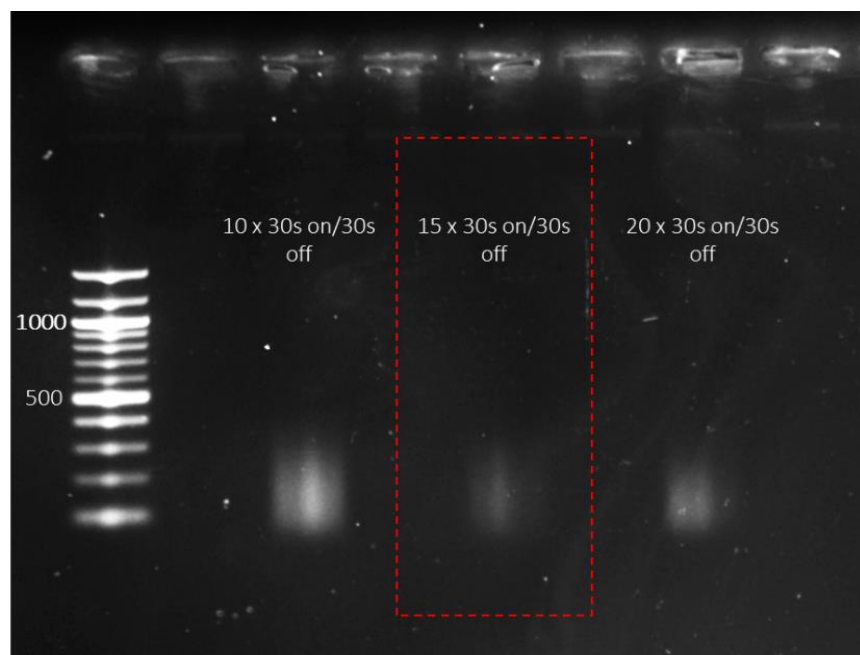
Appendix D5. Mapping of whole transcriptome sequencing data. Mapping of reads to a reference genome served as an additional post-sequencing quality check. Percentages of mapped and uniquely mapped reads, as well as the total number of detected genes in each sample are displayed.

Appendix D6

A



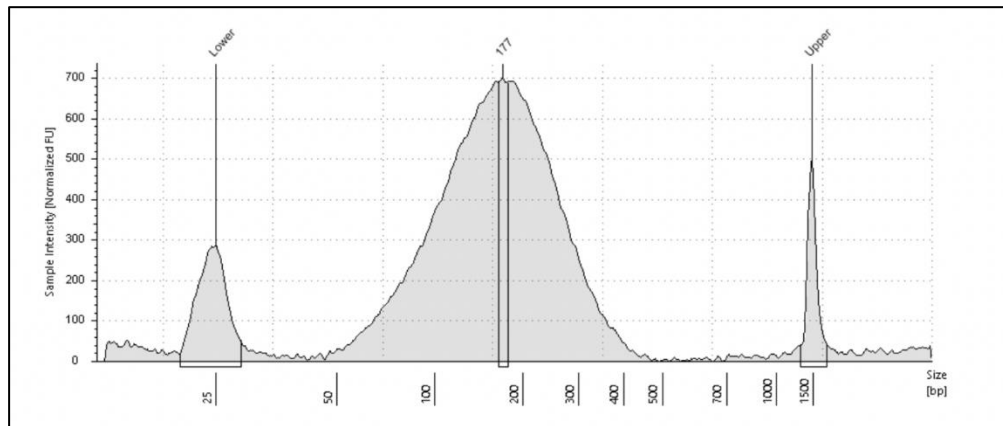
B



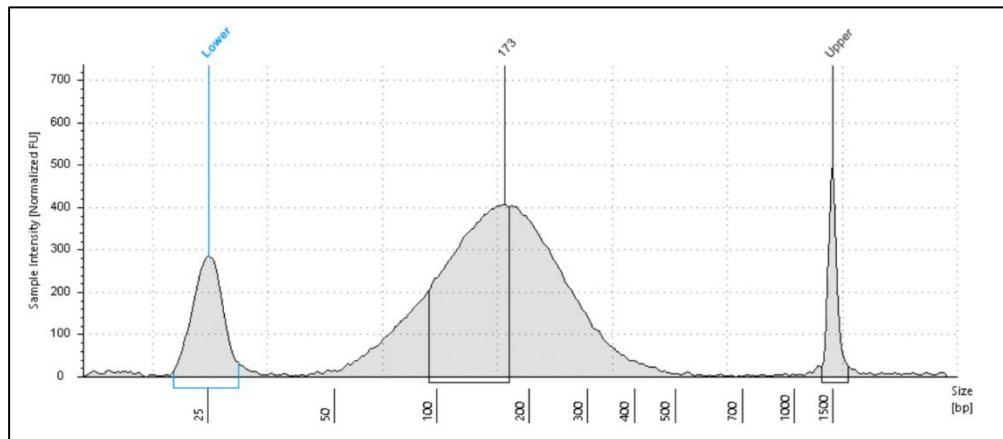
Appendix D6. Optimisation of sonication and cross-linking conditions for HDMB-03 and D283 cell lines using the Magna G CHIP kit. Purified, sheared chromatin isolated from fixed HDMB-03 (A) and D283 (B) cells were loaded onto a 1.5% agarose gel and electrophoresed at 120V. A cross-linking time of 1 minute and concentrations of 1% PFA was used for all test samples. Sonication parameters are displayed on the gel. Sonication for 15 minutes as 30 seconds on and 30 seconds off was selected for both cell lines as it produced fragments ranging between 100 bp and 500 bp however would likely avoid “over-shearing”.

Appendix D7

A



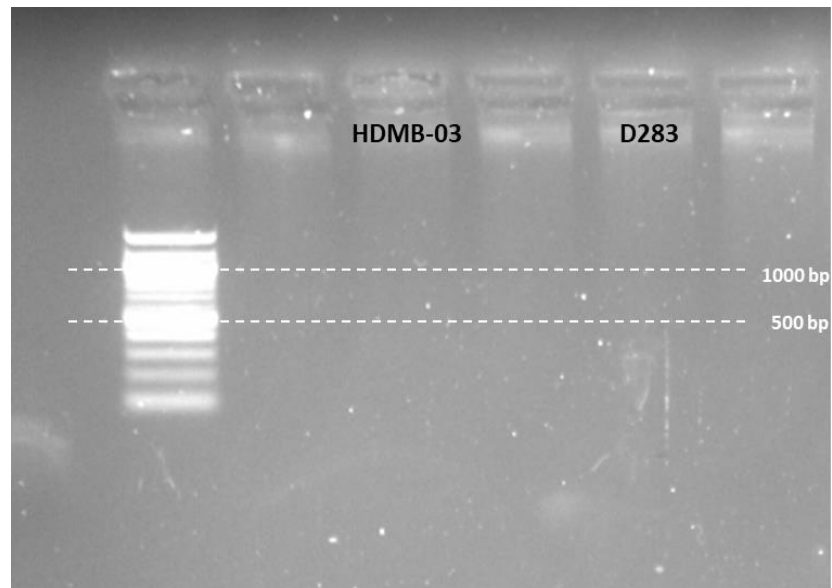
B



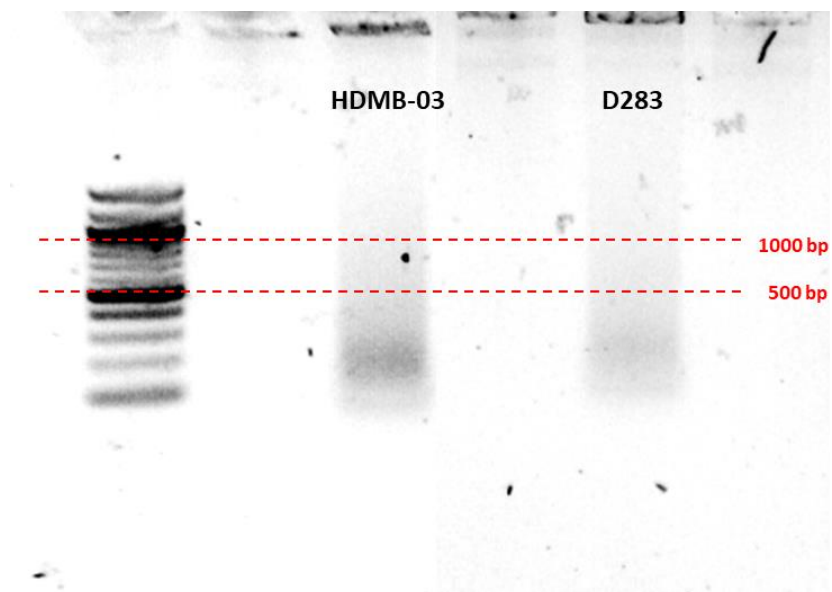
Appendix D7. Fragment size distribution (bp) of chromatin test samples prepared from HDMB-03 and D283 cell lines using the Magna G ChIP kit. Fragment distribution of each HDMB-03 (A) and D283 (B) test samples were assessed using an Agilent TapeStation. The central peak highlighted on the electropherogram represents the average fragment size, while lower and upper peaks represent the lower (25 bp) and upper (1500 bp) markers of the electronic ladder. Samples from both cell lines had an average fragment size of approximately 170 bp, which represents an ideal size to allow excellent resolution for ChIP sequencing.

Appendix D8

A

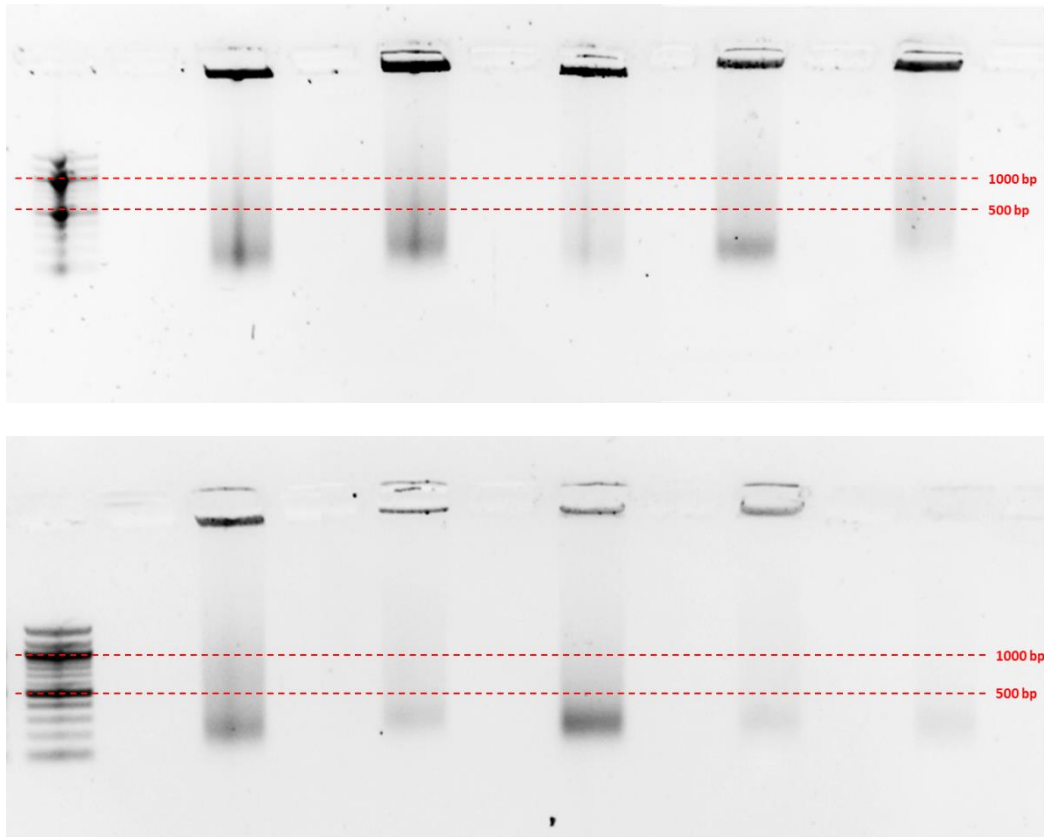


B



Appendix D8. Optimisation of Active Motif ChIP-IT High Sensitivity Kit. Purified, sheared chromatin isolated from fixed HDMB-03 and D283 cells were loaded onto a 1.5% agarose gel and electrophoresed at 120V. A cross-linking time of 1 minute and concentrations of 1% PFA was used for all test samples. Sonication was carried out at 15 s 30 seconds on/30 seconds off. A) Initial testing yielded no visible fragments on agarose gel. It was decided that this likely arose from poor cell and nuclear lysis resulting in limited chromatin release. As such the protocol was amended to include lysis through a 30 G syringe needle rather than a homogeniser as recommended. B) Samples drawn through a 30 G syringe needle yielded purified chromatin ranging predominantly between 100 bp and 600 bp in size with minimal fragments up to approximately 1000 bp.

Appendix D9



Appendix D9. Quality control of ChIP Sequencing samples. In order to ensure all samples submitted to sequencing were of appropriate fragment size, every input sample produced for ChIP sequencing was denatured and purified according to manufacturer's instructions, following which samples were run on a 1.5% agarose gel and electrophoresed at 120V. Any samples were sonication had not produced chromatin fragments of adequate size were re-synthesised and re-tested. All samples made using the Active Motif ChIP-IT High Sensitivity kit. Representative agarose gels depicting of 10 out of the submitted 36 samples shown.

Appendix D10

Number	Sample Name	Sample Concentration (ng/ μ L)	No. Required PCR Cycles
1	DT-HDMB-03-CIS N = 1	0.21	9
2	DT-HDMB-03-CIS N = 2	14.2	4
3	INPUT DT-HDMB-03-CIS	22.2	4
4	DT-HDMB-03-DMF N = 1	0.106	9
5	DT-HDMB-03-DMF N = 2	2.862	4
6	INPUT DT-HDMB-03-DMF	18.24	4
7	DT-D283-CIS N = 1	0.236	9
8	DT-D283-CIS N = 2	13.92	4
9	INPUT DT-D283-CIS	7.8	4
10	DT-D283-DMF N = 1	7.08	4
11	DT-D283-DMF N = 2	20.4	4
12	INPUT DT-D283-DMF	6.3	4
13	HDMB-03 + CIS N = 1	0.218	9
14	HDMB-03 + CIS N = 2	0.104	9
15	INPUT HDMB-03 CIS	23	4
16	HDMB-03 + DMF N = 1	0.302	9
17	HDMB-03 + DMF N = 2	1.69	4
18	INPUT HDMB-03 DMF	23.6	4
19	HDMB-03 + VIN N = 1	too low	9
20	HDMB-03 + VIN N = 2	11.4	4
21	INPUT HDMB-03 VIN	18.3	4
22	HDMB-03 + DMSO N = 1	too low	9
23	HDMB-03 + DMSO N = 2	3.94	4
24	INPUT HDMB-03 DMSO	16.6	4
25	D283 + CIS N = 1	0.124	9
26	D283 + CIS N = 2	0.456	9
27	INPUT D283 CIS	12.3	4
28	D283 + DMF N = 1	too low	9
29	D283 + DMF N = 2	11.8	4
30	INPUT D283 DMF	25	4
31	D283 + VIN N = 1	8.1	4
32	D283 + VIN N = 2	15.1	4
33	INPUT D283 VIN	27.4	4
34	D283 + DMSO N = 1	26.2	4
35	D283 + DMSO N = 2	7.94	4
36	INPUT D283 DMSO	23.4	4

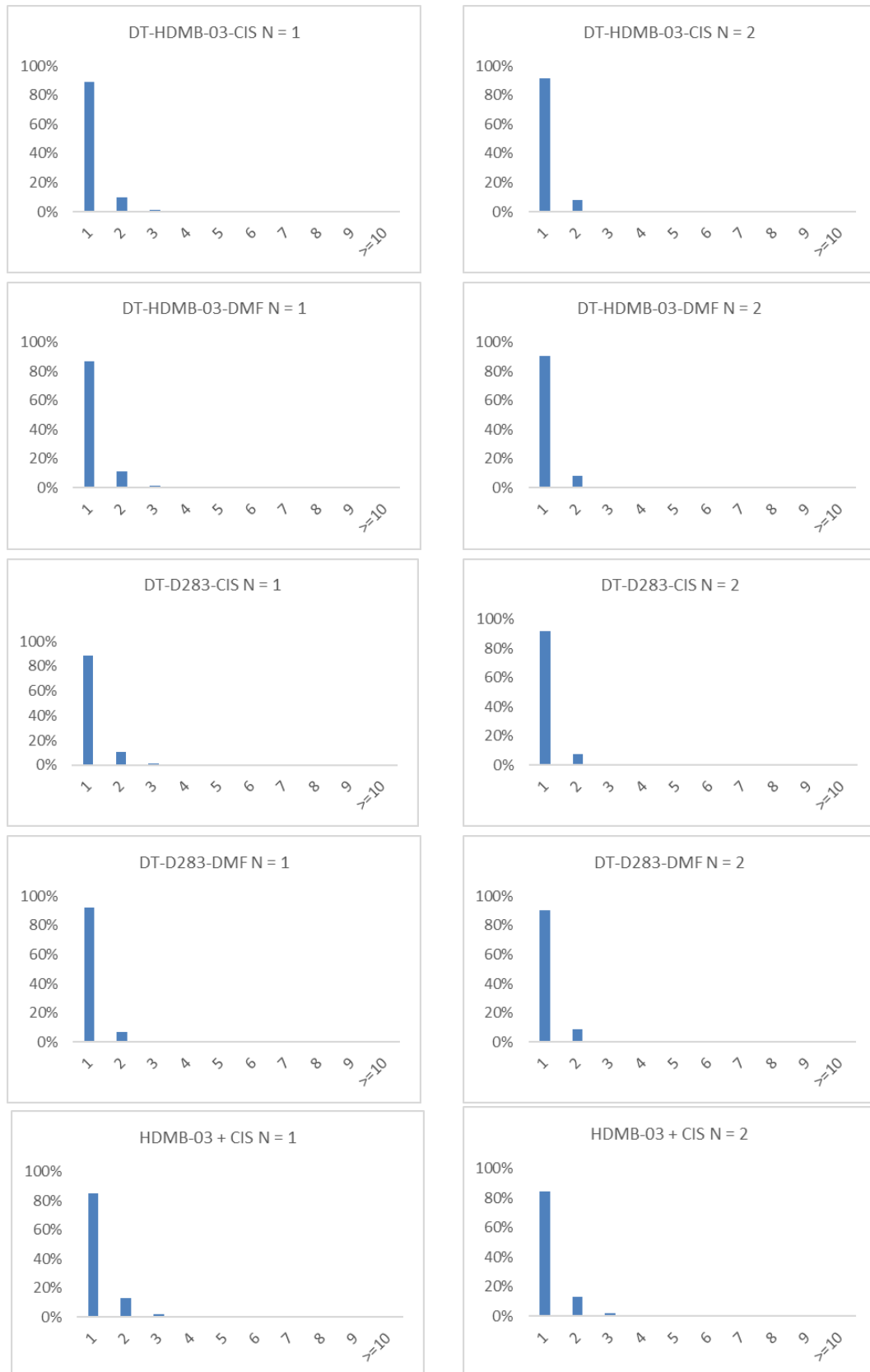
Appendix D10. ChIP-Seq sample concentrations. Prior to library preparation, all ChIP samples (input and IPs) were analysed using a Qubit Fluorometer to assess sample concentration. Samples with a concentration > 1.5 ng/ μ L underwent 4 cycles of PCR amplification while samples with lower concentrations underwent 9 PCR cycles to enrich resultant ChIP-Seq libraries.

Appendix D11

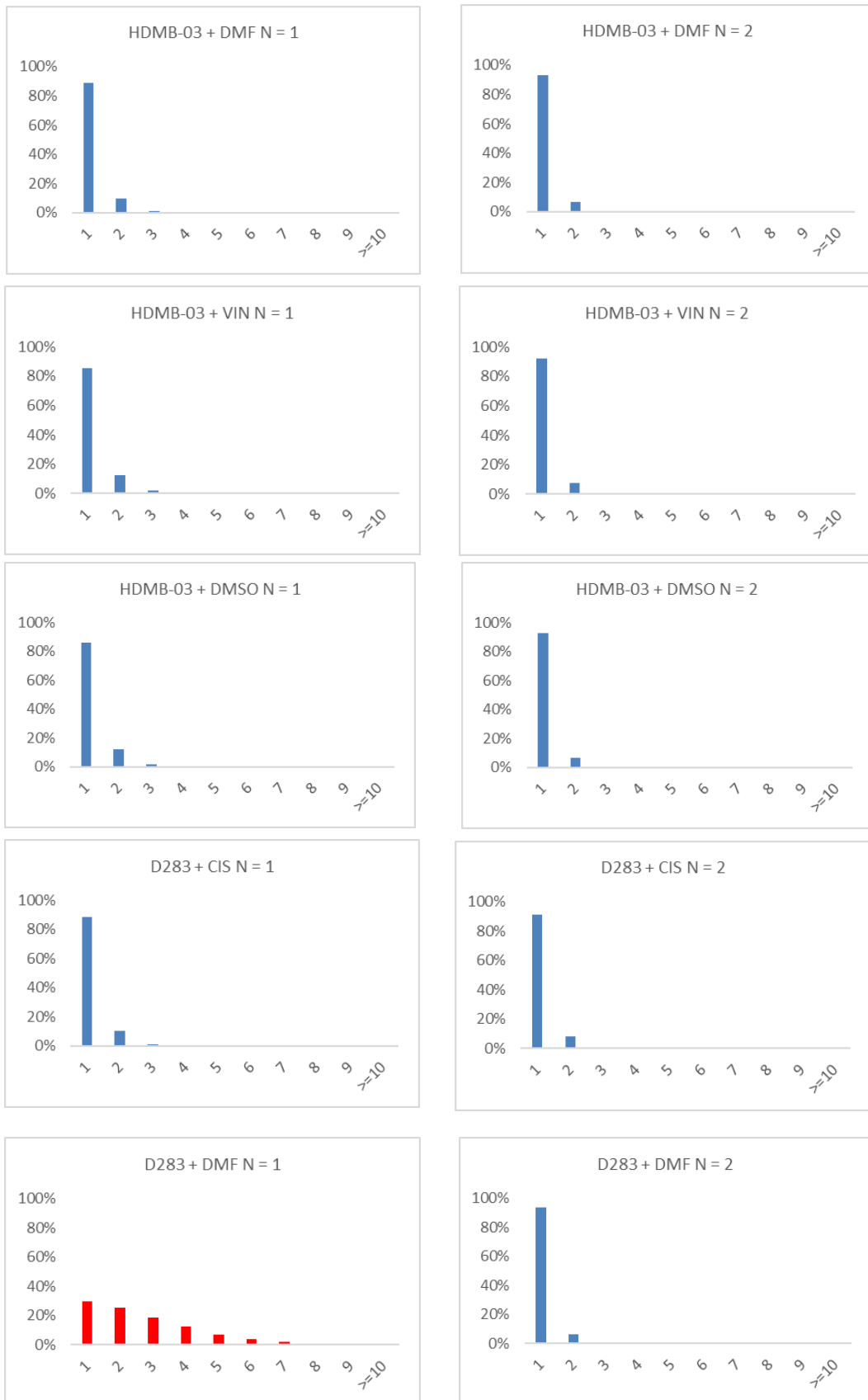
Number	Sample Name	Library Concentration (ng/ μ L)	Mean Fragment Size (bp)
1	DT-HDMB-03-CIS N = 1	7.9	573
2	DT-HDMB-03-CIS N = 2	2.9	601
3	INPUT DT-HDMB-03-CIS	3.74	506
4	DT-HDMB-03-DMF N = 1	3.66	563
5	DT-HDMB-03-DMF N = 2	2.96	591
6	INPUT DT-HDMB-03-DMF	4.12	529
7	DT-D283-CIS N = 1	4.96	625
8	DT-D283-CIS N = 2	3.14	562
9	INPUT DT-D283-CIS	4.6	511
10	DT-D283-DMF N = 1	2.76	579
11	DT-D283-DMF N = 2	3.36	609
12	INPUT DT-D283-DMF	4.3	506
13	HDMB-03 + CIS N = 1	6.96	591
14	HDMB-03 + CIS N = 2	3.32	581
15	INPUT HDMB-03 CIS	3.64	505
16	HDMB-03 + DMF N = 1	6.1	662
17	HDMB-03 + DMF N = 2	2.8	559
18	INPUT HDMB-03 DMF	3.94	479
19	HDMB-03 + VIN N = 1	3.08	545
20	HDMB-03 + VIN N = 2	2.4	554
21	INPUT HDMB-03 VIN	4.84	532
22	HDMB-03 + DMSO N = 1	3.56	588
23	HDMB-03 + DMSO N = 2	4.24	615
24	INPUT HDMB-03 DMSO	2.46	448
25	D283 + CIS N = 1	3.8	557
26	D283 + CIS N = 2	14.3	592
27	INPUT D283 CIS	2.84	501
28	D283 + DMF N = 1	1.44	540
29	D283 + DMF N = 2	2.28	603
30	INPUT D283 DMF	7.78	535
31	D283 + VIN N = 1	2.46	615
32	D283 + VIN N = 2	3.94	576
33	INPUT D283 VIN	2.7	441
34	D283 + DMSO N = 1	3.26	581
35	D283 + DMSO N = 2	2.8	559
36	INPUT D283 DMSO	3.16	528

Appendix D11. Quantification of prepared input and YB-1 ChIP libraries. Input samples are presented in blue.

Appendix D12



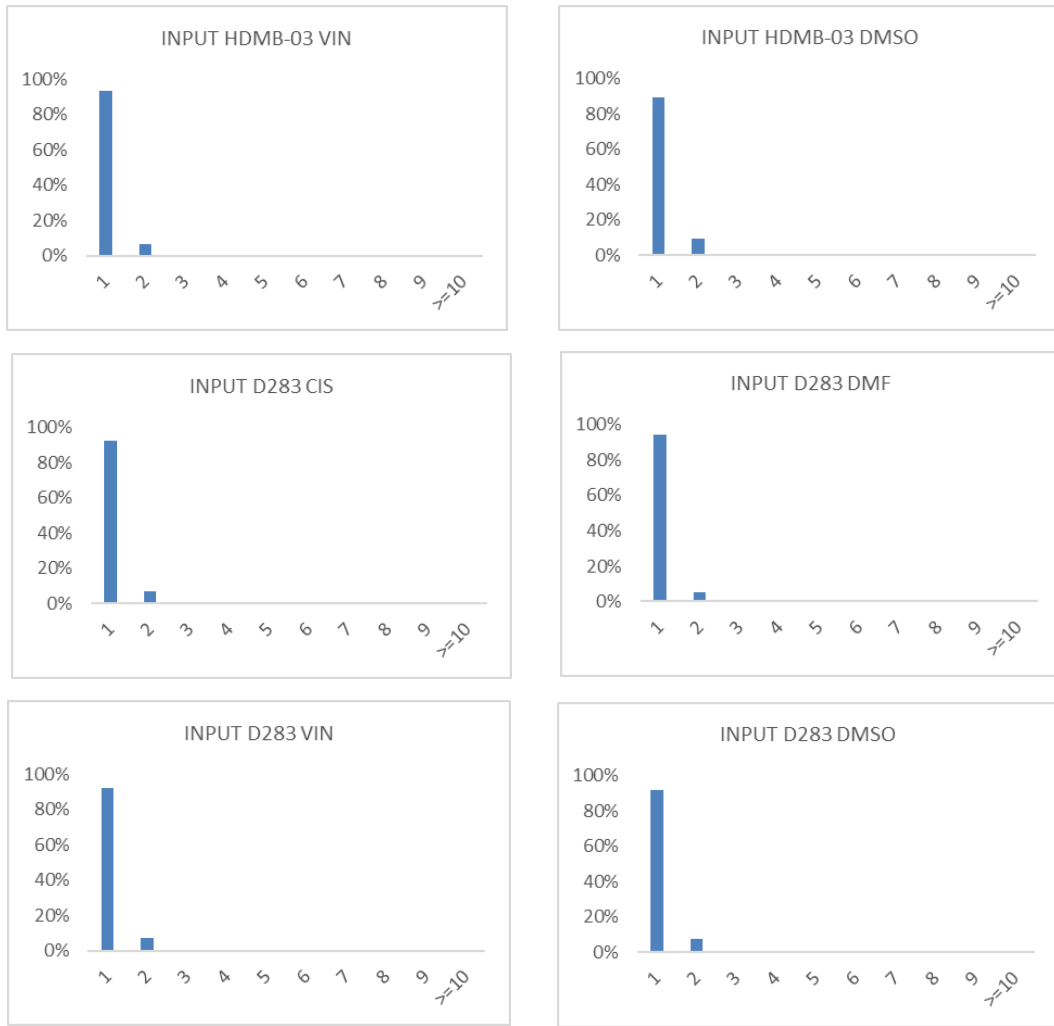
Appendix D12.1. Occurrence of duplicate reads from CHIP-Seq libraries. Frequency (%) of duplicate read occurrences.



Appendix D12.2. Occurrence of duplicate reads from ChIP-Seq libraries. Frequency (%) of duplicate read occurrences. Samples in red possessed a high occurrence of duplicate reads and were excluded from downstream analysis.



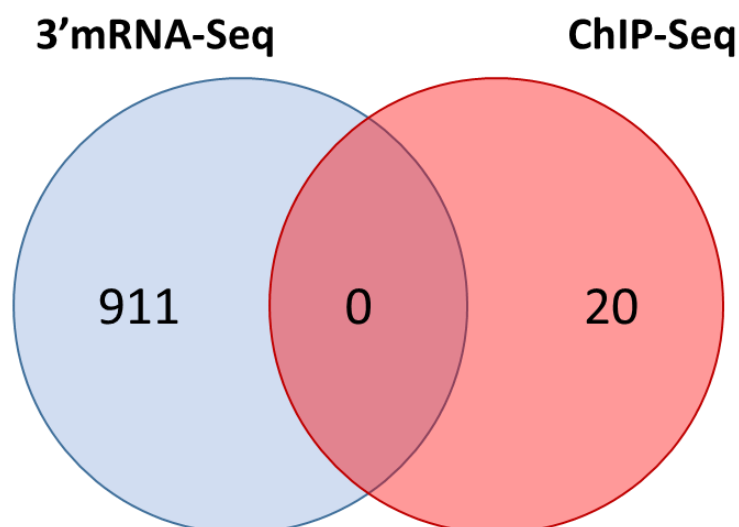
Appendix D12.3. Occurrence of duplicate reads from ChIP-Seq libraries. Frequency (%) of duplicate read occurrences.



Appendix D12.4. Occurrence of duplicate reads from ChIP-Seq libraries. Frequency (%) of duplicate read occurrences.

Appendix D13

A



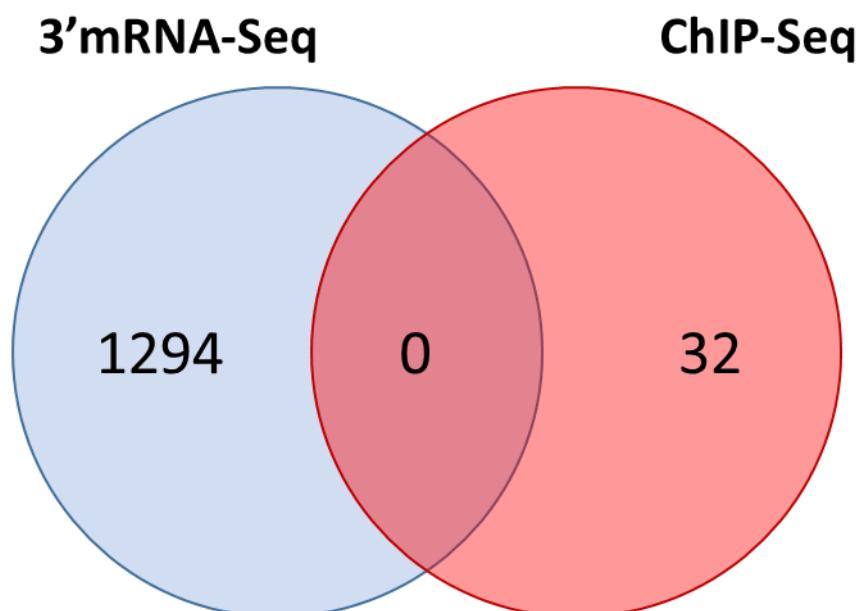
B

Unique Drug-Tolerant (DT-HDMB-03-CIS) Genes			
ENSG00000235070	GAPDHP49	ENSG00000279783	RN7SKP43
NBPF1	SCYGR9	TM4SF20	ENSG00000224414
RNA5SP19	RN7SL448P	ENSG00000240440	RNA5SP80
COL4A3	ENSG00000259136	ENSG00000230621	ENSG00000286272
RNU6-579P	IGKV1-13	MT-RNR1	ENSG00000239311

Appendix D13. Integration of unique DT-HDMB-03-CIS ChIP-Seq and 3'mRNA-Seq datasets revealed no overlap. Integration of YB-1 target genes identified as unique to DT-HDMB-03-CIS samples (i.e. not detected in DT-D283-DMF samples) and DEGs identified from 3'mRNA-Seq reveals no genes are common to both datasets. A) Venn diagram showing overlap of unique, drug-tolerant cell line genes and 3'mRNA-Seq DEGs. B) Table displaying the 20 YB-1 target genes identified as unique to DT-HDMB-03-CIS samples.

Appendix D14

A



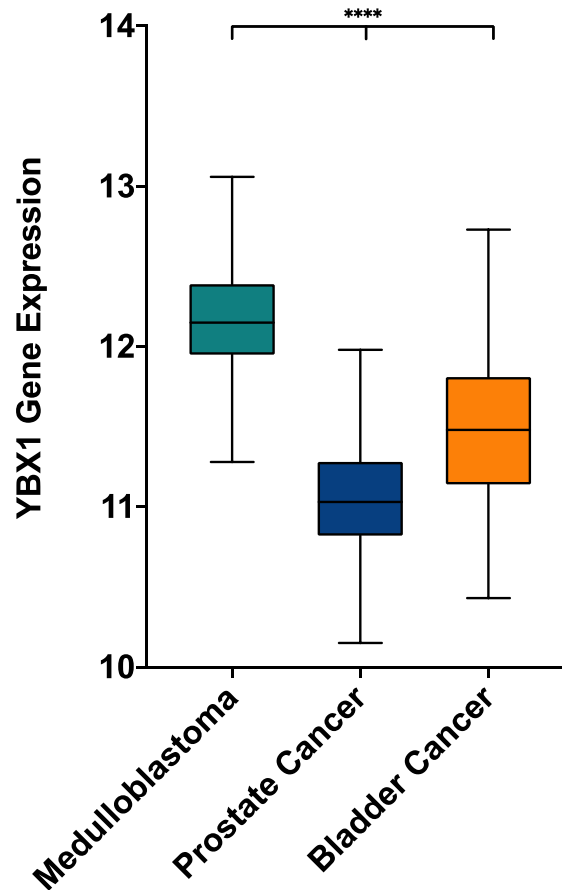
B

Unique Drug-Tolerant (DT-D283-CIS) Genes			
PKIA-AS1	ENSG00000253911	TMEM74	CNGB3
ENSG00000253214	NBN	OTUD6B	ENSG00000287208
ENSG00000254182	RNU6-748P	ENSG00000254001	ENSG00000253945
ENSG00000225885	ENSG00000253391	RPL32P4	NIPAL2
DUX4L37	PKHD1L1	RNA5SP274	ENSG00000286010
ENSG00000253122	RN7SKP231	DCSTAMP	ENSG00000253872
RNU6-690P	U2	RIPK2	LINC00534
TRHR	PDE4DIPP8	H2AZP7	PLEKHF2

Appendix D14. Integration of unique DT-D283-CIS ChIP-Seq and 3'mRNA-Seq datasets revealed no overlap. Integration of YB-1 target genes identified as unique to DT-D283-CIS samples (i.e. not detected in DT-D283-DMF samples) and DEGs identified from 3'mRNA-Seq reveals no genes are common to both datasets. A) Venn diagram showing overlap of unique, drug-tolerant cell line genes and 3'mRNA-Seq DEGs. B) Table displaying the 32 YB-1 target genes identified as unique to DT-HDMB-03-CIS samples.

Appendix E: Chapter 7 – Discussion

Appendix E1



Appendix E1. *YBX1* expression is significantly higher in medulloblastoma patients compared to prostate and bladder cancer patients. R2 Genomics Analysis was used to analyse differences in *YBX1* expression between different cancers in which YB-1 and its association with cisplatin resistance had been investigated. Medulloblastoma n = 223; prostate cancer n = 72; bladder cancer n = 93. Expression displayed as box plots showing minimum (lower line), lower quartile (bottom of box), median (line within box), upper quartile (top of box) and maximum (upper line). ****P > 0.0001. Significance assessed using Ordinary One-way ANOVA analyses with Tukey's multiple comparison test.

PhD Project Outputs

This project was funded by the Biotechnology and Biological Sciences Research Council (BBSRC) Doctoral Training Partnership (DTP), a four-year PhD programme in which a training month and three short research projects are completed in the first seven months, before starting the PhD project. During the programme, a three-month professional internship is also undertaken.

Laboratory Rotations

October – December 2017

A functional 3D biomimetic in vitro approach to assess brown fat thermogenesis.

Supervised by Prof Mike Symonds and Dr Virginie Sottile

January – February 2018

ABC transporters: a unifying force in tumour invasion and drug resistance?

Supervised by Dr Beth Coyle and Dr Ian Kerr

February – April 2018

Cell morphogenesis: The regulation of cell shape and behaviour in multiple cell types.

Supervised by Dr Marios Georgiou and Dr Ruman Rahman

List of publications

Original articles:

Taylor, L., Kerr, I., & Coyle, B. (2020). Y-Box Binding Protein-1: A Neglected Target in Pediatric Brain Tumors?. *Molecular Cancer Research*, 19(3), 375-387. doi: 10.1158/1541-7786.mcr-20-0655.

Conference abstracts:

SNO (Society for Neuro-Oncology), 2021, USA (in-person) – Taylor, L., Kerr, I., & Coyle, B. (2021): DDRE-37. YB-1 as a biomarker for drug resistance and tumour progression in medulloblastoma; *Neuro-Oncology* 23(Supplement_6):vi82

ISPNO (International Symposium On Paediatric Neuro-Oncology), 2020, Japan (virtual) - Taylor, L., Kerr, I., & Coyle, B. (2020): MBRS-42. YB-1 - a novel therapeutic target in high-risk medulloblastoma?; *Neuro-Oncology* 22(Supplement_3):iii405-iii405.

Grant Awards

July 2020 – UNICAS @ Graduate School Inter-disciplinary Grant; £4803.63; *'Elucidating the Role of YB-1 in Medulloblastoma Chemoresistance'*; Louisa Taylor, Matthew Carlile, Fei Sang.

January 2020 – The Stoneygate Children's Brain Tumour Research Fund Proof of Concept Award; 2020 – 2021; £35,568.00; *'Y Does Bra1n Tumour Therapy Fail?'*; Beth Coyle, Louisa Taylor; Ian Kerr; Franziska Linke.

Presentations

Oral Presentations

May 2021 - Children's Brain Tumour Research Centre Spring Research Day (15 min)

June 2019 - School of Medicine Postgraduate Research Forum (5 min)

April 2019 - Children's Brain Tumour Research Centre Spring Research Day (15 min)

April 2018 - BBSRC DTP Spring School Project Presentations (5 min)

Poster Presentations

November 2021 - Society for Neuro-Oncology Annual Meeting

December 2020 - International Symposium on Paediatric Neuro-Oncology

June 2019 - School of Medicine Postgraduate Research Forum

May 2019 – BBSRC DTP Spring School

Awards

May 2019 – Second Year Poster Prize at BBSRC DTP Spring School conference.

Professional Internship for PhD Students (PIPS)

Note to examiners

This statement is included as an appendix to the thesis in order that the thesis accurately captures the PhD training experienced by the candidate as a BBSRC Doctoral Training Partnership student. The Professional Internship for PhD Students is a compulsory 3-month placement which must be undertaken by DTP students. It is usually centred on a specific project and must not be related to the PhD project. This reflective statement is designed to capture the skills development which has taken place during the student's placement and the impact on their career plans it has had.

PIPS Reflective Statement

PIPS Reflective Statement; November 2019 – February 2020: *Assistant Producer of the Nottingham Festival of Science and Curiosity and Lab_13 Scientist in Residence with Ignite!.*

The requirement to undertake a three-month professional internship during my PhD was an exciting opportunity to build upon skills that are challenging to develop within a laboratory environment. Science outreach had always been an area that I was interested in exploring further. As Nottingham City Coordinator of Pint of Science I have had first-hand experience of seeing the benefits and importance of effective public engagement, both on the public and on the participating scientists. A significant barrier to effective public engagement is a misunderstanding of how to communicate knowledge and research, and importantly how to foster a mutual trust with the public. For this reason, my goals

for my internship were to experience working in the public engagement sector and to improve my science communication skills. With this in mind, I chose to spend my internship at Ignite!, a Nottingham-based education charity which aims to promote curiosity and STEM subjects across the East Midlands.

Ignite! functions at the intersection of creativity, curiosity and community. They work with schools, youth groups and communities, delivering a range of projects which aim to give families the opportunity to learn together, raise confidence in their own ideas and challenge preconceptions about the world. They also are the organisers of the Nottingham Festival of Science and Curiosity (FOSAC), a free and interactive science festival which takes place at numerous venues across Nottinghamshire. FOSAC is very different to other UK science festivals. Instead of using a big venue and hosting paid events with famous speakers, FOSAC holds free events in accessible venues such as local libraries, leisure centres and even the indoor market in Nottingham's Victoria Centre. The focus of the festival is to make STEM fun and most importantly, accessible for everyone, regardless of their background or social group.

My project at Ignite! was two-fold. First, I was the Assistant Producer of the festival, where I was the lead organiser of the festival's "Lates" programme – a series of STEM-themed events held in local pubs, bars and theatres aimed at adults. Outside of this role, I was also a "Scientist in Residence" for Ignite!'s Lab_13 BioCity project. Lab_13 BioCity is a partnership between Ignite! and BioCity where local primary school children are invited spend a day at the BioCity labs where they do experiments designed by a Scientist in Residence to investigate the

questions that matter to them.

I learnt a huge amount during my internship at Ignite!. Working with Year 5 pupils from local schools was a fantastic way to develop my communication skills. The students were extraordinarily curious and asked a lot of questions about my research. I had to learn how to explain complex ideas and difficult topics in a way that was interesting and understandable, a skill that is not only important when talking to the public, but also when conversing with other scientists outside of my field. In organising a science festival as big as FOSAC, I developed organisational and event management skills and learnt how to manage groups of interns and students who volunteered at the festival. Moreover, in the run up to the festival I was given the opportunity to appear on NottsTV where I spoke about the importance of science festivals, some of the events at FOSAC and even did a quick experiment live on air. I also took part in a podcast called NG Meets where I spoke about the festival as well as topics such as diversity in STEM and also wrote pieces about the festival for various local magazines. These opportunities were very valuable and greatly improved my communication skills and confidence in public speaking. Ignite! is a charity that relies on grant funding to support its projects and during my internship I also had the opportunity to write a grant application to fund some of the festival activities. The grant was successful and we were awarded £2000 from the UK Science Festival Network. As I was writing grants to support various sequencing experiments for my PhD project at the time, the experience of constructing a successful grant application was incredibly beneficial.

Overall, I thoroughly enjoyed my time with Ignite!. The opportunity to work in

STEM outreach and engagement gave me the opportunity to develop numerous transferable skills that I could take back to my PhD. Of equal importance, it allowed me to understand how to communicate science to the public, children and adults alike. I learnt what makes a successful science communicator and how important it is for scientists to take part in outreach, especially in projects that take place outside university walls, which can feel like a barrier to so many. Although spending time away from the lab bench did reinforce my love for research and the problem solving nature of scientific experiments, my internship made it very clear that I would like my future research-based career to include a public engagement role. As scientists, I believe that we have a responsibility to share our research with the public and working with Ignite! showed me how vital and rewarding this can be.

